The origin and magmatic evolution of the REE-rich Strange Lake A-type peralkaline granite, northern Québec-Labrador, Canada

KARIN SIEGEL

December 2017

Department of Earth & Planetary Sciences,

McGill University, Montreal

A thesis submitted to McGill University in partial fulfillment of the requirements of the degree of Doctor of Philosophy

ABSTRACT

Although it is well known that A-type granites are enriched in high field strength elements (HFSE), such as Zr, Nb and the REE, the magmatic processes controlling their unusual enrichment and the sources of these elements are still debated. The 1.24 Ga Strange Lake pluton in the Paleoproterozoic '*Core Zone'* of Québec-Labrador, which belongs to the large Nain Plutonic Suite, provides an extraordinary example of extreme HFSE-enrichment in a peralkaline A-type granite. In this study, unaltered samples from the center of the pluton were analyzed for their bulk rock and mineral major and trace element compositions (alkali feldspar, alkali amphibole, alkali zirconosilicates, primary REE-minerals). Two hypersolvus granite units (south and north) contain a perthitic alkali feldspar as the earliest major phase and, in addition to quartz, a sodic amphibole (mostly arfvedsonite) as a late interstitial phase. A transsolvus granite has separate microcline and albite crystals in addition to primary perthitic alkali feldspar, and the sodic amphibole occurs as phenocryst phase. The primary HFSE-minerals are zircon (Zr, HREE), monazite-(Ce) (LREE), pyrochlore group minerals (LREE, Nb), as well as gagarinite-(Ce) (LREE, Y), in the case of the transsolvus granite. Magma evolution progressed from the southern to the northern hypersolvus to the transsolvus granite, and is indicated by decreasing bulk Al (avg. 11.9, 11.7 and 10.3 wt. % Al_2O_3, respectively), and increasing Si, Fe, Rb, REE, Zr, Nb concentrations and alkalinity indices (avg. 1.13, 1.15 and 1.27, respectively). Perthitic alkali feldspar compositions mirror the bulk rock trend, i.e., decreasing Al contents match with increasing Si, Fe^{3+}, REE, Zr and Nb contents. The crystallization of alkali zircono- and titano-silicates marked a transition from miaskitic to agpaitic phase assemblages. The low viscosity (10^4–10^5 Pa·s) transsolvus granite formed in the magma chamber by the removal of the feldspar-rich hypersolvus granites, and the saturation in sodic amphibole, which, due to a release of F to

the melt, triggered a transition from hypersolvus to subsolvus conditions. The dark grey enclaves hosted by this unit are interpreted to represent the quenched and feldspar-rich margin of both the hypersolvus and transsolvus granite. The hypersolvus and transsolvus granite magmas evolved and concentrated the HFSE by a combination of perthitic alkali feldspar fractionation, low viscosity induced density segregation of early HFSE-minerals, and the early unmixing of a REE-rich fluoride melt.

The study of the amphibole-group minerals from Strange Lake was designed to gain a detailed insight into the evolving magma conditions. Compositions range from sodium-calcium amphibole (ferro-ferri-katophorite) in the least evolved southern hypersolvus granite to sodium amphibole (arfvedsonite, ferro-ferri-leakeite) in the other, more evolved units. High Na, Si, Li, and low Al and Ca concentrations in the phenocrysts of the transsolvus granite indicate that it crystallized from a more evolved magma than the hypersolvus granite, despite the fact that these crystals formed early. Increasing Fe^{3+}/Fe^{2+} ratios in the amphibole with granite evolution are interpreted to reflect crystal chemical effects (Na/Ca-ratio) and the product of increasing fO_2, F^- and OH^- in the melt. All the amphiboles have elevated Nb, Zr, Hf and REE concentrations compared to the bulk rock, suggesting that these elements were compatible, whereas the much lower Ti concentrations were due to saturation in sodium-titanosilicates. The amphibole REE concentrations vary greatly among the granite units. The amphibole of the southern and northern hypersolvus granite contains 0.16 and 0.07 wt. % ∑REE+Y, on average, and the crystals of the transsolvus granite only 0.01 wt. %, despite the more evolved nature of its host. The compositional difference may be due to the fact that the latter represents early phenocrysts, whereas the hypersolvus amphibole is a late interstitial phase. Variations in the chondrite-normalized LREE-profiles reflect the variable crystallization of primary LREE-bearing phases as well as the exsolution of a LREE-rich fluoride melt. The LREE are incompatible in the amphibole structure (apparent $D < 0.01$) and are preferably accommodated by the octahedral C-site, whereas the HREE occupy the B-site. The HREE profiles are steep and narrow, and display an increasing relative enrichment that culminates in compatible behavior for Yb and Lu (apparent $D > 1$), suggesting that their concentrations are controlled by partitioning (crystal chemical effects). Large proportions of the bulk HREE content (up to 70 %) reside in the amphibole and their later release through hydrothermal replacement helps explain the unusual HREE enrichmen of the Strange Lake pluton.

Age-corrected εNd values of the bulk samples and sodic amphiboles from the pluton reach from -0.6 to -5.7, and -0.3 to -5.3, respectively. The $^{147}Sm/^{144}Nd$ ratios of the suite are between 0.0967 and 0.1659, large variations that can be explained by in-situ fractionation of early LREE-minerals and late hydrothermal HREE remobilization. The measured $\delta^{18}O$ values for quartz are between +8.2 and +9.1, and are considerably higher than the mantle value of 5.7 ± 0.2 ‰. The negative εNd values and positive $\delta^{18}O$ values indicate that the magma experienced considerable crustal contamination. The underlying Archean Mistinibi (para-) gneiss complex, which is characterized by low εNd and high $\delta^{18}O$ values, has been considered as the major contaminant. Mixing of 5 – 15 % of such a gneiss, having an εNd value of -15 and a $\delta^{18}O$ value of +11, with a moderately enriched mantle source (εNd = +0.9, $\delta^{18}O = +6.3$) would produce values similar to those of the Strange Lake granites. Based on analogies between the Nain Plutonic Suite and the Gardar alkaline igneous province (SW-Greenland), the Strange Lake pluton and associated REE-mineralized anorogenic bodies are interpreted to be the result of a combination of subduction-induced fertilization of the sub-lithospheric mantle, crustal extension and in-situ magma evolution.

RESUME

Il est bien connu que les granites de type-A sont enrichis en éléments à champ électrostatique élevé (high field strength elements = HFSE), tels que le Zr, le Nb et les terres rares (rare earth elements = REE). Toutefois, les processus magmatiques qui contrôlent l'enrichissement inhabituel de ces éléments et leurs sources restent largement débattus. Le pluton de Strange Lake (1.24 Ga), qui appartient à la Suite Plutonique de Nain dans la 'Core Zone' Paléoprotérozoïque de Québec-Labrador, fournit un exemple d'enrichissement extrême en HFSE dans un granite peralcalin de type-A. Dans cette étude, des échantillons non altérés provenant du centre du pluton ont été analysés pour déterminer leur composition en roche totale, ainsi que leur composition minéralogique en éléments majeurs et en éléments en traces (feldspath alcalin, amphibole alcaline, zirconosilicates alcalins, minéraux de terres rares primaires). Deux unités de granite hypersolvus (sud et nord) contiennent un feldspath alcalin perthitique comme phase majeure précoce et, en plus du quartz, une amphibole sodique (principalement de l'arfvedsonite) en phase interstitielle tardive. Un granite transsolvus se caractérise par des cristaux distincts des cristaux distincts de microcline et d'albite en plus de la feldspath alcalin perthitique primaire, et par la présence d'amphibole sodique sous la forme de phénocristaux. Les principaux minéraux porteurs de HFSE sont le zircon (Zr, HREE), la monazite-(Ce) (LREE), les minéraux du groupe du pyrochlore (LREE, Nb), et la gagarinite-(Ce) (LREE, Y) dans le granite transsolvus. L'évolution magmatique a progressé depuis le granite hypersolvus au sud vers celui au nord, puis vers le granite transsolvus, et se caractérise par une diminution en Al (11.9, 11.7 et 10.3 $\%_{\text{poids}}$ Al_2O_3 en moyenne, respectivement), et par une augmentation des concentrations en Si, Fe, Rb, REE, Zr, Nb et de l'indice d'alcalinité (1.13, 1.15 et 1.27 en moyenne, respectivement). Les compositions de la feldspath alcalin perthitique reflètent les variations de la roche totale, à savoir

une diminution de la concentration en Al correspondant à une augmentation des concentrations en Si, $Fe^{3+,}$ REE, Zr et Nb. La cristallisation de zircono- et de titano-silicates alcalins marque une transition entre les assemblages de phase miaskitique et agpaïtique. Le granite transsolvus, d'une viscosité faible (10^4-10^5 Pa·s), s'est formé dans la chambre magmatique par l'évacuation des granites hypersolvus riches en feldspath, et par la saturation en amphibole sodique, qui, en raison d'une libération de F dans le magma, a déclenché une transition des conditions d'hypersolvus vers subsolvus. Les enclaves gris foncé présentes dans cette unité sont interprétées comme la marge trempée et riche en feldspath des granites hypersolvus et transsolvus. Les magmas granitiques hypersolvus et transsolvus ont évolué et concentré les HFSE par le fractionnement de la feldspath alcalin perthitique, par la ségrégation par densité des minéraux porteurs de HFSE induite par la viscosité faible, et par la ségrégation précoce d'un liquide fluoré enrichi en REE.

L'étude des minéraux du groupe des amphiboles de Strange Lake a été conçue pour permettre un suivi détaillé des conditions du magma en évolution. Les amphiboles varient en composition de sodique-calcique (ferro-ferri-katophorite) dans le granite hypersolvus du sud, le moins évolué, à sodique (arfvedsonite, ferro-ferri-leakeite) dans les autres unités plus évoluées. Les concentrations élevées en Na, Si, Li et les faibles teneurs en Al et Ca des phénocristaux d'amphibole dans le granite transsolvus indiquent que celui-ci a cristallisé à partir d'un magma plus évolué que le granite hypersolvus, malgré le fait que ces cristaux se soient formés tôt. La hausse des ratios de Fe^{3+}/Fe^{2+} dans les amphiboles pendant l'évolution granitique est le produit d'effets cristallochimiques (ratio Na/Ca) et de l'augmentation de $fO_{2,}$ F^- et OH^- dans le magma. Toutes les amphiboles ont des concentrations élevées de Nb, Zr, Hf et REE par rapport à la roche totale, suggérant que ces éléments étaient compatibles, alors que les concentrations de Ti plus faibles étaient dues à la saturation des titanosilicates de sodium. Les concentrations de REE dans les amphiboles varient considérablement entre les différentes unités de granite. Les amphiboles des granites hypersolvus du sud et du nord contiennent, en moyenne, 0.16 et 0.07 $\%_{\text{poids}}$ ΣREE + Y, respectivement, et les cristaux du granite transsolvus 0.01 $\%_{\text{poids}}$ seulement, malgré la nature plus évoluée la roche hôte. La différence de composition est peut être due au fait que ces derniers représentent des phénocristaux précoces, alors que l'amphibole hypersolvus est une phase interstitielle tardive. Les variations dans les profils de terres rares légères (LREE) normalisés aux chondrites reflètent la cristallisation variable des principales phases porteuses de LREE, ainsi que l'exsolution d'un liquide fluoré riche en LREE. Les LREE sont incompatibles dans la structure de l'amphibole ($D_{apparent} < 0.01$) et sont accommodés préférentiellement par le site octaédrique C, tandis que les HREE (terres rares lourdes) occupent le site B. Les profils de terres rares lourdes (HREE) sont abrupts et étroits, et présentent un enrichissement relatif qui aboutit à un comportement compatible du Yb et du Lu ($D_{apparent} > 1$), ce qui suggère que leurs concentrations sont contrôlées par le partitionnement (effets cristallochimiques). Une grande proportion de la teneur totale de la roche en HREE (jusqu'à 70%) réside dans l'amphibole et leur libération tardive par remplacement hydrothermal aide à expliquer les enrichissements inhabituels en HREE du pluton de Strange Lake.

Les valeurs corrigées de l'âge de εNd de la roche totale et des amphiboles sodiques du pluton se situent entre -0.6 et -5.7, et -0.3 et -5.3, respectivement. Les valeurs du ratio ^{147}Sm/^{144}Nd de la suite, entre 0.0967 et 0.1659, montrent de larges variations qui peuvent être expliquées par le fractionnement in-situ précoce de minéraux porteurs de LREE, et par la remobilisation hydrothermale tardive des HREE. Les valeurs mesurées de δ^{18}O du quartz sont comprises entre 8.2 et 9.1, et sont considérablement plus élevées que la valeur du manteau (5.7 ± 0.2 ‰). Les valeurs négatives de εNd et positives de δ^{18}O indiquent que le magma a subi une contamination

crustale. Le complexe Archéen sous-jacent de (para-)gneiss de Mistinibi, qui se caractérise par valeurs faibles de εNd et élevées de $\delta^{18}O$, est considéré comme le principal contaminant. Le mélange de 5-15% d'un tel gneiss, caractérisé par un εNd de -15 et un $\delta^{18}O$ de +11, avec une source mantellique modérément enrichie (εNd = +0.9, $\delta^{18}O$ = +6.3), produirait des valeurs semblables à ceux des granites de Strange Lake. Par analogie avec la Suite Plutonique de Nain et la province ignée alcaline de Gardar (sud-ouest Groenland), le pluton du Strange Lake et les intrusions anorogéniques associées minéralisées en REE, sont interprétés comme le résultat de la fertilisation du manteau sous-lithosphérique, induite par subduction, combinée à l’extension de la croûte et à l’évolution in-situ du magma.

ACKNOWLEDGEMENTS

Special thanks go to my supervisor Anthony E. Williams-Jones for his continuous support and advice as well as the creative environment he provides in his research group. I appreciated a high degree of freedom and independency throughout my Ph.D. I am grateful for Willy's trust in me, his strong hand in revising and editing of the manuscripts and the opportunity to participate in several international research conferences. The funding of the thesis was provided by grants from Quest Rare Minerals Ltd. and NSERC to Dr. Anthony E. Williams-Jones and financial support to the author from the Department of Earth and Planetary Sciences, McGill University.

During fieldwork I enjoyed to be accompanied by Angela Buchanan, a competent field assistant. I also thank Patrick Collins and Colin Hayes (former Quest Rare Minerals Ltd.) for the provision of data and logistics. Thanks to Penney Glen (Dept. of Natural Resources, Gov. of Newfoundland and Labrador) for granting access to the core storage center in Goose Bay, Labrador.

At the Department of Earth and Planetary Sciences (McGill University) I thank Lang Shi for his help, advice and fruitful discussions at the electron microprobe facility. I specially admire Vincent van Hinsberg for his extensive knowledge on any matter, and I'm grateful for in-depth discussions, help with data interpretation, modeling and the Iolite software. I am particularly grateful for knowing Robert Martin and to be able to benefit from his extensive experience, for lively debates, supplementary material and his advice. Special thanks go to Olga Vasyukova for countless hours of lively discussions, her scientific competence and her friendship. Thanks go also to Alexander Gysi (now CSM) for his advice and the sharing of samples. Bill Minarik is thanked for his help with the Iolite software. I am very grateful to Galen Halverson and his

group, including Peter Crockford, for their help at the GEOTOP laboratories and the use of their equipment.

At GEOTOP (Université de Québèc à Montréal, UQAM) I am deeply grateful to André Porier and Julien Gogot for their extensive help with the LA-ICP-MS facility, the use of the clean lab and wet chemistry procedures as well with the TIMS facilities.

Andy Kerr (former CSG), Mike Hamilton (UofTo) and David Corrigan (CSG) provided their time and interest for informative conversations on the fourth chapter. They also provided supplementary material which helped greatly in the understanding of the geology in Northern Québec and Labrador.

My fellow grad students Nicole Hurtig, Sebastian Fuchs, Sarah Bodeving, Ichiko Sugyiama, Nicolas Gaillard, Jason Coumans, Joel Trofanenko, Ryan Libbey, Gregor Lucic, Charlie Beard, Nils Backeberg and Volker Möller helped with analytical work and discussions, and I spent unforgettable times with them on field trips, field schools and conferences. I also shared wonderful experiences on field trips and conferences with the fellow students of the UQAM mineral deposits group.

My partner Perry Keijzer provided kind and continuous support during the publishing process of the manuscripts and the finalization of my Ph.D. My good friends Sarah Wörndle, Ichiko Sugyiama, Andres Felipe Peña Castro, Louise-Marie Meunier, Sarah Bodeving, Thomas Maguire and Jaana Vapaavuori were great listeners and supporters throughout my Ph.D. Also my sister Linda, my brother David as well as my parents and grandparents provided their constant encouragement and interest.

PREFACE

This research was performed in the Department of Earth and Planetary Sciences at McGill University, as well as in the GEOTOP laboratories at Université du Québec à Montréal (UQAM). Access to the field area was provided by Quest Rare Minerals Ltd. Fieldwork was accomplished in the summers of 2012 and 2013, assisted by Angela Buchanan and Patrick Collins, and included detailed mapping and core-logging. A set of additional rock samples and thin-sections were provided by Alexander Brosseau-Liard and Robert Fritscher, former graduate students, as well as Alexander Gysi and Olga Vasyukova, former post-doctoral fellows of the research group.

At McGill University, Lang Shi helped with the Electron microprobe mineral analyses and Anna Jung supervised mineral analysis at the Laser Ablation ICP MS facility. Analytical work at GEOTOP, including the use of the clean lab, the TIMS facilities as well as Laser Ablation ICP MS were supervised by André Poirier and Julien Gogot, who helped a great deal to improve the data quality. The oxygen isotope analyses were performed by the team of Fred Longstaffe at the Laboratory for Stable Isotope Science at University of Western Ontario (UWO) as well as at the Queen’s facility for Isotope Research (Queens University).

The author prepared the samples (grinding, milling and mineral separation), performed the laboratory work (column chemistry) and analyses (SEM, EMPA, LA-ICP-MS, TIMS), and carried out the data reduction and calculations. The author also interpreted the results and, with the help of Dr. A.E. Williams-Jones, wrote the manuscripts and published the research findings. The thesis abstract was translated by Nicolas Gaillard, a fellow student of the research group.

The thesis consists of three manuscripts, all of which are the product of scientific collaboration between the author and Dr. Anthony Williams-Jones, the supervisor of this research project.

Olga Vasyukova is a co-author on Chapter 2; her experience with and understanding of the nature of the Strange Lake magma made an essential contribution to the manuscript. Chapter 3 is co-authored by Vincent van Hinsberg, who contributed in the application of lattice strain theory to the inter-site partitioning of the REE in amphibole. The manuscript benefitted considerably from reviews by Dr. Nelson Eby, Dr. Massimo Tiepolo and Dr. Kathryn Goodenough. Chapter 4 was co-supervised by Ross Stevenson (UQAM); his help was crucial for the interpretation of the Nd-isotope data. Constructive reviews by Dr. Bernard Bonin and Dr. William J. Collins helped to improve this manuscript significantly.

The current status of the material contained in this thesis is as follows:

Chapter 2: IN REVIEW - Siegel, K., Vasyukova, O., Williams-Jones, A.E., Magmatic evolution and controls on rare earth mineralization of the Strange Lake A-type peralkaline granitic pluton, Québec-Labrador, Lithos.

Chapter 3: PUBLISHED – Siegel, K., Williams-Jones, A.E., van Hinsberg, V.J., The amphiboles of the REE-rich A-type peralkaline granitic Strange Lake pluton – fingerprints of magma evolution, Lithos (2017): 288-289, doi 10.1016/j.lithos.2017.07.012.

Chapter 4: PUBLISHED – Siegel, K., Williams-Jones, A. and Stevenson R., A Nd- and O-isotope study of the REE-rich peralkaline Strange Lake granite: implications for Mesoproterozoic A-type magmatism in the Core Zone (NE-Canada), Contributions to Mineralogy and Petrology (2017): 172 (54), doi: 10.1007/s00410-017-1373-x.

CONTENTS

LIST OF FIGURES

LIST OF TABLES

CHAPTER 1 - THESIS INTRODUCTION

1.1 A-TYPE GRANITES IN THE CONTEXT OF ALKALINE ROCKS

1.1.1 Characteristics of A-type granites

The Strange Lake pluton, owing to its unique mineralogy and alkaline composition, but particularly due to its extreme enrichment in the REE, Zr, Nb and F, is classified as an A-type granite. A-type granitoid rocks are members of a large group of alkaline igneous intrusive felsic rocks with a wide range of compositions and textures, and include silica-undersaturated alkali nepheline syenites, saturated quartz syenites and silica-oversaturated suites (Bailey and Schairer, 1966). The A-prefix originates from their alkaline character and/or their association with anorogenic rift settings (Bonin, 2007). It is well known that A-type granitic rocks are enriched in incompatible and high field strength elements such as the REE Zr, Nb, U, Ta, but also volatiles such as F, Cl and H_2O (Bonin, 2007). Chemically they are distinguished from other granitoid types (S- or I-type) by high alkali (Na+K) concentrations, high Fe/Mg, Ga/Al, Nb/Yb and Zr/Ti ratios and low Ca, Sr, and Ba concentrations (Eby, 1990; Frost et al., 2001a; Whalen et al., 1987). Their degree of alkalinity, even within the same intrusive suite, can range from subalkaline or metaluminous to peralkaline and agpaitic (Whalen et al., 1987).

Peralkaline granites represent a sub-group of A-type granitoids that are characterized by the occurrence of sodic pyroxene (e.g., aegirine) and amphibole (e.g., riebeckite or arfvedsonite) as major mafic phases. In addition, peralkaline granites are distinguished from other, more common A-type granites by having an agpaitic or alkalinity index (molar Na+K/Al) significantly greater than 1.0 (MacDonald, 1974). An important consequence of this high alkalinity is that alkali zircono- and/or titano-silicates crystallize in place of primary zircon and/or titanite (and ilmenite), respectively (Linthout, 1984). This change in phase assemblages, which is referred to as the miaskitic to agpaitic transition, has been applied mostly to silica-undersaturated alkaline suites (Linthout, 1984; Marks et al., 2011; Schonenberger and Markl, 2008) but, in principle, is also applicable to saturated and oversaturated alkaline igneous rocks. The agpaitic rocks are a subgroup of extreme alkalinity (agpaitic index >1.2) (Sorensen, 1997) with exotic mineralogy (Khomyakov, 1995). Well-known examples include Khibina (Kola Peninsula, Russia) (Kramm and Kogarko, 1994) and the Ilímaussaq complex of the Gardar Province, SW-Greenland (Ferguson, 1970; Andersen and Friis, 2015), as well as the Khaldzan Burgetey rare metal deposit, Mongolia, which is hosted in agpaitic granites (Kovalenko et al., 1995).

1.1.2 Hypotheses for the formation of A-type granitoids

Even though a large number of A-type granitoids have been thoroughly investigated, no single hypothesis for how they form has been agreed on. On the contrary, researchers have shown that A-type granites can be the product of a variety of processes, which are further reviewed below.

Some researchers have proposed that A-type granites can be produced by the fractionation of basaltic magmas of mantle origin. For example, the formation of the Fe-rich alkalic Sherman granitic batholith and the Red Mountain monzonitic to granitic pluton (Laramie Anorthosite Complex), based on Pb, Nd and Sr isotopic evidence, has been attributed to fractional crystallization of a ferrodioritic melt of mantle origin (Frost et al., 1999, 2001, 2002; Andersen et al., 2003). Frost and co-workers had previously suggested that A-type granites can be produced by partial melting of ferrodiorite, which originated from underplating of the crust by tholeiitic magmas (e.g. Frost and Frost, 1997). However, a ferrodiorite-related origin for the magmas has not been universally accepted. For example, on the basis of initial Sr- and Nd- isotope signatures and geochemical modeling, Schmitt et al. (2000) and Schmitt et al. (2002) proposed that the peralkaline granites of Brandberg, Namibia, crystallized from the residues of highly fractionated alkali-basaltic mantle melts. In the case of A-type ferroan granites and syenites associated with massive anorthosites (e.g., the Eastern Ghats Belt, India), it has been proposed that the magmas were the products of tholeiitic melts that underwent high pressure (~6.8 kb) differentiation (Kumar et al., 2007).

Several researchers have proposed that metasomatic processes play an essential role in the formation of A-type granites (Martin, 2006, 2012). For example, Woolley (1987) suggested that the coexistence of alkaline syenitic, granitic and carbonatitic rock groups of the Chilwa Province (Malawi) resulted from melting of metasomatized lithosphere at different depths. Indeed, numerous studies have provided evidence for the metasomatism of lherzolite and harzburgite unrelated to subduction in the form of elevated concentrations of volatiles such as F, CH_4 and CO_2. Moreover, these metasomatized mantle rocks have also been shown to be enriched in the HSFE, including the REE (Neumann et al., 2002; Zaccarini et al., 2004).

A few studies have concluded that A-type granites are exclusively of crustal origin, based on their εNd values, initial $^{87}Sr/^{86}Sr$ ratios and Sr and Rb concentrations. For example, owing to their strongly negative εNd values, the intraplate rapakivi A-type granites of Carajas, Brazil, are interpreted to have resulted from melting of Archean crust (Dall'Agnol et al., 2005). A-type granitoids of the Lachlan Fold Belt, Australia, on the basis of their anhydrous nature, highly variable initial $^{87}Sr/^{86}Sr$ ratios as well as high Sr and low Rb concentrations have been linked to the melting of a residual lower crust that had earlier generated an I-type granite (Collins et al., 1982). Given their data, Collins et al. (1982) ruled out the hypothesis that these A-type granitoids resulted from extensive fractionation (feldspar) of this earlier I-type granite.

Recently, liquid immiscibility has been proposed as a driving force of A-type granite evolution. For example, the Madeira peralkaline tin-mineralized albite-rich granite from Pitinga, Brazil, is interpreted to represent a F-rich peralkaline phase that separated from a metaluminous to peralkaline parental melt as an immiscible liquid (Costi et al., 2009). Melt inclusion studies of evolved tin-enriched peralkaline granites from the Erzgebirge (Germany), also have provided strong evidence that the peralkaline phase (enriched in Cl, P, B, F, Ca, Fe, and HFSE (Sn, W, Nb, Ta, Zr) and depleted in Si and Al), separated relatively early from a more silicic peraluminous melt (Thomas et al., 2005; 2006). The phase separation is not restricted to silicate melts. Indeed, in the case of the Strange Lake pluton, a recent melt inclusion study has provided strong evidence for the early separation of a REE-rich fluoride melt from the silicate melt, which accumulated during granite evolution and resulted in the hyper-enrichment of the pegmatites in the rare earth elements (Vasyukova and Williams-Jones, 2014, 2016).

Many studies have concluded that A-type granites are the product of a fertile mantle melt which underwent variable degrees of crustal contamination (Hegner et al., 2010; Landoll and Foland, 1996). Some researchers have suggested that potassic magmas are generated at deeper mantle levels, and sodic-potassic partial melts stem from higher, amphibole-rich, mantle levels (Lloyd and Bailey, 1975). Pre-enrichment of a depleted mantle may be produced by metasomatism related to subducted oceanic crust of predominantly basaltic composition (Bailey, 1987). For example, the rare-metal deposits of Khaldzan Burgetey and Khan Bogd (Mongolia) show isotopic and trace element evidence of an enriched mantle source that assimilated variable proportions of crust (Kovalenko et al., 2004; 2007; 2009). In Namibia, a series of A-type granites, namely the silicic Damaraland complexes and the Etendeka rhyodacites, display isotopic signatures of either crustal remelting or crustal assimilation. The mantle source for these granites was not an enriched subcontinental mantle, but rather an ocean-island-basalt-type (OIB; Tristan mantle plume) mantle of partially depleted nature (Trumbull et al., 2004a; Trumbull et al., 2004b).

The models presented above indicate that partial melting of depleted or enriched mantle, or lower crust, combined with fractional crystallization or liquid immiscibility, can result in the formation of A-type granites. It is particularly striking that in the same alkaline suites, different rock types (e.g. syenites, granites) may originate from different source regions (Sobolev et al., 2007). A particularly good example of this is the Gardar Province, which was interpreted to host alkaline rocks that are derivatives from both depleted and enriched mantle (Stevenson et al., 1997; Halama et al., 2003). Naturally, the plate tectonic framework plays a crucial role in where and how alkaline magmas are generated. This is discussed in the following section.

1.1.3 Plate tectonic environments that favor alkaline magmatism

The magmas producing A-type granites melts are generated in anorogenic intra-plate rift-settings. Some researchers have shown that, in a number of alkaline provinces, a hot spot (mantle plume) is responsible for the linear alignment of the intrusive bodies. An example of this is the alkaline intrusions of the Damaraland anorogenic complex, which researchers linked to the Tristan da Cunha plume on the basis of the mantle plume-like isotopic signatures of the mafic members (Milner and leRoex, 1996; Trumbull et al., 2004a). The Tristan da Cunha plume generated alkaline OIB-type lavas that form a series of islands in the South Atlantic, and was located in the rift zone during the Cretaceous breakup of Pangaea (Le Roex et al., 1990). Another example is the ~124 Ma Monteregian Igneous Province, which produced a roughly aligned array of nine under- to oversaturated alkaline and carbonatitic intrusions in southern Québec, Canada. The source of the intrusions, some of which exhibit an extraordinarily exotic mineralogy (e.g., Mont Saint Hilaire) is interpreted to have been a mantle plume, based on geochemical and isotopic OIB and HIMU signatures; the products of this plume extend to the New England seamounts in the Atlantic (Eby, 1985; Foland et al., 1988). However, owing to a lack of progressive eastward younging and, based on more recent Sr, Nd-, and Pb-isotope data, it was subsequently proposed that the Monteregian intrusions formed instead from an enriched subcontinental lithospheric mantle and were emplaced in a thinned crust, just prior to the opening of the North Atlantic Ocean (Roulleau and Stevenson, 2013).

Many other alkaline provinces are associated with crustal de-stressing following collisional events. For example, the large AMCG (Anorthosite-Mangerite-Charnockite-Granite) intrusions of the Nain Plutonic Suite and the Grenville in Labrador and Québec were emplaced during the waning stages of a sequence of orogenic events, e.g., the Labradorian, Elsonian and Grenvillian (Gower and Krogh, 2002; McLelland et al., 2010). Some researchers, therefore, have proposed that alkaline magmatism results from delamination of an orogenically thickened lithosphere followed by ascent of the asthenosphere and subsequent rifting (Bonin, 2004; Connelly and Ryan, 1999; Martin, 2012; McLelland et al., 2010). Others have concluded that the age and thickness of the lithosphere controls the degree of alkalinity and silica saturation of anorogenic-type intrusions, based on evaluations of the features of major alkaline provinces (Black et al., 1985). In addition, they have proposed that undersaturated alkaline within-plate magmas are generated in well-defined rifts and fault zones (e.g., the Gardar Province, Greenland), whereas oversaturated suites occur along reactivated ancient zones of crustal weakness or failed rifts, where they undergo a higher degree of crustal assimilation (Black et al., 1985; Stevenson et al., 1997; Upton, 2013a, b). The variable characteristics of A-type granites are due not only to multiple possible sources and a variety of plate tectonic conditions that favor anorogenic magmatism, but also to upper crustal emplacement processes, which are discussed in the following section.

1.1.4 Emplacement characteristics of A-type granitoids in the upper crust

A-type granitoids have several features that distinguish them from other alkaline intrusions, notably stoping of large country rock blocks and ring faulting. For example, several smaller Mesoproterozoic REE-rich intrusive bodies in Northern Québec can be easily identified on aeromagnetic maps by their ring-shape (Kerr and Hamilton, 2014). From studies of alkaline complexes in Corsica (Bonin, 1986) and Tertiary intrusive centers in Britain (Walker, 1975), ring-dikes are thought by many researchers to form through cauldron subsidence after an early volcanic or magmatic phase. The cauldron collapse generates a ring-fault along which a subsequent diapiric batch of magma intrudes. Commonly, the later emplaced units contain large fragments of host rock (roof pendants), which are assimilated upon emplacement (Bonin, 1986). This intrusive sequence can occur repeatedly, forming ring-dikes with several smaller interior rings (Bonin, 1986; Walker, 1975), e.g., the Misery Lake syenite to ferro-syenite intrusion (Petrella et al., 2014). The Strange Lake pluton also includes an intrusion in the shape of a ring, which is weakly defined in a recent aeromagnetic map (this study). As the latter is hyper-enriched in the REE and thus of interest to mineral exploration companies, the economic geology of the REE are discussed briefly below.

1.2 ECONOMIC GEOLOGY OF THE REE

1.2.1 Background information

The search for and understanding of REE-mineralized rocks has become increasingly important for a number of reasons. China, which hosts large rare-metal resources such as the Bayan Obo carbonate-hosted REE-Nb-Fe deposit (Yuan et al., 1992), has been responsible for the global supply of the REE since the early 1990'ies. However, rare-earth export quotas from the Chinese government during the early years of the millennium forced other nations to invest in developing their own resources (Simandl, 2014). In addition, the demand for the REE has increased in recent years. Thus, the estimated total global demand of TREO (total rare earth oxides) was 105 kt in 2011 and is expected to rise to 160 kt by the end of 2016 (Hatch, 2012). The REE are used in a large number of modern and energy-saving technologies, e.g., as hydrocarbon-cracking catalysts, automotive catalytic converters, polishing media for modern computer-, TV- or mobile phone-screens, permanent magnets, metal alloys and in rechargeable battery cells and LED- and LCD-light technologies (Hatch, 2012). The currently known global REO resources are hosted by China (43 %), Russia (10%), Australia (10%), Canada (8 %), Brazil (8%), Greenland (6%), USA (3 %) and other nations (12%). However, access and cost of transport and processing play a crucial role in determining whether a deposit can be exploited, or is economically feasible to exploit (Weng et al., 2015).

1.2.2 Current production

Rare earth ore can be produced from carbonatite or carbonatite-syenite complex related deposits (~51 % of global resources, e.g., Bayan Obo, Mountain Pass), weathered carbonatite (e.g., Tomtor, Russia; Mt. Weld, Australia), ion adsorption clay deposits (~10 % of global resources) monazite ± apatite veins (minor global resources) and peralkaline under- or oversaturated deposits (~13 % of global resources, e.g., Nechalacho, Kipawa and Strange Lake, Canada and Lovozero, Russia) (Weng et al., 2015). Currently, the REE are produced primarily from carbonatite and carbonatite-related deposits (Simandl, 2014), owing to the greater ease of extraction of the REE from carbonates, e.g., bastnäsite ($(Ce,La)(CO_3)F$), compared to phosphates and silicates. The REE-phosphate- (e.g., monazite), or silicate- (e.g. allanite)-dominant rare earth element deposits are more difficult to deal with due to high Th-concentrations (radioactivity) or the complex extraction process (Simandl, 2014).

Most of the producing deposits are rich in the LREE, and, with the notable exception of the South China ion adsorption clay deposits, only a few of them contain significant concentrations of the HREE. Among the latter elements, Gd, Tb, Dy, Er, Yb, Lu and Y are in high demand, as they are used for high technology applications involving lasers, lighting, and magnets as well as for medical applications (Chakhmouradian and Wall, 2012; Weng et al., 2015). The REE magnets are particularly important for green technologies because of their use in hybrid and electric vehicles, and in wind turbines. Owing to a strong HREE-enrichment in the pegmatites of the B-zone, Strange Lake is thus of special interest for potential exploitation (Kerr and Rafuse, 2012; Gysi and Williams-Jones, 2013). The hydrothermal processes of the HFSE enrichment of Strange Lake has been thoroughly studied (e.g. Salvi and Williams-Jones, 1990; 1992; 1997; 2006; Gysi and Williams-Jones, 2013; Vasyukova et al., 2016), however, the magmatic aspect of rare metal enrichment still requires detailed investigation. Some previous studies have been devoted to the igneous petrology of the Strange Lake pluton and are briefly reviewed in the next section.

1.3 PREVIOUS STUDIES OF THE IGNEOUS PETROLOGY OF THE STRANGE LAKE PLUTON

Previous work on the igneous aspects of the pluton commenced with the study of Pillet et al. (1992), who interpreted the in-situ evolution of the body to be the result of fractional crystallization of alkali feldspar, which was accompanied by an increase in fO_2. Boily and Williams-Jones (1994), on the basis of bulk rock compositions, concluded that the REE enrichment occurred through a combination of fractional crystallization, HFSE and REE complexation with fluorine and the heterogeneous dispersion of these complexes in the residual F-rich silicic melts.

Recently, Vasyukova and Williams-Jones (2014) used information from melt inclusions to show that an immiscible Ca-REE rich fluoride melt separated from the Zr-Nb-Ti-enriched silicate melt early in the history of the emplacement of the pluton. The former melt accumulated as coalescing droplets in the evolving silicate melt, culminating with its concentration in the pegmatites where it crystallized as complex REE-F-minerals and formed the potential REE ore zone (Vasyukova and Williams-Jones, 2016). The previous studies provide the foundation on which the present study is built upon, the objectives of which are elaborated upon in the following paragraph.

1.4 RESEARCH OBJECTIVES AND METHODOLOGY

The goal of the research presented in this thesis is to contribute to the understanding of the genesis of A-type granites, and to gain insight into the magmatic evolution of highly mineralized members of this group of rocks. The Strange Lake intrusion is an extraordinary example of a HFSE-enriched A-type peralkaline granitic pluton, as it has an exotic mineralogy and is hyper-mineralized in the REE, Zr and Nb and in the HREE in particular. This research project builds upon previous studies, and is distinguished from those in using a new set of tools to provide new and revise existing interpretations of the origin and evolution of the granites. The methods used include detailed fieldwork that concentrated on the central and unaltered part of the pluton. In addition to detailed petrography and the assessment of bulk rock data, the mineral compositions of perthitic alkali feldspar phenocrysts were used to trace the magmatic evolution of the pluton. An analysis of the major and trace element chemistry of the amphibole-group, the main mafic phase of the granitic suite, was carried out to reveal more detail of the magmatic evolution and crystallization conditions. The investigation of REE-partitioning in the crystal structure of the alkali amphiboles aimed to add to the understanding of magmatic REE enrichment in A-type granites. A neodymium isotope study on unaltered samples and arfvedsonite separates of the Strange Lake pluton, supported by oxygen isotope compositions of quartz separates, aimed to determine the magma sources of the pluton. The study considered a variety of hypotheses, including the derivation of the magma from both depleted and enriched mantle sources and mixing this magma with crustal material from the underlying Archean to Paleoproterozoic basement rocks. In addition, the isotope study aimed to link the Strange Lake pluton to the large Paleoproterozoic Nain Plutonic Suite (NPS) in northern Québec and Labrador, and also to the alkaline Gardar Province in SW-Greenland, which is similar in age and tectonic setting of magmatic activity.

1.5 THESIS ORGANIZATION

This thesis is manuscript-based and consists of five chapters, the first of which is the general introduction. Chapter two is a manuscript evaluating the magmatic evolution and HFSE-enrichment of the Strange Lake pluton, based on bulk rock and mineral major and trace element compositions. Chapter three focuses on the mineral chemistry of the amphibole-group minerals, and the distribution of the REE in their crystal structure. The fourth chapter is a radiogenic (Nd) and stable isotope (O) study which identifies the source of the Strange Lake magma. The chapter also discusses the Strange Lake pluton in the context of the large scale alkaline magmatic events in NE-Canada and SW-Greenland during the Mesoproterozoic. The fifth chapter reports the principal observations and conclusions of the study and provides a summary of contributions to the scientific community. The appendix consists of the tables containing the bulk rock and mineral compositions generated during this project as well as the calculated partitioning coefficients and melt compositions.

REFERENCES

Andersen, T., and Friis, H., 2015, The Transition from Agpaitic to Hyperagpaitic Magmatic Crystallization in the Ilimaussaq Alkaline Complex, South Greenland: Journal of Petrology, v. 56, no. 7, p. 1343-1363.

Anderson, I. C., Frost, C. D., and Frost, B. R., 2003, Petrogenesis of the Red Mountain pluton, Laramie anorthosite complex, Wyoming: implications for the origin of A-type granite: Precambrian Research, v. 124, no. 2-4, p. 243-267.

Bailey, D. K., 1987, Mantle metasomatism - perspective and prospect: Geological Society, London, v. 30, no. Special Publications, p. 1-13.

Bailey, D. K., and Schairer, J. F., 1966, System Na2o-Al2o3-Fe2o3-Sio2 at 1 Atmosphere and Petrogenesis of Alkaline Rocks: Journal of Petrology, v. 7, no. 1, p. 114-&.

Black, R., Lameyre, J., and Bonin, B., 1985, The Structural Setting of Alkaline Complexes: Journal of African Earth Sciences, v. 3, no. 1-2, p. 5-16.

Bonin, B., 1986, Ring complex granites and anorogenic magmatism, North Oxford Academic Publishers Ltd.

-, 2004, Do coeval mafic and felsic magmas in post-collisional to within-plate regimes necessarily imply two contrasting, mantle and crustal, sources? A review: Lithos, v. 78, no. 1-2, p. 1-24.

-, 2007, A-type granites and related rocks: Evolution of a concept, problems and prospects: Lithos, v. 97, no. 1-2, p. 1-29.

Chakhmouradian, A. R., and Wall, F., 2012, Rare earth elements: minerals, mines, magnets (and more). Elements, v. 8, p. 333-340.

Collins, W. J., Beams, S. D., White, A. J. R., and Chappell, B. W., 1982, Nature and Origin of a-Type Granites with Particular Reference to Southeastern Australia: Contributions to Mineralogy and Petrology, v. 80, no. 2, p. 189-200.

Connelly, J. N., and Ryan, A. B., 1999, Age and tectonic implications of Paleoproterozoic granitoid intrusions within the Nain Province near Nain, Labrador: Canadian Journal of Earth Sciences, v. 36, no. 5, p. 833-853.

Costi, H. T., Dall'Agnol, R., Pichavant, M., and Ramo, O. T., 2009, The Peralkaline Tin-Mineralized Madeira Cryolite Albite-Rich Granite of Pitinga, Amazonian Craton, Brazil: Petrography, Mineralogy and Crystallization Processes: Canadian Mineralogist, v. 47, no. 6, p. 1301-1327.

Dall'Agnol, R., Teixeira, N. P., Ramo, O. T., Moura, C. A. V., Macambira, M. J. B., and de Oliveira, D. C., 2005, Petrogenesis of the Paleoproterozoic rapakivi A-type granites of the Archean Carajas metallogenic province, Brazil: Lithos, v. 80, no. 1-4, p. 101-129.

Eby, G. N., 1985, Sr and Pb Isotopes, U and Th Chemistry of the Alkaline Monteregian and White Mountain Igneous Provinces, Eastern North-America: Geochimica Et Cosmochimica Acta, v. 49, no. 5, p. 1143-1153.

-, 1990, The A-type granitoids: a review of their occurrence and chemical characteristics and speculations on their petrogenesis: Lithos, v. 26, p. 115-134.

Ferguson, J., 1970, The differentiation of agpaitic magmas: the Ilimaussaq intrusion, south Greenland, p. 15.

Foland, K. A., Chen, J. F., Gilbert, L. A., and Hofmann, A. W., 1988, Nd and Sr Isotopic Signatures of Mesozoic Plutons in Northeastern North-America: Geology, v. 16, no. 8, p. 684-687.

Frost, B. R., Barnes, C. G., Collins, W. J., Arculus, R. J., Ellis, D. J., and Frost, C. D., 2001a, A geochemical classification for granitic rocks: Journal of Petrology, v. 42, no. 11, p. 2033-2048.

Frost, C. D., Bell, J. M., Frost, B. R., and Chamberlain, K. R., 2001b, Crustal growth by magmatic underplating: Isotopic evidence from the northern Sherman batholith: Geology, v. 29, no. 6, p. 515-518.

Frost, C. D., and Frost, B. R., 1997, Reduced rapakivi-type granites: The tholeiite connection: Geology, v. 25, no. 7, p. 647-650.

Frost, C. D., Frost, B. R., Bell, J. M., and Chamberlain, K. R., 2002, The relationship between A-type granites and residual magmas from anorthosite: evidence from the northern Sherman batholith, Laramie Mountains, Wyoming, USA: Precambrian Research, v. 119, no. 1-4, p. 45-71.

Frost, C. D., Frost, B. R., Chamberlain, K. R., and Edwards, B. R., 1999, Petrogenesis of the 43 Ga Sherman batholith, SE Wyoming, USA: A reduced, rapakivi-type anorogenic granite: Journal of Petrology, v. 40, no. 12, p. 1771-1802.

Gower, C. F., and Krogh, T. E., 2002, A U-Pb geochronological review of the Proterozoic history of the eastern Grenville Province: Canadian Journal of Earth Sciences, v. 39, no. 5, p. 795-829.

Gysi, A. P., and Williams-Jones, A. E., 2013, Hydrothermal mobilization of pegmatite-hosted REE and Zr at Strange Lake, Canada: A reaction path model: Geochimica et Cosmochimica Acta, v. 122, no. 2013, p. 324-352.

Halama, R., Wenzel, T., Upton, B. G. J., Siebel, W., and Markl, G., 2003, A geochemical and Sr-Nd-O isotopic study of the Proterozoic Eriksfjord Basalts, Gardar Province, South Greenland - Reconstruction of an OIB signature in crustally contaminated rift-related basalts: Mineralogical Magazine, v. 67, no. 6, p. 1338-1338.

Hatch, G. P., 2012, Dynamics in the Global Market for Rare Earths: Elements, v. 8, no. 5, p. 341-346.

Hegner, E., Emslie, R. F., Iaccheri, L. M., and Hamilton, M. A., 2010, Sources of the Mealy Mountains and Atikonak River Anorthosite-Granitoid Complexes, Grenville Province, Canada: Canadian Mineralogist, v. 48, no. 4, p. 787-808.

Kerr, A., and Hamilton, M. A., 2014, Rare-earth element (REE) mineralization in the Mistastin Lake and Smallwood Reservoir areas, Labrador: field relationships and preliminary U-Pb zircon ages from host granitoid rocks Current Research (1990) Newfoundland Department of Mines and Energy, Geological Survey v. 1, p. 45-62.

Kerr, A., and Rafuse, H., 2012, Rare-earth element (REE) geochemistry of the Strange Lake deposits: Implications for resource estimation and metallogenic models.: Current Research (2012) Newfoundland and Labrador Department of Natural Resources, v. 1, p. 39-60.

Khomyakov, A. P., 1995, Mineralogy of Hyperagpaitic Alkaline Rocks, Oxford, Clarendon Press, 188 p.:

Kovalenko, V. I., Tsaryeva, G. M., Goreglyad, A. V., Yarmolyuk, V. V., Troitsky, V. A., Hervig, R. L., and Farmer, G. L., 1995, The Peralkaline Granite-Related Khaldzan-Buregtey Rare-Metal (Zr, Nb, Ree) Deposit, Western Mongolia: Economic Geology and the Bulletin of the Society of Economic Geologists, v. 90, no. 3, p. 530-547.

Kovalenko, V. I., Yarmolyuk, V. V., Kovach, V. P., Kovalenko, D. V., Kozlovskii, A. M., Andreeva, I. A., Kotov, A. B., and Salnikova, E. B., 2009, Variations in the Nd isotopic ratios and canonical ratios of concentrations of incompatible elements as an indication of mixing sources of alkali granitoids and basites in the Khaldzan-Buregtei massif and the Khaldzan-Buregtei rare-metal deposit in western Mongolia: Petrology, v. 17, no. 3, p. 227-252.

Kovalenko, V. I., Yarmolyuk, V. V., Kovach, V. P., Sal'nikova, E. B., Kozlovskii, A. M., Kotov, A. B., and Khanchuk, A. I., 2004, Multiple magma sources for the peralkaline granitoids and related rocks of the Khaldzan Buregte group of massifs, western Mongolia: Isotopic (neodymium, strontium, and oxygen) and geochemical data: Petrology, v. 12, no. 6, p. 497-518.

Kovalenko, V. I., Yarmolyuk, V. V., Kozlovsky, A. M., Kovach, V. P., Sal'nikova, E. B., Kotov, A. B., and Vladykin, N. V., 2007, Two types of magma sources of rare-metal alkali granites: Geology of Ore Deposits, v. 49, no. 6, p. 442-466.

Kramm, U., and Kogarko, L. N., 1994, Nd and Sr Isotope Signatures of the Khibina and Lovozero Agpaitic Centers, Kola-Alkaline-Province, Russia: Lithos, v. 32, no. 3-4, p. 225-242.

Kumar, K. V., Frost, C. D., Frost, B. R., and Chamberlain, K. R., 2007, The Chimakurti, Errakonda, and Uppalapadu plutons, Eastern Ghats belt, India: An unusual association of tholeiitic and alkaline magmatism: Lithos, v. 97, no. 1-2, p. 30-57.

Landoll, J. D., and Foland, K. A., 1996, The formation of quartz syenite by crustal contamination at Mont Shefford and other Monteregian complexes, Quebec: Canadian Mineralogist, v. 34, p. 301-324.

Le Roex, A. P., Cliff, R. A., and Adair, B. J. I., 1990, Tristan da Cunha, South Atlantic: Geochemistry and Petrogenesis of a Basanite-Phonolite Lava Series: Journal of Petrology, v. 31, no. 4, p. 779-812.

Linthout, K., 1984, Alkali-Zirconosilicates in Peralkaline Rocks: Contributions to Mineralogy and Petrology, v. 86, no. 2, p. 155-158.

Lloyd, F. E., and Bailey, D. K., 1975, Light Element Metasomatism of the Continental Mantle: the Evidence and the Consequences: Physics and Chemistry of Earth, v. 9, p. 389-416.

MacDonald, R., 1974, Nomenclature and Petrochemistry of the Peralkaline Oversaturated Extrusive Rocks: Bulletin Volcanologique, v. 38.2, p. 489-516.

Marks, M. A. W., Hettmann, K., Schilling, J., Frost, B. R., and Markl, G., 2011, The Mineralogical Diversity of Alkaline Igneous Rocks: Critical Factors for the Transition from Miaskitic to Agpaitic Phase Assemblages: Journal of Petrology, v. 52, no. 3, p. 439-455.

Martin, R. F., 2006, A-type granites of crustal origin ultimately result from open-system fenitization-type reactions in an extensional environment: Lithos, v. 91, no. 1-4, p. 125-136.

-, 2012, The petrogenesis of anorogenic felsic magmas and AMCG suites: Insights on element mobility and mutual cryptic contamination from polythermal experiments: Lithos, v. 151, p. 35-45.

McLelland, J. M., Selleck, B. W., Hamilton, M. A., and Bickford, M. E., 2010, Late- to post-tectonic setting of some major proterozoic anorthosite - mangerite - charnockite - granite (AMCG) suites: Canadian Mineralogist, v. 48, no. 4, p. 729-750.

Milner, S. C., and leRoex, A. P., 1996, Isotope characteristics of the Okenyenya igneous complex, northwestern Namibia: Constraints on the composition of the early Tristan plume and the origin of the EM 1 mantle component: Earth and Planetary Science Letters, v. 141, no. 1-4, p. 277-291.

Neumann, E. R., Wulff-Pedersen, E., Pearson, N. J., and Spencer, E. A., 2002, Mantle xenoliths from Tenerife (Canary Islands): Evidence for reactions between mantle peridotites and silicic carbonatite melts inducing Ca metasomatism: Journal of Petrology, v. 43, no. 5, p. 825-857.

Petrella, L., Williams-Jones, A. E., Goutier, J., and Walsh, J., 2014, The Nature and Origin of the Rare Earth Element Mineralization in the Misery Syenitic Intrusion, Northern Quebec, Canada: Economic Geology, v. 109, no. 6, p. 1643-1666.

Pillet, D., Chenevoy, M., and Belanger, M., 1992, Petrology of Peralkaline Granite from Lake Brisson (Central Labrador, Nouveau-Quebec) .1. Intrusion and Chemical Evolution: Canadian Journal of Earth Sciences, v. 29, no. 2, p. 353-372.

Roulleau, E., and Stevenson, R., 2013, Geochemical and isotopic (Nd-Sr-Hf-Pb) evidence for a lithospheric mantle source in the formation of the alkaline Monteregian Province (Quebec): Canadian Journal of Earth Sciences, v. 50, no. 6, p. 650-666.

Schmitt, A. K., Emmerman, R., Trumbull, R. B., Buhn, B., and Henjes-Kunst, F., 2000, Petrogenesis and Ar-40/Ar-39 geochronology of the Brandberg complex, Namibia: Evidence for a major mantle contribution in metaluminous and peralkaline granites: Journal of Petrology, v. 41, no. 8, p. 1207-1239.

Schmitt, A. K., Trumbull, R. B., Dulski, P., and Emmermann, R., 2002, Zr-Nb-REE mineralization in peralkaline granites from the Amis Complex, Brandberg (Namibia): Evidence for magmatic pre-enrichment from melt inclusions: Economic Geology and the Bulletin of the Society of Economic Geologists, v. 97, no. 2, p. 399-413.

Schonenberger, J., and Markl, G., 2008, The magmatic and fluid evolution of the Motzfeldt intrusion in South Greenland: Insights into the formation of agpaitic and miaskitic rocks: Journal of Petrology, v. 49, no. 9, p. 1549-1577.

Simandl, G. J., 2014, Geology and market-dependent significance of rare earth element resources: Mineralium Deposita, v. 2014, no. 49, p. 889-904.

Sobolev, A. V., Hofmann, A. W., Kuzmin, D. V., Yaxley, G. M., Arndt, N. T., Chung, S. L., Danyushevsky, L. V., Elliott, T., Frey, F. A., Garcia, M. O., Gurenko, A. A., Kamenetsky, V. S., Kerr, A. C., Krivolutskaya, N. A., Matvienkov, V. V., Nikogosian, I. K., Rocholl, A., Sigurdsson, I. A., Sushchevskaya, N. M., and Teklay, M., 2007, The amount of recycled crust in sources of mantle-derived melts: Science, v. 316, no. 5823, p. 412-417.

Sorensen, H., 1997, The agpaitic rocks - an overview: Mineralogical Magazine, v. 61, no. 4, p. 485-498.

Stevenson, R., Upton, B. G. J., and Steenfelt, A., 1997, Crust-mantle interaction in the evolution of the Ilimaussaq complex, south Greenland: Nd isotopic studies: Lithos, v. 40, no. 2-4, p. 189-202.

Thomas, R., Forster, H. J., Rickers, K., and Webster, J. D., 2005, Formation of extremely F-rich hydrous melt fractions and hydrothermal fluids during differentiation of highly evolved tin-granite magmas: a melt/fluid-inclusion study: Contributions to Mineralogy and Petrology, v. 148, no. 5, p. 582-601.

Thomas, R., Webster, J. D., Rhede, D., Seifert, W., Rickers, K., Forster, H. J., Heinrich, W., and Davidson, P., 2006, The transition from peraluminous to peralkaline granitic melts: Evidence from melt inclusions and accessory minerals: Lithos, v. 91, no. 1-4, p. 137-149.

Trumbull, R. B., Harris, C., Frindt, S., and Wigand, A., 2004a, Oxygen and neodymium isotope evidence for source diversity in Cretaceous anorogenic granites from Namibia and implications for A-type granite genesis: Lithos, v. 73, no. 1-2, p. 21-40.

Trumbull, R. B., Harris, C., Frindt, S., and Wigand, M., 2004b, Source diversity in Cretaceous anorogenic granites from Namibia raises doubt on A-type classifications: Geochimica Et Cosmochimica Acta, v. 68, no. 11, p. A662-A662.

Upton, B. G. J., 2013a, Tectono-magmatic evolution of the younger Gardar southern rift, South Greenland: Geological Survey of Denmark and Greenland (GEUS).

-, 2013b, Uniqueness of the southern branch of the Gardar rift: Geological Survey of Denmark and Greenland Bulletin, no. 29, p. 9-+.

Vasyukova, O., and Williams-Jones, A. E., 2014, Fluoride–silicate melt immiscibility and its role in REE ore formation: Evidence from the Strange Lake rare metal deposit, Que´bec-Labrador, Canada: Geochimica et Cosmochimica Acta, v. 139, no. 2014, p. 110-130.

-, 2016, The evolution of immiscible silicate and fluoride melts: Implications for REE ore-genesis: Geochimica et Cosmochimica Acta, v. 172, p. 205-224.

Vasyukova, O. V., Williams-Jones, A. E., and Blamey, N. J. F., 2016, Fluid evolution in the Strange Lake granitic pluton, Canada: Implications for HFSE mobilization: Chemical Geology, v. 444, p. 83-100.

Walker, G. P. L., 1975, A new concept of the evolution of the British Tertiary intrusive centres: Journal of the Geological Society of London, v. 131, p. 121-141.

Weng, Z. H., Jowitt, S. M., Mudd, G. M., and Haque, N., 2015, A Detailed Assessment of Global Rare Earth Element Resources: Opportunities and Challenges: Economic Geology, v. 110, no. 8, p. 1925-1952.

Whalen, J. B., Currie, K. L., and Chappell, B. W., 1987, A-Type Granites - Geochemical Characteristics, Discrimination and Petrogenesis: Contributions to Mineralogy and Petrology, v. 95, no. 4, p. 407-419.

Woolley, A. R., 1987, Lithosphere Metasomatism and the Petrogenesis of the Chilwa Province of Alkaline Igneous Rocks and Carbonatites, Malawi: Journal of African Earth Sciences, v. 6, no. 6, p. 891-898.

Yuan, Z. X., Bai, G., Wu, C. Y., Zhang, Z. Q., and Ye, X. J., 1992, Geological Features and Genesis of the Bayan Obo Ree Ore Deposit, Inner-Mongolia, China: Applied Geochemistry, v. 7, no. 5, p. 429-442.

Zaccarini, F., Stumpfl, E. F., and Garuti, G., 2004, Zirconolite and Zr-Th-U minerals in chromitites of the Finero complex, Western Alps, Italy: evidence for carbonatite-type metasomatism in a subcontinental mantle plume: Canadian Mineralogist, v. 42, p. 1825-1845.

CHAPTER 2 -

MAGMATIC EVOLUTION AND CONTROLS ON RARE EARTH MINERALIZATION OF THE STRANGE LAKE A-TYPE PERALKALINE GRANITIC PLUTON, QUÉBEC-LABRADOR

PREFACE

In this chapter, we focus on the fresh rocks in the center of the pluton, and use a combination of bulk-rock and perthitic alkali feldspar chemistry, in conjunction with geochemical modeling, to reconstruct the magmatic evolution of the pluton. Expanding upon previous studies, we recognize separate southern and a more evolved northern hypersolvus granitic intrusion, both of which include a separate oikocrystic to pegmatitic facies. We also show that the subsolvus granite of previous studies is in fact a highly evolved, low-viscosity transsolvus granite. In addition, we determine the origin of the dark grey enclaves hosted by the latter unit, showing that they represent fragments of both, quenched hypersolvus and transsolvus granite. The identity of the primary REE-minerals is established in all granitic facies from least and to most evolved. A major thrust of the chapter is to determine the magmatic processes that occurred in the magma chamber. We reconstruct its in-situ evolution, which involved the crystallization of complex alkali zircono-silicates in place of primary zircon, and show that, in addition to fractional crystallization of perthitic alkali feldspar, low viscosity-induced density segregation and fluoride-silicate-melt immiscibility played critical roles in the magmatic pre-enrichment of the HFSE. This pre-enrichment provided the source for later hydrothermal re-mobilization of the REE and the formation of one of the richest rare-metal deposits in the world.

ABSTRACT

Although it is well known that A-type granites are enriched in the rare earth elements (REE) and other high field strength elements (HFSE), the magmatic processes that concentrate these elements are still poorly understood. The 1.24 Ga Strange Lake pluton in northern Québec-Labrador provides an extraordinary example of hyper-enrichment in the REE, Zr, and Nb in a peralkaline A-type granite. Unaltered samples from the center of the pluton were used for detailed petrography, and analyzed for their bulk rock and mineral major and trace element compositions (alkali feldspar, alkali zirconosilicates, primary REE-minerals). The pluton consists of two hypersolvus granite units (southern and northern) and a transsolvus granite, all of which contain perthitic alkali feldspar as the earliest major phase; the transsolvus granite also contains separate albite and microcline crystals. Arfvedsonite, a sodic amphibole, occurs exclusively as phenocrysts in the transsolvus granite, whereas in the hypersolvus granite it is present as a late, interstitial phase. The primary ore minerals are zircon (Zr, HREE), monazite-(Ce) (LREE) and the pyrochlore group minerals (LREE, Nb), as well as gagarinite-(Ce) (LREE, Y), in the case of the transsolvus granite. Magma evolution in the bulk rock was monitored by the alumina content, which decreases from the southern to the northern hypersolvus granite and is lowest in the transsolvus granite (avg. 11.9, 11.7 and 10.3 wt. % Al_2O_3, respectively). Alkalinity indices (avg. 1.13, 1.15 and 1.27, respectively) and bulk Si, Fe, Rb, REE, Zr, Nb concentrations show the opposite trend. Alkali feldspar compositions mirror the trend shown by the bulk rock, i.e., decreasing Al contents are accompanied by increasing Si, Fe^{3+}, REE, Zr and Nb contents. The emplacement of the southern hypersolvus granite in the upper crust was followed by that of the more evolved northern hypersolvus granite; both units underwent further in situ evolution. Quartz, arfvedsonite and alkali zircono- and titano-silicate minerals (in that sequence) crystallized after emplacement. The crystallization of alkali zircono- and titano-silicates marked a transition from miaskitic to agpaitic phase assemblages. Volatile-rich residual melts formed relatively barren oikocrystic- and pegmatitic-textured granites. After a substantial proportion of the feldspar-rich magma (hypersolvus granites) had been removed from the magma chamber to be emplaced in the upper crust, the remaining magma evolved progressively. It eventually saturated in arfvedsonite, which, due to a release of F to the melt, triggered a transition from hypersolvus to subsolvus conditions. This highly evolved, low viscosity ($10^4 – 10^5$ Pa·s) melt was emplaced as a single large magma batch. The dark grey enclaves hosted by this unit are interpreted to represent the quenched and feldspar-rich margin of both, hypersolvus and transsolvus granite. Arfvedsonite, microcline and albite continued to crystallize after emplacement. The evolution of the melt in the magma chamber was driven by alkali feldspar fractionation, whereas the main magmatic processes responsible for concentrating the HFSE were the early crystallization of HFSE- minerals, the gravity settling of these heavier HFSE minerals, and the unmixing of a REE-rich fluoride melt.

Keywords

Rare earth elements, Strange Lake, Peralkaline granite, Magma evolution

2.1 INTRODUCTION

Numerous studies have established that A-type granitic rocks are enriched in incompatible elements, such as the REE, Zr, Nb, U and Ta, and volatiles, such as F, Cl and CO_2 (Bonin, 2007; Eby, 1990; Eby, 1992). Some aspects of their formation, however, are still debated, in particular the processes by which A-type granites achieve potentially economic concentrations of critical metals, e.g., the REE and Nb. To explain the hyper-enrichment in these elements, some authors have proposed magmatic processes such as extreme fractional crystallization and others metasomatism (prior to melting or after crystallization) as the major driving forces. For example, in the case of the Zr-Nb-REE-rich (5.3 wt. % Zr, 0.8 wt. % Nb, 0.4 wt. % REE) Khaldzan-Buregtey peralkaline granite, Mongolia, Kovalenko et al. (1995) concluded that the mineralized rocks are the products of extreme fractional crystallization of a rare metal-bearing pantelleritic magma. Kempe et al. (1999) subsequently argued that the unusual rare metal enrichment resulted from a combination of magmatic and metasomatic processes, the latter due to exsolution of Ca-, F- and CO_2-rich fluids from the magma. A magmatic concentration model was also proposed for the aplite-hosted Zr-Nb-REE mineralization (1.7 wt. % Zr, 0.3 wt. % Nb, 0.5 wt. % REE) in the peralkaline Amis granite Complex, Brandberg, Namibia (Schmitt et al., 2002). Although the authors observed evidence of local hydrothermal remobilization, they concluded that hydrothermal processes did not concentrate the rare metals, including the REE. By contrast, Walters et al. (2013) showed that in the Loch Loyal syenite complex, Scotland, magmatic concentration of the REE in the form of early allanite-(Ce) was followed by hydrothermal concentration of the REE as late allanite-(Ce) and an unidentified REE-Sr-carbonate in hydrothermal biotite-magnetite veins (0.25-2.5 wt. % La+Ce). In all these examples, the essential conditions for hyper-enrichment of the HFSE were a combination of a fertile source and extreme fractionation of the magma leading to highly evolved melts that produced pegmatites and aplites, although post-magmatic hydrothermal processes may have contributed to further enrichment.

The Strange Lake granite (Québec-Labrador) is an example of an A-type granite that is hyper-enriched in the REE, Zr and Nb. Indeed, the enrichment resulted in indicated resource of 278 Mt of ore, grading 0.94 wt. % REE_2O_3 (38% heavy rare-earth oxides), 1.92 wt. % ZrO_2 and 0.18 wt. % Nb_2O_5 referred to as the B-Zone (Quest, 2012). The 1240 Ma (Miller et al., 1997) peralkaline granitic pluton is composed of both fresh and hydrothermally altered granitic units, as well as numerous pegmatites of NYF type. A large number of studies have been undertaken of the pluton, most of which have focused on the hydrothermal alteration and related rare-metal mineralization (Salvi and Williams-Jones, 1990; 1992; 1996; 1997; Gysi and Williams-Jones, 2013, 2016) and its unique and exotic mineralogy (Birkett et al., 1992; 1996; Jambor et al., 1996; 1998). A few studies, however, have been devoted to the igneous aspects of rare-metal concentration. Boily and Williams-Jones (1994) concluded that the REE enrichment occurred by a combination of fractional crystallization, REE complexation with F and heterogeneous dispersion of these complexes in the residual F-rich silicic melts. Recently, Vasyukova and Williams-Jones (2014; 2016) provided evidence for the separation of an immiscible fluoride melt from the silicate melt. The fluoride melt preferentially incorporated the LREE and accumulated in the fluorine-rich cores of the late pegmatites that host the bulk of the REE mineralization.

Owing to the unusual enrichment of the Strange Lake granites in the HFSE, including the REE, even distal to the potential ore zones, the Strange Lake pluton provides an ideal setting in which to study the magmatic processes that concentrate these elements to extreme levels. In this study, we focus on the fresh rocks in the center of the pluton and use a combination of bulk-rock and mineral chemistry, in conjunction with geochemical modeling, to reconstruct the magmatic evolution of the pluton. We show that, in addition to fractional crystallization of perthitic alkali feldspar (Boily and Williams-Jones, 1994), low viscosity-induced density segregation and fluoride-silicate-melt immiscibility played critical roles in the magmatic pre-enrichment of the HFSE. This pre-enrichment provided the source for later hydrothermal re-mobilization of the REE and the formation of one of the richest rare-metal deposits in the world.

2.2 GEOLOGIC SETTING

2.2.1 Regional geology

The Strange Lake pluton in northeastern Canada is a member of the Nain Plutonic Suite (~19,000 km^2), which comprises anorthositic, mangeritic, charnockitic, and granitic intrusions (AMCG) that straddle the boundary between Archean rocks to the East (Nain Province) and late Archean to Early Paleoproterozoic gneisses to the West (Churchill Province/Core Zone) (Emslie et al., 1994). The earliest members of the suite (1460-1420 Ma) are the Michikamau and Harp Lake anorthosites and the granitoid rocks of the Mistastin batholith (1420 Ma) (Emslie et al., 1994; McLelland et al., 2010). They were followed by the anorthosites, troctolites, norites, diorites and granitoids of the 1353-1290 Ma Nain complex and finally by silica under- and over-saturated alkaline to agpaitic intrusive and volcanic rocks, notably the 1270 Ma peralkaline Flowers River granite and volcanic suite (Hill, 1991), and the 1240 Ma Strange Lake granite pluton (Miller et al., 1997).

The Strange Lake pluton is hosted partly by the Napeu Kainiut amphibole-biotite quartz monzonite, which, owing to its similarity to the intrusions of the Mistastin batholith, is believed to represent a satellite of the latter (Miller et al., 1997). The Mistastin batholith is one of the largest and oldest (1420 Ma) members of the Nain Plutonic Suite, and was intruded by syenitic intrusions, such as the 1410 Ma Misery Lake ferrosyenite (David et al., 2012), which contains a potentially economic REE deposit (Petrella et al., 2014). The metaluminous quartz monzonite of the Napeu Kainiut intrusion is generally coarse-grained and equigranular, and consists mainly of quartz, K-feldspar, plagioclase and biotite. The other host to the Strange Lake pluton is an Archean to Paleoproterozoic gneiss complex belonging to the Core Zone, which is composed of quartzofeldspathic augen-gneisses, banded biotite gneisses and minor garnet-bearing and mafic gneisses.

2.2.2 The Strange Lake pluton

The Strange Lake pluton is located on the border between Québec and Labrador, and intruded along the boundary between the Napeu Kainiut quartz monzonite to the West and South, and the Core Zone gneisses to the East. The pluton consists of a sequence of peralkaline granites (described in detail below) forming a circular intrusive body with a diameter of about six km (Fig. 2-1). A radiometric U-Pb determination on primary zircon of the oldest unit, a hypersolvus granite, yielded an age of 1240 ± 2 Ma (Miller et al., 1997). The hypersolvus granite, so named because it contains a single perthitic alkali feldspar, forms the center of the pluton, and has been divided into a southern and northern subfacies (this study). A transsolvus granite, which contains two separate alkali feldspars (microcline and albite) in addition to perthitic alkali feldspar, occupies the bulk of the pluton, and in large part has been strongly altered by hydrothermal fluids (formerly referred to as exotic granite) (Miller, 1990). The unaltered part of this unit occurs in the center of the pluton and locally contains dark grey, fine-grained ovoid enclaves and relatively barren pegmatite pockets. In contrast, the altered transsolvus granite contains the highly mineralized pegmatites that have been the focus of mineral exploration. Finally, a dark grey porphyritic granite with a fine-grained matrix is observed in contact with bodies of country rock within the intrusion (Fig. 2-1).

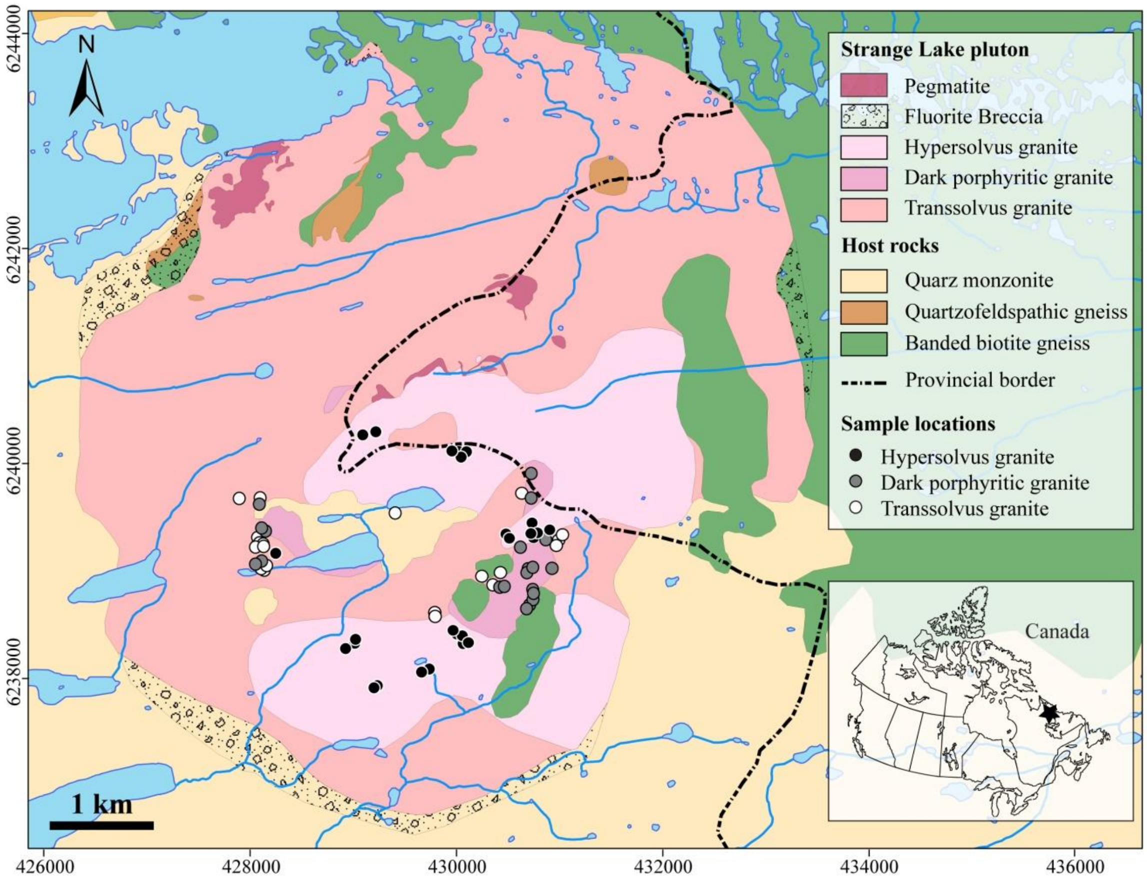

Fig. 2-1: Surface geological map of the Strange Lake pluton

Map showing the intrusive units mapped during this project and the locations of the samples used for this study.

2.2.2.1 Hypersolvus granite

The hypersolvus granite is divided into two subfacies. The northern subfacies is generally equigranular and fine-grained (Fig. 2-2a), and contrasts with the more variably textured southern hypersolvus granite. The latter varies from fine- to coarse-grained and pegmatitic, and locally is poikilitic, with anhedral arfvedsonite oikocrysts enclosing smaller crystals of perthitic alkali feldspar (Fig. 2-2b). In terms of major minerals, the northern and southern hypersolvus granite facies are indistinguishable, and are composed mainly of perthitic alkali feldspar, quartz and arfvedsonite. The perthitic alkali feldspar generally occurs as large crystals, and has minor inclusions of pyrochlore and monazite-(Ce). A second generation of perthitic alkali feldspar is present along the rims of some grains (represented as Afs 1 and 2 in Fig. 2-2c) or as smaller perthitic alkali feldspar crystals in the groundmass. Quartz and arfvedsonite both occur interstitially to the perthitic alkali feldspar, although the arfvedsonite appears to have crystallized later than the quartz as it wraps around the margins of the quartz crystals (Fig. 2-2d).

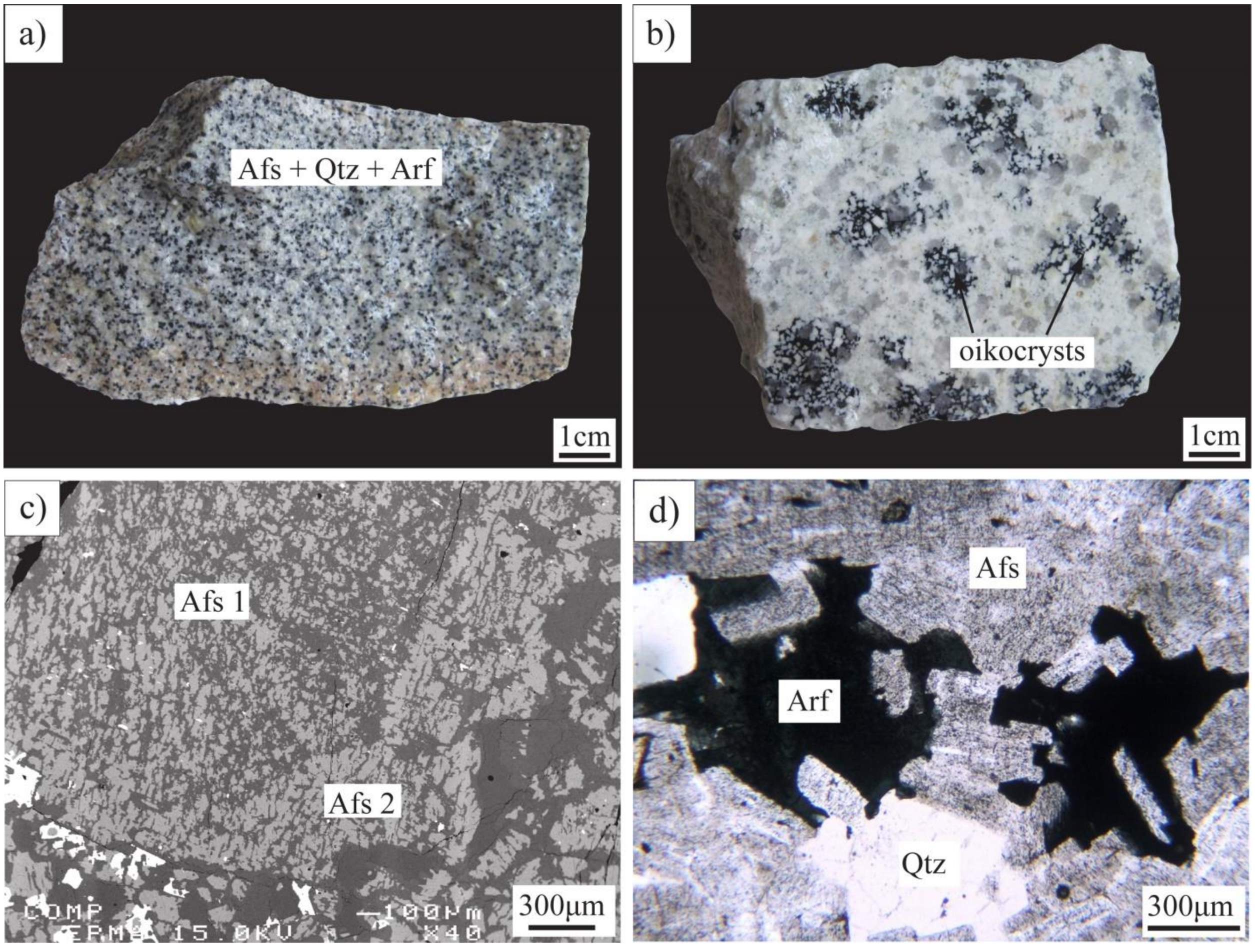

Fig. 2-2: Rock and thin section photographs of hypersolvus granite samples

a) A photograph of hypersolvus granite showing its typical fine-grained texture, b) a photograph of an oikocrystic textured sample with arfvedsonite (black) in interstitial pockets enclosing perthitic alkali feldspar grains, c) a backscattered electron image (BSE) of a large primary perthitic alkali feldspar grain (Afs 1) rimmed by secondary perthitic alkali feldspar (Afs 2), and d) a thin section photomicrograph showing arfvedsonite (Arf) interstitial to alkali feldspar and quartz.

In addition to the main rock-forming minerals, the hypersolvus granite contains a variety of Zr, Nb and rare-earth element (REE) minerals and fluorite. Minor proportions of late-crystallizing alkali zirconosilicate minerals, namely elpidite ($NaZrSi_6O_{15}•3(H_2O)$), vlasovite ($Na_2ZrSi_4O_{11}$) and dalyite ($K_2ZrSi_6O_{15}$) occur with relics of primary zircon ($ZrSiO_4$). The latter also occurs as separate, pristine crystals if they are included in other minerals, e.g., in quartz (Fig. 2-3a). Textural relationships among these minerals indicate that vlasovite and dalyite replaced zircon and were, in turn, replaced by elpidite (Fig. 2-3b) or catapleiite ($(NaCa)_2ZrSi_3O_9•2(H_2O)$). Sodium titanosilicates in the form of yellow fibrous astrophyllite ($K_2NaFe^{2+}{}_7Ti_2Si_8O_{26}(OH)_4$), and dark red aenigmatite ($Na_2Fe^{2+}{}_5TiO_2Si_6O_{18}$) replaced arfvedsonite; the latter is restricted to the northern hypersolvus granite. Fluorite is a common accessory mineral that is either disseminated interstitially or occurs as abundant round and translucent inclusions in arfvedsonite (Fig. 2-3c). In one sample, fluorite is present as round inclusions in perthitic alkali feldspar, some of which also contain astrophyllite and bastnäsite-(Ce) (Fig. 2-3d).

The primary REE-bearing minerals are monazite-(Ce) and pyrochlore-group minerals. The monazite-(Ce) crystals are small and euhedral to subhedral, and occur as inclusions in alkali feldspar (Fig. 2-3e). In contrast, the pyrochlore-group minerals take the form of yellow to dark brown octahedral pyramidal crystals (Fig. 2-3f) and usually are overgrown by a Ba-, Pb- and Si-rich and Nb-, Na- and F-poor variety of pyrochlore. The secondary REE-rich minerals are Y-rich fluorite, gagarinite-(Y) and bastnäsite-(Ce). Yttrium-rich fluorite forms rims around fluorite, and gagarinite-(Y) is observed as inclusions in fluorite (Fig. 2-3c) or arfvedsonite, where it replaced inclusions of fluorite. Bastnäsite-(Ce) locally replaced gagarinite-(Y). The minerals and their ideal chemical formulae are listed in Table 2-1.

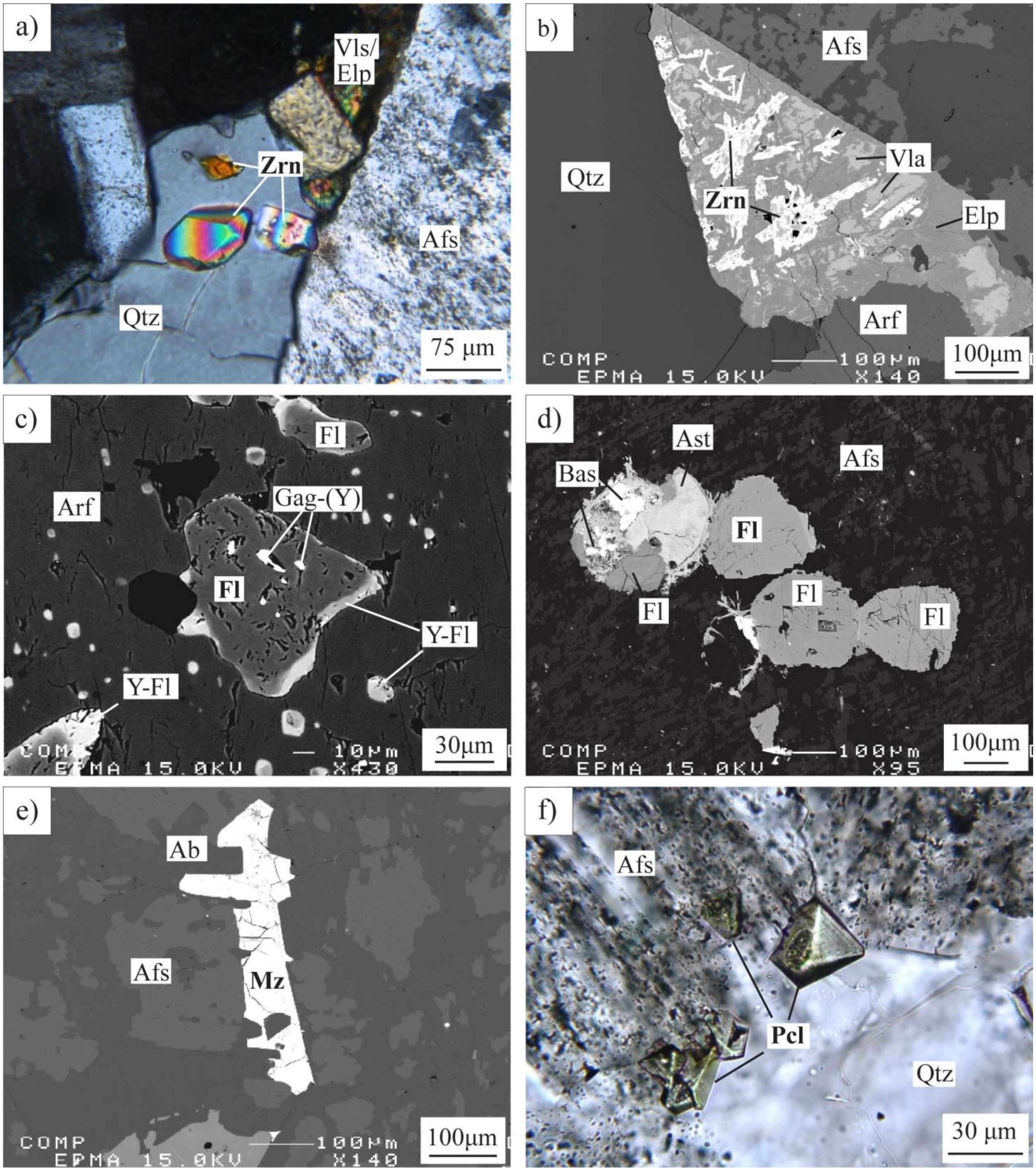

Fig. 2-3: Ore minerals of the hypersolvus granite

a) A thin section photomicrograph of primary zircon crystals enclosed in quartz, and alkali zirconosilicates (vlasovite and elpidite) interstitial to alkali feldspar and quartz, b) a backscattered electron (BSE) image showing alkali zirconosilicates (vlasovite and elpidite) and remnants of primary zircon (white) interstitial to quartz and alkali feldspar, c) a BSE image of fluorite (Fl) and Y-rich fluorite (Y-Fl, bright rims) as inclusions in arfvedsonite, and gagarinite-(Y) (Gag-Y) as inclusions in fluorite, d) a BSE image of fluorite globules with minor astrophyllite (Ast) and bastnäsite-(Ce) (Bas) as inclusions in perthitic alkali feldspar, e) a BSE image of monazite-(Ce) (Mz) as inclusions in perthitic alkali feldspar, and f) a thin section photomicrograph showing pyramidal fluornatropyrochlore (Pcl) crystals at the boundary between alkali feldspar and quartz.

Table 2-1: List of minerals identified in the fresh Strange Lake granites

Mineral name	Formula
Silicates	
Aegirine	$NaFe^{3+}Si_2O_6$
Albite	$NaAlSi_3O_8$
Arfvedsonite	$NaNa_2(Fe^{2+}{}_4Fe^{3+})Si_8O_{22}(OH,F)_2$
Fluorbritholite-(Ce)	$(LREE)_5(SiO_4,PO_4)_3(OH,F)$
Microcline	$KAlSi_3O_8$
Perthitic alkali feldspar	$KAlSi_3O_8$ - $NaAlSi_3O_8$
Quartz	SiO_2
Zirconosilicates	
Catapleiite	$(NaCa)_2ZrSi_3O_9$•$2(H_2O)$
Dalyite	$K_2ZrSi_6O_{15}$
Elpidite	$NaZrSi_6O_{15}$•$3(H_2O)$
Vlasovite	$Na_2ZrSi_4O_{11}$
Zircon	$ZrSiO_4$
Titanosilicates	
Aenigmatite	$Na_2Fe^{2+}{}_5TiO_2Si_6O_{18}$
Astrophyllite	$K_2Na(Fe^{2+},Mn)_7Ti_2Si_8O_{26}(OH)_4$
Narsarsukite	$Na_2(Ti,Fe^{3+})Si_4(O,F)_{11}$
Oxides	
Magnetite	Fe_3O_4
Fluorcalciopyrochlore	$(Ca,\square)_2Nb_2(O,OH)_6F$
Fluornatropyrochlore	$(Na,REE,Ca)_2Nb_2(O,OH)_6F$
REE-F-(CO_2)-minerals	
Bastnäsite-(Ce)	$(Ce,La)CO_3F$
Fluorite	CaF_2
Fluorite-fluocerite-$_{s.s.}$	CaF_2-$LREEF_3$
Gagarinite-(Y)	$NaCa(Y,Ce)F_6$
Gagarinite-(Ce)	$Na(LREE_xCa_{1-x})(REE_yCa_{1-y})F_6$
Phosphates	
Monazite-(Ce)	$(LREE)PO_4$

2.2.2.2 Transsolvus granite

The transsolvus granite surrounds and intruded the hypersolvus granite, and contains abundant fine-grained, dark grey ellipsoidal enclaves (Figs. 2-4a, b). Much of it has been strongly altered hydrothermally, although it is relatively fresh in the center of the pluton, adjacent to the hypersolvus granite. This granite is composed mainly of perthitic alkali feldspar, arfvedsonite, quartz, microcline and albite. The perthitic alkali feldspar occurs as phenocrysts, whereas the microcline and albite crystals are smaller and form the groundmass. The rims of the perthitic alkali feldspar and microcline crystals have been replaced by albite. The larger perthitic alkali feldspar phenocrysts locally have rims of microcline around a perthitic core (Fig. 2-4c). Arfvedsonite occurs as phenocrysts in this unit. They are prismatic and locally contain inclusions of microcline and albite in the center and more frequently along the rims (Fig. 2-4d). In a number of samples, arfvedsonite has been partially replaced by aegirine (Fig. 2-4e). Arfvedsonite crystals of this unit locally form cumulates in which the crystals are aligned, indicating flow. The quartz is anhedral to subhedral (Fig. 2-4e) and frequently occurs as globular grains displaying a ‘snowball texture’, in which albite crystals grew along the crystal faces. Locally quartz has inclusions of microcline, albite or arfvedsonite in the cores (Fig. 2-4f).

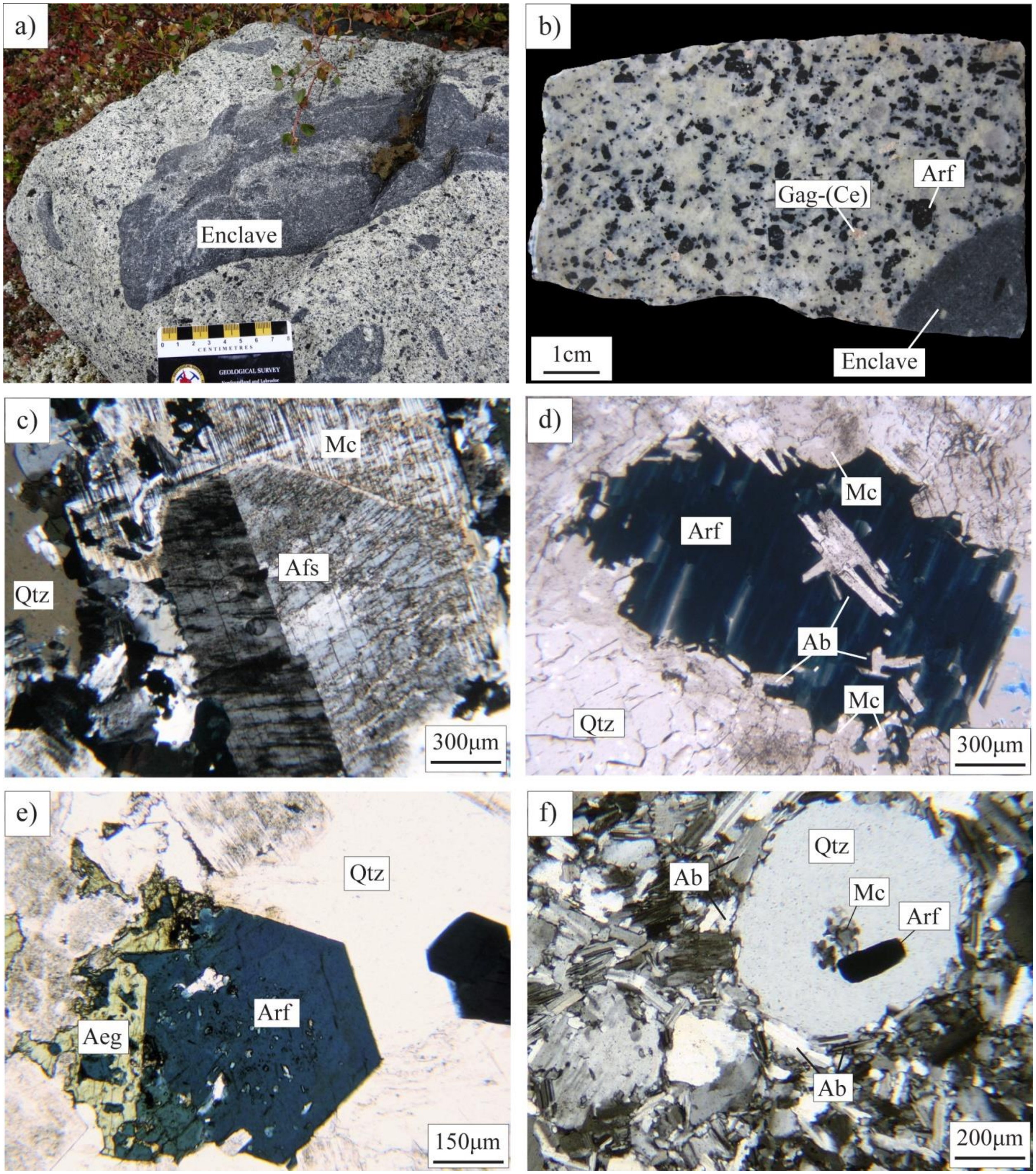

Fig. 2-4: Rock and thin section photographs of transsolvus granite

a) A photograph of a block of transsolvus granite containing a large dark grey ovoid enclave and several smaller enclaves, b) a photograph of a hand specimen of transsolvus granite containing typical arfvedsonite phenocrysts, gagarinite-(Ce) and part of an enclave, c) a photomicrograph showing a perthitic alkali feldspar crystal (Afs 1) with an overgrowth of microcline (Mc), d) a photomicrograph of an arfvedsonite phenocryst with albite (Ab) inclusions in the crystal center, and a rim with intergrowths of microcline and albite, e) a photomicrograph showing an arfvedsonite phenocryst partly replaced by aegirine, and f) a photomicrograph of a quartz ‘eye’ with arfvedsonite and alkali feldspar inclusions and albite laths along crystal surfaces in a matrix of fine microcline and albite crystals.

Like the hypersolvus granite, the transsolvus granite contains a variety of Zr-, Nb-, and REE-minerals. Alkali zirconosilicates, mostly vlasovite rimmed by minor proportions of elpidite (Fig. 2-5a), are the major Zr-bearing phases. Primary zircon is absent, however, secondary zircon formed locally as a result of the alteration of vlasovite to elpidite (Fig. 2-5a). In the transsolvus granite, the alkali zirconosilicates usually occupy a larger part of the rock volume compared to the hypersolvus granite, and invariably are interstitial, enclosing microcline and albite crystals. Narsarsukite ($Na_2(Ti,Fe^{3+})Si_4(O,F)_{11}$) is the only sodium titanosilicate present in the transsolvus granite, and forms large tabular poikilitic crystals in some samples. Fluorite occurs sparsely as a late (interstitial) phase. Pyrochlore-group minerals were relatively late crystallizing, as they occur as subhedral crystals along the margins of arfvedsonite and alkali feldspar crystals, or enclose microcline and albite crystals (Fig. 2-5b). They are less common than in the hypersolvus granite, but also are rimmed by a Ba-rich variety of pyrochlore. Monazite-(Ce) forms small inclusions in both perthitic alkali feldspar and arfvedsonite. Primary gagarinite-(Ce) (formerly named zajacite-(Ce)) Jambor et al. (1996)), is present as subhedral crystals, particularly among arfvedsonite cumulates, and was locally replaced by bastnäsite-(Ce) (Fig. 2-5c). Fluorbritholite-(Ce) crystals, in association with fluorite and remnants of bastnäsite-(Ce), were observed in a single sample in a matrix of microcline and albite (Fig. 2-5d).

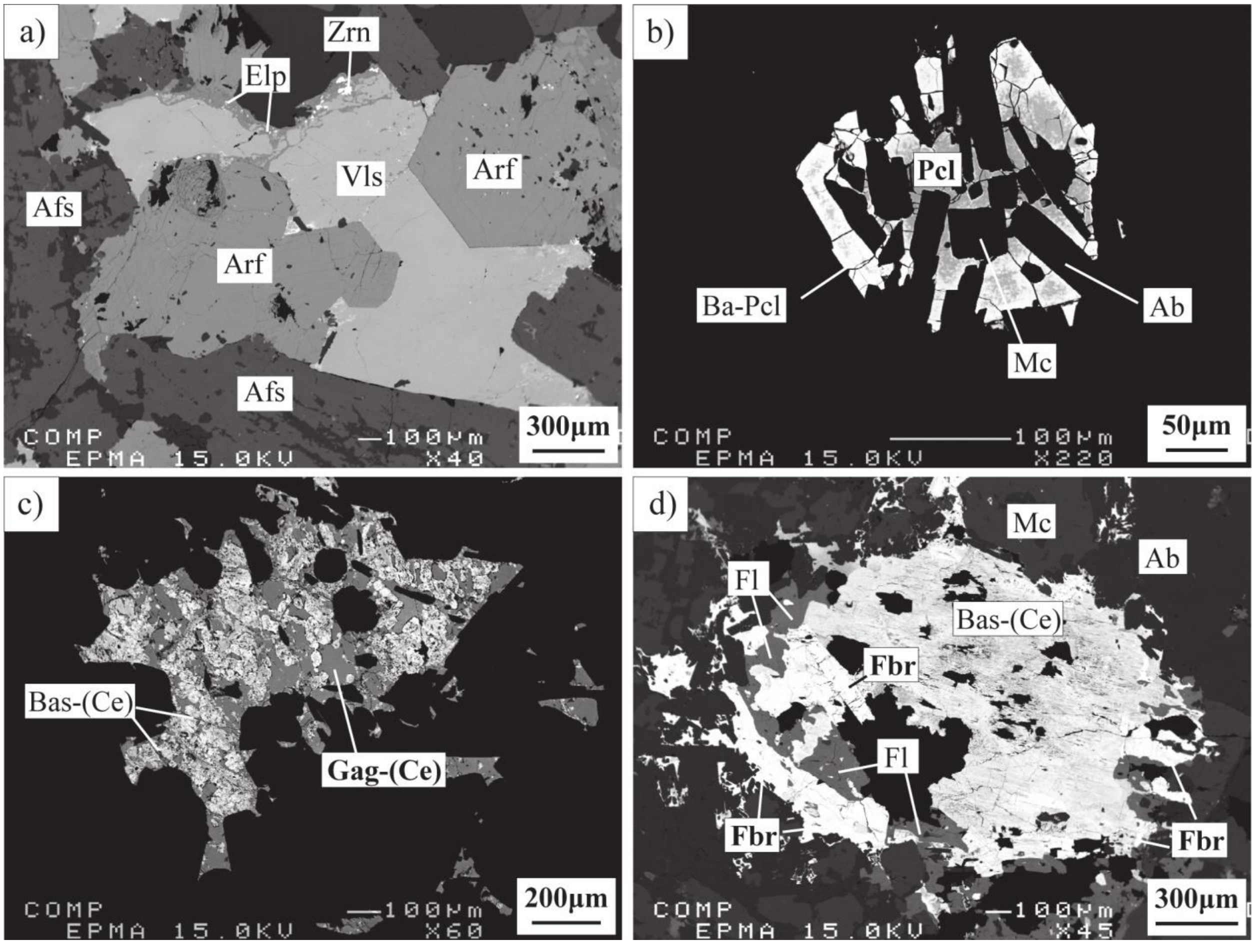

Fig. 2-5: Backscattered electron images of ore minerals of the transsolvus granite

a) Alkali zirconosilicates (vlasovite rimmed by elpidite) and secondary zircon interstitial to arfvedsonite and alkali feldspar, b) poikilitic fluornatropyrochlore with inclusions of microcline and albite, overgrown by a Ba-Pb-Si-rich pyrochlore, c) primary gagarinite-(Ce) locally replaced by bastnäsite-(Ce) (brighter), and d) fluorbritholite-(Ce) and fluorite replaced by bastnäsite-(Ce) (as fibrous remnants) in a matrix of alkali feldspar crystals.

2.2.2.3 Enclaves and dark porphyritic granite

The enclaves hosted by the transsolvus granite were assimilated by the latter to varying degrees and in varying proportions, e.g., the more assimilated enclaves appear as ghost-like patches and the less assimilated ones are dark with sharp contacts (Fig. 2-4a, b). They are most common in the center of the pluton and range from a few mm to 50 cm in diameter. Locally they occupy more than half the rock volume. As in the transsolvus granite, they contain phenocrysts of perthitic alkali feldspar, some of which have overgrowths of microcline (Fig. 2-6a). Approximately half of the enclaves sampled also contain arfvedsonite as well as narsarsukite phenocrysts (group 2), the latter of which occur as large white to beige tabular poikilitic crystals. The phenocrysts are embedded in a matrix of fine-grained quartz, microcline, albite and finely distributed subhedral arfvedsonite, which gives the enclaves their dark appearance.

The dark porphyritic granite, which is observed in outcrops adjacent to bodies of the host gneiss, contains phenocrysts of perthitic alkali feldspar and (locally) arfvedsonite, as well as round quartz crystals. These are set in a fine-grained matrix of subhedral arfvedsonite, microcline and albite (Fig. 2-6b). In some locations, the dark porphyritic granite is interlayered with ‘leucosomes’ of transsolvus granite creating a ‘marble cake’ texture (Fig. 2-6c). Elsewhere, it forms rounded blocks and was clearly intruded by the transsolvus granite (Fig. 2-6d). Significantly, the dark porpyritic granite is very similar in appearance to the enclaves hosted by the transsolvus granite. The paragenetic relationships of both, hypersolvus and transsolvus granite, are illustrated in Fig. 2-7.

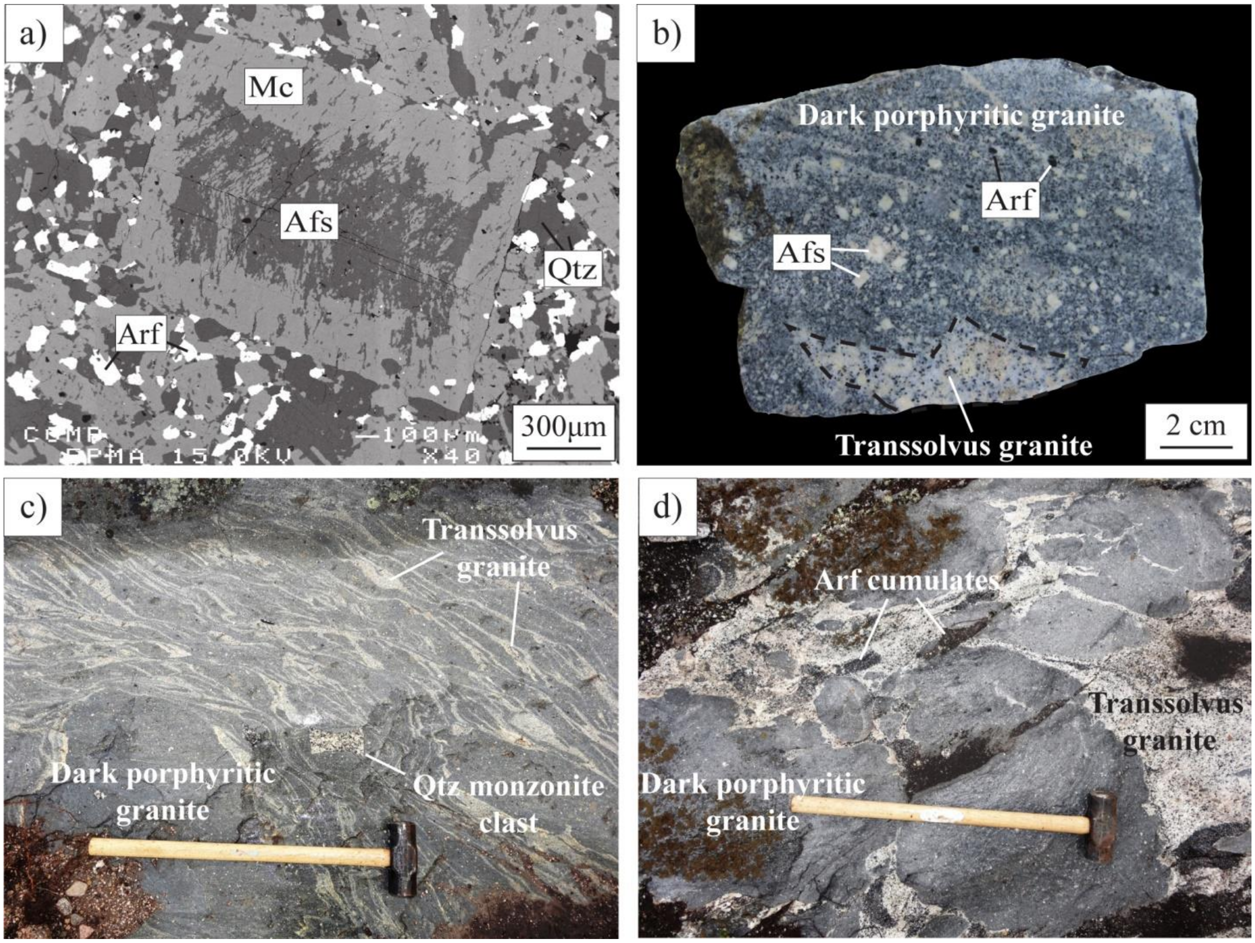

Fig. 2-6: Photographs of the dark grey porphyritic granite and enclaves

a) A backscattered electron image of an enclave showing perthitic alkali feldspar grain (Afs) rimmed by microcline in a matrix of fine-grained quartz, arfvedsonite, microcline and albite, b) a photograph of dark porphyritic granite showing perthitic alkali feldspar and minor arfvedsonite phenocrysts in a matrix of fine-grained quartz, arfvedsonite and alkali feldspar intermingled with some transsolvus granite (brighter); c) a photograph of an outcrop of porphyritic granite (dark grey) with ‘leucosomes’ (marble cake) and one angular clast of quartz monzonite (host rock), and d) dark porphyritic granite intruded by leucocratic transsolvus granite containing arfvedsonite cumulates.

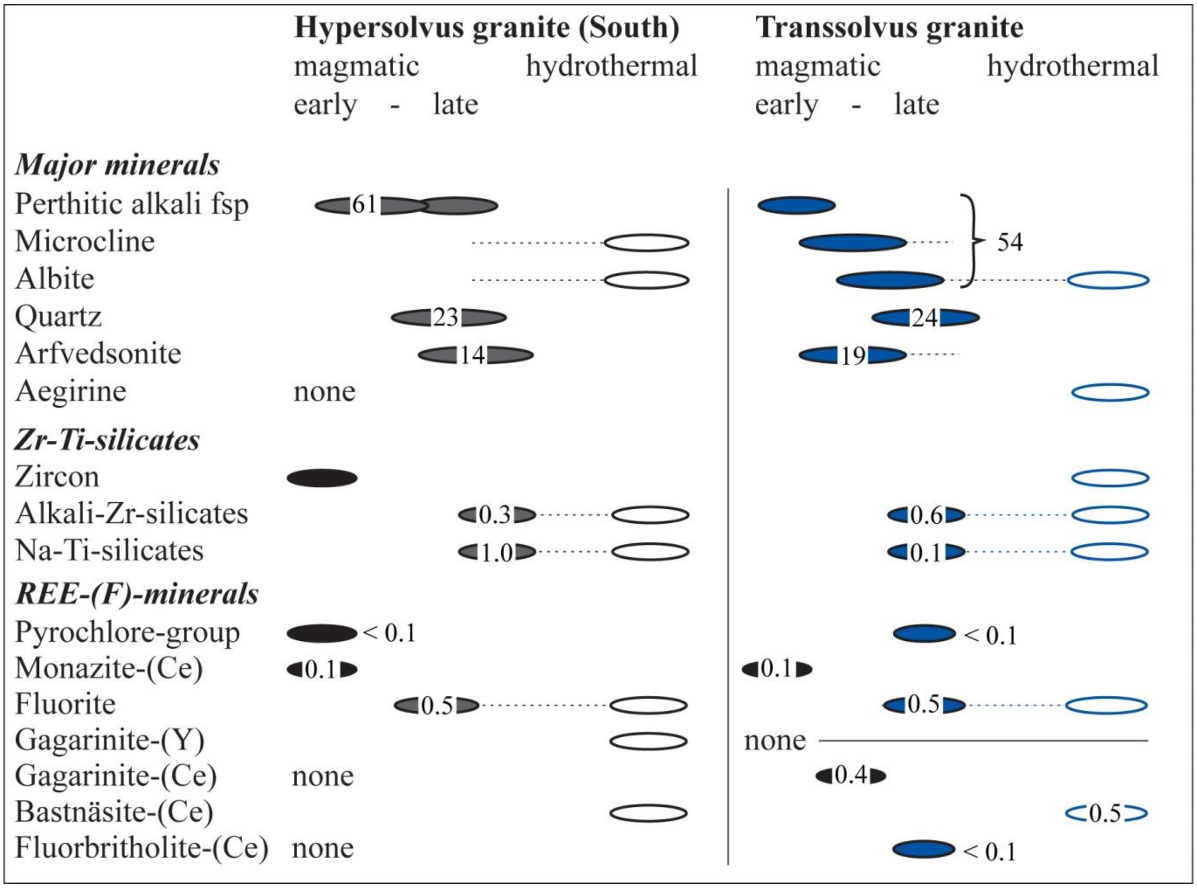

Fig. 2-7: Mineral parageneses in hypersolvus granite (south) and transsolvus granite

Modal mineral volumes (in wt. %) calculated using the MINSQ least square method. Black circles = early fractionated REE-, Zr- and Nb- minerals; dark grey and blue circles = magmatic minerals; white circles = hydrothermal phases. The dashed lines indicate prolonged mineral crystallization.

2.2.2.4 Pegmatites

The hypersolvus and transsolvus granites both contain pegmatites, which, on the basis of drill hole intersections, occur mainly as flat-lying sheets, and locally as subvertical dikes. In the hypersolvus granite, the pegmatites are composed of coarse-grained, comb-textured arfvedsonite, quartz, K-feldspar and minor proportions of alkali zirconosilicate minerals. The unaltered transsolvus granite locally contains bodies of pegmatite with K-feldspar, quartz, arfvedsonite and interstitial zirconosilicate minerals that contain inclusions of feldspar and arfvedsonite. In contrast, the altered transsolvus granite is host to numerous NYF-type pegmatites with border zones of K-feldspar, quartz, arfvedsonite partially altered to aegirine and/or hematite and pseudomorphs after zirconosilicates. Their cores are composed of quartz, fluorite and interstitial exotic REE minerals. The strongly altered pegmatites of the altered transsolvus granite are host to the bulk of the rare-metal mineralization in the deposit and have been the target of mineral exploration.

2.2.2.5 Fluorite-hematite breccia

A fluorite-hematite breccia is exposed in a single outcrop and in the core from a large number of holes that were drilled along the margins of the pluton. The bright purple and/or reddish colored breccia contains angular fragments ranging from a few mm to several cm in diameter of the host rock types observed in the proximity of the pluton. To the west and south, the fragments are of the adjacent Napeu Kainiut quartz monzonite, whereas to the east, they mainly comprise nearby Paleoproterozoic quartzofeldspathic gneisses and biotite-gneisses. The intensity of the fracturing of the host rocks decreases with distance to the pluton; the fractures are filled with purple fluorite and reddish hematite but are barren of any mineralization.

2.2.2.6 Roof pendants and remnants of wall rock

Fragments of Napeu Kainiut quartz monzonite occur as angular inclusions a few cm in diameter in the dark porphyritic granite (see Fig. 2-6c) or have been mapped as large outcrops in the center of the transsolvus granite (see map Fig. 2-1). The exposed quartz monzonite within the Strange Lake pluton has the same coarse-grained texture and mineralogy (plagioclase, perthitic alkali feldspar, quartz and biotite) observed in quartz monzonite outside the pluton, but exhibits features of recrystallization such as granophyric-textured intergrowths of quartz and alkali feldspar. To the east and in the northern part of the pluton, fragments in drill core and large outcrops consist mostly of banded biotite gneiss. The large outcrops of foreign rock types in the center of the pluton may represent roof pendants, but the larger, elongate exposures of the gneisses (see map, Fig. 2-1), are most likely remnants of the wall-rock. The latter is suggested by the observation that the foliation of the larger gneiss outcrops within the pluton generally matches that of the gneisses outside the pluton (NNW-SSE).

2.3 METHODS

The Strange Lake pluton and its host-rocks were mapped in detail during the course of this project; 25 samples of least-altered granite were collected for petrographic and chemical analysis. These samples were supplemented by an additional 46 samples that form part of a Strange Lake collection at McGill University. Enclaves were extracted from 12 transsolvus granite samples and treated separately. The bulk-rock chemical data were provided by Quest Rare Minerals Ltd., and represent the results of analyses by Actlabs using XRF (X-ray fluorescence) for Nb, ISE-MS (ion selective electrode) for F, fusion-ICP-OES for major elements and fusion ICP-MS for most trace elements.

The major-element composition of alkali feldspars, alkali zirconosilicates and the REE minerals, including fluorite, was determined on carbon-coated 30 μm thick polished sections, using a JEOL JXA-8900L electron microprobe (EMP) at the Department of Earth and Planetary Sciences, McGill University. The beam current was 30 nA for zircon, the REE minerals and fluorite and 20 nA for all other minerals. The acceleration voltage was 20 kV for the pyrochlore-group minerals and zircon, and 15 kV for feldspars, the alkali zirconosilicates, the REE minerals and fluorite. The beam diameter was 5 μm for zircon, 10 μm for microcline, albite and pyrochlore-group minerals, 15 μm for the REE minerals and fluorite and 50 μm for the alkali zirconosilicates, in order to avoid Na and volatile loss. A 200 μm beam diameter was used for perthitic alkali feldspar to facilitate the line- and multiple spot-analyses that were needed to obtain a reliable average composition for each grain. Counting times and standards used in the analyses, as well as detection limits based on repeated analyses of standards, are listed in the appendix (Table 2-10). Backscattered electron micrographs (BSE) were made with a 5 µm beam diameter and 20 nA acceleration voltage. Mineral identification was accomplished using an energy dispersive spectrometer (EDS) attached to the EMP.

Laser Ablation Inductively Coupled Plasma Mass Spectrometric (LA-ICP-MS) analyses were conducted on 15 samples using a NewWave 213 nm Nd-YAG laser-ablation system and a Thermo Finnigan iCapQ ICP-MS at the Department of Earth and Planetary Sciences at McGill University. The perthitic alkali feldspar crystals were analyzed for selected major and trace elements in the same 30 µm-thick polished sections. The NIST 610 glass was used as a standard and Si from the EMP analyses was used as internal standard. The analyses were performed as line traverses with a 10 Hz repetition rate, 20 µm beam diameter, a scan speed of 15 µm/s and an output rate of 45%. Data reduction was carried out using the software, Iolite, version 2.5, based on Igor Pro, version 6.34A. The estimated error was 5-10 % for each element.

2.4 RESULTS

2.4.1 Bulk rock compositions

The average bulk-rock major and trace element compositions of the unaltered Strange Lake granites are reported in Table 2-2. Totals < 100 wt. % are attributed to the presence of H_2O and CO_2, which were not analyzed. The agpaitic index (molar [(Na+K)/Al]) of the unaltered granites from the center of the pluton varies between 1.05 and 1.39 and hence classifies the rocks as peralkaline, whereas the quartz monzonite host-rock is classified as metaluminous with an average agpaitic index of 0.83. The Strange Lake granite samples generally have low concentrations of Ca and Mg and high concentrations of alkalis, Fe, F, Zn, Rb, Zr, Nb and REE. Alumina (as Al_2O_3) was chosen as monitor of magmatic evolution rather than the AI (alkalinity index) or ASI (alumina saturation index) as these indices include Na, K and Ca, elements which were involved in the alteration that affected even the freshest rocks of the pluton. Generally, the concentrations of incompatible elements, such as Ce (LREE) and Zr (HFSE), but also major elements, such as Si and Fe (Fig. 2-8a-c), increase with decreasing Al content and hence, with evolution. The agpaitic index also increases with evolution.

Compositionally, the hypersolvus granite can be divided into two Al_2O_3 populations, one averaging ~12 wt. %, and the other ~10.5 wt. % (Fig. 2-8; Table 2-2). Both populations are represented in the southern hypersolvus granite, whereas only the high alumina population is represented in the northern hypersolvus granite (sample set of this study). The high Al_2O_3 population of the southern hypersolvus granite is fine-grained and equigranular in texture and, as it has the lowest concentrations of Si, REE and Zr and the lowest agpaitic index (avg. 1.12) (see Table 2-2, Fig. 2-8 a, b), is interpreted to represent the least evolved rock unit. This population (high Al_2O_3) is referred to hereafter as the southern hypersolvus granite. Note that the low Al_2O_3 population of the same unit, which comprises medium-grained, and mostly oikocrystic to pegmatitic textured members, has higher Si and Fe concentrations, a higher average agpaitic index of 1.24, and only slightly elevated REE and Zr concentrations compared to the high alumina granite (Fig. 2-8 a, b, c; Table 2-2). The concentrations of the REE and Zr in the northern hypersolvus granite are consistently higher (e.g., avg. 700 ppm Ce and 3500 ppm Zr) than those in the southern hypersolvus granite (avg. 460 ppm Ce and 2400 ppm Zr) and the bulk K/Rb ratio is much lower. The Al_2O_3 content is also somewhat lower (avg. 11.7 vs. 11.9 wt. %), suggesting that it is more evolved.

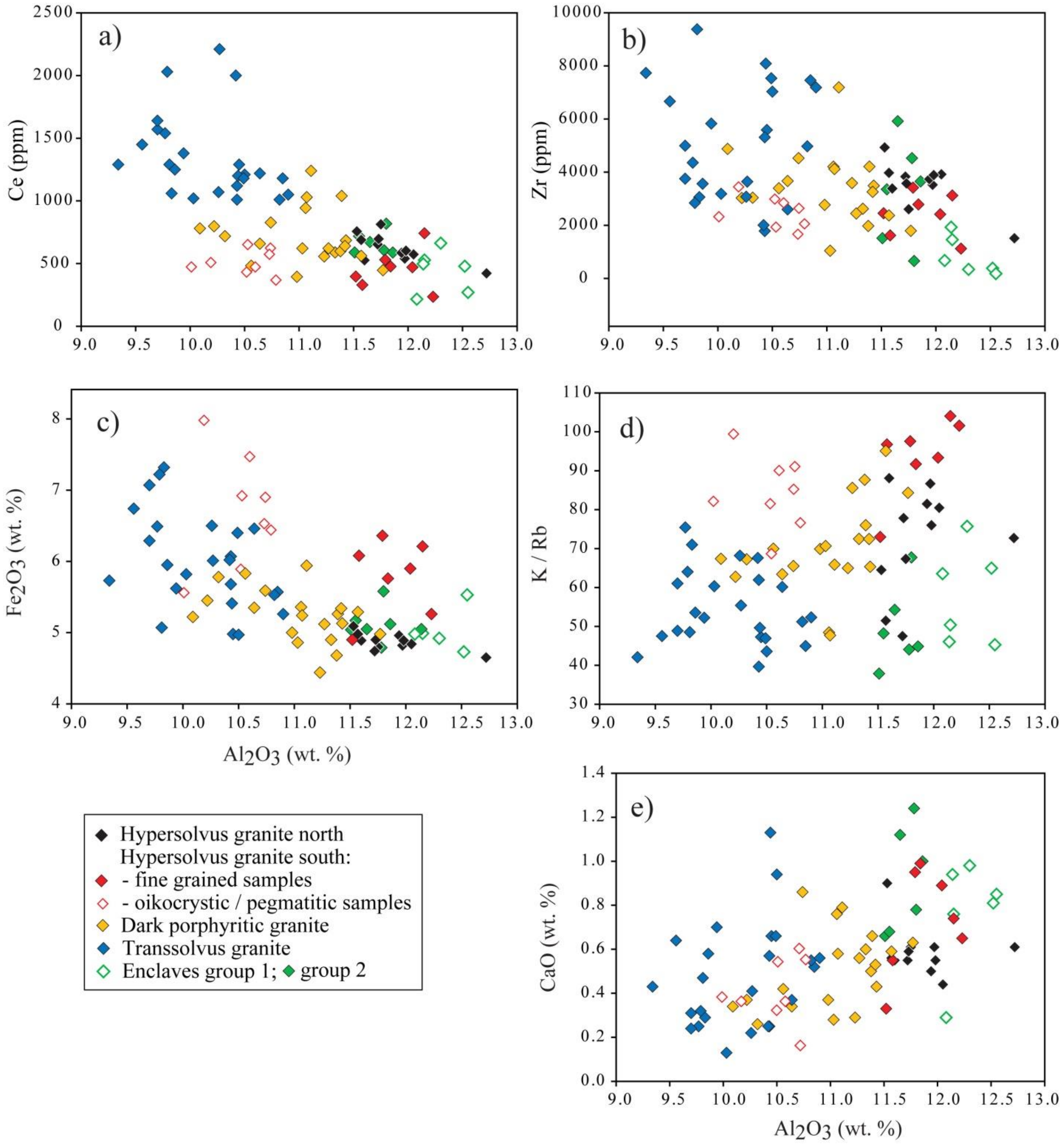

Fig. 2-8: Major element bulk rock compositions of the unaltered Strange Lake granites

Compositions displayed as a function of Al_2O_3 (wt. %) concentration (X-axis). a) cerium (LREE), b) zirconium, c) ferric iron, d) K/Rb ratio, e) calcium.

The transsolvus granite generally has higher Si, REE, Zr, Nb, Rb and F concentrations and significantly lower Al and Ca concentrations than the hypersolvus granite (Fig. 2-8, Table 2-2). On the basis of compositional and mineralogical differences, the dark grey enclaves can be subdivided into two groups. Group 1 has high Al, K and Rb, and low Na, Fe, Mn, Ti, Zr and Nb concentrations. This group is fine-grained and its phenocrysts are restricted to perthitic alkali feldspar. Group 2 has higher Na, Mn, Ti, Nb, Zr, and lower Al, K and Rb concentrations than group 1 (Table 2-2, Fig. 2-8). This group contains arfvedsonite and narsarsukite phenocrysts in addition to perthitic alkali feldspar. The dark grey porphyritic granite is intermediate in composition between the hypersolvus granite and the transsolvus granite (Fig. 2-8). The wide range in composition of this unit is attributed to varying degrees of intermixing of the dark grey facies with the leucocratic transsolvus granite (see Fig. 2-6b, c).

Chondrite-normalized (Sun and McDonough, 1989) trace element profiles of the unaltered granite facies are characterized by strong enrichments in U, Th, Nb, Ta and REE and depletions in Sr, Pb, Ba and Eu (Fig. 2-9). The northern hypersolvus granite has higher concentrations of REE and the HFSE (Th, U, Nb, Zr, Hf) than the southern hypersolvus granite (Figs. 2-9a, b). The bulk REE and other HFSE concentrations are highest for the transsolvus granite (Table 2-2), ranging for the LREE between 10^3 and 10^4 times chondrite values; the range in HREE and other HFSE concentrations is wider (Figs. 2-9c, d). The enclaves hosted by the transsolvus granite have LREE concentrations similar to that of the hypersolvus granites, a relatively wide range in HREE concentrations, and have overall slightly lower REE concentrations than those of the dark porphyritic granite (Figs. 2-9e). Enclave group 1 has slightly lower REE concentrations than group 2, and is relatively depleted in the HFSE (Zr, Nb, U, Th), whereas group 2 is enriched in these elements (Fig. 2-9 e, f).

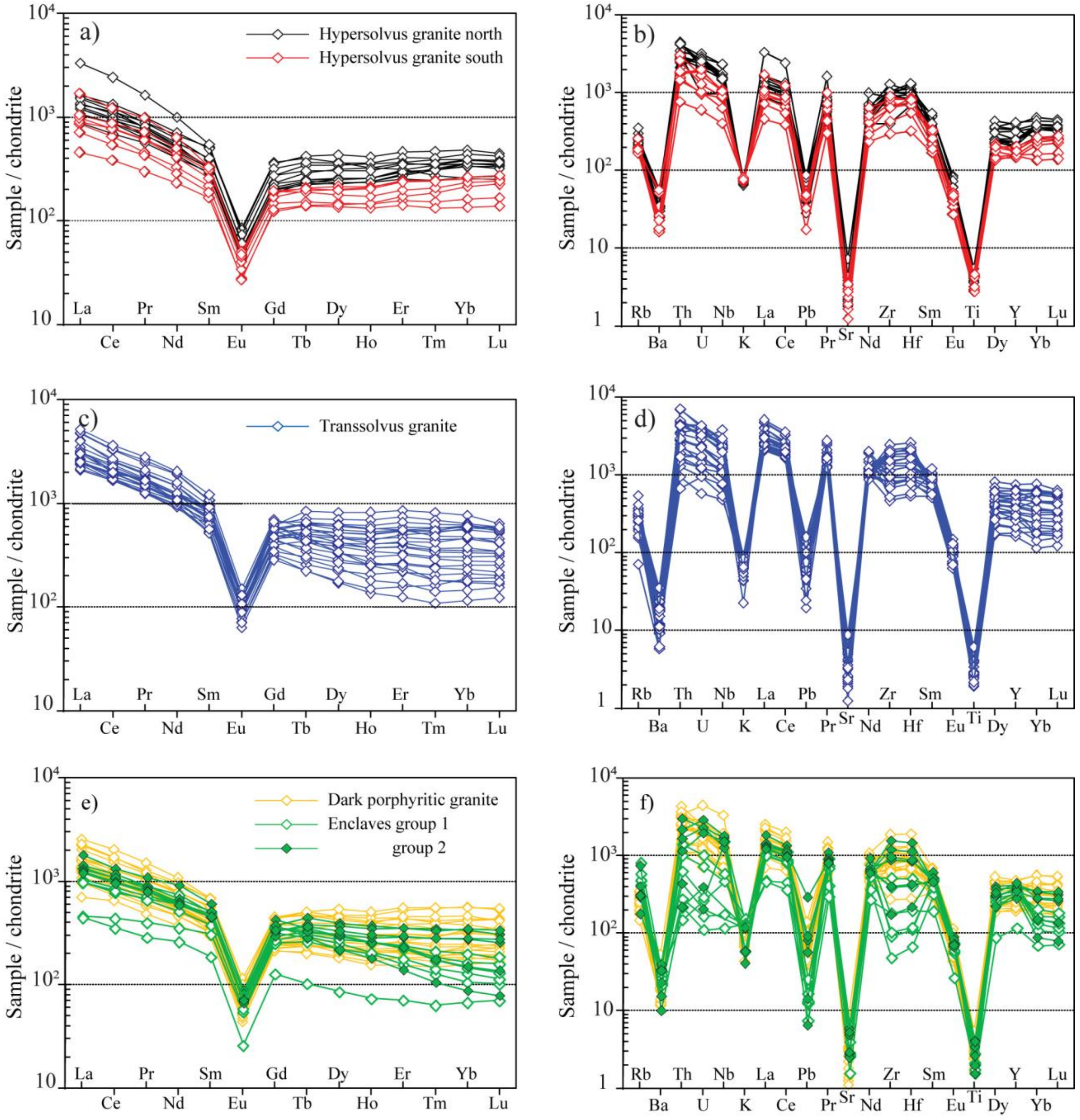

Fig. 2-9:Bulk rock REE and trace element profiles

Bulk rock chondrite-normalized (Sun and McDonough, 1989) REE (a, c, e) and trace element (b, d, f) profiles of the unaltered Strange Lake granites.

Table 2-2: Bulk rock compositions of the fresh Strange Lake granites

Average (median) bulk rock compositions with median absolute deviation (±) of unaltered granites from the center of the Strange Lake pluton. The quartz monzonite host-rock samples presented in this table are from outside the pluton (not metasomatized by Strange Lake fluids). *fgr = fine grained rocks and **pg = oikocrystic and pegmatitic textured rocks.

Unit	Hypersolvus granite S fgr*		Hypersolvus granite S pg**		Hypersolvus granite N		Transsolvus granite		Dark porphyritic granite		Enclave group 1		Enclave group 2		Quartz monzonite (host)	
Samples	*7*		*8*		*12*		*24*		*20*		*6*		*6*		*6*	
(wt. %)		±		±		±		±		±		±		±		±
SiO_2	69.04	0.89	70.57	0.56	70.68	0.36	71.28	0.53	70.64	0.51	68.96	0.58	69.81	0.64	70.88	0.19
Al_2O_3	11.88	0.26	10.57	0.17	11.74	0.21	10.27	0.39	11.09	0.32	12.23	0.12	11.72	0.12	12.64	0.20
Fe_2O_3	5.78	0.31	6.72	0.52	4.89	0.08	5.98	0.47	5.25	0.23	4.99	0.06	5.09	0.06	5.23	0.23
MnO	0.10	0.01	0.11	0.01	0.10	0.01	0.12	0.01	0.09	0.01	0.08	<0.01	0.12	0.02	0.07	0.01
MgO	0.04	0.01	0.02	0.01	0.05	0.01	0.03	0.01	0.04	0.01	0.04	0.01	0.04	0.02	0.34	0.05
CaO	0.73	0.19	0.37	0.11	0.57	0.03	0.45	0.18	0.52	0.15	0.83	0.09	0.89	0.22	1.36	0.06
Na_2O	4.92	0.17	5.11	0.05	5.09	0.10	5.08	0.35	4.90	0.34	3.08	0.28	5.72	0.57	3.07	0.07
K_2O	4.93	0.21	4.48	0.09	4.74	0.11	4.32	0.31	4.77	0.33	8.35	0.29	3.84	0.63	5.06	0.23
TiO_2	0.28	0.03	0.21	0.03	0.27	0.01	0.21	0.05	0.22	0.04	0.14	0.01	0.22	0.08	0.55	0.04
Nb_2O_5	0.03	0.01	0.05	0.01	0.06	<0.01	0.05	0.02	0.04	0.01	0.02	0.01	0.05	0.01	<0.01	<0.01
P_2O_5	0.02	<0.01	0.02	<0.01	0.02	0.01	0.01	0.01	0.01	0.01	<0.01	<0.01	<0.01	<0.01	0.12	0.01
F	0.44	0.02	0.37	0.09	0.46	0.04	0.51	0.06	0.44	0.08	0.56	0.05	0.46	0.01	0.07	0.01
TREO	0.17	0.03	0.19	0.02	0.24	0.03	0.48	0.06	0.24	0.05	0.23	0.03	0.28	0.02	0.06	<0.01
LREO	0.12	0.02	0.13	0.02	0.16	0.02	0.33	0.04	0.17	0.03	0.14	0.03	0.17	0.01	0.05	<0.01
HREO+Y	0.05	<0.01	0.06	0.01	0.08	0.01	0.11	0.04	0.08	0.02	0.08	0.01	0.10	0.01	0.01	<0.01
Total	98.53		99.19		99.14		99.20		98.49		98.97		98.09		99.50	
LOI	0.72	0.09	0.47	0.14	0.70	0.14	0.72	0.15	0.64	0.20	0.79	0.05	0.88	0.09	0.74	0.22
A.I.	1.13	0.02	1.23	0.02	1.15	0.03	1.27	0.03	1.19	0.03	1.14	0.01	1.17	0.01	0.83	0.02

Table 2-2: Bulk rock compositions of the fresh Strange Lake granites (continued)

Be *(ppm)*	36	8	40	14	53	11	54	22	39	8	26	8	34	3	4	<1
Zn	285	40	545	30	465	60	585	90	430	70	385	65	700	120	95	10
Ga	45	3	52	3	44	1	60	3	51	2	48	2	51	5	22	1
Rb	417	23	436	31	522	47	672	99	623	119	1080	189	706	124	188	5
Sr	18	5	15	5	21	7	21	8	13	3	20	5	28	9	134	3
Y	266	17	293	36	392	74	616	196	440	112	513	41	582	53	59	2
Zr	2413	667	2504	469	3656	268	4984	1917	3325	835	529	269	3503	1505	615	66
Sn	58	17	75	19	95	10	105	39	74	21	20	2	73	14	6	<1
Ba	76	13	43	8	85	18	43	15	48	11	57	6	67	21	1293	48
La	228	33	221	35	305	51	630	81	325	65	232	53	304	18	95	4
Ce	464	73	485	72	629	79	1235	170	650	112	488	108	639	51	194	9
Pr	56	14	60	7	73	10	149	20	74	16	62	13	77	3	23	1
Nd	191	42	207	27	240	35	527	52	271	50	254	56	292	14	86	2
Sm	39	10	51	6	49	6	115	16	60	11	62	10	68	1	16	0.4
Eu	2	0.4	3	0.4	3	0.4	6	1	3	0.5	4	0.4	4	0.2	2	0.1
Gd	33	5	44	7	45	7	100	18	54	9	62	10	66	5	12	0.4
Tb	6	1	8	1	10	1	17	4	10	2	11	1	13	1	2	<0.1
Dy	44	7	53	8	69	12	103	29	64	15	64	8	79	9	11	0.3
Ho	10	2	11	2	15	2	21	7	13	3	13	2	16	3	2	0.1
Er	33	6	36	7	50	6	64	24	42	11	32	5	47	10	7	0.1
Tm	5	1	6	1	8	1	9	4	7	2	4	1	7	2	1	<0.1
Yb	36	3	42	9	57	4	58	29	45	13	22	5	45	11	7	0.3
Lu	6	0.4	7	1	9	1	8	4	7	2	3	1	7	1	1	0.1
Hf	69	12	67	12	97	15	136	47	94	20	16	7	88	36	14	1
Ta	14	1	20	4	28	4	25	13	20	5	4	3	23	3	2	0.2
Pb	94	17	169	53	137	38	187	73	139	32	32	5	170	94	39	4
Th	54	9	69	20	88	15	84	40	72	23	13	8	40	25	21	1
U	10	3	14	3	19	2	17	8	13	4	2	1	16	3	4	0.4

2.4.2 Modal mineralogy

The proportions of the major and minor minerals for a representative sample of each granite were estimated using the MINSQ excel spreadsheet of Herrmann and Berry (2002), which relates the bulk rock composition to the mineral compositions. Both hypersolvus granite units and the enclaves contain high alkali feldspar proportions (>61 wt. %) in comparison to the transsolvus granite (~54 wt. %). The proportion of arfvedsonite differs between the southern and northern hypersolvus granite (~14 vs. 10 wt. %), as in the latter, arfvedsonite has been replaced locally by a higher proportion of titanosilicates. The transsolvus granite contains an elevated proportion of arfvedsonite (~19 wt. %) compared to the enclaves (~13 wt. %) for which the proportion is similar to that of the hypersolvus granites; both the transsolvus granite and the enclaves have low proportions of titanosilicates. The southern hypersolvus granite and enclave group 1 contain the smallest, and the transsolvus granite the highest proportion of REE minerals. The relative mineral proportions per unit are reported in Table 2-3 and illustrated in Figure 2-7.

Table 2-3: Relative proportion of primary minerals per granite unit

Unit	Hypersolvus granite S	Hypersolvus granite N	Transsolvus granite	Enclave Group 1	Enclaves Group 2
Sample	204771	204756	204720	10039	204712
Mineral (wt. %)					
Perthitic alkali feldspar	61	63	54	69	63
Microcline	-	-			
Albite	-	-			
Quartz	23	22	24	17	22
Arfvedsonite	14	10	19	13	13
Fluorite	0.5	0.7	0.5	0.9	0.8
Zircon/zircono-silicates	0.3	0.7	0.6	<0.05	0.3
Titano-silicates	1.0 (Ast)	2.5 (Aen/Ast)	0.1 (Nars)	0.7	<0.05 (Nars)
Monazite-(Ce)	0.1	0.2	0.1	<0.05	0.2
Pyrochlore group	<0.05	0.1	0.05	<0.05	0.2
Gagarinite-(Ce)	-	-	0.4	-	-
Bastnäsite-(Ce)	-	-	0.5	-	-
Total	99.9	99.4	98.9	100.6	99.5

2.4.3 Mineral chemistry

2.4.3.1 Alkali feldspar

The feldspars (perthitic alkali feldspar, microcline and albite) were analyzed for their major element and common trace element (Ba, Rb and Pb) proportions. In addition, the perthitic alkali feldspar was analyzed for the REE and other trace elements. The Al content of the perthitic alkali feldspar is highest in the fine-grained, equigranular samples of the southern hypersolvus granite with an average of 0.99 apfu, whereas the samples from the northern hypersolvus granite, the transsolvus granite and its enclaves have lower values, averaging 0.96 apfu (Fig. 2-10, Table 2-5). The Na concentration in the perthitic alkali feldspar of the southern hypersolvus granite varies between 0.37 and 0.69 apfu, and is higher on average (0.53 apfu) than in the perthitic alkali feldspar of the northern hypersolvus granite (avg. 0.47 apfu), which has a wider range of values, i.e., between 0.18 to 0.61 apfu (Fig. 2-10a). The perthitic alkali feldspar in the transsolvus granite and its enclaves has an exceptionally wide range in Na (0.09 to 0.90 apfu) and K (0.09 to 0.88 apfu) contents (Fig. 2-10a, b). The average orthoclase proportion (X_{Or}) of the perthitic alkali feldspar is 0.57 in the southern hypersolvus granite and 0.55 in the dark porphyritic granite, and 0.60 to 0.63 in the northern hypersolvus granite, transsolvus granite and the enclaves. The silica content of the perthitic alkali feldspar shows an overall increase with decreasing Al concentration and varies mainly between 2.98 and 3.08 apfu (Fig. 2-10c). The Fe^{3+} concentration is lowest in the perthitic alkali feldspar of the southern hypersolvus granite and increases progressively through the northern hypersolvus granite, the enclaves and the transsolvus granite. It is highest in the dark porphyritic granite (Table 2-4, Fig. 2-10d). The concentration of Ca is low or lies below the detection limit in all feldspars (perthitic alkali feldspar, microcline and albite) (Table 2-4).

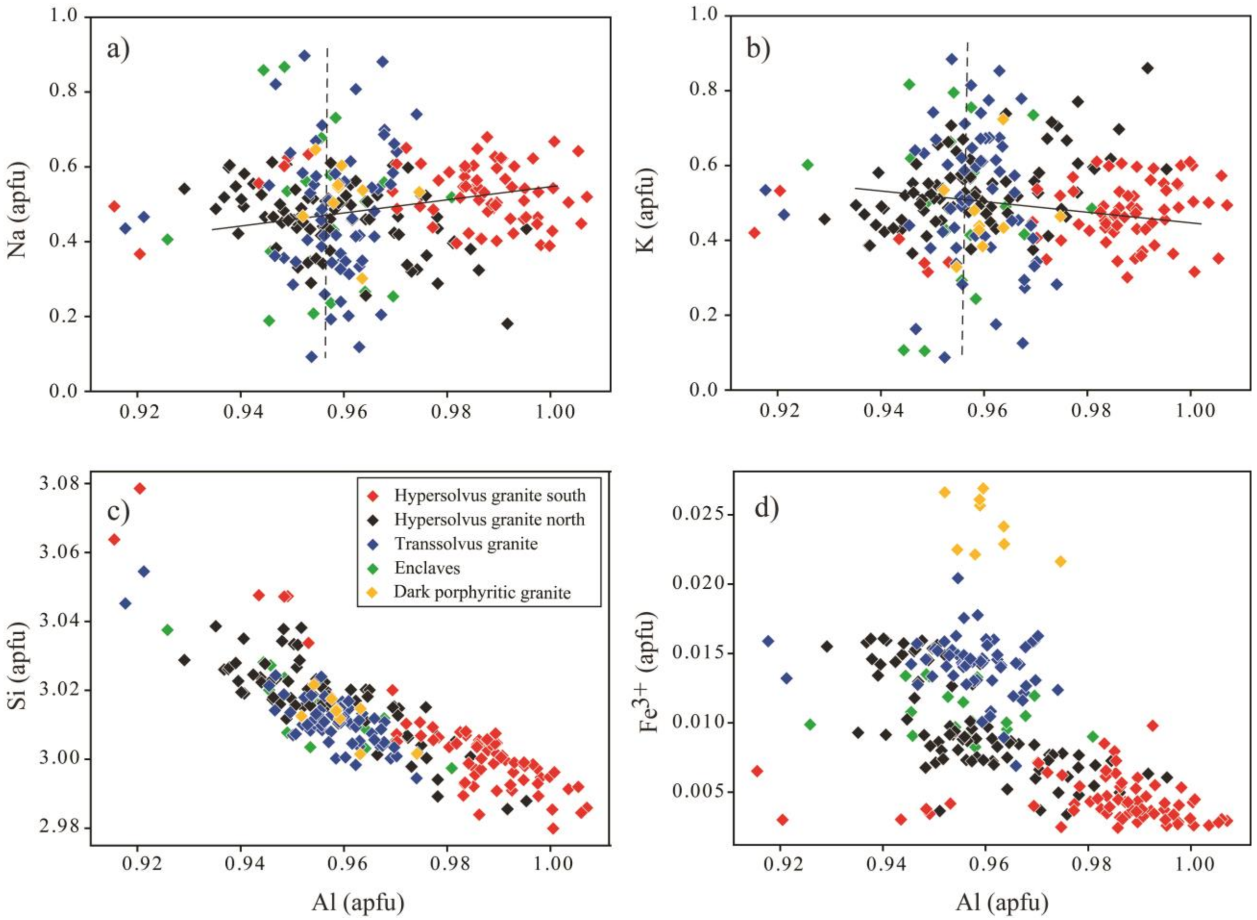

Fig. 2-10: Binary diagrams showing perthitic alkali feldspar compositions

Alkali feldspar compositions (in apfu) displayed with alumina concentrations as monitor of granite evolution (X axis). a) sodium, b) potassium, c) silica, d) ferric iron. The solid lines in a) and b) indicate the decreasing Na-, and increasing K-concentrations in the perthitic alkali feldspar with hypersolvus granite evolution (south to north); the dashed lines indicate the large range in Na and K concentrations in the perthitic alkali feldspar of the transsolvus granite and enclaves.

Concentrations of common trace elements in alkali feldspars (Rb, Ba and Pb) show no significant variation among the granite units and lie mostly below the detection limit. An exception is Rb, which reaches an average of 0.06 wt. % (Rb_2O) in the perthitic alkali feldspar of the enclaves and 0.03 wt. % in the transsolvus granite (Table 2-4); microcline in the transsolvus granite contains an average of 0.25 wt. % Rb_2O. The concentrations of other trace elements in the perthitic alkali feldspar differ significantly among the granite facies (Fig. 2-11). The total

REE concentration of the perthitic alkali feldspar is lowest for the southern hypersolvus granite (avg. 11 ppm), intermediate for the dark porphyritic granite (avg. 24 ppm) and northern hypersolvus granite (avg. 51 ppm) and is highest in the transsolvus granite and its enclaves (avg. 120, and 146 ppm, respectively) (Table 2-5). The chondrite-normalized REE profiles of the perthitic alkali feldspar vary greatly among the units, showing low concentrations and flat profiles for the southern hypersolvus and dark porphyritic granites and higher concentrations with decreasing trends towards the middle REE for the northern hypersolvus and transsolvus granites as well as the enclaves; all have a distinct negative Eu-anomaly (Fig. 2-11a). The HREE profiles are relatively flat and progressively depleted in the heaviest REE, Yb and Lu. The northern hypersolvus granite and dark porphyritic granite show a slight enrichment in the HREE (except for Yb and Lu), as well as a small negative Y-anomaly (Fig. 2-11b). The trace element profiles generally display distinct negative anomalies for Ba, Pb, Sr and Ti, and positive anomalies for Rb and Th (Fig. 2-11b).

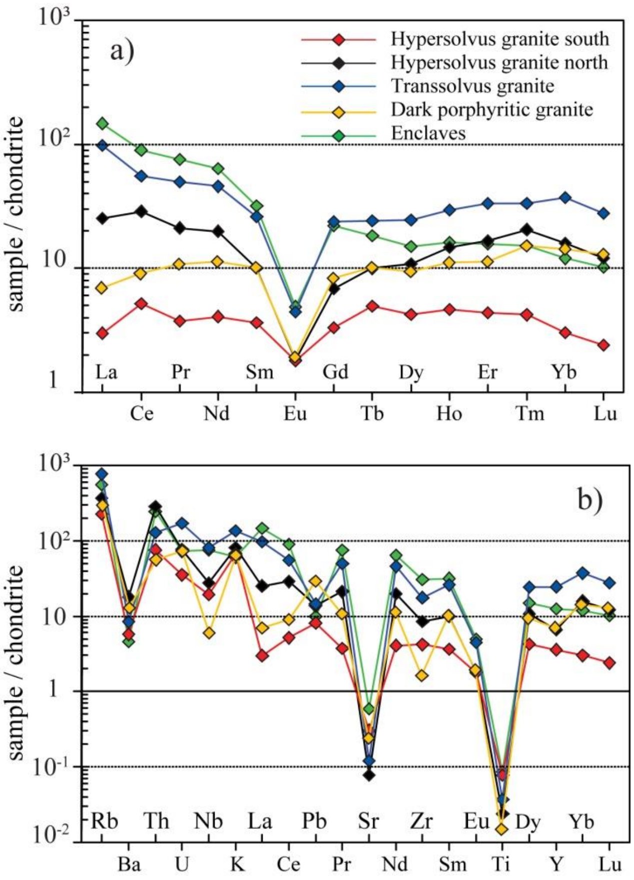

Fig. 2-11: REE and trace element profiles of perthitic alkali feldspar

Profiles normalized to chondrite (Sun and McDonough, 1989)

Table 2-4: Feldspar compositions (perthitic alkali feldspar, microcline and albite)

Average (median) elemental composition of feldspars (perthitic alkali feldspar, microcline and albite) and median absolute deviation (±) of each granite unit with relative Ab-Or (X_{Or}) component. *fine grained, equigranular samples, and **oikocrystic/pegmatitic samples, *n* = number of analyses.

Unit	Hypersolvus granite						Enclave group 1		Dark porph. granite		Transsolvus granite					
Type	South – fgr*		South – peg**		North											
Mineral *(n)*	Perthitic alkali feldspar *(67)*		Perthitic alkali feldspar *(95)*		Perthitic alkali feldspar *(82)*		Perthitic alkali feldspar *(19)*		Perthitic alkali feldspar *(9)*		Perthitic alkali feldspar *(58)*		Microcline *(34)*		Albite *(58)*	
(wt. %)		±		±		±		±		±		±		±		±
K_2O	8.26	1.03	7.87	0.81	9.08	0.85	8.72	2.52	7.65	0.71	9.11	2.04	16.01	0.07	0.10	0.02
Na_2O	6.12	0.77	6.24	0.50	5.34	0.59	5.82	1.91	6.17	0.40	5.29	1.36	0.50	0.09	11.63	0.09
CaO	0.04	0.02	0.02	0.01	0.02	0.01	0.08	0.02	0.02	0.01	0.02	0.01	-	-	0.01	0.01
Al_2O_3	18.65	0.17	18.02	0.19	17.96	0.17	17.86	0.15	17.96	0.08	17.86	0.19	17.71	0.15	19.35	0.65
BaO	-	-	0.01	0.01	-	-	-	-	-	-	-	-	0.01	0.01	0.01	0.01
SiO_2	66.90	0.59	67.01	0.52	67.05	0.55	66.31	0.65	66.60	0.25	66.27	0.55	64.82	0.10	68.54	0.38
Fe_2O_3	0.24	0.05	0.86	0.08	0.51	0.10	0.59	0.06	0.70	0.06	0.83	0.06	0.77	0.12	0.81	0.20
Rb_2O	-	-	-	-	-	-	0.06	0.06	0.01	0.01	0.03	0.03	0.25	0.05	-	-
PbO	-	-	0.01	0.01	0.01	0.01	-	-	-	-	0.01	0.01	-	-	-	-
Total	100.2		100.0		99.96		99.42		99.11		99.41		100.1		100.5	
X_{Or}	0.57		0.56		0.63		0.60		0.55		0.63		0.97		0.01	
Structural formulae																
K	0.47		0.45		0.52		0.50		0.44		0.52		0.95		0.01	
Rb	-		-		-		-		-		-		0.01		-	
Na	0.53		0.54		0.47		0.51		0.54		0.46		0.05		0.98	
Al	0.99		0.95		0.96		0.96		0.96		0.96		0.97		0.99	
Fe^{3+}	0.01		0.03		0.02		0.02		0.03		0.03		0.03		0.03	
Si	3.00		3.01		3.02		3.02		3.01		3.01		3.00		2.99	

Table 2-5: Trace element compositions of perthitic alkali feldspar

Average (median) trace element compositions of perthitic alkali feldspar for each granite unit with median absolute deviation (±).

Unit	Hypersolvus granite S		Hypersolvus granite N		Transsolvus granite		Enclave Group 1		Dark porphyritic granite	
Analyses	*n=14*		*n=15*		*n=29*		*n=7*		*n=4*	
		±		±		±		±		±
Sc *(ppm)*	22.5	1.3	22.7	0.8	20.0	2.5	24.4	0.4	27.2	0.5
Ti	33.9	15.5	10.4	4.8	16.1	4.0	37.7	13.3	6.3	0.7
Zn	14.8	3.7	35.8	8.6	65.7	32.2	63.4	6.7	44.4	12.8
Rb	523	82	848	97	1773	381	1280	417	686	16
Sr	2.21	1.51	0.56	0.30	0.87	0.33	4.27	1.43	1.70	0.60
Y	5.63	2.16	10.4	2.6	38.6	11.6	19.7	3.4	11.0	1.3
Zr	16.0	8.2	32.3	23.3	67.0	32.0	118	31	6.1	4.4
Nb	4.79	2.60	6.80	3.50	19.8	10.3	18.7	1.9	1.46	0.77
Ba	13.7	3.8	43.4	4.9	20.2	5.7	11.0	4.4	31.0	1.9
La	0.71	0.38	5.97	1.63	23.2	5.25	34.9	12.1	1.63	0.15
Ce	3.16	2.01	17.6	5.2	34.0	14.3	55.1	10.8	5.5	0.4
Pr	0.35	0.18	1.96	0.62	4.60	1.36	7.00	1.50	0.99	0.12
Nd	1.86	1.08	9.07	2.20	20.9	8.5	29.1	5.5	5.1	0.6
Sm	0.54	0.24	1.48	0.41	3.85	1.23	4.70	0.86	1.49	0.20
Eu	0.10	0.05	0.10	0.03	0.25	0.02	0.28	0.09	0.11	0.02
Gd	0.66	0.30	1.36	0.40	4.73	0.98	4.36	0.85	1.64	0.19
Tb	0.18	0.07	0.36	0.07	0.87	0.18	0.66	0.16	0.36	0.05
Dy	1.04	0.42	2.66	0.74	6.00	1.00	3.69	1.15	2.29	0.45
Ho	0.25	0.10	0.80	0.22	1.61	0.40	0.88	0.28	0.60	0.13
Er	0.70	0.24	2.65	0.94	5.35	1.55	2.51	0.51	1.79	0.35
Tm	0.11	0.03	0.52	0.29	0.85	0.24	0.39	0.16	0.38	0.06
Yb	0.48	0.11	2.55	2.01	5.99	1.69	1.93	0.77	2.28	0.18
Lu	0.06	0.01	0.30	0.23	0.68	0.20	0.25	0.11	0.32	0.01
Pb	20.1	10.2	33.8	23.5	36.0	15.7	24.4	8.3	72.1	7.6
Th	2.20	0.69	8.23	6.51	3.74	2.06	7.10	1.60	1.62	0.63
U	0.26	0.06	0.57	0.29	1.26	0.48	0.54	0.08	0.54	0.05
TREE	11.1	4.6	51.0	10.4	120	27	146	28	24.0	3.8
LREE	6.7	3.9	36.2	10.1	86.8	30.7	131	30.8	14.8	1.5
HREE+Y	9.1	3.4	21.6	7.4	64.7	17.8	34.4	7.4	20.6	2.7

2.4.3.2 Zirconosilicate minerals

Vlasovite is the most abundant alkali zirconosilicate mineral in all the granite units with the ZrO_2 content averaging 28.6 wt. % and the Na_2O content averaging 7.9 wt. %; concentrations of K_2O, CaO, TiO_2, FeO and SnO_2 are low (< 0.15 wt. %) (Table 2-6). Elpidite occurs almost exclusively along the rims of vlasovite crystals and contains a lower ZrO_2 concentration (avg. 19.7 wt. %), and significant proportions of SnO_2 (0.53 wt. %). The totals (avg. 89.6 wt. %) are low, consistent with the presence of H_2O in the crystal structure. Catapleiite was identified in a sample of southern hypersolvus granite and a sample of transsolvus granite. In both cases, the mineral has high concentrations of ZrO_2 (avg. 31.3 wt. %), contains significant proportions of HfO_2 (1.0 wt. %), CaO (2.2 wt. %) and TiO_2 (avg. 0.2 wt. %), and yields low analytical totals (avg. 89.0 wt. %) due to the presence of structural H_2O. Differences in composition among alkali zirconosilicates in the hypersolvus granite and those in the transsolvus granite are insignificant. Both elpidite and catapleiite have anomalously low concentrations of Na_2O, which resulted in less than half the ideal site occupation (see Table 2-6). Low Na concentrations (and high vacancies) were caused either by Na-loss during the analyses (minor effect) or hydrothermal alteration. The alkali zirconosilicate minerals all have REE concentrations below the detection limit (EMP). Primary zircon from the northern hypersolvus granite has an average ZrO_2 concentration of 64.3 wt. % and significant HREE concentrations (avg. 0.1 wt. % Dy_2O_3, 0.2 wt. % Er_2O_3, 0.2 wt. % Yb_2O_3 and 1.2 wt. % Y_2O_3) (Table 2-6).

Table 2-6: Compositions and formulae of the alkali zirconosilicate minerals and zircon

Average (median) compositions with median absolute deviation (±) of the alkali zirconosilicate minerals and zircon with formulae (ideal site occupation in brackets). Catapleiite, elpidite and vlasovite analyses are from both hypersolvus and transsolvus granite, whereas zircon analyses are from the hypersolvus granite exclusively.

Mineral	Catapleiite		Elpidite		Vlasovite		Zircon		
Analyses	*n=4*		*n=23*		*n=89*			*n=20*	
(*wt. %)*		±		±		±			±
SiO_2	50.16	0.83	64.33	0.87	61.41	0.83	SiO_2	32.55	0.11
ZrO_2	31.25	0.42	19.71	0.40	28.63	0.44	ZrO_2	64.28	0.47
HfO_2	1.01	0.21	0.34	0.09	0.79	0.09	HfO_2	1.14	0.04
Al_2O_3	0.01	0.01	0.05	0.04	-	-	P_2O_5	0.17	0.03
TiO_2	0.21	0.09	0.10	0.07	0.07	0.03	Dy_2O_3	0.10	0.02
FeO	0.29	0.06	0.12	0.09	0.01	0.01	Er_2O_3	0.16	0.02
SnO_2	0.39	0.06	0.53	0.49	0.14	0.05	Y_2O_3	1.15	0.12
Na_2O	2.27	0.34	3.07	0.70	7.86	1.69	Yb_2O_3	0.20	0.04
K_2O	0.05	0.01	0.10	0.07	0.13	0.03	CaO	0.02	0.01
CaO	2.22	0.28	0.06	0.05	0.01	0.01			
F	-	-	-	-	0.03	0.03	REE+Y	1.61	0.21
Total	88.99		89.61		99.28		Total	99.74	
Structural formulae									
Si *(apfu)*	3.00		6.00		4.00		Si	1.00	
Al	-		0.01		-		*Sum T*	*1.00*	*(1)*
Sum T	*3.00*	*(3)*	*6.01*	*(6)*	*4.00*	*(4)*	Zr	0.96	
Zr	0.90		0.90		0.91		Hf	0.01	
Hf	0.02		0.01		0.01		P	-	
Ti	0.01		0.01		-		Dy	-	
Fe	0.01		0.01		-		Er	-	
Sn	0.01		0.02		-		Y	0.02	
Sum Zr	*0.95*	*(1)*	*0.97*	*(1)*	*0.94*	*(1)*	Yb	-	
Na	0.26		0.54		0.98		Ca	-	
K	-		0.01		0.01		*Sum Zr*	*0.99*	*(1)*
Ca	0.14		0.01		-				
Sum Na,Ca	*0.40*	*(2)*	*0.58*	*(2)*	*0.99*	*(2)*			
F	-		-		0.01				
H_2O	2.00		3.00		-				
Sum anions	*2.02*	*(2)*	*3.00*	*(3)*	*0.01*	*(0)*			

2.4.3.3 REE-minerals and fluorite

The unaltered Strange Lake granites contain a variety of primary REE-minerals, compositions of which are specified below. The compositions of the REE-minerals do not differ significantly among the granite units. Monazite-(Ce) occurs in all the granite units, is strongly enriched in the LREE, more depleted in the HREE than the other primary REE minerals (Ce/Y of 506) and contains minor proportions of Si, Sm, Gd, Y, Th and F (Table 2-7; Fig. 2-12). The pyrochlore group minerals, with the general formula $A_2B_2O_6Y$, have high concentrations of La, Ce and Nd (avg. TREO 17.3 wt. %), whereas their HREE concentrations lie below the detection limit (Table 2-7). The Y-site is dominated by F (> 0.5 apfu), which assigns the majority of the analyses (70 %) a “fluor-“prefix (Atencio et al., 2010). The rest of the Y-site is occupied by OH, O or □. The A-site hosts the elements Na, Ca, Sr, Ba, U, Th, the LREE and □. The mineral group is moderately depleted in the HREE (Ce/Y of 62). There is a large variation in the Na concentration (0.01 to 1.14 apfu), which results in a high vacancy in the A-site in most cases. A positive correlation between Na and F (R^2 ~0.6) was observed. According to Yaroshevskii and Bagdasarov (2008), such a correlation may imply modification of the Y-site with OH^- replacing F^- as a result of hydrothermal alteration. The crystals with Na dominance at the A site classify as “fluornatropyrochlore”. This applies to the majority of cases. In three samples, two from the northern hypersolvus granite and the other from transsolvus granite, Ca is dominant in the A-site and hence the mineral is classified as “fluorcalciopyrochlore” (Atencio et al., 2010). In a number of samples, representing all granite facies, the fluornatropyrochlore was overgrown by a variety rich in Ba, Pb and Si and poor in Na, Nb and F. This variety has a lower total (avg. 92.4 vs. 94.6 wt. %), which is likely due to a higher proportion of H_2O in the structure (see Table 2-6). According to the latest classification scheme, the Ba- and Pb-rich pyrochlore is referred to as “zero-valent-dominant pyrochlore” (Atencio et al., 2010).

Fluorbritholite-(Ce) is enriched in the LREE and has relatively high concentrations of the middle to heavy REE and Y compared to the other primary REE minerals (Ce/Y of 15). The remaining REE-bearing minerals, fluorite, Y-rich fluorite and gagarinite-(Ce), all contain essential Ca, F and significant Na (Table 2-7). Fluorite contains minor concentrations of the LREE (avg. 0.55

wt. % LREO) and Y (avg. 0.27 wt. % Y_2O_3), and is relatively enriched in Pr and Sm compared to chondrite values (Fig. 2-12). In most samples, the fluorite is rimmed by a Y-rich variety (brighter in BSE images) that has significantly lower Ca and F, and higher Na, REE and Y concentrations than the ordinary fluorite (Table 2-7). This Y-rich fluorite is a member of the fluorite-fluocerite-(Ce) solid solution, also observed by Gysi and Williams-Jones (2013) in the cores of pegmatites from the altered part of the Strange Lake pluton. The chondrite-normalized REE profile of the fluorite-fluocerite-(Ce) solid solution is flat (Ce/Y of 0.4) with a small Eu anomaly (Fig. 2-12). Primary gagarinite-(Ce), which was identified exclusively in the transsolvus granite, is enriched in the LREE and has high proportions of Sm, Gd, Dy and Y (Ce/Y of 7) and a total REE oxide concentration, averaging 46 wt. %. The chondrite-normalized REE profile of gagarinite-(Ce) displays a relatively high LREE and MREE enrichment (Fig. 2-12).

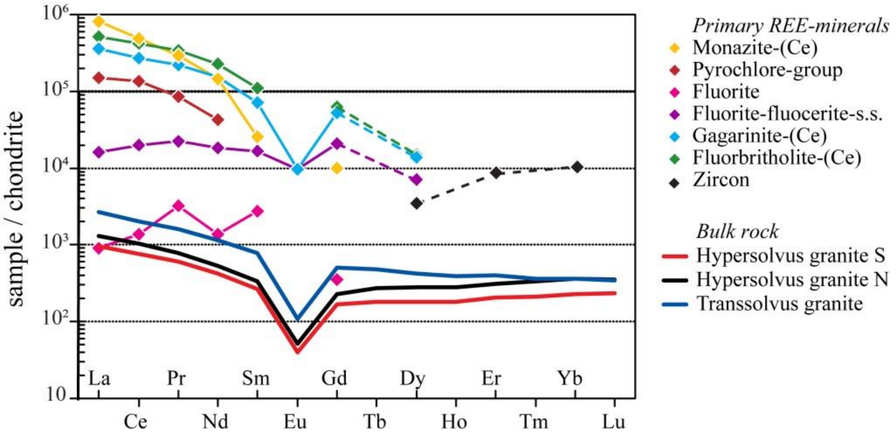

Fig. 2-12: REE profiles of the primary REE- minerals

Average REE profiles (chondrite-normalized, Sun and McDonough, 1989) of primary REE-bearing minerals identified in the unaltered Strange Lake granites. Elements not displayed lie below the (EMP) detection limit. Average bulk rock REE profiles for each granite unit are displayed for reference.

Table 2-7: Compositions and formulae of the primary REE-minerals

Elemental compositions (median) with median absolute deviation (±) and calculated formulae of the primary REE-minerals from the unaltered granites of the Strange Lake pluton. The low total of the pyrochlore mineral group and fluorbritholite-(Ce) can be accounted to the OH-component, which was not determined.

Mineral	Fluornatro-/calcio-pyrochlore		Zero-valent-dominant pyrochlore		Monazite-(Ce)		Fluorbritholite-(Ce)	
Analyses	*n = 64*		*n = 17*		*n = 39*		*n=5*	
(wt. %)		±		±		±		±
SiO_2	1.08	0.63	4.24	1.32	0.52	0.13	20.66	0.17
TiO_2	5.27	0.71	6.94	1.43	-	-	-	-
FeO	0.17	0.12	0.72	0.34	-	-	-	-
CaO	3.16	0.45	2.42	0.17	0.02	0.01	3.05	0.12
Na_2O	4.57	1.62	0.71	0.53	-	-	1.66	0.07
P_2O_5	-	-	-	-	30.28	0.29	1.10	0.56
Nb_2O_5	55.92	1.73	51.29	2.02	-	-	-	-
Ta_2O_5	2.53	0.37	1.72	0.41	-	-	-	-
PbO	0.18	0.07	3.52	1.47	0.03	0.01	0.91	0.09
SrO	0.03	0.02	0.22	0.10	-	-	0.08	0.01
BaO	0.09	0.06	2.50	0.81	-	-	-	-
ZrO_2	0.31	0.09	0.22	0.08	-	-	-	-
La_2O_3	4.20	0.21	3.84	0.21	22.54	2.53	14.32	0.29
Ce_2O_3	9.72	0.21	9.45	0.39	35.33	1.04	30.53	0.39
Pr_2O_3	0.93	0.05	0.86	0.09	3.19	0.27	3.70	0.04
Nd_2O_3	2.29	0.11	2.04	0.21	7.74	1.45	12.24	0.09
Sm_2O_3	-	-	-	-	0.44	0.25	1.89	0.09
Eu_2O_3	-	-	-	-	-	-	-	-
Gd_2O_3	-	-	-	-	0.23	0.09	1.44	0.10
Dy_2O_3	-	-	-	-	-	-	0.42	0.16
Y_2O_3	0.17	0.05	0.24	0.04	0.07	0.05	2.19	0.36
ThO_2	0.03	0.03	0.18	0.08	0.73	0.27	0.28	0.03
UO_2	0.46	0.13	0.77	0.14	-	-	-	-
F	3.71	0.39	1.29	0.51	0.55	0.04	2.09	0.12
Cl	-	-	-	-	0.01	<0.01	0.03	0.01
Total	94.55		92.44		101.662		96.59	
TREO	17.30		16.42		69.53		66.73	

Table 2-7: Compositions and formulae of the primary REE-minerals (continued)

Structural formulae (apfu)					
Si	0.07	0.30	0.02		3.03
Ti	0.28	0.37	-		-
Fe	0.01	0.05	-		-
Ca	0.23	0.19	-		0.46
Na	0.62	0.10	-		0.45
P	-	-	0.99		0.11
Nb	1.76	1.69	-		-
Ta	0.05	0.04	-		-
Pb	-	0.07	-		0.03
Sr	-	0.01	-		0.01
Ba	-	0.07	-		-
Zr	0.01	0.01	-		-
La	0.11	0.10	0.32		0.83
Ce	0.25	0.25	0.50		1.61
Pr	0.02	0.02	0.05		0.19
Nd	0.06	0.05	0.11		0.65
Sm	-	-	0.01		0.09
Gd	-	-	-		0.07
Dy	-	-	-		0.02
Y	0.01	0.01	-		0.18
Th	-	-	0.01		0.01
U	0.01	0.01	-		-
F	0.81	0.29	0.07		0.94
O	6.00	6.00	0.93	(=1-F)	4.00
OH (1-F)	0.19	0.71	-		-
∑REE	0.44	0.44	0.98		3.64

Table 2-8: Compositions and formulae of the F-REE-minerals

Average (median) compositions of fluorite and the F-REE-minerals from the unaltered granites of the Strange Lake pluton with median absolute deviation (±) and their structural formulae. The distinction between fluorite and the fluorite-fluocerite solid solution was made based on the Y-concentrations. Fluorite has < 0.4 wt. % Y and the fluorite-fluocerite solid solution has > 1.0 wt. % Y_2O_3.

Mineral	Fluorite		Fl-fluocerite-s.s.		Gagarinite-(Ce)	
Analyses	*n=21*		*n=32*		*n= 6*	
(wt. %)		±		±		±
CaO	50.28	0.22	42.46	1.26	10.43	0.14
Na_2O	0.11	0.03	1.79	0.19	6.46	0.44
SrO	-	-	-	-	0.08	0.02
La_2O_3	0.03	0.02	0.45	0.09	10.01	0.25
Ce_2O_3	0.10	0.04	1.43	0.31	19.45	0.15
Pr_2O_3	0.04	0.03	0.24	0.06	2.41	0.05
Nd_2O_3	0.07	0.05	0.98	0.19	8.26	0.12
Sm_2O_3	0.05	0.03	0.29	0.06	1.23	0.04
Eu_2O_3	-	-	0.06	0.05	0.06	0.05
Gd_2O_3	0.01	0.01	0.48	0.05	1.20	0.06
Dy_2O_3	-	-	0.20	0.05	0.39	0.06
Y_2O_3	0.27	0.06	3.78	0.46	3.26	0.29
F	48.98	0.21	47.47	0.36	35.46	0.36
Total	99.92		99.62		98.71	
TREO+Y	0.55		7.91		46.27	
Structural formulae (apfu)						
Ca	0.70		0.61		0.60	
Na	-		0.05		0.33	
F	2.00		2.00		6.00	
Y	0.002		0.03		0.05	
La	-		-		0.10	
Ce	-		0.01		0.19	
Pr	-		-		0.02	
Nd	-		-		0.08	
Sm	-		-		0.01	
Gd	-		-		0.01	
Dy	-		-		-	
∑REE+Y	0.003		0.04		0.48	

2.5 DISCUSSION

2.5.1 Emplacement of the Strange Lake pluton

2.5.1.1 Magma transport and emplacement

The circular surface shape of the pluton, which is defined by a ring fault delineated by a fluorite-hematite breccia that surrounds the pluton, and the occurrence of a ring-like magnetic feature (2012, Quest Rare Minerals Ltd.), suggests that the intrusion was emplaced as a ring dike. The emplacement of magma in the shape of ring dikes is typical of epizonal anorogenic intrusions in extensional tectonic settings (Bonin, 1986; 2007). Further evidence for this is provided by large remnants of host rock (roof pendants and walls) such as those observed in the central and eastern parts of the pluton (see map, Fig. 2-1). We infer that blocks of country rocks were engulfed by the ascending magma (stoping is a common feature of anorogenic intrusions; Bonin, 2007). A nearby analogue is provided by the 1.27 Ga peralkaline Flowers River peralkaline volcanic to plutonic suite, a member of the Nain Plutonic Suite (Hill, 1991).

2.5.1.2 P-T conditions of magma emplacement

The fine-grained to porphyritic nature of the granites as well as the brittle deformation of the host rocks evident from crosscutting Strange Lake dikes speak to a high level of intrusion. The pluton was emplaced in a zone of crustal weakness between the Napeu Kainiut quartz-monzonite and the Core Zone gneiss complex. Boily and Williams-Jones (1994) proposed that the least evolved hypersolvus granite formed by differentiation of a syenitic (trachytic) parental magma injected at shallow crustal levels (1-3 km). This is consistent with results of a recent fluid inclusion study showing that the pluton was emplaced at a pressure of 1.1 kbar, corresponding to a depth of ~3 km (Vasyukova et al., 2016).

In the hypersolvus granite, quartz and arfvedsonite are both late phases and thus oxygen isotope data for these minerals can provide estimates of the crystallization temperature. These data were obtained by Boily and Williams-Jones (1994) for a hypersolvus granite sample (28-A-1), and predict a crystallization temperature of 660°C (assuming equilibrium) using the quartz-hornblende thermometer of Bottinga and Javoy (1975). As the two minerals formed after emplacement, the temperature of the magma in the magma chamber was presumably higher (≥700 °C). A crystallization temperature could not be predicted for the transsolvus granite because arfvedsonite and quartz were not in equilibrium in this intrusion (the arfvedsonite occurs as phenocrysts).

2.5.1.3 Melt viscosity

Evidence of flow differentiation and high concentrations of fluxing and network modifying constituents (F, Cl, H_2O, excess alkalis and Fe), imply that the transsolvus granite magma had a relatively low viscosity. The above melt components served to lower the solidus temperature, melt density and viscosity (Bailey, 1977; Baker and Vaillancourt, 1995; Simmons and Webber, 2008). The melt viscosity of transsolvus granite sample #10024 was calculated using the equation for peralkaline melts derived from experiments of Baker and Vaillancourt (1995) and Giordano et al. (2008). Assuming the presence of 6-10 wt. % H_2O (Vasyukova and Williams-Jones, 2017) and 1-2 wt. % F in the melt (the F values correspond to those for melt inclusions in the transsolvus granite; Vasyukova and Williams-Jones, 2014), the calculated viscosity ranges between 10^4 – 10^5 Pa·s for temperatures between 600°-700°C. According to Baker and Vaillancourt (1995), pressure has a negligible effect on viscosity and was thus not considered. The calculated viscosity is typical for peralkaline granites, and significantly lower than that of peraluminous to metaluminous granite, even for the same F and H_2O concentrations (Baker and

Vaillancourt, 1995; Clemens et al., 1986; Dingwell et al., 1998). The hypersolvus granitic melt likely had lower concentrations of fluxing components, and thus presumably had a higher viscosity than the transsolvus granite.

The low viscosity promoted a rapid separation of the magma from its source region. For peralkaline melts, separation at 800°C takes place at a rate of ~1 mm/y, whereas for granites of metaluminous to peraluminous composition, the separation rate is much lower (0.03 to 0.1 mm/y) (Baker and Vaillancourt, 1995; McKenzie, 1985). The rapid separation of magma promotes the discharge of a relatively large melt volume (Baker and Vaillancourt, 1995), a process which may explain the apparently much greater proportion of transsolvus granite compared to hypersolvus granite (see map Fig. 2-1).

2.5.2 Early magma evolution

2.5.2.1 Granite evolution

The early peralkaline granitic melt produced a fine-grained hypersolvus granite with perthitic alkali feldspar as the sole alkali feldspar. Field observations and bulk rock chemistry provide evidence for two separate units of fine-grained hypersolvus granite (south and north); there is also a coarse oikocrystic to pegmatitic variety of southern hypersolvus granite. Higher bulk rock concentrations of Si, REE, Zr and Nb, a higher alkalinity index and the lower K/Rb ratio of the northern relative to the southern fine-grained hypersolvus granite (see Fig. 2-8) imply a more evolved composition for the former. Based on the similar compositions of the two granite units, and the almost identical mineralogy, we propose that the hypersolvus granitic magma evolved from a common source, i.e., the same magma chamber, and was emplaced in the upper crust as two separate batches.

A significant change in magma composition from the hypersolvus granite to the transsolvus granite is evident in the higher bulk concentrations of incompatible elements (REE, Zr and Nb), higher Si, Fe, F, and Rb concentrations and lower Al concentrations of the latter (see Figs. 2-8, 2-9). The increase in alkali content resulted in a higher agpaitic index for the transsolvus granite (avg. 1.27) than for the hypersolvus granite (avg. 1.13 and 1.15). Based on its significantly more evolved composition and distinctly different primary mineralogy, we propose that the transsolvus granite represents a separate later phase of intrusion. Owing to the overall similarity in bulk composition (peralkaline granitic) and mineralogy (alkali feldspars, arfvedsonite, quartz), we further propose that the transsolvus granite evolved in the same magma chamber as the hypersolvus granite.

Significantly, the transsolvus granite is compositionally similar to the coarse oikocrystic and pegmatitic textured hypersolvus granite in terms of bulk Al, Fe, Ca concentrations and agpaitic index (see Fig. 2-8, Table 2-2). This implies that the transsolvus granite evolved from the hypersolvus granitic melt. However, the two units differ significantly in alkali feldspar mineralogy, arfvedsonite morphology and the concentrations of some trace elements (Zr, F and REE). We therefore conclude that although the transsolvus granite unit evolved from the hypersolvus granitic magma, much of this evolution took place in the magma chamber.

2.5.2.2 Alkali feldspar chemistry – implications for melt evolution

Textural relationships among the minerals, i.e., the occurrence of perthitic alkali feldspar as phenocrysts, and zircon, monazite-(Ce) and the pyrochlore group minerals as inclusions in perthitic alkali feldspar, show that these were the earliest minerals to crystallize in the hypersolvus granite. They show also that these minerals crystallized prior to emplacement of the magma, i.e., in the magma chamber. It therefore follows that the composition of these minerals, and particularly that of the alkali feldspar, can provide important information on the early evolution of the magma.

Alkali feldspar from the (fine-grained) southern hypersolvus granite differs greatly in composition from that of the northern hypersolvus granite (see Figs. 2-10, 2-11). The observed evolution of a weakly potassic (avg. X_{Or} 0.57) to a more potassic alkali feldspar (avg. X_{Or} 0.64) (southern to northern hypersolvus granite) can be explained by a temperature decrease and/or an increase of ρH_2O in the magma (Parsons, 1978). The significantly lower alumina concentration in the perthitic alkali feldspar of the northern hypersolvus granite compared to that of the perthitic alkali feldspar in the southern intrusion (see Fig. 2-10) coincides with higher average silica and iron contents of the former, all of which indicate that it crystallized from a more evolved northern hypersolvus granite melt. The higher content of iron in the perthitic alkali feldspar of the northern hypersolvus granite compared to the southern hypersolvus granite may indicate that the corresponding magma was more oxidized. This is because only the oxidized form of iron, Fe^{3+}, is accepted by the alkali feldspar, in which it substitutes for Al^{3+} (Hofmeister and Rossman, 1984). It has been suggested that higher fO_2 can result from the separation of a fluid phase followed by the dissociation of H_2O and loss of H^+ by diffusion (Czamanske and Wones, 1973), however, there is no evidence that a fluid exsolved this early in the evolution of the system. Alternatively, simple cooling of the magma under non-buffered conditions (at this stage only feldspar crystals were present) could induce oxidation. The northern hypersolvus granite has two populations of alkali feldspar, namely large perthitic alkali feldspar crystals that in many cases are zoned (Afs 1 and 2 in Fig. 2-2c) and smaller perthitic crystals. This indicates two stages of crystal growth. The two populations have distinctly different iron concentrations, i.e., ~0.010 apfu Fe^{3+} and ~0.015 apfu Fe^{3+}, respectively (see Fig. 2-10d), suggesting that conditions changed during crystallization. We conclude that the first (low Fe^{3+}) generation formed in the magma chamber, whereas the second generation crystallized during or after emplacement in an environment of higher oxidation.

In the transsolvus granite, only a small proportion of the alkali feldspar is perthitic alkali feldspar. However, its composition differs from that of the hypersolvus granite, for example, it has a lower Al concentration (see Fig. 2-10) as well as a relatively high Rb concentration (avg. 1773 ppm), indicating a higher degree of evolution. The greater evolution of the transsolvus granite is also consistent with elevated Fe^{3+}, REE, Zn, Zr and Nb and contents in the perthitic alkali feldspar (see Figs. 2-10, 2-11; Table 2-5). High Fe^{3+} concentrations in the perthitic alkali feldspar were due to elevated OH^- and F^- concentrations in the melt, which allowed more Fe^{3+} to be present at a given fO_2 (Birkett et al., 1996; Giehl et al., 2013), or simple cooling of the magma under non-buffered conditions. As in the northern hypersolvus granite, the perthitic alkali feldspar of this unit has two populations of Fe^{3+} concentrations (~0.010 vs. 0.015 apfu), although the high Fe^{3+} population is significantly more important (see Fig. 2-10d). We propose that in the transsolvus granite, both of the Fe^{3+} populations originated in the magma chamber, meaning that no perthitic alkali feldspar crystallized after emplacement. Moreover, we suggest, that in contrast to the perthitic alkali feldspar of the hypersolvus granite (the high Fe^{3+} population is late), the dominant high Fe^{3+} population reflects the early stage of perthitic alkali feldspar growth in the transsolvus granite magma. The low Fe^{3+} population reflects a change in the magma due to the onset of amphibole crystallization, which consumed a significant proportion of Fe^{3+}.

2.5.2.3 Transition from hypersolvus to subsolvus conditions

The observation that microcline and albite occur as rims around primary perthitic alkali feldspar crystals (see Fig. 2-4c), as well as inclusions in arfvedsonite (see Fig. 2-4d), indicates that the transition from perthitic alkali feldspar to two separate feldspars occurred in the magma chamber before or contemporaneously with arfvedsonite crystallization. The crystallization of arfvedsonite phenocrysts in the transsolvus granite was triggered due to the OH^- enrichment in the melt, which had been caused by massive alkali feldspar crystallization. The importance of high OH^- concentration for the early saturation of arfvedsonite in peralkaline magmas has been demonstrated experimentally by Scaillet and MacDonald (2001). The arfvedsonite crystallization, in turn, contributed significantly to the increase in F^- concentration in the melt. This assumes that fluorine in silicate melts is mostly dissolved as NaF° (Mysen and Virgo, 1985a, b), and therefore the crystallization of arfvedsonite would destroy this species through the consumption of Na and release of F^- to the melt. Such an increase in F^- concentration in the melt could have triggered the transition from hypersolvus to subsolvus conditions. We propose that the hypersolvus to subsolvus transition occurred due to an increase in the partial pressure of H_2O (pH_2O) and/or F content in the melt (Tuttle and Bowen, 1958), which lowered the feldspar liquidus to its intersection with the two-feldspar field. Furthermore, we propose that the overgrowth of microcline on perthitic alkali feldspar crystals observed in the transsolvus granite (see Fig. 2-4c) as well as in some of the enclaves (see Fig. 2-6a) was mainly caused by the change in conditions in the magma chamber described above.

2.5.2.4 Early HFSE minerals

The early crystallized HFSE-bearing minerals of the hypersolvus granite (zircon, monazite-(Ce) and pyrochlore group minerals) provide information on the bulk HFSE concentrations hosted by these minerals. The average modal proportion of monazite-(Ce) in each granite unit was calculated assuming that all the bulk rock P_2O_5 is hosted by monazite-(Ce). Based on this calculation, the southern hypersolvus granite contains ~0.1 wt. % monazite-(Ce), and the northern equivalent ~0.07 wt. %. Similarly, assuming that nearly all of the bulk Nb_2O_5 is hosted by pyrochlore, there is ~0.05 wt. % of this mineral group in the southern and ~0.11 wt. % of it in the northern hypersolvus granite. From these proportions and the REE oxide concentrations in the minerals (see Tables 2-7, 2-8), we conclude that more than 40 % of the bulk REE oxides in the southern hypersolvus granite are hosted by monazite-(Ce), and only ~5% by the pyrochlore group. In the northern unit, about 20 % of the bulk REE is hosted by monazite-(Ce) and about 8 % by the pyrochlore group. The remaining LREE were either dissolved in the melt or had already partitioned into a separate REE-rich fluoride melt, as proposed by Vasyukova and Williams-Jones (2014). Indeed, the large fluorite crystals associated with bastnäsite-(Ce) in primary perthitic alkali feldspar (Afs 1) of a hypersolvus granite sample (see Fig. 2-3d) appear to represent globules of this immiscible fluoride melt. Their occurrence in the earliest phase (perthitic alkali feldspar) is consistent with the conclusion of Vasyukova and Williams-Jones (2014) that this fluoride melt exsolved early in the evolutionary history of Strange Lake. The bulk HREE were accommodated by zircon (~ 1 wt. % HREE) (see Table 2-6).

The transsolvus granite contains small proportions of monazite-(Ce) (~0.03 wt. %) and pyrochlore group minerals (~0.09 wt. %), which each host only ~5 %, and ~3 %, respectively, of the bulk REE. A large proportion of the remaining bulk REE in this unit is hosted by late magmatic gagarinite-(Ce), fluorbritholite-(Ce) and secondary bastnäsite-(Ce). This indicates that the REE were dissolved in the melt until a late stage (after emplacement), and/or accumulated as fluoride-melt globules, which crystallized later as REE minerals. These processes are discussed in detail below.

2.5.3 Mechanisms of magmatic HFSE enrichment

2.5.3.1 Crystal fractionation of alkali feldspar

As shown by Boily and Williams-Jones (1994), the fractional crystallization of ~20 wt. % alkali feldspar played an important role in concentrating the incompatible elements in the early Strange Lake magmas. In order to quantitatively evaluate to what extent the early magmatic evolution and unusual HFSE enrichment was controlled by perthitic alkali feldspar crystallization, we modeled the fractionation of this phase using (average) measured concentrations from this study. The intention of the modeling was to determine if the more evolved rock units are derivatives of the least evolved unit. In the model, the average alkali feldspar composition was removed in 1% increments from the bulk composition of the least evolved southern hypersolvus granite sample, until the Al_2O_3 content reached that of the more evolved northern hypersolvus granite. After each step, the masses of each element corresponding to the amount crystallized were subtracted from the masses of the hypothetical residual liquid.

The model satisfactorily reproduces the observed bulk rock trends for Al, Na, K and Ti concentrations between the southern and northern hypersolvus granite if ~ 8 wt. % perthitic alkali feldspar were crystallized and removed (Fig. 2-13a, b). However, the model does not reproduce the trends in bulk rock Si, Fe, Ca, F, REE, Zr and Nb concentrations. The Si concentration increases in the bulk rock, but not in the model, whereas Fe, Ca and F concentrations increase in the model but remain nearly constant in the bulk rock (Fig. 2-13c). This indicates that the excess modelled Fe, Ca and F were removed from the bulk rock, which could have occurred if a Fe- and a Ca-F-bearing mineral had crystallized, or if Fe, Ca and F had been leached by a fluid. There is much evidence for ferric- as well as Ca-F metasomatism at Strange Lake (Gysi et al., 2016; Salvi and Williams-Jones, 1996). This includes a fluorite-hematite breccia at the rim of the pluton, which indicates that Ca, F and Fe^{3+} partitioned into a hydrothermal fluid and migrated from the pluton center outwards, depleting the (unaltered) rock in these elements. Such fluid migration also helps explain the strong enrichment in Ca within the most altered parts of the transsolvus granite and the pegmatites (Salvi and Williams Jones 1990, 1996, Gysi et al, 2016). Previously, this enrichment was attributed to an external Ca-rich fluid (Salvi and Williams-Jones, 1996), however it is also possible that the fluid was of local origin. The progressive removal of Ca and F left an increasingly Si-rich melt behind, which is reflected in the disproportional bulk rock increase in Si, but not in the model.

In contrast, the bulk rock concentrations of the REE, Zr, and Nb in the northern hypersolvus are higher than predicted by the fractionation of perthitic alkali feldspar (Fig. 2-13d), indicating that an additional process contributed to the distribution of these components. We propose that early crystallized zircon, monazite-(Ce) and the pyrochlore group minerals were distributed unevenly between the southern and northern hypersolvus magma batches, due to gravity settling. Since monazite-(Ce) and the pyrochlore group minerals only contribute about 20, and 8 %, respectively, of the bulk REE, we suggest that the REE-rich fluoride melt (discussed in Vasyukova and Williams-Jones (2014)) also had separated by this stage. Indeed, it was shown by Vasyukova and Williams-Jones (2016), that the fluoride melt globules could have served as nucleation surfaces for minerals, such as zircon and chevkinite-(Ce). Monazite-(Ce) and pyrochlore group minerals also probably crystallized early along the boundaries between the fluoride and silicate melts. Thus, the separation of the REE-rich fluoride melt together with the phenomenon of heterogeneous nucleation and gravity settling could both have contributed to the concentration of the HFSE. This would explain why the extreme increase in bulk REE, Zr and Nb towards the northern hypersolvus granite could not be modelled with perthitic alkali feldspar fractionation.

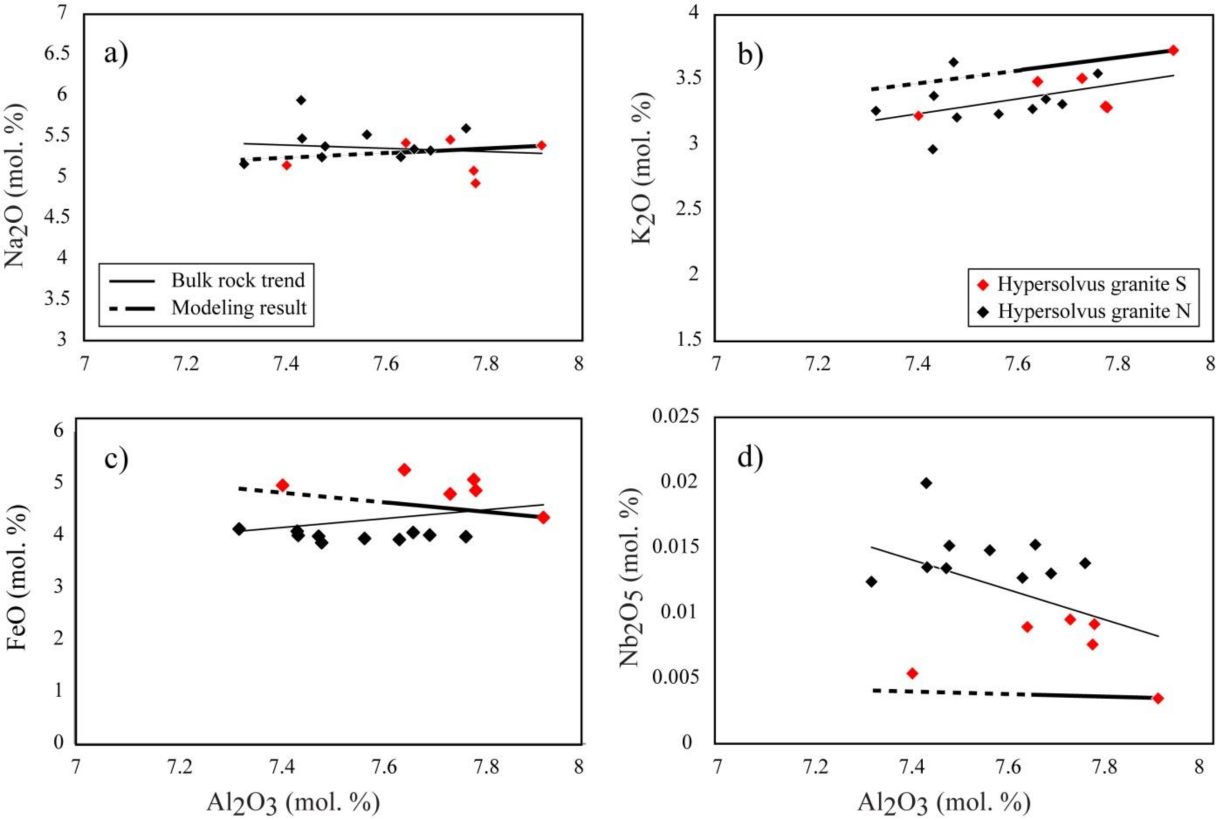

Fig. 2-13: Hypersolvus granite evolution by perthitic alkali feldspar fractionation

Binary oxide diagrams (in mol. %) showing the predicted trends of hypersolvus granite evolution (as a function of alumina concentration) by perthitic alkali feldspar fractionation (dashed line) compared to bulk rock composition (solid line, linear regression) for selected elements. a) sodium, b) potassium, c) iron and d) niobium.

The evolution of the transsolvus granite from the hypersolvus granite cannot be reconstructed using the same model because an unknown amount of the residual melt (and fluid) was removed from the transsolvus granite to form pegmatites. Owing to the imbalance in major mineral proportions due to gravity settling (high alkali feldspar and low arfvedsonite proportions in the enclaves vs. high arfvedsonite and low alkali feldspar proportions in the transsolvus granite) (see

Table 2-3), we conclude that the bulk composition of the transsolvus granite samples does not represent the true composition of this last and most evolved melt batch. For these reasons, the modeling of the transsolvus granite evolution by perthitic alkali feldspar fractionation would lead to an unreliable result.

2.5.3.2 Early melt HFSE concentrations

As the perthitic alkali feldspar was the earliest major mineral to crystallize in all granite units, its composition makes it possible to estimate the early magma composition. Approximate melt REE and trace element compositions were constrained using the measured perthitic alkali feldspar compositions and calculated mineral-melt partition coefficients (*D*) following White (2003). On the basis of a multivariate linear regression (MLR) analysis applied to bulk rock, feldspar and trace element partitioning data compiled by them, White et al. (2003) concluded that the partition coefficients between alkali feldspar and peralkaline melts for most cations (1+, 3+, 4+, 5+) are a function of the bulk rock alkalinity index as well as Si and Ca concentrations (White, 2003). The calculated coefficients (*D*) for the partitioning of elements between alkali feldspar and melt average 0.34 (±0.03) for Rb^+, 0.051 (±0.008) for Zr^{4+}, 0.047 (±0.009) for Nb^{5+} and between 0.034 and 0.052 (±0.009) for the REE^{3+}, except for Eu. The value for Eu is highly dependent on the bulk rock Na_2O/K_2O ratio and is significantly higher (avg. 0.644 ± 0.464) than those for the other REE due to its compatibility as the 2+ ion with the alkali feldspar structure. Melt compositions (in ppm) for each element were calculated from the relationship $C_l = C_{afs}/D$, where C_l is the concentration in the liquid (ppm) and C_{afs} is the concentration in the perthitic alkali feldspar (ppm).

A comparison of the reconstructed early melt composition (Table 2-9) and the bulk rock composition of the granites provides information on the crystallization processes. For example, the much lower concentrations of LREE, Zr and Nb in this melt compared to the bulk rock (southern hypersolvus granite; Fig. 2-14) indicate that alkali feldspar started crystallizing at a stage when a LREE-rich fluoride melt had already exsolved from the silicate melt, and a significant proportion of monazite-(Ce), pyrochlore minerals and zircon had fractionated. This is consistent with our earlier conclusions made on the basis of the feldspar fractionation model that the LREE, Zr and Nb were removed from the silicate melt by the separation of the immiscible LREE-rich fluoride melt and the crystallization of HFSE minerals at the interface between the two melts. The progressively smaller differences between the LREE, Zr and Nb contents of the melt and the bulk rock from the southern to the northern hypersolvus granite and to the transsolvus granite suggests that these melts were progressively more evolved and capable of dissolving higher concentrations of incompatible elements. The increased alkalinity, in particular, led to a partial dissolution of the HFSE-bearing phases and therefore the enrichment of the melts in these elements. The only exception is the larger difference in Nb content (melt vs. bulk rock) of the northern granite compared to the southern hypersolvus granite, as well as a consistently large difference in Zr concentrations in all the units. We conclude that an uneven distribution of pyrochlore and zircon crystals could have contributed to this, i.e., through gravity settling, a process discussed further below.

Melt HREE concentrations are consistently lower in the southern hypersolvus granite than the bulk rock (Fig. 2-14). This is consistent with our proposal that zircon crystallized earlier than perthitic alkali feldspar, thereby buffering the HREE content in the melt and increasing it in the bulk rock (zircon contains ~1 wt. % $HREE_2O_3$, Table 2-6).

Table 2-9: Melt REE and trace element compositions

(median and median absolute deviation ±)

Unit	Hypersolvus granite south		Hypersolvus granite north		Transsolvus granite	
Samples	3		2		5	
Analyses	*14*		*15*		*29*	
(ppm)		±		±		±
Rb	1429	166	2301	184	5695	1536
Zr	311	152	597	448	1228	641
Nb	118	59	130	77	442	218
La	13	7	92	18	516	194
Ce	67	36	319	86	721	361
Pr	7	3	35	11	78	30
Nd	49	26	195	39	440	211
Sm	23	10	44	12	112	32
Eu	0.07	0.02	0.19	0.05	1.20	0.22
Gd	25	10	39	11	117	22
Dy	33	16	70	20	152	32
Er	18	8	66	23	117	29
Yb	16	4	66	52	132	45
Y	184	108	267	64	983	262
TREE	434	228	1193	335	3369	1217

By contrast, in both the northern hypersolvus granite and the transsolvus granite, melt HREE concentrations exceed those in bulk rock. We speculate that a partial dissolution of zircon in a progressively more evolved (alkali- and F-rich) melt could account for the HREE enrichment in the later melts. The decoupling of the LREE and HREE observed at this stage indicates their different sources, i.e., immiscible fluoride melt globules preferentially scavenged the LREE (Vasyukova and Williams-Jones, 2014, 2016), whereas zircon was likely the sink for the HREE. Therefore, the crystallization and dissolution of these phases controlled the LREE and HREE contents of the melts. The highest HREE content would have been (dissolved) in the last residual melt, which migrated to the apical part of the pluton to form pegmatites. Such removal of residual melt from the transsolvus granite would explain the low HREE concentrations in the transsolvus bulk rock compared to the melt.

Although yttrium is a HREE, it partitioned into both the immiscible fluoride melt and zircon, in which the measured Y_2O_3 content was 1.3 and 1.2 wt. %, respectively (Table 1 in Vasyukova and Williams-Jones (2016) and Table 2-6). Moreover, zircon that crystallized on the boundary between the silicate and fluoride melts attained an extremely high Y content (4.8 wt. %, in the zircon core, Table 2 in Vasyukova and Williams-Jones, 2016). This behavior explains the decoupling of Y from the rest of the HREE in the northern hypersolvus granite. In the transsolvus granitic melt, the Y content is higher than that of the bulk rock (Fig. 2-14), which indicates, as for the LREE, that the more evolved magma was capable of dissolving higher concentrations of incompatible elements.

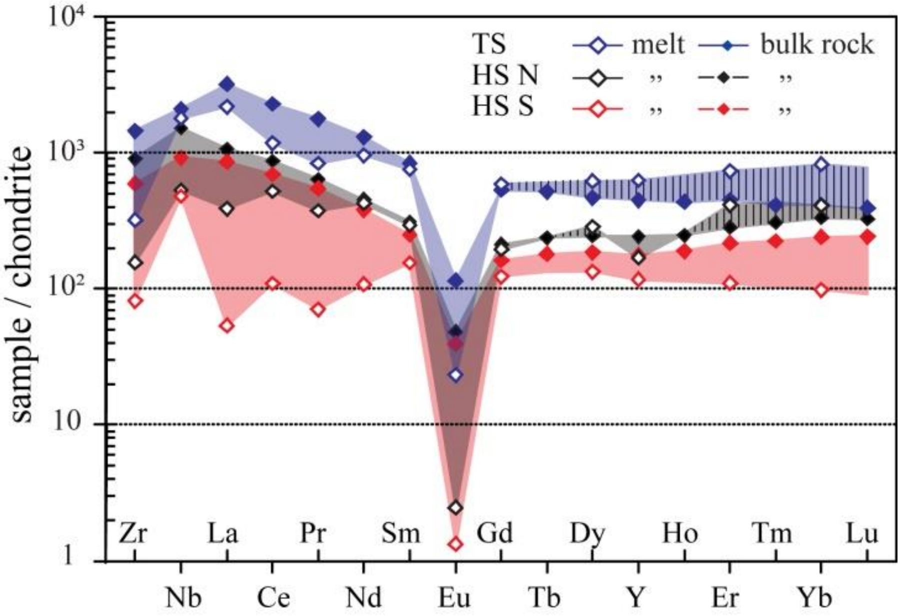

Fig. 2-14: Trace element profiles comparing melt and bulk rock compositions

Trace element profiles of average (calculated) melt and bulk rock compositions of the southern and northern hypersolvus granite and transsolvus granite (chondrite-normalized, Sun and McDonough, 1989). The shaded areas represent elements for which melt concentrations are higher than bulk rock concentrations, and clear areas represent elements for which the reverse is the case.

2.5.3.3 Gravity settling and flow differentiation

Gravity separation and flow differentiation were important processes in concentrating the REE, Zr and Nb with progressive magma evolution. As mentioned earlier, an uneven distribution of REE-, Zr- and Nb-bearing phases might have contributed to the unusual enrichment in these elements. In this section, we show how differences between melt and mineral density may have influenced the HFSE distribution in the melt. For example, rhyolitic melts typically have a density of ~2.35 g/cm^3 (Lange, 1994), however, peralkaline melts may have much lower density due to their high alkali and volatile (OH, CO_2, F) content. In fact, the addition of ~5.5 % H_2O to a haplogranitic (rhyolitic) melt at 750^{o}C, lowers the melt density to ~2.16 g/cm^3 (Lange, 1994). In low density peralkaline melts, settling rates are 10 to 100 m/y depending on the mineral, which is ~10 times higher than for the same minerals in peraluminous or metaluminous granitic melts (Baker and Vaillancourt, 1995).

As reported earlier, a REE-rich fluoride melt and HFSE minerals separated early from the silicate melt during hypersolvus granite evolution. The LREE-rich fluoride melt globules (especially when they were attached to crystals) were relatively heavy, because monazite-(Ce) and zircon have an average density (ρ) of 4.6 g/cm^3, and the pyrochlore group of ~5.3 g/cm^3. These globules therefore tended to settle in the magma chamber, whereas perthitic alkali feldspar with a density of ~ 2.5 g/cm^3 ($\rho_{sanidine}$) was likely to have remained in suspension.

Owing to the low viscosity of the transsolvus granite magma, gravity settling and flow differentiation played an even more important role in this unit. For example, the uneven distribution of heavier and lighter minerals depending on location is manifested in the relatively large scatter in Al, Fe and the HFSE (see Fig. 2-8) among the samples. This could reflect the separation of the denser arfvedsonite phenocrysts (ρ ~ 3.4 g/cm^3) from perthitic alkali feldspar (ρ

~ 2.5 g/cm^3), microcline (ρ ~ 2.56 g/cm^3) and albite (ρ ~ 2.62 g/cm^3). During ascent, the large mass and rapid movement of this magma batch likely resulted in a relatively high convection rate, which kept heavier phases in suspension. After emplacement, arfvedsonite crystals continued to grow and settled to form gravity settled and flow differentiated cumulates together with gagarinite-(Ce) (ρ ~ 4.5 g/cm^3) (see Fig. 2-6d).

2.5.4 In-situ evolution

2.5.4.1 Post-emplacement melt evolution

The hypersolvus granite evolved further after emplacement, and late minerals such as quartz, fluorite and arfvedsonite, as well as a variety of alkali zircono- and titanosilicates formed. Vlasovite and dalyite crystallized at the expense of primary zircon, and are commonly rimmed by elpidite and minor catapleiite (Fig. 2-3b), which are interpreted to be low-temperature hydrothermal phases (<600°C at 1 kbar) (Currie and Zaleski, 1985). Primary ilmenite and arfvedsonite were replaced by aenigmatite and astrophyllite (hydrothermal). Interestingly, in contrast to zircon, the alkali zirconosilicates do not contain detectable amounts of any of the REE (EMP analyses), thus the replacement of primary zircon likely released the HREE to a late stage fluid.

The groundmass of the transsolvus granite is composed of quartz, microcline, albite, alkali zirconosilicate minerals, mostly vlasovite and minor elpidite (see Fig. 2-5a), and locally, narsarsukite and pyrochlore minerals. The occurrence of quartz as anhedral to subhedral grains or as globular ‘eyes’ with inclusions of microcline, albite or arfvedsonite (see Fig. 2-4f), indicates that it crystallized relatively late (after emplacement). From textural observations, e.g., albite attached to the crystal faces of quartz eyes (snowball texture), we infer that albite mostly crystallized after emplacement. The presence of microcline and albite inclusions along the arfvedsonite rims in some samples (see Fig. 2-4d), suggests that arfvedsonite continued to grow after emplacement. This is in agreement with Siegel et al. (2017), who detected more evolved compositions in the rims compared to the cores of arfvedsonite phenocrysts. Crystallization of arfvedsonite was followed by the crystallization of zircono- and titano-silicate minerals as they are invariably interstitial.

2.5.4.2 The miaskitic to agpaitic transition

The zircono- and titano-silicates were the last magmatic minerals to crystallize in both, hypersolvus and transsolvus granite. In the hypersolvus granite, they crystallized at the expense of primary zircon and ilmenite, respectively, remnants of which were identified in this study (see Fig. 2-3b) and in Birkett et al. (1996). These relationships reflect a change from miaskitic to agpaitic conditions, in which, with increasing degree of peralkalinity, Zr^{4+} cations were progressively shielded by the large alkali cations, Na^+ and K^+, which inhibited the bonding of Zr^{4+} with SiO_4 tetrahedra to form zircon (Linthout, 1984). During this transition, primary zircon (see Fig. 2-3a) became unstable, and vlasovite and dalyite crystallized instead (see Fig. 2-3b). The miaskitic/agpaitic terminology has been restricted to peralkaline nepheline syenites, and used to describe the transition from zircon- and ilmenite-bearing alkaline rocks to rocks containing complex alkali-zircono- and sodium titano-silicates with increasing alkalinity (Marks et al., 2011; Sorensen, 1992). As evidence of the same transition is observed in the Strange Lake granites, we propose that the classification also be applicable to peralkaline granites. Similarly, the occurrence of sodium titanosilicates in the northern hypersolvus granite marks the beginning of the agpaitic stage, in which aenigmatite crystallized at the expense of ilmenite (Birkett et al., 1996). In the transsolvus granite, the lack of remnants of primary zircon or ilmenite, suggests that the magma was already agpaitic when emplaced. This means, that zircon had likely crystallized early in the magma chamber, but was re-dissolved in the melt once alkali activity surpassed the threshold to the agpaitic stage. Secondary zircon in this unit occurs in association with elpidite and vlasovite (see Fig. 2-5a) and is interpreted to be the result of the alteration of zirconosilicates.

2.5.4.3 Origin of the dark porphyritic granite and enclaves

On the basis of its fine-grained nature, and proximity to large bodies of the host gneisses, and Napeu Kainuit quartz monzonite, we interpret the dark porphyritic granite to represent a quenched facies. Compositionally, it is intermediate between and overlaps the hypersolvus and transsolvus granites (Fig. 2-8). This and its interlayering with transsolvus granite to produce the 'marble cake' texture (Fig. 2-6c), suggests that its composition was modified by mingling of a less evolved granite and transsolvus granite. This in turn indicates that the dark porphyritic granite represents quenched hypersolvus granite.

The dark and fine-grained nature and similar mineralogy of the enclaves suggest that they represent fragments of the quenched facies. As noted earlier, two distinct groups of enclaves (1 and 2) (see Table 2-2), can be identified on the basis of their mineralogy and bulk composition. Group 1 enclaves have bulk rock Al, Fe, Zr and REE contents that are very similar to those of the northern hypersolvus granite (Fig. 2-8). The high bulk Al, K, Rb and low Na, Fe, REE, Zr and Nb concentrations of group 1 enclaves points to a disproportionally high modal amount of perthitic alkali feldspar and microcline (high Al, K and Rb) accompanied by a smaller proportion of arfvedsonite (low Na and Fe), zircon and REE-minerals. This is supported by the calculated modal mineralogy, in which these enclaves contain ~69 wt. % alkali feldspar and 13 wt. % arfvedsonite. High alkali feldspar and low arfvedsonite proportions are also features of the northern hypersolvus granite (see Table 2-3). We therefore conclude on the basis of their bulk rock composition and mineralogy that the magma which formed the group 1 enclaves (and most of the dark porphyritic granite) represents a hypersolvus granite magma that was quenched along the cold wall rock.

The group 2 enclaves differ significantly from the group 1 by containing arfvedsonite and narsarsukite phenocrysts and a groundmass composed of microcline, albite, quartz and subhedral arfvedsonite, i.e., they are mineralogically similar to transsolvus granite (arfvedsonite is a late phase in the hypersolvus granite and narsarsukite is not observed in this unit). Their high Na, Fe, Mn and HFSE, and lower Al, K and Rb content compared to group 1 point to a more evolved nature of the magma. Moreover, the composition of the amphibole in these enclaves is similar for most elements to that of amphibole from the transsolvus granite. For example, in both units it has high Na (2.7-2.9), Li (0.1-1.2 apfu) concentrations, low Al (0.05-0.1 apfu), Ca (≤0.05 apfu), Ti (0.06-0.10 apfu), Mn (0.05-0.10 apfu) and REE (≤0.01apfu) concentrations and low $Fe^{2+/}Fe^{3+}$ ratios (0.6-1.5) in comparison to amphibole of the hypersolvus granite (2.0-2.8 apfu Na; ≤0.4 apfu Li; 0.1-0.5 apfu Al; 0.05-0.6 apfu Ca; 0.1-0.22 apfu Ti; 0.08-0.13 apfu Mn; 0.01-0.04 apfu REE and 0.1-2.5 $Fe^{2+/}Fe^{3+}$). Moreover, in both units (group 2 enclaves and transsolvus granite), the amphibole classifies as ferro-ferri-fluoro-leakeite, as opposed to the hypersolvus granite, where it classifies mostly as ‘fluoro-arfvedsonite’ (Siegel et al., 2017). The compositional overlap of group 2 enclaves with the northern hypersolvus granite in terms of Al, Fe, Zr and REE contents was likely the result of density settling in the magma chamber, which is suggested by the fact that they have higher alkali feldspar and lower arfvedsonite proportions than the rest of the transsolvus granite (see Table 2-3). Based on the evidence presented here, we conclude that group 2 enclaves represent fragments of early feldspar rich-, and arfvedsonite- (and HFSE-mineral-) poor quenched transsolvus granite. Both quenched units (hypersolvus and transsolvus granite) were broken up into plastic fragments by the rest of the transsolvus granite magma (see Fig. 2-6d) and dispersed to form the enclaves. Similar observations have been made by Bonin (1991), who described felsic micro-granular enclaves with the same mineralogy as the chilled margin facies of alkaline anorogenic granites in Corsica that were mechanically re-mobilized by granitic melt, which intruded the chilled facies.

2.5.4.4 Barren pegmatites and oikocrystic granite

The hypersolvus granite contains pegmatitic pockets and coarse-grained oikocrystic textured granites (see Fig. 2-2b). Their compositions indicate that the latter are slightly more evolved than their fine-grained counterparts (see Table 2-2; Fig. 2-8). We propose that these coarse-textured rocks were the products of in-situ fractional crystallization of the hypersolvus granite magma, and that this led to the formation of a volatile rich, but relatively barren residual melt. The textures indicate rapid crystallization and low nucleation rates due to the high volatile content of the melt (Simmons and Webber, 2008). Although these residual melts were evolved, they crystallized barren pegmatites because there was insufficient initial enrichment in the HFSE.

2.5.5 Fluid exsolution

Major exsolution of fluid occurred during the crystallization of the H_2O-rich transsolvus granite, which is evident in the replacement of primary minerals by secondary minerals (see below). The crystallization of arfvedsonite as a liquidus mineral buffered the H_2O-activity of the magma and inhibited fluid exsolution during ascent. It is likely that the crystallization of microcline, albite and quartz resulted in a buildup and release of the fluid after emplacement of the granite. These orthomagmatic fluids caused a succession of sodic, ferric, potassic, calcic, calcic-fluorine and acidic (phyllic) metasomatic subsolidus events (Gysi et al., 2016; Salvi and Williams-Jones, 1996). Sodic and ferric alteration is manifested by overgrowths on and replacement of perthitic alkali feldspar and microcline by albite (Na), arfvedsonite by aegirine (Na, Fe^{3+}) (see Fig. 2-4e) and magmatic zircon, vlasovite and dalyite by H_2O-bearing elpidite (Na) and catapleiite (Ca, Na) (see Figs. 2-4h; 2-5c). Replacement of ferrous iron by ferric iron was caused either by oxidation of the system due to the dissociation of H_2O and loss of H^+ ions by diffusion (Czamanske and Wones, 1973), or simply by isobaric cooling-induced oxidation (Vasyukova et al., 2016). The saline (NaCl) fluorine-bearing fluids remobilized the REE concentrated in primary minerals such as monazite-(Ce), the pyrochlore-group, gagarinite-(Ce) and zircon (HREE), which resulted in the formation of secondary REE-minerals like bastnäsite-(Ce) and gagarinite-(Y). These processes have been discussed in detail by Salvi and Williams-Jones (1990, 1996, 2006) and (Gysi and Williams-Jones, 2013; Gysi et al., 2016).

2.5.6 Model for the emplacement and magmatic evolution of the Strange Lake pluton

The Strange Lake pluton was emplaced as a ring dike accompanied by stoping at a depth of about 3 km. There were at least three magma batches, two of hypersolvus and one of transsolvus granite that all originated and evolved in a common magma chamber. The solidus temperature ranged between 660 and 700°C for the hypersolvus granite, and may have been lower for the transsolvus granite.

The major driving forces for the evolution of the hypersolvus magma were the early separation of a fluoride melt from the silicate melt and the crystallization of perthitic alkali feldspar and HFSE-rich phases (zircon, monazite-(Ce), pyrochlore minerals). Gravity settling played an important role by allowing the relatively light feldspar crystals to float to the upper part of the magma chamber and the heavier HFSE-rich phases to accumulate at the base. An alkali feldspar-rich (perthitic alkali feldspar) crystal-mush was emplaced as the first, and least evolved southern hypersolvus granite. A second batch of more evolved hypersolvus granite (northern unit) was released from the chamber somewhat later, which also contained a high proportion of alkali feldspar (perthitic alkali feldspar), but in addition an elevated proportion of heavier immiscible LREE-fluoride melt globules and (frequently attached) HFSE minerals (Fig. 2-15a). After emplacement, both hypersolvus granite intrusions (south and north) were quenched on the wall rock and cooled quickly. Both units evolved further in situ, crystallizing a second generation of perthitic alkali feldspar, followed by quartz, fluorite, arfvedsonite and the alkali zircono- and titano-silicates (in that sequence) (Fig. 2-15b). The latter minerals crystallized at the expense of primary zircon and ilmenite, which marked the transition from the miaskitic to the agpaitic stage. Volatile-rich melt pockets which represented the last residues of the evolved hypersolvus melt, formed the coarse oikocrystic and pegmatitic textured rocks observed in both the southern and northern facies.

The evolution of the hypersolvus granite resulted in significant changes in the magma feeding the intrusion. Massive fractionation of perthitic alkali feldspar led to the accumulation of OH^-, which triggered the crystallization of arfvedsonite phenocrysts (Fig. 2-15c). The latter, in turn, caused an increase in fluorine in the melt, which governed the transition from a hypersolvus to a subsolvus regime. High concentrations in the alkalis, OH^- and F^- caused a transition from miaskitic to agpaitic conditions and significantly increased the solubility of the HFSE (Aseri et al., 2015; Linthout, 1984). A mush of alkali feldspar (perthitic alkali feldspar and microcline), arfvedsonite and LREE-fluoride melt globules, and a melt containing high proportions of dissolved alkali- or F-REE-, Zr- and Nb-complexes, were emplaced in the upper crust as the transsolvus granite in a single large low viscosity surge (10^4–10^5 Pa·s). The feldspar-rich magma that developed due to gravity settling, was dragged into the conduit first, then quenched and assimilated by the rest of the transsolvus magma. Upon emplacement, arfvedsonite (and gagarinite-(Ce)) crystals settled and formed cumulates or flow differentiation textures, and continued to crystallize together with microcline, albite and quartz (Fig. 2-15d). At this stage, Nb, Zr and Ti were still dissolved in the melt and crystallized as late pyrochlore group, zircono- and titano-silicate minerals. The immiscible fluoride-melt crystallized as gagarinite-(Ce)-fluorite or fluorbritholite-(Ce)-fluorite assemblages; however, most of them accumulated in the volatile-rich residual melts. These melts migrated to the top of the pluton where they formed the F-REE-rich cores of the highly mineralized pegmatites in the altered parts of the transsolvus granite (Vasyukova and Williams-Jones, 2016).

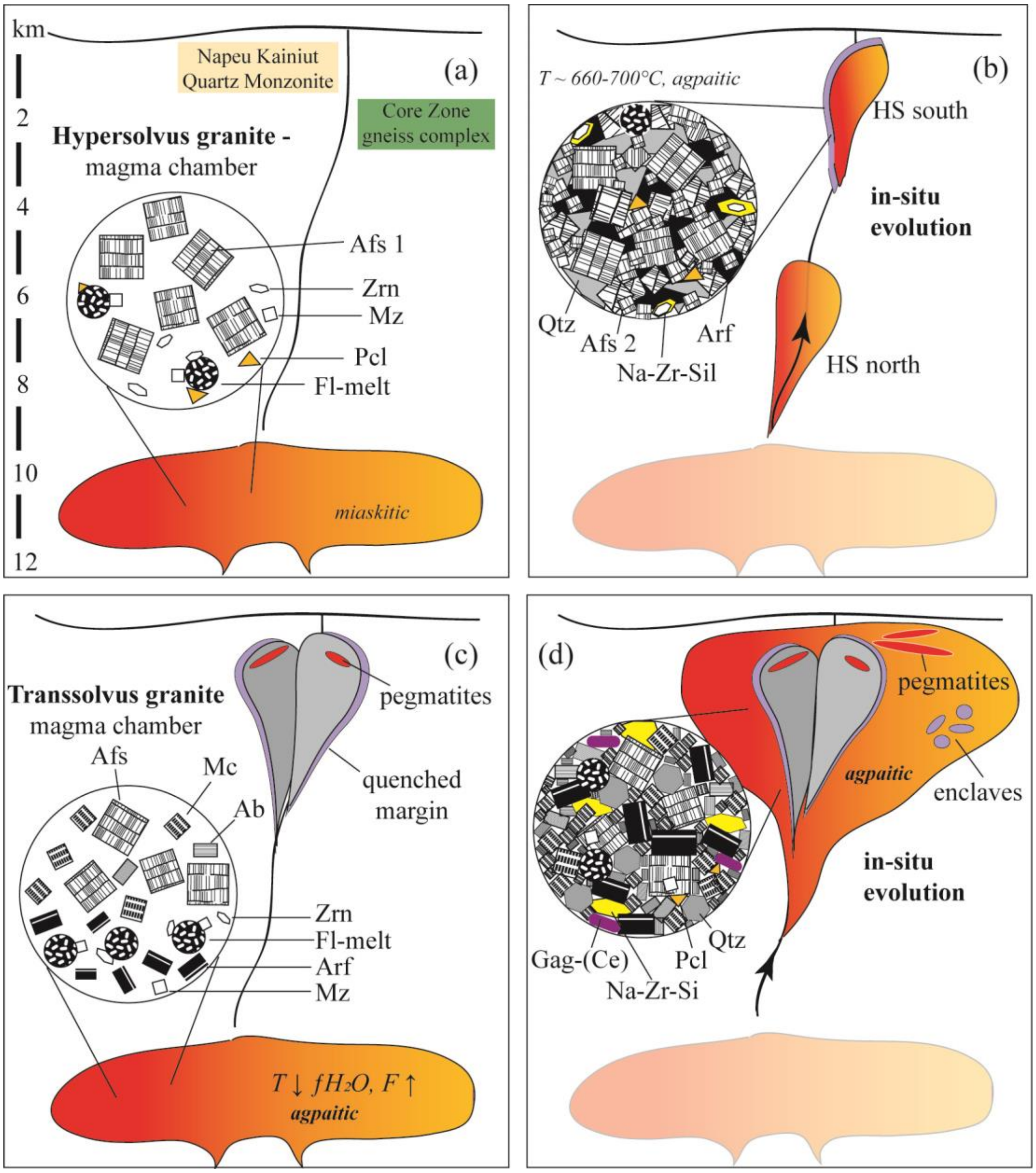

Fig. 2-15: Cartoon showing the magmatic evolution and emplacement sequence.

a) Early evolution of the hypersolvus granite, b) emplacement of the southern and northern hypersolvus granite with in-situ mineralogy and quenching along host rocks, c) early evolution of the transsolvus granite and d) emplacement of transsolvus granite with in-situ mineralogy and formation of the enclaves.

APPENDIX

Table 2-10: EMPA standards, counting times (Ct) and detection limits.

Element	Standard	Ct (s)	Detection limit (ppm) [a)]		
Feldspars			*Perthitic alkali feldspar*	*K-fsp*	*Albite*
Na	Albite	20	334	249	251
Fe	Hematite	20	437	412	385
Ca	Diopside	20	357	322	282
Si	Orthoclase	20	678	371	352
Rb	Rb-feldspar	80	1079	503	446
Ba	Ba-orthoclase	20	905	874	875
Pb	Vanadinite	80	374	364	337
Al	Orthoclase	20	540	312	311
K	Orthoclase	20	279	270	233
Zircon					
Zr	Zircon	20	850		
Si	Zircon	20	387		
Hf	Zircon	20	613		
Cl	Vanadinite	20	215		
Dy	MAC-Dy [b)]	20	542		
P	Fluorapatite	20	202		
Ca	Diopside	20	219		
Er	MAC-Er	20	537		
Y	MAC-Y	20	646		
Yb	MAC-Yb	20	1099		
Alkali zircono-silicates					
Na	Albite	20	396		
F	Fluorite	20	2920		
K	Orthoclase	20	431		
Zr	Zircon	20	1561		
Fe	Hematite	20	678		
Si	Zircon	20	644		
Al	Orthoclase	20	478		
Ca	Diopside	20	528		
Sn	Cassiterite	20	1034		
Ti	Titanite	20	680		
Hf	Zircon	20	2483		

Table 2-10: EMPA standards, counting times (Ct) and detection limits (continued)

Pyrochlore-group minerals							
Na	Pyrochlore	20	326				
F	Fluorite	20	2603				
Ca	Titanite	20	231				
Nb	Pyrochlore	20	830				
Ba	Ba-orthoclase	20	738				
Ti	Titanite	20	449				
Sr	Sr-feldspar	20	633				
Fe	Hematite	20	284				
U	Uraninite	20	1026				
Y	MAC-Y	20	1061				
Ce	MAC-Ce	20	732				
Th	Thorite	20	b.d.				
Zr	Zircon	20	857				
La	MAC-La	20	837				
Pb	Vanadinite	20	1048				
Si	Titanite	20	299				
Ta	Pyrochlore	20	950				
Mn	Spessartine	20	b.d.				
Nd	MAC-Nd	20	1307				
Pr	MAC-Pr	20	1473				
REE-(F)-minerals			*Mz-(Ce)*	*Fbr-(Ce)*	*Fl*	*Fl-Flc ss*	*Gag-(Ce)*
Na	Albite	20	298	269	152	154	198
F	Fluorapatite	20	2860	2819	2194	2090	1529
Cl	Vanadinite	20	218	201	162	147	183
P	Fluorapatite	20	453	368	169	150	164
La	MAC-La	20	1369	1238	741	707	978
Ca	Fluorapatite	20	369	256	270	233	235
Pb	Vanadinite	100	445	413	354	306	363
Ce	MAC-Ce	20	1269	1132	644	637	843
Th	Thorite	20	909	827	604	564	690
Si	Diopside	20	344	340	130	119	142
Dy	MAC-Dy	20	3350	3152	2032	2026	2549
U	Uraninite	100	573	528	383	365	437
Y	MAC-Y	20	965	912	625	556	689
Sm	MAC-Sm	20	2646	2484	1462	1500	1989
Sr	Sr-feldspar	20	754	738	725	636	631
Gd	MAC-Gd	20	2862	2677	1735	1701	2134
Pr	MAC-Pr	20	2450	2294	1338	1313	1793
Nd	MAC-Nd	20	2493	2223	1285	1262	1778
Eu	MAC-Eu	20	2625	2402	1493	1421	1917

a) Detection limits represent values of representative analyses
b) MAC: REE silicate glasses Micro Analysis Consultants
c) b.d. = below detection limit

ACKNOWLEDGEMENTS

Financial support for this study was provided by a grant from Quest Rare Minerals Ltd. and a matching grant from the NSERC Collaborative Research and Development Program, both to A.E W-J. Quest Rare Minerals Ltd. (Peter Cashin and Pierre Guay) provided access to the field area, drill core, internal data and assay data. Former Quest geologists Angela Buchanan and Patrick Collins provided essential geological information and assisted in the interpretation of field observations. Alexandre Brosseau-Liard and Robert Fritscher contributed a suite of surface samples collected in 2011. Alexander Gysi contributed samples and provided valuable advice on petrographic observations. Discussions with Robert F. Martin greatly helped to clarify our ideas on the evolution of the pluton. Lang Shi, André Poirier, Vincent van Hinsberg and Bill Minarik helped with the application of the analytical methods and the interpretation of results.

REFERENCES

Aseri, A. A., Linnen, R. L., Che, X. D., Thibault, Y., and Holtz, F., 2015, Effects of fluorine on the solubilities of Nb, Ta, Zr and Hf minerals in highly fluxed water-saturated haplogranitic melts: Ore Geology Reviews, v. 64, p. 736-746.

Atencio, D., Andrade, M. B., Christy, A. G., Giere, R., and Kartashov, P. M., 2010, The pyrochlore supergroup of minerals: nomenclature: Canadian Mineralogist, v. 48, no. 3, p. 673-698.

Bailey, J. C., 1977, Fluorine in granitic rocks and melts - review: Chemical Geology, v. 19, no. 1, p. 1-42.

Baker, D. R., and Vaillancourt, J., 1995, The low viscosities of F+H2O-bearing granitic melts and implications for melt extraction and transport: Earth and Planetary Science Letters, v. 132, no. 1-4, p. 199-211.

Birkett, T. C., Miller, R. R., Roberts, A. C., and Mariano, A. N., 1992, Zirconium-bearing minerals of the Strange Lake intrusive complex, Quebec-Labrador: Canadian Mineralogist, v. 30, p. 191-205.

Birkett, T. C., Trzcienski, W. E., and Stirling, J. A. R., 1996, Occurrence and compositions of some Ti-bearing minerals in the Strange Lake intrusive complex, Quebec-Labrador boundary: Canadian Mineralogist, v. 34, p. 779-801.

Boily, M., and Williams-Jones, A. E., 1994, The role of magmatic and hydrothermal processes in the chemical evolution of the Strange Lake plutonic complex, Quebec-Labrador: Contributions to Mineralogy and Petrology, v. 118, no. 1, p. 33-47.

Bonin, B., 1986, Ring complex granites and anorogenic magmatism, North Oxford Academic Publishers Ltd.

-, 1991, Enclaves and Granite Petrology, Amsterdam, The Netherlands, Elsevier Science Publishers B.V., Developments in Petrology.

-, 2007, A-type granites and related rocks: Evolution of a concept, problems and prospects: Lithos, v. 97, no. 1-2, p. 1-29.

Bottinga, Y., and Javoy, M., 1975, Oxygen Isotope Partitioning among Minerals in Igneous and Metamorphic Rocks: Reviews of Geophysics, v. 13, no. 2, p. 401-418.

Clemens, J. D., Holloway, J. R., and White, A. J. R., 1986, Origin of an a-Type Granite - Experimental Constraints: American Mineralogist, v. 71, no. 3-4, p. 317-324.

Currie, K. L., and Zaleski, E., 1985, The Relative Stability of Elpidite and Vlasovite - a P-T Indicator for Peralkaline Rocks: Canadian Mineralogist, v. 23, p. 577-582.

Czamanske, G. K., and Wones, D. R., 1973, Oxidation during Magmatic Differentiation, Finnmarka Complex, Oslo Area, Norway .2. Mafic Silicates: Journal of Petrology, v. 14, no. 3, p. 349-380.

David, J., Simard, M., Bandyayera, D., Goutier, J., Hammouche, H., Pilote, P., Leclerc, F., and Dion, C., 2012, Datations U-Pb effectuées dans les provinces du Supérieur et de Churchill en 2010-2011: Geologie Québec, Ministère des Ressources Naturelles et de la Faune (MRNF), v. RP 2012-01, p. 30.

Dingwell, D. B., Hess, K. U., and Romano, C., 1998, Extremely fluid behavior of hydrous peralkaline rhyolites: Earth and Planetary Science Letters, v. 158, no. 1-2, p. 31-38.

Eby, G. N., 1990, The A-type granitoids: a review of their occurrence and chemical characteristics and speculations on their petrogenesis: Lithos, v. 26, p. 115-134.

Eby, G. N., 1992, Chemical subdivision of the a-type granitoids - petrogenetic and tectonic implications: Geology, v. 20, no. 7, p. 641-644.

Emslie, R. F., Hamilton, M. A., and Theriault, R. J., 1994, Petrogenesis of a Midproterozoic anorthosite-mangerite-charnockite-granite (AMCG) complex - isotopic and chemical evidence from the Nain Plutonic Suite: Journal of Geology, v. 102, no. 5, p. 539-558.

Giehl, C., Marks, M., and Nowak, M., 2013, Phase relations and liquid lines of descent of an iron-rich peralkaline phonolitic melt: an experimental study: Contributions to Mineralogy and Petrology, v. 165, no. 2, p. 283-304.

Giordano, D., Russell, J. K., and Dingwell, D. B., 2008, Viscosity of magmatic liquids: A model: Earth and Planetary Science Letters, v. 271, no. 1-4, p. 123-134.

Gysi, A. P., and Williams-Jones, A. E., 2013, Hydrothermal mobilization of pegmatite-hosted REE and Zr at Strange Lake, Canada: A reaction path model: Geochimica et Cosmochimica Acta, v. 122, no. 2013, p. 324-352.

Gysi, A. P., Williams-Jones, A. E., and Collins, P., 2016, Lithogeochemical Vectors for Hydrothermal Processes in the Strange Lake Peralkaline Granitic REE-Zr-Nb-Deposit: Economic Geology and the Bulletin of the Society of Economic Geologists, v. 111, p. 1241-1276.

Herrmann, W., and Berry, R. F., 2002, MINSQ - a least squares spreadsheet method for calculating mineral proportions from whole rock major element analyses: Geochemistry: Exploration, Environment, Analysis, v. 2, no. 4, p. 361-368.

Hill, J. D., 1991, Emplacement and Tectonic Implications of the Midproterozoic Peralkaline Flowers River Igneous Suite, North-Central Labrador: Precambrian Research, v. 49, no. 3-4, p. 217-227.

Hofmeister, A. M., and Rossman, G. R., 1984, Determination of Fe-3+ and Fe-2+ Concentrations in Feldspar by Optical-Absorption and Electron-Paramagnetic-Res Spectroscopy: Physics and Chemistry of Minerals, v. 11, no. 5, p. 213-224.

Jambor, J. L., Roberts, A. C., Grice, J. D., Birkett, T. C., Groat, L. A., and Zajac, S., 1998, Gerenite-(Y), $(Ca,Na)_2(Y,REE)_3Si_6O_{18} * 2H_2O$, a new mineral species, and an associated Y-bearing gadolinite-group mineral, from the Strange Lake peralkaline complex, Quebec-Labrador: Canadian Mineralogist, v. 36, p. 793-800.

Jambor, J. L., Roberts, A. C., Owens, D. R., and Grice, J. D., 1996, Zajacite-(Ce), a new rare-earth fluoride from the Strange Lake deposit, Quebec-Labrador: Canadian Mineralogist, v. 34, p. 1299-1304.

Kempe, U., Goetze, J., Dandar, S., and Habermann, D., 1999, Magmatic and metasomatic processes during formation of the Nb-Zr-REE deposits Khaldzan Buregte and Tsakhir (Mongolian Altai): Indications from a combined CL-SEM study: Mineralogical Magazine, v. 63 no. 2, p. 165-177.

Kovalenko, V. I., Tsaryeva, G. M., Goreglyad, A. V., Yarmolyuk, V. V., Troitsky, V. A., Hervig, R. L., and Farmer, G. L., 1995, The Peralkaline Granite-Related Khaldzan-Buregtey Rare-Metal (Zr, Nb, Ree) Deposit, Western Mongolia: Economic Geology and the Bulletin of the Society of Economic Geologists, v. 90, no. 3, p. 530-547.

Lange, R. A., 1994, The Effect of H2o, Co2 and F on the Density and Viscosity of Silicate Melts: Volatiles in Magmas, v. 30, p. 331-369.

Linthout, K., 1984, Alkali-Zirconosilicates in Peralkaline Rocks: Contributions to Mineralogy and Petrology, v. 86, no. 2, p. 155-158.

Marks, M. A. W., Hettmann, K., Schilling, J., Frost, B. R., and Markl, G., 2011, The Mineralogical Diversity of Alkaline Igneous Rocks: Critical Factors for the Transition from Miaskitic to Agpaitic Phase Assemblages: Journal of Petrology, v. 52, no. 3, p. 439-455.

McKenzie, D., 1985, The extraction of magma from the crust and mantle: Earth and Planetary Science Letters, v. 74, no. 1, p. 81-91.

McLelland, J. M., Selleck, B. W., Hamilton, M. A., and Bickford, M. E., 2010, Late- to post-tectonic setting of some major proterozoic anorthosite - mangerite - charnockite - granite (AMCG) suites: Canadian Mineralogist, v. 48, no. 4, p. 729-750.

Miller, R. R., 1990, The Strange Lake Pegmatite - Aplite - hosted Rare-Metal Deposit, Labrador: Current Research (1990) Newfoundland Department of Mines and Energy, Geological Survey Branch, v. Report 90-1, p. 171-182.

Miller, R. R., Heaman, L. M., and Birkett, T. C., 1997, U-Pb zircon age of the Strange Lake peralkaline complex: Implications for Mesoproterozoic peralkaline magmatism in north-central Labrador: Precambrian Research, v. 81, no. 1-2, p. 67-82.

Mysen, B. O., and Virgo, D., 1985a, Interaction between Fluorine and Silica in Quenched Melts on the Joins SiO_2-AlF_3 and SiO_2-Naf Determined by Raman-Spectroscopy: Physics and Chemistry of Minerals, v. 12, no. 2, p. 77-85.

-, 1985b, Structure and Properties of Fluorine-Bearing Aluminosilicate Melts - the System Na_2O-Al_2O_3-SiO_2-F at 1-Atm: Contributions to Mineralogy and Petrology, v. 91, no. 3, p. 205-220.

Parsons, I., 1978, Feldspars and Fluids in Cooling Plutons: Mineralogical Magazine, v. 42, no. 321, p. 1-17.

Petrella, L., Williams-Jones, A. E., Goutier, J., and Walsh, J., 2014, The Nature and Origin of the Rare Earth Element Mineralization in the Misery Syenitic Intrusion, Northern Quebec, Canada: Economic Geology, v. 109, no. 6, p. 1643-1666.

Quest, 2012, Quest announces that a revised resource estimate for the Strange Lake B-Zone REE deposit shows a doubling of tonnage, http://questareminerals.com/news.php, Volume 2016: Toronto, Quest Rare Minerals Ltd.

Salvi, S., and Williams-Jones, A. E., 1990, The Role of Hydrothermal Processes in the Granite-Hosted Zr, Y, Ree Deposit at Strange Lake, Quebec Labrador - Evidence from Fluid Inclusions: Geochimica et Cosmochimica Acta, v. 54, no. 9, p. 2403-2418.

Salvi, S., and Williams-Jones, A. E., 1992, Reduced Orthomagmatic C-O-H-N-Nacl Fluids in the Strange Lake Rare-Metal Granitic Complex, Quebec Labrador, Canada: European Journal of Mineralogy, v. 4, no. 5, p. 1155-1174.

Salvi, S., and Williams-Jones, A. E., 1996, The role of hydrothermal processes in concentrating high-field strength elements in the Strange Lake peralkaline complex, northeastern Canada: Geochimica et Cosmochimica Acta, v. 60, no. 11, p. 1917-1932.

Salvi, S., and Williams-Jones, A. E., 1997, Fischer-Tropsch synthesis of hydrocarbons during sub-solidus alteration of the Strange Lake peralkaline granite, Quebec/Labrador, Canada: Geochimica Et Cosmochimica Acta, v. 61, no. 1, p. 83-99.

Salvi, S., and Williams-Jones, A. E., 2006, Alteration, HFSE mineralisation and hydrocarbon formation in peralkaline igneous systems: Insights from the Strange Lake Pluton, Canada: Lithos, v. 91, p. 19-34.

Scaillet, B., and MacDonald, R., 2001, Phase relations of peralkaline silicic magmas and petrogenetic implications: Journal of Petrology, v. 42, no. 4, p. 825-845.

Schmitt, A. K., Trumbull, R. B., Dulski, P., and Emmermann, R., 2002, Zr-Nb-REE mineralization in peralkaline granites from the Amis Complex, Brandberg (Namibia): Evidence for magmatic pre-enrichment from melt inclusions: Economic Geology and the Bulletin of the Society of Economic Geologists, v. 97, no. 2, p. 399-413.

Siegel, K., Williams-Jones, A. E., and Van Hinsberg, V. J., 2017, The Amphiboles of the REE-rich A-type peralkaline Strange Lake pluton - fingerprints of magma evolution Lithos, v. 288-289, p. 156-174.

Simmons, W. B., and Webber, K. L., 2008, Pegmatite genesis: state of the art: European Journal of Mineralogy, v. 20, no. 4, p. 421-438.

Sorensen, H., 1992, Agpaitic Nepheline Syenites - a Potential Source of Rare Elements: Applied Geochemistry, v. 7, no. 5, p. 417-427.

Sun, S. S., and McDonough, W. F., 1989, Chemical and isotopic systematics of oceanic basalts: implications for mantle composition and processes: Geological Society, London, Special Publications, v. 42, p. 313-345.

Tuttle, O. F., and Bowen, N. L., 1958, Origin of granite in the light of experimental studies in the system $NaAlSi_3O_8$-$KAlSi_3O_8$-SiO_2-H_2O, Geological Society of America, Memoir 74, 146 p.

Vasyukova, O., and Williams-Jones, A. E., 2014, Fluoride–silicate melt immiscibility and its role in REE ore formation: Evidence from the Strange Lake rare metal deposit, Que´bec-Labrador, Canada: Geochimica et Cosmochimica Acta, v. 139, no. 2014, p. 110-130.

-, 2016, The evolution of immiscible silicate and fluoride melts: Implications for REE ore-genesis: Geochimica et Cosmochimica Acta, v. 172, p. 205-224.

-, 2017 The roles of magma and fluid in concentrating HFSE/REE at Strange Lake, Québec. Proceedings of the 14th Biennial SGA Meeting Québec City, p. 1261-1264.

Vasyukova, O. V., Williams-Jones, A. E., and Blamey, N. J. F., 2016, Fluid evolution in the Strange Lake granitic pluton, Canada: Implications for HFSE mobilization: Chemical Geology, v. 444, p. 83-100.

Walters, A. S., Goodenough, K. M., Hughes, H. S. R., Roberts, N. M. W., Gunn, A. G., Rushton, J., and Lacinska, A., 2013, Enrichment of Rare Earth Elements during magmatic and post-magmatic processes: a case study from the Loch Loyal Syenite Complex, northern Scotland: Contributions to Mineralogy and Petrology, v. 166, no. 4, p. 1177-1202.

White, J. C., 2003, Trace-element partitioning between alkali feldspar and peralkalic quartz trachyte to rhyolite magma. Part II: Empirical equations for calculating trace-element partition coefficients of large-ion lithophile, high field-strength, and rare-earth elements: American Mineralogist, v. 88, no. 2-3, p. 330-337.

White, J. C., Holt, G. S., Parker, D. F., and Ren, M. H., 2003, Trace-element partitioning between alkali feldspar and peralkalic quartz trachyte to rhyolite magma. Part I: Systematics of trace-element partitioning: American Mineralogist, v. 88, no. 2-3, p. 316-329.

Yaroshevskii, A., and Bagdasarov, Y., 2008, Geochemical diversity of minerals of the pyrochlore group: Geochemistry International, v. 46, no. 12, p. 1245-1266.

CHAPTER 3 -

THE AMPHIBOLES OF THE REE-RICH A-TYPE PERALKALINE GRANITIC STRANGE LAKE PLUTON – FINGERPRINTS OF MAGMA EVOLUTION

PREFACE

The previous chapter (2) identified three consecutive granitic intrusions of the Strange Lake pluton. The first emplaced and least evolved unit is a fine grained southern hypersolvus granite, followed by the more evolved northern hypersolvus granite. The last emplaced and most evolved transsolvus granite has significantly higher concentrations of HFSE. Chapter 3 focuses on the major and trace element compositions of the amphibole-group minerals of the least altered rocks of the Strange Lake pluton. It contains the first report of alkali species such as katophorite and Li-rich ferro-ferri-(fluoro)-leakeite, besides (fluoro)-arfvedsonite in the Strange Lake granites. The evolutionary trends shown in Chapter 2 are traced with the amphibole chemistry; in addition, calculated Fe^{2+}/Fe^{3+} ratios in the amphibole provide information on fO_2 and OH^- and F^- melt concentrations. Some of the amphibole species have shown to carry significant concentrations of the REE and the HREE in particular. Consequently, the partitioning of the REE between alkali amphibole and melt is discussed in detail.

ABSTRACT

Major and trace element compositions of amphibole in igneous environments commonly reflect evolving magma compositions. In this study, we use the amphibole-group minerals from the Strange Lake, REE-enriched peralkaline granitic pluton to gain insights into the evolution of the magma. This 1240 Ma old pluton consists of two main intrusive facies, an early hypersolvus granite, which occurs as separate northern and southern intrusions, and a more evolved transsolvus granite. In the hypersolvus granite the amphibole is a late interstitial phase, whereas in the transsolvus granite, it is present as phenocrysts. The compositions vary from sodium-calcium amphibole (ferro-ferri-katophorite) in the southern hypersolvus granite to sodium amphibole (arfvedsonite, ferro-ferri-leakeite) in the other, more evolved granitic units. High Na, Si, Li, and low Al and Ca concentrations in the amphibole phenocrysts of the transsolvus granite indicate formation from a more evolved magma compared to the hypersolvus granite, despite the fact that these crystals formed early. We interpret the increasing Fe^{3+}/Fe^{2+} ratios in the amphibole of the hypersolvus granite to reflect crystal chemical effects (Na/Ca-ratio) and increasingly oxidizing conditions in the magma, whereas in the phenocrysts of the transsolvus granite, the increasing ratio was the product of increasing proportions of F^- and OH^- in the melt. The amphiboles of all the granite units have elevated Nb, Zr, Hf and REE concentrations compared to the bulk rock, suggesting that these elements are compatible in amphibole. By contrast the much lower Ti concentration was due to saturation of the magma in sodium-titanosilicates. The amphibole REE concentrations vary greatly among the granite units. Amphibole of the southern and northern hypersolvus granite contains 0.16 and 0.07 wt. % ∑REE+Y, on average, respectively, and in the transsolvus granite, the average $\sum$REE content is only 0.01 wt. %, despite the more evolved nature of its host transsolvus granite. We intrepret this compositional difference to be due to the fact that the latter represents phenocrysts, which crystallized early, whereas the hypersolvus arfvedsonite is a late interstitial phase. Chondrite-normalized REE profiles emphasise the wide range in LREE-, and the narrow range in HREE-concentrations of the amphiboles. The variations in the LREE-profiles reflect the variable crystallization of primary LREE-bearing phases, including monazite-(Ce), pyrochlore group minerals and gagarinite-(Ce), prior to or contemporaneous with the amphibole, as well as the exsolution of a LREE-rich fluoride melt. The LREE are incompatible in the amphibole structure (apparent $D < 0.01$) and are preferably accommodated by the octahedral C-site, whereas the HREE occupy the B-site. The chondrite-normalized HREE profiles are steep and display an increasing relative enrichment that culminates in compatible behavior for Yb and Lu (apparent $D > 1$). Owing to their small ionic radius and their compatibility with the amphibole structure, HREE concentrations were more controlled by partitioning (crystal chemical effects) than by the concentrations in the corresponding magma. Large proportions of the bulk HREE content (up to 70 %) reside in the amphibole, and their later release through hydrothermal replacement helps to explain the extreme and unusual HREE enrichment of the Strange Lake pluton.

Keywords

Amphibole, REE, Strange Lake, Peralkaline granite, Magma evolution

3.1 INTRODUCTION

Our understanding of the genesis of intra-plate rift-generated intrusions that produce A-type granites is still incomplete. In particular, the reasons for the extremely high REE-, F- and other HFSE-concentrations in many of these peralkaline rocks are poorly known. In addition to the need for a highly fertile magma source, magmatic evolution by fractional crystallization appears to play a critical role in the enrichment of these elements (e.g., Kovalenko et al., 1995; Mungall and Martin, 1996). The chemistry of a major mineral, such as amphibole, which adapts to its *P*-*T*-*X* environment, and is capable of hosting most cation sizes and charges, can potentially record this and any other processes that might have operated in the magma chamber. As a phenocryst, the amphibole would record the conditions prior to intrusion, and as a late crystallizing phase, the in-situ crystal fractionation processes.

The well-known ability of minerals of the amphibole super-group to accommodate a wide variety of elements with highly variable ionic radius and charge, including alkali elements, high field strength elements (HFSE) and the rare earth elements (REE), makes it an ideal monitor of magma evolution (Abdel-Rahman, 1994; Marks et al., 2004). In this study, we use the occurrence and composition of amphibole-group minerals in the Strange Lake pluton, Québec-Labrador, Canada, to trace the evolution of a peralkaline granitic magma that is unusually enriched in the REE, Zr and Nb. This magma was the source of a large REE/HFSE resource (indicated resources: 278 million tons grading 0.93 wt. % REE_2O_3, 0.18 wt. % Nb_2O_5 and 1.92 wt. % ZrO_2; Quest Rare Minerals Ltd., 2012) that is currently being considered for exploitation. In this study, the Na, Ca, Li, Fe^{3+} and REE contents of the amphibole-group minerals are used to gain information on the composition of the magma and conditions prior to, during and after its emplacement. The results show that fractional crystallization of a perthitic alkali feldspar, gravity settling of REE-minerals and zircon as well as the exsolution of a LREE-rich fluoride melt played a major role in the evolution of the magma and in concentrating the ore elements. They also show that the amphibole-group minerals host a significant proportion of the REE, and were the principal carriers of the HREE in some parts of the pluton.

3.2 BACKGROUND INFORMATION

A number of studies have traced evolutionary trends in alkaline rock suites using the crystal chemistry of the dominant mafic minerals (Davidson, 1982; Marks et al., 2004). In peralkaline rocks, which are defined by a molar excess of alkalis in respect to aluminum, the mafic minerals are usually of a sodic nature, e.g., amphiboles, such as arfvedsonite and riebeckite, or pyroxenes such as aegirine. The amphiboles of alkaline complexes generally trend from calcic through sodic-calcic to sodic members with differentiation, reflecting the increasing alkalinity of the melt from which they crystallized (Giret et al., 1980; Piilonen et al., 2013). They also display significant variations in REE and HFSE concentrations with magmatic differentiation, as shown, for example, by Marks et al. (2004) for the Gardar alkaline province (SW-Greenland). Similar conclusions have been reached for amphibole phenocrysts in alkaline basalts from the Rhine graben valley, Germany (Mayer et al., 2014).

Lithium has proven to be a particularly important constituent of alkali amphiboles (Camara et al., 2010; Hawthorne et al., 1993). Owing to its incompatible character in common rock-forming minerals, its concentration in amphibole may reflect the degree of melt differentiation. This case has been made for lithium-bearing amphiboles from Hurricane Mountain, New Hampshire, where the amphiboles vary from early Li-rich leakeite to late Li-poor riebeckite (Hawthorne et al., 1996). The progressive depletion in lithium in crystals growing into miarolitic cavities in granitic pegmatites is consistent with the idea that a highly evolved melt with a high Li content formed the earlier leakeite, and that progressive fluid exsolution resulted in the removal of lithium and the growth of Li-poor riebeckite.

The 1240 Ma Strange Lake pluton (Miller et al., 1997) is an extraordinary example of hyper-REE-, Zr-, and Nb- enrichment in a peralkaline granite, and is composed of a sequence of granitic intrusions, two earlier hypersolvus granites and a later transsolvus granite (this study). The last of these intrusions is host to numerous NYF-type pegmatites with extremely high concentrations of the REE, particularly the heavy REE (HREE), Zr and Nb. Most of the previous studies of the pluton have focused on the hydrothermal alteration and the rare-metal mineralized pegmatites (Gysi et al., 2016; Gysi and Williams-Jones, 2013; Kerr and Rafuse, 2012; Salvi and Williams-Jones, 1990; 1992; 1996; 1997; 2006; Vasyukova et al., 2016). Several studies, however, have addressed its magmatic evolution. Boily and Williams-Jones (1994) proposed that the REE-enrichment was due to a combination of fractional crystallization, and the heterogeneous distribution of F-rich residual melts, in which the REE and HFSE were transported as fluoro-complexes. Vasyukova and Williams-Jones (2014; 2016) provided evidence for the early separation of a REE- and Y-rich immiscible fluoride melt from the silicate melt, which accumulated in the highly evolved residual melts that formed the mineralized pegmatites.

Previous studies of the mafic minerals of the Strange Lake pluton concluded that the amphiboles are enriched in Li and Zn, are associated with Ti-silicates and crystallized under relatively low fO_2 (Pillet et al., 1993; Roelofsen, 1997). Hawthorne et al. (2001) showed that Li is an essential component of the amphiboles and identified lithian arfvedsonite and lithian manganoan arfvedsonite.

3.3 GEOLOGIC SETTING

The Strange Lake pluton is part of the Nain Plutonic AMCG suite, which comprises anorthosites, mangerites, charnockites and granites (Miller, 1996; Gower and Krogh, 2002). Rocks of the Nain suite were emplaced along the boundary between the Archean Nain province and the Archean to Early Paleoproterozoic Churchill province (Emslie et al., 1994), more recently referred to as the Core Zone (James and Dunning, 2000). The Nain Plutonic Suite covers an area of ~19,000 km^2, and was emplaced between 1460 and 1240 Ma, with the Strange Lake pluton (1240 ± 2 Ma) representing the youngest intrusive body (Gower and Krogh, 2002).

To the south and west, the Strange Lake pluton intrudes the Napeu Kainiut quartz monzonite, which is interpreted to represent a satellite body of the Mistastin batholith (Miller et al., 1997). The Napeu Kainiut intrusion, which is composed mainly of quartz, K-feldspar, plagioclase and biotite, also occurs within the Strange Lake pluton as xenoliths and large roof pendants. The Mistastin batholith consists of pyroxene- and fayalite-bearing Rapakivi-textured granites, which were cut by younger biotite-hornblende-bearing granites and minor syenitic intrusions, such as the Misery Lake syenite, which hosts abundant REE mineralization (Petrella et al., 2014). Dated at 1420 Ma (Emslie and Stirling, 1993), the Mistastin batholith represents one of the oldest members of the Nain Plutonic Suite. The other host rock to the Strange Lake pluton is an Archean to Paleoproterozoic gneiss complex belonging to the Core Zone (Churchill Province), comprising quartzofeldspathic augen-gneiss, banded biotite gneiss and minor garnet-bearing paragneiss and mafic gneiss.

3.3.1 The Strange Lake pluton

The circular (in outcrop), ~ 6 km in diameter, Strange Lake pluton is located on the border between Québec and Labrador, and consists of a sequence of alkaline granitic intrusive units

(Fig. 3-1). The earliest phase of the pluton is a hypersolvus granite (Pillet et al., 1992), implying its formation at conditions above the alkali feldspar solvus (Tuttle and Bowen, 1958). The hypersolvus granite occurs in the center and southern part of the pluton, and has been subdivided into a northern and a southern unit, based on bulk rock and mineral compositional differences. The third major unit, formerly classified as subsolvus granite (Boily and Williams-Jones, 1994; Salvi and Williams-Jones, 1996; Gysi and Williams-Jones, 2013), is now classified as transsolvus granite, and contains perthitic alkali feldspar phenocrysts as well as separate albite and K-feldspar crystals in the groundmass. It occupies much of the pluton, and has been strongly affected by hydrothermal activity. A smaller, unaltered part of the transsolvus granite is exposed in the center of the pluton and provided the samples for this study. The transsolvus granite commonly contains dark grey, fine-grained ovoid enclaves and barren pegmatite pockets; the altered transsolvus granite is host to highly REE/HFSE-enriched pegmatites. A dark grey porphyritic microgranite with a fine-grained matrix occurs in contact with remnants of country rock within the pluton and is interpreted to represent quenched hypersolvus granite. The enclaves in the transsolvus granite, some of which are compositionally similar to the hypersolvus granite, are interpreted to represent fragments of this quenched material; the other fragments represent quenched transsolvus granite. The pluton is surrounded by a purple to dark red fluorite-hematite breccia, delineating a ring-fault that contains angular fragments of the host rocks.

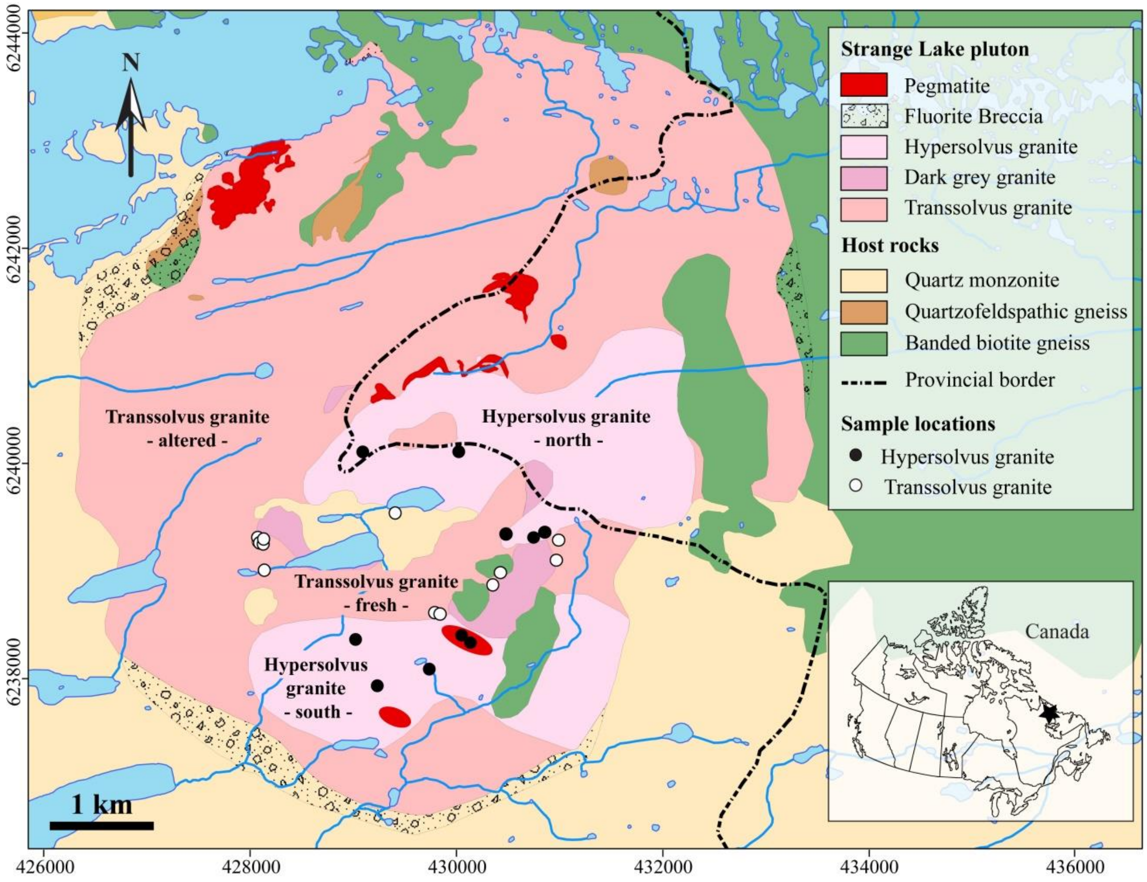

Fig. 3-1: Geological map of the Strange Lake pluton.

A geological map of the Strange Lake pluton showing the distribution of the major lithological units. Locations of the samples used in this study are indicated.

3.3.2 Hypersolvus granite

The hypersolvus granite has been subdivided into an equigranular and fine-grained northern part and a variably textured fine- to coarse-grained southern part (this study). Locally, the southern hypersolvus granite is coarse-grained and displays poikilitic to pegmatitic textures, which are also observed in drill core of the northern hypersolvus granite (not sampled). These poikilitic textured samples contain anhedral arfvedsonite oikocrysts enclosing smaller crystals of perthitic alkali feldspar, whereas the pegmatitic samples are coarse-grained and contain comb-textured arfvedsonite, quartz, K-feldspar and minor proportions of alkali zirconosilicate minerals. Both the northern and southern hypersolvus granite units are composed of perthitic feldspar, quartz, and sodic amphibole. Minor microcline and albite are present in the groundmass, either reflecting evolution of the magma to conditions in the two-feldspar stability field or subsolidus hydrothermal crystallization. A number of alkali feldspar crystals of the southern hypersolvus granite contain inclusions of fibrous astrophyllite. The quartz and sodic amphibole both occur interstitially to the perthitic alkali feldspar, and the amphibole appears to have crystallized later than the quartz (Fig. 3-2a). In most of the southern hypersolvus granite samples, the amphibole exhibits swapped margins with perthitic alkali feldspar (Fig. 3-2b). The amphibole contains numerous inclusions of fluorite and a Y-rich fluorite-fluocerite solid solution, particularly in the cores of crystals (Fig. 3-3a). In addition to the silicates mentioned above, a variety of interstitial zirconosilicate minerals, e.g., vlasovite, elpidite, dalyite and catapleiite replaced primary zircon (remnants of zircon in crystal cores). Titanosilicates occur mostly in the northern hypersolvus granite, and locally replaced the sodic amphibole. These minerals comprise dark red aenigmatite ($Na_2Fe^{2+}{}_5TiSi_6O_{20}$) and yellow fibrous astrophyllite ($(K,Na)_3(Fe^{2+})_7Ti_2Si_8O_{26}(OH)_4$) (Figs. 3-2c, 3-3b). The primary REE-minerals of both the northern and southern hypersolvus granite are monazite-(Ce) and fluornatropyrochlore. The monazite-(Ce) crystals are small and euhedral, and occur as inclusions in the perthitic alkali feldspar. Fluornatropyrochlore is more abundant, and occurs as pyramidal crystals in the groundmass, or as inclusions in the alkali feldspar. The oikocrystic and pegmatitic textured samples contain a much smaller proportion of primary REE minerals than the fine-grained varieties of the same unit. Fluorite is an abundant accessory mineral and forms small to large, rounded, translucent to purple inclusions in sodic amphibole or is disseminated interstitially through the rock. It is usually rimmed by the Y-rich fluorite-fluocerite solid solution, which is brighter in BSE images (Fig. 3-3a). Locally, gagarinite-(Y) occurs in association with fluorite and the fluorite-fluocerite solid solution, and is interpreted to be secondary.

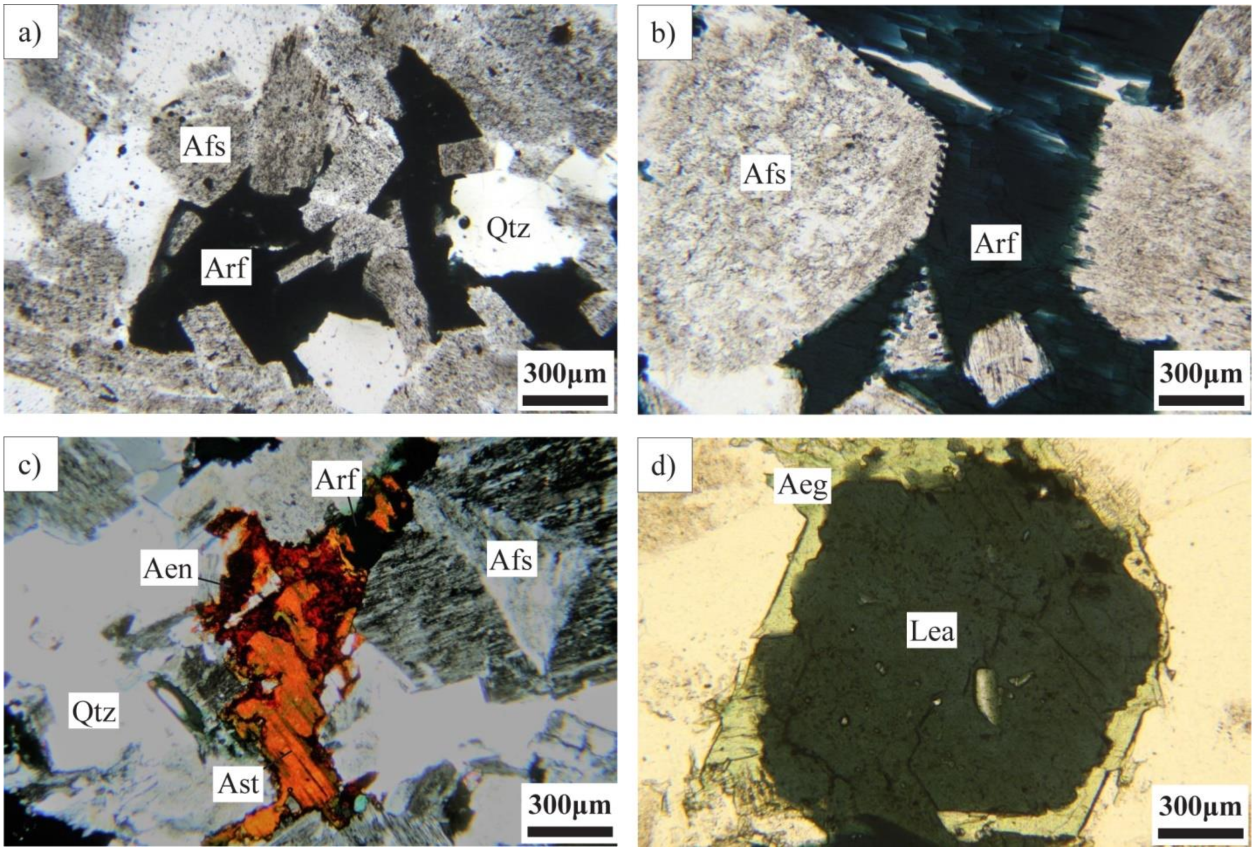

Fig. 3-2: Thin section photomicrographs of the amphibole group minerals

Thin section photomicrographs showing a) amphibole in hypersolvus granite (Arf), occupying interstices between alkali-feldspar (perthitic alkali feldspar) (Afs) and quartz (Qtz) (ppl view), b) amphibole in hypersolvus granite showing swapped margin texture with alkali-feldspar (ppl), c) interstitial amphibole in the northern hypersolvus granite that has been largely replaced by aenigmatite (red) (Aen) and astrophyllite (orange) (Ast) (xpl) and d) a Li-bearing amphibole (Lea) phenocryst in transsolvus granite that has been partly replaced by aegirine (Aeg) along its rim (ppl).

3.3.3 Transsolvus granite and enclaves

The transsolvus granite unit, which contains abundant fine-grained, dark grey ellipsoidal enclaves, surrounds and partially intruded the hypersolvus granite. The unaltered part of this intrusion at the center of the pluton is composed of the same major minerals as the hypersolvus granite, i.e., perthitic alkali feldspar, arfvedsonite and quartz. However, in contrast to the hypersolvus granite, microcline and albite form an essential part of the groundmass, indicating that the transsolvus granite crystallized at a lower temperature and/or higher pH_2O than the hypersolvus granite (Tuttle and Bowen, 1958). Amphibole in this granitic facies forms prismatic phenocrysts that locally contain inclusions of microcline and albite (Fig. 3-3c), but in contrast to amphibole in the hypersolvus granite, they rarely contain fluorite inclusions. Locally, the amphibole has been replaced by aegirine (Fig. 3-2d) and, in the more heavily altered parts of the pluton, hematite. Quartz forms round crystals that display a snowball texture, in which primary albite nucleated on the faces of the crystal. Alkali zirconosilicates, such as vlasovite and elpidite, occur intersitially, and usually occupy a larger proportion of the rock volume than in the hypersolvus granite. Narsarsukite ($Na_2(Ti,Fe^{3+})Si_4(O,F)_{11}$), the sole sodium-titanosilicate, occurs as large tabular beige poikilitic crystals, and is observed in the dark grey enclaves and in a number of transsolvus granite samples. Titanite has been reported to occur in the altered parts (Birkett et al., 1996), and is an abundant phase in the pegmatites of the transsolvus granite (Gysi et al., 2016). The primary REE minerals are fluornatropyrochlore, monazite-(Ce) and gagarinite-(Ce), which was replaced by bastnäsite-(Ce). Fluorbritholite-(Ce) occurs sparsely and interstitially in association with fluorite. Fluorite occurs as a late magmatic, interstitial (translucent) or hydrothermal (purple) phase, and is less abundant than in the hypersolvus granite. The transsolvus granite hosts a large number of NYF-type pegmatites with border zones of K-feldspar, quartz, sodic amphibole and alkali zirconosilicates, and a strongly altered core with quartz, fluorite and exotic REE minerals, as well as zircon and pyrochlore (Gysi and Williams-Jones, 2013). These pegmatites host the bulk of the rare metal mineralization in the deposit and have been the target of recent mineral exploration.

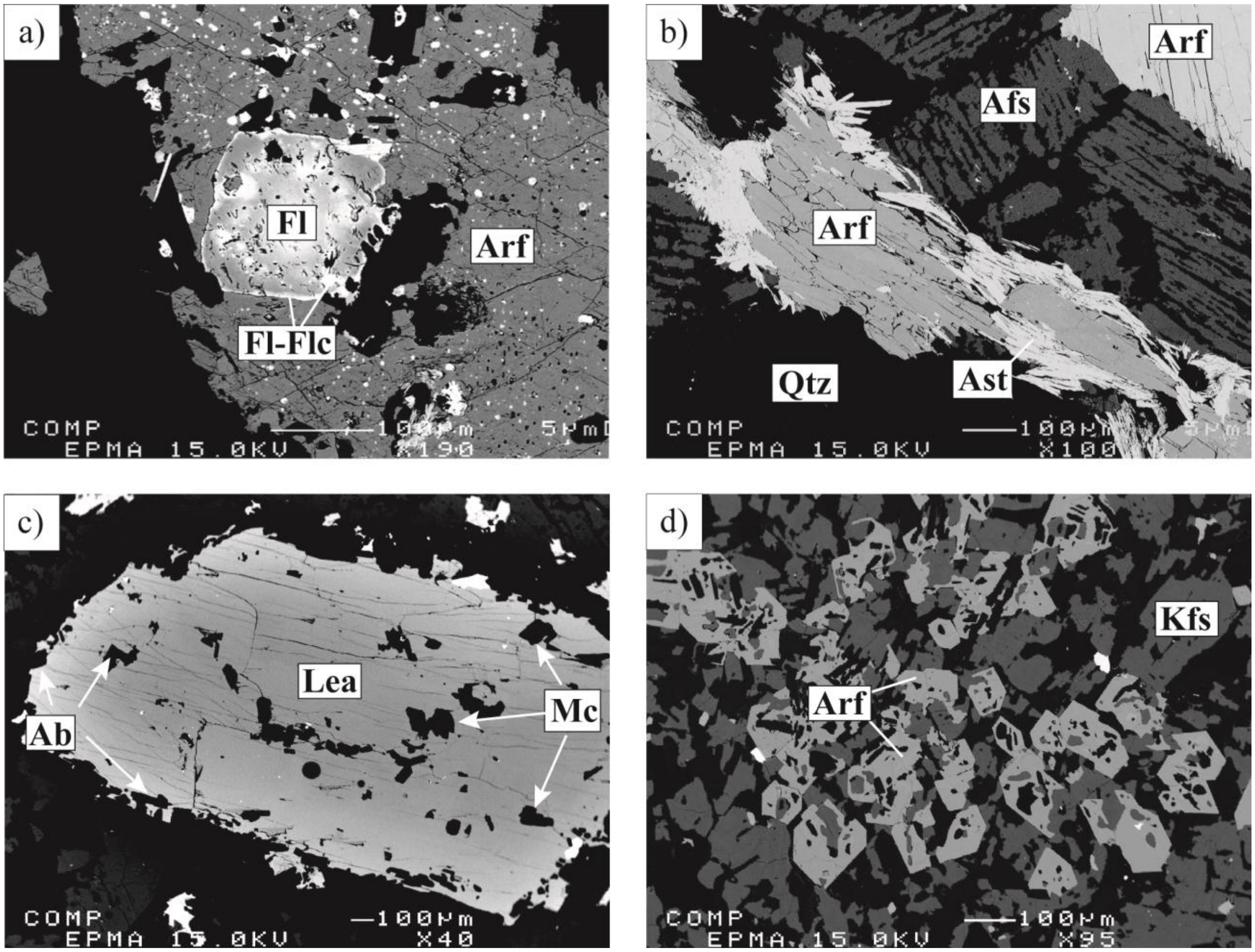

Fig. 3-3: Backscattered electron images of the amphibole-group minerals

a) Arfvedsonite with one large and numerous small fluorite (Fl) and fluorite-fluocerite solid solution (Fl-Flc) (brighter) inclusions (hypersolvus granite), b) amphibole interstitial to perthitic alkali feldspar and quartz (hypersolvus granite), replaced by fibrous astrophyllite along the rim, c) an euhedral Li-bearing alkali amphibole (ferro-ferri-fluoro-leakeite) crystal (transsolvus granite) containing numerous microcline (Mc) and albite (Ab) inclusions and, d) small subhedral amphibole crystals among K-feldspar (Ksp) and quartz crystals (enclave).

A dark grey, porphyritic microgranite exposed within the Strange Lake pluton contains perthitic alkali feldspar phenocrysts, quartz eyes and fine-grained subhedral to phenocrystic arfvedsonite in the groundmass (Fig. 3-3d). Locally, this unit was intruded by a leucocratic transsolvus granite, which, texturally and mineralogically, is similar to the dark grey enclaves observed in the transsolvus granite. This unit has a bulk composition slightly less evolved than, and a mineralogy similar to that of the transsolvus granite. The fine-grained, dark grey enclaves hosted by the transsolvus granite are ellipsoidal in shape, range from a few cm up to 50 cm in diameter and have sharp edge contacts in most cases. These enclaves are composed of perthitic alkali feldspar phenocrysts embedded in a matrix of fine-grained quartz, microcline, albite and finely distributed subhedral and locally phenocrystic sodic amphibole, which gives them their dark appearance.

3.4 METHODS

3.4.1 Material

The major and trace element compositions of the amphibole-group minerals were determined in 22 least-altered rock samples. All granite types occurring in the unaltered portion of the Strange Lake pluton were considered (Fig. 3-1). Bulk-rock compositions of the samples were provided by Quest Rare Minerals Ltd., and represent the results of analyses by Actlabs using XRF (X-ray fluorescence) for Nb, ISE-MS (ion selective electrode) for F, fusion-ICP-OES for major elements and fusion ICP-MS for most trace elements.

3.4.2 Electron-microprobe analyses

The composition of the amphibole-group minerals in 30µm thick, carbon-coated polished thin sections was determined using a JEOL JXA-8900L electron microprobe (EMP) at the Department of Earth and Planetary Sciences, McGill University. The beam current was 20 nA, the acceleration voltage 20 kV, and the beam diameter 10 µm. Counting times and standards used for analyses as well as detection limits based on repeated standard analyses are listed in the appendix (Table 3-7). To ensure analysis of the same spots by both EMP and LA-ICP-MS (see below), backscattered electron micrographs (BSE) of the analyzed grains were taken.

3.4.3 Laser-ablation analyses

Laser ablation ICP–MS (LA-ICP-MS) analyses were conducted on 16 samples using a NewWave 213 nm Nd-YAG laser-ablation system and a Thermo Finnigan iCapQc quadrupole ICP-MS at the Department of Earth and Planetary Sciences, McGill University. Six samples were analyzed at Université du Québec à Montreal (UQAM) using a Photon Machine G2 short-pulse (4ns) laser-ablation system (193 nm excimer) and a Nu AttoM high-resolution magnetic sector ICP-MS. The amphibole-group minerals were analyzed for selected major and trace elements in the same 30 µm-thick polished sections. NIST SRM 610 glass was used as the primary standard, and EMP data for both Si and Ti were used as internal references. The analyses were performed with a 5 Hz repetition rate, on material ablated from a 20 µm diameter pit. Data reduction was carried out using the software, Iolite, version 2.5. The estimated precision is 5-10 % for each element.

3.4.4 Amphibole formulae

The amphibole-group mineral formulae were calculated on the basis of O + OH + F = 24 atoms per formula unit (apfu) and OH = 2-2Ti, using the amount of Ti^{4+} as a proxy for the (maximum) oxy-component in the mineral structure (Hawthorne et al., 2012). The formula calculation was performed following the latest IMA 2012 recommendations (Hawthorne et al., 2012; Oberti et al., 2012) using the Excel spreadsheet of Locock (2014). On the basis of a preliminary formula calculation after Leake et al. (1997), the following cation normalization schemes were chosen:

Si-Ca+Li ≤ 15, Si-Na ≥ 15 and Si-K ≤ 16. As some fluorite inclusions in the amphibole from the hypersolvus granite were too small to be detected by imaging, analyses returning high concentrations of both Ca (> 3 wt. %) and F (> 2 wt. %) were removed from the dataset.

Table 3-1: Compositions of the unaltered Strange Lake granites

Average (median) bulk rock major and trace element compositions of the unaltered granites from the center of the pluton (*fgr = fine grained, $^+$pg = oikocrystic and pegmatitic samples)

Unit	Hypersolvus granite S fgr*		Hypersolvus granite S pg$^+$		Hypersolvus granite N		Transsolvus granite		Enclaves	
Samples	*7*		*8*		*12*		*24*		*12*	
(wt. %)		±		±		±		±		±
SiO_2	69.04	0.89	70.57	0.56	70.68	0.36	71.28	0.53	69.36	0.60
Al_2O_3	11.88	0.26	10.57	0.17	11.74	0.21	10.27	0.39	11.97	0.25
Fe_2O_3	5.78	0.31	6.72	0.52	4.89	0.08	5.98	0.47	5.05	0.10
MnO	0.10	0.01	0.11	0.01	0.10	0.01	0.12	0.01	0.09	0.02
MgO	0.04	0.01	0.02	0.01	0.05	0.01	0.03	0.01	0.04	0.02
CaO	0.73	0.19	0.37	0.11	0.57	0.03	0.45	0.18	0.83	0.15
Na_2O	4.92	0.17	5.11	0.05	5.09	0.10	5.08	0.35	3.60	0.98
K_2O	4.93	0.21	4.48	0.09	4.74	0.11	4.32	0.31	7.60	1.61
TiO_2	0.28	0.03	0.21	0.03	0.27	0.01	0.21	0.05	0.15	0.04
Nb_2O_5	0.03	0.01	0.05	0.01	0.06	0.005	0.05	0.02	0.02	0.02
P_2O_5	0.02	0.00	0.02	-	0.02	0.01	0.01	0.01	-	-
F	0.44	0.02	0.37	0.09	0.46	0.04	0.51	0.06	0.49	0.07
TREO	0.17	0.03	0.19	0.02	0.24	0.03	0.48	0.06	0.25	0.03
LREO	0.12	0.02	0.13	0.02	0.16	0.02	0.33	0.04	0.16	0.02
HREO+Y	0.05	0.005	0.06	0.01	0.08	0.01	0.11	0.04	0.09	0.01
LOI	0.72		0.47		0.70		0.72		0.83	
Total	98.53		99.19		99.14		99.20		99.68	
Agp index	1.13	0.02	1.23	0.02	1.15	0.03	1.27	0.03	1.17	0.02
Be *(ppm)*	36	8	40	14	53	11	54	22	31	7
Zn	285	40	545	30	465	60	585	90	465	145
Ga	45	3	52	3	44	1	60	3	48	5
Rb	417	23	436	31	522	47	672	99	925	241
Sr	18	5	15	5	21	7	21	8	21	5
Y	266	17	293	36	392	74	616	196	556	48
Zr	2413	667	2504	469	3656	268	4984	1917	1488	1126
Ba	76	13	43	8	85	18	43	15	58	14
La	228	33	221	35	305	51	630	81	286	47
Ce	464	73	485	72	629	79	1235	170	589	88
Pr	56	14	60	7	73	10	149	20	74	10
Nd	191	42	207	27	240	35	527	52	282	23
Sm	39	10	51	6	49	6	115	16	68	5
Eu	2	0.4	3	0.4	3	0.4	6	1	4	0.2
Gd	33	5	44	7	45	7	100	18	66	7
Tb	6	1	8	1	10	1	17	4	12	1
Dy	44	7	53	8	69	12	103	29	72	10
Ho	10	2	11	2	15	2	21	7	14	3
Er	33	6	36	7	50	6	64	24	37	10
Tm	5	1	6	1	8	1	9	4	5	2
Yb	36	3	42	9	57	4	58	29	25	10
Lu	6	0.4	7	1	9	1	8	4	4	1
Hf	69	12	67	12	97	15	136	47	42	31
Ta	14	1	20	4	28	4	25	13	7	5
Pb	94	17	169	53	137	38	187	73	38	21
Th	54	9	69	20	88	15	84	40	23	17
U	10	3	14	3	19	2	17	8	4	3

3.5 RESULTS

3.5.1 Bulk rock compositions

The average (median) major and trace element bulk-rock compositions of the unaltered Strange Lake granites are reported in Table 3-1. The agpaitic indices (molar [Na+K)/Al]) of all units are >1 and hence classify the rocks as peralkaline. The granites generally have low Ca and Mg and high alkali, Fe, F, Zn, Rb, Zr, Nb and REE concentrations. The evolution of the granites is reflected by decreasing Al, and increasing Si, Fe and incompatible element concentrations (i.e., REE, Nb, Zr). The agpaitic index also increases with evolution. The fine-grained southern hypersolvus granite, based on the above mentioned element concentrations, is interpreted to represent the least evolved rock unit. The oikocrystic / pegmatitic textured members of this unit has higher Si and Fe concentrations, a higher agpaitic index and slightly elevated REE and Zr concentrations. The concentrations of the HFSE (REE, Th, U, Nb, Zr, Hf) in the northern hypersolvus granite are higher, whereas Al concentrations are lower than those in the southern hypersolvus granite, suggesting that it is more evolved. The transsolvus granite generally has high Si, REE, Zr, Nb, Rb and F concentrations and significantly lower Al and Ca concentrations than the hypersolvus granite, and is considered to be the most evolved member of the suite. The dark grey enclaves hosted in the transsolvus granite have high Al, K and Ca, and low Na, Fe, Ti, Zr and Nb concentrations compared to the other granite types. Their REE concentrations are lower than those of their host, but higher than those of the hypersolvus granites.

3.5.2 Formula assignments

The amphibole-group minerals have the general structural formula, $AB_2C_5T_8O_{22}W_2$. The A-site of the Strange Lake amphiboles is occupied by Na^+ and minor K^+, and the B-site by Na^+ and Ca^{2+}, which assigns them to the alkali group. The octahedral C-site is occupied by Ti^{4+}, Zr^{4+},

Al^{3+}, REE^{3+}, Fe^{3+}, Zn^{2+}, Mn^{2+}, Fe^{2+}, Mg^{2+} and Li^{+}. The tetrahedral T-site is occupied by Si^{4+}, $^{T}Al^{3+}$ and in some cases $^{T}Ti^{4+}$. The W-site is dominated by the anions F^{-}, Cl^{-} and OH^{-}, which assigns the amphiboles to the hydroxy-fluoro-chloro-group, where ^{W}F > ^{W}OH, ^{W}Cl, and a “fluoro“-prefix is assigned to the amphibole name, which was the case for the majority of the crystals analyzed (see Table 3-2). In the matter of nomenclature, we have followed the latest IMA recommendations (Hawthorne et al., 2012; Oberti et al., 2012).

The C-site has a consistent under-occupancy (< 5 apfu), whereas the A-site has an over-occupancy (> 1 apfu) (see Table 3-2). Despite using a variety of calculation procedures (Hawthorne et al., 2012; Leake et al., 1997; Oberti et al., 2012), normalization schemes, and varying the Fe^{2+}/Fe^{3+} ratios and oxo-components, we were unable to reduce the under-occupancy and over-occupancy of the C- and A-sites, respectively. This issue has been reported to be common for alkali amphiboles in peralkaline rocks, such as arfvedsonite or riebeckite, by other researchers, who have deemed it to be an irresolvable artefact (Czamanske and Dillet, 1988; Hawthorne, 1976; Hawthorne et al., 1993). Hawthorne (1976) suggested that some of the B-site cations, notably Ca^{2+}, theoretically could be accommodated in the C-site on the basis of bond-length constraints. This would result in a total C-site occupation closer to 5 apfu, and shift the excess A-site cations to the B-site.

Table 3-2: Calculated formulae of the amphibole group minerals

Average calculated formulae and cation assignments (in apfu) of amphibole group minerals, based on 24 oxygens. Ideal site occupation is noted in brackets. The rock units are: HS S fgr (hypersolvus granite south, fine grained), HS N (hypersolvus granite north), EN (enclaves), TS (transsolvus granite).

Species	Arfved-sonite	'fluoro-arfvedsonite'	Ferro-ferri-leakeite	Ferro-ferri-fluoro-leakeite	Ferro-ferri-kato-phorite
Unit	HS S	all units	HS N	HS N, TS	HS S fgr
Analyses	*n=12*	*n=56*	*n=5*	*n=70*	*n=6*
Formula Assignments					
Si	7.64	7.83	7.64	7.74	7.53
Al	0.23	0.10	0.11	0.07	0.36
Ti	0.09	0.09	0.11	0.09	0.11
Fe^{3+}	0.10	0.03	0.15	0.12	-
T (8)	8.00	8.00	8.00	8.00	8.00
Ti	0.09	0.06	-	0.03	0.10
Zr	0.01	0.01	0.02	0.01	-
Al	0.10	0.05	-	-	-
REE	0.02	0.01	0.01	-	0.03
Fe^{3+}	1.66	1.70	1.99	2.01	1.36
Zn	0.08	0.04	0.11	0.05	0.06
Mn^{2+}	0.09	0.10	0.09	0.08	0.10
Fe^{2+}	2.62	2.49	1.96	2.00	3.02
Mg	0.06	0.04	0.05	0.02	0.09
Li	0.29	0.31	0.71	0.74	0.15
C (5)	4.87	4.75	4.94	4.92	4.91
Li	-	-	0.07	0.08	-
Ca	0.23	0.10	0.09	0.03	0.57
Na	1.77	1.90	1.87	1.95	1.43
B (2)	2.00	2.00	2.00	2.00	2.00
Na	0.79	0.89	0.87	0.86	0.69
K	0.28	0.31	0.31	0.33	0.26
A (0-1)	1.07	1.20	1.18	1.19	0.95
OH	1.05	0.70	0.93	0.61	1.14
F	0.72	1.07	0.85	1.20	0.44
Cl	0.01	-	-	-	0.01
O	0.23	0.22	0.21	0.19	0.41
W (2)	2.00	2.00	2.00	2.00	2.00

The occupancy of the A- and B-sites determines whether the amphiboles analyzed belong to the sodium subgroup (arfvedsonite, leakeite) or the sodium-calcium subgroup (katophorite), in which $^{B}Ca > 0.5$. Ferro-ferri-katophorite was identified in the least evolved fine- to medium-grained samples of the southern hypersolvus granite, exclusively. All the other amphiboles belong to the sodic subgroup, and in the cases of a calculated Fe^{2+}/Fe^{3+} ratio of 1.1 to 2.3, have been classified as arfvedsonite. The solid solution between the endmembers, arfvedsonite and katophorite, is displayed in Figure 3-4a. In principle, the location of endmember arfvedsonite could lie anywhere on the Na-K axis, as a potassic endmember has not been shown to exist in nature. The occupancy of the C-site divides the sodic amphibole subgroup into arfvedsonite and ferro-ferri-leakeite; the latter has $^{C}Li > 0.5$ apfu and a Fe^{2+}/Fe^{3+} ratio between 0.7 and 1.3. Ferro-ferri-leakeite is the principal amphibole in the transsolvus granite but also occurs in the northern hypersolvus granite. The fluoride-rich-variety (ferro-ferri-fluor-leakeite) was detected mainly in the transsolvus granite and its enclaves, whereas the fluoride-poor variety occurs predominantly in the northern hypersolvus granite. The composition of the analyzed solid-solution between the endmembers, arfvedsonite and ferro-ferri-leakeite, is displayed in Figure 3-4b. The slope of the trend from the arfvedsonite to leakeite endmembers indicates an increase in Fe^{3+} with increasing Li^{+}. The end-member stoichiometric formulae of the amphibole-group minerals present in the unaltered granites of the Strange Lake pluton are listed in Table 3-3.

Table 3-3: Amphibole and Ti-bearing minerals with their endmember structural formulae

Mineral name	Formula
Amphibole-group minerals	
(Fluoro)-arfvedsonite	$NaNa_2(Fe^{2+}{}_4Fe^{3+})Si_8O_{22}(OH,F)_2$
Ferro-ferri-(fluoro)-katophorite	$Na(NaCa)(Fe^{2+}{}_4Fe^{3+})Si_7AlO_{22}(OH,F)_2$
Ferro-ferri-(fluoro)-leakeite	$NaNa_2(Fe^{2+})_2(Fe^{3+})_2LiSi_8O_{22}(OH,F)_2$
Clinopyroxenes	
Aegirine	$NaFe^{3+}Si_2O_6$
Titano-silicates and Ti-oxide mineral	
Aenigmatite	$Na_2Fe^{2+}{}_5TiSi_6O_{20}$
Astrophyllite	$(K,Na)_3(Fe^{2+})_7Ti_2Si_8O_{26}(OH)_4$
Narsarsukite	$Na_2(Ti,Fe^{3+})Si_4(O,F)_{11}$
Titanite	$CaTiSiO_5$
Ilmenite	$Fe^{3+}TiO_3$

Table 3-4: Compositions of the amphibole group minerals

Average (median) major and trace element compositions with median absolute deviation (±) of the amphibole group minerals from the unaltered part of the pluton (*fgr = fine grained, $^+$pg = oikocrystic and pegmatitic samples)

Unit	Hypersolvus granite S fgr*		Hypersolvus granite S pg$^+$		Hypersolvus granite N		Enclaves		Transsolvus granite	
Analyses	*n=13*		*n=19*		*n=39*		*n=9*		*n=72*	
(wt. %)		±		±		±		±		±
SiO_2	48.29	0.51	49.97	0.80	50.71	0.19	50.71	0.93	51.02	0.52
Al_2O_3	1.47	0.30	0.99	0.15	0.50	0.08	0.36	0.01	0.34	0.05
TiO_2	1.45	0.30	0.84	0.12	1.09	0.14	0.92	0.08	0.71	0.09
FeO	33.67	0.42	33.80	0.41	32.06	0.27	31.78	0.22	32.47	0.38
MgO	0.72	0.05	0.64	0.05	0.85	0.03	0.71	0.08	0.56	0.04
MnO	0.34	0.07	0.10	0.08	0.22	0.03	0.09	0.03	0.08	0.03
ZnO	0.62	0.16	0.24	0.05	0.45	0.04	0.60	0.11	0.30	0.05
ZrO_2	0.04	0.02	0.06	0.03	0.17	0.04	0.13	0.03	0.11	0.03
Nb_2O_5	0.07	0.02	0.02	0.01	0.02	0.02	0.02	0.01	0.01	0.004
Na_2O	7.25	0.54	9.18	0.20	9.36	0.09	9.34	0.19	9.57	0.13
K_2O	1.27	0.15	1.28	0.12	1.59	0.11	1.73	0.09	1.65	0.09
CaO	2.79	0.69	1.11	0.50	0.47	0.08	0.13	0.05	0.13	0.03
F	1.29	0.31	1.97	0.27	2.08	0.12	2.05	0.18	2.56	0.15
Cl	0.03	0.01	0.02	0.01	0.01	0.01	-	-	0.01	0.005
Total	99.18		100.5		99.87		98.84		99.93	
Li *(ppm)*	1613	772	1450	615	3099	549	4802	931	5775	1260
Rb	58.8	17.8	20.9	6.3	61.8	9.4	88.7	15.5	84.3	18.6
Sr	23.3	6.8	8.5	3.0	11.7	3.7	4.0	1.4	1.4	0.5
Y	471	145	70.9	26.0	107	27	92.0	32.0	27.7	5.5
Zr	1208	653	647	124	2648	450	2073	234	1356	339
Sn	160	80.3	21.3	8.9	156	49	90.1	36.2	137	41
La	96.0	11.2	31.9	9.5	32.4	5.9	24.1	8.5	2.8	1.2
Ce	282	24	91.6	14.7	85.9	22.6	45.3	9.7	6.6	2.8
Pr	44.4	4.9	13.5	2.8	13.7	4.3	6.9	1.6	1.0	0.4
Nd	218	25	60.1	15.7	62.3	20.5	32.5	8.0	4.7	2.2
Sm	59.7	7.3	13.8	2.7	11.6	4.5	6.2	1.3	0.91	0.47
Eu	4.0	0.3	0.85	0.22	0.68	0.30	0.37	0.17	0.05	0.02
Gd	50.0	5.8	9.6	2.0	7.6	3.1	9.3	3.9	0.67	0.33
Tb	10.6	1.5	1.7	0.5	1.6	0.6	1.7	0.7	0.21	0.08
Dy	71.7	13.8	12.4	2.3	18.3	5.7	11.4	3.0	2.6	0.6
Ho	17.1	3.7	3.1	0.5	7.7	1.8	3.2	0.9	1.2	0.3
Er	69.7	21.2	15.1	2.9	48.5	12.3	14.9	1.2	8.1	1.4
Tm	14.2	4.4	4.3	1.0	17.5	4.8	4.6	0.8	2.7	0.5
Yb	144	52	53.1	11.8	215	53	52.4	5.7	35.9	6.3
Lu	29.5	11.6	11.7	2.6	50.1	11.5	12.8	3.1	8.6	1.9
Hf	60.3	35.8	27.5	7.0	130	25	85.0	20.6	63.6	17.6
Ta	9.0	1.7	2.2	0.4	2.9	0.8	1.9	0.6	1.1	0.3
Pb	77.9	8.0	8.9	5.1	34.5	10.5	10.7	4.6	5.8	1.7
Nb	468	116	124	51	214	34	109	20	92.4	13.8
Ba	10.5	6.3	3.4	2.5	6.0	2.4	1.9	0.9	0.43	0.26
Th	1.7	1.4	0.75	0.66	0.51	0.47	2.9	2.5	0.02	0.02
U	0.13	0.10	0.13	0.11	0.03	0.03	0.16	0.15	0.01	0.01
TREE+Y	1634	297	395	91	708	174	389	117	110	19

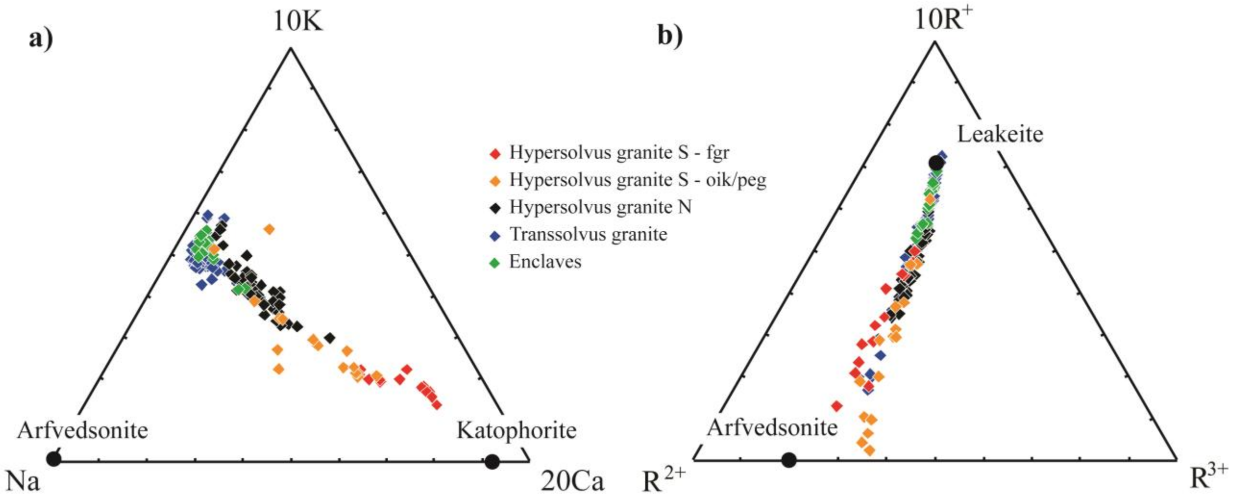

Fig. 3-4: Ternary diagrams of the amphibole group A-, B, and C-site occupancies.

Ternary diagrams showing a) the A-and B-site occupancy of the sodium-calcium to sodium amphibole-group minerals of the Strange Lake pluton (in apfu) (note that theoretically, endmember arfvedsonite can have any composition along the Na-K tie-line), and b) the C-site occupation of the amphibole-group minerals. The diagram (b) organizes the compositional data according to the valence state of the cations, where $R^+ = {}^{C}Li^+$, $R^{2+} = Fe^{2+}$, Mn^{2+}, Mg^{2+}, Zn^{2+} and $R^{3+} = Fe^{3+}$, ${}^{C}Al^{3+}$. The endmember compositions of katophorite (sodium-calcium), arfvedsonite and leakeite (sodium) are indicated on the diagrams. In the legend “fgr” (southern hypersolvus granite) refers to the fine-grained rocks of the unit, whereas “peg” stands for the oikocrystic to pegmatitic textured rocks.

3.5.3 Major elements

The major element compositions of the analyzed amphibole are reported in Table 3-4 (median values) and illustrated in Figure 3-5 relative to their Al content. Aluminum was chosen because the Al content of amphibole is commonly a reliable indicator of the differentiation of the corresponding magma, if alkali feldspar fractionation (perthitic alkali feldspar phenocrysts) was the major control on magma evolution (Hawthorne et al., 2001; Piilonen et al., 2013). As shown in Figure 3-5a, the Ca content decreases with decreasing Al content in a ratio slightly greater than 1:1, and is highest and shows the greatest range (~ 0.3 to 0.6 apfu) in the amphibole of the fine-grained granite from the southern hypersolvus granite. The Ca content is lower in the pegmatitic and oikocrystic textured samples of the same unit (0.1 to 0.35 apfu). Amphibole of the northern hypersolvus granite has a much lower Ca concentration, between 0.05 and 0.2 apfu. The lowest Ca concentrations are for amphibole in the enclaves and the transsolvus granite (≤ 0.1 apfu) (Fig. 3-5a). Sodium exhibits the opposite trend to Ca, with concentrations increasing with decreasing Al content. In the fine- to medium-grained samples of the southern hypersolvus granite, Na-contents are relatively low, between 2.1 and 2.6 apfu, whereas in the oikocrystic to pegmatitic samples, the Na contents are consistently higher, between 2.6 and 2.9 apfu, and are similar to those of the amphibole from the northern hypersolvus granite, the enclaves and the transsolvus granite (Fig. 3-5b). The Ti content of amphibole in the fine- to medium-grained samples of the southern hypersolvus granite has a similar range to that in the northern hypersolvus granite, i.e., from 0.08 to 0.22 apfu versus 0.1 to 0.21 apfu, but because of the much lower Al content of the amphibole in the northern hypersolvus granite samples, the two datasets display separate Ti-Al trends (Fig. 3-5c). Amphiboles in the oikocrystic to pegmatitic samples of the southern hypersolvus granite, the transsolvus granite and the enclaves all have relatively low Ti contents (0.06 to 0.16 apfu) (Fig. 3-5c). Silica in amphibole behaves similarly to Na, increasing in concentration with decreasing Al concentration. The lowest silica concentrations are those of the fine- to medium-grained samples of the southern hypersolvus granite (7.4 to 7.7 apfu) (Fig. 3-5d); the oikocrystic to pegmatitic samples display the largest range in amphibole Si content, from 7.4 to 8.0 apfu. Amphibole in the northern hypersolvus granite, the enclaves and the transsolvus granite has Si contents from 7.7 to 7.9, 7.6 to 7.9 and 7.6 to 8 apfu, respectively (Fig. 3-5d).

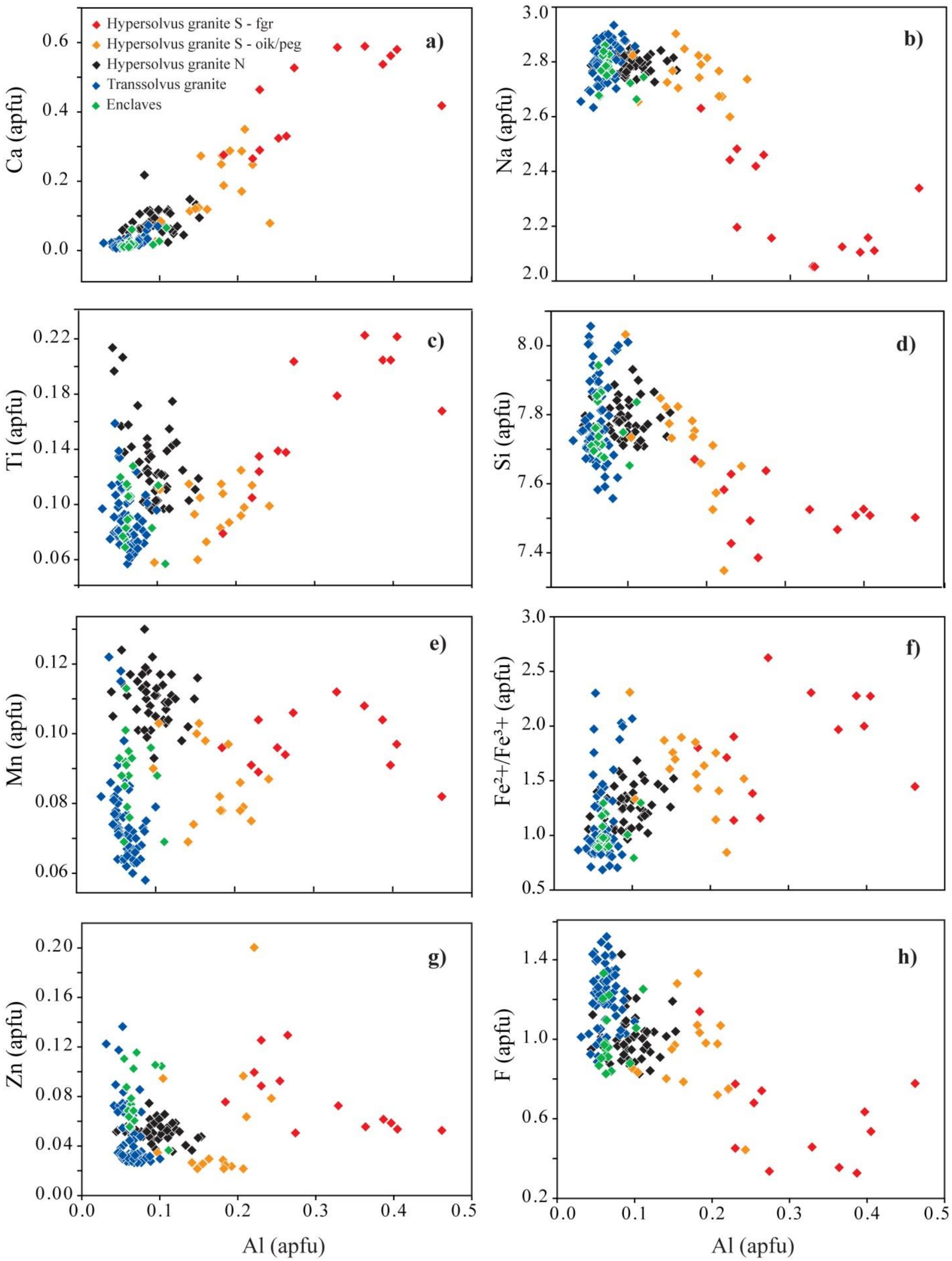

Hypersolvus granite S - fgr
Hypersolvus granite S - oik/peg
Hypersolvus granite N
Transsolvus granite
Enclaves
a)
Ca (apfu)
0.0
0.2
0.4
0.6
b)
Na (apfu)
2.0
2.2
2.4
2.6
2.8
3.0
c)
Ti (apfu)
0.06
0.10
0.14
0.18
0.22
d)
Si (apfu)
7.4
7.6
7.8
8.0
e)
Mn (apfu)
0.06
0.08
0.10
0.12
f)
Fe²+/Fe³+ (apfu)
0.5
1.0
1.5
2.0
2.5
3.0
g)
Zn (apfu)
0.00
0.04
0.08
0.12
0.16
0.20
h)
F (apfu)
0.2
0.6
1.0
1.4
0.0
0.1
0.2
0.3
0.4
0.5
Al (apfu)
0.0
0.1
0.2
0.3
0.4
0.5
Al (apfu)

Fig. 3-5: Binary diagrams of the amphibole group elemental compositions

Binary diagrams showing major and minor element concentrations of amphibole in atoms per formula unit (apfu), all as a function of Al concentration (X-axis). The decreasing Al content monitors the differentiation of the magma.

Manganese contents of amphibole are highest in the northern hypersolvus granite (0.09 – 0.12) and show the greatest range in the transsolvus granite (0.06 – 0.12) (Fig. 3-5e). They are broadly similar for amphibole from the enclaves and the southern oikocrystic to pegmatitic hypersolvus granite (0.07 – 0.10), and range from 0.08 to 0.11 for amphibole from the fine-grained southern hypersolvus granite. The calculated Fe^{2+}/Fe^{3+} ratios correlate weakly with the Al concentrations. Amphibole from the fine-grained southern hypersolvus granite generally has the highest Fe^{2+}/Fe^{3+} ratio; amphibole from the enclaves, the northern hypersolvus granite and many of the transsolvus granite samples has a low ratio (Fig. 3-5f). Zinc concentrations are slightly elevated for the amphibole from the fine-grained samples of the southern hypersolvus granite (avg. 0.08 apfu) and the enclaves (avg. 0.07 apfu), compared to the amphibole of the northern hypersolvus granite, the transsolvus granite and the oikocrystic and pegmatitic samples of the southern hypersolvus granite (all avg. 0.05 apfu) (Fig. 3-5g). Fluorine concentration is highest in the amphibole of the transsolvus granite (1.0 - 1.4 apfu), lowest for the crystals of the (fine-grained) southern hypersolvus granite (0.2 – 0.8 apfu) and is intermediate (avg. ~ 1 apfu) for all the other granite units.

The amphibole phenocrysts of the transsolvus granite differ only slightly in composition from core to rim (Fig. 3-6; Table 3-5). The phenocryst cores have total Al and Si contents averaging 0.06 (apfu) and 7.9 (apfu), respectively, a considerable range in Ca concentration (~0.1 to 0.5 apfu, avg. 0.03 apfu), Na and K contents averaging 2.8 and 0.33 apfu, respectively, a Fe^{3+} content averaging 1.8 apfu, a Mg content averaging 0.03 apfu, a total Ti content of 0.09 apfu (avg.), Mn and Zn contents averaging 0.07 and 0.05 apfu (avg.), respectively, and a F content averaging 1.2 apfu. The phenocryst rims have lower concentrations of Al (avg. 0.06 apfu), Si (7.7 apfu), Ca (avg. 0.02 apfu), Na (avg. 2.8 apfu), Mg (avg. 0.02) and F (avg. 1.1 apfu), and higher concentrations of total Fe^{3+} (avg. 2.2 apfu), K (avg. 0.4 apfu), total Ti (0.1 apfu), Mn and Zn (avg. 0.09 and 0.07 apfu, respectively).

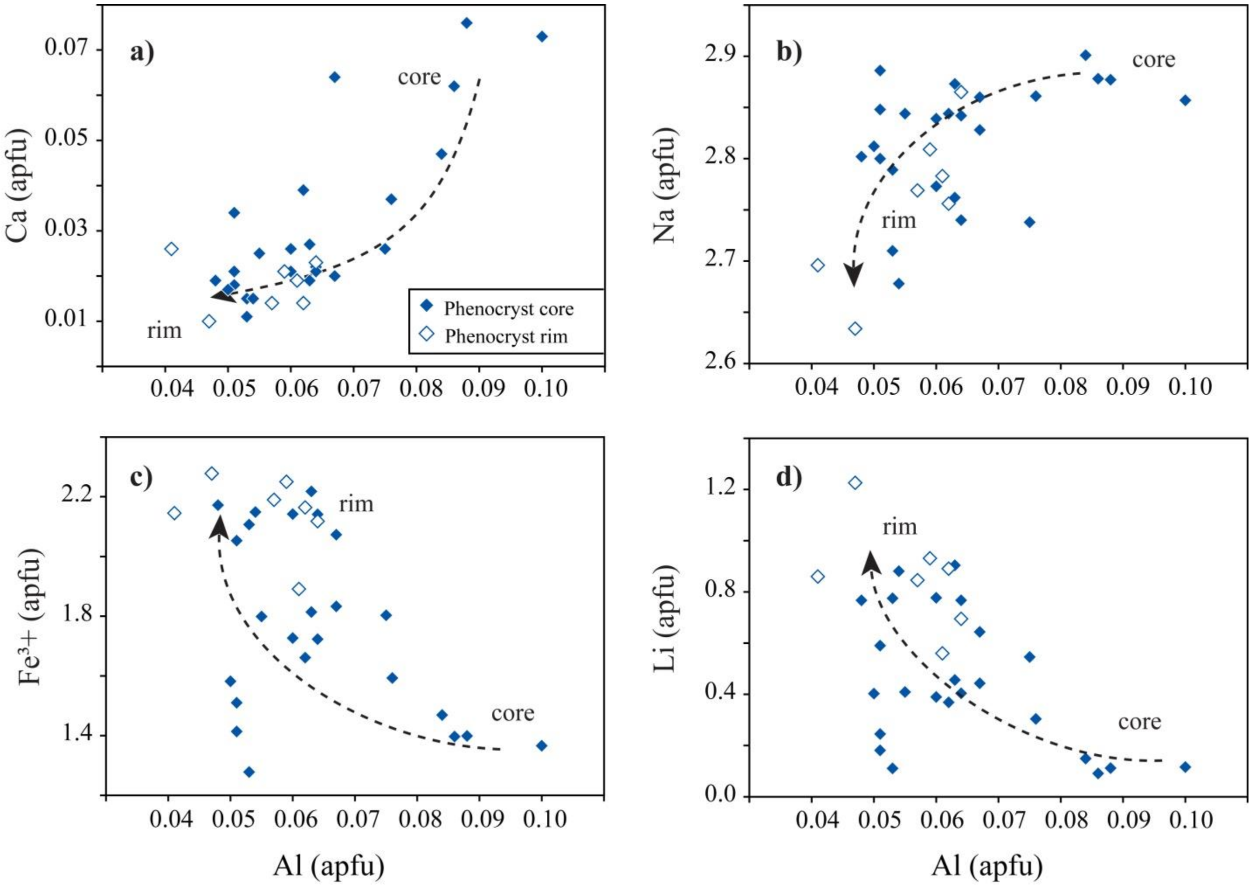

Fig. 3-6: Diagram showing core and rim elemental concentrations of amphibole phenocrysts

Binary diagrams showing the changing concentration (apfu) of selected elements as a function of Al concentration (dashed arrows) from the cores to rims of amphibole phenocrysts in the transsolvus granite.

Table 3-5: Core and rim compositions of amphibole phenocrysts

Average (median) core and rim compositions (in apfu) with median absolute deviation (±) of selected phenocrysts from the transsolvus granite

Location	Core		Rim	
Analyses	*n=24*		*n=7*	
		±		±
^{T}Si *(apfu)*	7.906	0.102	7.716	0.039
^{T}Al	0.059	0.006	0.059	0.003
^{T}Ti	0.072	0.010	0.083	0.008
^{T}Fe^{3+}	0.143	0.030	0.135	0.025
^{C}Ti	0.084	0.016	0.001	-
^{C}Zr	0.008	0.003	0.008	0.002
^{C}Al	0.052	0.019	-	-
^{C}REE	0.002	0.001	0.002	-
^{C}Fe^{3+}	1.763	0.215	2.022	0.007
^{C}Zn	0.034	0.006	0.072	0.015
^{C}Mn^{2+}	0.072	0.004	0.081	0.007
^{C}Fe^{2+}	2.441	0.321	1.952	0.058
^{C}Mg	0.026	0.006	0.014	0.001
^{C}Li	0.407	0.232	0.825	0.044
^{B}Li	0.051	0.024	0.066	0.024
^{B}Ca	0.024	0.006	0.019	0.005
^{B}Na	1.973	0.009	1.964	0.017
^{A}Na	0.867	0.042	0.838	0.037
^{A}K	0.317	0.011	0.347	0.050
^{W}F	1.205	0.057	1.027	0.122
total Ti	0.156	0.026	0.083	0.008
total Al	0.111	0.025	0.059	0.003
total Fe^{3+}	0.074	0.011	2.164	0.046
total Na	1.906	0.245	2.769	0.040
total Li	8.034	0.006	0.860	0.071
total Fe	0.156	0.020	0.825	0.044
Fe^{2+}/Fe^{3+}	2.449	0.324	2.134	0.040

3.5.4 The REE and other trace elements

The shapes of the chondrite-normalized amphibole REE profiles (Sun and McDonough, 1989) are similar for all the granite units and, in general, are characterized by relatively flat light and middle REE parts, a marked negative Eu-anomaly (Eu/Eu* = 0.04-0.66) and an enrichment in the HREE (Fig. 3-7). However, the absolute REE concentrations differ considerably. The amphiboles of the fine-grained samples of the southern hypersolvus granite have the highest total REE concentration, on average (median value) 0.16 ± 0.03 wt. % (Table 3-4). By contrast, oikocrystic to pegmatitic samples of the same unit have much lower amphibole REE concentrations, on average, 0.04 ± 0.01 wt. %. The total REE concentrations of amphibole in the northern hypersolvus granite are intermediate between those of the fine-grained and oikocrystic to pegmatitic southern hypersolvus granite, averaging 0.07 ± 0.02 wt. %. Amphiboles of the transsolvus granite and its enclaves have much lower total REE concentrations, averaging 0.01 ± 0.002 wt. % and 0.04 ± 0.01 wt. %, respectively (Table 3-4). The amphibole REE concentrations are between 10^2 and 10^3 times the chondrite values (Fig. 3-7c, e).

The contents of the individual REE in the amphiboles are significantly lower (in the case of the light REE (LREE), more than an order of magnitude lower) than their respective bulk host rock concentrations, except for the heaviest of the REE, Yb and Lu, which are significantly higher (Fig. 3-7). In the case of the fine-grained southern hypersolvus granite, the exception extends to the middle REE and for Yb and Lu the content in amphibole is about four times higher than the bulk rock content (Fig. 3-7a). The concentrations of Yb and Lu of the amphiboles from the northern hypersolvus granite exceed the bulk rock concentrations to a similar degree (Fig. 3-7c). The largest difference between amphibole and bulk rock REE concentrations is exhibited by the transsolvus granite, which has considerably higher concentrations in the bulk rock except for Yb and Lu; the amphibole in this unit also shows the steepest chondrite-normalized rise in HREE concentration (Fig. 3-7e). The amphiboles in the dark-grey enclaves hosted by this unit have elevated light to middle REE compositions compared to that of amphibole in the transsolvus granite, whereas the Tm, Yb and Lu concentrations are within the range of their host (Fig. 3-7e).

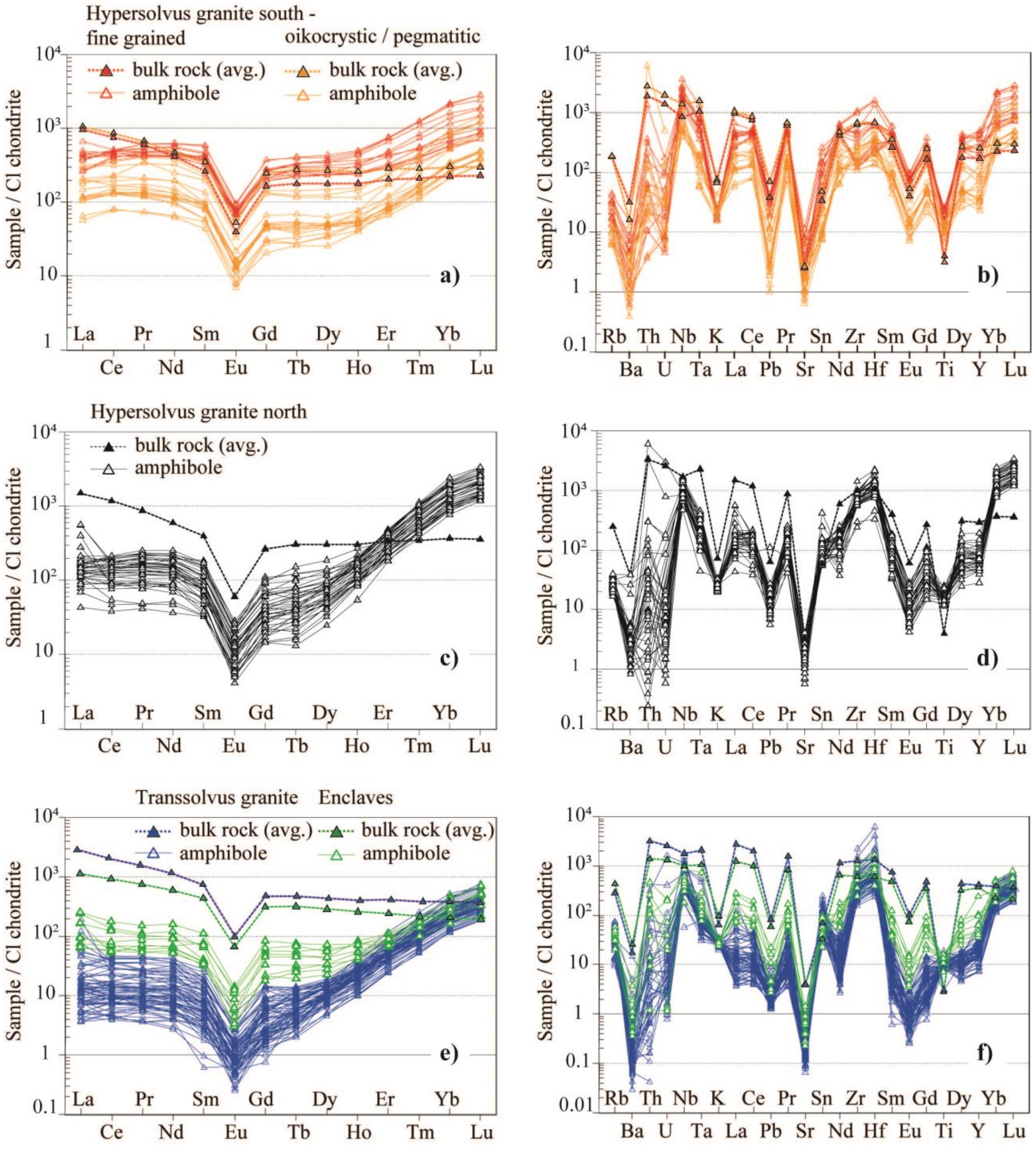

Fig. 3-7: Chondrite-normalized REE-and trace element profiles of the amphibole group

Profiles of the amphibole group minerals are displayed with the average bulk rock profiles of the respective units. a) REE- and b) trace element spider diagram for the southern hypersolvus granite; c) REE- and d) trace element spider diagram for the northern hypersolvus granite; and e) REE- and f) trace element spider diagram for the transsolvus granite and enclaves. The chondrite values are from Sun and McDonough, 1989.

As is the case for the REE, the contents of most of the other trace elements are considerably lower in the amphibole-group minerals than in the average bulk-rock (other than in the southern fine- to medium-grained hypersolvus granite). Conspicuous exceptions are Nb, Zr and Hf, which in addition to being present in zircon, monazite-(Ce) and the pyrochlore group minerals, are also accommodated by the amphibole. The chondrite-normalized trace element profiles for the amphiboles in all granite units have negative Ba, U, K, Pb, Sr, Eu, Ti and Y anomalies, and positive Th, Nb, Ta, Sn, REE, Zr and Hf anomalies, whereas the average bulk rock has negative Ba, K, Pb, Sr, Eu, and Ti and positive Th, U, Nb, Ta, REE, Zr, Hf and Y anomalies (Fig. 3-7). Thus, although the behavior of most elements in the amphibole is similar to that in the host rock, U and Y show opposite behavior, i.e., their concentrations are anomalously low in the amphibole and high in the bulk rock. Zirconium concentrations are lowest in amphibole from the southern hypersolvus granite (avg. 0.07 to 0.12 wt. %), and reach more than double these concentrations in amphibole from the northern hypersolvus granite (~0.26 wt. %). Concentrations are intermediate between these extremes in the amphibole of the transsolvus granite (~0.14 wt. %) and enclaves (~0.21 wt. %). Lithium concentrations, on average, are lowest in amphibole of the southern hypersolvus granite (avg. 0.15 to 0.16 wt. %), significantly higher in amphibole of the northern hypersolvus granite (avg. 0.31 wt. %) and by far the highest in amphibole of the transsolvus granite (avg. 0.58 wt. %) and enclaves (avg. 0.48 wt. %). However, they vary greatly among samples, and, to a lesser extent, among crystals in the same sample (see Table 3-4).

Differences in the chondrite-normalized REE profile are particularly marked among the five amphibole types identified in this study. Sodium- and calcium-rich ferro-ferri-katophorite as well as arfvedsonite have the highest total REE concentrations; their average La_N/Yb_N ratios are 0.23 and 0.49, respectively (Fig. 3-8). ‘fluoro-arfvedsonite’ and Li-rich ferro-ferri-leakeite both have intermediate REE concentrations and a more prominent HREE enrichment with an average La_N/Yb_N ratio of 0.09 and 0.14, respectively. Ferro-ferri-fluoro leakeite has by far the lowest total REE concentration, and it exhibits the strongest relative HREE enrichment with an average La_N/Yb_N ratio of. 0.04.

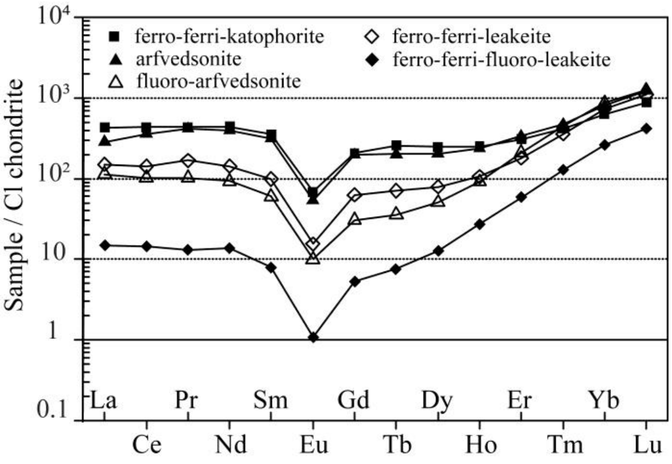

Fig. 3-8: Chondrite-normalized REE-profiles of the amphibole species

Chondrite-normalized REE-spider diagrams showing the average distribution of the elements corresponding to the amphibole species identified in the Strange Lake pluton. The chondrite values are from Sun and McDonough, 1989.

3.6 DISCUSSION

3.6.1 Amphibole composition as a tracer of granite differentiation

The variations in the major and trace element chemistry of amphibole in the Strange Lake pluton are interpreted to reflect the evolution of the granitic melt. The earliest intrusive phase was the hypersolvus granite, which has been subdivided into a southern and a northern part on the basis of compositional and mineralogical differences. In both units, the amphiboles, mainly (fluoro)-arfvedsonite’ (n=49) and minor (fluoro)-katophorite (n=6), occur interstitially to perthitic alkali feldspar and quartz, and thus were the last of the main rock-forming minerals to crystallize. By contrast, in the more evolved transsolvus granite, the amphibole, mostly ‘fluoro-arfvedsonite’ and ferro-ferri-(fluoro)-leakeite (n=55), occurs as phenocrysts together with minor perthitic alkali feldspar, and therefore crystallized prior to the emplacement of this granite facies. This difference in the timing of crystallization of the amphibole, as we will show below, played a crucial role in determining the extent to which incompatible elements, such as the REE and other HFSE, were incorporated in its crystal structure.

3.6.2 Magma evolution monitored by A-and B-site occupancy

In the hypersolvus granite, the A- and B-sites are occupied mainly by Na, but also by considerable Ca in some samples of the southern hypersolvus granite (see Fig. 3-4a). The high density of fluorite inclusions also suggests that the early melt was relatively rich in Ca. The occupation of the B-site by the bivalent Ca ion was balanced by Al^{3+} at the T-site. With increasing degree of differentiation, Na^+ substituted for Ca^{2+} and Si^{4+} for Al^{3+} (see Figs. 3-5a, b, d). This coupled substitution can be expressed by the relationship:

$$^{B}Ca^{2+} + {}^{T}Al^{3+} \rightarrow {}^{B}Na^{+} + {}^{T}Si^{4+}$$

A similar correlation of decreasing Ca and increasing Si in amphibole with magmatic evolution has been documented for silica-undersaturated alkaline intrusive suites, namely Ilímaussaq in southern Greenland (Marks et al., 2004), the Khibiny complex in the Kola Peninsula of Russia (Konopleva et al., 2008), and the alkaline pegmatites of the silica-undersaturated to -saturated Larvik plutonic suite of the Oslo Rift in Southern Norway (Piilonen et al., 2013). In these three locations, the amphibole composition evolved from calcic to sodic-calcic to sodic varieties with increasing degree of differentiation, reflecting the increasing alkalinity of the corresponding magma.

As the Ca content is highest in amphibole of the fine- to medium-grained southern hypersolvus granite (see Fig. 3-5a), we interpret this unit to be the earliest and least evolved intrusive facies of the Strange Lake pluton. The much lower content of Ca in amphibole of the oikocrystic to pegmatitic textured granites from the same unit is consistent with the interpretation that these rocks crystallized from residual melts. Consistent with these interpretations, the northern hypersolvus granite, in which amphibole has a relatively low Ca (and Al) concentration, represents the intrusion of a separate and more evolved batch of magma.

The amphibole of the transsolvus granite generally has low Ca- and Al-, as well as high Na- and Si-concentrations (see Fig. 3-5a, b, d), which all point towards a significantly more evolved melt. As the amphibole of this unit crystallized early (it occurs as phenocrysts), as opposed to the hypersolvus granite, the transsolvus granitic melt was more evolved from the outset. The evolution of this melt is monitored by the compositional differences between phenocryst cores and rims. For example, Ca, Na and Al concentrations decrease from core to rim (see Fig. 3-6, Table 3-4). Decreasing Ca and Al concentrations mirror the evolution to a more alkaline magma composition, which was caused by alkali feldspar fractionation (Boily and Williams-Jones, 1994). The unexpected depletion of Na in the rims, however, is likely an artefact of the exsolution of a Na-rich fluid at a later stage of crystallization (Salvi and Williams-Jones, 1996; Roelofsen, 1997; Gysi et al., 2016), and/or the onset of albite crystallization. Not surprisingly, given the generally very low Ca and Al contents (close to zero) (Fig. 3-5a) and very high Na (Fig. 3-5b) content of the amphibole, compared to those of the hypersolvus granite, the transsolvus granite is the most evolved of the intrusive units considered in this study. The enclaves in this unit contain amphibole with slightly higher Ca, and Al, and lower K and F concentrations than the crystals in the host granite (see Fig. 3-5), which points to a slightly less evolved composition. Nonetheless, their close compositional resemblance to the crystals of the transsolvus granite, indicates that they may be part of the same intrusion.

3.6.3 Magma evolution monitored by the C-site occupancy

3.6.3.1 Implications of the Fe^{2+}/Fe^{3+} ratio

The C-site of the amphibole-group minerals in the Strange Lake complex mainly hosts Fe^{2+} and Fe^{3+}, but also Li^{+}, Mg^{2+}, Mn^{2+}, Zn^{2+}, Ti^{4+} and Zr^{4+} in significant proportions. The Fe^{2+}/Fe^{3+} ratio of a magma is controlled by the fO_2, and may be recorded by the amphibole composition. However, Fe^{3+} also becomes more or less compatible in the amphibole structure depending on its overall composition, and the exchange vectors that operate. In particular, the incorporation of Na at the expense of Ca is charge-balanced by 3+ elements in the exchange vector: Ca + (Mg, Fe^{2+}) = Na + (Al, Fe^{3+}). When Al contents are depleted in the melt (e.g., increasing peralkalinity), Fe^{3+} becomes progressively more important in this exchange vector. In this case, the amphibole Fe^{2+}/Fe^{3+} ratio will vary with the Na/Ca ratio in rocks with the same major mineral paragenesis. In the late amphibole of the hypersolvus granite, Fe^{2+}/Fe^{3+} ratios of the northern unit are lower and have higher Na/Ca ratios than the amphibole of the southern unit (Fig. 3-9), which suggests that incorporation of Fe^{3+} in the structure, to some degree, was tied to the lower Ca content of the amphibole. However, as the correlation between Fe^{2+}/Fe^{3+} and Na/Ca is not 1:1, it is likely that there was an additional effect on the Fe^{2+}/Fe^{3+} ratio, e.g., oxidation. Oxidation of a magma commonly occurs following fluid exsolution from the magma, due to decomposition of H_2O to H_2 and ½O_2, and the subsequent loss of the much faster diffusing H_2 (Czamanske and Wones, 1973). As the amphibole crystallized late in this facies, it can be inferred that the cooling intrusion had experienced some degassing and subsequent fluid loss at this point. Even in the freshest units (e.g., the hypersolvus granite) of the Strange Lake pluton, there is evidence of

H_2O-saturation at a late stage of in-situ evolution, e.g., the albitization of K-feldspar, the hydrothermal alteration of primary REE-minerals and the crystallization of hydrothermal REE-phases, such as gagarinite-(Y) after fluorite (Gysi et al., 2016; Vasyukova and Williams-Jones, 2016).

The amphibole of the transsolvus granite and enclaves generally has a low Fe^{2+}/Fe^{3+} ratio (see Fig. 3-5f). In addition, the phenocrysts rims have elevated Fe^{3+} concentrations compared to their cores (see Fig. 3-6c) which can be related to increasing fO_2. The amphibole rims may have continued to crystallize after emplacement, when the magma experienced degassing and oxidation. In addition, some correlation between Fe^{2+}/Fe^{3+} and Na/Ca suggests that crystal chemical effects (high Na/Ca ratio), partially caused the low Fe^{2+}/Fe^{3+} ratio (Fig. 3-9). However, as the correlations are not 1:1, this indicates that a process, in addition to crystal chemical effects and oxidation, caused the high Fe^{3+} content. In peralkaline igneous systems, high concentrations of F^- and OH^- in the melt allow more Fe^{3+} to be present at a given fO_2 (Birkett et al., 1996; Giehl et al., 2013). The high proportion of Fe^{3+} in the amphibole was likely caused by an increasing proportion of anions, notably F^- and OH^- in the evolving melt. This is manifested by significantly higher F concentrations in the amphibole phenocrysts, compared to the amphiboles of the hypersolvus granite (see Table 3-3).

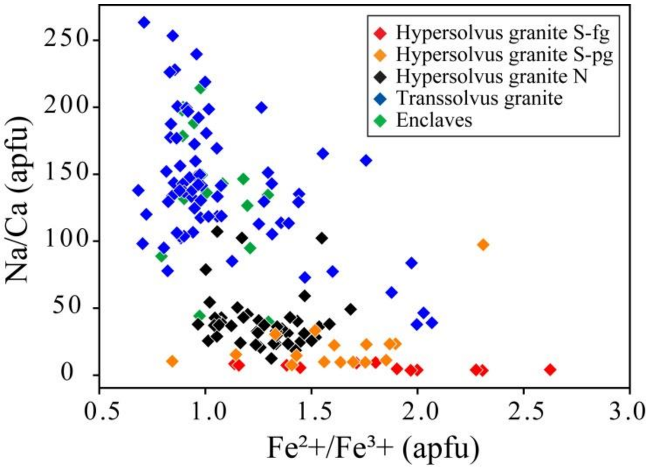

Fig. 3-9: The amphibole Fe^{2+}/Fe^{3+} ratio as a function of the Na/Ca ratio Binary diagram showing the amphibole Fe^{2+}/Fe^{3+} ratio as a function of the Na/Ca ratio in both, hypersolvus and transsolvus granite indicating a (low degree) coupled behavior of the ratios in rocks with the same major phase paragenesis.

3.6.3.2 Titanium, manganese and zinc concentrations

The titanium concentration of the amphibole-group minerals in alkaline rocks is an important indicator of the melt evolution owing to the incompatible nature of Ti. Indeed Ti^{4+} was preferentially incorporated into the late crystallizing amphibole of the hypersolvus granite and much less so in the phenocrysts of the transsolvus granite (see Fig. 3-5c). From bulk rock compositions, we know that both the southern and northern hypersolvus granitic magmas were relatively enriched in TiO_2 (on average, 0.3 wt. % in both units). However, the amphibole of the southern unit has a much higher TiO_2 concentration (avg. 1.5 wt. %) than the northern unit (avg.1.1 wt. %).

The proportion of the amphibole in each granite unit was estimated using the MINSQ excel spreadsheet of Herrmann and Berry (2002), which applies a least squares method to bulk rock and mineral compositions in order to determine the normative mineralogy of a sample.

Proportions of the bulk TiO_2 contributed by the mineral group were estimated from the amphibole proportion and the TiO_2 content. The fine-grained southern hypersolvus granite contains ~14 wt. % amphibole, which hosts ~70 % of the bulk TiO_2. The northern hypersolvus granite contains only ~11 wt. % amphibole, which hosts about 40 % of the bulk TiO_2. The remaining titanium is concentrated in aenigmatite and astrophyllite, sodium-titanosilicate minerals, which are present almost exclusively in the northern hypersolvus granite (see Fig. 3-2d). In the southern hypersolvus granite, the missing 30 % is concentrated mostly in secondary astrophyllite, which occurs as inclusions in the alkali feldspar. Both the transsolvus granite and its enclaves have bulk rock Ti concentrations of ~0.2 wt. % and significantly lower concentrations in amphibole (0.7 and 0.9 wt. %, respectively). As the amphibole is a phenocryst phase, it did not incorporate the relatively incompatible Ti^{4+}. However, a slight increase in total Ti concentration from phenocryst cores to rims (avg. 0.09 to 0.1 apfu) is consistent with the internal evolution of this unit. In both the transsolvus granite and its enclaves, about 58 % of the bulk TiO_2 is hosted by the amphibole. The transsolvus granite has an elevated proportion of amphibole (~18 wt. %), whereas the enclaves contain much lower proportions of the mineral (~12 wt. %), due to density separation that occurred in the magma chamber. The remaining TiO_2 in this unit is concentrated mostly in the Na-Ti-silicate, narsarsukite.

Several studies have reported a strong positive correlation between Ti^{4+} and O^{2-} concentrations in amphibole, which is reflected in the relationships, ${}^{C}Ti = Ti$ and $O^{2-} = 2Ti^{4+}$ with the limit of ${}^{W}[2-(OH, F, Cl)]$. This means, that if the F, Cl and Ti concentrations of the amphibole are measured, and a maximum of 2 apfu for the W-site is assigned, the OH- (and O-) proportion can be estimated using the relationship OH = 2 – (2Ti – F – Cl) (Hawthorne et al., 2012; King et al., 1999; Leake, 1968; Oberti et al., 2012). Following this protocol, hydroxyl (OH^-) and oxygen

(O^{2-}) are essential components of the amphibole from the southern hypersolvus granite (>1 apfu) (Fig. 3-10), whereas in the other, more evolved granite units, F^- is the dominant W-site anion (see Figs. 3-5h, 3-11b). Abundant fluorite inclusions in the amphibole of this unit (see Fig. 3-3a) indicate that fluorite saturated prior to the amphibole. This suggests that in the early and least evolved magma, the late amphibole crystallized from a water-rich, F-poor, residual magma. In the northern hypersolvus residual granitic melt, more F^-, in addition to oxygen, was available to be incorporated in the amphibole (see Figs. 3-5h, Fig. 3-10). In both hypersolvus granite units (south and north), high Ti^{4+} concentrations required significant proportions of O^{2-} (0.2 to 0.45 apfu) to balance the higher charge of the C site. The phenocrysts of the transsolvus granite have high proportions of F^-, and low proportions of O^{2-} and OH^- occupying the W-site (see Figs. 3-5h, 3-10). This implies a highly F-enriched melt from the outset (phenocryst cores).

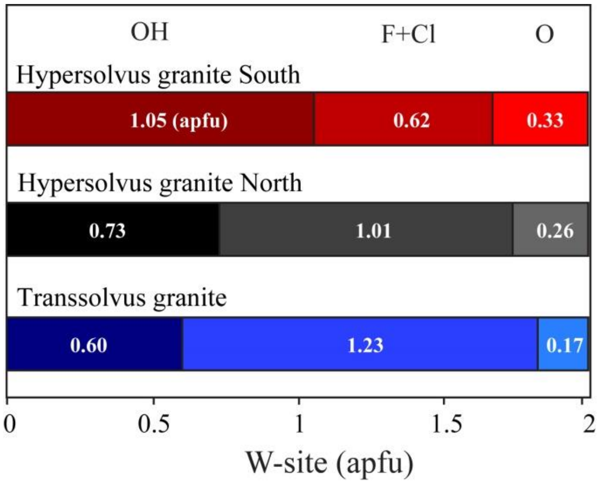

Fig. 3-10: Anion occupation of the W-site

Bar diagram showing the (average) relative proportion of the anions occupying the W-site for each granite unit.

Elevated Mn-concentrations in the amphibole of the northern hypersolvus granite compared to those of amphibole in the fine-grained samples of the southern unit (see Fig. 3-5e) point to a progressive increase in Mn^{2+} concentration with hypersolvus granite evolution. The relatively incompatible behavior of Mn^{2+} compared to Fe^{2+} was likely caused by the larger ionic radius of $^{C}Mn^{2+}$ (r=0.83Å) over Fe^{2+} (r=0.78Å) (Hawthorne et al., 2001; Shannon, 1976). Amphibole Zn^{2+} concentrations decrease with hypersolvus granite differentiation (see Fig. 3-5g), due either to the co-crystallization of another Zn-bearing phase or the progressive replacement of the relatively compatible Zn^{2+} ion by more incompatible cations, such as Fe^{3+}. The amphibole phenocrysts of the transsolvus granite generally have low but highly variable Mn^{2+}- and Zn^{2+}-concentrations, from 0 to 0.12 apfu, and 0.02 to 0.14 apfu, respectively. The latter is due to the much higher Mn and Zn concentrations of the phenocryst rims compared to the cores (see Table 3-4), which reflects increasing evolution of the magma. A progressive build-up in both Mn and Zn in the Strange Lake amphiboles with evolution was reported by Hawthorne et al. (2001), whereas we observe this trend separately for each granite unit.

3.6.3.3 The role of lithium

Lithium is a significant component of the Strange Lake amphiboles and has been reported to be an important constituent in alkali amphiboles of highly evolved alkaline rocks elsewhere (e.g., Hawthorne et al., 1993; Hawthorne et al., 1996; Marks et al., 2004). Owing to the incompatibility of lithium in common rock-forming minerals, its concentration reflects the degree of melt differentiation. The amphiboles of the Strange Lake pluton have an average Li concentration of 0.3 apfu, but concentrations reach > 1.0 apfu in some transsolvus granite samples. Lithium concentrations of >0.5 apfu classify a sodic amphibole as ferro-ferri-(fluoro)-leakeite, which is the case for most of the amphibole in the more evolved units. Hawthorne et al. (2001), who reported Li concentrations of up to 0.4 apfu for amphibole in the most evolved members of the Strange Lake pluton, concluded that the elevated Li concentration was due to its high content in the magma rather than the structure of the mineral. The generally low content of Li in amphibole of both the southern and northern hypersolvus granite (avg. 0.16 and 0.31 wt. %, respectively) compared to the transsolvus granite (avg. 0.58 wt. %) (see Table 3-4), despite the fact that amphibole in the hypersolvus granite was a late crystallizing phase, suggests that the hypersolvus granite magma was relatively poor in Li. In contrast, the occurrence of ferro-ferri-(fluoro)-leakeite as phenocrysts in the transsolvus granite suggests that the corresponding magma was more evolved. Of significance in this regard is the large range in Li-concentrations of the amphibole phenocrysts (0.1 to 1.2 apfu) (Fig. 3-11), which suggests that they record a large part of the evolution of the magma, a conclusion that is supported by the elevated Li concentrations of crystal rims relative to their cores (see Fig. 3-6d).

As noted earlier, the Li^+ concentration of the amphiboles correlates positively with the C-site occupancy (R^2 ~0.8), and hence knowledge of the concentration of this ion is essential to reliably evaluate the amphibole formula. In particular, the calculation of the Fe^{3+} concentration, which is highly dependent on Li^+ for charge balance, can only be performed accurately if the Li^+ concentration is known (Hawthorne et al., 1993). The lithium concentration in the amphiboles correlates strongly with the Fe^{3+} concentration (R^2=0.92 for the transsolvus granite, R^2=0.83 for the hypersolvus granite) (Fig. 3-11), and, with increasing degree of evolution, can be expressed by the coupled substitution reaction

$$^{C}Fe^{2+} + {}^{C}Fe^{2+} \rightarrow {}^{C}Fe^{3+} + {}^{C}Li^{+}$$

The progressive increase in Li^+ and Fe^{3+} with evolution is consistent with the increase in fO_2 in the hypersolvus granite, and also with the increase in melt F^- and OH^- in the transsolvus granite, both of which were discussed earlier.

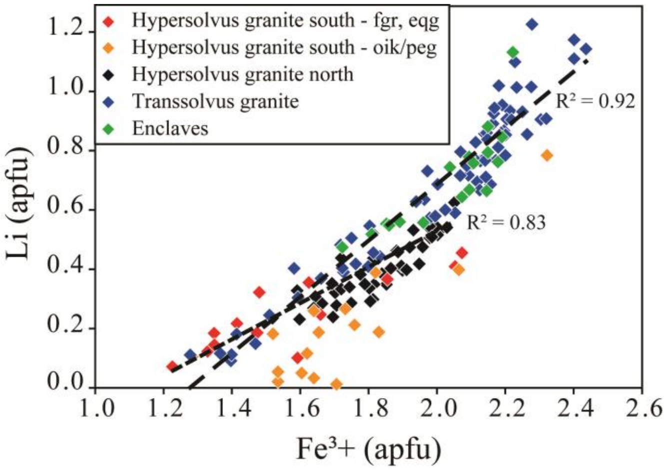

Fig. 3-11: Amphibole group Fe^{3+} and Li^+ concentrations

Binary diagram illustrating the positive correlation between Fe^{3+} and Li^+ in amphibole from the different granite facies. Linear trend lines and correlation coefficients have been added to distinguish amphibole in the hypersolvus granite from that in the transsolvus granite. Lithium concentrations are consistently lower in the hypersolvus granite than in the transsolvus granite.

3.6.4 Distribution of the REE and other trace elements

The trace element composition of amphibole-group minerals is a function of the magma composition and the structure of the mineral (i.e., the preference of its sites for ions of a particular size and charge). In the Strange Lake granites, for example, the negative Ba, Pb, Sr, and Eu anomalies in both the amphibole and bulk rock are likely due to voluminous plagioclase fractionation early in the crystallization history. This process is interpreted to have produced the large Mesoproterozoic anorthosite complexes of the Nain Plutonic Suite (Emslie et al., 1994; McLelland et al., 2010). Consistently low Rb concentrations, and negative U and Y anomalies in the amphibole, but not in bulk rock, on the other hand, are interpreted to have been caused by within-pluton-fractionation of K-feldspar (substitution of Rb for K) and of Y- and U-rich minerals, such as gagarinite-(Y), the fluorite-fluocerite solid solution and small amounts of U-bearing thorite.

The behavior of the REE in amphibole-group minerals is governed by a combination of crystal chemical constraints and magmatic processes. Several studies have concluded that the trace element composition of amphibole is dependent on the major element distribution, and, to a lesser extent, on the P, T and fO_2 conditions (Bottazzi et al., 1999; Dalpé and Baker, 2000). In the Gardar Province (Ilímaussaq, Puklen and Grønnedal-Ika intrusions), for example, Ca-rich amphibole- group minerals are strongly enriched in the LREE (order of magnitude), compared to the Na-rich members of the same mineral group (Marks et al., 2004). Consistent with this observation, the Ca-rich ferro-ferri-katophorite at Strange Lake is enriched in the REE by 10^2 to 10^3 times the chondrite values, whereas the Na-rich fluor-arfvedsonite and ferro-ferri-(fluoro)-leakeite have much lower total REE concentrations, and show a stronger relative enrichment in the HREE (see Fig. 3- 8).

The Ca-rich amphiboles are members of the earlier, less evolved hypersolvus granite, in which they crystallized as a late, interstitial phase from a small proportion of residual liquid. The residual liquid of this overall less evolved unit was relatively enriched in incompatible elements such as the REE, whereas the amphibole phenocrysts of the more evolved transsolvus granite crystallized from a relatively ‘dilute’ magma with low incompatible element concentrations. In contrast, the amphiboles of the Gardar Province all are late, near solidus phases in all rock types that have been investigated, e.g., augite-syenites, alkali granites, agpaites and nepheline syenites (Markl et al., 2001; Marks et al., 2004). Thus, the fact that the LREE are tied to Ca-rich amphiboles implies that another factor, in addition to the magma composition, may have been important in accommodating the REE in the crystal structure. Rare earth element concentrations in the Strange Lake amphiboles correlate positively with Al^{3+} (R^2=0.59) and Ca^{2+} (R^2 = 0.61) concentrations, and negatively with Na^+ (R^2= 0.57), F^- (R^2 = 0.51) (Fig. 3-12) and Si^{4+} concentrations. This suggests that overall the REE become less compatible in the amphibole structure with increasing degree of magma evolution, or alternatively, that the nature of the major elements in the mineral structure control the accommodation of the REE.

Interestingly, the amphiboles of the oikocrystic and pegmatitic samples of the southern hypersolvus granite have much lower REE concentrations (avg. ~0.04 wt. %) than their host (avg. 0.16 wt. %), but similar to those of amphiboles in the northern hypersolvus granite (avg. ~0.07 wt. %) (see Table 3-3). In the latter amphiboles, however, the Al and Ca contents are significantly lower (0.5 vs 1.0 wt. % Al_2O_3 and 0.5 vs. 1.1 wt. % CaO). This is consistent with the interpretation that the oikocrystic and pegmatitic granites crystallized from volatile-rich melt pockets that evolved in-situ, and is further evidence that the northern hypersolvus granite evolved from the southern hypersolvus granite. The decoupling of REE concentrations from those of Ca and Al observed in these two rock units speaks to a factor other than the degree of magma evolution in controlling the incorporation of the REE in amphibole.

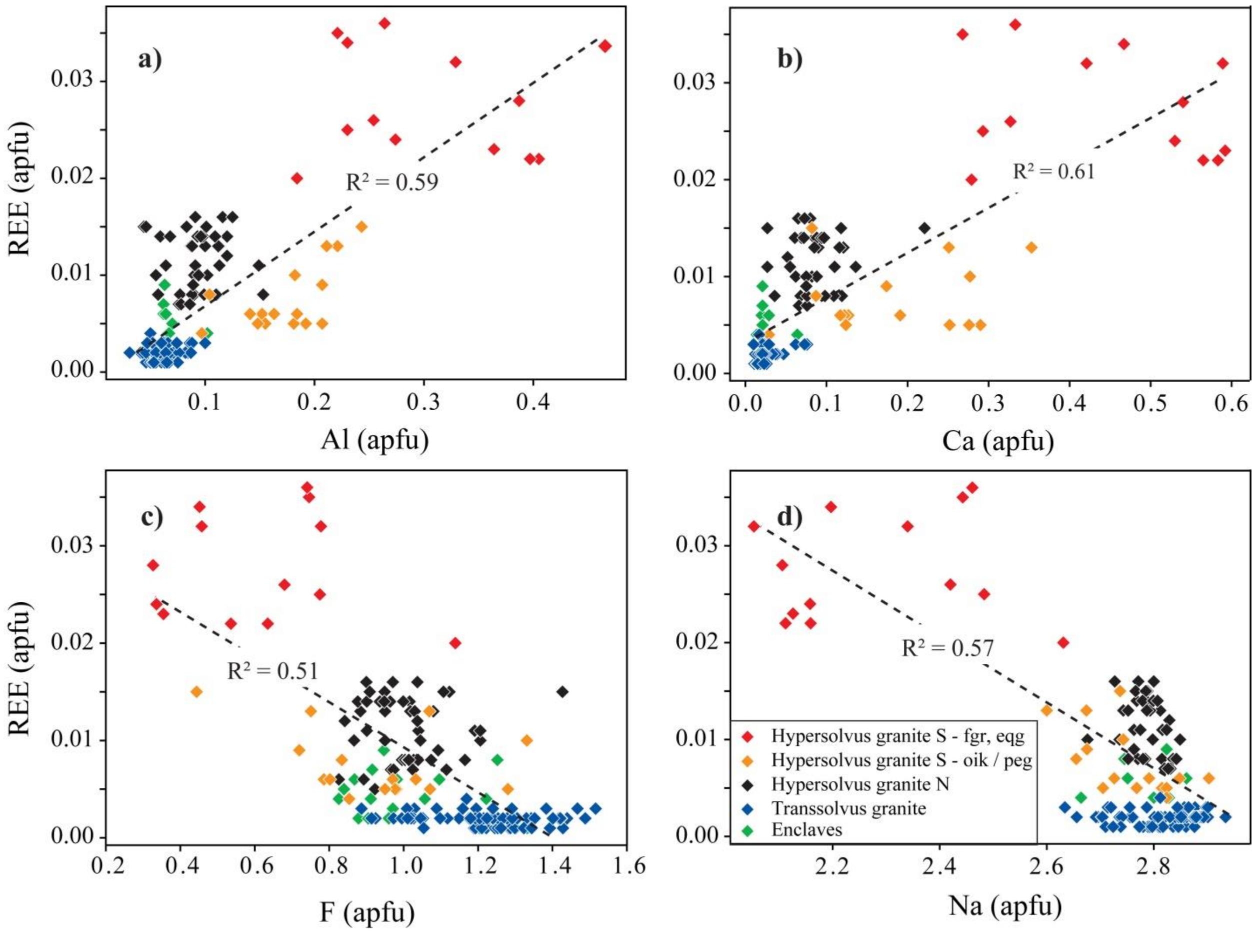

Fig. 3-12: Diagrams of the amphibole REE concentrations against selected major elements

Binary diagrams showing the total REE concentration in amphibole of the different granite facies as a function of the concentration of selected major elements. Also shown are the corresponding trend lines and correlation coefficients (R^2).

3.6.5 REE inter-site partitioning

Previous studies have concluded that the REE in the amphibole structure are distributed over the B and C sites and that this distribution depends on the nature of the major elements that reside in these sites (Bottazzi et al., 1999; Tiepolo et al., 2007; Tiepolo et al., 2000). These conclusions were reached from studies of the partitioning of the REE between amphibole and melt, with the D_{REE} showing systematic behavior controlled by the B and C site dimensions (*cf.* Blundy and Wood, 2003). Unfortunately, these data do not extend to the amphibole compositions encountered at Strange Lake. In order to obtain a first-order estimate of the localization of the REE in sodic amphibole, apparent mineral-melt partition coefficients were calculated from the bulk rock and median sodic amphibole compositions of transsolvus granite sample 204720. Amphibole was the first major phase to crystallize in this sample, but inclusions of pyrochlore group minerals and monazite-(Ce) indicate that these minerals had likely already saturated. The median compositions of these minerals at their respective modes were subtracted from the bulk composition to obtain an estimate of the melt composition at the time of amphibole crystallization. This assumes that sample 204720 acted as a closed system, that it represents a melt composition, that all pyrochlore group minerals and monazite-(Ce) crystallized prior to amphibole, and that all amphibole formed at the same time. However, deviations from these assumptions mainly impact the absolute D values, whereas their systematics are unaffected.

A plot of the partition coefficients against the radii of the REE (6-fold and 8-fold coordinated radii for the C and B-sites, respectively, as given in Shannon 1976) is shown in Figure 3-13. The LREE in the sodic amphiboles from Strange Lake are most compatible with the B-site (Fig. 3-13), as also has been shown for calcium and sodium-calcium amphiboles (Bottazzi et al., 1999). The lightest of the lanthanides, La and Ce, which have ionic radii of 1.16 Å and 1.14 Å (at 8-fold coordination) are closest to the ideal radius of the B-site and are thus preferentially incorporated. For reference, the major elements occupying this site are Na and Ca, which with ionic radii of 1.12 Å and 1.18 Å, respectively, are slightly smaller or larger than the ideal radius. The HREE, which have ionic radii between 0.86 to 0.94 Å, on the other hand, are compatible with the 6-fold coordinated C-site, and their compatibility increases exponentially with increasing atomic number (Fig. 3-13). Thus, the ‘heaviest’ of the REE, Yb and Lu are preferentially incorporated in the crystal structure ($D^{amph\text{-}bulk}_{Yb,\ Lu} > 1.0$), which, indeed, is what is observed in the chondrite-normalized REE profiles (Fig. 3-7). The middle REE, e.g., Gd, has the lowest apparent partition coefficient as its radius is furthest from that of the ideal radii of both the B and C sites and hence fits in neither site (in Fig. 3-13 it is shown at its 6-fold coordinated radius). The apparent D values also suggest that $D_{LREE} < D_{HREE}$, in agreement with Tiepolo et al. (2000), who showed that the LREE are incompatible in amphibole ($D^{amph/l}{}_{La}$ = 0.06 to 0.5), whereas the HREE are relatively compatible ($D^{amph/l}{}_{Yb}$ = 0.25 to 2.0). The apparent (calculated) $D^{amph\text{-}bulk}$ and ionic radii at 6- and 8-fold coordination are given in Table 3-6.

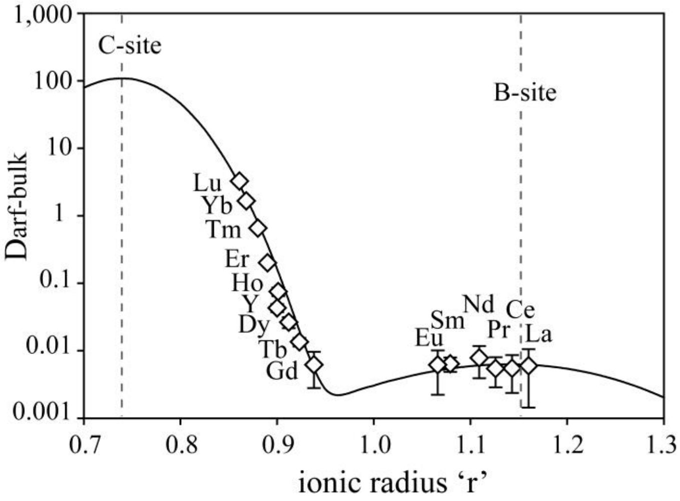

Fig. 3-13: The ionic radii of the REE versus the apparent partition coefficient $D_{amph\text{-}bulk}$

Diagram showing the ionic radii of the REE either in 6-fold (C-site) or 8-fold (B-site) coordination versus the apparent partition coefficient $D_{arf\text{-}bulk}$ (median REE content of amphibole / REE content of the bulk rock, sample 204720), plotted with error bars (median absolute deviation). Also shown is a Lattice-Strain Theory fit through these data (solid line).

Table 3-6: Apparent melt-amphibole partition coefficients, ionic radii and ideal radii

Apparent melt-amphibole partition coefficients ($D_{amph-bulk}$), ionic radii ‘r’ in 6- and 8-fold coordination, ideal radius (r) for each element and median absolute deviation (MAD)

	$D_{amph-bulk}$	r_{6-fold}	r_{8-fold}	r	MAD[*]
La	0.006	1.03	1.16	1.2	0.005
Ce	0.005	1.01	1.14	1.1	0.003
Pr	0.005	0.99	1.13	1.1	0.003
Nd	0.008	0.98	1.11	1.1	0.004
Sm	0.006	0.96	1.08	1.1	0.002
Eu	0.006	0.95	1.07	1.1	0.004
Gd	0.006	0.94	1.05	0.9	0.003
Tb	0.014	0.92	1.04	0.9	0.002
Dy	0.027	0.91	1.03	0.9	0.005
Y	0.043	0.90	1.02	0.9	0.006
Ho	0.075	0.90	1.02	0.9	0.011
Er	0.201	0.89	1.00	0.9	0.016
Tm	0.657	0.88	0.99	0.9	0.053
Yb	1.664	0.87	0.99	0.9	0.165
Lu	3.261	0.86	0.98	0.9	0.321

[*] The Median Absolute Deviation (MAD) is reported (plotted as error bars in Fig. 3-13) instead of the standard deviation, as the median amphibole concentration was used instead of the mean concentration.

3.6.6 The role of amphibole in concentrating HREE in the pluton

A significant proportion of the bulk REE content of the Strange Lake granites is contained in amphibole. Indeed, the REE content of amphibole in both fine-grained and oikocrystic and pegmatitic samples of the southern hypersolvus granite is similar to or exceeds that of the bulk rock, except for La and Ce; the contents of the heaviest of the REE, Yb and Lu, are four times higher than in the bulk rock.

Proportions of the bulk REE hosted by the mineral group were estimated from the proportion of the amphibole in each granite facies and the REE contents of the corresponding amphiboles. The amphibole of the southern hypersolvus granite (fine-grained) (~ 14 wt. %) contains about 10 % of the bulk LREE (avg. 0.1 wt. %) and more than 35 % of the bulk HREE (avg. 0.01 wt. %) (Fig. 3-14). In the case of Yb and Lu, the proportions increase to 55 and 70 wt. %, respectively. In the northern hypersolvus granite, REE concentrations are considerably lower than the bulk rock concentrations, except for Tm, Yb and Lu. On average, 2 % of the bulk LREE (avg. 0.15 wt. %), and 17 % of the bulk HREE (avg. 0.02 wt. %) are hosted by amphibole in this unit (~11 wt. %) (Fig. 3-14). As the bulk rock LREE concentrations of this unit are relatively high (~10^3 times chondrite values), this points to a major LREE bearing phase, e.g., monazite-(Ce), and/or pyrochlore group minerals having crystallized prior to the amphibole or that there was another sink for the LREE. The latter would be consistent with the findings of Vasyukova and Williams-Jones (2014, 2016) that the hypersolvus granite magma saturated with (exsolved) a fluoride liquid into which the LREE partitioned preferentially.

Amphibole proportions in the transsolvus granite are relatively high (~18 wt. %), whereas their REE concentrations are particularly low (> 1 and < 100 times the chondrite value). In this unit, only 0.1% of the bulk LREE (avg. 0.28 wt. %) and 4 % of the HREE (avg. 0.03 wt. %), on average, are hosted by the amphibole (Fig. 3-14). As the amphiboles occur as phenocrysts in the transsolvus granite, they largely record information about the pre-emplacement composition of the magma. Given the low LREE content of the amphibole, it is possible that an early fractionating phase depleted the melt in the LREE. These phases were monazite-(Ce) and gagarinite-(Ce), which crystallized prior to or contemporaneously with the amphibole.

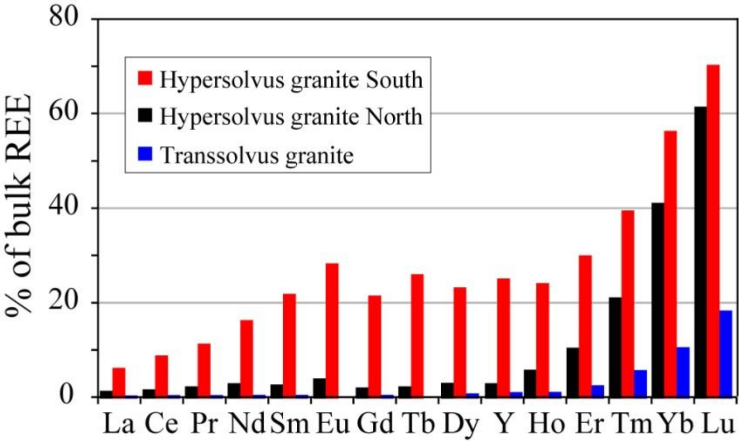

Fig. 3-14: Relative proportions of the bulk rock REE concentrations hosted by amphibole

Chart comparing the relative proportions of the bulk rock REE concentrations hosted by amphibole (average values) for each granite facies (see text for details). The chart for the southern hypersolvus granite only considers the fine-grained samples.

As mentioned earlier, some of the enclaves hosted by the transsolvus granite are interpreted to represent the quenched margin of this intrusion. Accordingly, amphibole phenocrysts in these enclaves and the host intrusion should have similar compositions. Indeed, their major element concentrations match closely those of the transsolvus granite (see Fig. 3-5). However, the light and middle REE contents of the amphiboles from the enclaves are generally higher than those of amphiboles in their host (see Fig. 3-7e); the chondrite-normalized profiles of the bulk enclaves are parallel to those of the bulk host granite, but their absolute values are slightly lower. The consistently higher light and middle REE concentrations of amphibole in the enclaves compared to their host could indicate that the amphibole crystallized from a melt relatively enriched in these elements. However, much of the amphibole in the enclaves crystallized after emplacement (quenching), which means that it crystallized from the very first and least evolved transsolvus granite magma (lower bulk REE profile, see Fig. 3-7e). We therefore suggest that amphibole in the enclaves crystallized slightly later than the phenocrysts in the magma chamber (transsolvus granite), resulting in an amphibole more enriched in the REE.

The amphibole in the more altered localities of the transsolvus granite was replaced extensively by aegirine and/or hematite during hydrothermal alteration (Gysi and Williams-Jones, 2013; Gysi et al., 2016; Salvi and Williams-Jones, 1990, 1996; Vasyukova et al., 2016). As the REE content of the aegirine is orders of magnitude lower than that of the amphibole, it is very likely that the replacement of amphibole by aegirine (and hematite) led to the release of the REE, particularly the HREE to the hydrothermal fluid and the development of potentially exploitable zones of HREE mineralization.

3.7 CONCLUSIONS

We have shown that the major and trace-element compositions of amphiboles of the Strange Lake granite complex reflect the magmatic evolution of the pluton. The differentiation of the magma proceeded from the southern hypersolvus granite to the more evolved northern hypersolvus granite, two separate intrusions which both contain amphibole as a late, interstitial phase (Fig. 3-15a). The most evolved unit, a transsolvus granite, contains early crystallizing amphibole in the form of phenocrysts (Fig. 3-15b). Compositions vary from sodium-calcium amphiboles (ferro-ferri-katophorite) in the least evolved southern hypersolvus granite to sodium amphiboles ((fluoro)-arfvedsonite, ferro-ferri-(fluoro)-leakeite) in the other, more evolved granites. The increasing Fe^{3+} concentration in amphibole with hypersolvus granite evolution was a result of crystal chemical effects (Na/Ca proportion) and increasing fO_2 through degassing. The same trend in the phenocrysts of the transsolvus granite implies a higher compatibility of Fe^{3+} with increasing Na/Ca proportions and an increase in OH^- and F^- concentrations in the evolving melt. Variations in Ti-concentrations indicate the presence of Na-Ti-silicates, such as aenigmatite, astrophyllite and narsarsukite, which replaced the amphibole to varying degrees in each unit. In the transsolvus granite, magma evolution is manifested by increasing Ti, Mn and Zn concentrations from amphibole cores to rims. The phenocrysts of the transsolvus granite also contain significant Li (ferro-ferri-fluoro-leakeite) that correlates positively with Fe^{3+}, indicating that this most evolved melt was already enriched in Li at an early stage.

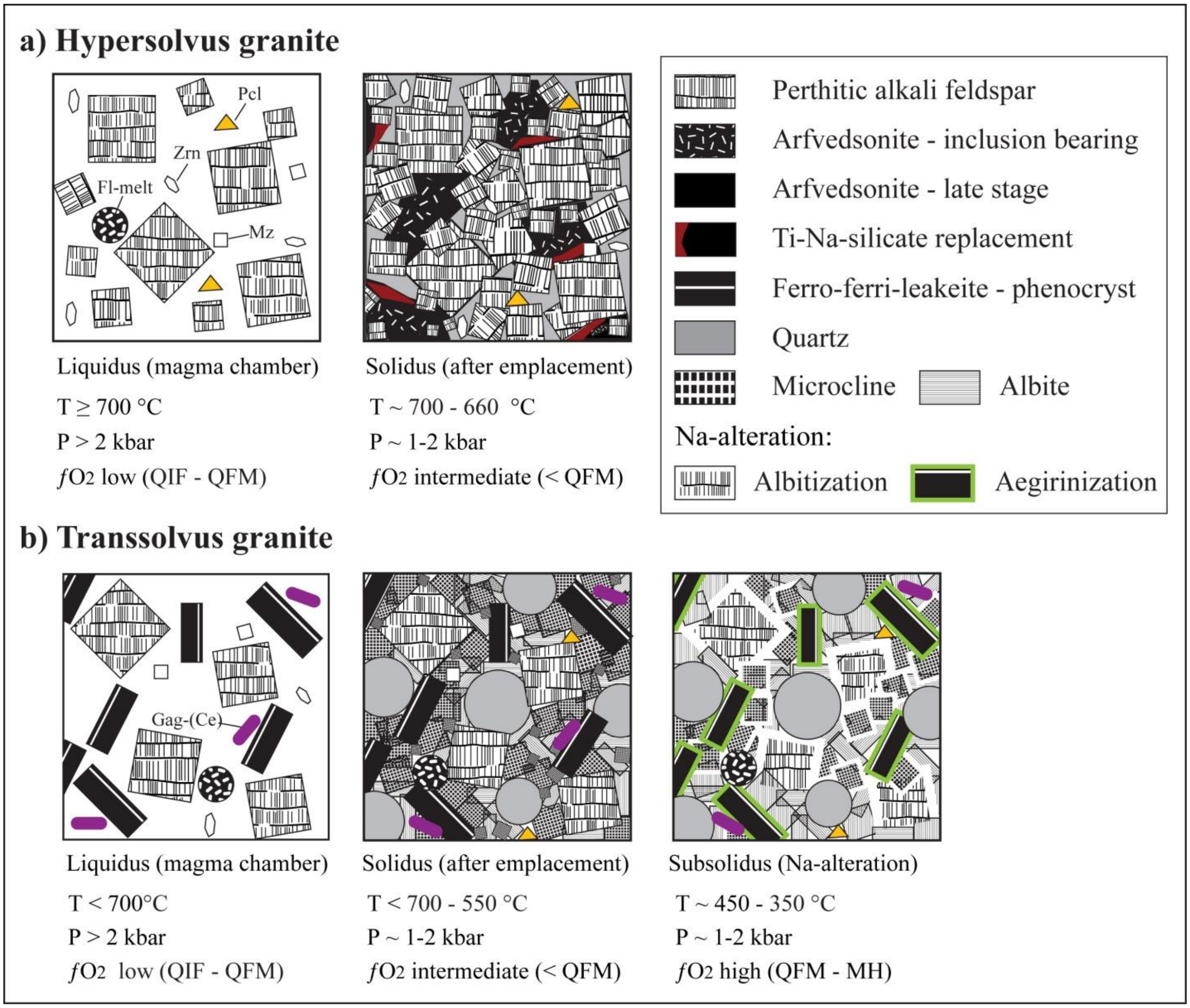

Fig. 3-15: Cartoon showing the textural parageneses of the amphibole group minerals

Cartoon showing the evolution of amphibole in the context of the textural development of a) hypersolvus and b) transsolvus granite, from liquidus to solidus stages and the subsolidus Na-alteration that affected the transsolvus granite. Crystallization temperature-, pressure- and oxygen fugacity ranges are given, and were taken from the studies of the Strange Lake pluton by Salvi and Williams-Jones (1992) and Vasyukova et al. (2016). The fO_2 ranges are indicated in respect to the iron oxide buffers, MH (magnetite-hematite), QFM (quartz-fayalite-magnetite) and QIF (quartz-iron-fayalite).

The amphiboles of all units are enriched in Nb, Zr and Hf and the HREE compared to the bulk rock, reflecting a combination of magmatic compositional and crystal chemical effects. In the hypersolvus granite, the late crystallization of amphiboles from a small proportion of residual magma resulted in high incompatible element concentrations, whereas the early crystallization of amphiboles in the transsolvus granite ensured relatively low concentrations of these elements, despite the overall more evolved nature of the magma. The concentrations of the relatively incompatible LREE ($D_{amph\text{-}bulk} < 0.01$) are positively coupled to the amphibole Ca concentration, with the LREE preferentially incorporated in the larger B-site. The HREE were preferred by the C-site and increased in compatibility ($D_{amph\text{-}bulk} > 0.1$) with increasing atomic number and decreasing ionic radius. Variations in the LREE concentrations of the amphiboles were controlled by the relative timing of crystallization of amphibole and the presence of primary LREE minerals, such as monazite-(Ce), pyrochlore group minerals and gagarinite-(Ce), as well as the exsolution of a LREE-rich fluoride melt. The uptake of the HREE by amphibole was controlled by their relative compatibility in the structure of this mineral due to their smaller radii. A significant proportion of the bulk HREE content of the Strange Lake granites was carried by the amphibole, which during subsequent hydrothermal alteration was released to the fluid and contributed to the development of potentially exploitable HREE mineralization.

APPENDIX

Table 3-7: EMPA standards, counting time and detection limits for the amphibole group

Element	Standard	Counting time (s)	Detection limit (ppm)
Na	Albite	20	267
Fe	Hematite	20	264
Mn	Spessartine	20	413
Ti	Rutile	20	370
Zr	Zircon	20	653
Si	Diopside	20	363
Ca	Diopside	20	243
Mg	Diopside	20	266
Al	Orthoclase	20	216
K	Orthoclase	20	205
Cl	Vanadinite	20	218
F	Fluorite	100	1501
Zn	Willemite	20	427

Detection limits and standard deviations (2 $\boldsymbol{\sigma}$) represent average detection limits calculated from repeated analyses of standards during the analytical runs.

ACKNOWLEDGEMENTS

A grant by Quest Rare Minerals Ltd. and a matching grant from the NSERC Collaborative Research and Development Program, both to A. E. Williams-Jones, provided financial support for this study. Quest Rare Minerals Ltd. granted access to the field area, drill core, logistical support and assay data. The sample suite used for this study included outcrop samples collected by Alexandre Brosseau-Liard and Robert Fritscher. Discussions with Robert F. Martin and Jeanne Paquette contributed greatly to our understanding of the amphibole chemistry. Olga Vasyukova provided valuable insights into the evolution of the Strange Lake magma from her own research on the pluton. Lang Shi, André Poirier, Bill Minarik and Anna Jung provided essential support by guiding the mineral chemical analyses and helping in the interpretation of the results. The manuscript benefited considerably from thoughtful reviews by Massimo Tiepolo and Kathryn Goodenough.

REFERENCES

Abdel-Rahman, A. F. M., 1994, Alkali Amphibole: A Potential Source of Rare Earth Elements in Felsic Alkaline Rocks: Exploration and Mining Geology, v. 3, no. 2, p. 81-94.

Birkett, T. C., Trzcienski, W. E., and Stirling, J. A. R., 1996, Occurrence and compositions of some Ti-bearing minerals in the Strange Lake intrusive complex, Quebec-Labrador boundary: Canadian Mineralogist, v. 34, p. 779-801.

Blundy, J., and Wood, B., 2003, Partitioning of trace elements between crystals and melts: Earth and Planetary Science Letters, v. 210, no. 3-4, p. 383-397.

Boily, M., and Williams-Jones, A. E., 1994, The role of magmatic and hydrothermal processes in the chemical evolution of the Strange Lake plutonic complex, Quebec-Labrador: Contributions to Mineralogy and Petrology, v. 118, no. 1, p. 33-47.

Bottazzi, P., Tiepolo, M., Vannucci, R., Zanetti, A., Brumm, R., Foley, S. F., and Oberti, R., 1999, Distinct site preferences for heavy and light REE in amphibole and the prediction of D-Amph/L(REE): Contributions to Mineralogy and Petrology, v. 137, no. 1-2, p. 36-45.

Cámara, F., Hawthorne, F. C., Ball, N. A., Bekenova, G., Stepanov, A. V., and Kotel'nikov, P. E., 2010, Fluoroleakeite, $NaNa_2(Mg_2Fe_2^{3+}Li)Si_8O_{22}F_2$, a new mineral of the amphibole group from the Verkhnee Espe deposit, Akjailyautas Mountains, Eastern Kazakhstan District, Kazakhstan: description and crystal structure: Mineralogical Magazine, v. 74, no. 3, p. 521-528.

Czamanske, G. K., and Dillet, B., 1988, Alkali amphibole, tetrasilicic mica, and sodic pyroxene in peralkaline siliceous rocks, Questa Caldera, New Mexico: American Journal of Science, v. 288-A, no. 1988, p. 358-392.

Czamanske, G. K., and Wones, D. R., 1973, Oxidation during Magmatic Differentiation, Finnmarka Complex, Oslo Area, Norway .2. Mafic Silicates: Journal of Petrology, v. 14, no. 3, p. 349-380.

Dalpé, C., and Baker, D. R., 2000, Experimental investigation of large-ion-lithophile-element-, high-field-strength-element- and rare-earth-element-partitioning between calcic amphibole and basaltic melt: the effects of pressure and oxygen fugacity: Contributions to Mineralogy and Petrology, v. 140, no. 2, p. 233-250.

Davidson, A., 1982, Petrochemistry of the Blachford Lake Complex near Yellowknife, Northwest Territories.: Maurice, E. T. (ed.) Uranium in Granites. Geological Survey of Canada, p. 71-79.

Emslie, R. F., Hamilton, M. A., and Theriault, R. J., 1994, Petrogenesis of a Midproterozoic anorthosite-mangerite-charnockite-granite (AMCG) complex - isotopic and chemical evidence from the Nain Plutonic Suite: Journal of Geology, v. 102, no. 5, p. 539-558.

Emslie, R. F., and Stirling, J. A. R., 1993, Rapakivi and Related Granitoids of the Nain Plutonic Suite - Geochemistry, Mineral Assemblages and Fluid Equilibria: Canadian Mineralogist, v. 31, p. 821-847.

Giehl, C., Marks, M., and Nowak, M., 2013, Phase relations and liquid lines of descent of an iron-rich peralkaline phonolitic melt: an experimental study: Contributions to Mineralogy and Petrology, v. 165, no. 2, p. 283-304.

Giret, A., Bonin, B., and Leger, J. M., 1980, Amphibole Compositional Trends in Oversaturated and Undersaturated Alkaline Plutonic Ring-Complexes: Canadian Mineralogist, v. 18, p. 481-495.

Gower, C. F., and Krogh, T. E., 2002, A U-Pb geochronological review of the Proterozoic history of the eastern Grenville Province: Canadian Journal of Earth Sciences, v. 39, no. 5, p. 795-829.

Gysi, A. P., and Williams-Jones, A. E., 2013, Hydrothermal mobilization of pegmatite-hosted REE and Zr at Strange Lake, Canada: A reaction path model: Geochimica et Cosmochimica Acta, v. 122, no. 2013, p. 324-352.

Gysi, A. P., Williams-Jones, A. E., and Collins, P., 2016, Lithogeochemical Vectors for Hydrothermal Processes in the Strange Lake Peralkaline Granitic REE-Zr-Nb-Deposit: Economic Geology and the Bulletin of the Society of Economic Geologists, v. 111, p. 1241-1276.

Hawthorne, F. C., 1976, The crystal chemistry of amphiboles: V. the structure and chemistry of arfvedsonite: Canadian Mineralogist, v. 14, p. 346-356.

Hawthorne, F. C., Oberti, R., Cannillo, E., Ottolini, L., Roelofsen, J. N., and Martin, R. F., 2001, Li-bearing arfvedsonitic amphiboles from the Strange Lake peralkaline granite, Quebec: Canadian Mineralogist, v. 39, p. 1161-1170.

Hawthorne, F. C., Oberti, R., Harlow, G. E., Maresch, W. V., Martin, R. F., Schumacher, J. C., and Welch, M. D., 2012, Nomenclature of the amphibole supergroup: American Mineralogist, v. 97, no. 11-12, p. 2031-2048.

Hawthorne, F. C., Oberti, R., Ottolini, L., and Foord, E. E., 1996, Lithium-bearing fluor-arfvedsonite from Hurricane Mountain, New Hampshire: A crystal-chemical study: Canadian Mineralogist, v. 34, p. 1015-1019.

Hawthorne, F. C., Ungaretti, L., Oberti, R., Bottazzi, P., and Czamanske, G. K., 1993, Li - an Important Component in Igneous Alkali Amphiboles: American Mineralogist, v. 78, no. 7-8, p. 733-745.

Herrmann, W., and Berry, R. F., 2002, MINSQ - a least squares spreadsheet method for calculating mineral proportions from whole rock major element analyses: Geochemistry: Exploration, Environment, Analysis, v. 2, no. 4, p. 361-368.

James, D. T., and Dunning, G. R., 2000, U-Pb geochronological constraints for paleoproterozoic evolution of the core zone, southeastern Churchill Province, northeastern laurentia: Precambrian Research, v. 103, no. 1-2, p. 31-54.

Kerr, A., and Rafuse, H., 2012, Rare-earth element (REE) geochemistry of the Strange Lake deposits: Implications for resource estimation and metallogenic models.: Current Research (2012) Newfoundland and Labrador Department of Natural Resources, v. 1, p. 39-60.

King, P. L., Hervig, R. L., Holloway, J. R., Vennemann, T. W., and Righter, K., 1999, Oxy-substitution and dehydrogenation in mantle-derived amphibole megacrysts: Geochimica Et Cosmochimica Acta, v. 63, no. 21, p. 3635-3651.

Konopleva, N. G., Ivanyuk, G. Y., Pakhomovsky, Y. A., Yakovenchuk, V. N., Men'shikov, Y. P., and Korchak, Y. A., 2008, Amphiboles of the Khibiny alkaline pluton, Kola Peninsula, Russia: Geology of Ore Deposits, v. 50, no. 8, p. 720-731.

Kovalenko, V. I., Tsaryeva, G. M., Goreglyad, A. V., Yarmolyuk, V. V., Troitsky, V. A., Hervig, R. L., and Farmer, G. L., 1995, The Peralkaline Granite-Related Khaldzan-Buregtey Rare-Metal (Zr, Nb, Ree) Deposit, Western Mongolia: Economic Geology and the Bulletin of the Society of Economic Geologists, v. 90, no. 3, p. 530-547.

Leake, B. E., 1968, A Catalog of Analyzed Calciferous and Subcalciferous Amphiboles Together with Their Nomenclature and Associated Minerals: Geological Society of America, Special Papers 1968, v. 98, p. 1-44.

Leake, B. E., Woolley, A. R., Arps, C. E. S., Birch, W. D., Gilbert, M. C., Grice, J. D., Hawthorne, F. C., Kato, A., Kisch, H. J., Krivovichev, V. G., Linthout, K., Laird, J., Mandarino, J. A., Maresch, W. V., Nickel, E. H., Rock, N. M. S., Schumacher, J. C., Smith, D. C., Stephenson, N. C. N., Ungaretti, L., Whittaker, E. J. W., and Guo, Y. Z., 1997, Nomenclature of amphiboles: Report of the subcommittee on amphiboles of the International Mineralogical Association, Commission on New Minerals and Mineral Names: Canadian Mineralogist, v. 35, p. 219-246.

Locock, A. J., 2014, An Excel spreadsheet to classify chemical analyses of amphiboles following the IMA 2012 recommendations: Computers & Geosciences, v. 62, p. 1-11.

Markl, G., Marks, M., Schwinn, G., and Sommer, H., 2001, Phase equilibrium constraints on intensive crystallization parameters of the Ilimaussaq complex, South Greenland: Journal of Petrology, v. 42, no. 12, p. 2231-2258.

Marks, M., Halama, R., Wenzel, T., and Markl, G., 2004, Trace element variations in clinopyroxene and amphibole from alkaline to peralkaline syenites and granites: implications for mineral-melt trace-element partitioning: Chemical Geology, v. 211, no. 3-4, p. 185-215.

Mayer, B., Jung, S., Romer, R. L., Pfander, J. A., Klugel, A., Pack, A., and Groner, E., 2014, Amphibole in alkaline basalts from intraplate settings: implications for the petrogenesis of alkaline lavas from the metasomatised lithospheric mantle: Contributions to Mineralogy and Petrology, v. 167, no. 989.

McLelland, J. M., Selleck, B. W., Hamilton, M. A., and Bickford, M. E., 2010, Late- to post-tectonic setting of some major proterozoic anorthosite - mangerite - charnockite - granite (AMCG) suites: Canadian Mineralogist, v. 48, no. 4, p. 729-750.

Miller, R. R., 1996, Structural and textural evolution of the Strange Lake peralkaline rare-element (NYF) granitic pegmatite, Quebec-Labrador: Canadian Mineralogist, v. 34, p. 349-371.

Miller, R. R., Heaman, L. M., and Birkett, T. C., 1997, U-Pb zircon age of the Strange Lake peralkaline complex: Implications for Mesoproterozoic peralkaline magmatism in north-central Labrador: Precambrian Research, v. 81, no. 1-2, p. 67-82.

Mungall, J. E., and Martin, R. F., 1996, Extreme differentiation of peralkaline rhyolite, Terceira, Azores: A modern analogue of Strange Lake, Labrador?: Canadian Mineralogist, v. 34, p. 769-777.

Oberti, R., Cannillo, E., and Toscani, G., 2012, How to name amphiboles after the IMA2012 report: rules of thumb and a new PC program for monoclinic amphiboles: Periodico Di Mineralogia, v. 81, no. 2, p. 257-267.

Petrella, L., Williams-Jones, A. E., Goutier, J., and Walsh, J., 2014, The Nature and Origin of the Rare Earth Element Mineralization in the Misery Syenitic Intrusion, Northern Quebec, Canada: Economic Geology, v. 109, no. 6, p. 1643-1666.

Piilonen, P. C., Mcdonald, A. M., Poirier, G., Rowe, R., and Larsen, A. O., 2013, Mafic Minerals of the Alkaline Pegmatites in the Larvik Plutonic Complex, Oslo Rift, Southern Norway: Canadian Mineralogist, v. 51, no. 5, p. 735-770.

Pillet, D., Chenevoy, M., and Belanger, M., 1992, Petrology of Peralkaline Granite from Lake Brisson (Central Labrador, Nouveau-Quebec) .1. Intrusion and Chemical Evolution: Canadian Journal of Earth Sciences, v. 29, no. 2, p. 353-372.

-, 1993, Petrology of Peralkaline Granite from Lake Brisson (Quebec-Labrador) .2. Mineralogy and Modes of Crystallization: Canadian Journal of Earth Sciences, v. 30, no. 12, p. 2423-2435.

Quest, 2012, Quest announces that a revised resource estimate for the Strange Lake B-Zone REE deposit shows a doubling of tonnage, http://questareminerals.com/news.php, Volume 2016: Toronto, Quest Rare Minerals Ltd.

Roelofsen, J. N., 1997, The primary and secondary mafic silicates of two alkaline anorogenic complexes: Strange Lake (Québec-Labrador) and Amba Dongar (Gujarat, India) [Ph.D.: McGill University, 321 p.

Salvi, S., and Williams-Jones, A. E., 1990, The Role of Hydrothermal Processes in the Granite-Hosted Zr, Y, Ree Deposit at Strange Lake, Quebec Labrador - Evidence from Fluid Inclusions: Geochimica et Cosmochimica Acta, v. 54, no. 9, p. 2403-2418.

Salvi, S., and Williams-Jones, A. E., 1992, Reduced Orthomagmatic C-O-H-N-Nacl Fluids in the Strange Lake Rare-Metal Granitic Complex, Quebec Labrador, Canada: European Journal of Mineralogy, v. 4, no. 5, p. 1155-1174.

Salvi, S., and Williams-Jones, A. E., 1996, The role of hydrothermal processes in concentrating high-field strength elements in the Strange Lake peralkaline complex, northeastern Canada: Geochimica et Cosmochimica Acta, v. 60, no. 11, p. 1917-1932.

Salvi, S., and Williams-Jones, A. E., 1997, Fischer-Tropsch synthesis of hydrocarbons during sub-solidus alteration of the Strange Lake peralkaline granite, Quebec/Labrador, Canada: Geochimica Et Cosmochimica Acta, v. 61, no. 1, p. 83-99.

Salvi, S., and Williams-Jones, A. E., 2006, Alteration, HFSE mineralisation and hydrocarbon formation in peralkaline igneous systems: Insights from the Strange Lake Pluton, Canada: Lithos, v. 91, p. 19-34.

Shannon, R. D., 1976, Revised Effective Ionic-Radii and Systematic Studies of Interatomic Distances in Halides and Chalcogenides: Acta Crystallographica Section A, v. 32, no. Sep1, p. 751-767.

Sun, S. S., and McDonough, W. F., 1989, Chemical and isotopic systematics of oceanic basalts: implications for mantle composition and processes: Geological Society, London, Special Publications, v. 42, p. 313-345.

Tiepolo, M., Oberti, R., Zanetti, A., Vannucci, R., and Foley, S. F., 2007, Trace-element partitioning between amphibole and silicate melt: Amphiboles: Crystal Chemistry, Occurrence, and Health Issues, v. 67, p. 417-451.

Tiepolo, M., Vannucci, R., Bottazzi, P., Oberti, R., Zanetti, A., and Foley, S., 2000, Partitioning of rare earth elements, Y, Th, U, and Pb between pargasite, kaersutite, and basanite to trachyte melts: Implications for percolated and veined mantle: Geochemistry Geophysics Geosystems, v. 1.

Tuttle, O. F., and Bowen, N. L., 1958, Origin of granite in the light of experimental studies in the system $NaAlSi_3O_8$-$KAlSi_3O_8$-SiO_2-H_2O, Geological Society of America, Memoir 74, 146 p.:

Vasyukova, O., and Williams-Jones, A. E., 2014, Fluoride–silicate melt immiscibility and its role in REE ore formation: Evidence from the Strange Lake rare metal deposit, Que´bec-Labrador, Canada: Geochimica et Cosmochimica Acta, v. 139, no. 2014, p. 110-130.

-, 2016, The evolution of immiscible silicate and fluoride melts: Implications for REE ore-genesis: Geochimica et Cosmochimica Acta, v. 172, p. 205-224.

Vasyukova, O. V., Williams-Jones, A. E., and Blamey, N. J. F., 2016, Fluid evolution in the Strange Lake granitic pluton, Canada: Implications for HFSE mobilization: Chemical Geology, v. 444, p. 83-100.

SUPPLEMENTARY ON-LINE MATERIAL

Table 3-8: Amphibole group EMP and LA-ICP-MS analyses with formulae

EMP and LA-ICP-MS analyses

Unit	Hypersolvus granite south – fine grained samples														
Sample	2047 71-1	2047 71-2	2047 71-3	2047 71-4	2047 71-6	2047 68-2	2047 68-3	2047 68-4	2047 68-5	2047 68-6	2047 68-7	2047 68-8	20476 8-10	Mdn	MAD
Major and minor elements (wt. %)															
SiO_2	48.37	47.70	48.81	47.27	48.68	47.71	47.60	48.83	47.81	48.42	48.29	47.49	48.72	48.29	0.51
TiO_2	1.20	1.06	0.90	1.18	0.67	1.51	1.87	1.15	1.73	1.72	1.75	1.88	1.45	1.45	0.30
Al_2O_3	1.39	1.25	1.21	1.43	0.99	1.77	2.18	1.25	2.09	1.47	2.16	1.97	2.55	1.47	0.30
FeO	34.10	34.01	34.62	33.90	33.84	33.77	32.96	32.87	33.63	33.67	32.54	33.25	30.86	33.67	0.42
MnO	0.73	0.67	0.69	0.71	0.72	0.84	0.72	0.79	0.78	0.80	0.69	0.81	0.63	0.72	0.05
MgO	0.34	0.34	0.32	0.27	0.23	0.35	0.45	0.36	0.33	0.26	0.52	0.41	1.11	0.34	0.07
ZnO	0.80	1.09	0.86	1.12	0.65	0.62	0.46	0.76	0.52	0.43	0.51	0.48	0.46	0.62	0.16
ZrO_2	0.03	0.04	0.15	0.05	0.20	0.06	0.03	0.03	0.04	0.08	0.00	0.05	0.01	0.04	0.02
Nb_2O_5	0.05	0.05	0.09	0.09	0.04	0.08	0.07	0.13	0.09	0.06	0.06	0.05	0.07	0.07	0.02
Na_2O	8.05	8.22	8.11	8.12	8.61	6.71	6.90	7.25	6.91	7.05	7.14	6.97	7.83	7.25	0.54
K_2O	1.07	1.03	1.11	1.12	1.08	1.07	1.38	1.64	1.41	1.37	1.35	1.27	1.34	1.27	0.15
CaO	1.97	1.75	1.61	1.99	1.65	3.48	3.45	2.79	3.21	3.14	3.38	3.51	2.55	2.79	0.69
F	1.39	1.57	1.52	1.50	2.28	0.92	1.07	0.92	0.66	0.67	1.29	0.71	1.60	1.29	0.31
Cl	0.03	0.03	0.02	0.03	0.03	0.02	0.05	0.03	0.04	0.01	0.04	0.04	0.02	0.03	0.01
Total	99.52	98.81	100.0	98.77	99.67	98.89	99.19	98.78	99.24	99.14	99.70	98.89	99.18	99.18	0.34
Trace elements (ppm)															
Li	2730	3376	1839	3025	738	1345	900	2385	1067	522	1613	1370	2668	1613	772
Rb	76.6	48.6	50.1	58.8	31.1	37.2	41.0	66.2	92.9	39.3	71.8	74.9	101	58.8	17.8
Sr	19.4	16.5	17.9	20.0	15.1	18.1	29.0	23.3	59.1	39.8	47.4	56.2	83.5	23.3	6.8
Y	361	316	554	571	248	693	326	764	643	399	410	471	775	471	145
Zr	1631	1738	4010	3720	1438	1208	562	1956	571	470	519	457	555	1208	653
Sn	160	99.2	248	240	46.4	149	80.7	189	370	102	76.3	254	441	160	80.3
La	105	90.8	87.7	87.4	64.4	62.7	96.0	62.6	117	108	96.9	107	158	96.0	11.2
Ce	305	286	308	313	245	258	274	226	282	302	253	259	313	282	24
Pr	50.8	50.1	57.1	56.7	44.4	38.7	45.0	39.5	40.6	45.7	40.8	39.5	44.1	44.4	4.9
Nd	259	251	287	281	216	195	218	189	193	228	207	187	218	218	25
Sm	70.0	67.0	86.5	84.7	59.7	61.9	54.2	62.5	47.1	53.8	51.4	48.6	56.8	59.7	7.3
Eu	4.6	3.9	5.2	5.4	4.0	3.9	3.9	4.1	3.9	4.3	3.5	3.4	4.3	4.0	0.3
Gd	55.0	50.0	74.4	73.7	47.9	53.1	41.2	51.7	41.3	45.9	38.9	38.4	55.8	50.0	5.8
Tb	11.1	9.3	14.5	14.8	8.4	12.2	9.1	12.0	10.6	9.6	8.0	8.3	12.0	10.6	1.5
Dy	77.0	62.6	98.0	107	57.2	85.3	57.7	90.5	71.7	62.1	57.9	59.0	87.7	71.7	13.8
Ho	18.5	17.1	26.3	27.2	13.7	23.4	13.0	24.5	16.4	13.4	13.1	14.0	20.2	17.1	3.7
Er	74.5	78.1	119	121	53.6	107	50.3	118	66.4	46.2	46.5	48.5	69.7	69.7	21.2
Tm	18.6	21.2	31.4	31.9	13.6	27.4	10.9	31.6	14.2	9.0	10.3	10.1	13.7	14.2	4.4
Yb	187	227	352	346	144	263	108	328	127	84.9	95.2	92.2	111	144	52
Lu	36.9	44.5	68.7	69.2	29.5	47.2	21.6	59.9	24.8	17.7	21.9	17.9	21.0	29.5	11.6
Hf	61.6	71.8	162	161	60.3	71.1	28.4	138	31.6	21.2	23.0	21.2	24.5	60.3	35.8
Ta	6.9	5.7	9.1	10.3	4.8	9.0	9.3	17.9	10.8	7.2	6.8	7.3	9.5	9.0	1.7
Pb	60.0	48.8	77.9	77.8	44.3	94.4	73.6	85.9	84.8	79.0	106	76.9	166	77.9	8.0
Nb	331	352	656	634	305	531	489	881	598	394	419	381	468	468	116
Ba	11.1	10.5	3.6	2.8	2.8	5.0	7.3	1.5	16.8	11.6	15.1	20.9	37.3	10.5	6.3
Th	0.62	4.6	0.30	0.11	1.9	9.1	0.87	0.31	10.4	1.6	1.7	6.1	38.6	1.7	1.4
U	0.13	0.64	0.18	0.06	0.38	0.72	0.06	0.03	0.28	0.04	0.06	0.11	1.3	0.13	0.10
REE+Y	1634	1574	2170	2189	1249	1931	1329	2064	1699	1430	1354	1404	1960	1634	297

Table 3-8: Amphibole group EMP and LA-ICP-MS analyses with formulae (continued)

Formulae

Unit	Hypersolvus granite south – fine grained												
Sample	20477 1-1	20477 1-2	20477 1-3	20477 1-4	20477 1-6	20476 8-2	20476 8-3	20476 8-4	20476 8-5	20476 8-6	20476 8-7	20476 8-8	20476 8-10
Species*	arf	arf	arf	arf	fl-arf	kat	kat	arf	kat	kat	kat	kat	arf
(apfu)													
Si	7.50	7.43	7.59	7.39	7.67	7.53	7.51	7.63	7.51	7.64	7.53	7.47	7.51
Al	0.25	0.23	0.22	0.26	0.18	0.33	0.41	0.23	0.39	0.27	0.40	0.36	0.46
^{T}Ti	0.14	0.12	0.11	0.14	0.08	0.14	0.08	0.14	0.10	0.09	0.07	0.17	0.03
^{T}Fe^{3+}	0.11	0.22	0.09	0.21	0.06								
T (8)	8.00	8.00	8.00	8.00	8.00	8.00	8.00	8.00	8.00	8.00	8.00	8.00	8.00
^{C}Ti						0.04	0.14		0.10	0.12	0.13	0.06	0.14
Zr			0.01		0.02	0.01				0.01			
REE+Y	0.03	0.03	0.04	0.04	0.02	0.03	0.02	0.03	0.03	0.02	0.02	0.02	0.03
^{C}Fe^{3+}	1.75	1.86	1.57	1.85	1.53	1.35	1.33	1.48	1.35	1.23	1.42	1.47	1.63
Zn	0.09	0.13	0.10	0.13	0.08	0.07	0.05	0.09	0.06	0.05	0.06	0.06	0.05
Mn^{2+}	0.10	0.09	0.09	0.09	0.10	0.11	0.10	0.10	0.10	0.11	0.09	0.11	0.08
Fe^{2+}	2.57	2.36	2.84	2.38	2.87	3.11	3.02	2.82	3.07	3.22	2.83	2.90	2.35
Mg	0.08	0.08	0.07	0.06	0.05	0.08	0.11	0.09	0.08	0.06	0.12	0.10	0.26
Li	0.37	0.46	0.25	0.41	0.10	0.18	0.12	0.32	0.15	0.07	0.22	0.19	0.36
C (5)	4.97	4.99	4.97	4.96	4.76	4.98	4.89	4.93	4.94	4.88	4.88	4.91	4.89
Ca	0.33	0.29	0.27	0.33	0.28	0.59	0.58	0.47	0.54	0.53	0.57	0.59	0.42
^{B}Na	1.67	1.71	1.73	1.67	1.72	1.41	1.42	1.53	1.46	1.47	1.44	1.41	1.58
B (2)	2.00	2.00	2.00	2.00	2.00	2.00	2.00	2.00	2.00	2.00	2.00	2.00	2.00
^{A}Na	0.75	0.78	0.71	0.79	0.91	0.64	0.70	0.66	0.65	0.69	0.72	0.72	0.76
K	0.21	0.21	0.22	0.22	0.22	0.22	0.28	0.33	0.28	0.28	0.27	0.25	0.26
A (≤1)	0.96	0.98	0.93	1.02	1.13	0.86	0.97	0.99	0.93	0.96	0.99	0.97	1.03
OH	1.03	0.97	1.04	0.98	0.70	1.18	1.01	1.27	1.25	1.25	0.95	1.19	0.88
F	0.68	0.78	0.75	0.74	1.14	0.46	0.54	0.45	0.33	0.34	0.64	0.36	0.78
Cl	0.01	0.01		0.01	0.01		0.01	0.01	0.01		0.01	0.01	
O	0.28	0.25	0.21	0.28	0.16	0.36	0.45	0.27	0.41	0.41	0.41	0.45	0.34
W (2)	2.00	2.00	2.00	2.00	2.00	2.00	2.00	2.00	2.00	2.00	2.00	2.00	2.00

*Amphibole group mineral species are abbreviated as: arf = arfvedsonite, fl-arf = fluor-arfvedsonite, kat = ferro-ferri-katophorite, lea = ferro-ferri-leakeite, fl-lea = ferro-ferri-fluoro-leakeite

Table 3-8: Amphibole group EMP and LA-ICP-MS analyses with formulae (continued)

EMP and LA-ICP-MS analyses

Unit	Hypersolvus granite south – oikocrystic / pegmatitic																	
Sample	100 16-1	100 16-2	100 16-3	100 16-5	100 16-7	100 16-8	100 18-4	100 18-5	100 18-7	100 18-8	100 18-9	204 773-2	204 773-4	204 773-5	204 773-6	204 773-12	Mdn	MAD
Species	fl-arf	fl-arf	fl-arf	arf	fl-arf	arf	arf	fl-arf	fl-arf	fl-arf	fl-arf	lea	arf	fl-arf	arf	arf		
Major and minor elements (wt. %)																		
SiO_2	50.26	49.14	49.98	50.46	49.68	51.98	51.03	50.74	49.97	50.19	50.93	48.61	49.34	48.29	48.58	48.28	49.97	0.80
TiO_2	0.52	0.74	0.71	0.62	0.78	0.50	0.99	0.95	0.90	0.99	0.80	1.00	0.85	0.83	1.07	0.92	0.84	0.12
Al_2O_3	0.84	1.04	0.99	0.89	1.13	0.53	0.78	1.02	0.85	1.00	0.82	1.24	1.33	1.14	1.13	0.55	0.99	0.15
FeO	34.96	34.50	33.61	34.28	34.02	32.87	33.90	32.92	33.74	32.83	33.28	33.85	34.13	33.57	34.13	31.64	33.80	0.41
MnO	0.76	0.73	0.62	0.74	0.65	0.69	0.53	0.60	0.78	0.60	0.57	0.59	0.66	0.59	0.59	0.76	0.64	0.05
MgO	0.00	0.03	0.02	0.01	0.04	0.00	0.13	0.24	0.34	0.30	0.22	0.11	0.14	0.12	0.10	0.04	0.10	0.08
ZnO	0.21	0.20	0.25	0.25	0.19	0.30	0.23	0.21	0.22	0.18	0.19	1.79	0.68	0.55	0.84	0.79	0.24	0.05
ZrO_2	0.06	0.02	0.12	0.08	0.09	0.23	0.09	0.09	0.03	0.18	0.06	0.03	0.06	0.07	0.03	-	0.06	0.03
Nb_2O_5	0.03	0.04	-	-	0.02	0.04	0.01	0.02	0.03	-	-	0.02	0.02	0.02	0.02	0.02	0.02	0.01
Na_2O	9.68	9.31	9.35	9.47	9.19	9.42	9.14	9.42	9.01	9.18	9.29	8.87	9.10	8.79	8.90	8.55	9.18	0.20
K_2O	0.79	1.10	1.15	0.98	1.17	1.80	1.36	1.32	1.12	1.23	1.40	1.43	1.39	1.27	1.29	2.73	1.28	0.12
CaO	0.77	1.74	1.51	0.74	1.74	0.18	0.71	1.17	1.66	1.68	0.75	1.55	0.49	2.10	1.05	0.51	1.11	0.50
F	1.99	1.99	2.18	1.60	1.99	1.75	1.65	2.14	2.62	2.73	1.96	1.57	0.91	2.16	1.47	1.65	1.97	0.27
Cl	0.03	0.03	0.01	0.02	0.03	0.01	0.01	0.03	0.01	0.01	0.02	0.02	0.02	0.01	0.02	-	0.02	0.01
Total	100.9	100.6	100.5	100.1	100.7	100.3	100.6	100.9	101.3	101.1	100.3	100.7	99.11	99.49	99.22	96.43	100.5	0.34
Trace elements (ppm)																		
Li	256	101	1500	424	427	850	1720	1999	821	1400	1830	5995	1577	1388	2972	2810	1450	615
Rb	8.4	16.1	15.5	8.3	23.9	34.6	16.4	14.2	21.3	14.9	20.4	57.4	30.6	24.3	58.4	30.2	20.9	6.3
Sr	5.6	8.8	7.9	4.7	6.0	8.2	13.3	11.5	8.0	18.4	8.0	13.7	12.5	45.1	6.9	11.9	8.5	3.0
Y	73.2	63.4	68.6	77.5	42.6	53.2	96.5	54.9	44.6	196	103	144	136	107	41.3	49.8	70.9	26.0
Zr	585	433	466	525	994	967	580	546	670	593	978	772	701	623	1089	874	647	124
Sn	16.5	12.6	16.3	12.1	23.4	43.6	19.1	17.6	18.7	13.5	40.1	81.2	34.3	35.7	57.4	46.1	21.3	8.9
La	28.6	32.2	31.5	25.7	28.5	15.3	26.8	35.0	23.6	42.6	12.7	49.3	73.4	72.8	44.9	48.9	31.9	9.5
Ce	93.6	89.5	89.3	81.0	83.3	61.0	84.6	101.3	73.6	136.5	45.3	141	214	192	120	103	91.6	14.7
Pr	13.7	13.2	13.3	11.7	11.1	6.8	13.1	14.7	10.6	19.7	6.7	32.7	37.5	31.1	19.4	16.3	13.5	2.8
Nd	60.9	56.9	56.9	51.1	45.6	28.0	60.0	60.2	43.2	89.7	29.2	114	174	150	88.7	69.9	60.1	15.7
Sm	15.0	13.8	13.8	12.1	10.2	6.0	14.2	12.2	8.2	19.9	7.5	29.5	35.6	32.8	14.5	13.5	13.8	2.7
Eu	0.76	0.83	0.86	0.67	0.65	0.34	1.1	0.88	0.42	1.2	0.44	1.9	2.1	2.3	0.94	0.67	0.85	0.22
Gd	10.0	11.3	9.7	10.3	7.2	4.9	9.4	9.4	4.0	13.2	5.7	26.0	28.7	26.2	9.1	9.5	9.6	2.0
Tb	1.9	2.0	2.0	1.8	1.1	0.88	1.7	1.6	0.88	2.5	1.2	4.5	5.2	4.2	1.4	1.4	1.7	0.5
Dy	12.7	11.1	13.7	12.1	8.9	8.2	12.3	12.6	6.0	15.6	9.3	31.4	36.6	28.5	10.8	12.4	12.4	2.3
Ho	3.6	2.6	3.1	3.0	2.5	2.8	3.4	2.9	2.1	4.2	2.6	7.9	8.7	6.4	4.1	3.2	3.1	0.5
Er	16.2	10.9	13.4	13.3	12.0	15.1	15.1	14.4	12.4	18.8	12.9	39.2	39.1	28.6	27.7	19.0	15.1	2.9
Tm	4.3	2.9	3.1	3.4	3.6	5.0	4.0	4.3	4.0	4.6	3.2	11.6	10.3	8.3	10.1	6.3	4.3	1.0
Yb	52.4	36.6	36.8	41.5	45.1	57.8	45.5	55.1	51.4	53.7	41.0	151	130	87.0	131	83.4	53.1	11.8
Lu	11.8	8.4	8.0	9.6	9.7	13.4	10.8	12.2	11.4	11.6	8.7	35.5	29.4	20.3	30.7	20.1	11.7	2.6
Hf	21.0	14.8	14.7	16.9	33.3	32.9	23.2	20.1	24.7	21.8	35.7	44.5	39.3	33.7	51.3	30.3	27.5	7.0
Ta	0.8	1.0	0.9	0.8	2.5	1.1	2.3	2.3	2.2	2.6	2.1	1.8	2.2	2.2	2.7	1.7	2.2	0.4
Pb	3.1	6.2	5.8	2.5	9.6	8.4	6.4	4.5	9.4	5.2	19.6	27.3	29.8	46.9	28.7	16.4	8.9	5.1
Nb	196	259	-	-	154	287	98	133	196	-	-	122	115	111	146	125	124	51
Ba	0.26	2.3	2.1	0.83	0.76	0.90	12.2	3.7	1.8	5.4	3.0	5.7	7.5	9.6	7.2	9.3	3.4	2.5
Th	-	0.11	0.53	0.02	0.49	0.81	1.8	1.2	3.2	4.4	156	0.68	0.46	0.69	3.2	1.4	0.75	0.66
U	-	0.08	0.07	0.01	0.03	0.04	0.18	0.05	0.21	0.07	3.5	0.29	0.28	0.95	1.0	0.25	0.13	0.11
REE+Y	399	356	364	355	312	279	398	392	296	630	290	820	960	797	554	457	395	91

Table 3-8: Amphibole group EMP and LA-ICP-MS analyses with formulae (continued)

Formulae

Unit	Hypersolvus granite south – oikocrystic / pegmatitic															
Sample	10016-1	10016-2	10016-3	10016-5	10016-7	10016-8	10018-4	10018-5	10018-7	10018-8	10018-9	204773-2	204773-4	204773-5	204773-6	204773-12
Species	fl-arf	fl-arf	fl-arf	arf	fl-arf	arf	arf	fl-arf	fl-arf	fl-arf	fl-arf	lea	arf	fl-arf	arf	arf
(apfu)																
Si	7.78	7.66	7.79	7.83	7.71	8.03	7.85	7.76	7.74	7.74	7.83	7.35	7.65	7.58	7.53	7.74
Al	0.15	0.19	0.18	0.16	0.21		0.14	0.18	0.16	0.18	0.15	0.22	0.24	0.21	0.21	0.10
^{T}Ti	0.06	0.09	0.03	0.01	0.08		0.01	0.06	0.11	0.08	0.03	0.11	0.10	0.10	0.13	0.11
^{T}Fe^{3+}	0.01	0.06							0.01			0.31	0.00	0.12	0.14	0.05
T (8)	8.00	8.00	8.00	8.00	8.00	8.03	8.00	8.00	8.00	8.00	8.00	8.00	8.00	8.00	8.00	8.00
^{C}Ti			0.05	0.06	0.01	0.06	0.11	0.05		0.04	0.07					
Zr			0.01	0.01	0.01	0.02	0.01	0.01		0.01				0.01		
^{C}Al						0.10										
REE+Y	0.01	0.01	0.01	0.01	0.01		0.01	0.01	0.01	0.01	0.01	0.01	0.02	0.01	0.01	0.01
^{C}Fe^{3+}	1.63	1.65	1.54	1.54	1.60	1.28	1.52	1.73	1.62	1.65	1.64	2.01	1.76	1.72	1.92	1.77
Zn	0.02	0.02	0.03	0.03	0.02	0.03	0.03	0.02	0.03	0.02	0.02	0.20	0.08	0.06	0.10	0.09
Mn^{2+}	0.10	0.10	0.08	0.10	0.09	0.09	0.07	0.08	0.10	0.08	0.07	0.08	0.09	0.08	0.08	0.10
Fe^{2+}	2.88	2.79	2.84	2.91	2.81	2.97	2.84	2.48	2.75	2.58	2.64	1.96	2.67	2.58	2.36	2.42
Mg		0.01	0.01		0.01		0.03	0.06	0.08	0.07	0.05	0.03	0.03	0.03	0.02	0.01
^{C}Li	0.03	0.01	0.02	0.05	0.05	0.11	0.18	0.27	0.12	0.19	0.26	0.71	0.21	0.19	0.40	0.39
C (5)	4.68	4.58	4.58	4.70	4.61	4.66	4.79	4.69	4.69	4.65	4.76	5.00	4.85	4.67	4.89	4.80
^{B}Li												0.07				
Ca	0.13	0.29	0.25	0.12	0.29	0.03	0.12	0.19	0.28	0.28	0.12	0.25	0.08	0.35	0.17	0.09
^{B}Na	1.87	1.71	1.75	1.88	1.71	1.97	1.88	1.81	1.72	1.72	1.88	1.68	1.92	1.65	1.83	1.91
B (2)	2.00	2.00	2.00	2.00	2.00	2.00	2.00	2.00	2.00	2.00	2.00	2.00	2.00	2.00	2.00	2.00
^{A}Na	1.03	1.11	1.08	0.97	1.06	0.85	0.84	0.98	0.98	1.02	0.89	0.92	0.82	1.03	0.85	0.74
K	0.16	0.22	0.23	0.19	0.23	0.36	0.27	0.26	0.22	0.24	0.27	0.28	0.28	0.25	0.26	0.56
A (≤1)	1.19	1.33	1.31	1.16	1.29	1.21	1.11	1.24	1.20	1.26	1.17	1.20	1.09	1.28	1.10	1.30
OH	0.90	0.84	0.76	1.06	0.83	1.03	0.97	0.74	0.51	0.44	0.86	1.02	1.35	0.73	1.03	0.94
F	0.97	0.98	1.07	0.79	0.98	0.85	0.80	1.03	1.28	1.33	0.95	0.75	0.44	1.07	0.72	0.83
Cl	0.01	0.01		0.01	0.01			0.01			0.01					
O	0.12	0.17	0.17	0.15	0.18	0.12	0.23	0.22	0.21	0.23	0.19	0.23	0.20	0.20	0.25	0.22
W (2)	2.00	2.00	2.00	2.00	2.00	2.00	2.00	2.00	2.00	2.00	2.00	2.00	2.00	2.00	2.00	2.00

Table 3-8: Amphibole group EMP and LA-ICP-MS analyses with formulae (continued)

EMP and LA-ICP-MS analyses

Unit	Hypersolvus granite north (1/3)															
Sample	2047 46-2	2047 46-3	2047 46-4	2047 46-6	2047 46-7	2047 46-8	2047 46-10	2047 56-3	2047 56-9	2047 56-10	2047 54-1	2047 54-2	2047 54-3	2047 54-4	2047 54-5	2047 54-6
Species	fl-arf	fl-arf	fl-arf	fl-arf	fl-lea	fl-lea	fl-arf	fl-arf	fl-arf	fl-arf	fl-arf	fl-arf	fl-arf	fl-arf	fl-lea	fl-arf
Major and minor elements (wt. %)																
SiO_2	50.83	50.92	50.85	50.73	50.78	50.66	51.08	50.97	51.21	50.28	50.71	50.87	50.71	50.84	50.81	50.63
TiO_2	1.16	1.19	1.09	1.28	1.53	1.79	1.50	1.06	1.20	1.22	1.01	1.19	1.24	1.05	1.86	1.02
Al_2O_3	0.50	0.50	0.48	0.48	0.67	0.31	0.42	0.55	0.33	0.38	0.50	0.62	0.66	0.43	0.24	0.84
FeO	31.99	31.69	31.97	32.11	31.89	31.27	31.95	32.63	32.31	32.68	32.59	31.21	32.33	32.76	31.81	32.50
MnO	0.91	0.91	0.92	0.87	0.91	0.96	0.83	0.81	0.88	0.90	0.81	0.78	0.86	0.88	0.87	0.89
MgO	0.31	0.29	0.25	0.19	0.27	0.19	0.21	0.39	0.29	0.28	0.13	0.25	0.19	0.17	0.20	0.22
ZnO	0.53	0.49	0.54	0.41	0.52	0.49	0.45	0.43	0.46	0.47	0.39	0.43	0.47	0.42	0.45	0.41
ZrO_2	0.21	0.17	0.27	0.19	0.16	0.16	0.23	0.17	0.23	0.31	0.28	0.13	0.18	0.25	0.13	0.19
Nb_2O_5	0.02	-	0.02	-	0.02	0.04	-	0.05	0.03	-	0.03	0.03	0.04	0.03	0.02	0.02
Na_2O	9.41	9.35	9.24	9.45	9.61	9.54	9.60	9.48	9.36	9.37	9.29	9.17	9.32	9.23	9.40	9.26
K_2O	1.49	1.83	1.70	1.56	1.65	1.98	1.68	1.55	1.75	1.63	1.58	2.20	1.44	1.46	2.02	1.31
CaO	0.50	0.72	0.71	0.52	0.32	0.22	0.40	0.55	0.42	0.51	0.49	0.17	0.37	0.66	0.16	0.59
F	1.96	2.12	2.23	2.40	1.75	2.09	2.32	1.83	1.99	1.80	1.85	2.12	1.93	2.05	1.96	2.13
Cl	0.02	0.02	0.02	-	0.01	0.01	0.01	0.02	0.01	-	0.03	-	-	0.02	0.01	0.02
Total	99.83	100.2	100.3	100.2	100.1	99.70	100.7	100.5	100.5	99.81	99.70	99.16	99.75	100.2	99.93	100.0
Trace elements (ppm)																
Li	2939	2550	3290	2901	4002	3893	3608	2159	2424	2189	2871	2441	3494	2502	3824	2128
Rb	67.4	70.3	69.2	52.3	89.4	72.3	84.0	54.9	56.2	59.9	63.6	42.9	57.3	46.8	78.7	38.2
Sr	7.7	4.1	8.8	6.3	10.2	4.9	5.0	14.3	17.4	17.1	9.3	5.2	10.4	12.2	26.0	14.1
Y	98.5	95.2	193	107	153	100	102	129	134	143	205	86.8	123	75.8	140	78.5
Zr	3365	2845	3421	2122	3550	3192	2717	3377	3826	3630	3894	1135	2629	2661	5420	2350
Sn	132	134	139	154	146	205	187	245	263	270	156	261	204	118	220	92.8
La	26.1	20.6	34.2	18.6	37.9	16.5	10.2	30.4	31.5	32.4	35.5	27.0	34.9	23.0	45.0	26.5
Ce	77.9	57.6	98.2	47.4	91.4	28.9	23.6	75.3	78.5	82.9	107	33.5	103	53	109	58.9
Pr	12.3	8.2	15.9	7.3	14.2	4.5	3.8	12.1	11.5	12.8	19.1	4.5	18.8	8.9	14.7	9.1
Nd	60.4	39.9	73.8	31.4	62.3	21.6	16.8	56.1	54.2	56.7	89.8	23.8	82.8	36.7	69.6	41.6
Sm	11.3	8.8	16.4	6.9	12.4	4.9	4.8	11.6	9.9	14.4	27.4	5.1	17.1	5.2	11.5	5.7
Eu	0.59	0.76	1.0	0.35	0.85	0.28	0.40	0.64	0.68	0.59	1.4	0.38	0.83	0.34	0.46	0.30
Gd	6.1	7.2	11.9	6.8	7.9	4.0	4.3	5.9	5.7	8.7	22.0	3.4	8.8	4.5	7.6	4.0
Tb	1.1	1.3	2.8	1.5	2.2	1.0	1.2	1.6	1.4	2.0	4.4	1.3	1.8	0.7	1.6	0.8
Dy	12.6	13.5	24.5	14.3	20.3	14.1	12.2	19.6	22.6	24.0	34.0	11.7	16.7	10.8	19.2	10.7
Ho	5.9	5.6	8.1	6.1	8.5	5.9	5.9	10.2	10.8	11.0	11.9	5.1	7.7	5.2	9.8	4.9
Er	46.8	33.7	48.5	37.5	53.1	40.2	38.6	74.2	76.0	75.2	68.2	47.0	65.3	38.3	78.1	39.6
Tm	16.4	11.2	16.2	13.4	18.4	14.3	13.1	26.8	28.0	26.6	21.2	23.3	23.0	13.4	27.3	13.6
Yb	211	138	208	165	238	177	167	333	340	310	268	337	298	190	355	176
Lu	50.1	32.4	50.4	36.8	55.5	39.4	38.6	67.7	72.6	66.2	61.6	77.8	60.1	40.0	80.9	40.1
Hf	130	108	134	82.1	129	112	140	160	212	218	154	33.9	139	106	228	92.7
Ta	3.4	4.9	3.0	2.1	3.1	3.6	2.4	1.9	2.9	2.2	3.6	0.60	4.5	1.4	3.0	1.3
Pb	30.7	42.2	30.7	22.9	30.6	43.8	26.9	47.1	50.6	48.5	36.5	16.7	32.2	30.9	66.9	27.0
Nb	260	211	270	200	248	226	200	198	209	202	335	115	322	170	315	164
Ba	3.5	4.8	5.3	3.8	7.1	6.8	3.6	8.6	7.0	9.0	4.6	13.9	2.9	6.0	13.0	6.7
Th	0.03	97.7	0.15	0.57	0.20	8.8	0.01	0.08	0.01	0.02	0.29	1.2	0.97	0.65	3.4	0.03
U	-	5.8	-	-	0.04	1.2	-	-	-	0.02	0.05	0.14	-	0.07	0.10	-
REE+Y	637	474	803	500	776	473	443	853	877	866	977	688	862	506	969	510

Table 3-8: Amphibole group EMP and LA-ICP-MS analyses with formulae (continued)

Formulae

Unit	Hypersolvus granite north (1/3)															
Sample	2047 46-2	2047 46-3	2047 46-4	2047 46-6	2047 46-7	2047 46-8	2047 46-10	2047 56-3	2047 56-9	2047 56-10	2047 54-1	2047 54-2	2047 54-3	2047 54-4	2047 54-5	2047 54-6
Species	fl-arf	fl-arf	fl-arf	fl-arf	fl-lea	fl-lea	fl-arf	fl-arf	fl-arf	fl-arf	fl-arf	fl-arf	fl-arf	fl-arf	fl-lea	fl-arf
(apfu)																
Si	7.80	7.82	7.79	7.80	7.71	7.77	7.77	7.80	7.85	7.77	7.80	7.90	7.76	7.82	7.77	7.81
Al	0.09	0.09	0.09	0.09	0.12	0.06	0.08	0.10	0.06	0.07	0.09	0.10	0.12	0.08	0.04	0.15
^{T}Ti	0.11	0.09	0.13	0.12	0.17	0.18	0.16	0.10	0.09	0.14	0.11		0.12	0.10	0.19	0.04
^{T}Fe^{3+}										0.02						
T (8)	8.00	8.00	8.00	8.00	8.00	8.00	8.00	8.00	8.00	8.00	8.00	8.00	8.00	8.00	8.00	8.00
^{C}Ti	0.02	0.05		0.03	0.01	0.03	0.02	0.02	0.05		0.01	0.14	0.03	0.02	0.03	0.08
Zr	0.02	0.01	0.02	0.01	0.01	0.01	0.02	0.01	0.02	0.02	0.02	0.01	0.01	0.02	0.01	0.01
^{C}Al												0.02				
REE+Y	0.01	0.01	0.01	0.01	0.01	0.01	0.01	0.01	0.01	0.01	0.02	0.01	0.01	0.01	0.02	0.01
^{C}Fe^{3+}	1.82	1.75	1.83	1.84	2.01	2.00	1.96	1.75	1.70	1.78	1.78	1.59	1.88	1.72	1.98	1.66
Zn	0.06	0.06	0.06	0.05	0.06	0.06	0.05	0.05	0.05	0.05	0.05	0.05	0.05	0.05	0.05	0.05
Mn^{2+}	0.12	0.12	0.12	0.11	0.12	0.12	0.11	0.11	0.11	0.12	0.11	0.10	0.11	0.12	0.11	0.12
Fe^{2+}	2.29	2.33	2.27	2.29	2.05	2.01	2.11	2.43	2.44	2.42	2.42	2.46	2.26	2.49	2.09	2.53
Mg	0.07	0.07	0.06	0.04	0.06	0.04	0.05	0.09	0.07	0.06	0.03	0.06	0.04	0.04	0.05	0.05
Li	0.39	0.34	0.44	0.39	0.53	0.52	0.48	0.29	0.32	0.29	0.38	0.33	0.46	0.33	0.51	0.28
C (5)	4.79	4.72	4.80	4.77	4.84	4.80	4.79	4.75	4.77	4.76	4.81	4.77	4.86	4.80	4.84	4.79
Ca	0.08	0.12	0.12	0.09	0.05	0.04	0.07	0.09	0.07	0.09	0.08	0.03	0.06	0.11	0.03	0.10
^{B}Na	1.92	1.88	1.88	1.91	1.95	1.96	1.93	1.91	1.93	1.92	1.92	1.97	1.94	1.89	1.97	1.90
B (2)	2.00	2.00	2.00	2.00	2.00	2.00	2.00	2.00	2.00	2.00	2.00	2.00	2.00	2.00	2.00	2.00
^{A}Na	0.88	0.90	0.86	0.90	0.88	0.87	0.90	0.90	0.85	0.89	0.85	0.79	0.83	0.86	0.81	0.87
K	0.29	0.36	0.33	0.31	0.32	0.39	0.33	0.30	0.34	0.32	0.31	0.44	0.28	0.29	0.40	0.26
A (≤1)	1.17	1.26	1.19	1.21	1.20	1.26	1.22	1.21	1.19	1.21	1.16	1.23	1.11	1.15	1.21	1.13
OH	0.78	0.69	0.67	0.54	0.81	0.57	0.54	0.87	0.76	0.84	0.86	0.68	0.78	0.76	0.62	0.72
F	0.95	1.03	1.08	1.17	0.84	1.01	1.12	0.88	0.96	0.88	0.90	1.04	0.94	1.00	0.95	1.04
Cl			0.01					0.01			0.01			0.00	0.00	0.01
O	0.27	0.28	0.25	0.30	0.35	0.41	0.34	0.24	0.28	0.28	0.23	0.28	0.29	0.24	0.43	0.24
W (2)	2.00	2.00	2.00	2.00	2.00	2.00	2.00	2.00	2.00	2.00	2.00	2.00	2.00	2.00	2.00	2.00

Table 3-8: Amphibole group EMP and LA-ICP-MS analyses with formulae (continued)

EMP and LA-ICP-MS analyses

Unit	Hypersolvus granite north (2/3)														
Sample	204754-7	204754-8	204754-9	204754-10	204779-4	204779-6	204779-7	204779-8	204779-9	204779-10	10040-2	10040-5	10040-7	10040-8	10040-10
Species	fl-arf	fl-arf	fl-arf	fl-arf	fl-arf	fl-arf	fl-arf	fl-arf	fl-arf	fl-arf	fl-arf	fl-arf	fl-arf	fl-arf	fl-arf
Major and minor elements (wt. %)															
SiO_2	50.52	50.96	50.92	50.57	50.14	50.35	50.84	51.05	50.69	50.51	49.73	50.27	50.71	50.59	50.46
TiO_2	0.96	1.09	1.36	1.06	0.95	0.98	1.70	1.38	0.90	0.96	1.32	1.23	1.05	1.17	1.25
Al_2O_3	0.82	0.48	0.30	0.56	0.54	0.63	0.26	0.36	0.56	0.62	0.63	0.48	0.61	0.51	0.69
FeO	32.66	32.32	31.98	32.23	33.08	33.08	31.94	32.43	32.89	33.04	32.05	32.46	32.76	32.45	32.06
MnO	0.85	0.84	0.88	0.85	0.71	0.82	0.81	0.86	0.85	0.84	0.83	0.85	0.80	0.83	0.84
MgO	0.12	0.26	0.23	0.17	0.16	0.20	0.22	0.21	0.20	0.19	0.25	0.22	0.18	0.25	0.26
ZnO	0.41	0.46	0.45	0.41	0.39	0.49	0.46	0.43	0.44	0.50	0.51	0.49	0.41	0.51	0.45
ZrO_2	0.13	0.19	0.13	0.22	0.18	0.21	0.12	0.20	0.14	0.21	0.18	0.12	0.04	0.21	0.16
Nb_2O_5	0.05	0.04	0.05	0.01	0.03	0.07	-	0.02	0.05	0.03	0.06	0.06	0.02	0.03	0.04
Na_2O	9.48	9.20	8.95	9.12	9.31	9.26	9.30	9.40	9.37	9.44	9.29	9.28	9.36	9.31	9.13
K_2O	1.40	1.65	1.96	1.68	1.54	1.29	2.14	1.78	1.47	1.34	1.56	1.50	1.79	1.47	1.59
CaO	0.83	0.46	0.38	0.53	0.54	0.73	0.16	0.34	0.72	0.71	0.39	0.51	0.42	0.57	0.44
F	2.46	2.20	2.14	2.46	2.08	2.10	2.32	1.87	2.28	1.97	1.98	2.10	2.07	2.05	2.13
Cl	0.01	0.01	0.01	0.01	0.01	-	-	-	0.02	0.01	0.02	0.02	-	0.01	0.01
Total	100.7	100.2	99.71	99.87	99.65	100.2	100.3	100.3	100.6	100.4	98.80	99.59	100.2	99.95	99.51
Trace elements (ppm)															
Li	2638	2312	3287	2632	2965	3099	3452	3597	2635	3171	2962	2506	3042	2632	3284
Rb	52.4	47.4	63.8	60.5	71.9	67.6	87.3	89.9	59.0	64.5	51.3	44.4	63.1	90.1	71.6
Sr	6.2	15.4	17.2	12.4	10.1	11.7	8.6	12.1	12.6	11.1	13.6	11.1	16.8	23.4	29.2
Y	95.7	72.3	90.6	98.6	122	114	118	100	170	111	154	103	62.0	106	135
Zr	2522	2799	3554	3682	3012	2450	2140	3380	2476	2608	2523	2197	917	3450	2610
Sn	176	116	156	156	231	237	717	426	213	211	188	205	126	220	266
La	28.3	26.6	30.4	27.2	40.0	37.4	66.2	29.9	40.4	37.4	40.2	31.2	95.1	132	133
Ce	85.9	55.2	68.6	66.9	122	119	55.0	71.8	126	128	131	91.7	51.7	110	102
Pr	14.5	8.0	9.8	11.0	20.4	20.0	7.1	11.2	21.1	21.9	23.4	15.5	8.0	16.3	15.5
Nd	67.4	37.4	49.2	51.6	97.4	98.1	42.0	52.6	104	105	116	72.2	36.2	75.9	70.5
Sm	13.6	7.1	7.9	11.1	23.3	22.6	16.8	11.3	25.9	23.8	25.5	14.2	9.0	13.9	12.5
Eu	0.71	0.31	0.28	0.56	1.3	1.2	1.2	0.75	1.6	1.5	1.2	0.58	0.53	0.80	0.73
Gd	8.6	3.0	3.5	6.4	13.7	13.6	13.5	9.1	18.1	13.9	15.2	8.0	6.0	6.9	8.9
Tb	1.4	0.6	0.9	1.3	2.8	2.5	3.8	2.2	3.6	2.0	2.9	1.7	1.4	1.5	2.3
Dy	15.5	8.9	12.3	14.5	22.9	21.0	29.6	18.9	32.9	19.3	28.5	19.6	13.8	18.3	22.4
Ho	7.0	4.8	6.8	6.5	9.1	8.6	9.3	7.7	10.7	9.0	10.7	9.3	5.0	8.7	10.0
Er	48.4	42.2	48.8	43.9	59.2	56.0	68.1	50.2	65.3	60.8	73.6	70.6	33.5	63.2	68.4
Tm	17.5	15.8	18.7	15.3	20.3	20.3	28.7	19.1	21.7	21.2	25.1	25.6	11.6	22.3	26.4
Yb	215	202	239	197	247	240	391	236	256	246	304	312	154	265	320
Lu	45.9	43.4	55.0	45.8	53.2	50.0	82.9	50.3	51.0	51.4	59.7	63.1	34.0	55.2	63.1
Hf	137	110	150	153	178	139	76.5	223	142	147	157	130	47	158	146
Ta	3.8	1.6	1.9	2.5	5.5	4.6	5.9	2.4	4.7	5.2	6.2	5.4	1.9	3.0	4.4
Pb	30.0	28.5	43.1	46.2	54.0	47.3	270	45.0	42.4	49.6	42.8	34.5	43.1	55.1	45.0
Nb	278	175	214	233	374	316	226	211	326	355	398	330	180	277	356
Ba	2.9	6.6	7.7	6.3	3.4	4.6	43.0	8.4	3.9	2.2	2.7	4.5	63.0	93.0	91.0
Th	1.0	0.06	0.27	8.6	0.25	0.94	175	0.05	1.2	0.06	1.3	0.43	1.3	2.7	4.4
U	0.01	0.01	-	1.3	0.04	0.08	22.0	0.02	0.03	-	0.01	0.01	0.15	0.63	0.11
REE+Y	665	527	642	598	854	824	933	671	948	851	1010	838	522	896	991

Table 3-8: Amphibole group EMP and LA-ICP-MS analyses with formulae (continued)

Formulae

Unit	Hypersolvus granite north (2/3)														
Sample	204754-7	204754-8	204754-9	204754-10	204779-4	204779-6	204779-7	204779-8	204779-9	204779-10	10040-2	10040-5	10040-7	10040-8	10040-10
Species	fl-arf	fl-arf	fl-arf	fl-arf	fl-arf	fl-arf	fl-arf	fl-arf	fl-arf	fl-arf	fl-arf	fl-arf	fl-arf	fl-arf	fl-arf
(apfu)															
Si	7.74	7.86	7.86	7.83	7.74	7.72	7.80	7.77	7.77	7.71	7.73	7.79	7.77	7.79	7.78
Al	0.15	0.09	0.06	0.10	0.10	0.11	0.05	0.06	0.10	0.11	0.12	0.09	0.11	0.09	0.13
^{T}Ti	0.11	0.05	0.09	0.07	0.11	0.11	0.16	0.16	0.10	0.11	0.16	0.13	0.12	0.12	0.10
^{T}Fe^{3+}					0.06	0.05			0.02	0.07					
T (8)	8.00	8.00	8.00	8.00	8.00	8.00	8.00	8.00	8.00	8.00	8.00	8.00	8.00	8.00	8.00
^{C}Ti		0.07	0.07	0.06			0.04					0.02		0.02	0.05
Zr	0.01	0.01	0.01	0.02	0.01	0.02	0.01	0.02	0.01	0.02	0.01	0.01	0.00	0.02	0.01
^{C}Al															
REE+Y	0.01	0.01	0.01	0.01	0.01	0.01	0.02	0.01	0.02	0.01	0.02	0.01	0.01	0.01	0.02
^{C}Fe^{3+}	1.85	1.64	1.72	1.69	1.84	1.84	1.89	1.92	1.79	1.88	1.91	1.80	1.87	1.79	1.81
Zn	0.05	0.05	0.05	0.05	0.05	0.06	0.05	0.05	0.05	0.06	0.06	0.06	0.05	0.06	0.05
Mn^{2+}	0.11	0.11	0.12	0.11	0.09	0.11	0.11	0.11	0.11	0.11	0.11	0.11	0.10	0.11	0.11
Fe^{2+}	2.33	2.53	2.41	2.48	2.37	2.35	2.21	2.21	2.40	2.27	2.25	2.40	2.33	2.39	2.32
Mg	0.03	0.06	0.05	0.04	0.04	0.05	0.05	0.05	0.05	0.04	0.06	0.05	0.04	0.06	0.06
Li	0.35	0.31	0.44	0.35	0.40	0.41	0.46	0.47	0.35	0.42	0.40	0.34	0.40	0.35	0.44
C (5)	4.74	4.80	4.87	4.81	4.81	4.84	4.83	4.83	4.77	4.81	4.82	4.80	4.81	4.80	4.86
Ca	0.14	0.08	0.06	0.09	0.09	0.12	0.03	0.06	0.12	0.12	0.07	0.09	0.07	0.09	0.07
^{B}Na	1.86	1.92	1.94	1.91	1.91	1.88	1.97	1.95	1.88	1.88	1.94	1.92	1.93	1.91	1.93
B (2)	2.00	2.00	2.00	2.00	2.00	2.00	2.00	2.00	2.00	2.00	2.00	2.00	2.00	2.00	2.00
^{A}Na	0.95	0.83	0.74	0.82	0.87	0.87	0.79	0.83	0.90	0.91	0.87	0.87	0.85	0.87	0.80
K	0.27	0.32	0.39	0.33	0.30	0.25	0.42	0.35	0.29	0.26	0.31	0.30	0.35	0.29	0.31
A (≤1)	1.23	1.15	1.12	1.16	1.18	1.13	1.21	1.18	1.19	1.17	1.17	1.17	1.20	1.16	1.11
OH	0.58	0.67	0.64	0.55	0.76	0.76	0.48	0.78	0.68	0.83	0.71	0.68	0.75	0.73	0.67
F	1.19	1.07	1.05	1.21	1.02	1.02	1.12	0.90	1.11	0.95	0.97	1.03	1.00	1.00	1.04
Cl									0.01		0.01				
O	0.22	0.25	0.32	0.25	0.22	0.23	0.39	0.32	0.21	0.22	0.31	0.29	0.24	0.27	0.29
W (2)	2.00	2.00	2.00	2.00	2.00	2.00	2.00	2.00	2.00	2.00	2.00	2.00	2.00	2.00	2.00

Table 3-8: Amphibole group EMP and LA-ICP-MS analyses with formulae (continued)

EMP and LA-ICP-MS analyses

Unit	Hypersolvus granite north (3/3)									
Sample	204743-1	204743-4	204743-5	204743-7	204743-9	204743-10	204743-11	204743-12	Mdn	MAD
Species	lea	fl-lea	fl-lea	fl-lea	lea	fl-lea	fl-lea	fl-lea		
Major and minor elements (wt. %)										
SiO_2	50.70	50.22	50.49	50.55	51.01	51.14	50.47	50.73	50.71	0.19
TiO_2	0.84	0.85	0.86	1.14	0.85	0.92	0.89	1.07	1.09	0.14
Al_2O_3	0.61	0.50	0.53	0.43	0.53	0.48	0.55	0.49	0.50	0.08
FeO	32.06	31.74	32.04	31.85	31.87	31.73	31.91	31.95	32.06	0.27
MnO	0.88	0.82	0.94	0.78	0.79	0.78	0.85	0.76	0.85	0.03
MgO	0.19	0.22	0.23	0.20	0.63	0.22	0.25	0.21	0.22	0.03
ZnO	0.47	0.44	0.57	0.41	0.34	0.42	0.54	0.36	0.45	0.04
ZrO_2	0.13	0.15	0.12	0.23	0.15	0.15	0.09	0.16	0.17	0.04
Nb_2O_5	-	-	0.04	0.02	0.02	-	-	0.02	0.02	0.02
Na_2O	9.44	9.47	9.45	9.48	9.72	9.58	9.54	9.29	9.36	0.09
K_2O	1.56	1.77	1.48	1.67	1.56	1.82	1.50	1.73	1.59	0.11
CaO	0.44	0.67	0.59	0.40	0.46	0.47	0.46	0.46	0.47	0.08
F	1.86	2.48	1.96	1.99	1.81	2.02	2.08	2.25	2.08	0.12
Cl	0.01	0.01	-	-	0.02	0.01	0.02	-	0.01	0.01
Total	99.19	99.33	99.28	99.16	99.74	99.74	99.16	99.50	99.87	0.34
Trace elements (ppm)										
Li	4096	4063	4090	4094	4780	4138	3831	4014	3099	549
Rb	53.4	51.2	57.1	67.2	61.8	59.0	49.4	71.5	61.8	9.4
Sr	19.7	17.1	15.9	7.4	16.5	10.5	9.9	11.0	11.7	3.7
Y	234	139	301	79.2	112	44.4	70.1	76.7	107	27
Zr	2198	2302	2280	2648	2163	2467	2381	2726	2648	450
Sn	103	106	130	131	112	95.6	95.5	122	156	49
La	50.8	47.3	41.9	21.2	50.6	31.9	31.1	35.0	32.4	5.9
Ce	130	113	92.7	55.5	107	84.0	91.2	90.2	85.9	22.6
Pr	20.8	17.5	14.9	8.6	18.0	12.9	14.4	13.7	13.7	4.3
Nd	97.3	89.6	86.9	40.0	82.6	59.3	67.2	63.3	62.3	20.5
Sm	21.0	17.0	19.2	8.8	16.8	7.9	10.5	10.8	11.6	4.5
Eu	1.3	1.0	1.3	0.51	0.96	0.23	0.41	0.33	0.68	0.30
Gd	20.4	12.2	18.8	5.2	10.1	2.9	2.9	4.9	7.6	3.1
Tb	4.5	2.8	5.5	1.5	2.5	0.48	0.57	0.98	1.6	0.6
Dy	34.9	24.3	45.9	12.4	18.3	6.1	7.9	10.0	18.3	5.7
Ho	9.3	7.5	14.6	5.1	6.5	3.0	4.6	5.0	7.7	1.8
Er	44.2	39.1	53.9	30.0	33.5	28.9	32.9	32.9	48.5	12.3
Tm	12.6	11.3	13.5	9.7	11.7	11.3	11.1	11.9	17.5	4.8
Yb	165	151	147	125	151	148	142	154	215	53
Lu	35.1	35.0	30.2	28.9	34.6	34.7	33.8	36.4	50.1	11.5
Hf	86.2	88.8	91.0	107	86.0	100	98.3	108	130	25
Ta	2.1	2.4	2.3	2.2	2.6	2.3	2.0	2.9	2.9	0.8
Pb	25.0	19.5	13.8	17.7	20.2	21.3	21.0	23.5	34.5	10.5
Nb	190	191	181	182	179	185	183	215	214	34
Ba	6.4	7.6	4.7	4.3	12.2	3.6	2.0	3.5	6.0	2.4
Th	0.51	0.77	2.6	0.23	2.3	0.13	0.04	0.05	0.51	0.47
U	0.08	0.06	0.13	0.01	0.05	0.04	-	0.02	0.03	0.03
REE+Y	881	708	887	431	656	476	521	546	708	174

Table 3-8: Amphibole group EMP and LA-ICP-MS analyses with formulae (continued)

Formulae

Unit	Hypersolvus granite north (3/3)							
Sample	204743-1	204743-4	204743-5	204743-7	204743-9	204743-10	204743-11	204743-12
Species	lea	fl-lea	fl-lea	fl-lea	lea	fl-lea	fl-lea	fl-lea
(apfu)								
Si	7.75	7.73	7.73	7.76	7.71	7.78	7.75	7.78
Al	0.11	0.09	0.10	0.08	0.09	0.09	0.10	0.09
Ti	0.10	0.10	0.10	0.13	0.10	0.11	0.10	0.12
$^{T}Fe^{3+}$	0.04	0.08	0.07	0.03	0.10	0.03	0.05	0.01
T (8)	8.00	8.00	8.00	8.00	8.00	8.00	8.00	8.00
Zr	0.01	0.01	0.01	0.02	0.01	0.01	0.01	0.01
REE+Y	0.01	0.01	0.01	0.01	0.01	0.01	0.01	0.01
$^{C}Fe^{3+}$	1.93	1.95	1.92	1.97	1.96	1.95	1.94	1.92
Zn	0.05	0.05	0.06	0.05	0.04	0.05	0.06	0.04
Mn^{2+}	0.11	0.11	0.12	0.10	0.10	0.10	0.11	0.10
Fe^{2+}	2.13	2.06	2.11	2.09	1.98	2.06	2.11	2.17
Mg	0.04	0.05	0.05	0.05	0.14	0.05	0.06	0.05
Li	0.54	0.54	0.54	0.54	0.63	0.55	0.51	0.53
C (5)	4.83	4.77	4.83	4.82	4.86	4.77	4.81	4.83
Ca	0.07	0.11	0.10	0.07	0.08	0.08	0.08	0.08
^{B}Na	1.93	1.89	1.90	1.93	1.93	1.92	1.92	1.93
B (2)	2.00	2.00	2.00	2.00	2.00	2.00	2.00	2.00
^{A}Na	0.87	0.93	0.90	0.89	0.92	0.90	0.92	0.84
K	0.31	0.35	0.29	0.33	0.30	0.35	0.29	0.34
A (≤1)	1.18	1.28	1.19	1.21	1.23	1.26	1.21	1.18
OH	0.90	0.60	0.86	0.77	0.94	0.81	0.78	0.66
F	0.90	1.21	0.95	0.97	0.87	0.97	1.01	1.09
Cl								
O	0.19	0.20	0.20	0.26	0.19	0.21	0.21	0.25
W (2)	2.00	2.00	2.00	2.00	2.00	2.00	2.00	2.00

Table 3-8: Amphibole group EMP and LA-ICP-MS analyses with formulae (continued)

EMP and LA-ICP-MS analyses

Unit	Transsolvus granite (1/5)														
Sample	1001 4-1	1001 4-2	1001 4-4	1001 4-5	1001 4-6	1001 4-7	1001 4b-1	1001 4b-2	1001 4b-3	1001 4b-6	1003 5-10	1003 5-4	1003 5-5	1003 5-6	1003 5-7
Species	fl-arf	fl-arf	fl-arf	fl-arf	fl-arf	fl-arf	fl-lea	fl-lea	fl-lea	fl-lea	fl-arf	fl-arf	fl-arf	fl-arf	fl-arf
Major and minor elements (wt. %)															
SiO_2	51.62	52.11	52.11	51.40	51.65	51.69	51.90	51.92	51.96	51.93	51.56	51.58	52.07	52.09	52.21
TiO_2	0.53	0.70	0.62	0.66	0.64	0.99	0.71	0.73	0.71	0.70	0.61	0.92	0.87	0.83	0.85
Al_2O_3	0.37	0.34	0.36	0.30	0.33	0.29	0.37	0.34	0.37	0.35	0.46	0.47	0.49	0.55	0.28
FeO	33.25	33.21	33.05	33.11	32.96	32.36	31.88	31.38	31.73	31.64	32.63	32.67	32.61	32.57	32.68
MnO	0.50	0.55	0.52	0.54	0.55	0.61	0.66	0.77	0.66	0.68	0.56	0.55	0.58	0.61	0.57
MgO	0.02	0.09	0.07	0.12	0.06	0.08	0.05	0.07	0.06	0.06	0.07	0.12	0.14	0.12	0.12
ZnO	0.23	0.29	0.26	0.27	0.24	0.35	0.44	0.48	0.40	0.39	0.26	0.25	0.24	0.26	0.27
ZrO_2	0.07	0.05	0.04	0.19	0.08	0.10	0.13	0.10	0.15	0.09	0.07	0.14	0.08	0.06	0.10
Nb_2O_5	-	-	-	-	0.02	0.05	0.05	0.03	0.05	0.04	0.04	0.01	0.04	0.01	-
Na_2O	9.67	9.64	9.64	9.58	9.56	9.23	9.70	9.46	9.64	9.71	9.66	9.58	9.65	9.58	9.55
K_2O	1.64	1.59	1.64	1.60	1.66	2.15	1.67	1.87	1.75	1.91	1.65	1.57	1.55	1.52	1.64
CaO	0.13	0.13	0.13	0.15	0.15	0.06	0.15	0.09	0.12	0.08	0.29	0.37	0.46	0.44	0.21
F	2.53	2.48	2.59	2.68	2.59	2.42	2.53	2.68	2.46	2.46	2.35	2.44	2.12	2.24	2.50
Cl	-	0.01	0.01	-	-	0.01	-	0.01	0.01	0.01	0.01	0.02	0.01	-	0.02
Total	100.6	101.2	101.0	100.6	100.5	100.4	100.2	99.92	100.1	100.0	100.2	100.7	100.9	100.9	101.0
Trace elements (ppm)															
Li	3350	2970	3070	3090	3170	830	4850	5580	4790	5250	1050	642	795	825	1290
Rb	63.1	75.7	78.8	80.5	43.6	80.5	21.5	27.8	23.6	64.3	32.5	29.0	30.2	31.3	56.2
Sr	2.1	1.8	1.2	1.6	0.81	0.94	1.1	0.56	1.1	1.1	3.3	3.2	3.4	3.5	1.5
Y	13.5	16.0	11.8	13.8	11.2	11.9	23.8	20.0	30.2	26.6	40.4	48.2	38.7	46.2	32.7
Zr	688	1265	764	1244	738	1104	975	1073	1149	904	601	805	694	867	920
Sn	64.0	98.1	63.9	72.9	61.7	70.9	139	105	119	92.4	36.6	38.8	39.2	42.5	67.2
La	2.9	1.9	0.9	1.3	1.0	0.9	2.2	2.7	1.9	8.1	5.7	8.1	7.3	7.1	2.3
Ce	8.6	5.8	3.1	4.5	3.9	3.1	6.3	7.8	5.7	18.5	20.7	28.0	26.4	25.7	8.7
Pr	1.2	0.77	0.53	0.66	0.56	0.48	0.87	1.0	0.79	2.3	3.2	4.2	4.0	3.8	1.3
Nd	4.7	3.1	1.8	2.4	2.6	1.8	3.3	3.8	3.4	9.5	13.8	18.2	16.6	16.4	5.1
Sm	0.92	0.74	0.45	0.53	0.53	0.32	0.55	1.2	0.68	2.3	2.8	4.1	3.0	3.6	1.1
Eu	0.07	0.04	0.01	0.04	0.03	0.04	0.04	0.06	0.07	0.08	0.15	0.28	0.14	0.16	0.08
Gd	0.81	0.37	0.28	0.41	0.33	0.20	0.27	0.85	0.48	1.2	1.8	2.9	1.6	2.4	0.83
Tb	0.17	0.14	0.09	0.13	0.09	0.08	0.07	0.15	0.11	0.22	0.32	0.50	0.24	0.46	0.19
Dy	1.7	1.8	1.2	1.5	1.2	1.3	1.1	1.7	1.6	2.1	2.9	4.3	2.6	4.1	2.1
Ho	0.65	0.84	0.55	0.68	0.54	0.62	0.75	0.56	0.81	0.72	1.00	1.5	1.1	1.3	0.80
Er	4.0	5.9	3.8	4.8	3.9	4.4	6.5	3.9	6.6	5.3	6.4	8.2	7.1	7.1	5.2
Tm	1.3	2.0	1.4	1.6	1.4	1.4	2.2	1.6	2.3	2.0	1.9	2.6	2.4	2.2	1.7
Yb	18.8	27.0	18.4	21.7	18.3	19.7	33.8	20.8	32.2	29.9	23.8	32.8	30.7	28.3	21.6
Lu	4.6	6.4	4.6	5.7	4.6	4.9	8.3	5.2	7.8	6.9	5.7	7.7	7.2	6.8	5.3
Hf	39.1	69.3	34.5	65.1	31.1	68.2	99.0	51.8	81.6	42.0	23.9	32.6	27.6	32.9	40.8
Ta	1.3	1.7	0.90	1.1	0.84	0.84	1.7	1.5	1.4	1.6	0.34	0.45	0.37	0.51	0.92
Pb	5.8	5.6	3.4	4.1	3.1	3.6	5.4	6.6	4.3	13.9	3.2	5.9	4.1	7.7	3.1
Nb	-	-	-	14.0	168	377	322	175	377	287	294	41.9	252	90.9	-
Ba	0.18	0.34	0.09	0.15	0.43	0.31	0.85	0.78	1.3	1.7	0.81	1.0	0.68	1.3	0.32
Th	0.23	-	-	-	-	-	1.3	12.1	0.28	9.0	0.01	0.40	0.02	0.21	0.03
U	0.04	-	-	-	-	-	0.35	3.0	0.29	11.9	-	-	-	-	-
REE+Y	63.9	72.7	48.8	59.9	50.0	51.1	89.9	71.3	94.7	116	131	171	149	156	88.9

Table 3-8: Amphibole group EMP and LA-ICP-MS analyses with formulae (continued)

Formulae

Unit	Transsolvus granite (1/5)														
Sample	1001 4-1	1001 4-2	1001 4-4	1001 4-5	1001 4-7	1001 4a-6	1001 4b-1	1001 4b-2	1001 4b-3	1001 4b-6	1003 5-10	1003 5-4	1003 5-5	1003 5-6	1003 5-7
Species	fl-arf	fl-arf	fl-arf	fl-arf	fl-arf	fl-arf	fl-lea	fl-lea	fl-lea	fl-lea	fl-arf	fl-arf	fl-arf	fl-arf	fl-arf
(apfu)															
Si	7.87	7.91	7.92	7.87	8.06	7.90	7.86	7.87	7.87	7.85	7.99	7.99	8.00	8.01	8.03
$^{\mathrm{T}}$Al	0.07	0.06	0.06	0.06		0.06	0.07	0.06	0.07	0.06	0.01	0.01			
$^{\mathrm{T}}$Ti	0.06	0.03	0.01	0.08		0.04	0.08	0.08	0.06	0.08					
$^{\mathrm{T}}$Fe^{3+}										0.01					
T (8)	8.00	8.00	8.00	8.00	8.06	8.00	8.00	8.00	8.00	8.00	8.00	8.00	8.00	8.01	8.03
$^{\mathrm{C}}$Ti		0.05	0.06		0.12	0.03		0.01	0.02		0.07	0.11	0.10	0.10	0.10
Zr	0.01			0.01	0.01	0.01	0.01	0.01	0.01	0.01	0.01	0.01	0.01	0.01	0.01
$^{\mathrm{C}}$Al					0.05						0.07	0.08	0.09	0.10	0.05
REE+Y															
$^{\mathrm{C}}$Fe^{3+}	1.83	1.73	1.72	1.80	1.28	1.76	1.96	1.97	1.94	1.99	1.47	1.40	1.40	1.37	1.41
Zn	0.03	0.03	0.03	0.03	0.04	0.03	0.05	0.05	0.04	0.04	0.03	0.03	0.03	0.03	0.03
Mn^{2+}	0.07	0.07	0.07	0.07	0.08	0.07	0.09	0.10	0.08	0.09	0.07	0.07	0.08	0.08	0.07
Fe^{2+}	2.41	2.49	2.48	2.44	2.94	2.45	2.07	2.00	2.08	2.00	2.76	2.83	2.79	2.82	2.79
Mg	0.01	0.02	0.02	0.03	0.02	0.01	0.01	0.02	0.01	0.01	0.02	0.03	0.03	0.03	0.03
$^{\mathrm{C}}$Li	0.44	0.39	0.40	0.41	0.11	0.42	0.64	0.73	0.63	0.69	0.15	0.09	0.11	0.12	0.18
C (5)	4.79	4.79	4.78	4.79	4.65	4.79	4.83	4.89	4.82	4.83	4.64	4.65	4.64	4.65	4.67
$^{\mathrm{B}}$Li															
Ca	0.02	0.02	0.02	0.03	0.01	0.03	0.02	0.01	0.02	0.01	0.05	0.06	0.08	0.07	0.03
$^{\mathrm{B}}$Na	1.98	1.98	1.98	1.98	1.99	1.98	1.98	1.99	1.98	1.99	1.95	1.94	1.92	1.93	1.97
B (2)	2.00	2.00	2.00	2.00	2.00	2.00	2.00	2.00	2.00	2.00	2.00	2.00	2.00	2.00	2.00
$^{\mathrm{A}}$Na	0.88	0.86	0.86	0.87	0.80	0.86	0.87	0.79	0.85	0.86	0.95	0.94	0.95	0.93	0.88
K	0.32	0.31	0.32	0.31	0.43	0.32	0.32	0.36	0.34	0.37	0.33	0.31	0.30	0.30	0.32
A (≤1)	1.20	1.17	1.18	1.18	1.23	1.18	1.19	1.16	1.19	1.23	1.27	1.25	1.26	1.23	1.20
OH	0.66	0.65	0.61	0.55	0.57	0.60	0.63	0.55	0.66	0.66	0.71	0.59	0.77	0.72	0.58
F	1.22	1.19	1.25	1.30	1.19	1.25	1.21	1.28	1.18	1.18	1.15	1.20	1.03	1.09	1.22
Cl															
O	0.12	0.16	0.14	0.15	0.23	0.15	0.16	0.17	0.16	0.16	0.14	0.21	0.20	0.19	0.20
W (2)	2.00	2.00	2.00	2.00	2.00	2.00	2.00	2.00	2.00	2.00	2.00	2.00	2.00	2.00	2.00

Table 3-8: Amphibole group EMP and LA-ICP-MS analyses with formulae (continued)

EMP and LA-ICP-MS analyses

Unit	Transsolvus granite (2/5)														
Sample	1003 5-8	1003 5-9	1003 9-4	1003 9-5	1003 9-7	1003 9-8	1003 9-9	2047 13-1	2047 13-4	2047 13-5	2047 13-7	2047 13-8	2047 13-9	20471 3-10	2047 15-3
Species	fl-arf	fl-arf	fl-arf	fl-lea	fl-arf	fl-arf	fl-arf	fl-lea	fl-lea	fl-lea	fl-lea	fl-lea	fl-lea	fl-lea	fl-lea
Major and minor elements (wt. %)															
SiO_2	52.19	51.84	52.46	52.11	52.39	52.08	51.88	51.02	51.59	51.49	50.94	51.68	51.38	51.70	50.87
TiO_2	0.67	0.79	0.98	0.97	0.67	0.50	0.80	0.71	0.95	0.71	0.72	0.63	0.67	0.80	0.82
Al_2O_3	0.28	0.42	0.31	0.31	0.28	0.35	0.34	0.29	0.27	0.26	0.28	0.32	0.29	0.30	0.33
FeO	32.44	32.26	30.77	30.90	31.61	32.84	32.03	32.40	32.51	32.44	32.44	32.86	32.93	32.89	32.91
MnO	0.59	0.52	0.92	0.89	0.61	0.55	0.54	0.60	0.65	0.63	0.61	0.51	0.50	0.58	0.55
MgO	0.08	0.13	0.08	0.11	0.28	0.11	0.31	0.03	0.04	0.04	0.03	0.03	0.04	0.07	0.05
ZnO	0.28	0.31	0.58	0.62	0.33	0.26	0.28	0.29	0.32	0.30	0.30	0.25	0.26	0.27	0.67
ZrO_2	0.17	0.16	0.11	0.12	0.10	0.10	0.15	0.16	0.24	0.22	0.20	0.08	0.07	0.08	0.11
Nb_2O_5	0.01	0.04	0.02	0.03	0.02	0.02	0.02	0.02	-	-	-	0.03	-	0.01	0.01
Na_2O	9.70	9.61	9.68	9.55	9.49	9.77	9.58	9.56	9.80	9.56	9.56	9.71	9.61	9.77	9.61
K_2O	1.77	1.69	1.93	1.85	1.82	1.63	1.58	1.97	1.72	1.81	1.85	1.56	1.72	1.66	1.54
CaO	0.11	0.23	0.14	0.15	0.10	0.12	0.24	0.09	0.10	0.09	0.11	0.09	0.12	0.10	0.13
F	2.01	2.30	2.19	2.06	2.42	2.11	2.27	2.69	3.04	3.00	2.91	3.15	2.72	2.70	2.50
Cl	-	0.01	-	-	0.01	0.01	0.01	-	-	0.01	-	-	-	-	-
Total	100.3	100.3	100.2	99.67	100.1	100.4	100.0	99.84	101.2	100.6	99.94	100.9	100.3	100.9	100.1
Trace elements (ppm)															
Li	1770	2200	3140	3540	2610	2900	2520	6620	7220	6580	6560	7840	5854	7020	7150
Rb	49.6	50.4	77.9	91.3	98.4	65.1	79.7	136	136	131	123	125	89.3	115	118
Sr	3.8	6.6	4.5	1.5	2.3	2.0	3.0	0.62	0.97	0.97	1.2	2.3	0.82	0.81	1.8
Y	32.5	41.4	43.3	46.7	113	49.9	45.4	22.6	30.8	20.7	21.3	46.4	21.1	24.5	28.1
Zr	917	911	1071	921	1042	1125	1034	1666	1711	3870	3207	1349	1683	1871	2340
Sn	62.7	55.4	56.1	93.3	228	71.6	59.3	184	182	267	223	359	135	162	180
La	4.6	4.7	3.4	0.9	1.3	1.5	1.9	1.8	1.2	1.1	1.4	3.5	1.9	1.6	3.2
Ce	17.0	14.5	10.3	2.6	4.8	5.5	6.4	2.4	3.6	2.4	2.8	7.8	3.2	4.7	6.4
Pr	2.4	1.9	1.4	0.35	0.64	0.76	0.93	0.51	0.53	0.33	0.33	1.1	0.60	0.60	0.59
Nd	10.2	7.0	5.9	1.3	2.5	3.3	3.7	2.1	2.5	1.2	1.8	4.7	2.3	2.6	3.7
Sm	1.4	1.6	0.84	0.28	0.41	0.90	0.90	0.54	0.41	0.14	0.09	0.76	0.41	0.44	0.53
Eu	0.09	0.09	0.06	0.05	0.08	0.06	0.05	0.03	0.04	0.03	0.04	0.05	0.03	0.03	0.03
Gd	0.42	1.5	0.54	0.26	0.61	0.49	0.54	0.15	0.30	0.36	0.28	0.90	0.46	0.33	1.3
Tb	0.12	0.34	0.12	0.10	0.26	0.13	0.20	0.21	0.20	0.07	0.13	0.30	0.11	0.11	0.31
Dy	1.7	3.4	1.8	1.9	4.0	2.0	2.3	2.7	2.6	2.2	2.4	3.5	2.6	3.0	3.3
Ho	0.91	1.1	0.91	0.95	2.4	1.1	0.92	1.2	1.8	1.1	1.2	2.1	1.0	1.3	1.4
Er	6.8	6.7	6.9	6.7	19.4	6.7	5.9	7.9	11.9	8.1	8.3	14.9	7.9	9.3	8.4
Tm	2.5	2.0	2.3	2.4	6.6	2.2	2.1	2.5	4.3	2.9	2.6	4.9	2.6	3.4	3.7
Yb	33.1	26.0	30.6	30.5	85.6	26.5	26.7	33.5	57.5	41.2	39.1	55.8	37.9	41.9	47.6
Lu	7.5	6.1	7.1	6.7	17.4	5.9	6.4	7.7	14.2	9.7	10.7	12.0	9.6	11.0	11.8
Hf	48.2	36.9	43.6	38.7	45.9	53.3	44.0	75.2	57.8	234	175	56.0	69.7	78.1	117
Ta	0.42	0.57	0.62	0.60	0.59	0.87	0.55	1.0	1.2	1.4	1.2	1.2	0.96	1.2	1.1
Pb	3.9	6.2	5.0	4.3	5.5	3.3	3.6	10.8	8.8	6.2	7.9	16.9	5.1	6.2	8.7
Nb	41.9	266	147	189	147	147	133	85.3	90.4	94.8	90.8	193	82.2	101	104
Ba	0.63	0.91	0.62	0.55	1.3	0.31	0.31	0.07	0.30	-	1.1	0.91	0.14	0.42	0.43
Th	0.03	0.35	-	-	0.04	-	0.01	0.28	0.03	0.07	-	0.01	-	-	0.04
U	-	-	-	-	0.04	-	0.05	0.12	0.03	0.03	0.03	0.10	0.02	0.01	0.08
REE+Y	121	118	116	102	259	107	104	85.7	92.3	159	105	131	129	127	95.7

Table 3-8: Amphibole group EMP and LA-ICP-MS analyses with formulae (continued)

Formulae

Unit	Transsolvus granite (2/5)														
Sample	1003 5-8	1003 5-9	1003 9-4	1003 9-5	1003 9-7	1003 9-8	1003 9-9	2047 13-1	2047 13-4	2047 13-5	2047 13-7	2047 13-8	2047 13-9	20471 3-10	2047 15-3
Species	fl-arf	fl-arf	fl-arf	fl-lea	fl-arf	fl-arf	fl-arf	fl-lea	fl-lea	fl-lea	fl-lea	fl-lea	fl-lea	fl-lea	fl-lea
(apfu)															
Si	8.01	7.96	7.97	7.95	8.01	7.90	7.94	7.73	7.71	7.76	7.73	7.72	7.77	7.72	7.67
^{T}Al		0.04	0.03	0.06		0.06	0.06	0.05	0.05	0.05	0.05	0.06	0.05	0.05	0.06
^{T}Ti						0.04		0.08	0.11	0.08	0.08	0.07	0.08	0.09	0.09
^{T}Fe^{3+}								0.14	0.14	0.11	0.14	0.16	0.11	0.14	0.18
T (8)	8.01	8.00	8.00	8.00	8.01	8.00	8.00	8.00	8.00	8.00	8.00	8.00	8.00	8.00	8.00
^{C}Ti	0.08	0.09	0.11	0.11	0.08	0.02	0.09								
Zr	0.01	0.01	0.01	0.01	0.01	0.01	0.01	0.01	0.02	0.02	0.02	0.01	0.01	0.01	0.01
^{C}Al	0.05	0.03	0.03	0.00	0.05		0.01								
REE+Y															
^{C}Fe^{3+}	1.51	1.59	1.72	1.75	1.58	1.81	1.66	2.06	2.08	2.03	2.05	2.08	2.02	2.07	2.07
Zn	0.03	0.04	0.07	0.07	0.04	0.03	0.03	0.03	0.04	0.03	0.03	0.03	0.03	0.03	0.07
Mn^{2+}	0.08	0.07	0.12	0.12	0.08	0.07	0.07	0.08	0.08	0.08	0.08	0.06	0.06	0.07	0.07
Fe^{2+}	2.65	2.55	2.19	2.19	2.46	2.35	2.44	1.91	1.85	1.95	1.93	1.87	2.04	1.91	1.90
Mg	0.02	0.03	0.02	0.03	0.06	0.02	0.07	0.01	0.01	0.01	0.01	0.01	0.01	0.02	0.01
^{B}Li	0.25	0.30	0.48	0.51	0.40	0.46	0.37	0.87	0.93	0.86	0.86	0.95	0.77	0.90	0.87
C (5)	4.68	4.71	4.74	4.78	4.76	4.77	4.75	4.96	5.00	4.97	4.97	5.00	4.93	5.00	5.00
^{C}Li									0.01			0.07		0.01	0.06
Ca	0.02	0.04	0.02	0.03	0.02	0.02	0.04	0.01	0.02	0.01	0.02	0.02	0.02	0.02	0.02
^{B}Na	1.98	1.96	1.98	1.98	1.98	1.98	1.96	1.99	1.98	1.99	1.98	1.92	1.98	1.98	1.92
B (2)	2.00	2.00	2.00	2.00	2.00	2.00	2.00	2.00	2.00	2.00	2.00	2.00	2.00	2.00	2.00
^{A}Na	0.90	0.90	0.87	0.85	0.83	0.89	0.88	0.82	0.86	0.81	0.83	0.90	0.84	0.85	0.89
K	0.35	0.33	0.37	0.36	0.36	0.32	0.31	0.38	0.33	0.35	0.36	0.30	0.33	0.32	0.30
A (≤1)	1.25	1.23	1.25	1.21	1.18	1.21	1.19	1.20	1.19	1.16	1.19	1.19	1.17	1.17	1.19
OH	0.87	0.70	0.73	0.78	0.68	0.87	0.72	0.55	0.35	0.41	0.44	0.37	0.55	0.54	0.62
F	0.97	1.12	1.05	1.00	1.17	1.01	1.10	1.29	1.44	1.43	1.39	1.49	1.30	1.28	1.19
Cl															
O	0.16	0.18	0.22	0.22	0.16	0.11	0.18	0.16	0.21	0.16	0.16	0.14	0.15	0.18	0.19
W (2)	2.00	2.00	2.00	2.00	2.00	2.00	2.00	2.00	2.00	2.00	2.00	2.00	2.00	2.00	2.00

Table 3-8: Amphibole group EMP and LA-ICP-MS analyses with formulae (continued)

EMP and LA-ICP-MS analyses

Unit	Transsolvus granite (3/5)														
Sample	204715-4	204715-5	204715-7	204715-8	204715-9	204715-10	204805-1	204805-2	204805-3	204805-4	204805-5	204805-6	204805-7	204805-8	204805-9
Species	fl-lea	fl-lea	fl-lea	fl-lea	fl-lea	fl-lea	fl-lea	fl-lea	fl-lea	fl-lea	fl-lea	fl-lea	fl-lea	fl-lea	fl-lea
Major and minor elements (wt. %)															
SiO_2	50.79	50.71	50.67	50.77	50.38	50.43	50.52	49.39	49.84	50.19	49.10	48.99	50.01	49.04	49.98
TiO_2	0.71	0.65	0.63	0.72	0.70	0.70	0.65	0.71	0.64	0.76	0.67	0.61	0.62	0.67	0.58
Al_2O_3	0.36	0.23	0.33	0.35	0.27	0.28	0.41	0.45	0.39	0.46	0.48	0.39	0.42	0.39	0.36
FeO	33.06	31.53	32.63	32.65	32.69	32.78	32.62	32.43	32.43	32.64	32.35	32.10	32.26	32.42	32.00
MnO	0.49	0.94	0.54	0.55	0.60	0.56	0.49	0.49	0.47	0.52	0.44	0.51	0.51	0.49	0.56
MgO	0.13	0.06	0.12	0.06	0.06	0.12	0.13	0.10	0.10	0.08	0.12	0.11	0.10	0.11	0.09
ZnO	0.70	0.64	0.62	0.62	0.63	0.48	0.29	0.27	0.28	0.27	0.27	0.27	0.23	0.23	0.30
ZrO_2	0.12	0.08	0.12	0.14	0.19	0.11	0.05	0.05	0.08	0.08	0.06	0.18	0.13	0.09	0.09
Nb_2O_5	0.01	0.01	0.01	0.01	0.01	0.01	0.01	0.01	0.02	0.01	0.01	0.01	0.01	0.01	0.01
Na_2O	9.43	9.09	9.38	9.35	9.45	9.37	9.90	9.59	9.75	9.43	9.57	9.48	9.28	9.59	9.53
K_2O	1.52	2.33	1.75	1.49	1.73	1.68	1.53	1.57	1.50	1.55	1.43	1.57	1.53	1.48	1.49
CaO	0.17	0.16	0.16	0.09	0.12	0.13	0.13	0.18	0.15	0.17	0.22	0.12	0.20	0.11	0.12
F	2.54	2.12	2.69	2.66	2.55	2.58	2.56	2.11	2.79	2.16	2.53	2.87	2.57	2.45	2.68
Cl	-	0.01	0.02	-	-	-	-	0.01	0.01	0.01	0.01	0.01	0.02	0.01	-
Total	100.0	98.55	99.68	99.45	99.39	99.22	99.27	97.36	98.45	98.31	97.26	97.21	97.88	97.07	97.79
Trace elements (ppm)															
Li	6920	6506	5892	6773	5800	4430	5190	8630	8430	6440	6740	6329	4245	6753	6380
Rb	113	85.5	97.5	81.3	101	60.8	58.6	105	101	93.9	89.6	83.1	49.0	81.8	85.3
Sr	1.6	0.84	1.3	1.7	0.90	0.84	1.6	1.6	1.9	1.5	0.68	1.3	1.2	1.1	1.6
Y	27.2	24.7	23.2	34.7	21.6	21.9	31.1	32.3	32.9	23.9	29.2	32.4	22.7	26.8	28.7
Zr	1586	1706	1403	1729	3570	1448	1318	1350	1552	1313	1238	1290	1311	1285	2366
Sn	153	139	132	127	219	101	127	159	170	139	149	136	96	134	156
La	3.8	2.3	2.8	5.0	1.2	1.7	5.8	3.6	3.0	2.5	3.0	4.4	3.9	2.7	3.2
Ce	5.7	5.2	5.3	13.7	2.8	4.9	12.9	10.9	8.6	6.0	9.7	10.5	9.3	9.6	9.2
Pr	0.85	0.91	0.90	1.8	0.40	0.62	2.2	2.0	1.3	0.91	1.5	2.1	1.3	1.2	1.5
Nd	4.0	4.2	4.1	9.2	1.9	3.3	12.2	8.4	6.4	4.7	8.2	10.3	7.0	6.1	7.9
Sm	1.1	1.0	0.8	1.7	0.5	0.4	3.1	1.9	1.3	0.8	0.4	2.7	1.1	2.7	1.8
Eu	0.05	0.07	0.05	0.06	0.03	0.03	0.15	0.03	0.04	0.10	0.03	0.15	0.04	0.05	0.06
Gd	0.50	0.80	0.55	1.7	0.44	0.35	2.8	1.9	0.97	0.52	1.4	2.7	1.2	1.1	1.1
Tb	0.24	0.20	0.19	0.45	0.18	0.13	0.37	0.39	0.43	0.30	0.14	0.48	0.17	0.27	0.35
Dy	2.7	3.0	2.2	4.1	2.3	2.4	3.8	3.0	3.5	2.6	3.2	3.8	2.5	3.4	3.5
Ho	1.3	1.2	1.2	1.7	1.1	1.1	1.6	1.5	1.4	1.4	1.6	1.6	1.1	1.5	1.4
Er	8.9	8.4	8.2	10.9	8.5	8.1	7.7	9.9	11.0	7.6	9.3	8.9	7.7	8.1	8.0
Tm	2.8	2.8	2.7	3.7	3.0	3.2	2.7	3.3	3.3	2.7	3.6	2.6	2.4	2.2	2.7
Yb	38.0	37.0	33.5	46.3	40.3	39.7	35.7	40.2	43.0	33.5	41.7	32.8	34.5	32.1	32.7
Lu	9.5	9.0	8.2	11.2	10.7	9.7	8.9	9.3	10.3	8.2	9.4	7.9	8.3	7.1	7.8
Hf	75.8	105	61.1	71.7	215	62.5	70.8	58.8	69.7	58.6	55.4	55.8	91.7	61.9	151
Ta	1.1	0.98	0.88	1.3	1.2	1.2	1.7	0.98	1.3	0.96	0.93	1.1	2.2	0.98	0.97
Pb	5.0	7.5	6.6	6.6	5.8	4.8	3.9	4.1	4.6	4.4	4.3	4.6	3.8	5.8	3.5
Nb	95.4	77.0	82.6	95.7	88.3	70.0	92.3	101	116	90.6	88.6	92.4	87.4	90.6	76.3
Ba	1.4	0.65	0.36	0.07	0.33	0.20	0.40	0.67	1.1	0.43	0.44	-	0.34	0.26	0.51
Th	0.06	0.02	0.07	7.2	-	-	0.19	-	1.2	-	0.02	-	-	-	0.62
U	0.04	0.02	0.03	0.01	0.01	-	0.06	0.01	0.27	0.02	0.02	-	0.01	0.01	0.81
REE+Y	122	123	103	105	110	100	131	129	127	95.7	122	123	103	105	110

Table 3-8: Amphibole group EMP and LA-ICP-MS analyses with formulae (continued)

Formulae

Unit	Transsolvus granite (3/5)														
Sample	204715-4	204715-5	204715-7	204715-8	204715-9	204715-10	204805-1	204805-2	204805-3	204805-4	204805-5	204805-6	204805-7	204805-8	204805-9
Species	fl-lea	fl-lea	fl-lea	fl-lea	fl-lea	fl-lea	fl-lea	fl-lea	fl-lea	fl-lea	fl-lea	fl-lea	fl-lea	fl-lea	fl-lea
(apfu)															
Si	7.67	7.76	7.73	7.72	7.71	7.77	7.73	7.56	7.60	7.69	7.62	7.65	7.80	7.62	7.72
^{T}Al	0.06	0.04	0.06	0.06	0.05	0.05	0.07	0.08	0.07	0.08	0.09	0.07	0.08	0.07	0.07
^{T}Ti	0.08	0.08	0.07	0.08	0.08	0.08	0.07	0.08	0.07	0.09	0.08	0.07	0.07	0.08	0.07
^{T}Fe^{3+}	0.18	0.13	0.14	0.14	0.17	0.10	0.13	0.28	0.26	0.14	0.21	0.21	0.05	0.23	0.15
T (8)	8.00	8.00	8.00	8.00	8.00	8.00	8.00	8.00	8.00	8.00	8.00	8.00	8.00	8.00	8.00
^{C}Ti															
Zr	0.01	0.01	0.01	0.01	0.01	0.01			0.01	0.01	0.01	0.01	0.01	0.01	0.01
^{C}Al															
REE+Y															
^{C}Fe^{3+}	2.03	2.02	2.00	2.03	2.01	1.95	2.03	2.16	2.14	2.06	2.09	2.06	1.93	2.09	2.04
Zn	0.08	0.07	0.07	0.07	0.07	0.05	0.03	0.03	0.03	0.03	0.03	0.03	0.03	0.03	0.03
Mn^{2+}	0.06	0.12	0.07	0.07	0.08	0.07	0.06	0.06	0.06	0.07	0.06	0.07	0.07	0.06	0.07
Fe^{2+}	1.96	1.89	2.02	1.99	2.01	2.17	2.02	1.72	1.73	1.98	1.90	1.93	2.23	1.89	1.95
Mg	0.03	0.01	0.03	0.01	0.01	0.03	0.03	0.02	0.02	0.02	0.03	0.03	0.02	0.03	0.02
^{B}Li	0.83	0.86	0.78	0.82	0.77	0.59	0.69	1.00	1.00	0.84	0.89	0.86	0.57	0.89	0.85
C (5)	5.00	4.98	4.97	5.00	4.96	4.88	4.86	5.00	5.00	5.00	5.00	4.98	4.86	5.00	4.98
^{C}Li	0.08			0.07				0.14	0.11	0.01	0.01			0.02	
Ca	0.03	0.03	0.03	0.01	0.02	0.02	0.02	0.03	0.02	0.03	0.04	0.02	0.03	0.02	0.02
^{B}Na	1.90	1.97	1.97	1.92	1.98	1.98	1.98	1.83	1.87	1.96	1.95	1.98	1.97	1.96	1.98
B (2)	2.00	2.00	2.00	2.00	2.00	2.00	2.00	2.00	2.00	2.00	2.00	2.00	2.00	2.00	2.00
^{A}Na	0.86	0.72	0.80	0.84	0.82	0.82	0.96	1.02	1.01	0.84	0.93	0.89	0.84	0.93	0.88
K	0.29	0.46	0.34	0.29	0.34	0.33	0.30	0.31	0.29	0.30	0.28	0.31	0.30	0.29	0.29
A (≤1)	1.16	1.18	1.14	1.13	1.16	1.15	1.26	1.32	1.30	1.14	1.21	1.20	1.15	1.22	1.17
OH	0.62	0.82	0.55	0.56	0.61	0.58	0.61	0.82	0.51	0.78	0.60	0.44	0.58	0.64	0.56
F	1.22	1.03	1.30	1.28	1.23	1.25	1.24	1.02	1.34	1.05	1.24	1.42	1.27	1.20	1.31
Cl			0.01										0.01		
O	0.16	0.15	0.15	0.17	0.16	0.16	0.15	0.16	0.15	0.18	0.16	0.14	0.15	0.16	0.13
W (2)	2.00	2.00	2.00	2.00	2.00	2.00	2.00	2.00	2.00	2.00	2.00	2.00	2.00	2.00	2.00

Table 3-8: Amphibole group EMP and LA-ICP-MS analyses with formulae (continued)

EMP and LA-ICP-MS analyses															
Unit	Transsolvus granite (4/5)														
Sample	204805-10	204720-1	204720-2	204720-3	204720-4	204720-5	204720-6	204720-7	204720-8	204720-9	204720-10	204722-5	204722-6	204722-7	204722-8
Species	fl-lea	fl-lea	fl-lea	fl-lea	fl-lea	fl-lea	fl-lea	fl-lea	fl-lea	fl-lea	fl-lea	fl-lea	fl-lea	fl-lea	fl-lea
Major and minor elements (wt. %)															
SiO_2	50.87	50.71	50.95	50.98	50.61	51.02	50.98	51.38	51.72	51.58	51.14	50.95	50.95	50.93	50.76
TiO_2	0.56	0.80	0.72	0.90	0.67	0.62	0.70	0.90	1.19	0.59	0.60	1.00	0.70	0.85	1.18
Al_2O_3	0.40	0.36	0.36	0.35	0.35	0.35	0.33	0.37	0.29	0.38	0.37	0.24	0.28	0.18	0.30
FeO	32.53	32.31	33.01	32.49	32.82	33.01	32.27	32.56	32.12	32.80	32.03	32.33	31.65	31.85	32.06
MnO	0.56	0.60	0.53	0.57	0.55	0.55	0.60	0.56	0.56	0.54	0.51	0.67	0.70	0.64	0.56
MgO	0.13	0.06	0.07	0.11	0.04	0.05	0.07	0.04	0.09	0.07	0.08	0.05	0.06	0.10	0.07
ZnO	0.29	0.30	0.24	0.29	0.27	0.28	0.27	0.26	0.28	0.29	0.34	0.79	0.47	1.09	0.74
ZrO_2	0.17	0.17	0.13	0.39	0.09	0.13	0.09	0.17	0.10	0.02	0.05	0.14	0.12	0.14	0.18
Nb_2O_5	0.01	0.01	0.01	0.02	0.01	0.01	0.01	0.01	0.03	0.01	0.01	0.02	0.01	0.01	0.02
Na_2O	9.57	9.67	9.66	10.05	9.73	9.78	9.84	9.67	9.84	9.80	9.83	9.12	9.30	9.03	9.30
K_2O	1.64	1.78	1.81	1.53	1.65	1.63	1.71	1.59	1.68	1.57	1.57	1.92	1.82	2.17	1.70
CaO	0.12	0.14	0.12	0.13	0.13	0.11	0.13	0.15	0.07	0.10	0.13	0.09	0.09	0.16	0.07
F	2.95	2.09	3.16	2.94	2.95	2.63	2.70	2.77	2.94	2.72	3.05	1.92	2.15	2.11	1.91
Cl	0.01	0.01	-	-	-	-	-	0.01	0.01	0.01	0.01	-	0.02	-	0.01
Total	99.79	99.00	100.8	100.7	99.87	100.2	99.69	100.4	100.9	100.5	99.72	99.22	98.33	99.24	98.85
Trace elements (ppm)															
Li	5440	5260	5080	9120	5951	5420	6180	4400	5490	4580	5750	5899	3890	7050	7275
Rb	81.3	85.8	78.6	151	98.0	89.1	83.2	73.9	129	66.2	58.7	172	87.2	109	143
Sr	1.9	3.6	6.9	1.4	0.97	1.2	1.7	0.81	0.65	0.91	3.2	0.56	0.47	1.3	0.47
Y	24.7	30.5	30.2	38.4	23.4	22.4	29.4	23.4	23.9	21.6	30.4	26.4	15.4	33.3	24.4
Zr	1283	1945	3149	1848	1554	1528	1642	1165	2980	1237	2389	2662	832	1872	1488
Sn	131	143	268	212	132	134	141	95.6	287	124	99	317	141	164	230
La	3.1	28.9	45.5	10.8	2.8	1.7	13.5	2.2	1.9	4.0	18.2	1.8	1.5	3.2	1.6
Ce	7.3	21.5	13.6	18.0	5.9	4.4	23.6	6.2	4.5	10.2	22.0	4.3	3.4	5.8	4.5
Pr	1.0	2.5	1.6	2.5	0.89	1.1	2.5	0.82	0.68	1.2	3.4	0.70	0.50	0.81	0.75
Nd	5.7	11.4	8.9	11.8	4.5	3.4	14.6	4.7	3.3	6.6	16.2	2.9	2.1	3.5	3.0
Sm	1.1	1.2	1.3	2.0	1.2	0.77	1.6	1.1	0.64	1.1	2.2	0.26	0.35	0.83	0.57
Eu	0.05	0.03	0.10	0.20	0.04	0.08	0.11	0.01	0.04	-	0.08	0.05	-	0.04	0.02
Gd	0.47	2.5	1.4	2.9	0.51	0.38	1.7	0.61	0.34	0.73	1.1	0.61	0.41	0.80	0.37
Tb	0.21	0.29	0.27	0.42	0.15	0.17	0.29	0.21	0.26	0.27	0.39	0.13	0.10	0.29	0.12
Dy	2.5	2.7	3.5	3.8	1.9	2.1	3.5	2.6	2.2	2.5	3.1	2.4	1.5	3.7	2.6
Ho	1.4	1.6	1.6	1.8	1.2	1.1	1.5	1.3	1.3	1.1	1.4	1.5	0.8	1.7	1.3
Er	7.9	10.6	10.5	11.0	8.3	8.4	8.7	9.2	8.9	7.3	9.4	12.7	5.9	12.1	10.4
Tm	2.8	3.7	3.5	3.7	2.9	2.6	3.1	3.2	3.5	3.0	3.2	4.6	2.3	4.1	4.1
Yb	33.8	46.2	47.1	47.3	37.4	36.0	40.2	41.8	48.8	34.2	44.1	71.3	36.0	51.7	61.8
Lu	8.3	10.4	10.6	11.6	8.8	8.4	9.9	9.5	13.3	8.1	10.5	18.8	9.6	11.7	15.9
Hf	56.6	75.7	178	86.0	68.2	66.2	65.2	41.8	146	59.6	145	138	29.0	81.1	51.0
Ta	1.2	0.77	1.6	1.6	1.0	0.94	1.1	2.6	6.4	1.7	1.2	1.6	1.0	1.0	1.3
Pb	4.7	8.5	7.7	22.0	5.9	5.2	6.5	6.0	7.6	5.3	6.5	10.0	5.2	8.5	7.4
Nb	91.6	87.6	99.1	124	86.3	80.2	98.4	80.3	224	87.3	83.5	149	92.3	101	135
Ba	-	12.0	35.0	1.2	0.5	0.2	0.2	-	0.3	-	5.9	0.46	0.24	1.4	0.17
Th	-	0.23	0.11	-	-	-	0.01	-	0.02	-	0.05	0.10	0.02	0.34	0.02
U	0.01	0.05	0.09	0.08	-	-	-	-	-	-	0.06	0.02	-	0.13	-
REE+Y	100	174	180	166	100	93.0	154	107	113	102	166	148	79.9	133	131

Table 3-8: Amphibole group EMP and LA-ICP-MS analyses with formulae (continued)

Formulae

Unit	Transsolvus granite (4/5)														
Sample	204805-10	204720-1	204720-2	204720-3	204720-4	204720-5	204720-6	204720-7	204720-8	204720-9	204720-10	204722-5	204722-6	204722-7	204722-8
Species	fl-lea	fl-lea	fl-lea	fl-lea	fl-lea	fl-lea	fl-lea	fl-lea	fl-lea	fl-lea	fl-lea	fl-lea	fl-lea	fl-lea	fl-lea
(apfu)															
Si	7.76	7.75	7.74	7.59	7.71	7.74	7.74	7.82	7.80	7.82	7.78	7.76	7.90	7.73	7.70
^{T}Al	0.07	0.06	0.06	0.06	0.06	0.06	0.06	0.07	0.05	0.07	0.07	0.04	0.05	0.03	0.05
^{T}Ti	0.06	0.09	0.08	0.10	0.08	0.07	0.08	0.10	0.14	0.07	0.07	0.11	0.05	0.10	0.13
^{T}Fe^{3+}	0.11	0.10	0.11	0.25	0.15	0.13	0.13	0.02	0.02	0.05	0.08	0.09		0.14	0.11
T (8)	8.00	8.00	8.00	8.00	8.00	8.00	8.00	8.00	8.00	8.00	8.00	8.00	8.00	8.00	8.00
^{C}Ti													0.03		
Zr	0.01	0.01	0.01	0.03	0.01	0.01	0.01	0.01	0.01			0.01	0.01	0.01	0.01
^{C}Al															
REE+Y															
^{C}Fe^{3+}	1.99	2.02	2.01	2.15	2.05	2.01	2.05	1.98	2.05	1.98	2.02	2.01	1.81	2.02	2.08
Zn	0.03	0.03	0.03	0.03	0.03	0.03	0.03	0.03	0.03	0.03	0.04	0.09	0.05	0.12	0.08
Mn^{2+}	0.07	0.08	0.07	0.07	0.07	0.07	0.08	0.07	0.07	0.07	0.07	0.09	0.09	0.08	0.07
Fe^{2+}	2.06	2.01	2.07	1.64	1.98	2.04	1.92	2.15	1.98	2.13	1.98	2.03	2.29	1.88	1.88
Mg	0.03	0.01	0.02	0.02	0.01	0.01	0.02	0.01	0.02	0.02	0.02	0.01	0.02	0.02	0.02
^{B}Li	0.72	0.70	0.67	1.05	0.78	0.71	0.81	0.58	0.72	0.60	0.76	0.77	0.52	0.86	0.86
C (5)	4.91	4.87	4.87	5.00	4.93	4.89	4.91	4.83	4.88	4.83	4.88	5.00	4.83	5.00	5.00
^{C}Li				0.12								0.01		0.06	0.10
Ca	0.02	0.02	0.02	0.02	0.02	0.02	0.02	0.02	0.01	0.02	0.02	0.01	0.01	0.03	0.01
^{B}Na	1.98	1.98	1.98	1.86	1.98	1.98	1.98	1.98	1.99	1.98	1.98	1.98	1.99	1.91	1.89
B (2)	2.00	2.00	2.00	2.00	2.00	2.00	2.00	2.00	2.00	2.00	2.00	2.00	2.00	2.00	2.00
^{A}Na	0.85	0.89	0.86	1.04	0.90	0.89	0.91	0.88	0.89	0.90	0.92	0.71	0.81	0.74	0.84
K	0.32	0.35	0.35	0.29	0.32	0.32	0.33	0.31	0.32	0.30	0.30	0.37	0.36	0.42	0.33
A (≤1)	1.17	1.24	1.22	1.33	1.22	1.21	1.25	1.18	1.21	1.20	1.23	1.09	1.17	1.16	1.17
OH	0.45	0.80	0.32	0.42	0.43	0.60	0.55	0.46	0.33	0.56	0.39	0.85	0.78	0.79	0.81
F	1.42	1.01	1.52	1.38	1.42	1.26	1.29	1.33	1.40	1.31	1.47	0.93	1.05	1.01	0.91
Cl													0.01		
O	0.13	0.18	0.16	0.20	0.15	0.14	0.16	0.21	0.27	0.13	0.14	0.23	0.16	0.19	0.27
W (2)	2.00	2.00	2.00	2.00	2.00	2.00	2.00	2.00	2.00	2.00	2.00	2.00	2.00	2.00	2.00

Table 3-8: Amphibole group EMP and LA-ICP-MS analyses with formulae (continued)

EMP and LA-ICP-MS analyses

Unit	Transsolvus granite (5/5)													
Sample	2047 22-9	2047 22-10	2047 22-11	2047 64-2	2047 64-3	2047 64-4	2047 64-5	2047 64-6	2047 64-7	2047 64-8	2047 64-9	2047 64-10	Mdn	MAD
Species	fl-lea	lea	fl-lea	fl-lea	fl-lea	fl-lea	fl-lea	fl-lea	fl-lea	fl-lea	fl-lea	fl-lea		
Major and minor elements (wt. %)														
SiO_2	51.17	50.82	51.11	50.59	50.77	51.03	50.61	51.12	50.94	50.96	50.89	51.11	51.02	0.52
TiO_2	0.80	0.89	1.22	0.69	0.59	0.77	0.59	0.72	0.62	0.54	1.09	1.41	0.71	0.09
Al_2O_3	0.26	0.29	0.29	0.34	0.42	0.31	0.36	0.42	0.30	0.36	0.42	0.27	0.34	0.05
FeO	31.68	31.63	31.61	32.82	33.24	32.94	33.22	32.37	33.27	33.05	31.93	31.03	32.47	0.38
MnO	0.58	0.66	0.62	0.50	0.49	0.55	0.50	0.53	0.55	0.53	0.51	0.64	0.56	0.04
MgO	0.10	0.08	0.08	0.04	0.03	0.04	0.06	0.09	0.04	0.09	0.12	0.08	0.08	0.03
ZnO	0.60	1.22	0.66	0.61	0.60	0.64	0.59	0.41	0.63	0.57	0.77	1.05	0.30	0.05
ZrO_2	0.34	0.65	0.06	0.15	0.07	0.13	0.09	0.06	0.28	0.10	0.30	0.10	0.11	0.03
Nb_2O_5	0.01	0.02	0.02	0.01	0.01	0.01	0.01	0.01	0.01	0.01	0.02	0.03	0.01	0.00
Na_2O	9.36	9.27	9.50	9.27	9.18	9.19	9.27	9.16	9.21	9.23	9.44	9.05	9.57	0.13
K_2O	1.96	1.70	1.69	1.81	1.58	1.56	1.62	1.57	1.60	1.61	1.29	2.17	1.65	0.09
CaO	0.10	0.07	0.07	0.13	0.12	0.14	0.13	0.16	0.09	0.14	0.18	0.06	0.13	0.03
F	2.45	1.86	2.59	2.70	2.81	2.55	2.68	2.71	2.63	2.79	2.43	2.72	2.56	0.15
Cl	0.01	0.01	0.02	0.01	-	0.01	0.01	0.01	-	-	0.01	-	0.01	0.00
Total	99.41	99.16	99.53	99.65	99.92	99.87	99.73	99.34	100.2	99.99	99.40	99.72	99.93	0.54
Trace elements (ppm)														
Li	6050	7800	7215	7760	6380	6314	5820	4096	5903	5690	8443	9440	5775	1260
Rb	164	128	137	114	94.8	90.0	83.1	66.3	96.1	75.3	79.9	95.6	84.3	18.6
Sr	0.85	4.5	0.30	1.8	1.8	1.6	1.1	0.66	0.88	0.91	3.1	1.5	1.4	0.5
Y	22.4	36.7	33.3	41.2	30.7	34.2	24.0	16.2	22.4	20.7	47.5	33.9	27.7	5.5
Zr	5810	8520	1510	1481	1376	2289	1257	1880	1361	1142	1903	2898	1356	339
Sn	177	416	224	147	152	197	129	204	137	118	154	228	137	41
La	1.9	4.1	1.1	8.1	5.9	4.6	3.7	1.2	1.9	2.8	12.7	11.3	2.8	1.2
Ce	4.4	8.7	3.6	17.0	8.3	9.6	7.6	2.7	5.4	6.8	25.0	21.5	6.6	2.8
Pr	0.60	1.1	0.58	2.6	1.2	1.2	1.2	0.33	0.74	1.1	3.8	3.4	1.0	0.4
Nd	2.7	6.2	2.3	12.9	5.8	7.1	5.6	1.8	3.6	6.1	19.8	16.0	4.7	2.2
Sm	0.34	1.1	0.41	2.1	0.88	1.4	1.2	0.32	0.60	1.5	3.0	2.5	0.91	0.47
Eu	0.02	0.05	-	0.16	0.10	0.08	0.07	0.03	0.03	0.09	0.14	0.08	0.05	0.02
Gd	0.35	1.2	0.61	1.6	1.0	1.1	0.99	0.44	0.51	0.72	1.8	1.2	0.67	0.33
Tb	0.16	0.33	0.18	0.41	0.36	0.43	0.21	0.21	0.21	0.20	0.51	0.15	0.21	0.08
Dy	2.6	4.2	3.0	4.2	3.7	4.4	3.0	2.5	2.4	2.5	4.8	3.2	2.6	0.6
Ho	1.2	2.3	1.8	1.9	1.5	1.6	1.1	0.89	1.1	1.1	2.1	1.7	1.2	0.3
Er	8.8	13.3	14.7	11.8	8.0	10.8	8.1	6.0	7.2	7.0	14.3	13.2	8.1	1.4
Tm	3.4	5.4	5.4	3.5	2.6	4.0	2.6	2.1	2.7	2.2	4.9	5.0	2.7	0.5
Yb	47.9	71.3	78.0	46.7	33.0	52.6	31.1	28.3	33.6	29.4	67.1	75.3	35.9	6.3
Lu	11.7	16.5	18.9	10.7	7.4	12.8	7.7	6.7	7.8	7.1	16.6	16.2	8.6	1.9
Hf	423	633	57.7	64.7	61.5	124	54.2	103	60.1	53.5	120	135	63.6	17.6
Ta	2.4	1.6	1.5	0.76	1.2	1.7	0.84	1.9	0.84	0.82	2.8	7.6	1.1	0.3
Pb	9.6	22.5	9.3	7.7	12.5	11.3	4.5	4.2	4.6	5.2	8.6	7.5	5.8	1.7
Nb	98.5	134	144	87.0	88.0	104	81.2	70.2	83.2	74.3	152	231	92.4	13.8
Ba	0.27	1.4	0.25	1.5	2.0	0.99	0.15	0.25	0.30	0.15	1.2	0.66	0.43	0.26
Th	-	2.4	-	0.36	1.6	0.47	0.05	0.02	-	0.16	0.22	0.10	0.02	0.02
U	-	0.46	-	0.19	0.28	0.15	0.03	-	0.01	0.02	0.11	0.02	0.01	0.01
REE+Y	109	173	164	165	110	146	98.0	69.7	90.1	89.0	224	205	110	19

Table 3-8: Amphibole group EMP and LA-ICP-MS analyses with formulae (continued)

Formulae

Unit	Transsolvus granite (5/5)											
Sample	2047 22-9	2047 22-10	2047 22-11	2047 64-2	2047 64-3	2047 64-4	2047 64-5	2047 64-6	2047 64-7	2047 64-8	2047 64-9	2047 64-10
Species	fl-lea	lea	fl-lea	fl-lea	fl-lea	fl-lea	fl-lea	fl-lea	fl-lea	fl-lea	fl-lea	fl-lea
(apfu)												
Si	7.79	7.68	7.74	7.66	7.71	7.74	7.72	7.88	7.73	7.75	7.66	7.68
^{T}Al	0.05	0.05	0.05	0.06	0.08	0.06	0.06	0.08	0.05	0.07	0.07	0.05
^{T}Ti	0.09	0.10	0.14	0.08	0.07	0.09	0.07	0.05	0.07	0.06	0.12	0.16
^{T}Fe^{3+}	0.08	0.17	0.07	0.21	0.14	0.12	0.15		0.14	0.12	0.14	0.12
T (8)	8.00	8.00	8.00	8.00	8.00	8.00	8.00	8.00	8.00	8.00	8.00	8.00
^{C}Ti								0.04				
Zr	0.03	0.05		0.01	0.01	0.01	0.01	0.01	0.02	0.01	0.02	0.01
^{C}Al												
REE+Y												
^{C}Fe^{3+}	1.99	2.01	2.10	2.07	2.01	2.00	1.99	1.80	1.96	1.97	2.09	2.16
Zn	0.07	0.14	0.07	0.07	0.07	0.07	0.07	0.05	0.07	0.06	0.09	0.12
Mn^{2+}	0.07	0.08	0.08	0.06	0.06	0.07	0.07	0.07	0.07	0.07	0.07	0.08
Fe^{2+}	1.96	1.82	1.84	1.88	2.08	2.07	2.10	2.37	2.12	2.12	1.79	1.62
Mg	0.02	0.02	0.02	0.01	0.01	0.01	0.01	0.02	0.01	0.02	0.03	0.02
^{B}Li	0.80	0.89	0.89	0.90	0.78	0.78	0.76	0.55	0.75	0.75	0.92	1.00
C (5)	4.94	5.00	5.00	5.00	5.00	5.00	5.00	4.90	5.00	5.00	5.00	5.00
^{C}Li		0.13	0.05	0.12	0.06	0.05	0.01		0.03		0.18	0.23
Ca	0.02	0.01	0.01	0.02	0.02	0.02	0.02	0.03	0.02	0.02	0.03	0.01
^{B}Na	1.98	1.85	1.94	1.86	1.92	1.92	1.97	1.97	1.96	1.98	1.79	1.76
B (2)	2.00	2.00	2.00	2.00	2.00	2.00	2.00	2.00	2.00	2.00	2.00	2.00
^{A}Na	0.78	0.86	0.85	0.86	0.79	0.78	0.77	0.76	0.75	0.75	0.97	0.88
K	0.38	0.33	0.33	0.35	0.31	0.30	0.32	0.31	0.31	0.31	0.25	0.42
A (≤1)	1.16	1.19	1.18	1.21	1.09	1.08	1.08	1.07	1.06	1.06	1.21	1.29
OH	0.64	0.91	0.48	0.55	0.51	0.60	0.57	0.51	0.60	0.53	0.59	0.39
F	1.18	0.89	1.24	1.29	1.35	1.22	1.29	1.32	1.26	1.34	1.16	1.29
Cl												
O	0.18	0.20	0.28	0.16	0.14	0.18	0.14	0.17	0.14	0.12	0.25	0.32
W (2)	2.00	2.00	2.00	2.00	2.00	2.00	2.00	2.00	2.00	2.00	2.00	2.00

Table 3-8: Amphibole group EMP and LA-ICP-MS analyses with formulae (continued)

EMP and LA-ICP-MS analyses

Unit	Enclaves										
Sample	1003 9-2	2047 20-12	2047 20-13	2047 64-12	2047 64-13	2047 12-2	2047 12-3	2047 12-9	2047 12-11	Mdn	MAD
Species	fl-arf	fl-lea	fl-lea	fl-lea	fl-lea	fl-lea	lea	fl-lea	fl-lea		
Major and minor elements (wt. %)											
SiO_2	52.30	51.64	51.61	50.71	50.66	49.69	49.74	49.77	51.03	50.71	0.93
TiO_2	0.99	0.74	1.02	1.00	0.49	0.90	1.10	0.91	0.92	0.92	0.08
Al_2O_3	0.36	0.35	0.35	0.58	0.61	0.36	0.38	0.37	0.35	0.36	0.01
FeO	31.13	32.13	32.01	31.56	32.11	31.92	31.62	31.54	31.78	31.78	0.22
MnO	0.88	0.71	0.79	0.69	0.53	0.72	0.71	0.58	0.60	0.71	0.08
MgO	0.09	0.06	0.05	0.10	0.23	0.07	0.08	0.54	0.20	0.09	0.03
ZnO	0.66	0.49	0.51	0.93	0.32	0.89	1.01	0.53	0.60	0.60	0.11
ZrO_2	0.07	0.08	0.09	0.14	0.13	0.13	0.32	0.14	0.06	0.13	0.03
Nb_2O_5	0.01	-	0.02	0.02	0.01	0.02	0.03	0.01	0.02	0.02	0.01
Na_2O	9.59	9.72	9.71	9.10	9.15	9.34	9.24	9.41	9.21	9.34	0.19
K_2O	1.91	1.74	1.73	1.61	1.50	1.82	1.74	1.47	1.69	1.73	0.09
CaO	0.13	0.12	0.13	0.19	0.42	0.09	0.13	0.39	0.18	0.13	0.05
F	1.97	2.05	1.93	2.21	2.56	1.86	1.72	2.49	2.25	2.05	0.18
Cl	-	0.02	-	0.01	0.02	-	0.01	-	-	-	-
Total	100.1	99.85	99.94	98.84	98.73	97.81	97.84	98.16	98.87	98.84	1.00
Trace elements (ppm)											
Li	3610	4242	5990	8670	3871	5700	5950	4802	4150	4802	931
Rb	80.3	125	103	88.7	71.1	94.5	104	65.8	44.1	88.7	15.5
Sr	9.4	1.8	1.5	2.9	4.8	2.6	4.0	4.4	6.0	4.0	1.4
Y	354	93.0	92.0	64.0	152	52.9	69.8	60.0	141	92.0	32.0
Zr	1283	1842	2160	3120	869	2183	4000	2073	1839	2073	234
Sn	72.3	90.1	156	126	36.5	144	143	74.2	65.9	90.1	36.2
La	18.7	58.7	39.8	15.7	62.3	41.6	24.1	16.3	22.6	24.1	8.5
Ce	43.6	87.0	78.0	37.0	112	33.8	45.3	35.6	50.6	45.3	9.7
Pr	6.6	10.8	9.9	5.8	14.6	6.9	5.3	5.2	8.4	6.9	1.6
Nd	32.5	56.8	46.0	30.0	76.0	30.5	26.7	24.5	42.6	32.5	8.0
Sm	11.8	10.0	6.2	5.7	17.2	5.8	4.9	5.3	10.9	6.2	1.3
Eu	0.64	0.34	0.26	0.51	0.82	0.18	0.20	0.37	0.74	0.37	0.17
Gd	11.8	10.3	9.3	6.8	17.3	4.4	4.5	3.8	13.2	9.3	3.9
Tb	2.1	1.8	1.7	1.2	2.8	0.73	1.0	0.9	2.6	1.7	0.7
Dy	15.6	11.4	11.4	8.4	18.4	5.7	8.7	7.1	14.2	11.4	3.0
Ho	4.0	3.2	4.8	2.3	4.2	2.2	3.0	2.5	4.1	3.2	0.9
Er	18.1	14.9	18.4	11.2	11.7	13.7	14.4	15.6	14.9	14.9	1.2
Tm	4.6	3.9	5.4	3.8	2.7	4.6	4.6	5.3	3.7	4.6	0.8
Yb	46.9	40.0	77.2	52.4	27.2	56.1	54.1	71.5	46.7	52.4	5.7
Lu	9.7	8.4	17.8	12.8	5.6	13.2	13.9	18.1	12.8	12.8	3.1
Hf	64.4	75.6	110	158	38.4	90.4	161	85.0	82.9	85.0	20.6
Ta	0.97	1.3	2.3	2.5	3.6	1.8	9.3	1.5	1.9	1.9	0.6
Pb	10.3	24.3	51.0	6.2	37.2	10.7	25.3	10.6	7.3	10.7	4.6
Nb	41.9	88.6	138	109	70.7	116	199	103	115	109	20
Ba	1.2	8.3	1.9	1.0	4.1	2.5	1.9	0.79	0.95	1.9	0.9
Th	1.0	4.6	12.7	0.25	7.0	3.3	2.9	0.37	0.03	2.9	2.5
U	0.13	0.16	1.5	-	0.49	0.27	1.4	0.01	0.01	0.16	0.15
REE+Y	581	411	418	258	525	272	281	272	389	389	117

Table 3-8: Amphibole group EMP and LA-ICP-MS analyses with formulae (continued)

Formulae

Unit	Enclaves								
Sample	10039-2	204720-12	204720-13	204764-12	204764-13	204712-2	204712-3	204712-9	204712-11
Species	fl-arf	fl-lea	fl-lea	fl-lea	fl-lea	fl-lea	lea	fl-lea	fl-lea
(apfu)									
Si	7.95	7.84	7.77	7.66	7.84	7.68	7.68	7.72	7.86
^{T}Al	0.06	0.06	0.06	0.10	0.11	0.07	0.07	0.07	0.06
^{T}Ti		0.08	0.12	0.11	0.05	0.11	0.13	0.11	0.08
^{T}Fe^{3+}		0.01	0.06	0.13		0.15	0.12	0.11	
T (8)	8.00	8.00	8.00	8.00	8.00	8.00	8.00	8.00	8.00
^{C}Ti	0.11				0.01				0.03
Zr	0.01	0.01	0.01	0.01	0.01	0.01	0.02	0.01	
^{C}Al	0.01								
REE+Y	0.01	0.01	0.01		0.01		0.01		0.01
^{C}Fe^{3+}	1.72	1.95	2.04	2.09	1.81	2.03	2.03	1.96	1.85
Zn	0.07	0.05	0.06	0.10	0.04	0.10	0.12	0.06	0.07
Mn^{2+}	0.11	0.09	0.10	0.09	0.07	0.10	0.09	0.08	0.08
Fe^{2+}	2.23	2.12	1.93	1.76	2.35	1.95	1.93	2.02	2.24
Mg	0.02	0.01	0.01	0.02	0.05	0.02	0.02	0.12	0.05
^{B}Li	0.47	0.56	0.78	0.91	0.52	0.76	0.79	0.64	0.55
C (5)	4.77	4.80	4.93	5.00	4.86	4.97	5.00	4.90	4.88
^{C}Li				0.22			0.01		
Ca	0.02	0.02	0.02	0.03	0.07	0.01	0.02	0.06	0.03
^{B}Na	1.98	1.98	1.98	1.75	1.93	1.99	1.97	1.94	1.97
B (2)	2.00	2.00	2.00	2.00	2.00	2.00	2.00	2.00	2.00
^{A}Na	0.85	0.88	0.85	0.91	0.81	0.81	0.79	0.89	0.78
K	0.37	0.34	0.33	0.31	0.30	0.36	0.34	0.29	0.33
A (≤1)	1.22	1.22	1.19	1.22	1.11	1.17	1.14	1.18	1.11
OH	0.83	0.84	0.85	0.71	0.63	0.88	0.90	0.57	0.69
F	0.95	0.98	0.92	1.06	1.25	0.91	0.84	1.22	1.10
Cl		0.01			0.01				
O	0.23	0.17	0.23	0.23	0.11	0.21	0.26	0.21	0.21
W (2)	2.00	2.00	2.00	2.00	2.00	2.00	2.00	2.00	2.00

CHAPTER 4 -

A ND- AND O-ISOTOPE STUDY OF THE REE-RICH PERALKALINE STRANGE LAKE GRANITE: IMPLICATIONS FOR MESOPROTEROZOIC A-TYPE MAGMATISM IN THE CORE ZONE (NE-CANADA)

PREFACE

Chapters 2 and 3 focused on the internal magmatic evolution of the Strange Lake pluton, based on petrography including textural evidence, and more importantly, bulk rock and mineral compositions. The chapter that follows (4) takes the reader on a more regional and past-regional journey. Applying radiogenic Nd- and stable O-isotopes, the magma sources of the Strange Lake pluton are assessed in the context of existing theories of how A-type granitic magmas can be produced. Scenarios of depleted versus enriched-mantle sources and assimilation of varying amounts of underlying Archean and Paleoproterozoic crust belonging to the Core Zone (Churchill Province) are discussed. In addition, the Strange Lake pluton is placed in the context of the Mesoproterozoic Nain Plutonic Suite (Northern Québec and Labrador) as well as the alkaline intrusions of the Gardar Province (SW-Greenland). Plate tectonic reconstructions provide the background for a sequence of processes, namely the subduction induced fertilization of the subcontinental lithospheric mantle, crustal contamination and rifting, that favor the genesis of extremely HFSE-rich magmas.

ABSTRACT

It is well established that A-type granites enriched in high field strength elements, such as Zr, Nb and the REE, form in anorogenic tectonic settings. The sources of these elements and the processes controlling their unusual enrichment, however, are still debated. They are addressed here using neodymium and oxygen isotope analyses of samples from the 1.24 Ga Strange Lake pluton in the Paleoproterozoic Core Zone of Québec-Labrador, an A-type granitic body characterised by hyper-enrichment in the REE, Zr, and Nb. Age-corrected εNd values for bulk rock samples and sodic amphiboles (mainly arfvedsonite) from the pluton range from -0.6 to -5.7, and -0.3 to -5.3, respectively. The εNd values for the Napeu Kainiut quartz monzonite, which hosts the pluton, range from -4.8 to -8.1. The $^{147}Sm/^{144}Nd$ ratios of the suite and the host quartz monzonite range from 0.0967 to 0.1659, large variations that can be explained by in-situ fractionation of early LREE-minerals (Strange Lake), and late hydrothermal HREE remobilization. Oxygen isotope analyses of quartz of both Strange Lake and the host yielded $\delta^{18}O$ values between +8.2 and +9.1, which are considerably higher than the mantle value of 5.7 ± 0.2 ‰. Bulk rock oxygen isotope analyses of biotite-gneisses in the vicinity of the Strange Lake pluton yielded $\delta^{18}O$ values of 6.3, 8.6 and 9.6 ‰. The negative εNd values and positive $\delta^{18}O$ values of the Strange Lake and Napeu Kainiut samples indicate that both magmas experienced considerable crustal contamination. The extent of this contamination was estimated, assuming that the contaminants were sedimentary-derived rocks from the underlying Archean Mistinibi (para-) gneiss complex, which is characterized by low εNd and high $\delta^{18}O$ values. Mixing of 5 – 15 % of a gneiss, having an εNd value of -15 and a $\delta^{18}O$ value of +11, with a moderately enriched mantle source (εNd = +0.9, $\delta^{18}O$ = +6.3) would produce values similar to those obtained for the Strange Lake granites. Based on analogies between the Nain Plutonic Suite and the Gardar alkaline igneous province (SW-Greenland), we conclude that the Strange Lake pluton and associated REE-mineralized anorogenic bodies formed from a combination of subduction-induced fertilization of the sublithospheric mantle, crustal extension and in-situ magma evolution.

Keywords

Nd isotopes, O isotopes, Strange Lake, REE, Core Zone, Nain Plutonic Suite

4.1 INTRODUCTION

Although it is well known that A-type granitic rocks are enriched in incompatible and high field strength elements (HFSE), such as the rare earth elements (REE), Zr, Nb, U, Ta and volatiles such as F and Cl (Eby 1990; 1992; Bonin 2007), the reasons for this enrichment continue to be a matter of considerable debate. Some researchers, on the basis of Pb, Nd and Sr isotopic evidence and trace element modeling, have concluded that A-type granites are produced by the fractionation of basaltic magmas of mantle origin (Frost et al. 1997; 1999; 2001; Anderson et al. 2003) . Other researchers have interpreted them to result from melting of lower crustal material that has been metasomatized by fertile mantle-derived fluids (Woolley 1987; Martin 2006; 2012) . A few studies, noting the variability of initial $^{87}Sr/^{86}Sr$ ratios and other trace element variations, have proposed that A-type granites are exclusively of crustal origin (Collins et al. 1982; Dall'Agnol et al. 2005; Dall'Agnol and de Oliveira 2007). Finally, a considerable number of studies have argued that A-type granites crystallize from fertile mantle melts that have undergone variable degrees of crustal assimilation (Kovalenko et al. 2004; 2007; 2009; Hegner et al. 2010). According to this interpretation, an initially depleted mantle is metasomatically enriched in the REEs and alkalis as well as in volatiles such as H_2O, CO_2 CH_4 and F (Bailey, 1987).

Most A-type granitic intrusions are emplaced in anorogenic intra-plate rift-settings, e.g., settings of crustal de-stressing following collisional events. For example, the large AMCG (Anorthosite-Mangerite-Charnockite-Granite) intrusions of the Nain Plutonic Suite (NPS) in Labrador and northern Québec were emplaced during the waning stages of a series of orogenies, i.e., the Pinwarian (1.52-1.46 Ga), the Elsonian (1.46-1.23 Ga) and the Grenvillian (1.08-0.99 Ga) orogenies (Gower and Krogh, 2002; McLelland et al., 2010). Some researchers have proposed that the emplacement of anorogenic intrusive suites is the result of a combination of tectonic processes, e.g., continent-continent collision followed by the delamination of a thickened lithosphere, the ascent of asthenosphere and subsequent rifting (Connelly and Ryan 1999; Bonin 2007; McLelland et al. 2010).

This study investigates the genesis of A-type granites using the Strange Lake pluton in northern Québec-Labrador, which is composed of highly evolved peralkaline granitic intrusions, and late pegmatites that host two potentially economic REE-Zr-Nb deposits. One of the deposits, the B-zone, which is currently being evaluated for exploitation, is estimated to contain a resource of 278 Mt of ore, grading 0.93 wt. % REE_2O_3 (39% heavy rare-earth oxides), 1.92 wt. % ZrO_2 and 0.18 wt. % Nb_2O_5 (Quest, 2012). The Strange Lake pluton is the youngest representative of the alkaline Nain Plutonic Suite, which was emplaced in Québec and Labrador between 1.46 and 1.24 Ga (Miller et al. 1997; Gower and Krogh 2002). Based on the data presented in this paper and the generally accepted plate tectonic framework for Mesoproterozoic alkaline magmatism in northeastern Laurentia, we have developed a model for the formation of the hyper REE- and HFSE-mineralized Strange Lake pluton and, by extension, for other alkaline plutons in the Nain and Gardar (a postulated equivalent of the Nain plutonic province in southern Greenland) igneous provinces.

Using a set of radiogenic neodymium, and stable oxygen isotope data for the unaltered Strange Lake granites from the Québec side (this study) and additional isotopic data from the Labrador side of the pluton (Kerr, 2015), we show that the corresponding magmas originated from partial melting of a fertile mantle and evolved by the assimilation of continental crust. A combination of low degrees of partial melting of an enriched mantle, fractional crystallization and assimilation of underlying Archean gneiss satisfactorily explain the hyper-enrichment in the REE and the isotope signatures that we have obtained. In addition, published Nd and O isotope data and interpretations of the Nain Plutonic Suite and the Gardar alkaline province are consistent with our results, namely that the isotopic signature of the intrusions was greatly affected by the age (Archean vs. Paleoproterozoic) and the nature (metasedimentary) of the underlying crust.

4.2 GEOLOGIC SETTING

4.2.1 Regional geology

As noted above, the Strange Lake pluton is part of the Nain Plutonic Suite, a large igneous province in northeastern Canada (Fig. 4-1). This province comprises anorthositic-mangeritic-charnockitic-granitic intrusive rocks (AMCG complexes) and straddles the boundary between Archean rocks of the Nain Province to the east and late Archean and Early Paleoproterozoic rocks of the southeastern Churchill Province to the west; the latter has more recently been referred to as the 'Core Zone' (Emslie et al. 1994; James et al. 1996) . Beginning with the Michikamau and Harp Lake anorthosites and the Mistastin granitoid rocks (1.46-1.42 Ga), large batholiths were emplaced over a time span of about 220 Ma (Gower and Krogh, 2002). These early intrusions were followed by the emplacement of anorthosites, troctolites, norites, diorites and granitoids (1.35-1.29 Ga) to the east. They, in turn, were crosscut by alkaline and peralkaline volcanics and plutons, e.g., Flowers River (1.27 Ga), and the Strange Lake pluton (1.24 Ga) (Fig. 4-1). The anorthosites, troctolites and norites were also intruded by small masses of ferrodiorite, which are interpreted to have formed from the residual liquids of anorthosite crystallization (Emslie et al. 1994; McLelland et al. 2010).

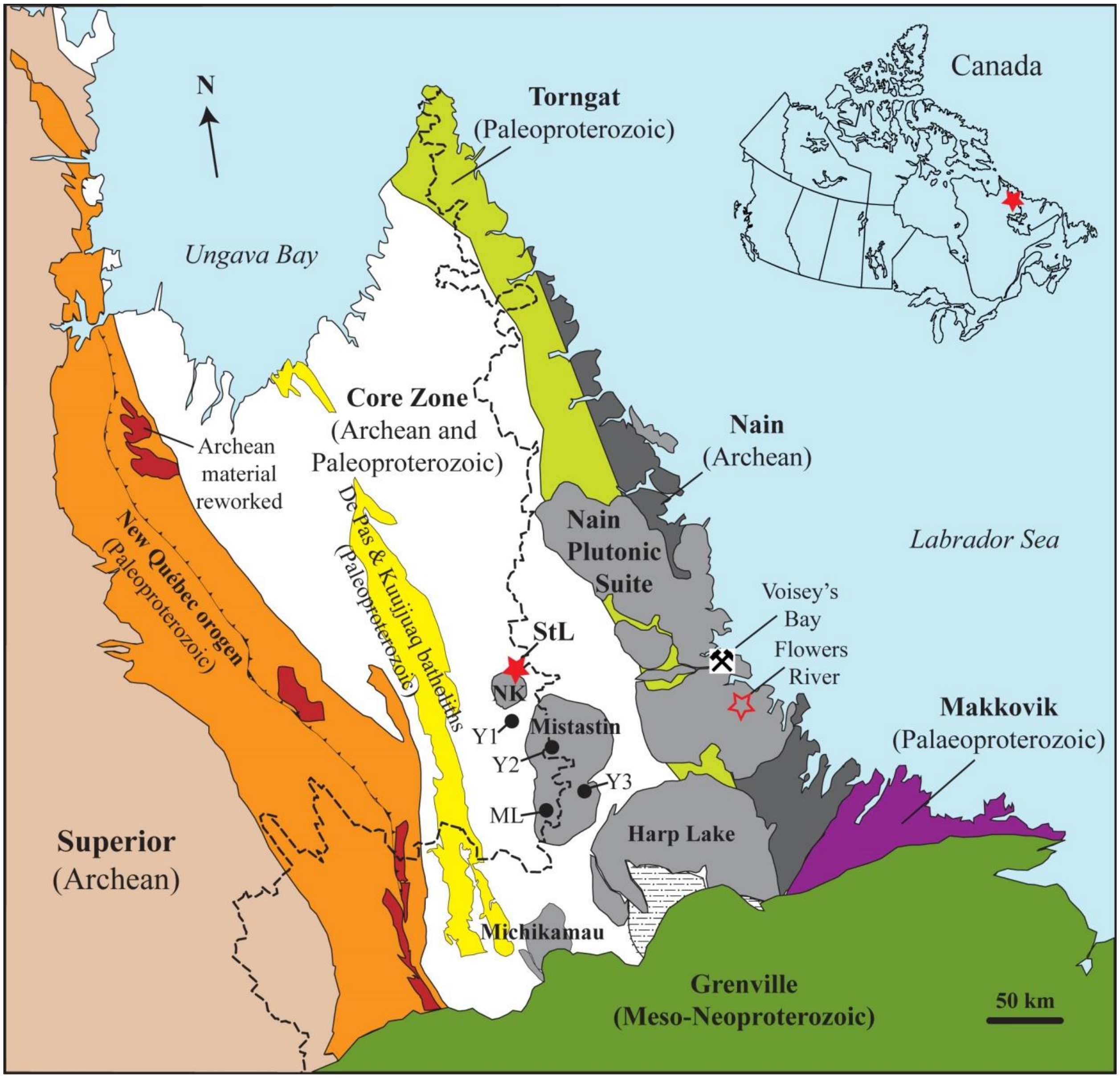

Fig. 4-1: Terrane map of Northeastern Québec and Labrador

An Archean and Paleoproterozoic terrane map of Northeastern Québec and Labrador showing the Nain Plutonic (AMCG) Suite and other Elsonian intrusions (grey), the Napeu Kainiut quartz monzonite (NK), and the locations of the Strange Lake (StL), Flowers River, Misery Lake (ML) and Ytterby (Y) 1, 2 and 3 REE-rich intrusions (modified after Emslie et al. 1994 and David et al. 2011).

The Strange Lake pluton is hosted partly by the Napeu Kainiut quartz monzonite, a satellite intrusion of the Mistastin batholith. Although the age of the Napeu Kainiut intrusion is unknown, the Mistastin batholith has been dated at 1.42 Ga (Emslie and Stirling, 1993). It is one of the largest and oldest intrusions of the Nain Plutonic Suite, and covers a surface area of about 5,000 km^2. The Mistastin batholith is composed dominantly of pyroxene- and olivine-bearing Rapakivi type granites, which are cut by younger biotite-hornblende-bearing granites. It is host to several smaller REE-rich intrusions, notably the Misery Lake syenite at 1.41 Ma (Petrella et al. 2014) and the Ytterby 2 granite and Ytterby 3 syenite-granite dated at 1.44 and 1.42 Ga, respectively (Kerr and Hamilton, 2014). The Napeu Kainiut quartz monzonite is a biotite-bearing monzonitic to granitic rock. It is coarse-grained, equigranular, consists mainly of quartz, K-feldspar, plagioclase and biotite, and is of metaluminous composition.

The other host to the Strange Lake pluton is an Archean to Paleoproterozoic gneiss complex in the Core Zone (southeastern Churchill Province), composed of quartzofeldspathic augen-gneisses, banded biotite-gneisses and minor garnet-bearing para-gneisses and mafic gneisses. This part of the Core Zone represents a poorly constrained collage of at least three Archean to Paleoproterozoic crustal lenses and domains bounded by shear zones, which represent former sutures (James and Dunning, 2000). The crustal rocks near Strange Lake are dominantly (meta-) volcanics (2.3 to 2.5 Ga) of the Mistinibi-Raude domain, crosscut by younger gabbroic rocks, and represent former accreted volcanic arcs and products of later rifting events (Girard 1990; Corrigan et al. 2016). The Archean blocks are exotic and do not belong to any of the larger Archean terranes of the Rae, Nain or Superior Provinces, as earlier believed (Corrigan et al. 2009; James and Duning, 2000). The crustal lenses in which Strange Lake is located, formed at middle to lower crustal levels (≥ 10 km depth) and underwent amphibolite to granulite facies metamorphism (Van der Leeden et al. 1990). They are underlain by an Archean (~2.7 Ga) tonalitic to metasedimentary gneiss package belonging to the Mistinibi Complex (Girard 1990; Van der Leeden et al. 1990).

The eastern foreland of the Core Zone underwent eastward subduction beneath the Archean Nain craton at 1.91-1.87 Ga, resulting in the N-S-trending Torngat orogen (1.87-1.84 Ga), the calc-alkaline Burwell Domain and a broad belt of Tasiuyak paragneiss, a former sedimentary wedge (Scott, 1998; Wardle et al., 2002). The Torngat event was followed by eastwards subduction of the eastern foreland of the Archean Superior Province under the Core Zone (1.84-1.82 Ga), and subsequent continent-continent collision (1.82-1.77 Ga), which produced the N-S trending New Québec orogen (1.87-1.79 Ga). This also led to the emplacement of large syn- and post-collisional intrusive bodies (see Fig. 4-1), notably the N-S trending calc-alkaline De Pas and Kuujjuaq batholiths (Hoffman, 1988; Wardle et al., 2002).

A number of authors (e.g., Blaxland and Curtis 1977; Myers et al. 2008) have argued that the Nain Plutonic Suite and the Gardar Province of Southwest Greenland belong to a larger igneous suite that was divided in two parts by the rifting event that created the Labrador sea during the late Mesozoic to early Tertiary (Royden and Keen, 1980). It is important to note, however, that the onset of the magmatic activity responsible for the Nain Plutonic Suite (ca 1.46 to 1.24 Ga) preceded Gardar magmatism (ca 1.35 to 1.12 Ga). The latter produced a series of alkaline gabbros, granites and nepheline syenites plus several small carbonatites (Bailey, 2001; Upton et al., 2003). Evidence that the two alkaline provinces were linked is provided by anorthosite xenoliths in the Gardar intrusions, which are compositionally similar to the large anorthosite complexes in Labrador (Bridgwater, 1967). It is also noteworthy that the 1.276 Ga mafic dike swarms (Nain Dikes) and the 1.273 Ga Harp Dikes of the Nain Province, are remarkably similar to the 1.273 Ga ‘Brown Dikes’ in the Gardar Province (Cadman et al. 1993; Carlson et al. 1993; Bartels et al. 2015) . Further evidence that the two provinces constitute a single larger province is provided by the basement to the intrusions of the Gardar Province, which is composed of the calc-alkaline Julianehåb batholith (1.80-1.77 Ga). This intrusion was emplaced during and following the Paleoproterozoic Ketilidian orogeny (1.85 to 1.80 Ga), which is represented by the Makkovik province (orogeny 1.895 to 1.870 Ga) in Labrador (Garde et al., 2002).

4.2.2 The Strange Lake pluton

The Strange Lake peralkaline granitic pluton is located on the border of Québec and Labrador and intruded along the boundary between the Mesoproterozoic Napeu Kainiut quartz monzonite to the West and a Paleoproterozoic gneiss complex of the Core Zone, to the East (Fig. 4-2). The pluton consists of a series of peralkaline granitic intrusions forming a cylindrical intrusive body with a diameter of about 6 km. A radiometric U-Pb determination on zircon for the oldest unit, a hypersolvus granite, yielded an age of 1240 ± 2 Ma (Miller et al., 1997). The hypersolvus granite, so-named because of the occurrence of a single perthitic alkali feldspar, forms the center of the pluton, and is divided into a less evolved southern and a more evolved northern unit , the latter evident from higher bulk Si, Zr, Nb, REE and lower Al concentrations (Table 4-1). The hypersolvus granite was succeeded by the most evolved unit, a transsolvus granite, which is distinguished from it by the presence of separate crystals of albite and K-feldspar in addition to perthitic alkali feldspar. This granite occupies most of the pluton, is heavily altered except in the center of the pluton and is host to REE/HFSE mineralized pegmatites that have been the target of recent exploration (Gysi and Williams-Jones, 2013; Gysi et al., 2016). A dark grey porphyritic granite is present between the transsolvus granite and large bodies of wall rocks, and is interpreted as the quenched margin of the former intrusion (Siegel et al., in review). This granite is also represented by dark grey, fine-grained ovoid enclaves that frequently occur in the transsolvus granite. A ring-fault and a fluorite-hematite breccia coincide with the margins of the pluton.

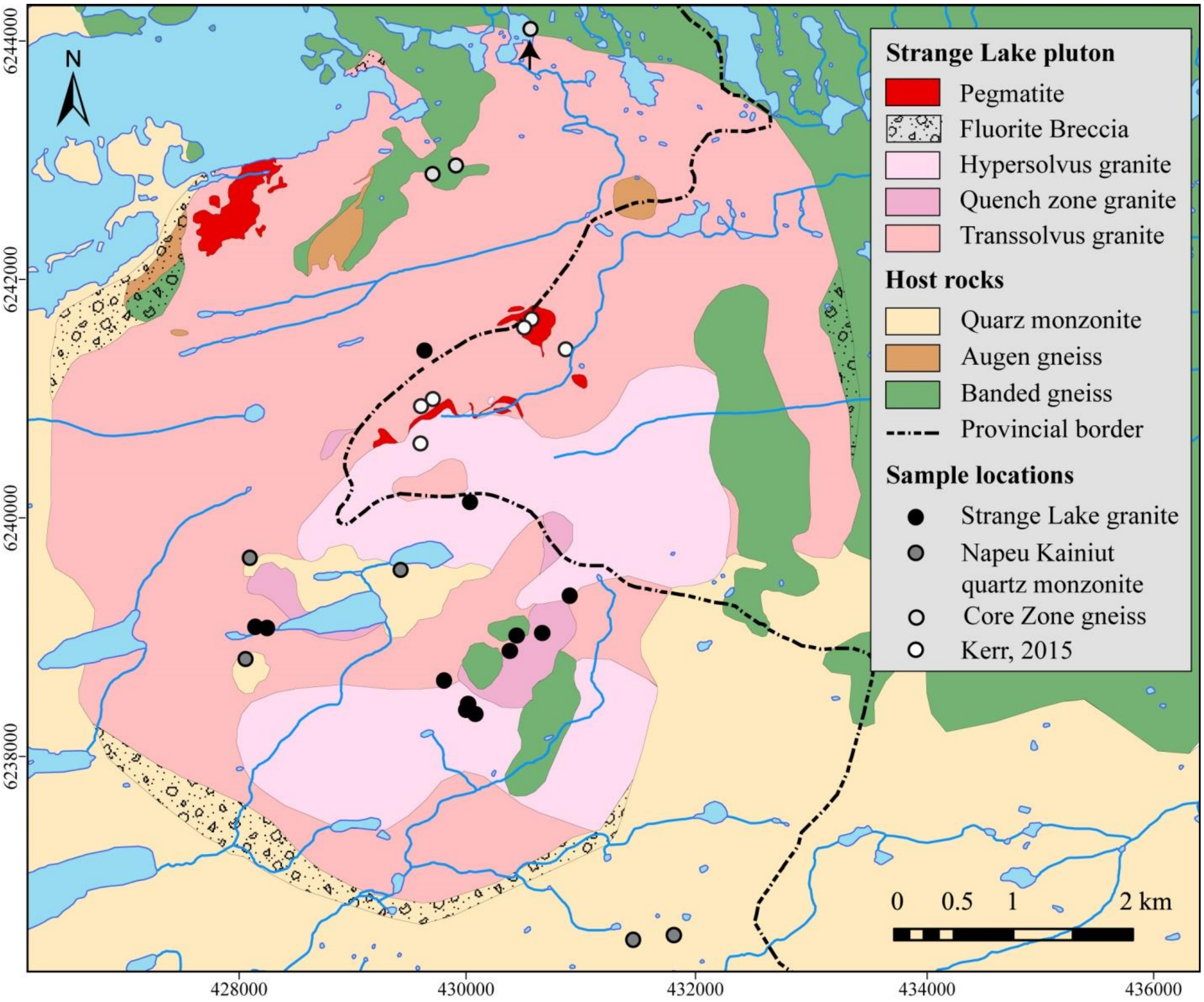

Fig. 4-2: Geological map of the Strange Lake pluton and host rocks

A geological map of the Strange Lake pluton, host Napeu Kainiut quartz monzonite and Core Zone gneisses. Also shown are the locations of the samples used for this study. The white dots represent the sampling locations of Kerr (2015) on the Labrador side of the pluton.

Table 4-1: Bulk rock compositions of samples used for the isotope study

Bulk rock major element and trace element (except REE and Y) concentrations of representative samples from the different lithological units sampled in this study.

Unit	Strange Lake				Napeu Kainiut	
Rock type	Hyper-solvus granite S	Hyper-solvus granite N	Quench zone granite	Trans-solvus granite	Quartz monzonite inside SL	Quartz monzonite outside SL
Sample	10032	10040	10036	10039	10118	10216
(*wt. %)*						
SiO_2	69.13	71.16	70.62	71.61	75.26	70.92
Al_2O_3	12.23	11.97	11.33	10.82	11.84	12.69
Fe_2O_3	5.26	4.82	4.90	5.53	2.44	5.19
MnO	0.07	0.10	0.09	0.12	0.03	0.08
MgO	0.03	0.05	0.03	0.03	0.08	0.26
CaO	0.65	0.61	0.60	0.55	0.75	1.68
Na_2O	5.06	5.00	5.15	6.56	2.98	3.02
K_2O	5.31	4.74	4.47	2.88	5.67	5.05
TiO_2	0.21	0.27	0.19	0.21	0.21	0.56
Nb_2O_5	0.01	0.05	0.04	0.14	0.004	0.004
P_2O_5	-	0.02	0.01	-	0.01	0.11
F	0.42	0.41	0.44	0.49	0.17	0.07
TREO	0.11	0.21	0.24	0.41	0.09	0.06
LREO	0.06	0.14	0.16	0.27	0.07	0.05
HREO+Y	0.04	0.07	0.08	0.14	0.02	0.01
Total	98.59	99.63	98.36	99.75	99.72	99.95
LOI	0.33	0.49	0.24	0.29	0.43	0.41
AI	1.15	1.12	1.17	1.29	0.93	0.82
Be *ppm*	14	47	51	96	9	4
Zn	210	300	350	520	40	90
Ga	45	40	50	60	24	22
Rb	434	454	512	467	311	188
Sr	12	17	22	13	46	134
Zr	1122	3524	2620	4971	349	640
Sn	31	69	65	103	5	6
Cs	2	6	1	4	3	2
Ba	39	73	53	45	313	1374
Hf	33	83	77	136	11	14
Ta	7	20	18	43	2	1
Pb	43	97	129	206	42	33
Th	22	80	74	98	38	18
U	4	15	13	21	8	3

4.3 METHODS

4.3.1 Samples

Twenty two samples were collected and prepared for Sm-Nd isotope analyses. These include seven bulk rock samples from the unaltered center of the Strange Lake pluton (four samples of hypersolvus granite, two of transsolvus granite and one of quench zone granite) and five bulk rock samples from the Napeu Kainiut quartz monzonite host rock. Three of the host rock samples were collected within the borders of the pluton from large outcrops interpreted to represent roof pendants, and two samples were from outside the pluton (see Fig. 4-2). In addition, ten samples of sodic amphibole (arfvedsonite) were separated manually from the Strange Lake granites with the aid of a binocular microscope. Four of these separates are from samples that were analyzed for their bulk rock Sm-Nd isotopic composition. The other six separates were prepared from samples not subjected to this analysis, because arfvedsonite grains in the remaining samples that had been analyzed for their Nd-Sm isotopic composition contain abundant inclusions of fluorite and other minerals. This is a common feature of arfvedsonite in the hypersolvus granite. Quartz crystals from six granite samples (three of hypersolvus granite, one of quench zone granite, and two transsolvus granite samples) and two samples of quartz monzonite (one from inside, and the other from outside the Strange Lake pluton) were separated manually for oxygen isotope analysis; quartz is considered to best reflect magmatic δ^{18}O values in granitic intrusions (Gregory et al., 1989). Samples of the Strange Lake bulk rock were not considered for oxygen isotope analyses because of the high probability that late stage hydrothermal fluids affected the δ^{18}O values of the feldspar. Three samples of biotite gneiss, including a garnet-bearing variety, from the gneiss complex partly hosting the Strange Lake pluton were analyzed for their bulk rock oxygen isotope composition. One of the samples was collected about 1 km north of the pluton and the other two from wall rock outcropping immediately to the north of the pluton. The gneiss samples were prepared (crushed and ground) and analyzed at the Queen's University Facility for Isotope Research. The bulk rock samples used for the Nd isotope analyses were crushed and ground to fine powders using a jaw crusher and tungsten carbide mill at McGill University, whereas the arfvedsonite and quartz separates were crushed and ground manually in agate mortars. The bulk-rock chemical data were provided by Quest Rare Minerals Ltd., and represent the results of analyses by Actlabs using fusion-ICP-OES for major elements, XRF (X-ray fluorescence) for Nb, ISE-MS (ion selective electrode) for F, and fusion-ICP-MS for the REE and other trace elements.

4.3.2 Analytical methods

4.3.2.1 Radiogenic isotopes

All radiogenic isotope analyses were performed at GEOTOP (Université de Québec à Montréal, UQAM). About 40 - 80 mg of powder of each sample was spiked with a ^{150}Nd-^{149}Sm tracer solution in order to accurately determine Sm and Nd concentrations through isotope dilution. The rock powders were dissolved in acidic HF and HNO_3 solutions on a hot plate for six days. In order to decompose insoluble fluorides, HNO_3 acid was added and the solutions evaporated repeatedly. The elements, Sm and Nd, were separated by ion-exchange chromatographic techniques under clean laboratory conditions using doubly distilled acids. Iron was removed using ion-exchange polyprep columns with AG1X8 resin. The rare earth elements (REE) were concentrated using Eichrom TRU spec resin, and Sm and Nd were subsequently separated using columns prepared with two ml of Eichrom LN spec resin.

The samples were loaded onto Re-filaments and analyzed on a thermal ionization TRITON PLUS mass spectrometer (TIMS). A double filament assemblage was used, in which each sample was evaporated from the Re-filament on the left side of the sample wheel and ionized by a blank counterpart Re-filament on the right side. Both Sm and Nd were analyzed in static mode. The $^{143}Nd/^{144}Nd$ values were corrected internally for fractionation using a $^{146}Nd/^{144}Nd$ value of 0.7219, assuming exponential fractionation behavior. Repeated measurements of the Nd standard, JNdi, returned a mean value of 0.512097 ± 7 (n = 5, 2σ mean), which is comparable to the published value of 0.512115 ± 7 (Tanaka et al., 2000). Initial $^{143}Nd/^{144}Nd$ values for the Strange Lake samples were calculated using a U-Pb zircon age of 1.24 Ga (Miller et al., 1997), whereas the 1.42 Ga age of the Misastin batholith (Emslie and Stirling, 1993) was assumed for the Napeu Kainiut quartz monzonite samples. The Sm-Nd concentrations were determined using the isotope dilution technique. The εNd values were calculated from the measured $^{143}Nd/^{144}Nd$ ratios relative to the chondritic uniform reservoir value (CHUR) using the present-day ratios of $^{143}Nd/^{144}Nd = 0.512638$ (Goldstein et al., 1984) and $^{147}Sm/^{144}Nd = 0.1967$ (Jacobsen and Wasserburg, 1980). The average total chemical blank concentration measured on the TIMS was 150 pg for Nd and Sm, which is considered negligible.

4.3.2.2 Oxygen isotopes

The oxygen isotope analyses on quartz were carried out at the Laboratory for Stable Isotope Science (LSIS) at the University of Western Ontario (UWO) using a method similar to that described by Polat and Longstaffe (2014). Approximately 8-10 mg of powder from each sample was weighed into spring-loaded sample holders and dried overnight at ca. 150°C. The holders were then placed in nickel reaction vessels and heated in vacuo for a further three hours at 300°C to remove surface water. The samples were subsequently reacted with ClF_3 overnight at ca. 580°C to release silicate-bound oxygen (Borthwick and Harmon, 1982; Clayton and Mayeda, 1963). The oxygen was converted to CO_2 over red-hot graphite for isotopic measurement using a

Prism II dual-inlet, stable-isotope-ratio mass-spectrometer. The oxygen isotope measurements were made using a Thermo Fisher Delta V Plus mass spectrometer in dual inlet mode. The gneiss samples were analyzed for their bulk rock $\delta^{18}O$ compositions at the Queen's Facility for Isotope Research (Queens University). Oxygen was extracted from 5mg samples at 550-600°C using the BrF5 procedure of (Clayton and Mayeda, 1963) and analyzed in dual inlet mode with a Thermo-Finnigan DeltaPlus XP Isotope-Ratio Mass Spectrometer.

Oxygen isotope compositions are reported in the standard delta (δ) notation in units of permil (‰), expressed relative to the Vienna Standard Mean Ocean Water (VSMOW) international standard. All samples were analyzed with a precision of 0.1‰. The $\delta^{18}O$ values for laboratory standards analyzed at the same time as the Strange Lake quartz samples were: quartz, 11.5 ± 0.24 ‰ (n=5); basalt, 7.5 ± 0.25 ‰ (n=4); and CO_2, 10.3 ± 0.05 ‰ (n=5). The accepted values for these standards are 11.5 ‰, 7.5 ‰ and 10.3 ‰, respectively. The accuracy for the gneiss bulk rock values was 0.1 ‰, based upon primary or secondary standard analyses.

4.4 RESULTS

4.4.1 Rare earth element contents

Chondrite-normalized (Sun and McDonough, 1989) REE-profiles for the Strange Lake bulk rock samples used in the Sm-Nd isotope study all display modest LREE enrichment, a strong negative Eu-anomaly and a flat HREE distribution (Fig. 4-3). The absolute REE concentrations are lowest in the least evolved southern hypersolvus granite, considerably higher in the northern hypersolvus granite and highest in the most evolved transsolvus granite (almost twice as high as in the southern hypersolvus granite; Table 4-2). The chondrite-normalized REE profiles of the Napeu Kainiut quartz monzonite samples display very similar LREE enrichment to the Strange Lake granites and absolute LREE concentrations similar to those of the southern hypersolvus granite. In contrast, the HREE are relatively depleted and the absolute HREE concentrations considerably lower than those of the Strange Lake granites. Interestingly, the quartz monzonite samples collected from within the Strange Lake pluton (roof pendants) have higher REE contents than the samples from outside the pluton.

Table 4-2: Bulk rock REE concentrations of samples used for the isotope study

Bulk rock REE and Y concentrations of representative samples from the lithological units sampled in this study.

Unit	Strange Lake				Napeu Kainiut	
Rock type	Hyper-solvus granite S	Hyper-solvus granite N	Quench zone granite	Trans-solvus granite	Quartz monzonite inside SL	Quartz monzonite outside SL
Sample	10032	10040	10036	10039	10118	10216
La *(ppm)*	108	252	291	493	136	96
Ce	235	540	589	1010	272	193
Pr	28	62	71	120	31	22
Nd	106	221	265	438	113	88
Sm	25	49	59	100	20	16
Eu	2	3	4	6	1	2
Gd	24	45	55	95	17	12
Tb	5	9	11	18	3	2
Dy	33	63	72	116	17	11
Ho	7	14	16	25	3	2
Er	23	48	50	75	10	7
Tm	3	8	8	11	2	1
Yb	22	53	50	73	10	6
Lu	3	8	7	10	2	1
Y	245	395	460	773	92	58
LREE	527	1171	1333	2262	591	430
HREE	96	203	213	329	46	30
REE	624	1374	1546	2590	637	460

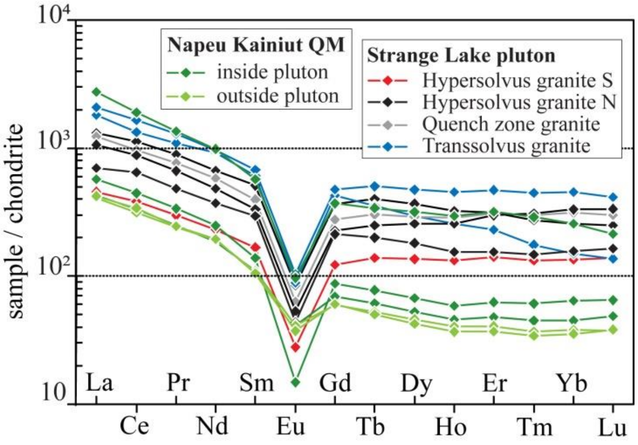

Fig. 4-3: Chondrite normalized REE-profiles of the bulk rock samples

Chondrite normalized REE-profiles for the bulk rock samples used in this study. The normalization was done using the chondrite data of Sun and McDonough (1989).

4.4.2 Sm–Nd isotope geochemistry

Bulk rock concentrations of Sm and Nd for the Strange Lake granites range from 10 to 61 ppm and from 45 to 291 ppm, respectively (Table 4-3). They are lowest in the hypersolvus and quench zone granites (Sm: 10 – 40 ppm and Nd: 45 – 188 ppm) and highest in the transsolvus granite (Sm: 50 – 61 ppm and Nd: 291 - 310 ppm), reflecting the more evolved nature of the latter unit (Fig. 4-4). Samarium and neodymium concentrations in the arfvedsonite samples show no obvious trends with granite evolution, and range from 4 to 27 ppm and 19 to 121 ppm, respectively. This is probably because arfvedsonite was a late crystallizing mineral in the hypersolvus granite and crystallized as an early phase in the transsolvus granite. The Napeu Kainiut quartz monzonite samples have significantly lower Sm and Nd concentrations of 14 to 18 ppm, and 70 to 107 ppm, respectively, with the exception of sample 10120, which contains 28 ppm Sm and 120 ppm Nd, and was collected inside the Strange Lake pluton.

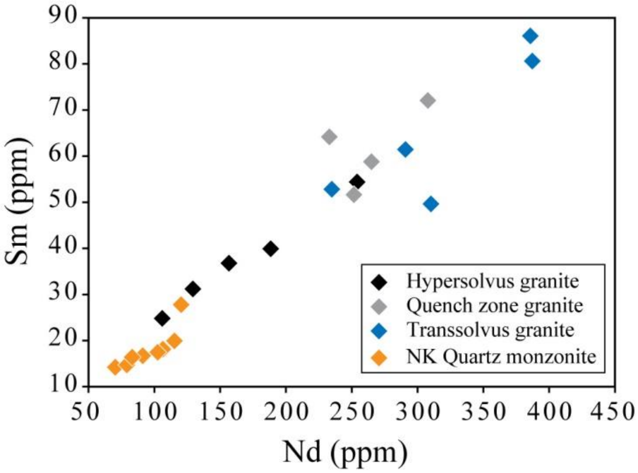

Fig. 4-4: Diagram showing bulk rock Sm and Nd concentrations

Binary diagram showing bulk rock concentrations of Sm and Nd in the Strange Lake granites (this study and Kerr 2015) and the host Napeu Kainiut quartz monzonite. Concentrations of both elements increase with increasing evolution of the granites.

The ^{147}Sm/^{144}Nd ratios of the unaltered Strange Lake granites and arfvedsonite separates range from 0.0967 to 0.1654 (most values are clustered between 0.124 and 0.146), and there is no discernible difference between the values for the hypersolvus granite and the transsolvus granite (Fig. 4-5). In contrast, the quartz monzonite values are lower, clustering between 0.1029 and 0.1220, except for sample 10120, which has a ratio of 0.1394. Note that values > 0.13 are unusual in plutonic rocks (De Paolo, 1988). The altered and mineralized Strange Lake samples analyzed by Kerr (2015) have much higher ^{147}Sm/^{144}Nd ratios than the unaltered samples analyzed in this study, and range between 0.1683 and 0.3903. The measured ^{143}Nd/^{144}Nd compositions of the Strange Lake granites and the arfvedsonite separates (this study) range between 0.511748 and 0.512304, and do not distinguish hypersolvus granite from transsolvus granite. These ratios for the Napeu Kainiut quartz monzonite are all considerably lower, between 0.511411 and 0.511527, except for the one sample (10120) with anomalously high Sm and Nd concentrations (Fig. 4-5, Table 4-3). This sample has a ^{143}Nd/^{144}Nd ratio similar to that of the

Strange Lake granites, of 0.511882. Arfvedsonite separates of some of the bulk rock samples have $^{147}Sm/^{144}Nd$ and $^{143}Nd/^{144}Nd$ ratios that differ considerably from those of their host rocks (Table 4-4), indicating a fractionation of Sm from Nd between the melt and arfvedsonite. For example, the bulk rock sample #10010, has a $^{147}Sm/^{144}Nd$ ratio of 0.1280 and a $^{143}Nd/^{144}Nd$ ratio of 0.511935, whereas the arfvedsonite separate of the same sample has ratios of 0.1659 and 0.512263, respectively.

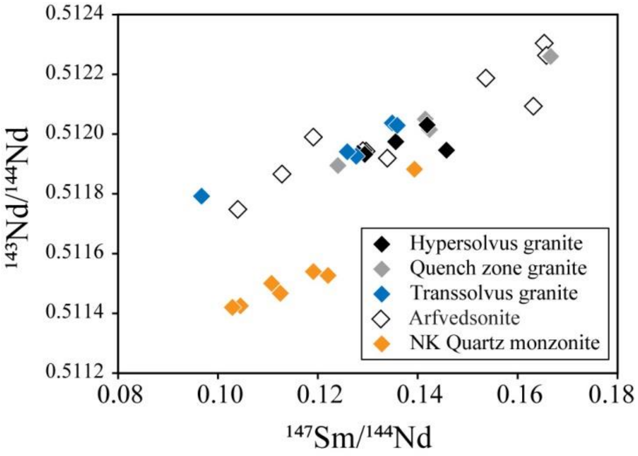

Fig. 4-5: Diagram showing bulk rock and arfvedsonite $^{147}Sm/^{144}Nd$ and $^{143}Nd/^{144}Nd$ ratios
Binary diagram showing bulk rock and arfvedsonite $^{147}Sm/^{144}Nd$ and $^{143}Nd/^{144}Nd$ ratios for the Strange Lake granites (this study and Kerr 2015), and the Napeu Kainiut quartz monzonite. The data for the Strange Lake granite define a single linear correlation that is roughly parallel to a linear correlation for the Napeu Kainiut quartz monzonite but at a significantly higher $^{143}Nd/^{144}Nd$ ratio.

The εNd (t) values for the Strange Lake samples were calculated using the crystallization age of the pluton of 1.24 Ga (Miller et al., 1997). These values vary considerably, from - 0.6 to - 5.7 for the bulk rock samples, and from -0.3 to -5.3 for the arfvedsonite separates (Table 4-3). However, the majority of the values of both bulk rock samples and arfvedsonite separates lie between -1.4 and -4. Similar results were reported recently by Kerr (2015) for bulk rock samples from the Labrador side of the Strange Lake pluton. His values lie between -1.5 and -5.5, with the majority being between -2 and -3. Although the age of the Napeu Kainiut quartz monzonite is unknown, as noted above, the intrusion is widely considered to be a satellite of the nearby (and compositionally similar) Mistastin batholith. Thus, the age of the latter (1.42 Ga) was used to calculate the εNd (t) values for the quartz monzonite samples. They are between - 6.6 and - 8.1, except for sample #10120, which has a εNd value of -4.8 (Table 4-3). If the age of the Strange Lake granite (1.24 Ga) was used instead, the εNd (t) values would be more negative by about two units (εNd = -8.6 to -9.9 and -6.8 for sample #10120).

Table 4-3: Sm-Nd concentrations, isotope data and depleted mantle model ages

Sm-Nd concentrations, isotope data and ages for the Strange Lake granitic pluton and the Napeu Kainiut quartz monzonite including depleted mantle model ages (T_{DM}).

Sample	Rock type	Sm (ppm)	Nd (ppm)	Sm/Nd	^{147}Sm/^{144} Nd	^{143}Nd/^{144}Nd	T (Ga)	εNd (t)	T_{DM}
Strange Lake amphibole separates									
10010-A	Hypersolvus granite - north	17.21	65.63	0.2622	0.1659	0.512263 ± 03	1.24	-1.43	2.82
10014-A	Transsolvus granite	20.78	120.73	0.1722	0.1041	0.511748 ± 06	1.24	-2.66	1.95
10016-A	Hypersolvus granite - south	5.33	27.03	0.1972	0.1192	0.511990 ± 39	1.24	-0.34	1.87
10032-A	Hypersolvus granite - south	15.11	68.18	0.2217	0.1340	0.511919 ± 11	1.24	-4.07	2.35
10036-A	Quench zone granite	6.41	29.88	0.2146	0.1297	0.511943 ± 07	1.24	-2.94	2.19
10039-A	Transsolvus granite	19.29	89.98	0.2144	0.1296	0.511935 ± 13	1.24	-3.06	2.20
10218-A	Hypersolvus granite - south	8.90	32.52	0.2736	0.1654	0.512304 ± 23	1.24	-1.55	2.66
204773-A	Hypersolvus granite - south	26.56	104.46	0.2543	0.1537	0.512187 ± 04	1.24	-1.98	2.44
OV-16-A	Hypersolvus pegmatite	3.56	19.05	0.1868	0.1129	0.511866 ± 06	1.24	-1.75	1.94
OV-92-A	Hypersolvus pegmatite	6.51	24.12	0.2700	0.1632	0.512093 ± 04	1.24	-5.32	3.18
Strange Lake granites bulk rock									
10010-WR	Hypersolvus granite - north	39.92	188.45	0.2118	0.1280	0.511935 ± 03	1.24	-2.81	2.16
10032-WR	Hypersolvus granite - south	10.09	44.98	0.2243	0.1356	0.511974 ± 61	1.24	-3.25	2.29
10035-WR	Transsolvus granite	61.44	290.86	0.2113	0.1277	0.511926 ± 03	1.24	-3.13	2.18
10036-WR	Quench zone granite	20.19	85.75	0.2355	0.1424	0.512015 ± 12	1.24	-3.53	2.42
10039-WR	Transsolvus granite	49.64	310.23	0.1600	0.0967	0.511792 ± 17	1.24	-0.62	1.77
10040-WR	Hypersolvus granite - north	31.19	129.35	0.2411	0.1458	0.511946 ± 12	1.24	-5.67	2.72
10043-WR	Hypersolvus granite - north	36.79	156.74	0.2347	0.1419	0.512031 ± 21	1.24	-3.31	2.39
Napeu Kainiut host rock									
10118-WR	Quartz monzonite - inside StL	18.13	106.51	0.1702	0.1029	0.511411 ± 05	1.42	-6.88	2.38
10119-WR	Quartz monzonite - inside StL	14.21	70.36	0.2019	0.1220	0.511527 ± 09	1.42	-8.12	2.69
10120-WR	Quartz monzonite - inside StL	27.77	120.44	0.2305	0.1394	0.511882 ± 04	1.42	-4.79	2.43
10216-WR	Quartz monzonite - outside StL	16.71	91.23	0.1832	0.1107	0.511500 ± 46	1.42	-6.57	2.64
206133-WR	Quartz monzonite - outside StL	14.72	79.12	0.1861	0.1125	0.511467 ± 05	1.42	-7.65	2.53

Analytical errors for ^{147}Sm/^{144}Nd are estimated to be less than 0.1% (~ 0.0001 to 0.0004), and for ^{143}Nd/^{144}Nd are estimated to be less than 0.002% (~0.00001) at 2 sigma. The calculation of model ages in respect to the depleted mantle was based on the model of Jacobson, 1984.

The initial isotope compositions for the Strange Lake granites were calculated using the 1.24 Ma U-Pb age from Miller et al. (1997). The values for the Napeu Kainiut quartz monzonite host rock were calculated assuming an age of 1.42 Ga, the age of the Mistastin batholith (Emslie & Stirling, 1993).

4.4.3 Oxygen isotope ratios

The oxygen isotope ratios ($\delta^{18}O$) for quartz from the Strange Lake samples (Table 4-4) are lowest for the least evolved southern hypersolvus granite (8.2 and 8.4 ‰), higher for the quench zone granite and the more evolved northern hypersolvus granite (8.4 and 8.7 ‰) and highest for the transsolvus granite (8.8 and 8.9 ‰). These values largely overlap with three oxygen isotope values determined by Boily and Williams-Jones (1994) for quartz separates from the northern hypersolvus granite (8.5 and 8.6 ‰) and the transsolvus granite (9.1 ‰). The quartz monzonite quartz samples have slightly higher $\delta^{18}O$ values of 8.9 and 9.1 ‰. The bulk rock biotite-gneiss samples have $\delta^{18}O$ values of 8.6 and 9.6 ‰, and the garnet-biotite-gneiss sample has a $\delta^{18}O$ value of 6.3 ‰.

Table 4-4: Oxygen isotope compositions

Oxygen isotope compositions of quartz separates from the Strange Lake pluton (StL), the Napeu Kainiut quartz monzonite (QM) with location (NK-i = inside; NK-o = outside the Strange Lake pluton) and bulk samples of gneiss with location (GN-i = inside; GN-o = outside the Strange Lake pluton).

Sample	Unit	Rock type	Material	$\delta^{18}O$ (‰)
10010-Q	StL	Hypersolvus granite - north	Quartz	8.7
10014-Q	StL	Transsolvus granite	Quartz	8.8
10016-Q	StL	Hypersolvus granite - south	Quartz	8.4
10039-Q	StL	Transsolvus granite	Quartz	8.9
204749-Q	StL	Quench zone granite	Quartz	8.4
204773-Q	StL	Hypersolvus granite - south	Quartz	8.2
46-B-3	StL	Transsolvus granite	Quartz	8.6 *
48-A-1	StL	Hypersolvus granite - north	Quartz	8.5 *
MBTR-3	StL	Transsolvus granite	Quartz	9.1 *
10118-Q	NK-i	Quartz monzonite	Quartz	8.9
206133-Q	NK-o	Quartz monzonite	Quartz	9.1
204812-B	GN-o	Biotite gneiss banded	Bulk	8.6
204824-B	GN-i	Biotite gneiss banded	Bulk	9.6
206127-B	GN-i	Garnet-biotite gneiss banded	Bulk	6.3

* data from Boily and Williams-Jones (1994)

4.5 DISCUSSION

4.5.1 The isotopic signature of the Strange Lake pluton

The fact that the hypersolvus and transsolvus granites cannot be distinguished on the basis of their εNd values (-1.4 to -4.1), suggests that the magmas responsible for these two granite types originated in the same reservoir. This means that the geochemical differences between the hypersolvus and transsolvus granites did not result from an external process like crustal assimilation, but instead from internal magmatic processes such as fractional crystallization. The bulk rock Sm and Nd concentrations are linearly distributed (see Fig. 4-4), consistent with an evolution of the magmas by fractional crystallization, i.e., they are lower in the hypersolvus granite and higher in the transsolvus granite. The highest concentrations of these elements, however, are in the altered rocks (see Fig. 4-6a), reflecting the important role of hydrothermal fluids in mobilizing the REE (Salvi and Williams-Jones 1996; Gysi et al. 2016).

Variations in the Sm/Nd ratios among the Strange Lake samples resulted either from fractionation induced by the crystallization of LREE-bearing minerals, hydrothermal activity or a combination of the two processes. The main reservoirs of Sm and Nd in the unaltered Strange Lake granites are monazite-(Ce), fluornatropyrochlore and arfvedsonite (Siegel et al., in review; Siegel et al., 2017). Experimentally determined partition coefficients between monazite-(Ce) and melt are consistently higher for Nd than for Sm over a wide range of pressure-temperature conditions and melt-H_2O contents (Stepanov et al., 2012). The same is true for Nd and Sm partition coefficients between pyrochlore group minerals and silicate melts (Zhao et al., 2002). Arfvedsonite, a major phase in the granite (~15 vol. %), also has a slight preference for Nd over Sm (calculated $D_{arf\text{-}melt}$ Nd ~0.009 vs. $D_{arf\text{-}melt}$ Sm ~0.008). Thus, all primary (magmatic) REE-bearing minerals at Strange Lake preferentially incorporated Nd over Sm.

Evidence that the magmatic Sm/Nd signature was affected by hydrothermal activity is provided by quartz monzonite sample #10120, which was collected from a Napeu Kainiut roof pendant located in close proximity to a mineralized Strange Lake pegmatite dike. This sample underwent strong hydrothermal alteration, resulting in anomalously high total Rare Earth oxide (0.4 wt. %), F (1.4 wt. %) and CaO (2.7 wt. %) concentrations, whereas the other quartz monzonite samples, which were only weakly altered (samples from within the Strange Lake pluton) or not altered at all (samples from outside the pluton) have very low total Rare Earth oxide (0.06 – 0.09 wt. %), F (0.07 – 0.17 wt. %) and CaO (0.75 – 1.68 wt. %) contents. Therefore, we conclude that the much higher Sm and Nd concentrations of sample #10120 compared to those of the other quartz monzonite samples, as well as its high ^{147}Sm/^{144}Nd ratio (0.1394), were likely the result of interaction with REE-rich fluids that were exsolved from the nearby Strange Lake pegmatite. These fluids must have had higher Sm/Nd ratios than the unaltered rock. Kerr (2015) also noted that highly mineralized samples (e.g., aplites, pegmatites) from the Labrador side of the Main Zone deposit had ^{147}Sm/^{144}Nd ratios as high as 0.1683 to 0.3903 (see Fig. 4-6b). These mineralized samples show evidence of intense hydrothermal alteration, and the REE are hosted dominantly in secondary minerals, such as gerenite-(Y), kainosite-(Y) and gadolinite-(Y) (Kerr and Rafuse, 2012). The high ^{147}Sm/^{144}Nd ratios indicate that the Sm-Nd system in these altered samples is highly disturbed. Indeed, they result in depleted mantle model ages (T_{DM}) that are younger than the intrusion or even lie in the future (Kerr, 2015). Mass-balance calculations and geochemical modeling suggest that low-temperature hydrothermal fluids preferentially mobilized the LREE over the HREE (Salvi and Williams-Jones 1996; Gysi and Williams-Jones 2013; Gysi et al. 2016). A fluid containing both Sm and Nd would preferentially enrich an unaltered rock in the slightly ‘heavier’ and less mobile Sm, whereas Nd is lighter and would be transported further

(Migdisov et al., 2016). This explains the unusually high $^{147}Sm/^{144}Nd$ ratios of the altered granites and pegmatites.

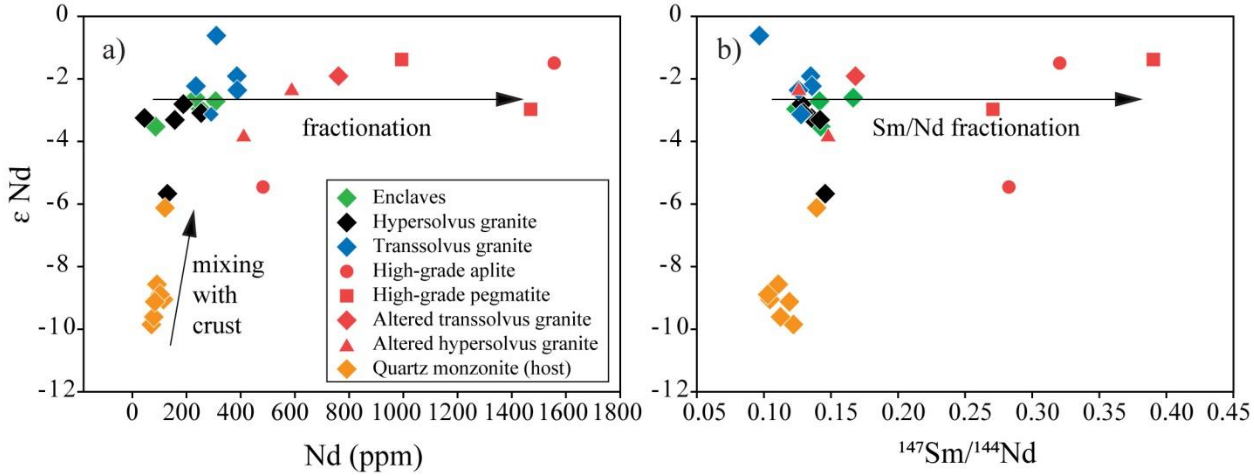

Fig. 4-6: Diagrams showing εNd vs Nd concentration and εNd vs. $^{147}Sm/^{144}Nd$

Binary diagrams showing a) εNd vs Nd concentration and b) εNd vs. $^{147}Sm/^{144}Nd$. The Nd concentration increases with granite evolution reflecting in-situ crystal fractionation by LREE-minerals and is accompanied by a similar increase in the $^{147}Sm/^{144}Nd$ ratio.

4.5.2 Model ages

Model ages are a function of the $^{147}Sm/^{144}Nd$ ratio and the model used for the mantle (depleted vs. enriched). As the $^{147}Sm/^{144}Nd$ ratios of the Strange Lake granites are highly variable, and as choice of the mantle model is made difficult by the fact that the composition of the mantle beneath Strange Lake is unknown, ages calculated for this mantle should be treated with caution. Applying the depleted model (T_{DM}) would require that there had been extensive melting of the mantle prior to the alkaline magmatism. The enriched or T_{CHUR} (chondritic evolution) model (De Paolo and Wasserburg, 1976) would require the assumption that the mantle beneath Strange Lake had not experienced appreciable depletion (e.g., by melting to produce crust) prior to the alkaline magmatism or that it had been enriched metasomatically.

The calculated depleted model ages (T_{DM}) for the full Strange Lake dataset are between 1.77 and 3.18 Ga. However, in order to exclude samples that may have been affected by non-magmatic Sm-Nd fractionation, we restricted the data to $^{147}Sm/^{144}Nd$ ratios < 0.13 (De Paolo, 1988). This restriction reduced the T_{DM} range to between 1.77 and 2.20 Ga (Fig. 4-7). For reference, the corresponding range of enriched mantle model ages (T_{CHUR}) (De Paolo, 1988) is between 1.27 and 1.74 Ga. The variability in both the depleted and enriched mantle model ages indicates that the Strange Lake samples were highly affected by fractionation. In addition the samples were also affected by crustal contamination, as shown by the relatively low initial $^{143}Nd/^{144}Nd$ and εNd values.

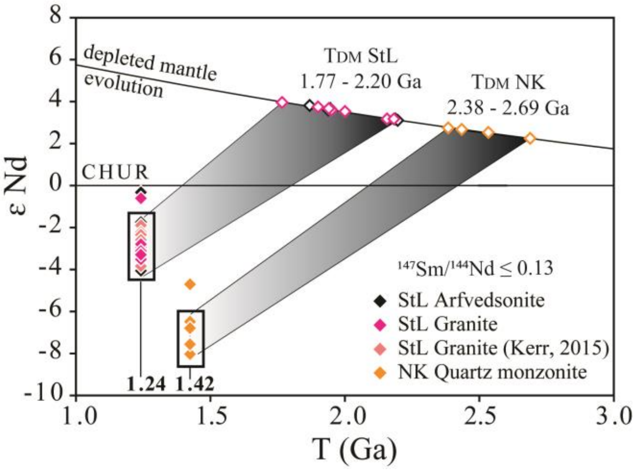

Fig. 4-7: Diagram showing the model ages (T_{DM}) vs. εNd (t)

A plot of model ages (T_{DM}) vs. εNd (t) for the Strange Lake granites (bulk rock, this study and Kerr (2015), and arfvedsonite) for $^{147}Sm/^{144}Nd \leq 0.13$ at t = 1.24 Ga, and for the Napeu Kainiut quartz monzonite at t = 1.42 Ga. The line and curve representing CHUR and depleted mantle, respectively, are from De Paolo (1988).

The Napeu Kainiut quartz monzonite samples have depleted mantle model ages (T_{DM}) from 2.38 to 2.69 Ga, whereas their enriched mantle model ages (T_{CHUR}) are between 1.99 and 2.26 Ga, both of which are significantly older than the model ages for Strange Lake (Fig. 4-7). For the reasons given above, the model ages and their geological significance should be treated with caution. Nonetheless, the large gap in model ages (enriched and depleted) predicted for the mantle by the Napeu Kainiut quartz monzonite and Strange Lake granites is significant and suggests that the two rock suites followed separate evolutionary paths. This is further elaborated upon below.

4.5.3 Relationship of the Strange Lake granites to the Napeu Kainiut quartz monzonite

The quartz monzonite samples from within and outside the Strange Lake pluton have lower εNd (-4.8 to -8.1, at t=1.42 Ga) and slightly higher $\delta^{18}O$ (8.9, 9.1 ‰) values than most of the Strange Lake samples. These differences can be explained by a higher degree of crustal contamination for the Napeu Kainiut pluton or its formation from crustal melts. The similarity in the mineralogy of the Napeu Kainiut pluton to that of the 1.42 Ga Mistastin batholith (Miller et al., 1997), and obvious differences in their isotopic signatures from those of the Strange Lake granites, as noted above, suggests that the magmas forming the Strange Lake pluton followed a different evolutionary path from those producing the former intrusions. In addition, the model ages reveal that initial melt extraction from the mantle may have been much later for the Strange Lake granites than for the rocks of the Napeu Kainiut pluton (Fig. 4-7). It is important to note, however, that this does not exclude the possibility that both intrusions were the products of the same large-scale tectonic processes or had the same primary magma source albeit with a greater mantle contribution in the case of the Strange Lake granites. Indeed, a common source is supported by the similarity of the shapes of the chondrite-normalized REE profiles of the Napeu Kainiut samples from outside the Strange Lake pluton to those of the Strange Lake granites. However, the Eu anomalies of the latter are stronger and their HREE trends flatter (see Fig. 4-3). Theoretically, it is possible that the extreme REE, Zr, Nb and alkali enrichment of the Strange

Lake pluton could have originated from the melting of crustal material. However, on the basis of the data presented, we suggest that it is much more likely that this enrichment was due to the involvement of a mantle melt or, as suggested by Martin (2006), metasomatism of the crust by alkali-, REE-, F-, CO_2, OH-rich mantle fluids prior to melting. A large number of isotopic studies of alkaline suites (e.g., Kerr and Fryer 1993; Stevenson et al. 1997; Kovalenko et al. 2009; Hegner et al. 2010) have concluded that the trace element enrichment of these suites was the product of combined crustal contamination and fractional crystallization of mantle-derived melts. On the basis of our data, we propose a similar origin for the silica-oversaturated Strange Lake pluton, which is examined in the following sections. However, the formation of the pluton from crustal melts metasomatically altered by mantle degassing (Martin, 2006) cannot be ruled out, as granitoid rocks produced in this manner would have isotopic signatures that would be indistinguishable from those produced by crustally contaminated mantle melts.

4.5.4 Nature of the mantle underlying the Core Zone

In order to evaluate the impact of crustal processes on the evolution of the Strange Lake pluton from a magma of mantle origin, it was first necessary to gain insights into the nature of the underlying mantle, which elsewhere in the Core Zone has been described as being either depleted or enriched (Ashwal et. al 1986; Amelin et al. 2000; Bédard 2001). Important insights into this nature can be gained from the behavior of the REE, which depends on the presence (or absence) of minerals that can sequester them and whether these minerals preferentially accept the LREE or the HREE. Most of the intrusions of the Nain Plutonic Suite (e.g., Emslie et al. 1994; Petrella and Williams-Jones 2014), including the Strange Lake granites, have chondrite-normalized REE profiles, which show some LREE enrichment, a pronounced negative Eu-anomaly and a flat HREE pattern (see Fig. 4-3). Thus, the mafic rocks (olivine gabbro, troctolites, gabbroic anorthosites) have chondrite-normalized La/Lu_N ratios between 0.8 and 1.0 (Emslie et al. 1994), and the least evolved Strange Lake granites have La/Lu_N ratios between 3 and 5. These low Lu/La ratios rule out a garnet-bearing mantle, because low degrees of partial melting of such a mantle would produce melts enriched in the LREE and depleted in the HREE due to retention of the latter by garnet (De Paolo, 1988). For comparison, low degrees of melting (1-3 %) of a garnet lherzolite would produce La/Lu_N ratios between ~200 and 400 in the resulting magma (calculated assuming a mantle composed of 50 % olivine, 30 % orthopyroxene, 10 % clinopyroxene and 10 % garnet and using mineral-melt partition coefficients from De Paolo (1988)). The REE profiles for the Nain Plutonic rocks, including the Strange Lake granites, are thus consistent with fractionation of a parental melt from a garnet-poor lherzolite or garnet-free lherzolite at depths less than those for which garnet is stable; < 85 km (Robinson and Wood, 1998). Moreover, such shallow melting could be promoted by the addition of water from subducted oceanic crust (Green, 1973). The isotopic compositions of olivine-bearing mafic intrusions and large mafic dike swarms exposed in the region should, in principle, be closest to those of the underlying mantle (higher degrees of partial melting). The 1.33 Ga mafic Voisey’s Bay intrusions, which lie about 150 km to the east of Strange Lake, are some of the most mafic intrusions of the Nain Plutonic Suite, and thus closest in composition to mantle (Amelin et al., 1999). The least contaminated samples are olivine-gabbros and troctolites that have εNd values from +0.9 to -2.1 (Table 4-5) and have been interpreted to represent either melting of an enriched subcontinental mantle or a depleted mantle contaminated by minor proportions of crustal material (Amelin et al., 2000). The olivine-bearing basaltic ‘Nain Dikes’ of the Nain Plutonic Suite, with εNd values of -0.2 and -1.2 and $\delta^{18}O$ values of 6.6 and 6.8 ‰, also have been interpreted to represent an enriched mantle source (Carlson et al., 1993). Carson et al. (1993), however, did not entertain the possibility of a depleted mantle contaminated by crust.

Table 4-5: Nd-concentrations, isotope values and ages of basement rocks

Average Nd-concentrations (ppm), average age corrected εNd (t) values and ages of basement rocks (T, in Ga), as well as average depleted mantle model ages ($T_{DM,}$ in Ga).

Rock type *(n)*	Location	Nd	T	εNd	Range	T_{DM}	Reference
Churchill Province / Core Zone (Paleoproterozoic)							
Gneiss (granitoid) *(2)*	near Strange Lake	15	1.24	-12.7	-12.4, -13.0	2.37	Kerr, 2015
Orthogneiss granitoid*(10)*	Core Zone	-*	1.30	-14.6	-11.1 to -18.3	2.70	Emslie et al., 1994
Enderbitic orthogneiss *(3)*	near Voiseys Bay	-	1.32	-4.0	-2.8 to -5.7	-	Amelin et al., 2000
Tasiuyak paragneiss *(4)*	near Voiseys Bay	30	1.32	-9.2	-8.3 to -10.1	-	Amelin et al., 2000
Nain Province (Archean)							
TTG and felsic gneiss *(8)*	near Kiglapait	15	1.30	-21.9	-14.2 to -28.1	3.20	Emslie et al., 1994
Orthogneiss *(5)*	near Voisey's Bay	50	1.32	-14.2	-11.6 to -18.3	-	Amelin et al., 2000
(Banded) orthogneiss*(3)*	Makkovik Prov.	25	1.72	-15.6	-14.8 to -16.5	3.10	Kerr & Fryer, 1993
Gneiss Archean *(1)*	Gardar Province	36	1.29	-17.8	-17.8	-	Bartels et al., 2015
Least contaminated mafic magmas							
Ol-gabbro, troctolites *(22)*	Voiseys Bay	-	1.32	-1.2	+0.9 to -2.1	-	Amelin et al., 2000
Ol-bearing mafic dikes *(5)*	Nain Province	40	1.28	-3.0	-0.2 to -4.6	2.16	Carlson et al., 1993
Mafic dike swarm *(12)*	Gardar Province	21	1.29	-2.3	-0.5 to -4.4	-	Bartels et al., 2015
Eriksfijord basalt *(6)*	Gardar Province	18	1.17	+2.1	+2.0 to 2.2	-	Paslick et al., 1993

t = age for the calculated εNd (t), which does not necessarily represent the age of the rock.
* Where no value is reported, the isotopic analysis was done on a mineral fraction.

As noted earlier, the Nain Plutonic Suite is interpreted to belong to a larger igneous province that includes SW-Greenland. Thus, studies of the Gardar Province could provide insights into the nature of the mantle beneath the Nain Plutonic Suite. Stevenson et al. (1997) attributed the εNd variations in the Gardar igneous rocks to crustal contamination of a depleted mantle. This interpretation was based on εNd values of +2.1 to +2.4 for the Eriksfjord basalts (Paslick et al., 1993) and a εHf value of +3.2 for an eudialyte sample from Ilímaussaq (Patchett et al., 1981). Negative εSr values and εNd values between +1 and +5 for the Igaliko carbonatite and associated lamprophyre dikes also suggest a depleted mantle (Pearce and Leng 1996; Halama et al. 2003). However, phonolites and oversaturated rocks of the same suite have signatures indicative of crustal contamination, such as strongly positive εSr values (26 and 115), only slightly positive εNd values (1.2 and 1.3) and a wide range in $\delta^{18}O$ values (6.1 to 15.9 ‰). In contrast, mafic dikes in the vicinity of the main intrusions of the Gardar Province (e.g., the 1.276 Ga Brown Dikes) with εNd values between -4.4 and -0.5 and a relatively flat HREE profile have been interpreted to originate from an enriched mantle that underwent partial melting at depths less than those of the garnet stability field (< 85 km) (Bartels et al., 2015). Other evidence of an enriched lithospheric mantle is provided by the occurrence of peridotitic mantle xenoliths (Igdlutalik) with high Zr and Nb contents and low Zr/Nb values (< 4) (Upton, 1991). Significantly, ultramafic lamprophyres and carbonatites in the younger southern Gardar rift have similarly low Zr/Nb (< 4) ratios (Upton et al. 2003; Upton 2013). In order to reconcile the apparently contradictory conclusions over whether the mantle underlying the Gardar Province is depleted or enriched, a number of researchers have argued for a mantle that initially was broadly similar (depleted) but became heterogeneous due to locally variable degrees of mantle metasomatism (Goodenough et al. 2002; Upton et al. 2003; Bartels et al. 2015). This interpretation of metasomatism of the lithospheric mantle beneath the Gardar Province is based on trace element concentrations that differ from common intraplate OIB (ocean island basalt) distributions, and are ascribed to the infiltration of subduction-related alkali and volatile rich fluids associated with the 1.80 Ga Ketilidian orogeny (Goodenough et al., 2002; Upton, 2013).

Evidence of the Ketilidian orogeny is absent in northern Québec-Labrador, with the exception of the Makkovik Province (Kerr and Fryer, 1994). However, the alkaline magmatism of the Nain Province was preceded by the eastward subduction of the foreland of the Superior craton under the Core Zone in the Paleoproterozoic at 1.84 to 1.82 Ga (Van Kranendonk et al., 1993; Wardle et al., 2002). In both northern Québec-Labrador and southern Greenland, there was enrichment of the subcontinental lithospheric mantle through subduction of an ocean floor that contributed to the extreme enrichment in F, alkalis and REE of the Gardar and Strange Lake intrusions (Goodenough et al., 2002; Upton, 2013). We conclude, on the basis of the evidence presented for both the Gardar and Nain Provinces that the mantle underlying the Strange Lake pluton was initially depleted and subsequently enriched by metasomatic fluids produced by subduction-related melts.

4.5.5 The composition of the crust beneath Strange Lake

As discussed earlier, the isotopic data provide compelling evidence that the Strange Lake magmas experienced crustal contamination. Here we evaluate possible sources of this contamination in the basement hosting the pluton, i.e., in the reworked Archean and Paleoproterozoic crustal lenses that constitute the Core Zone.

Seismic surveys and gravity data indicate that the crust of the Core Zone has a thickness of 35 to 40 km, of which the middle to lower part is composed mostly of refractory Archean lithosphere (Wardle et al., 2002). The upper crust of the Core Zone is composed of largely undifferentiated Archean to Paleoproterozoic gneisses of amphibolite to granulite facies (Wardle et al., 2002), which appear as separate blocks, commonly of metavolcanic arc material that are separated by shear zones (Girard 1990; James et al. 1996). The gneissic rocks in the proximity of the Strange Lake pluton consist dominantly of Paleoproterozoic gneisses, such as banded biotite paragneiss and quartzofeldspathic (augen-) orthogneiss and subordinate proportions of garnet-biotite paragneiss and mafic gneisses.

Only the quartzofeldspathic orthogneisses in the vicinity of Strange Lake have been analyzed for Sm-Nd isotopes and only the biotite-gneisses for oxygen isotopes. The quartzofeldspathic (granitoid) gneisses have an average εNd value of -12.7 at 1.24 Ga (Kerr, 2015), and the biotite- (and one garnet-biotite-) gneisses have $\delta^{18}O$ values between 6.3 and 9.6 ‰ (this study). Except for a single sample of biotite gneiss, these $\delta^{18}O$ values of the gneisses are lower than those for the Strange Lake granites; the exception has a $\delta^{18}O$ value of 9.6 ‰ (Table 4-5). This therefore likely rules them out as contaminants of the Strange Lake magma. Other Paleoproterozoic gneisses further from Strange Lake, for which oxygen isotopic data are available, are the Tasiuyak paragneisses located about 100 km to the east, which have $\delta^{18}O$ values between 8.3 and 16.1 ‰. This unit would have been a plausible contaminant, if it had been present in the vicinity of Strange Lake.

The Archean component of the western Core Zone at middle to lower crustal levels (> 6-10 km depth) is represented by the Mistinibi complex, which consists of intercalated ~2.7 Ga old tonalitic gneiss and paragneiss (Girard, 1990; Van der Leeden et al., 1990; Wardle et al., 2002). The Mistinibi complex, which underlies the Core Zone in the Strange Lake region, is a plausible contaminant because it is predicted to have strongly negative εNd values due to its Archean age, and positive $\delta^{18}O$ values due to the large sedimentary component. This proposal is supported by the observation that the De Pas batholith, located about 50 km to the west of Strange Lake, has similar εNd values to the Strange Lake granites (-3 to -7), and is interpreted to have experienced significant contamination by the same Archean crustal material (Kerr et al., 1994; Wardle et al., 2002).

4.5.6 Modeling the evolution of δ^{18}O and εNd

The extent of crustal assimilation by the Strange Lake magmas is evaluated here using a combined fractional crystallization and assimilation (AFC) model applied to the δ^{18}O and εNd data. Oxygen isotope compositions provide a reliable means for evaluating magma sources because they are relatively unaffected by the degree of partial melting or extent of fractional crystallization (Taylor, 1978). Mantle rocks, whether depleted or enriched, have a δ^{18}O value of 5.7 ± 0.2 ‰ (Ito et al., 1987). Thus, magmatic rocks originating from the mantle with values of $\delta^{18}O > 7$ are interpreted to reflect assimilation of crust, with the higher values corresponding to higher proportions of sediment-derived material (see Fig. 4-8) (Taylor, 1978). The oxygen isotopic fractionation between magma and silicate minerals is small at magmatic temperatures ($1 > \alpha > -1$). A value of 0.8 for was calculated for the fractionation between quartz and rhyolitic melt ($\Delta^{18}O_{quartz-melt}$) at 750°C using the empirically derived equation of Zhao and Zheng (2003).

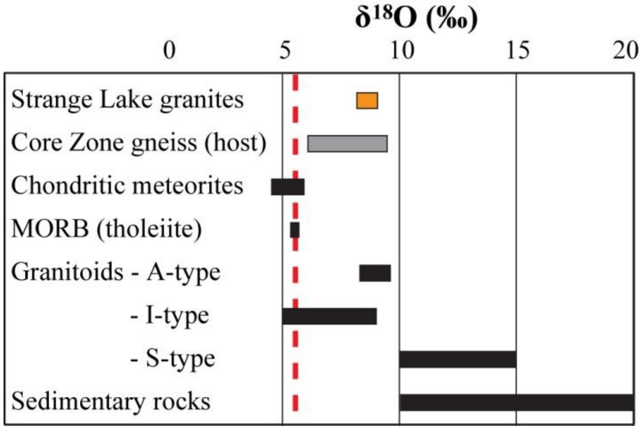

Fig. 4-8: The δ^{18}O values of this study in the context of global reservoirs

Diagram comparing the range of δ^{18}O values (Table 4-4) for the Strange Lake granites and Core Zone gneiss (this study) to corresponding values for global reservoirs. The mantle value of 5.7 ‰ ± 0.2 (Ito et al. 1987) is shown by the red dashed line. The data for the global reservoirs were taken from Onuma et al. (1972); O'Neil (1977); Radain et al. (1981); Harmon and Hoefs (1985); Hoefs (1987); and Wu et al. (2003).

We employed the AFC model of De Paolo (1981) to evaluate the combined effects of fractional crystallization and the assimilation of wall rock on the isotopic evolution of the Strange Lake granites. In this model, the ratio between the mass assimilation rate (M_a) and fractional crystallization rate (M_c) is defined as 'r', where M_a in common igneous systems is a fraction of M_c (De Paolo, 1981). We assumed, in the case of the oxygen isotope data, that the $\delta^{18}O$ value of the least contaminated Voisey's Bay mafic intrusion (6.3 ‰) was the starting value for the magma and assigned values for the contaminant that could explain the $\delta^{18}O$ values of the Strange Lake granites. As is evident from Figure 4-9a, only contaminants with $\delta^{18}O$ values ≥ 10 ‰ can explain the $\delta^{18}O$ values of the Strange Lake granites. Moreover, a contaminant of 10 ‰, would require that the 'r' value be ≥ 0.6, which is unrealistically high (De Paolo, 1981). In order to be able to use a more reasonable value of 'r', for example 0.3 or 0.4, it would be necessary to call on a contaminant with a $\delta^{18}O$ value of ~ 11 ‰ (Fig. 4-9a). Such a contaminant would produce the desired range of $\delta^{18}O$ values (8.2 – 9.1 ‰) after between 60% and 85% crystallization. Clearly, the $\delta^{18}O$ values of the biotite gneisses in the immediate vicinity of the Strange Lake pluton are too low for them to have been the contaminant; the maximum value obtained for these gneisses was 9.6 ‰ (Table 4-4). On the other hand, Churchill Province Paleoproterozoic paragneisses of the Tasiuyak formation near Voisey's Bay, which have $\delta^{18}O$ values between 8.3 and 16.1 ‰ and an average $\delta^{18}O$ value of 10.9 ‰, would have been ideal contaminants (Table 4-5). As noted above, however, we consider it more likely that the contaminant was an Archean paragneiss of the Mistinibi Complex, which is thought to underlie the Strange Lake pluton. Unfortunately, the oxygen isotope data required to evaluate this possibility are not available. For comparison, simple fractional crystallization without contamination leads to a small decrease in $\delta^{18}O$ (Fig. 4-9b).

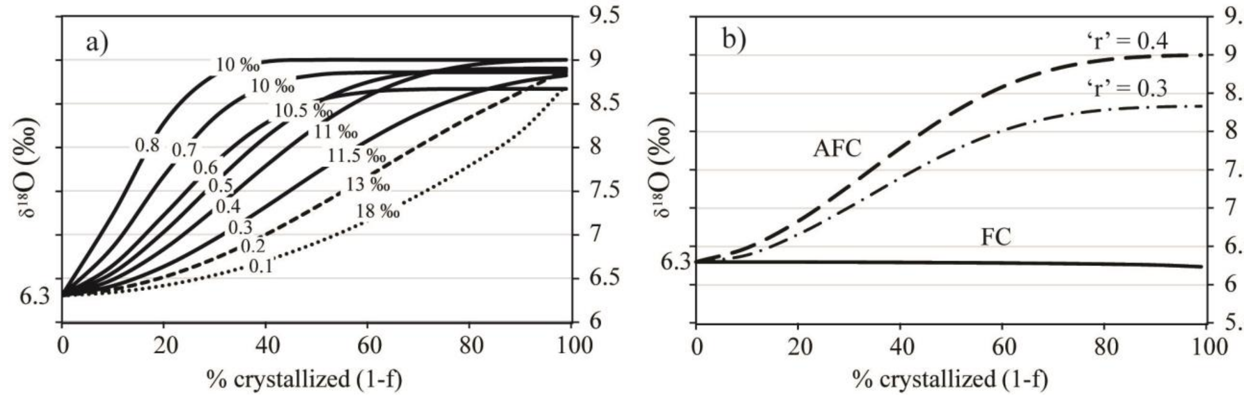

Fig. 4-9: Diagrams of the 'FC' and 'AFC' models

a) Diagram for the AFC model showing the dependence of the evolutionary path for $\delta^{18}O$ on the $\delta^{18}O$ value of the contaminant (10 to 18 ‰) and the value of 'r', the ratio between the mass assimilation rate and the fractional crystallization rate (0.1 to 0.8). The range of $\delta^{18}O$ values for the Strange Lake granites is best explained by a contaminant with a $\delta^{18}O$ value of 11‰ and a 'r' value between 0.3 and 0.4 (see text section 5.6 for further detail); b) A diagram comparing the effect of fractional crystallization 'FC' (Rayleigh fractionation) with the combined effects of fractional crystallization and assimilation 'AFC' on the $\delta^{18}O$ evolution of a magma with an initial $\delta^{18}O$ value of 6.3 ‰ and a contaminant with a $\delta^{18}O$ of 11‰.

In the case of the Nd isotope data, the very small coefficients ($D_{Nd} << 1$) for the partitioning of Nd between early crystallizing minerals (olivine, pyroxenes and plagioclase) and the melt, allow the distribution coefficient (D) to be excluded from the AFC equations of De Paolo (1981). The Nd melt concentration (starting at 40 ppm, the average composition of olivine-bearing basaltic dykes in the Nain Province, Carlson et al. 1993) thus increases exponentially with crystal fractionation, even though a significant proportion of crustal material (5, 10, 15 and 25 %) with a slightly lower Nd concentration (30 ppm, see below) is assimilated (Fig. 4-10). As starting compositions for the combined εNd - $\delta^{18}O$ AFC model, we used a εNd value of +0.9 and a $\delta^{18}O$ value of 6.3 ‰, which represent the highest εNd composition, and lowest $\delta^{18}O$ composition, respectively, of the least contaminated mafic rock series at Voisey's Bay (Amelin et al., 2000) and olivine bearing basaltic dikes in the Nain Province (Carlson et al., 1993) (Tables 4-5; 4-6). Crustal material with a $\delta^{18}O$ value of 11 ‰ was used as the contaminant (see previous paragraph). Data published on Core Zone Paleoproterozoic to Archean gneisses provided the εNd isotopic composition (avg. -15) (Emslie et al., 1994) and Nd-concentration (avg. 30 ppm) (Kerr and Fryer 1993; Amelin et al. 2000; Kerr 2015) of the contaminant. The 'r' value was set at 0.35 (this value yields the observed Strange Lake $\delta^{18}O$ values and a realistic degree of fractional crystallization, see above) and the proportions of assimilated crustal material were fixed at 5, 10, 15 and 25 %. The parameters and equations used for the mixing calculations are reported in the appendix and in Table 4-7.

Table 4-6: Bulk rock $\delta^{18}O$ values of Archean and Paleoproterozoic rocks in the Churchill and Nain Provinces.

Rock type *(n)*	Location	$\delta^{18}O$ avg. (‰)	$\delta^{18}O$ range (‰)	Reference
Churchill Province / Core Zone (Paleoproterozoic)				
Enderbitic (ortho) gneiss *(28)*	near Voiseys Bay	7.2	6.7 - 8.7	Ripley et al., 2000
Tonalite / biotite gneiss *(2)*	near Voiseys Bay	6.8	6.1, 7.5	Peck et al., 2010
Tasiuyak paragneiss *(26)*	near Voiseys Bay	10.9	8.3 - 16.1	Ripley et al., 2000
Tasiuyak paragneiss *(2)*	near Voiseys Bay	9.5	9.2, 9.7	Peck et al., 2010
Nain Province (Archean)				
Mafic gneiss *(14)*	near Voiseys Bay	7.3	5.7 - 8.5	Ripley et al., 2000
Qtz-diorite gneiss / migmatite *(4)*	near Voiseys Bay	6.4	5.4 - 7.4	Peck et al., 2010
Quartzofeldspathic gneiss *(2)*	near Voiseys Bay	9.6	9.5, 9.6	Ripley et al., 2000
Least contaminated mafic magmas				
Olivine-gabbro, troctolites *(106)*	Voiseys Bay intrusion	6.3	4.6 - 8.2	Ripley et al., 2000
Olivine-bearing mafic dikes *(5)*	Nain Province	6.8	6.3 - 7.9	Carlson et al., 1993

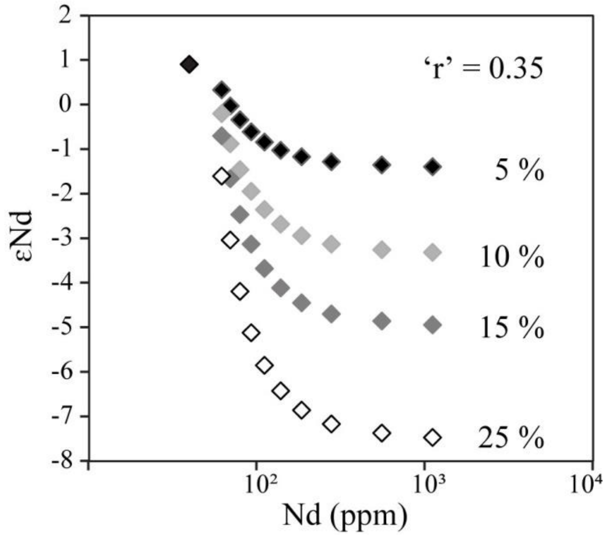

Fig. 4-10:A diagram of εNd versus Nd concentration

A plot of εNd versus Nd concentration showing the exponential increase in melt Nd concentration with decreasing εNd value upon fractional crystallization and assimilation of 5, 10, 15 and 25 % of crustal material. See text section 5.6 for further detail.

Four mixing scenarios were evaluated (Fig. 4-11). Mixing of a melt of basaltic dike composition with 5, 10 or 15 % of contaminant material produced the εNd and δ^{18}O values determined for the Strange Lake granites (pink box in Fig. 4-11). In order to model the isotopic values for the Napeu Kainiut quartz monzonite, a higher proportion of assimilated crustal material (~25 %) was required (orange line in Fig. 4-11). Note that the evolution of the εNd values from slightly positive values to as low as -5 depends on the proportion of contaminant (up to 15 %), and to a much lesser extent on fractional crystallization, which has a negligible effect on the Nd-isotopic composition. In contrast, the δ^{18}O values increase independently of the contaminant proportions, and instead reflect the interplay between the rate of addition of contaminant and the extent of crystallization of the magma.

In summary, the Nd and oxygen isotopic compositions of the Strange Lake granites are satisfactorily explained by fractional crystallization of a reasonably enriched mantle melt that assimilated between 5 and 15 % crust represented by paragneiss with a highly positive $\delta^{18}O$ value (~ 11) and strongly negative εNd value. As neither the Paleoproterozoic gneisses in the vicinity of Strange Lake or gneisses elsewhere in the Core Zone (except for the Tasiuyak paragneiss) could be the source of this contamination, we consider it much more likely that rocks of the Archean Mistinibi tonalite–paragneiss complex underlying the central and western Core Zone were the source. This view is supported by the observation that the De Pas batholith is interpreted to have been contaminated by the latter rocks and has εNd values (-3 to -5) similar to those of the Strange Lake granites (Kerr et al., 1994; Wardle et al., 2002). Assimilation of additional upper crustal material is likely (e.g., biotite-paragneiss and quartzofeldspathic orthogneiss). However, because the isotopic signatures are similar to or lower than those of the Strange Lake pluton, such assimilation would not be evident in the isotopic record of the final product.

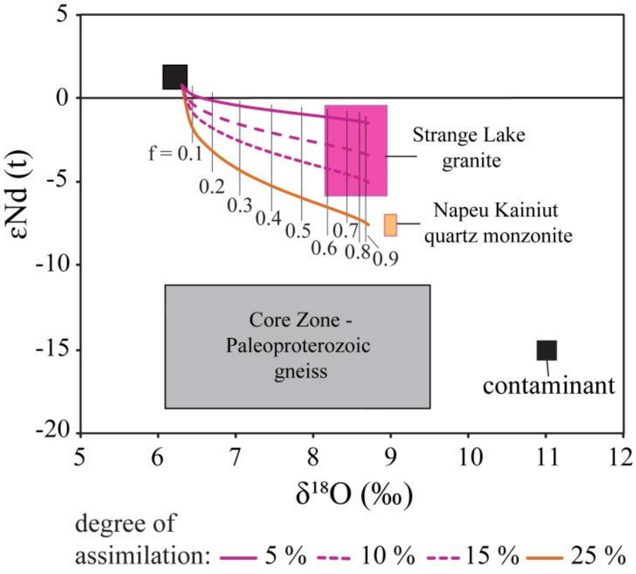

Fig. 4-11: Evolving εNd and δ^{18}O isotopic composition with AFC

Diagram showing the evolving εNd and δ^{18}O isotopic composition with assimilation and fractional crystallization (AFC) of a basaltic starting composition corresponding to the least contaminated Voisey's Bay intrusion (olivine gabbro) (εNd = +0.9 and δ^{18}O = +6.3) with a contaminant having the composition εNd = -15 and δ^{18}O = +11 (see text section 5.6 for references and further explanation). The evolution of the isotopic composition is displayed as a function of melt fraction crystallized (f). The compositional range of the main gneiss types in the vicinity of the Strange Lake pluton and elsewhere in the Core Zone (biotite paragneiss, enderbitic and quartzofeldspathic orthogneiss) is displayed as a grey box for reference.

4.5.7 Plate tectonic controls on the formation of A-type granites

An environment conducive to the generation of mineralized A-type granitoid rocks, such as the Strange Lake pluton as well as other silica-saturated and undersaturated REE-rich rocks, develops as a result of the following tectonic processes: 1) subduction of basaltic (alkali- and volatile-rich) oceanic crust; 2) fertilization of subcontinental mantle with alkalis and volatiles (F, Cl, H_2O, CO_2); 3) continent-continent collision; 4) crustal thickening (orogeny) with the emplacement of syn- and post-collisional calc-alkaline plutons, and perhaps the delamination of a thickened lithosphere; and 5) crustal extension induced either by post-collisional de-stressing or other rifting processes that favor alkaline magmatism (failed rifts) (Black et al., 1985; Martin, 2006; McLelland et al., 2010). The geological history of Laurentia during the Paleo- and Mesoproterozoic records this sequence of tectonic processes.

In the eastern foreland of the Superior Province, the above sequence began with Paleoproterozoic rifting at 2.2 to 2.1 Ga and possibly again at 1.88 Ga, leading to the generation of juvenile oceanic crust (Wardle et al., 2002) that was subducted eastwards under the Core Zone between 1.84 and 1.82 Ga and metasomatized the subcontinental mantle (Fig. 4-12a and b). The collision between the Superior province and the Core Zone resulted in the New Québec orogen and produced large syn-and post-collisional 1.84–1.81 Ga calk-alkaline intrusions (De Pas and Kuujjuaq batholiths) (Fig. 4-12c). This thickening of the crust exerted significant pressure on the underlying lithospheric mantle, which resulted in a low degree of partial melting.

The collisional events at ~1.82 Ga were followed by a long period of tectonic quiescence within the Core Zone until the beginning of the Nain magmatism at ~1.46 Ga. Partial melting began about 360 Ma after the collision, and was most likely induced by decompression of the mantle due to repeated rifting (Fig. 4-12d) in the waning stages of the Elsonian orogenic event (Gower and Krogh, 2002). Although the Core Zone remained relatively quiescent, tectonic activity continued along the southern margin of the Superior and North Atlantic (e.g., Nain Province) cratons with the formation of a marginal basin and the accretion of magmatic arcs during pre-Labradorian (> 1.71 Ga) and Labradorian events (1.71-1.62 Ga) (Gower and Krogh, 2002). This was followed by a change to north-trending flat subduction beneath the Core Zone during the Pinwarian (1.52-1.46 Ga) and Elsonian (1.46-1.23 Ga) orogenies that terminated with the Grenville collision at 1.08-0.98 Ga (Gower and Krogh, 2002). The Elsonian event gave rise to at least three stages of large-scale magmatism related to post-collisional crustal extension. These produced the 1.46–1.41 Ga Mistastin, Harp Lake and Michikamau intrusions, the 1.35–1.29 Ga

Nain plutons and the 1.29–1.24 Ga Harp and Nain dikes, as well as highly evolved Flowers River and Strange Lake peralkaline rhyolitic / granitic suites (Gower and Krogh, 2002).

There is compelling tectonic and geochronological evidence that the plutonic activity of the southern Nain Province was influenced by a mantle enriched through Paleo- and Mesoproterozoic pre-Grenvillian northward subduction, such as the Makkovikian event at ca. 1.80 Ga (Kerr and Fryer, 1994) and the Pinwarian event at ca. 1.50 Ga (Gower and Krogh, 2002). An argument could even be made for a multi-stage-fertilization of the mantle underlying the Core Zone, starting with the eastward subduction at ~1.82 Ga associated with the Superior Craton followed by the two above mentioned pre-Grenvillian subduction events. Although much of this activity occurred some 400 km to the south of Strange Lake, it is noteworthy, for comparison, that Andean volcanism occurs up to 500 km from the trench along the South American coast (Mamani et al., 2010).

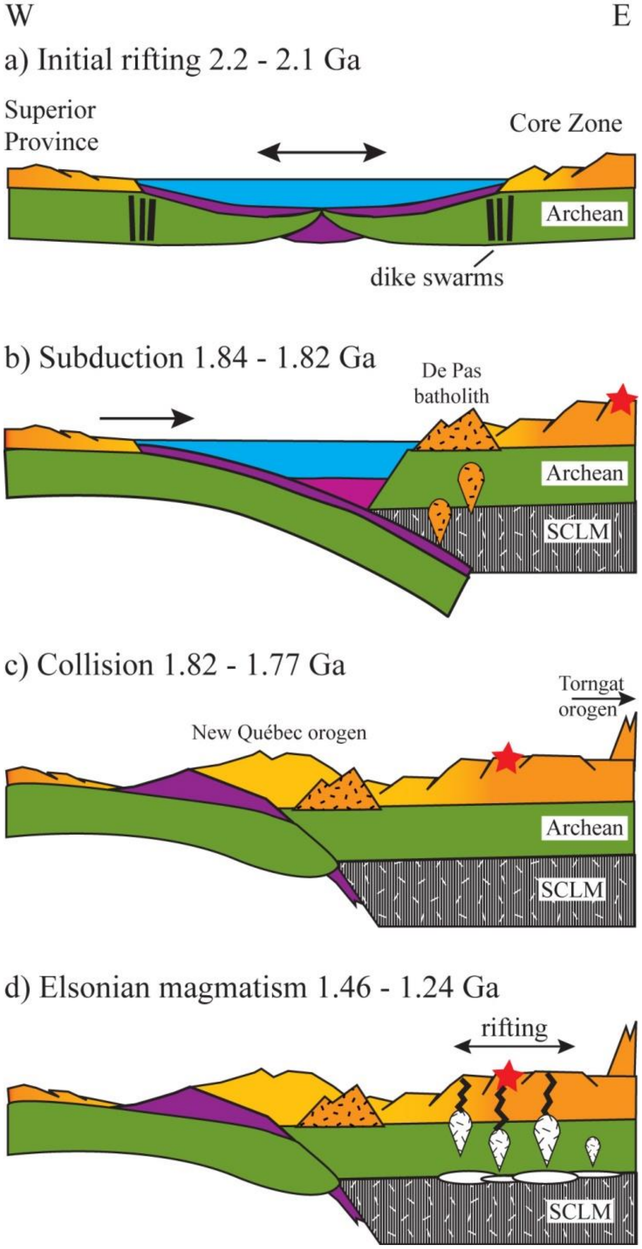

Fig. 4-12: Sketches of the tectonic processes that affected the Core Zone (2.2 to 1.24 Ga).

Sketches illustrating a) Initial rifting, b) Subduction, c) Continent-continent collision, and d) Elsonian magmatism. The red star represents the location of the Strange Lake pluton. SCLM = subcontinental lithospheric mantle.

4.5.8 Correlations between Strang Lake and other REE-mineralized intrusions

A number of smaller, mostly silica-saturated and REE-mineralized intrusions are either hosted by the 1.42 Ga old Mistastin batholith or are associated with the older Nain magmatism (1.45 to 1.41 Ga). These include the Ytterby 1, 2 and 3 intrusions (Kerr and Hamilton (2014) and the REE-rich Misery Lake ferro-syenite (Petrella et al., 2014).

The relative proximity of these REE mineralized bodies to each other suggests that they may be products of the same fertile source. The negative εNd values of the Strange Lake granites and those of a 1.42 Ga granite (εNd = -9.1) and a 1.44 Ga quartz syenite (εNd = -8.8) from REE-enriched intrusive bodies within the Mistastin batholith (Kerr and Hamilton, 2014) indicate that all of these mineralized intrusions underwent significant crustal assimilation. However, the fact that most of the REE-rich bodies to the south are silica-saturated syenites, whereas Strange Lake is silica-oversaturated, could indicate that there was greater crustal assimilation towards the North (Kay and Gast, 1973; Sobolev et al., 2007). The older ages of the Ytterby and Misery Lake intrusions (1.41 to 1.44 Ga) (David et al., 2012; Kerr and Hamilton, 2014) compared to Strange Lake (1.24 Ga) may reflect thickening of the crust with time, allowing greater contamination and silica-saturation of the Strange Lake parental magma. Further work is required to constrain these possible relationships.

4.5.9 Similarities and differences between the Nain and Gardar igneous provinces

We have argued that the source for the alkaline magmatism in Labrador (Nain Plutonic Suite) was likely a heterogeneous, and partially enriched subcontinental mantle, and that fertilization of this mantle occurred during the subduction of the eastern Superior Province foreland beneath the Core Zone at 1.84 - 1.82 Ga. A similar conclusion can be drawn for the Gardar Province, where there is also evidence for a highly heterogeneous mantle characterized by locations that are enriched and locations that are depleted (Stevenson et al. 1997; Halama et al. 2003; Sobolev et al. 2007). Basaltic magmas emplaced early in the evolution of the Gardar Province have geochemical signatures of subduction-related melts, i.e., high LILE, LREE and low Nb concentrations (Goodenough et al., 2002; Köhler et al., 2009), which have been attributed to the 1.85-1.80 Ga Ketilidian subduction (Garde et al., 2002; Upton, 2013).

On both sides of the present Labrador Sea, a tectonic quiescence of several hundred million years separated the subduction events from the large-scale alkaline magmatic periods. In the Gardar Province, more than 500 Ma elapsed between the Ketilidian subduction at ~1.8 Ga and the start of alkaline magmatism at ~1.3 Ga, whereas on the Labrador side, the interval was ≤ 400 Ma between the end of the Superior subduction at ~1.82 Ga and the start of Nain plutonism at 1.46 Ga. Both sides of the Labrador Sea experienced several stages of rifting along different axes, resulting in crustal thinning and low degrees of partial melting that produced small melt fractions with high volatile and incompatible element concentrations (e.g., Upton et al. 2003; Myers et al. 2008). The repetition of this rifting is particularly evident in the occurrence of several generations of mafic dikes in the Nain Province, some of which extend into the Gardar Province (Cadman et al. 1993; Bartels et al. 2015). The main stage of emplacement of the Nain Plutonic Suite (1.35-1.29 Ga) was controlled by a N-S trending zone of crustal weakness, parallel to the suture between the Archean Nain Province and the Core Zone (Myers et al., 2008). In contrast, the main intrusions of the Gardar Province, the Ilímaussaq and Tuutoq intrusions, are aligned along an old SW-NE trending lineament of lithospheric weakness (Upton et al., 2003). In addition, the large Gardar-Voisey's Bay lithospheric-scale fault zone (Fig. 4-13) aligns with and may be related to the major phases of alkaline magmatism (e.g., the Strange Lake pluton) that were localized along an extension of this fault zone (Myers et al., 2008).

There are several important differences between the Nain and Gardar igneous provinces. For example, the Nain Province magmatism is overall slightly older (1.46 to 1.24 Ga) and less alkaline than the Gardar province, which was emplaced between 1.35 to 1.12 Ga and produced highly agpaitic rocks. The main phase of Nain magmatism (1.35 to 1.29 Ga), however, coincides temporally with the earlier phase of Gardar magmatism (1.35 to 1.30 Ga) (Upton et al. 2003; Myers et al. 2008). There are compositional differences between the two provinces with nepheline syenites predominating in the Gardar Province (Upton and Blundell, 1978) and anorthosites, norites, ferrodiorites, monzonites and granites being prevalent in the Nain Province (Gower and Krogh, 2002). The differences in compositions (e.g., degree of alkalinity and silica saturation) and timing of magmatism in the two provinces may be due to several factors. Any enrichment of the mantle underlying the two provinces would have resulted from separate subduction events, namely the Ketilidian (Gardar Province) and the Superior (Nain Plutonic Suite) subduction. The nature and extent of fertilization of the subcontinental mantle under each province would therefore likely have differed because of differences in the compositions of the subducted slabs. Also, the Ketilidian crust, e.g., the Julianehåb batholith (Gardar Province), and the crust of the Core Zone (Nain Plutonic Suite), which are both the hosts and the contaminants of the intruding melts, differ in their proportions of intrusive, volcanic and sedimentary rocks. In addition, crustal extension was not homogenous throughout Eastern Laurentia, as implied by extensive dike swarms of several generations and axial orientations. The similarities between the settings of the two igneous provinces, however, exceed the differences and, in both cases, the tectonic environment was favorable for the generation and emplacement of alkaline rocks highly enriched in the REE and other HFSE.

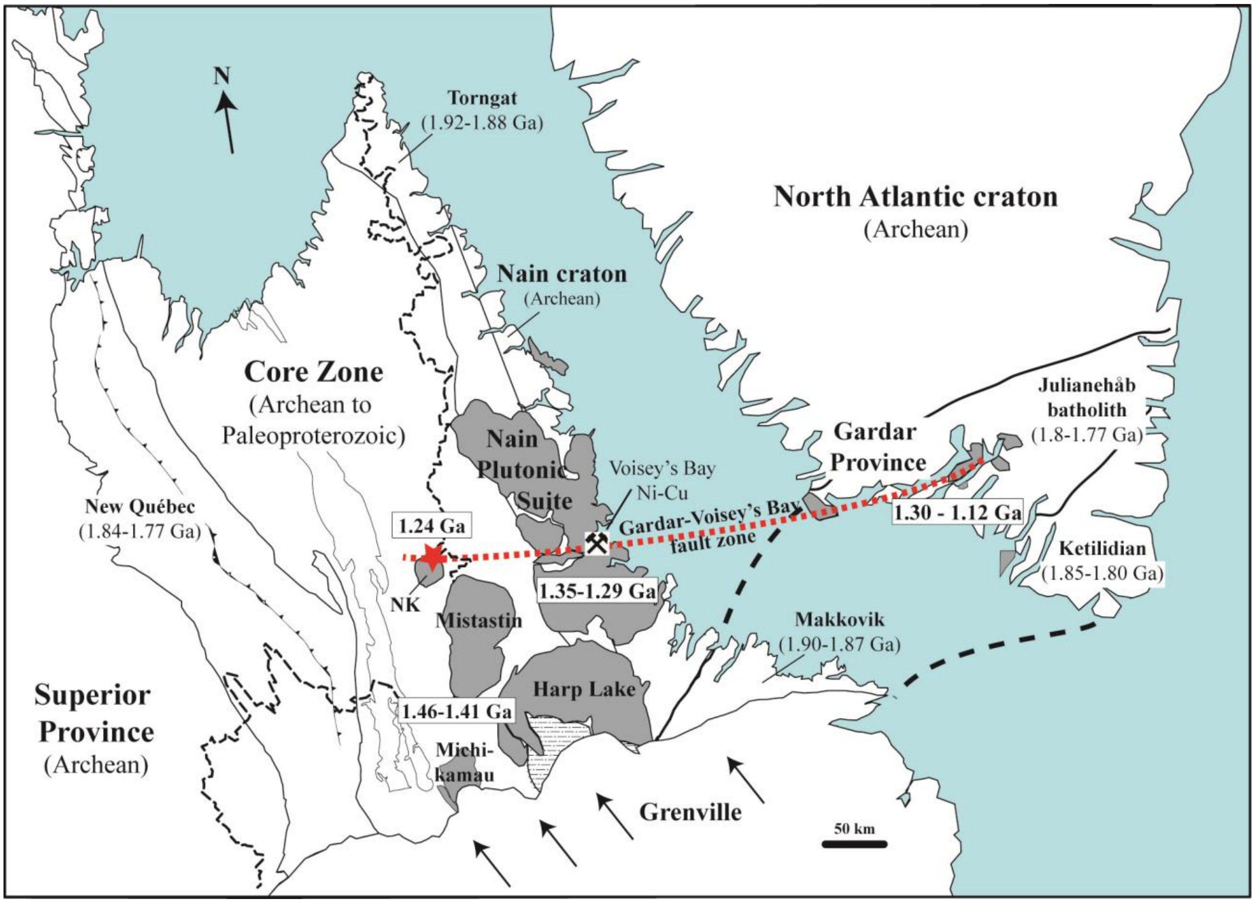

Fig. 4-13: A simplified map showing the tectonic units of northeastern Laurentia.

The distance between NE-Canada and SW-Greenland is disproportional. The locations of the Nain Plutonic Suite (Québec-Labrador) and the Gardar alkaline intrusions (SW-Greenland) are shown in grey, the inferred link between the Ketilidian and Makkovik provinces by *black dashed lines*, and the Gardar-Voisey's Bay Ni-Cu-deposit and fault zone connecting both provinces by a *red dashed line.*

4.6 CONCLUSIONS

The Nd- and O-isotope ratios for the unaltered Strange Lake granites presented in this study are consistent and differ from those of the surrounding Napeu Kainiut quartz monzonites, indicating different evolutionary paths for the two intrusions. The isotopic signatures of the Strange Lake samples can be explained by a combination of crustal assimilation and in-situ Sm-Nd fractionation, involving the crystallization of primary LREE-minerals and arfvedsonite and later hydrothermal remobilization of the REE.

The numerous reports of rocks with enriched isotope signatures among otherwise uncontaminated mafic rocks of the Nain Plutonic Suite (Emslie et al. 1994; Amelin et al. 2000; Peck et al. 2010; Kerr and Hamilton 2014), suggest that the Strange Lake magma was derived from a mantle that locally was metasomatically enriched in incompatible elements. Fractional crystallization of this magma and accompanying assimilation of 5-15 % of Archean paragneiss yielded the εNd and δ^{18}O values preserved by the Strange Lake granites. Generation of REE-mineralized A-type granites, as well as other silica-saturated members of the Nain Plutonic Suite, was likely due to a combination of tectonic events, including the 1.84-1.82 Ga subduction of oceanic crust of the Superior province foreland, which metasomatized the subcontinental mantle. This subduction was followed by continent-continent collision and the New Québec orogeny, which was accompanied by calc-alkaline magmatism. Rifting of the Nain Province during the waning stages of the Elsonian event between 1.46 and 1.24 Ga produced alkaline melts which were generated via low degrees of partial melting.

The alkaline intrusions of the Gardar province in SW-Greenland are similar to the Nain Plutonic Suite in nature and timing, but metasomatism of the Gardar mantle was related to the 1.85-1.80 Ga Ketilidian subduction and the Core Zone mantle to the 1.84 - 1.82 Ga Superior subduction. In addition, the underlying crust and main contaminant of the Gardar suites was the Paleoproterozoic calc-alkaline Julianehåb batholith, whereas for the Nain Plutonic Suite it was a highly heterogeneous mixture of Archean and Paleoproterozoic crust. A link between the two provinces is indicated by the extensive supra-regional dike swarms (Nain-, Harp-, Brown-dikes) as well as the shared Gardar-Voisey's Bay fault zone that led to the emplacement of both the Nain and Gardar magmas in the upper crust.

This study identifies a sequence of plate tectonic and evolutionary processes that favored the generation of highly REE-enriched alkaline silica-undersaturated and oversaturated melts. These processes are consistent with the tectonic framework that produced the alkaline magmatism of the Mesoproterozoic Nain and Gardar Provinces, and help constrain exploration models for REE-mineralized intrusive bodies.

APPENDIX

εNd - δ^{18}O endmember mixing

Eq (A.1)

Because $D_{Nd} << 1$:

$$\frac{\varepsilon_m-\varepsilon_m^0}{\varepsilon_a-\varepsilon_a^0} = 1/(1+\frac{C_m{}^0\cdot M_m}{C_a\cdot M_a})$$

with

$$\frac{C_m}{C_m^0} \sim F^{-1}\left[1 - \frac{C_a}{C_m^0}\cdot\frac{r}{r-1}\right]$$

Eq (A.2)

Because D δ^{18}O ~ 1 and $r \neq 1$

$$\delta_m - \delta_0 = (\delta_a - \delta_0 - \frac{\Delta}{r})\cdot(1-F^{(-z)})$$

with

$$z = \frac{r}{r-1}$$

Table 4-7: Parameters used for mixing calculations

	parameter
Source	
c Nd_l	40 ppm
εNd_i	+ 0.9
$\delta^{18}O_i$	6.3 ‰
Contaminant	
c Nd_c	30 ppm
εNd_c	-15.0
$\delta^{18}O_c$	+11 ‰
rate 'r'	0.35

ACKNOWLEDGEMENTS

Financial support for the research was provided by a grant from Quest Rare Minerals Ltd. and a matching grant from the NSERC Collaborative Research and Development program. Quest Rare Minerals Ltd. also provided essential logistical support in the field. André Poirier and Julien Gogot helped with the Nd isotope analyses, which were carried out in the GEOTOP laboratories (Université de Québec à Montréal). Galen Halverson (Earth & Planetary Sciences, McGill University) made his equipment in the clean laboratories available to the project and Peter Crockford helped with the wet column chemistry and the preparation of samples for the TIMS analyses (Sm-Nd-isotope analyses). Mike Hamilton (University of Toronto), Andy Kerr (formerly of the Newfoundland and Labrador Geological Survey), David Corrigan (Geological Survey of Canada) and Robert F. Martin (McGill University) contributed from their extensive knowledge and experience with alkaline igneous rocks, and provided supplementary data (unpublished maps and literature).

REFERENCES

Amelin, Y., Li, C. S., and Naldrett, A. J., 1999, Geochronology of the Voisey's Bay intrusion, Labrador, Canada, by precise U-Pb dating of coexisting baddeleyite, zircon, and apatite: Lithos, v. 47, no. 1-2, p. 33-51.

Amelin, Y., Li, C. S., Valeyev, O., and Naldrett, A. J., 2000, Nd-Pb-Sr isotope systematics of crustal assimilation in the Voisey's Bay and Mushuau intrusions, Labrador, Canada: Economic Geology and the Bulletin of the Society of Economic Geologists, v. 95, no. 4, p. 815-830.

Anderson, I. C., Frost, C. D., and Frost, B. R., 2003, Petrogenesis of the Red Mountain pluton, Laramie anorthosite complex, Wyoming: implications for the origin of A-type granite: Precambrian Research, v. 124, no. 2-4, p. 243-267.

Ashwal, L. D., Wooden, J. L., and Emslie, R. F., 1986, Sr, Nd, and Pb Isotopes in Proterozoic Intrusives Astride the Grenville Front in Labrador - Implications for Crustal Contamination and Basement Mapping: Geochimica Et Cosmochimica Acta, v. 50, no. 12, p. 2571-2585.

Bailey, D. K., 1987, Mantle metasomatism - perspective and prospect: Geological Society, London, v. 30, no. Special Publications, p. 1-13.

Bailey, J. C., Gwozdz, R., Rose-Hansen, J., Sorensen, H., 2001, Geochemical overview of the Ilimaussaq alkaline complex, South Greenland: Geology of Greenland Survey Bulletin, v. 190, p. 35-53.

Bartels, A., Nielsen, T. F. D., Lee, S. R., and Upton, B. G. J., 2015, Petrological and geochemical characteristics of Mesoproterozoic dyke swarms in the Gardar Province, South Greenland: Evidence for a major sub-continental lithospheric mantle component in the generation of the magmas: Mineralogical Magazine, v. 79, no. 4, p. 909-939.

Bédard, J. H., 2001, Parental magmas of the Nain Plutonic Suite anorthosites and mafic cumulates: a trace element modelling approach: Contributions to Mineralogy and Petrology, v. 141, no. 6, p. 747-771.

Black, R., Lameyre, J., and Bonin, B., 1985, The Structural Setting of Alkaline Complexes: Journal of African Earth Sciences, v. 3, no. 1-2, p. 5-16.

Blaxland, A. B., and Curtis, L. W., 1977, Chronology of Red Wine Alkaline Province, Central Labrador: Canadian Journal of Earth Sciences, v. 14, no. 8, p. 1940-1946.

Boily, M., and Williams-Jones, A. E., 1994, The role of magmatic and hydrothermal processes in the chemical evolution of the Strange Lake plutonic complex, Quebec-Labrador: Contributions to Mineralogy and Petrology, v. 118, no. 1, p. 33-47.

Bonin, B., 2007, A-type granites and related rocks: Evolution of a concept, problems and prospects: Lithos, v. 97, no. 1-2, p. 1-29.

Borthwick, J., and Harmon, R. S., 1982, A Note Regarding Cif3 as an Alternative to Brf5 for Oxygen Isotope Analysis: Geochimica Et Cosmochimica Acta, v. 46, no. 9, p. 1665-1668.

Bridgwater, D., 1967, Feldspathic inclusions in the Gardar igneous rocks of South Greenland and their relevance to their formation of major anorthosites in the Canadian Shield: Canadian Journal of Earth Sciences, v. 4, no. 6, p. 995-1014.

Cadman, A. C., Heaman, L., Tarney, J., Wardle, R., and Krogh, T. E., 1993, U-Pb Geochronology and Geochemical Variation within 2 Proterozoic Mafic Dyke Swarms, Labrador: Canadian Journal of Earth Sciences, v. 30, no. 7, p. 1490-1504.

Carlson, R. W., Wiebe, R. A., and Kalamarides, R. I., 1993, Isotopic Study of Basaltic Dikes in the Nain Plutonic Suite - Evidence for Enriched Mantle Sources: Canadian Journal of Earth Sciences, v. 30, no. 6, p. 1141-1146.

Clayton, R. N., and Mayeda, T. K., 1963, The Use of Bromine Pentafluoride in the Extraction of Oxygen from Oxides and Silicates for Isotopic Analysis: Geochimica Et Cosmochimica Acta, v. 27, no. Jan, p. 43-52.

Collins, W. J., Beams, S. D., White, A. J. R., and Chappell, B. W., 1982, Nature and Origin of a-Type Granites with Particular Reference to Southeastern Australia: Contributions to Mineralogy and Petrology, v. 80, no. 2, p. 189-200.

Connelly, J. N., and Ryan, A. B., 1999, Age and tectonic implications of Paleoproterozoic granitoid intrusions within the Nain Province near Nain, Labrador: Canadian Journal of Earth Sciences, v. 36, no. 5, p. 833-853.

Corrigan, D., Pehrsson, S., Wodicka, N., and de Kemp, E., 2009, The Palaeoproterozoic Trans-Hudson Orogen: a prototype of modern accretionary processes: Geological Society, London, v. 237, no. Special publications 2009, p. 457-479.

Corrigan, D., Wodicka, N., McFarlane, C., Lafrance, I., Bandyayera, D., Bilodeau, C., and van Rooyen, D., The Core Zone: A ribbon continent accreted to the western edge of the North Atlantic Craton in Canada, *in* Proceedings NAC+ 2016: The North Atlantic Craton and surrounding belts: a craton-specific approach to exploration targeting, Edinburgh, UK, 2016, The Mineralogical Society of Great Britain and Ireland, p. 29.

Dall'Agnol, R., and de Oliveira, D. C., 2007, Oxidized, magnetite-series, rapakivi-type granites of Carajas, Brazil: Implications for classification and petrogenesis of A-type granites: Lithos, v. 93, no. 3-4, p. 215-233.

Dall'Agnol, R., Teixeira, N. P., Ramo, O. T., Moura, C. A. V., Macambira, M. J. B., and de Oliveira, D. C., 2005, Petrogenesis of the Paleoproterozoic rapakivi A-type granites of the Archean Carajas metallogenic province, Brazil: Lithos, v. 80, no. 1-4, p. 101-129.

David, J., Simard, M., Bandyayera, D., Goutier, J., Hammouche, H., Pilote, P., Leclerc, F., and Dion, C., 2012, Datations U-Pb effectuées dans les provinces du Supérieur et de Churchill en 2010-2011: Geologie Québec, Ministère des Ressources Naturelles et de la Faune (MRNF), v. RP 2012-01, p. 30.

De Paolo, D. J., 1981, Trace-Element and Isotopic Effects of Combined Wallrock Assimilation and Fractional Crystallization: Earth and Planetary Science Letters, v. 53, no. 2, p. 189-202.

-, 1988, Neodymium Isotope Geochemistry: An Introduction, Springer Verlag, 187 p.:

De Paolo, D. J., and Wasserburg, G. J., 1976, Nd Isotopic Variations and Petrogenetic Models: Geophysical Research Letters, v. 3, no. 5, p. 249-252.

Eby, G. N., 1990, The A-type granitoids: a review of their occurrence and chemical characteristics and speculations on their petrogenesis: Lithos, v. 26, p. 115-134.

Eby, G. N., 1992, Chemical subdivision of the a-type granitoids - petrogenetic and tectonic implications: Geology, v. 20, no. 7, p. 641-644.

Emslie, R. F., Hamilton, M. A., and Theriault, R. J., 1994, Petrogenesis of a Midproterozoic anorthosite-mangerite-charnockite-granite (AMCG) complex - isotopic and chemical evidence from the Nain Plutonic Suite: Journal of Geology, v. 102, no. 5, p. 539-558.

Emslie, R. F., and Stirling, J. A. R., 1993, Rapakivi and Related Granitoids of the Nain Plutonic Suite - Geochemistry, Mineral Assemblages and Fluid Equilibria: Canadian Mineralogist, v. 31, p. 821-847.

Frost, C. D., Bell, J. M., Frost, B. R., and Chamberlain, K. R., 2001, Crustal growth by magmatic underplating: Isotopic evidence from the northern Sherman batholith: Geology, v. 29, no. 6, p. 515-518.

Frost, C. D., and Frost, B. R., 1997, Reduced rapakivi-type granites: The tholeiite connection: Geology, v. 25, no. 7, p. 647-650.

Frost, C. D., Frost, B. R., Chamberlain, K. R., and Edwards, B. R., 1999, Petrogenesis of the 43 Ga Sherman batholith, SE Wyoming, USA: A reduced, rapakivi-type anorogenic granite: Journal of Petrology, v. 40, no. 12, p. 1771-1802.

Garde, A. A., Hamilton, M. A., Chadwick, B., Grocott, J., and McCaffrey, K. J. W., 2002, The Ketilidian orogen of South Greenland: geochronology, tectonics magmatism and fore-arc accretion during Palaeoproterozoic oblique convergence: Canadian Journal of Earth Sciences, v. 39, no. 5, p. 765-793.

Girard, R., 1990, Evidence d'un magmatisme d'arc Proterozoique inferieur (2.3 Ga) sur le plateau de la riviere George: Geoscience Canada v. 17, no. 4, p. 265-268.

Goldstein, S. L., Onions, R. K., and Hamilton, P. J., 1984, A Sm-Nd Isotopic Study of Atmospheric Dusts and Particulates from Major River Systems: Earth and Planetary Science Letters, v. 70, no. 2, p. 221-236.

Goodenough, K. M., Upton, B. G. J., and Ellam, R. M., 2002, Long-term memory of subduction processes in the lithospheric mantle: evidence from the geochemistry of basic dykes in the Gardar Province of South Greenland: Journal of the Geological Society, v. 159, p. 705-714.

Gower, C. F., and Krogh, T. E., 2002, A U-Pb geochronological review of the Proterozoic history of the eastern Grenville Province: Canadian Journal of Earth Sciences, v. 39, no. 5, p. 795-829.

Green, D. H., 1973, Experimental Melting Studies on a Model Upper Mantle Composition at High-Pressure under Water-Saturated and Water-Undersaturated Conditions: Earth and Planetary Science Letters, v. 19, no. 1, p. 37-53.

Gregory, R. T., Criss, R. E., and Taylor, H. P., 1989, Oxygen Isotope Exchange Kinetics of Mineral Pairs in Closed and Open Systems - Applications to Problems of Hydrothermal Alteration of Igneous Rocks and Precambrian Iron Formations: Chemical Geology, v. 75, no. 1-2, p. 1-42.

Gysi, A. P., and Williams-Jones, A. E., 2013, Hydrothermal mobilization of pegmatite-hosted REE and Zr at Strange Lake, Canada: A reaction path model: Geochimica et Cosmochimica Acta, v. 122, no. 2013, p. 324-352.

Gysi, A. P., Williams-Jones, A. E., and Collins, P., 2016, Lithogeochemical Vectors for Hydrothermal Processes in the Strange Lake Peralkaline Granitic REE-Zr-Nb-Deposit: Economic Geology and the Bulletin of the Society of Economic Geologists, v. 111, p. 1241-1276.

Halama, R., Wenzel, T., Upton, B. G. J., Siebel, W., and Markl, G., 2003, A geochemical and Sr-Nd-O isotopic study of the Proterozoic Eriksfjord Basalts, Gardar Province, South Greenland - Reconstruction of an OIB signature in crustally contaminated rift-related basalts: Mineralogical Magazine, v. 67, no. 6, p. 1338-1338.

Hegner, E., Emslie, R. F., Iaccheri, L. M., and Hamilton, M. A., 2010, Sources of the Mealy Mountains and Atikonak River Anorthosite-Granitoid Complexes, Grenville Province, Canada: Canadian Mineralogist, v. 48, no. 4, p. 787-808.

Hoffman, P. F., 1988, United Plates of America, the Birth of a Craton - Early Proterozoic Assembly and Growth of Laurentia: Annual Review of Earth and Planetary Sciences, v. 16, p. 543-603.

Ito, E., White, W. M., and Gopel, C., 1987, The O, Sr, Nd and Pb Isotope Geochemistry of Morb: Chemical Geology, v. 62, no. 3-4, p. 157-176.

Jacobsen, S. B., and Wasserburg, G. J., 1980, Sm-Nd Isotopic Evolution of Chondrites: Earth and Planetary Science Letters, v. 50, no. 1, p. 139-155.

James, D. T., Connelly, J. N., Wasteneys, H. A., and Kilfoil, G. J., 1996, Paleoproterozoic lithotectonic divisions of the southeastern Churchill Province, western Labrador: Canadian Journal of Earth Sciences, v. 33, no. 2, p. 216-230.

James, D. T., and Dunning, G. R., 2000, U-Pb geochronological constraints for paleoproterozoic evolution of the core zone, southeastern Churchill Province, northeastern laurentia: Precambrian Research, v. 103, no. 1-2, p. 31-54.

Kay, R. W., and Gast, P. W., 1973, Rare-Earth Content and Origin of Alkali-Rich Basalts: Journal of Geology, v. 81, no. 6, p. 653-682.

Kerr, A., 2015, Sm-Nd Isotopic Geochemistry of Rare-Earth-Element (REE) Mineralization and Associated Peralkaline Granites of the Strange Lake Intrusion, Labrador: Current Research (2015) Newfoundland and Labrador Department of Natural Resources, v. 1, p. 63-83.

Kerr, A., and Fryer, B. J., 1993, Nd Isotope Evidence for Crust Mantle Interaction in the Generation of a-Type Granitoid Suites in Labrador, Canada: Chemical Geology, v. 104, no. 1-4, p. 39-60.

-, 1994, The Importance of Late-Orogenic and Postorogenic Crustal Growth in the Early Proterozoic - Evidence from Sm-Nd Isotopic Studies of Igneous Rocks in the Makkovik Province, Canada: Earth and Planetary Science Letters, v. 125, no. 1-4, p. 71-88.

Kerr, A., and Hamilton, M. A., 2014, Rare-earth element (REE) mineralization in the Mistastin Lake and Smallwood Reservoir areas, Labrador: field relationships and preliminary U-Pb zircon ages from host granitoid rocks Current Research (1990) Newfoundland Department of Mines and Energy, Geological Survey v. 1, p. 45-62.

Kerr, A., James, D. T., and Fryer, B. J., 1994, Nd isotopic and geochemical studies in the Labrador Shield: a progress report and preliminary data from the Churchill (Rae) Province: Eastern Canadian Shield Onshore-Offshore Transsect (ECSOOT), Report of the 1994 Transect Meeting.

Kerr, A., and Rafuse, H., 2012, Rare-earth element (REE) geochemistry of the Strange Lake deposits: Implications for resource estimation and metallogenic models.: Current Research (2012) Newfoundland and Labrador Department of Natural Resources, v. 1, p. 39-60.

Köhler, J., Schonenberger, J., Upton, B., and Markl, G., 2009, Halogen and trace-element chemistry in the Gardar Province, South Greenland: Subduction-related mantle metasomatism and fluid exsolution from alkalic melts: Lithos, v. 113, no. 3-4, p. 731-747.

Kovalenko, V. I., Yarmolyuk, V. V., Kovach, V. P., Kovalenko, D. V., Kozlovskii, A. M., Andreeva, I. A., Kotov, A. B., and Salnikova, E. B., 2009, Variations in the Nd isotopic ratios and canonical ratios of concentrations of incompatible elements as an indication of mixing sources of alkali granitoids and basites in the Khaldzan-Buregtei massif and the

Khaldzan-Buregtei rare-metal deposit in western Mongolia: Petrology, v. 17, no. 3, p. 227-252.

Kovalenko, V. I., Yarmolyuk, V. V., Kovach, V. P., Sal'nikova, E. B., Kozlovskii, A. M., Kotov, A. B., and Khanchuk, A. I., 2004, Multiple magma sources for the peralkaline granitoids and related rocks of the Khaldzan Buregte group of massifs, western Mongolia: Isotopic (neodymium, strontium, and oxygen) and geochemical data: Petrology, v. 12, no. 6, p. 497-518.

Kovalenko, V. I., Yarmolyuk, V. V., Kozlovsky, A. M., Kovach, V. P., Sal'nikova, E. B., Kotov, A. B., and Vladykin, N. V., 2007, Two types of magma sources of rare-metal alkali granites: Geology of Ore Deposits, v. 49, no. 6, p. 442-466.

Mamani, M., Worner, G., and Sempere, T., 2010, Geochemical variations in igneous rocks of the Central Andean orocline (13 degrees S to 18 degrees S): Tracing crustal thickening and magma generation through time and space: Geological Society of America Bulletin, v. 122, no. 1-2, p. 162-182.

Martin, R. F., 2006, A-type granites of crustal origin ultimately result from open-system fenitization-type reactions in an extensional environment: Lithos, v. 91, no. 1-4, p. 125-136.

Martin, R. F., Sokolov, M., and Magaji, S. S., 2012, Punctuated anorogenic magmatism: Lithos, v. 152, p. 132-140.

McLelland, J. M., Selleck, B. W., Hamilton, M. A., and Bickford, M. E., 2010, Late- to post-tectonic setting of some major proterozoic anorthosite - mangerite - charnockite - granite (AMCG) suites: Canadian Mineralogist, v. 48, no. 4, p. 729-750.

Migdisov, A. A., Williams-Jones, A. E., Brugger, J., and Caporuscio, F. A., 2016, Hydrothermal transport, deposition, and fractionation of the REE: Experimental data and thermodynamic calculations: Chemical Geology, v. 439, p. 13-42.

Miller, R. R., Heaman, L. M., and Birkett, T. C., 1997, U-Pb zircon age of the Strange Lake peralkaline complex: Implications for Mesoproterozoic peralkaline magmatism in north-central Labrador: Precambrian Research, v. 81, no. 1-2, p. 67-82.

Myers, J. S., Voordouw, R. J., and Tettelaar, T. A., 2008, Proterozoic anorthosite-granite Nain batholith: structure and intrusion processes in an active lithosphere-scale fault zone, northern Labrador: Canadian Journal of Earth Sciences, v. 45, no. 8, p. 909-934.

Paslick, C. R., Halliday, A. N., Davies, G. R., Mezger, K., and Upton, B. G. J., 1993, Timing of Proterozoic Magmatism in the Gardar Province, Southern Greenland: Geological Society of America Bulletin, v. 105, no. 2, p. 272-278.

Patchett, P. J., Kouvo, O., Hedge, C. E., and Tatsumoto, M., 1981, Evolution of Continental-Crust and Mantle Heterogeneity - Evidence from Hf Isotopes: Contributions to Mineralogy and Petrology, v. 78, no. 3, p. 279-297.

Pearce, N. J. G., and Leng, M. J., 1996, The origin of carbonatites and related rocks from the Igaliko Dyke Swarm, Gardar Province, South Greenland: Field, geochemical and C-O-Sr-Nd isotope evidence: Lithos, v. 39, no. 1-2, p. 21-40.

Peck, W. H., Clechenko, C. C., Hamilton, M. A., and Valley, J. W., 2010, Oxygen Isotopes in the Grenville and Nain Amcg Suites: Regional Aspects of the Crustal Component in Massif Anorthosites: Canadian Mineralogist, v. 48, no. 4, p. 763-786.

Petrella, L., Williams-Jones, A. E., Goutier, J., and Walsh, J., 2014, The Nature and Origin of the Rare Earth Element Mineralization in the Misery Syenitic Intrusion, Northern Quebec, Canada: Economic Geology, v. 109, no. 6, p. 1643-1666.

Polat, A., and Longstaffe, F. J., 2014, A juvenile oceanic island arc origin for the Archean (ca. 2.97 Ga) Fisken ae sset anorthosite complex, southwestern Greenland: Evidence from oxygen isotopes: Earth and Planetary Science Letters, v. 396, p. 252-266.

Quest, 2012, Quest announces that a revised resource estimate for the Strange Lake B-Zone REE deposit shows a doubling of tonnage, http://questareminerals.com/news.php, Volume 2016: Toronto, Quest Rare Minerals Ltd.

Ripley, E. M., Park, Y. R., Li, C. S., and Naldrett, A. J., 2000, Oxygen isotope studies of the Voisey's Bay Ni-Cu-Co deposit, Labrador, Canada: Economic Geology and the Bulletin of the Society of Economic Geologists, v. 95, no. 4, p. 831-844.

Robinson, J. A. C., and Wood, B. J., 1998, The depth of the spinel to garnet transition at the peridotite solidus: Earth and Planetary Science Letters, v. 164, no. 1-2, p. 277-284.

Royden, L., and Keen, C. E., 1980, Rifting Process and Thermal Evolution of the Continental-Margin of Eastern Canada Determined from Subsidence Curves: Earth and Planetary Science Letters, v. 51, no. 2, p. 343-361.

Salvi, S., and Williams-Jones, A. E., 1996, The role of hydrothermal processes in concentrating high-field strength elements in the Strange Lake peralkaline complex, northeastern Canada: Geochimica et Cosmochimica Acta, v. 60, no. 11, p. 1917-1932.

Scott, D. J., 1998, An overview of the U-Pb geochronology of the Paleoproterozoic Torngat Orogen, Northeastern Canada: Precambrian Research, v. 91, no. 1-2, p. 91-107.

Siegel, K., Vasyukova, O. V., and Williams-Jones, A. E., in review, Magmatic evolution and emplacement controls on rare metal-enrichment of the A-type peralkaline granitic Strange Lake pluton, Québec-Labrador.

Siegel, K., Williams-Jones, A. E., and Van Hinsberg, V. J., 2017, The Amphiboles of the REE-rich A-type peralkaline Strange Lake pluton - fingerprints of magma evolution Lithos, v. 288-289, p. 156-174.

Sobolev, A. V., Hofmann, A. W., Kuzmin, D. V., Yaxley, G. M., Arndt, N. T., Chung, S. L., Danyushevsky, L. V., Elliott, T., Frey, F. A., Garcia, M. O., Gurenko, A. A., Kamenetsky, V. S., Kerr, A. C., Krivolutskaya, N. A., Matvienkov, V. V., Nikogosian, I. K., Rocholl, A., Sigurdsson, I. A., Sushchevskaya, N. M., and Teklay, M., 2007, The amount of recycled crust in sources of mantle-derived melts: Science, v. 316, no. 5823, p. 412-417.

Stepanov, A. S., Hermann, J., Rubatto, D., and Rapp, R. P., 2012, Experimental study of monazite/melt partitioning with implications for the REE, Th and U geochemistry of crustal rocks: Chemical Geology, v. 300, p. 200-220.

Stevenson, R., Upton, B. G. J., and Steenfelt, A., 1997, Crust-mantle interaction in the evolution of the Ilimaussaq complex, south Greenland: Nd isotopic studies: Lithos, v. 40, no. 2-4, p. 189-202.

Sun, S. S., and McDonough, W. F., 1989, Chemical and isotopic systematics of oceanic basalts: implications for mantle composition and processes: Geological Society, London, Special Publications, v. 42, p. 313-345.

Tanaka, T., Togashi, S., Kamioka, H., Amakawa, H., Kagami, H., Hamamoto, T., Yuhara, M., Orihashi, Y., Yoneda, S., Shimizu, H., Kunimaru, T., Takahashi, K., Yanagi, T., Nakano, T., Fujimaki, H., Shinjo, R., Asahara, Y., Tanimizu, M., and Dragusanu, C., 2000, JNdi-1: a neodymium isotopic reference in consistency with LaJolla neodymium: Chemical Geology, v. 168, no. 3-4, p. 279-281.

Taylor, H. P., 1978, Oxygen and Hydrogen Isotope Studies of Plutonic Granitic Rocks: Earth and Planetary Science Letters, v. 38, no. 1, p. 177-210.

Upton, B. G. J., 1991, Gardar mantle xenoliths: Igdlutalik, South Greenland: Rapp. Gronland geol. Unders., v. 150, p. 37-43.

-, 2013, Tectono-magmatic evolution of the younger Gardar southern rift, South Greenland: Geological Survey of Denmark and Greenland (GEUS).

Upton, B. G. J., and Blundell, D. J., 1978, The Gardar Igneous Province: evidence for Proterozoic continental rifting, *in* Neumann, E. R., and Ramberg, I. B., eds., Petrology and Geochemistry of Continental Rifts, Reidel, Dordrecht, p. 163-172.

Upton, B. G. J., Emeleus, C. H., Heaman, L. M., Goodenough, K. M., and Finch, A. A., 2003, Magmatism of the mid-Proterozoic Gardar Province, South Greenland: chronology, petrogenesis and geological setting: Lithos, v. 68, no. 1-2, p. 43-65.

Van der Leeden, J., Belanger, M., Danis, D., Girard, R., and Martelain, J., 1990, Lithotectonic domains in the high-grade terrain east of the Labrador Trough (Québec) *in* Lewry, J. G., and Stauffer, M. R., eds., The Early Proterozoic Trans-Hudson Orogen of North America, Volume Special Paper 37, Geological Association of Canada, p. 371-386.

Van Kranendonk, M. J., Stonge, M. R., and Henderson, J. R., 1993, Paleoproterozoic Tectonic Assembly of Northeast Laurentia through Multiple Indentations: Precambrian Research, v. 63, no. 3-4, p. 325-347.

Wardle, R. J., James, D. T., Scott, D. J., and Hall, J., 2002, The southeastern Churchill Province: synthesis of a Paleoproterozoic transpressional orogen: Canadian Journal of Earth Sciences, v. 39, no. 5, p. 639-663.

Woolley, A. R., 1987, Lithosphere Metasomatism and the Petrogenesis of the Chilwa Province of Alkaline Igneous Rocks and Carbonatites, Malawi: Journal of African Earth Sciences, v. 6, no. 6, p. 891-898.

Zhao, Z. F., and Zheng, Y. F., 2003, Calculation of oxygen isotope fractionation in magmatic rocks: Chemical Geology, v. 193, no. 1-2, p. 59-80.

Zhao, Z. H., Xiong, X. L., Hen, X. D., Wang, Y. X., Qiang, W., Bao, Z. W., and Jahn, B., 2002, Controls on the REE tetrad effect in granites: Evidence from the Qianlishan and Baerzhe granites, China: Geochemical Journal, v. 36, no. 6, p. 527-543.

CHAPTER 5 - CONCLUSIONS

5.1 GENERAL CONCLUSIONS

The detailed mapping, bulk rock, mineral and isotope study of the unaltered rocks of the REE-, Zr- and Nb-rich peralkaline A-type granitic Strange Lake pluton revealed a number of new discoveries. These are summarized in the following paragraphs.

This study provides new insights into the sources of the magma, the emplacement processes and magmatic evolution which resulted in the extraordinary enrichment in the REE, Zr and Nb in the Strange Lake pluton. Evidence was found that the pluton was emplaced as a ring dike accompanied by stoping at about 3 km depth. Three magma batches were identified, two of hypersolvus granite (south and north), and one of transsolvus granite, which all evolved in a common magma chamber. The hypersolvus granite solidified at temperatures between 660-700°C, whereas the transsolvus granite may have been cooler. The evolution of the hypersolvus magma is interpreted to have been driven by perthitic alkali feldspar fractionation, accompanied by the crystallization of HFSE-rich phases (zircon, monazite-(Ce), pyrochlore group minerals), and the early separation of a LREE-rich fluoride melt from the silicate melt. An alkali feldspar-rich (perthitic alkali feldspar) crystal-mush was emplaced first, forming the southern hypersolvus granite. This was followed by emplacement of the more evolved northern hypersolvus granite. Owing to gravity settling, the latter contained an elevated proportion of heavier HFSE-minerals (frequently) attached to immiscible LREE-fluoride melt globules. After emplacement, both hypersolvus granite melts were quenched on the wall rock and evolved further in situ, crystallizing more perthitic alkali feldspar, as well as quartz, fluorite and arfvedsonite. The occurrence of late alkali zircono- and titano-silicates, which crystallized at the expense of primary zircon and ilmenite, marked the transition from the miaskitic to the agpaitic stage.

Coarse oikocrystic and pegmatitic textured rocks observed in both the southern and northern facies are interpreted to represent volatile-rich pockets of evolved residual hypersolvus granite melts.

The massive fractionation of perthitic alkali feldspar led to the accumulation of OH^- in the melt, which triggered the crystallization of arfvedsonite phenocrysts in the transsolvus granite. This, in turn, caused an increase in F^- in the melt, which resulted in the transition from hypersolvus towards subsolvus conditions. High alkali to alumina proportions led to the miaskitic to an agpaitic transition, which significantly increased the solubility of the HFSE. A crystal mush of alkali feldspar (perthitic alkali feldspar and microcline), and arfvedsonite, LREE-fluoride melt globules and a melt with high proportions of dissolved alkali- or F-REE-, Zr- and Nb-complexes, was emplaced in the upper crust in a single large low viscosity (10^4–10^5 Pa·s) surge. The feldspar-rich magma that developed due to gravity settling, was dragged into the conduit first, then quenched and assimilated by the rest of the transsolvus magma (enclaves). Upon emplacement of the magma, arfvedsonite crystals settled and formed cumulates or flow differentiation textures, and continued to crystallize together with microcline, albite and quartz. Niobium, Zr and Ti crystallized as late pyrochlore group minerals, zircono- and titano-silicate minerals, whereas the REE crystallized as gagarinite-(Ce)-fluorite and fluorbritholite-(Ce)-fluorite assemblages from immiscible fluoride-melt drops. A large proportion of these fluoride-melt drops accumulated in the volatile-rich residual melts and ultimately formed the F-REE-rich cores of the highly mineralized pegmatites in the altered parts of the transsolvus granite.

Evidence was presented that the major and trace-element compositions of amphibole in the unaltered Strange Lake granites reflect the magmatic evolution of the pluton. Compositions vary from sodium-calcium amphibole (ferro-ferri-katophorite) in the least evolved southern hypersolvus granite to sodium amphibole ((fluoro)-arfvedsonite) and Li-rich amphibole (ferro-ferri-(fluoro)-leakeite) in the other, more evolved granites. The increasing Fe^{3+} concentration in amphibole with evolution was a result of crystal chemical effects (Na/Ca proportion), increasing fO_2 through degassing, and an increase in OH^- and F^- concentrations in case of the transsolvus granite. All amphiboles are enriched in Nb, Zr and Hf and the HREE compared to the bulk rock, reflecting a combination of magmatic compositional and crystal chemical effects. Variations in Ti-concentrations indicate the presence of Na-Ti-silicates, such as aenigmatite, astrophyllite and narsarsukite, which replaced the amphibole to variable extents. In the hypersolvus granite, amphibole crystallized late from a small proportion of residual magma resulting in high incompatible element concentrations, whereas in the transsolvus granite, it formed early resulting in much lower concentrations of the HFSE, despite the overall more evolved nature of the magma. The LREE were relatively incompatible ($D_{arf\text{-}bulk} < 0.01$) and preferentially hosted by the larger B-site, which also accommodated Ca. The HREE were preferred by the C-site and increase in compatibility ($D_{arf/bulk} > 0.1$) with increasing atomic number and decreasing ionic radius, culminating in the compatible behavior of La and Lu and ($D_{arf/bulk} > 1.0$).Variations in the LREE concentrations of the amphiboles were controlled by the presence of primary LREE minerals and the exsolution of a LREE-rich fluoride melt, whereas the uptake of the HREE was controlled by their relative compatibility in the amphibole. The amphibole hosts a significant proportion of the bulk HREE content of the Strange Lake granites and released HREE through hydrothermal alteration to a late-stage fluid, which contributed to the extreme and unusual HREE mineralization in the pegmatites.

The Nd- and O-isotope study of the Strange Lake samples provided new insights into possible magma sources and the origin of the HFSE. For example, it showed that the isotopic signatures of the Strange Lake samples can be interpreted as resulting from a combination of crustal assimilation and in-situ Sm-Nd fractionation, involving the crystallization of primary LREE-minerals and arfvedsonite and later hydrothermal remobilization of the REE. Reports of mafic rocks with enriched isotope signatures of the Nain Plutonic Suite (Amelin et al. 2000; Carlson et al. 1993), suggest that the Strange Lake magma was derived from a locally metasomatized mantle, enriched in incompatible elements. Fractional crystallization of this magma and accompanying assimilation of 5-15 % of underlying Archean paragneiss yielded the εNd and $\delta^{18}O$ isotopic signature of the Strange Lake granites. The genesis of REE-mineralized A-type granites and other silica-saturated members of the Nain Plutonic Suite likely resulted from a combination of tectonic events, such as the 1.84-1.82 Ga subduction of the Superior Province foreland, which metasomatized the subcontinental mantle. This subduction was followed by continent-continent collision and the New Québec orogeny, accompanied by calc-alkaline magmatism. During the waning stages of the Elsonian event, rifting of the Nain Province between 1.46 and 1.24 Ga produced alkaline melts, which were generated by low degrees of partial melting. The alkaline Gardar Province in SW-Greenland is in nature and timing, similar to the Nain Plutonic Suite, but metasomatism of the Gardar mantle was related to the 1.85-1.80 Ga Ketilidian subduction, whereas the mantle beneath the Core Zone was influenced by the 1.84-1.82 Ga Superior subduction. Moreover, the main contaminant of the Gardar suites was the Paleoproterozoic calc-alkaline Julianehåb batholith, whereas for the Nain Plutonic Suite it was a highly heterogeneous mixture of Archean and Paleoproterozoic crust. A link between the two provinces is indicated by the extensive supra-regional dike swarms (Nain-, Harp-, Brown-dikes) as well as the shared Gardar-Voisey’s bay fault zone that led to the emplacement of both the Nain and Gardar magmas in the upper crust.

5.2 CONTRIBUTIONS TO THE SCIENTIFIC COMMUNITY

This study of the unaltered rocks of the REE-rich Strange Lake peralkaline granite presents a number of new findings, which contribute to the understanding of REE-mineralized A-type granite genesis. In Chapter 2, the internal magmatic processes were identified which, together, can lead to significant pre-enrichment in the HFSE (REE, Zr, Nb) in a peralkaline granite, i.e., perthitic alkali feldspar fractionation, density segregation of heavier HFSE-minerals and the unmixing of a LREE-fluoride melt from the silicate melt. The detailed study of the amphibole chemistry showed how the mafic phases in these granites are capable of carrying significant amounts of the HREE, which, during hydrothermal alteration, can contribute to their hyper-enrichment in the late stage melts and fluids. Finally, with the help of Nd- and O-isotopes, the study identified a sequence of plate tectonic and evolutionary processes that favored the generation of highly REE-enriched alkaline melts. These processes are consistent with the tectonic framework that produced the alkaline magmatism of the Mesoproterozoic Nain and Gardar Provinces, and help constrain genetic models for REE-mineralized intrusive bodies.

REFERENCES

Amelin, Y., Li, C. S., Valeyev, O., and Naldrett, A. J., 2000, Nd-Pb-Sr isotope systematics of crustal assimilation in the Voisey's Bay and Mushuau intrusions, Labrador, Canada: Economic Geology and the Bulletin of the Society of Economic Geologists, v. 95, no. 4, p. 815-830.

Emslie, R. F., Hamilton, M. A., and Theriault, R. J., 1994, Petrogenesis of a Midproterozoic anorthosite-mangerite-charnockite-granite (AMCG) complex - isotopic and chemical evidence from the Nain Plutonic Suite: Journal of Geology, v. 102, no. 5, p. 539-558.

Kerr, A., and Hamilton, M. A., 2014, Rare-earth element (REE) mineralization in the Mistastin Lake and Smallwood Reservoir areas, Labrador: field relationships and preliminary U-Pb zircon ages from host granitoid rocks Current Research (1990) Newfoundland Department of Mines and Energy, Geological Survey v. 1, p. 45-62.

Peck, W. H., Clechenko, C. C., Hamilton, M. A., and Valley, J. W., 2010, Oxygen Isotopes in the Grenville and Nain Amcg Suites: Regional Aspects of the Crustal Component in Massif Anorthosites: Canadian Mineralogist, v. 48, no. 4, p. 763-786.

CHAPTER 6 - APPENDICES

APPENDIX 1: BULK ROCK DATA

Table 6-1: Bulk rock data of least altered Strange Lake granites

Unit	Hypersolvus granite south – fine grained								
Sample	10013	10017	10032	204768	204771	204772	204774		
Geologist*	1	1	1	2	2	2	2		
Texture**	fgr, dk gr	fgr, eg	fgr, eg	fgr, eg	mgr, eg	mgr, eg	fgr, eg		
Easting	430673	429588	429956	429691	428973	428980	429586		
Northing	6238868	6238128	6238511	6238177	6238427	6238425	6238138	Mdn	MAD
(wt. %)									
SiO_2	70.02	67.64	69.13	69.07	70.42	69.38	67.63	69.04	0.89
Al_2O_3	11.52	11.84	12.23	12.04	11.58	12.15	11.79	11.88	0.26
Fe_2O_3	4.90	5.76	5.26	5.90	6.08	6.21	6.36	5.78	0.31
MnO	0.09	0.11	0.07	0.12	0.10	0.11	0.12	0.10	0.01
MgO	0.02	0.05	0.03	0.06	0.04	0.04	0.06	0.04	0.01
CaO	0.33	0.99	0.65	0.89	0.55	0.74	0.95	0.73	0.19
Na_2O	4.86	5.08	5.06	4.63	4.89	4.82	5.08	4.92	0.17
K_2O	5.17	4.96	5.31	4.69	4.65	4.75	4.96	4.93	0.21
TiO_2	0.22	0.33	0.21	0.32	0.31	0.24	0.34	0.28	0.03
Nb_2O_5	0.03	0.04	0.01	0.04	0.02	0.03	0.04	0.03	0.01
P_2O_5	0.02	0.03	<0.01	0.03	0.03	0.03	0.03	0.02	0.00
F	0.31	0.44	0.42	0.44	0.45	0.52	0.51	0.44	0.02
TREO	0.15	0.18	0.11	0.18	0.13	0.24	0.19	0.17	0.03
LREO	0.10	0.12	0.06	0.12	0.09	0.19	0.14	0.12	0.02
HREO+Y	0.04	0.05	0.04	0.06	0.04	0.05	0.05	0.05	0.00
Total	97.78	97.62	98.59	98.59	99.38	99.50	98.25	98.53	0.80
LOI	1.17	0.46	0.33	0.69	0.84	0.75	0.80	0.72	0.09
AI	1.18	1.16	1.15	1.05	1.13	1.08	1.16	1.13	0.02
Be *(ppm)*	23	34	14	54	36	42	33	36	8
Zn	320	250	210	270	290	330	360	285	40
Ga	52	43	45	42	49	46	42	45	3
Ge	3	4	3	2	2	3	3	3	0
As	7	9	11	10	25	6	6	11	2
Rb	588	449	434	417	399	379	422	417	23
Sr	9	22	12	25	14	17	20	18	5
Y	247	281	245	318	230	245	275	266	17
Zr	2454	2784	1122	2415	1620	3121	3417	2413	667
Sn	52	35	31	70	113	56	42	58	17
Cs	1	3	2	7	12	9	3	6	3
Ba	42	124	39	63	43	55	134	76	13
La	203	213	108	231	168	400	246	228	33
Ce	397	477	235	470	330	742	530	464	73
Pr	42	56	28	56	40	91	66	56	14
Nd	150	205	106	186	131	289	228	191	42
Sm	32	45	25	38	28	49	48	39	10
Eu	2	3	2	2	2	3	3	2	0
Gd	29	37	24	34	26	38	39	33	5
Tb	6	8	5	7	5	7	7	6	1
Dy	37	53	33	49	35	43	49	44	7
Ho	8	12	7	11	8	9	11	10	2
Er	25	38	23	39	28	32	38	33	6
Tm	4	6	3	6	5	5	6	5	1
Yb	26	41	22	41	34	38	42	36	3
Lu	4	6	3	6	6	6	7	6	0
Hf	73	71	33	87	56	84	82	69	12
Ta	13	15	7	22	13	14	16	14	1
Tl	3	2	3	2	5	2	2	3	0
Pb	107	82	43	124	115	119	80	94	17
Th	45	51	22	86	42	73	53	54	9
U	7	14	4	12	8	9	14	10	3

*Geologist: 1 = Karin Siegel and Angela Buchanan (2012, 2013); 2 = Robert Fritscher, Alexander Brosseau-Liard (2010, 2011); 3 = Alexander Gysi (2011, 2012)

**Texture: fgr = fine grained, mgr = medium grained, cgr = coarse grained, eg = equigranular, pp = porphyritic, dk gr = dark grey, peg = pegmatitic, oik = oikiocrystic, mgr+en = medium grained, enclave bearing

LOI = loss of ignition; AI = agpaitic index (molar Na+K / Al); Mdn = median; MAD = median absolute deviation

Table 6-1: Bulk rock data of least altered Strange Lake granites (continued)

Unit	Hypersolvus granite south – oikocrystic / pegmatitic samples									
Sample	10018	10031	10214	10218	204766	204769	204770	204773		
Geologist*	1	1	1	1	2	2	2	2		
Texture**	oik	mgr	mgr	peg	oik	mgr	mgr	mgr		
Easting	429189	429956	428158	429970	430000	429202	428865	430019		
Northing	6238017	6238511	6239260	6238500	6238503	6238036	6238341	6238422	Mdn	MAD
(wt. %)										
SiO_2	70.91	70.35	71.51	70.78	69.77	69.80	70.36	72.31	70.57	0.56
Al_2O_3	10.52	10.74	10.79	10.60	10.19	10.53	10.73	10.01	10.57	0.17
Fe_2O_3	5.89	6.90	6.44	7.47	7.98	6.92	6.53	5.56	6.72	0.52
MnO	0.10	0.11	0.11	0.11	0.12	0.13	0.13	0.10	0.11	0.01
MgO	0.02	-	0.03	-	0.01	0.02	0.04	0.02	0.02	0.01
CaO	0.32	0.16	0.55	0.36	0.36	0.54	0.60	0.38	0.37	0.11
Na_2O	4.90	5.14	5.08	5.17	5.39	5.15	5.08	4.34	5.11	0.05
K_2O	4.42	4.71	4.56	4.44	4.58	4.11	4.52	3.95	4.48	0.09
TiO_2	0.30	0.22	0.20	0.18	0.19	0.25	0.32	0.19	0.21	0.03
Nb_2O_5	0.05	0.06	0.04	0.03	0.03	0.06	0.06	0.05	0.05	0.01
P_2O_5	0.02	0.02	0.02	<0.01	0.01	0.03	0.02	0.02	0.02	0.00
F	0.32	0.25	0.37	0.36	0.50	0.53	0.50	0.30	0.37	0.09
TREO	0.18	0.21	0.14	0.17	0.18	0.30	0.20	0.24	0.19	0.02
LREO	0.11	0.16	0.09	0.12	0.13	0.18	0.15	0.12	0.13	0.02
HREO+Y	0.07	0.06	0.05	0.05	0.05	0.12	0.06	0.11	0.06	0.01
Total	98.12	99.08	99.98	99.84	99.50	98.67	99.30	97.70	99.19	0.59
LOI	0.40	-0.04	0.33	0.34	0.73	0.89	0.61	0.54	0.47	0.14
AI	1.22	1.26	1.23	1.26	1.36	1.23	1.23	1.14	1.23	0.02
Be *(ppm)*	25	77	20	40	39	27	48	63	40	14
Zn	300	540	450	560	580	520	620	550	545	30
Ga	47	58	50	55	52	52	47	51	52	3
Ge	4	5	3	4	4	4	3	3	4	1
As	7	12	12	6	5	12	<5	9	8	4
Rb	451	430	495	410	383	498	441	400	436	31
Sr	8	9	36	15	15	12	16	60	15	5
Y	373	288	273	247	267	685	298	610	293	36
Zr	3013	2663	2076	2872	3478	1951	1682	2345	2504	469
Sn	73	101	59	52	64	113	76	98	75	19
Cs	2	4	2	2	2	5	3	2	2	0
Ba	44	31	43	23	19	47	65	43	43	8
La	200	277	171	203	224	325	309	217	221	35
Ce	425	618	361	466	502	646	568	467	485	72
Pr	48	66	40	55	63	82	68	57	60	7
Nd	169	238	136	204	214	278	210	185	207	27
Sm	38	56	30	50	52	74	44	52	51	6
Eu	2	3	2	3	3	4	2	3	3	0
Gd	36	50	27	42	46	76	39	57	44	7
Tb	8	9	6	7	8	16	8	14	8	1
Dy	57	58	41	43	46	109	49	103	53	8
Ho	13	12	9	8	9	24	11	24	11	2
Er	43	38	30	25	28	74	35	79	36	7
Tm	7	6	5	4	4	11	6	12	6	1
Yb	50	43	37	28	31	69	40	79	42	9
Lu	7	7	5	4	5	10	7	11	7	1
Hf	75	69	55	79	100	53	45	65	67	12
Ta	18	22	14	15	15	26	31	22	20	4
Tl	2	4	4	3	2	3	2	2	2	0
Pb	143	194	99	84	112	217	212	243	169	53
Th	79	81	53	37	45	124	60	134	69	20
U	13	16	10	10	12	15	17	19	14	3

Table 6-1: Bulk rock data of least altered Strange Lake granites (continued)

Unit	Hypersolvus granite north													
Sample	10010	10011	10040	10203	10205	204746	204753	204754	204756	204791	204792	204801		
Geologist*	1	1	1	1	1	2	2	2	2	2	2	2		
Texture**	fgr, eg	fgr, eg	fgr, eg	fgr, eg	fgr, eg	fgr, eg	fgr, eg	fgr, eg	fgr, eg	fgr, eg	fgr, eg	fgr, eg		
Easting	430846	430694	429974	430600	429040	430697	430693	430417	430874	430030	429974	430043		
Northing	6239454	6239425	6240270	6239514	6240436	6239427	6239390	6239478	6239146	6240292	6240273	6240322	Mdn	MAD
(wt. %)														
SiO_2	70.32	70.11	71.16	71.38	70.90	70.78	70.67	70.31	70.68	69.81	70.22	70.70	70.68	0.36
Al_2O_3	11.57	11.75	11.97	11.72	11.53	10.87	11.73	11.94	11.60	12.05	11.98	12.72	11.74	0.21
Fe_2O_3	4.98	4.80	4.82	4.74	5.09	5.81	4.90	4.96	4.89	4.84	4.89	4.65	4.89	0.08
MnO	0.13	0.12	0.10	0.10	0.12	0.14	0.10	0.11	0.10	0.10	0.10	0.10	0.10	0.01
MgO	0.03	0.04	0.05	0.03	0.14	0.05	0.05	0.06	0.04	0.06	0.06	0.05	0.05	0.01
CaO	0.56	0.61	0.61	0.55	0.90	0.58	0.59	0.50	0.55	0.44	0.55	0.61	0.57	0.03
Na_2O	5.62	5.21	5.00	5.12	4.94	4.99	5.00	5.06	5.19	5.28	5.04	5.50	5.09	0.10
K_2O	4.26	4.64	4.74	4.64	4.74	4.51	5.26	4.82	4.86	5.08	4.76	4.51	4.74	0.11
TiO_2	0.21	0.34	0.27	0.27	0.35	0.40	0.27	0.31	0.28	0.27	0.27	0.27	0.27	0.01
Nb_2O_5	0.08	0.06	0.05	0.06	0.05	0.08	0.06	0.06	0.06	0.06	0.05	0.03	0.06	0.00
P_2O_5	0.01	0.02	0.02	0.02	0.03	0.06	0.01	<0.01	0.01	0.02	0.02	0.02	0.02	0.01
F	0.42	0.46	0.41	0.38	0.46	0.58	0.51	0.46	0.41	0.41	0.48	0.45	0.46	0.04
TREO	0.28	0.33	0.21	0.23	0.29	0.48	0.25	0.24	0.20	0.21	0.24	0.17	0.24	0.03
LREO	0.18	0.21	0.14	0.17	0.19	0.36	0.17	0.15	0.13	0.15	0.16	0.11	0.16	0.02
HREO+Y	0.09	0.12	0.07	0.07	0.10	0.11	0.07	0.09	0.07	0.06	0.08	0.06	0.08	0.01
Total	97.77	97.70	98.80	98.64	98.79	98.28	98.64	98.13	98.26	98.01	97.94	99.16	99.14	0.37
LOI	0.26	0.57	0.49	1.53	0.63	0.99	0.87	0.84	0.69	0.64	0.71	0.75	0.70	0.14
AI	1.20	1.16	1.12	1.15	1.15	1.20	1.19	1.13	1.19	1.18	1.12	1.10	1.15	0.03
Be *(ppm)*	69	165	47	43	71	79	41	50	65	44	52	53	53	11
Zn	640	490	300	530	510	680	390	480	410	450	450	370	465	60
Ga	53	48	40	44	45	51	45	44	44	44	44	43	44	1
Ge	4	4	4	3	4	5	3	3	3	3	3	3	3	0
As	20	14	12	18	7	13	11	10	5	8	9	7	11	3
Rb	687	572	454	811	610	478	561	491	458	524	520	515	522	47
Sr	31	24	17	30	53	28	31	16	13	17	15	15	21	7
Y	530	619	395	370	521	652	371	496	368	326	388	309	392	74
Zr	3975	2606	3524	3831	4929	3334	3576	3736	3385	3920	3890	1511	3656	268
Sn	90	99	69	88	79	133	129	83	103	79	101	102	95	10
Cs	3	12	6	8	4	9	4	7	4	7	7	10	7	2
Ba	78	119	73	60	136	122	110	85	118	82	73	84	85	18
La	311	387	252	321	371	781	355	282	254	285	299	207	305	51
Ce	688	813	540	654	757	1480	697	586	527	573	603	422	629	79
Pr	83	93	62	73	82	151	73	63	57	70	76	52	73	10
Nd	305	322	221	246	281	454	233	211	194	227	258	182	240	35
Sm	75	73	49	46	58	80	49	48	43	50	60	43	49	6
Eu	5	5	3	3	4	4	3	3	3	3	3	3	3	0
Gd	72	71	45	37	54	63	40	46	40	45	54	42	45	7
Tb	14	15	9	8	13	13	9	10	8	9	11	9	10	1
Dy	90	106	63	56	84	89	61	77	57	61	75	58	69	12
Ho	18	23	14	13	20	20	14	18	13	14	17	13	15	2
Er	50	74	48	45	59	65	49	58	44	47	56	40	50	6
Tm	7	12	8	8	10	10	9	9	8	8	9	6	8	1
Yb	42	77	53	58	63	70	61	57	54	57	62	43	57	4
Lu	6	11	8	8	9	10	9	8	8	9	9	7	9	1
Hf	116	75	83	104	107	88	129	82	97	98	135	70	97	15
Ta	38	31	20	27	23	50	30	36	27	29	26	21	28	4
Tl	3	4	4	5	4	4	3	4	2	3	3	4	4	0
Pb	197	153	97	160	175	198	217	120	100	117	117	70	137	38
Th	62	127	80	78	84	101	121	71	129	77	124	91	88	15
U	23	16	15	18	19	21	22	21	17	20	19	7	19	2

Table 6-1: Bulk rock data of least altered Strange Lake granites (continued)

Unit	Transsolvus granite (1/2)												
Sample	10009	10020	10022	10023	10039	10046	10202	10209	10212	122705	122709	122712	204710
Geologist*	1	1	1	1	1	3	1	1	1	3	3	3	2
Texture**	mgr + en	mgr + en	fgr	mgr	mgr + en	fgr + en	mgr + en	mgr	mgr + en	mgr + en	mgr + en	mgr + en	mgr + en
Easting	430951	428103	430633	430639	430378	428068	430672	430895	430325	428090	428090	428090	428042
Northing	6239477	6239389	6240095	6239831	6239106	6239759	6239844	6239473	6238971	6239129	6239129	6239129	6239493
(wt. %)													
SiO_2	69.89	71.82	69.90	71.25	71.61	72.98	68.93	69.74	71.60	72.87	71.60	71.58	71.79
Al_2O_3	10.85	10.43	9.81	10.45	10.82	10.03	9.56	10.50	10.26	10.42	9.83	9.77	9.70
Fe_2O_3	5.57	6.07	5.07	4.98	5.53	5.82	6.74	4.97	6.50	6.02	7.32	6.49	7.07
MnO	0.12	0.09	0.12	0.12	0.12	0.10	0.14	0.12	0.10	0.09	0.12	0.11	0.11
MgO	0.03	0.02	0.03	0.06	0.03	0.01	0.04	0.04	0.03	0.03	0.03	0.02	0.04
CaO	0.52	0.25	0.47	0.66	0.55	0.13	0.64	0.94	0.22	0.25	0.29	0.25	0.24
Na_2O	6.03	4.73	5.42	5.20	6.56	4.79	5.15	4.91	5.81	5.68	5.79	6.99	5.36
K_2O	3.58	4.88	4.32	4.56	2.88	4.17	4.23	4.47	2.94	3.55	3.25	1.49	3.61
TiO_2	0.31	0.14	0.40	0.29	0.21	0.16	0.31	0.30	0.20	0.16	0.20	0.22	0.20
Nb_2O_5	0.08	0.02	0.08	0.09	0.14	0.04	0.09	0.10	0.04	0.03	0.02	0.04	0.04
P_2O_5	<0.01	<0.01	0.03	0.02	<0.01	<0.01	0.03	0.02	0.01	<0.01	<0.01	<0.01	<0.01
F	0.52	0.41	0.45	0.43	0.49	0.29	0.44	0.52	0.36	0.48	0.50	0.43	0.54
TREO	0.45	0.32	0.46	0.50	0.41	0.33	0.53	0.53	0.33	0.62	0.35	0.51	0.50
LREO	0.31	0.27	0.33	0.34	0.27	0.27	0.38	0.32	0.28	0.54	0.29	0.41	0.43
HREO+Y	0.14	0.04	0.13	0.16	0.14	0.06	0.15	0.22	0.05	0.08	0.06	0.09	0.07
Total	96.97	98.45	95.66	97.67	98.45	98.23	95.86	96.11	97.70	99.10	98.45	96.96	98.16
LOI	0.61	0.11	0.40	0.41	0.29	0.62	0.50	0.57	0.32	0.84	0.69	0.81	0.87
AI	1.27	1.25	1.39	1.29	1.29	1.24	1.37	1.23	1.24	1.27	1.33	1.34	1.31
Be *(ppm)*	64	27	72	105	96	47	52	59	30	29	25	20	38
Zn	540	330	490	550	520	490	670	770	480	440	490	500	640
Ga	57	62	52	61	60	61	57	51	63	61	56	62	60
Ge	5	5	5	5	5	6	5	4	4	5	4	4	4
As	9	7	8	9	8	14	8	9	12	<5	12	23	13
Rb	661	654	739	801	467	574	739	852	358	436	380	164	491
Sr	29	9	15	36	13	26	56	52	13	18	14	9	16
Y	767	255	681	872	773	324	842	1187	280	431	330	524	409
Zr	7458	1785	9375	5589	4971	3184	6665	7032	3075	2004	3060	4358	3755
Sn	143	41	144	139	103	73	181	172	64	38	43	53	96
Cs	2	1	4	3	4	5	3	3	1	1	0	0	1
Ba	43	23	61	71	45	55	46	69	28	29	22	14	15
La	568	560	628	632	493	555	743	590	604	1120	594	826	963
Ce	1180	1010	1290	1290	1010	1020	1450	1210	1070	2000	1060	1540	1570
Pr	138	116	145	149	120	115	161	134	117	226	123	176	181
Nd	498	442	507	550	438	420	570	479	440	874	477	669	670
Sm	112	79	103	123	100	77	124	120	76	156	92	128	118
Eu	7	4	6	7	6	4	6	7	4	7	4	7	5
Gd	104	62	91	114	95	64	109	121	57	122	76	108	90
Tb	20	8	18	23	18	9	23	30	8	16	10	15	13
Dy	129	42	113	148	116	55	137	200	43	83	58	95	71
Ho	27	7	24	31	25	11	29	45	8	14	10	19	14
Er	86	20	79	94	75	35	88	137	25	35	27	53	42
Tm	14	3	13	15	11	5	15	21	4	5	4	8	6
Yb	90	19	92	94	73	34	97	123	30	28	23	49	40
Lu	13	3	14	14	10	5	13	16	5	4	4	8	6
Hf	218	55	269	172	136	87	178	195	86	60	92	132	103
Ta	33	9	41	39	43	16	40	45	17	11	11	22	20
Tl	3	2	3	4	2	3	5	3	2	2	2	1	2
Pb	201	48	380	350	206	129	338	275	86	60	129	146	135
Th	139	28	103	126	98	49	124	202	45	38	20	56	72
U	23	4	29	25	21	13	26	32	9	7	7	12	11

Table 6-1: Bulk rock data of least altered Strange Lake granites (continued)

Unit	Transsolvus granite (2/2)											
Sample	204712	204713	204715	204717	204720	204722	204743	204751	204752	204760	204805		
Geologist*	2	2	2	2	2	2	2	2	2	2	2		
Texture**	mgr + en	mgr + en	mgr	mgr	mgr + en	cgr, peg	fgr + en	mgr + en	mgr + en	mgr + en	mgr + en		
Easting	428041	428053	428055	428096	428090	428101	430939	430663	430894	430201	429365		
Northing	6239399	6239399	6239378	6239782	6239382	6239128	6239417	6239847	6239477	6239058	6239682	Mdn	MAD
(wt. %)													
SiO_2	70.85	70.75	71.33	71.70	69.73	70.59	70.66	71.30	69.51	68.97	71.56	71.28	0.53
Al_2O_3	10.43	9.34	9.70	9.86	9.79	10.27	10.90	9.94	10.44	10.49	10.64	10.27	0.39
Fe_2O_3	5.68	5.73	6.29	5.95	7.22	6.01	5.26	5.62	5.41	6.40	6.46	5.98	0.47
MnO	0.11	0.12	0.11	0.10	0.12	0.11	0.12	0.12	0.13	0.14	0.10	0.12	0.01
MgO	0.03	0.03	0.02	0.08	0.02	0.02	0.04	0.13	0.05	0.04	0.03	0.03	0.01
CaO	0.57	0.43	0.31	0.58	0.32	0.41	0.56	0.70	1.13	0.66	0.37	0.45	0.18
Na_2O	4.03	4.71	5.06	4.33	4.81	5.09	5.06	4.51	4.82	4.66	5.40	5.08	0.35
K_2O	5.97	4.36	4.02	4.52	4.99	4.31	4.62	4.51	4.62	5.44	4.31	4.32	0.31
TiO_2	0.19	0.21	0.19	0.15	0.18	0.21	0.30	0.25	0.45	0.21	0.16	0.21	0.05
Nb_2O_5	0.05	0.08	0.05	0.04	0.03	0.05	0.08	0.08	0.10	0.07	0.03	0.05	0.02
P_2O_5	0.01	0.02	<0.01	<0.01	0.02	<0.01	0.02	0.04	0.02	0.01	<0.01	0.02	0.01
F	0.53	0.47	0.47	0.58	0.71	0.67	0.54	0.57	0.72	0.61	0.52	0.51	0.06
TREO	0.42	0.54	0.56	0.44	0.64	0.72	0.38	0.54	0.46	0.50	0.41	0.48	0.06
LREO	0.31	0.35	0.45	0.35	0.55	0.59	0.27	0.37	0.31	0.33	0.33	0.33	0.04
HREO+Y	0.11	0.19	0.11	0.09	0.09	0.12	0.11	0.18	0.15	0.17	0.08	0.11	0.04
Total	97.91	95.79	97.08	97.30	97.22	97.07	97.61	97.20	96.68	97.09	99.06	99.22	0.61
LOI	0.73	0.85	0.79	0.95	0.70	1.03	0.84	0.92	1.14	0.90	0.65	0.72	0.15
AI	1.26	1.33	1.31	1.22	1.36	1.27	1.22	1.24	1.24	1.29	1.27	1.27	0.03
Be *(ppm)*	76	108	54	26	33	54	70	102	116	59	36	54	22
Zn	680	830	650	580	580	650	690	640	720	790	590	585	90
Ga	57	59	61	60	66	69	55	54	50	52	54	60	3
Ge	4	4	4	4	6	6	5	5	4	4	4	5	1
As	10	10	14	17	15	18	12	14	12	19	9	12	3
Rb	1250	860	683	701	647	646	733	717	773	962	595	672	99
Sr	23	31	19	42	13	38	17	26	64	17	24	21	8
Y	625	1027	606	500	517	702	591	982	850	990	472	616	196
Zr	5311	7733	4997	3565	2841	3643	7188	5830	8086	7533	2597	4984	1917
Sn	107	182	97	76	72	109	146	164	227	132	72	105	39
Cs	3	3	1	1	2	1	2	2	5	3	1	2	1
Ba	28	37	25	27	37	42	64	57	85	48	46	43	15
La	613	700	945	755	1140	1220	512	723	580	591	716	630	81
Ce	1120	1290	1640	1250	2030	2210	1050	1380	1200	1180	1220	1235	170
Pr	134	153	194	148	240	258	116	155	138	159	154	149	20
Nd	498	557	720	555	880	929	399	547	473	570	489	527	52
Sm	109	131	141	105	159	179	92	127	110	136	83	115	16
Eu	6	7	7	5	8	8	5	7	6	7	4	6	1
Gd	96	124	115	86	122	139	78	114	95	132	69	100	18
Tb	16	26	18	13	17	21	16	23	19	24	11	17	4
Dy	99	172	104	81	83	115	102	153	129	151	66	103	29
Ho	20	37	20	17	15	22	22	33	28	31	14	21	7
Er	62	118	61	51	39	66	68	105	88	89	41	64	24
Tm	9	18	9	7	5	9	11	16	14	12	6	9	4
Yb	56	103	54	45	29	60	74	100	96	76	37	58	29
Lu	8	15	8	7	4	8	11	14	15	10	5	8	4
Hf	146	210	136	96	91	105	230	170	233	217	80	136	47
Ta	24	40	22	18	13	26	46	39	53	34	12	25	13
Tl	4	3	2	2	2	2	3	3	3	4	2	2	1
Pb	171	347	187	149	115	186	295	343	395	248	113	187	73
Th	80	205	82	66	43	86	122	144	131	126	49	84	40
U	18	30	17	13	9	17	32	27	32	24	9	17	8

Table 6-1: Bulk rock data of least altered Strange Lake granites (continued)

Unit	Enclaves													
Sample	10035	10052	10213	122714	204711	10039EN	204712EN	204742EN	ALT11003-1	AW12001-3	AW12003-1	AW12003-2		
Geologist*	1	3	1	3	2	1	1	1	1	1	1	1		
Texture**	fg, dk gr	fg, dk gr	fg, dk gr	fg, dk gr	fg, dk gr	fg, dk gr	fg, dk gr	fg, dk gr	fg, dk gr	fg, dk gr	fg, dk gr	fg, dk gr		
Easting	430321	430325	430325	428090	428056	430378	428041	no data	429799	428797	428684	428684		
Northing	6238972	6238974	6238971	6239129	6239458	6239106	6239399	no data	6240625	6240868	6240674	6240674	Mdn	MAD
(wt. %)														
SiO_2	69.02	68.79	69.13	67.71	69.38	68.22	69.33	70.66	71.30	69.63	70.66	69.99	69.36	0.60
Al_2O_3	11.80	12.30	12.08	12.52	12.15	12.55	11.51	11.55	12.14	11.65	11.78	11.86	11.97	0.25
Fe_2O_3	5.58	4.92	4.98	4.73	4.99	5.53	5.04	5.17	5.05	5.05	4.79	5.12	5.05	0.10
MnO	0.09	0.08	0.08	0.08	0.08	0.14	0.10	0.14	0.09	0.13	0.11	0.14	0.09	0.02
MgO	0.02	0.03	0.03	0.02	0.05	0.04	0.02	0.05	0.05	0.06	0.04	0.03	0.04	0.02
CaO	0.78	0.98	0.29	0.81	0.76	0.85	0.66	0.68	0.94	1.12	1.24	1.00	0.83	0.15
Na_2O	3.65	3.14	2.99	3.02	3.54	2.24	3.10	5.56	5.86	6.60	5.88	5.97	3.60	0.98
K_2O	7.48	8.50	8.19	8.53	7.95	9.87	7.71	3.89	3.69	2.66	3.79	3.77	7.60	1.61
TiO_2	0.14	0.15	0.13	0.11	0.13	0.15	0.11	0.19	0.20	0.30	0.25	0.30	0.15	0.04
Nb_2O_5	<0.003	<0.003	0.01	0.05	0.02	0.02	<0.003	0.06	0.02	0.06	0.04	0.05	0.02	0.02
P_2O_5	<0.01	0.02	0.02	<0.01	<0.01	<0.01	<0.01	<0.01	<0.01	0.03	<0.01	0.01	<0.01	<0.01
F	0.61	0.60	0.27	0.52	0.60	0.59	0.45	0.45	0.45	0.58	0.44	0.46	0.49	0.07
TREO	0.32	0.27	0.09	0.23	0.25	0.16	0.23	0.31	0.22	0.28	0.26	0.27	0.25	0.03
LREO	0.23	0.19	0.06	0.14	0.15	0.08	0.16	0.19	0.14	0.18	0.17	0.16	0.16	0.02
HREO+Y	0.09	0.08	0.03	0.09	0.10	0.08	0.07	0.11	0.08	0.11	0.09	0.11	0.09	0.01
Total	98.56	98.91	97.92	97.59	99.04	99.61	97.58	97.95	99.34	97.29	98.58	98.24	99.68	0.57
LOI	0.25	0.46	0.44	0.74	0.83	0.84	0.89	1.03	0.83	0.65	0.87	0.88	0.83	0.08
AI	1.20	1.17	1.14	1.13	1.19	1.14	1.17	1.16	1.12	1.18	1.17	1.17	1.17	0.02
Be *(ppm)*	22	17	19	28	34	23	21	36	44	33	36	34	31	7
Zn	310	280	340	380	390	730	460	830	470	800	600	810	465	145
Ga	54	43	50	48	48	42	55	57	47	42	43	48	48	5
Ge	5	4	3	3	3	4	4	4	3	4	4	4	4	0
As	7	13	<5	<5	<5	<5	6	5	11	21	9	13	7	7
Rb	917	932	1070	1090	1310	1810	1690	670	665	407	714	698	925	241
Sr	20	28	11	18	20	19	18	21	46	35	42	38	21	5
Y	564	523	178	572	597	491	438	653	503	599	547	688	556	48
Zr	655	341	674	383	1460	179	1516	3354	1928	5919	4525	3651	1488	1126
Sn	27	19	18	20	35	20	22	89	47	85	78	68	31	13
Cs	2	2	2	1	1	2	1	1	1	1	2	4	1	0
Ba	55	68	52	61	52	75	24	37	50	82	94	79	58	14
La	432	323	106	231	246	109	286	340	233	310	297	286	286	47
Ce	818	663	216	479	528	270	589	719	497	672	606	588	589	88
Pr	102	83	27	63	67	37	74	84	61	79	76	74	74	10
Nd	421	340	119	272	279	162	297	311	235	287	284	271	282	23
Sm	90	74	28	68	71	45	67	76	56	68	67	68	68	5
Eu	5.0	4.1	1.5	4.0	4.0	3.1	3.9	4.6	3.3	4.1	3.7	3.9	4.0	0
Gd	85	73	25	69	71	50	64	75	54	65	59	67	66	7
Tb	13	10	4	12	12	9	10	16	11	14	12	13	12	1
Dy	73	61	21	74	71	54	54	97	68	91	76	82	72	10
Ho	14	11	4	14	14	11	10	20	14	19	16	17	14	3
Er	37	29	11	36	37	25	22	57	38	57	46	47	37	10
Tm	4	4	2	4	5	3	3	9	5	8	7	7	5	2
Yb	24	21	11	24	26	17	14	55	32	56	44	45	25	10
Lu	3	3	2	3	4	2	2	8	4	8	6	7	4	1
Hf	22	11	20	12	41	7	44	86	51	150	116	90	42	31
Ta	3	1	3	2	8	6	3	23	10	27	24	24	7	5
Tl	4	5	4	4	4	9	6	3	3	2	4	4	4	0
Pb	35	31	18	40	32	30	16	139	61	716	200	223	38	21
Th	13	6	8	18	29	4	6	86	40	63	48	33	23	17
U	2	1	1	2	5	2	3	17	7	21	17	14	4	3

Table 6-1: Bulk rock data of least altered Strange Lake granites (continued)

Unit	Dark porphyritic granite (1/2)										
Sample	10012	10021	10034	10036	10037	10038	10043	10048	10051	10201	10204
Geologist*	1	1	1	1	1	1	1	2	2	1	1
Texture**	fgr, dk gr	mgr + en	mgr + en	pp+ts gr	pp+ts gr	pp+ts gr	pp+ts gr	pp+ts gr	pp+ts gr	fgr, dk gr	fgr, dk gr
Easting	430667	428103	430322	430602	430683	430668	428110	428068	430594	430628	430580
Northing	6238799	6239389	6238969	6239128	6238934	6238788	6239183	6239759	6239110	6239831	6240084
(wt. %)											
SiO_2	70.65	70.43	71.74	70.62	70.16	68.12	74.33	71.17	71.81	69.44	69.37
Al_2O_3	11.43	10.64	10.56	11.33	11.77	11.11	10.98	11.03	11.38	11.06	11.07
Fe_2O_3	5.13	5.35	5.83	4.90	4.98	5.94	5.00	4.86	4.68	5.36	5.24
MnO	0.10	0.10	0.10	0.09	0.08	0.13	0.08	0.08	0.08	0.12	0.12
MgO	0.03	0.02	0.03	0.03	0.05	0.10	0.02	0.02	0.04	0.10	0.04
CaO	0.43	0.34	0.42	0.60	0.63	0.79	0.37	0.28	0.50	0.76	0.58
Na_2O	5.26	4.59	5.95	5.15	5.17	4.82	4.91	3.43	5.34	4.98	5.43
K_2O	4.87	5.04	2.84	4.47	4.51	5.23	4.63	6.63	4.32	4.62	4.55
TiO_2	0.25	0.23	0.23	0.19	0.18	0.40	0.15	0.12	0.18	0.23	0.28
Nb_2O_5	0.05	0.07	0.05	0.04	0.02	0.12	0.02	0.02	0.02	0.04	0.07
P_2O_5	0.02	0.02	<0.01	0.01	0.02	0.01	<0.01	0.01	0.01	0.03	0.03
F	0.38	0.37	0.43	0.44	0.46	0.59	<0.01	0.29	0.38	0.49	0.47
TREO	0.23	0.31	0.20	0.24	0.19	0.43	0.16	0.22	0.23	0.38	0.40
LREO	0.17	0.18	0.13	0.16	0.12	0.32	0.10	0.16	0.16	0.26	0.28
HREO+Y	0.05	0.14	0.07	0.08	0.07	0.11	0.05	0.06	0.07	0.12	0.13
Total	98.21	96.82	97.75	97.43	97.58	96.77	100.5	97.66	98.36	96.74	96.78
LOI	0.39	0.22	0.09	0.24	0.42	0.63	0.02	0.54	0.45	0.75	0.64
AI	1.22	1.22	1.22	1.17	1.14	1.22	1.19	1.16	1.18	1.19	1.25
Be *(ppm)*	99	93	62	51	33	34	32	38	27	47	77
Zn	410	590	350	350	260	400	360	450	350	640	680
Ga	51	56	60	50	51	45	56	49	50	51	53
Ge	4	4	3	4	4	5	3	4	5	4	4
As	31	14	9	12	8	14	<5	<5	6	6	15
Rb	619	660	337	512	444	659	550	779	409	792	792
Sr	11	9	13	22	19	25	10	23	13	24	16
Y	302	742	391	460	384	604	324	355	390	690	722
Zr	3489	3666	3393	2620	1791	7191	2769	1041	1976	4206	4115
Sn	77	108	145	65	43	84	46	48	44	73	95
Cs	4	4	4	1	1	2	1	2	1	1	4
Ba	47	43	34	53	58	127	31	49	53	45	70
La	331	306	237	291	227	599	166	316	302	480	523
Ce	685	659	483	589	447	1240	395	621	599	944	1030
Pr	75	75	56	71	53	139	45	69	69	109	118
Nd	260	285	212	265	209	494	170	248	253	428	438
Sm	53	71	49	59	47	102	44	49	56	100	100
Eu	3	4	3	4	3	6	2	3	3	6	6
Gd	42	70	44	55	45	89	42	48	53	88	89
Tb	8	16	9	11	8	17	7	9	9	17	18
Dy	47	115	57	72	55	108	45	55	55	104	112
Ho	9	26	13	16	12	22	8	11	11	22	24
Er	29	83	43	50	35	69	25	33	33	61	71
Tm	5	14	7	8	5	11	4	5	5	9	10
Yb	35	90	55	50	32	69	25	30	31	54	61
Lu	6	13	9	7	5	11	4	4	5	8	8
Hf	103	94	105	77	54	197	66	29	56	119	109
Ta	19	23	23	18	11	49	11	9	10	21	31
Tl	3	3	1	3	2	2	2	4	3	4	4
Pb	157	178	111	129	99	119	94	111	76	259	226
Th	93	126	76	74	41	98	32	32	31	62	89
U	13	18	12	13	7	33	8	5	8	15	19

Table 6-1: Bulk rock data of least altered Strange Lake granites (continued)

Unit	Dark porphyritic granite (2/2)										
Sample	122711	122713	204709	204721	204724	204748	204749	204757	204758		
Geologist*	3	3	2	2	2	2	2	2	2		
Texture**	pp, dk grey	pp, dk grey	pp, dk grey	mgr + en	pp, dk grey	fgr, dk grey	pp+ts gr	pp+ts gr	pp+ts gr		
Easting	428090	428090	428044	428095	428090	430516	430601	430669	430683		
Northing	6239129	6239129	6239493	6239133	6239235	6239394	6239126	6238795	6238940	Mdn	MAD
(wt. %)											
SiO_2	70.77	71.06	72.56	71.56	70.00	70.46	70.66	70.59	70.62	70.64	0.51
Al_2O_3	10.09	10.22	11.23	10.32	10.74	11.39	11.27	11.42	11.57	11.09	0.32
Fe_2O_3	5.22	5.45	4.44	5.78	5.59	5.26	5.12	5.34	5.29	5.25	0.23
MnO	0.09	0.10	0.07	0.09	0.09	0.13	0.08	0.10	0.09	0.09	0.01
MgO	0.02	0.02	0.04	0.03	0.02	0.06	0.04	0.04	0.04	0.04	0.01
CaO	0.34	0.37	0.29	0.26	0.86	0.66	0.56	0.53	0.59	0.52	0.15
Na_2O	3.98	3.89	4.43	4.79	4.47	4.33	4.90	4.90	5.21	4.90	0.34
K_2O	6.08	6.16	5.12	4.35	5.57	5.74	4.67	5.01	4.65	4.77	0.33
TiO_2	0.28	0.26	0.13	0.18	0.22	0.28	0.19	0.26	0.20	0.22	0.04
Nb_2O_5	0.04	0.06	0.04	0.03	0.05	0.05	0.03	0.04	0.03	0.04	0.01
P_2O_5	0.02	<0.01	<0.01	0.02	<0.01	0.04	<0.01	0.02	<0.01	0.02	0.01
F	0.36	0.34	0.30	0.41	0.71	0.58	0.57	0.52	0.51	0.44	0.07
TREO	0.32	0.36	0.22	0.25	0.32	0.37	0.25	0.24	0.22	0.24	0.05
LREO	0.21	0.22	0.14	0.19	0.22	0.26	0.17	0.17	0.15	0.17	0.03
HREO+Y	0.11	0.14	0.07	0.06	0.10	0.11	0.08	0.07	0.07	0.08	0.02
Total	96.94	97.58	98.35	97.41	97.61	98.39	97.53	98.25	98.29	98.50	0.66
LOI	0.84	0.80	0.63	0.68	1.14	1.32	0.76	0.86	0.67	0.64	0.20
AI	1.30	1.28	1.14	1.22	1.25	1.17	1.16	1.18	1.18	1.19	0.03
Be *(ppm)*	25	19	47	38	40	43	33	47	35	39	8
Zn	460	570	450	450	500	400	360	460	360	430	70
Ga	46	48	51	60	57	47	50	49	50	51	2
Ge	4	4	3	4	4	4	3	4	4	4	0
As	12	29	5	12	11	6	13	25	8	12	4
Rb	749	815	654	537	706	627	453	574	406	623	119
Sr	11	11	13	8	60	37	13	11	16	13	3
Y	579	757	401	332	590	612	456	393	424	440	112
Zr	4877	3029	3592	3038	4527	4210	2445	3257	2370	3325	835
Sn	75	106	73	65	91	153	53	80	52	74	21
Cs	1	1	1	1	1	2	1	1	1	1	0
Ba	43	70	28	28	29	69	48	47	59	48	11
La	401	383	253	368	401	544	323	326	286	325	65
Ce	781	798	557	719	827	1040	621	640	562	650	112
Pr	93	94	61	82	97	112	74	72	65	74	16
Nd	359	348	229	295	359	354	276	256	245	271	50
Sm	81	86	55	62	84	68	62	58	56	60	11
Eu	4.6	4.9	3.0	3.2	4.6	3.7	3.4	3.0	3.0	3.3	0
Gd	77	85	51	51	75	56	55	48	49	54	9
Tb	14	18	10	9	14	13	10	9	9	10	2
Dy	95	132	63	50	81	92	64	54	57	64	15
Ho	20	28	13	10	17	21	13	11	12	13	3
Er	61	88	42	29	50	72	41	34	36	42	11
Tm	10	14	6	4	7	12	6	5	5	7	2
Yb	67	89	40	29	52	74	38	38	35	45	13
Lu	11	13	6	4	8	10	5	6	5	7	2
Hf	135	86	98	90	136	108	71	93	70	94	20
Ta	24	27	18	16	26	24	14	21	12	20	5
Tl	3	4	2	2	3	2	2	3	2	3	1
Pb	246	253	141	135	149	344	102	136	143	139	32
Th	62	107	75	42	70	91	41	75	47	72	23
U	16	17	13	11	16	21	10	13	9	13	4

APPENDIX 2: MINERAL ANALYSES AND FORMULAE

Perthitic alkali feldspar

Table 6-2: Perthitic alkali feldspar microprobe analyses

Unit	Hypersolvus granite south – fine grained (1/5)															
Sample	204768	204768	204768	204768	204768	204768	204768	204768	204768	204768	204768	204768	204768	204768	204768	204768
Grain/line	gr1-1	gr1-2	gr2-1	gr2-2	gr3-1	gr3-2	gr4-1	gr4-2	gr5-1	gr5-2	gr5-3	gr5-4	gr6-1	gr6-2	gr6-3	gr7-1
(wt. %)																
SiO$_2$	65.98	64.91	73.97	73.68	64.23	62.96	67.82	67.33	66.13	66.62	66.32	65.53	72.30	72.73	72.90	64.80
Al$_2$O$_3$	18.60	18.36	18.77	18.68	18.38	17.94	18.82	18.74	18.82	18.76	18.75	18.44	18.99	19.22	19.25	18.53
K$_2$O	9.54	10.20	10.03	7.92	8.33	8.34	6.98	8.55	8.68	7.80	9.52	9.64	7.51	5.91	6.37	9.75
Na$_2$O	5.24	4.37	4.55	6.13	5.77	5.92	6.89	5.91	5.76	6.27	5.32	5.21	6.80	7.69	7.43	5.02
Fe$_2$O$_3$	0.22	0.31	0.19	0.42	0.17	0.15	0.28	0.19	0.15	0.58	0.17	0.21	0.19	0.22	0.24	0.18
CaO	0.02	0.03	0.08	0.49	0.04	0.16	0.06	0.01	0.02	0.07	0.05	0.07	-	0.01	0.01	0.05
Rb$_2$O	0.02	-	-	0.04	-	-	-	-	0.02	-	-	0.04	0.03	0.01	0.02	-
BaO	0.04	-	-	-	-	-	-	-	-	-	-	-	0.01	0.04	-	-
PbO	-	0.02	-	0.03	-	0.01	-	0.02	-	-	0.01	-	-	-	-	0.01
Total	99.66	98.19	107.58	107.37	96.90	95.46	100.86	100.76	99.58	100.10	100.13	99.14	105.84	105.81	106.22	98.33
X$_{Or}$	0.54	0.61	0.59	0.46	0.49	0.48	0.40	0.49	0.50	0.45	0.54	0.55	0.42	0.34	0.36	0.56

Unit	Hypersolvus granite south – fine grained (2/5)															
Sample	204768	204768	204768	204768	204768	204768	204768	204771	204771	204771	204771	204771	204771	204771	204771	204771
Grain/line	gr7-2	gr8-1	gr8-2	gr8-3	gr9-1	gr9-2	gr9-3	gr1-1	gr1-2	gr1-3	gr1-4	gr2-1	gr2-2	gr2-3	gr2-4	gr3-1
(wt. %)																
SiO$_2$	64.44	66.36	66.61	66.37	67.08	67.30	66.39	65.27	65.08	65.47	65.37	66.22	66.41	66.01	65.70	61.40
Al$_2$O$_3$	18.32	18.74	18.76	18.80	18.58	18.33	18.58	18.21	18.27	18.29	18.24	18.14	18.18	18.43	18.32	17.22
K$_2$O	10.15	9.57	9.29	10.59	7.46	7.85	8.99	7.93	7.34	7.24	8.42	6.02	7.04	8.14	7.79	8.55
Na$_2$O	4.77	5.11	5.33	4.44	6.75	6.15	5.60	6.12	6.70	6.81	6.17	7.38	6.92	6.13	6.49	5.76
Fe$_2$O$_3$	0.24	0.16	0.15	0.18	0.26	0.24	0.25	0.37	0.35	0.46	0.49	0.38	0.42	0.43	0.36	0.29
CaO	0.03	0.02	0.05	0.04	0.04	0.02	0.04	0.07	0.04	0.03	0.02	0.04	0.02	0.07	0.13	-
Rb$_2$O	-	0.05	0.03	-	0.03	0.03	-	-	-	-	-	-	0.01	-	-	-
BaO	0.02	-	-	-	0.07	0.01	0.01	0.02	0.01	0.01	0.02	-	-	0.01	0.08	-
PbO	0.01	-	-	-	-	0.02	-	0.01	0.01	-	-	0.01	0.01	-	-	0.02
Total	97.97	100.00	100.23	100.43	100.26	99.93	99.86	97.99	97.79	98.31	98.74	98.19	99.02	99.22	98.87	93.24
X$_{Or}$	0.58	0.55	0.53	0.61	0.42	0.46	0.51	0.46	0.42	0.41	0.47	0.35	0.40	0.47	0.44	0.49

Table 6-2: Perthitic alkali feldspar microprobe analyses (continued)

Unit	Hypersolvus granite south – fine grained (3/5)															
Sample	204771	204771	204771	204771	204771	204771	204771	10017	10017	10017	10017	10017	10017	10017	10017	10017
Grain/line	gr3-2	gr3-3	gr3-4	gr3-5	gr4-1	gr4-2	gr4-3	gr1-1	gr1-2	gr1-3	gr1-4	gr1-5	gr1-6	gr2-1	gr2-2	gr2-3
(wt. %)																
SiO_2	65.86	66.57	66.43	67.19	66.07	66.19	66.23	67.57	67.28	67.36	67.18	67.36	66.74	67.06	67.33	67.43
Al_2O_3	18.04	18.56	18.34	18.48	18.71	18.56	18.62	18.84	18.65	18.81	18.76	18.58	18.67	18.74	18.96	18.89
K_2O	9.22	7.57	7.67	7.00	8.45	7.43	10.26	8.15	8.34	9.12	8.57	9.32	10.40	8.47	8.02	6.53
Na_2O	5.51	6.91	6.42	7.02	6.07	6.46	4.81	6.17	5.97	5.57	5.78	5.62	4.61	5.80	6.28	7.23
Fe_2O_3	0.41	0.39	0.32	0.37	0.24	0.28	0.20	0.26	0.23	0.21	0.22	0.25	0.26	0.17	0.18	0.19
CaO	-	-	-	0.02	0.04	0.02	0.02	0.04	0.04	0.04	0.05	0.04	-	0.07	0.06	0.08
Rb_2O	0.02	-	-	-	-	-	-	-	-	-	-	-	-	-	0.04	-
BaO	0.03	0.03	-	-	-	-	-	0.04	0.02	0.03	-	-	-	0.02	-	0.06
PbO	-	-	-	0.01	0.01	-	-	-	-	0.04	0.02	0.03	-	-	-	-
Total	99.09	100.02	99.18	100.09	99.60	98.93	100.14	101.06	100.54	101.17	100.57	101.19	100.68	100.32	100.87	100.41
X_{Or}	0.52	0.42	0.44	0.40	0.48	0.43	0.58	0.46	0.48	0.52	0.49	0.52	0.60	0.49	0.46	0.37

Unit	Hypersolvus granite south – fine grained (4/5)															
Sample	10017	10017	10017	10017	10017	10017	10017	10017	10017	10017	10017	10017	10017	10017	10017	10017
Grain/line	gr2-4	gr3-line1	gr3-line2	gr3-line3	gr3-line4	gr3-line5	gr3-line6	gr3-line7	gr3-line8	gr3-line9	gr3-line10	gr4-1	gr4-2	gr4-3	gr4-4	gr5-1
(wt. %)																
SiO_2	67.28	67.08	67.08	67.75	67.01	67.03	68.57	67.92	68.00	67.63	67.74	66.90	67.44	67.09	67.15	66.85
Al_2O_3	18.48	18.84	18.68	18.93	18.59	19.11	18.28	19.25	18.96	19.07	18.97	18.69	18.98	18.73	18.50	18.53
K_2O	9.10	6.78	6.03	6.21	7.76	6.17	6.05	5.61	5.34	6.44	6.35	10.57	8.50	8.26	9.95	10.65
Na_2O	5.70	6.94	7.47	7.29	6.29	7.42	7.39	7.80	7.93	7.24	7.27	4.71	5.91	5.72	5.04	4.54
Fe_2O_3	0.15	0.33	0.27	0.32	0.21	0.17	0.25	0.27	0.26	0.20	0.23	0.34	0.25	0.21	0.22	0.27
CaO	0.04	0.02	0.04	0.03	0.02	0.05	0.04	0.02	0.05	0.09	0.20	0.03	0.01	0.08	-	0.01
Rb_2O	-	-	-	0.04	-	-	0.01	-	-	0.01	-	0.05	0.02	0.01	-	-
BaO	-	0.04	0.07	-	0.04	-	0.03	-	0.07	-	0.04	-	0.02	0.08	0.05	0.05
PbO	-	-	-	0.01	-	0.02	-	0.01	-	-	0.01	0.02	-	-	0.01	-
Total	100.75	100.03	99.61	100.57	99.93	99.96	100.62	100.89	100.60	100.68	100.81	101.30	101.13	100.17	100.92	100.90
X_{Or}	0.51	0.39	0.35	0.36	0.45	0.35	0.35	0.32	0.31	0.37	0.36	0.60	0.49	0.49	0.56	0.61

Table 6-2: Perthitic alkali feldspar microprobe analyses (continued)

Unit	Hypersolvus granite south – fine gr. (5/5)					Hypersolvus granite south – oikocrystic/pegmatitic samples (1/7)										
Sample	10017	10017	10017			204773	204773	204773	204773	204773	204773	204773	204773	204773	204773	204773
Grain/line	gr5-2	gr5-3	gr5-4	Mdn	MAD	gr1-line1	gr1-line2	gr1-line3	gr1-line4	gr1-line5	gr1-line6	gr1-line7	gr1-line8	gr1-line9	gr1-line10	gr1-line11
(wt. %)																
SiO_2	66.47	67.16	66.85	66.90	0.59	67.37	66.90	66.99	66.85	67.13	67.16	66.15	67.80	67.57	66.80	65.78
Al_2O_3	18.55	18.70	18.61	18.65	0.17	18.17	17.96	17.93	17.80	17.81	18.12	17.77	18.31	18.44	18.02	18.02
K_2O	10.52	7.71	10.46	8.26	1.03	6.25	7.78	9.17	7.60	9.07	7.90	8.42	5.91	5.93	5.87	9.70
Na_2O	4.66	6.51	4.86	6.12	0.77	7.45	6.45	5.58	6.27	5.54	5.98	5.93	7.64	7.57	7.62	4.75
Fe_2O_3	0.18	0.14	0.23	0.24	0.05	0.79	0.86	0.89	1.05	1.01	0.96	0.88	0.31	0.30	0.98	0.84
CaO	0.06	0.10	0.07	0.04	0.02	0.01	0.01	0.03	0.04	0.03	0.04	0.03	0.03	0.02	0.01	-
Rb_2O	0.02	-	-	-	-	-	-	0.01	-	-	0.03	0.01	0.06	-	-	-
BaO	0.03	-	0.02	-	-	-	-	-	0.02	-	-	-	-	0.04	0.05	-
PbO	-	0.01	0.03	-	-	-	0.02	-	-	0.02	0.02	-	0.02	-	-	-
Total	100.49	100.34	101.13	100.17	0.69	100.04	99.97	100.59	99.64	100.61	100.21	99.18	100.06	99.86	99.35	99.09
X_{Or}	0.60	0.44	0.59	0.47	0.06	0.36	0.44	0.52	0.44	0.52	0.47	0.48	0.34	0.34	0.34	0.57

Unit	Hypersolvus granite south – oikocrystic/pegmatitic (2/7)															
Sample	204773	204773	204773	204773	204773	204773	204773	204773	204773	204773	204773	204773	204773	204773	204773	204773
Grain/line	gr1-line12	gr1-line13	gr1-line14	gr1-line15	gr1-line16	gr2-line1	gr2-line2	gr2-line3	gr2-line4	gr2-line5	gr2-line6	gr2-line7	gr3-line1	gr3-line2	gr3-line3	gr3-line4
(wt. %)																
SiO_2	66.76	66.32	66.90	66.81	66.97	66.33	67.68	66.91	66.04	66.16	67.88	68.21	67.55	65.98	67.29	67.96
Al_2O_3	17.87	17.91	17.93	18.05	18.06	18.15	17.93	17.75	17.82	17.46	18.43	17.86	17.95	17.43	17.73	18.16
K_2O	7.65	8.44	7.69	7.31	8.93	7.27	6.46	8.48	7.68	10.03	6.15	6.94	7.07	8.01	8.75	7.57
Na_2O	6.47	5.47	6.46	6.68	5.90	6.62	6.87	5.90	6.30	4.18	7.53	6.61	6.75	6.11	5.66	6.44
Fe_2O_3	0.91	0.92	0.83	0.90	0.87	0.61	0.92	0.91	0.72	0.86	0.70	0.86	0.86	0.74	0.88	0.74
CaO	0.01	0.02	0.01	0.01	-	0.02	0.02	0.05	0.02	0.06	-	0.02	0.03	0.02	0.01	0.02
Rb_2O	-	0.02	-	0.01	-	-	-	-	0.02	-	-	0.04	-	-	0.02	0.07
BaO	0.02	0.01	-	0.01	-	0.02	-	-	-	-	-	-	-	0.03	0.02	0.01
PbO	-	0.02	0.03	-	-	-	-	0.02	0.02	-	0.02	0.03	0.04	0.03	0.01	-
Total	99.68	99.15	99.85	99.78	100.74	99.01	99.88	100.02	98.61	98.76	100.70	100.56	100.24	98.36	100.35	100.97
X_{Or}	0.44	0.50	0.44	0.42	0.50	0.42	0.38	0.49	0.45	0.61	0.35	0.41	0.41	0.46	0.50	0.44

Table 6-2: Perthitic alkali feldspar microprobe analyses (continued)

Unit	Hypersolvus granite south – oikocrystic/pegmatitic (3/7)															
Sample	204773	204773	204773	204773	204773	204773	204773	204773	204773	204773	204773	204773	204773	204773	204773	204773
Grain/line	gr3-line5	gr3-line6	gr3-line7	gr3-line8	gr3-line9	gr3-line10	gr3-line11	gr3-line12	gr4-line1	gr4-line2	gr4-line3	gr4-line4	gr4-line5	gr4-line6	gr4-line7	gr4-line8
(wt. %)																
SiO_2	67.01	67.41	66.63	67.09	66.86	67.40	67.66	67.02	68.17	67.75	67.48	67.38	67.52	67.62	67.67	67.23
Al_2O_3	17.81	17.59	17.59	18.18	18.30	18.66	18.36	18.44	18.27	18.21	18.16	18.06	18.01	17.79	18.21	17.83
K_2O	10.82	9.54	8.94	9.34	9.03	7.87	9.94	9.04	6.12	7.51	6.58	7.13	7.41	7.28	7.32	8.77
Na_2O	4.38	5.03	5.59	5.33	5.55	6.30	4.80	5.63	7.33	6.70	7.36	6.70	6.71	6.57	6.62	5.68
Fe_2O_3	0.88	0.82	0.48	0.25	0.21	0.21	0.15	0.10	0.91	0.97	1.08	0.91	1.01	0.91	0.97	0.96
CaO	0.01	0.01	0.02	0.02	0.01	0.01	-	0.01	0.03	0.08	0.02	0.02	0.03	-	-	0.03
Rb_2O	-	-	0.02	-	-	0.05	-	-	-	-	-	-	0.08	0.02	-	0.02
BaO	0.02	0.04	0.03	0.02	-	0.07	-	-	0.02	-	-	0.01	0.05	0.03	0.01	-
PbO	0.03	0.02	-	-	0.02	0.01	-	0.01	0.06	0.02	0.04	-	0.01	0.04	0.04	0.04
Total	100.96	100.45	99.29	100.22	99.98	100.58	100.91	100.26	100.91	101.24	100.71	100.19	100.82	100.25	100.84	100.55
X_{Or}	0.62	0.56	0.51	0.54	0.52	0.45	0.58	0.51	0.35	0.42	0.37	0.41	0.42	0.42	0.42	0.50

Unit	Hypersolvus granite south – oikocrystic/pegmatitic (4/7)															
Sample	204773	204773	204773	204773	204773	204773	204773	204773	204773	204773	204773	204773	204773	204773	204773	204773
Grain/line	gr4-line9	gr4-line10	gr4-line11	gr4-line12	gr4-line13	gr4-line14	gr4-line15	gr4-line16	gr4-line17	gr4-line18	gr4-line19	gr4-line20	gr4-line21	gr4-line22	gr5-line1	gr5-line2
(wt. %)																
SiO_2	67.20	66.92	66.22	66.80	66.93	66.76	66.44	67.39	67.33	67.16	68.01	66.88	67.41	68.41	66.44	66.63
Al_2O_3	18.20	17.96	17.84	17.98	18.24	18.15	17.74	17.86	17.63	17.81	18.12	17.76	18.18	18.17	17.63	18.02
K_2O	8.04	8.19	9.76	7.40	9.49	8.33	10.56	8.16	6.78	7.57	6.39	8.00	7.05	5.15	9.62	8.73
Na_2O	6.27	5.97	4.99	6.50	5.34	5.99	4.45	6.29	6.95	6.35	7.14	6.20	6.88	8.07	4.84	5.83
Fe_2O_3	0.93	1.00	0.93	0.78	0.71	0.81	0.82	0.89	1.05	0.90	0.92	0.93	0.86	1.02	0.77	0.80
CaO	-	0.02	0.01	0.05	-	0.01	0.04	0.03	0.03	-	0.02	0.01	0.01	0.07	0.07	0.05
Rb_2O	-	-	-	0.05	-	0.04	-	-	-	-	0.06	-	0.03	-	-	-
BaO	0.02	0.05	0.03	0.03	-	-	0.02	0.01	-	-	-	0.01	-	0.06	0.01	-
PbO	0.03	0.03	0.04	0.03	0.02	-	0.05	-	0.02	0.03	0.01	-	0.01	0.02	0.03	0.06
Total	100.68	100.13	99.81	99.62	100.73	100.10	100.11	100.62	99.78	99.82	100.66	99.77	100.42	100.96	99.42	100.12
X_{Or}	0.46	0.47	0.56	0.43	0.54	0.48	0.61	0.46	0.39	0.44	0.37	0.46	0.40	0.30	0.57	0.50

Table 6-2: Perthitic alkali feldspar microprobe analyses (continued)

Unit	Hypersolvus granite south – oikocrystic/pegmatitic (5/7)															
Sample	204773	204773	204773	204773	204773	204773	204773	204773	204773	204773	204773	204773	204773	204773	204773	204773
Grain/line	gr5-line3	gr5-line4	gr5-line5	gr5-line6	gr5-line7	gr5-line8	gr5-line9	gr5-line10	gr6-line1	gr6-line2	gr6-line3	gr6-line4	gr6-line5	gr6-line6	gr6-line7	gr6-line8
(wt. %)																
SiO_2	66.75	66.89	66.58	65.95	66.35	66.03	67.17	66.59	67.63	68.00	67.37	67.36	68.18	67.55	67.68	67.18
Al_2O_3	17.92	17.93	17.84	18.03	17.87	17.83	17.86	18.09	17.79	17.94	17.85	17.76	17.90	17.81	18.10	17.72
K_2O	7.87	8.75	7.97	9.09	8.84	8.76	7.75	7.30	9.76	8.03	8.89	7.83	7.42	8.95	7.43	9.18
Na_2O	6.14	5.61	6.10	5.64	5.85	5.76	6.18	6.76	5.14	6.41	5.39	6.15	6.57	5.48	6.64	5.26
Fe_2O_3	0.83	0.91	0.85	0.89	0.96	0.96	0.81	0.73	0.93	0.86	0.80	0.90	0.94	0.94	0.98	0.99
CaO	0.04	0.03	-	0.04	-	0.03	0.01	0.03	-	0.02	0.03	0.04	0.02	0.06	0.02	0.02
Rb_2O	0.03	0.05	-	-	0.01	-	0.03	-	-	-	-	0.04	0.02	-	-	0.05
BaO	-	0.02	0.01	0.03	0.04	0.02	0.04	0.03	0.06	-	-	0.02	0.03	0.01	-	-
PbO	0.04	0.03	0.02	0.02	0.01	0.07	-	0.01	0.01	0.03	0.01	0.01	0.02	0.01	-	0.03
Total	99.62	100.21	99.36	99.69	99.92	99.45	99.84	99.53	101.33	101.28	100.35	100.11	101.10	100.81	100.84	100.43
X_{Or}	0.46	0.51	0.46	0.51	0.50	0.50	0.45	0.42	0.56	0.45	0.52	0.46	0.43	0.52	0.42	0.53

Unit	Hypersolvus granite south – oikocrystic/pegmatitic (6/7)															
Sample	204773	204773	204773	204773	10018	10018	10018	10018	10018	10018	10018	10018	10018	10018	10018	10018
Grain/line	gr6-line9	gr6-line10	gr6-line11	gr6-line12	gr1-1	gr1-2	gr1-3	gr1-4	gr1-5	gr2-1	gr2-2	gr2-3	gr2-4	gr2-5	gr3-1	gr3-2
(wt. %)																
SiO_2	68.28	67.50	67.81	68.39	66.48	65.63	65.80	65.69	65.42	66.31	66.48	66.99	66.13	66.45	66.16	66.56
Al_2O_3	18.07	18.13	18.21	17.68	18.60	18.73	18.72	18.50	18.70	18.52	18.67	18.68	18.64	18.72	18.19	18.45
K_2O	5.50	7.64	7.90	7.65	8.34	8.41	7.27	8.95	8.54	8.44	6.35	7.01	9.56	6.59	7.22	7.31
Na_2O	7.92	6.24	6.58	5.96	6.19	5.63	6.72	5.67	5.75	5.74	6.84	6.82	5.03	7.02	6.66	6.70
Fe_2O_3	0.87	0.79	0.82	0.61	0.17	0.15	0.20	0.14	0.22	0.41	0.30	0.31	0.23	0.20	0.75	0.72
CaO	0.01	0.05	0.05	0.03	0.01	0.05	0.07	0.05	0.03	-	-	0.04	0.04	0.01	0.02	0.01
Rb_2O	-	-	0.05	0.05	0.08	-	-	0.01	0.02	0.01	0.01	0.02	-	-	-	-
BaO	-	-	0.01	0.03	0.02	0.02	-	0.05	0.02	0.03	-	0.07	-	0.02	-	-
PbO	0.01	-	0.01	-	0.02	0.02	0.03	-	-	0.01	0.02	-	-	-	-	-
Total	100.66	100.35	101.44	100.39	99.90	98.63	98.81	99.06	98.70	99.47	98.66	99.94	99.63	99.02	99.00	99.76
X_{Or}	0.31	0.45	0.44	0.46	0.47	0.50	0.42	0.51	0.49	0.49	0.38	0.40	0.56	0.38	0.42	0.42

Table 6-2: Perthitic alkali feldspar microprobe analyses (continued)

Unit	Hypersolvus granite south – oik/peg (7/7)						Hypersolvus granite north (1/6)									
Sample	10018	10018	10018	10018			10040	10040	10040	10040	10040	10040	10040	10040	10040	10040
Grain/line	gr3-3	gr3-4	gr3-5	gr3-6	Mdn	MAD	gr1-1	gr1-2	gr1-3	gr1-4	gr2-line1	gr2-line2	gr2-line3	gr2-line4	gr3-line1	gr3-line2
(wt. %)																
SiO_2	67.13	67.89	68.57	64.90	67.01	0.52	63.64	63.93	62.43	61.89	63.55	64.00	64.36	63.88	66.49	67.04
Al_2O_3	18.43	18.84	18.64	18.06	18.02	0.19	17.77	17.61	17.31	17.44	17.64	17.47	17.83	17.59	18.17	17.87
K_2O	7.65	7.06	7.19	5.30	7.87	0.81	11.61	8.07	12.60	13.98	10.09	9.29	10.00	11.76	9.00	9.51
Na_2O	6.14	6.69	6.76	7.61	6.24	0.50	3.55	5.75	3.10	1.93	4.78	4.64	4.38	3.58	5.99	4.99
Fe_2O_3	0.75	0.53	0.79	0.80	0.86	0.08	0.28	0.44	0.27	0.35	0.43	0.34	0.31	0.28	0.50	0.51
CaO	0.01	0.01	0.03	-	0.02	0.01	0.02	0.04	0.01	0.02	0.21	0.11	0.11	0.07	0.02	0.03
Rb_2O	0.02	0.03	-	-	-	-	-	-	-	0.03	-	-	0.07	0.04	-	-
BaO	-	-	-	-	0.01	0.01	0.07	-	-	0.02	-	0.03	-	0.01	-	0.01
PbO	0.02	-	-	-	0.01	0.01	-	0.02	-	-	0.02	-	-	-	0.01	0.02
Total	100.14	101.04	101.97	96.67	100.11	0.49	96.92	95.86	95.71	95.67	96.72	95.87	97.07	97.22	100.17	99.98
X_{Or}	0.45	0.41	0.41	0.31	0.45	0.04	0.68	0.48	0.73	0.83	0.58	0.57	0.60	0.68	0.50	0.56

Unit	Hypersolvus granite north (2/6)															
Sample	10040	10040	10040	10040	10040	10040	10040	10040	10040	10040	10040	10040	10040	10040	204754	204754
Grain/line	gr3-line3	gr3-line4	gr3-line5	gr3-line6	gr4-1	gr4-2	gr5-line1	gr5-line2	gr5-line3	gr5-line4	gr6-1	gr6-2	gr6-3	gr6-4	gr1-1	gr1-2
(wt. %)																
SiO_2	67.03	66.72	66.75	66.45	66.75	66.76	67.60	66.00	67.53	67.29	67.01	67.06	66.07	66.78	64.07	65.43
Al_2O_3	17.75	18.01	17.95	17.88	17.94	17.79	18.15	17.54	18.24	18.47	17.83	18.42	17.90	18.24	17.65	18.06
K_2O	9.03	9.19	9.79	10.65	8.42	8.83	9.26	8.73	8.56	7.22	11.35	8.08	12.66	10.09	12.00	9.00
Na_2O	5.33	5.58	5.03	4.27	5.79	5.30	5.38	5.14	5.74	6.90	3.77	6.00	2.89	4.79	3.53	5.23
Fe_2O_3	0.60	0.44	0.52	0.56	0.51	0.47	0.44	0.41	0.43	0.46	0.21	0.20	0.30	0.22	0.44	0.39
CaO	0.06	0.10	0.05	-	0.02	0.04	0.03	0.03	0.05	0.02	0.05	0.04	-	0.07	0.05	0.02
Rb_2O	-	-	-	0.06	0.02	-	0.04	-	-	-	-	0.01	0.02	-	0.07	-
BaO	0.04	-	0.04	0.06	0.07	0.04	-	-	-	-	-	0.02	-	0.01	-	0.04
PbO	-	-	-	-	-	-	-	-	-	-	0.01	0.02	-	-	-	0.01
Total	99.83	100.04	100.12	99.93	99.50	99.23	100.89	97.85	100.56	100.36	100.23	99.84	99.85	100.19	97.80	98.18
X_{Or}	0.53	0.52	0.56	0.62	0.49	0.52	0.53	0.53	0.50	0.41	0.66	0.47	0.74	0.58	0.69	0.53

Table 6-2: Perthitic alkali feldspar microprobe analyses (continued)

Unit	Hypersolvus granite north (3/6)															
Sample	204754	204754	204754	204754	204754	204754	204754	204754	204756	204756	204756	204756	204756	204756	204756	204756
Grain/line	gr1-3	gr1-4	gr2-1	gr2-2	gr2-3	gr3-1	gr3-2	gr3-3	gr1-1	gr1-2	gr1-3	gr1-4	gr1-5	gr2-1	gr2-2	gr2-3
(wt. %)																
SiO_2	64.72	64.92	65.20	65.47	64.07	70.63	70.27	67.54	66.83	66.68	67.36	66.67	66.69	67.44	66.87	67.26
Al_2O_3	17.75	17.99	18.00	18.23	18.11	18.77	18.63	18.43	17.76	17.87	18.15	17.74	17.97	18.21	18.28	18.20
K_2O	11.33	10.01	11.36	10.57	9.92	8.25	9.24	6.58	10.46	9.33	6.59	9.58	9.81	8.84	9.17	9.65
Na_2O	3.75	4.46	4.07	4.28	4.80	5.87	5.38	6.98	4.37	5.17	7.03	5.32	5.25	5.85	5.35	5.27
Fe_2O_3	0.42	0.40	0.35	0.42	0.35	0.46	0.56	0.50	0.76	0.87	0.76	0.69	0.43	0.43	0.39	0.41
CaO	0.02	0.02	0.03	-	0.02	0.03	0.02	0.01	0.01	0.02	-	-	-	0.01	0.03	0.01
Rb_2O	-	0.01	0.02	0.04	-	0.04	0.08	0.02	-	-	0.04	-	-	-	-	0.03
BaO	0.02	-	-	0.01	-	0.05	-	-	-	-	-	0.03	-	0.06	-	-
PbO	-	-	-	0.01	0.01	-	0.01	0.03	-	0.01	0.02	0.03	0.01	0.03	0.01	-
Total	98.01	97.81	99.03	99.01	97.26	104.10	104.20	100.08	100.20	99.95	99.94	100.06	100.16	100.87	100.10	100.85
X_{Or}	0.67	0.60	0.65	0.62	0.58	0.48	0.53	0.38	0.61	0.54	0.38	0.54	0.55	0.50	0.53	0.55

Unit	Hypersolvus granite north (4/6)															
Sample	204756	204756	204756	204756	204756	204756	204756	204756	204756	204756	204756	204756	204756	204756	204756	204756
Grain/line	gr2-4	gr2-5	gr2-6	gr2-7	gr3-line1	gr3-line2	gr3-line3	gr3-line4	gr4-1	gr4-2	gr4-3	gr4-4	gr4-5	gr4-6	gr4-7	gr5-1
(wt. %)																
SiO_2	68.09	67.92	66.99	68.07	66.45	67.06	66.88	67.06	66.97	67.16	67.07	67.19	67.81	67.88	67.35	66.44
Al_2O_3	17.78	18.35	18.20	18.03	17.80	17.99	17.86	17.69	17.94	18.17	18.08	18.07	18.35	17.85	18.08	17.87
K_2O	8.68	8.32	9.71	8.43	11.44	9.89	9.11	10.10	11.08	7.83	9.05	9.91	7.59	8.51	10.08	11.56
Na_2O	5.63	6.08	5.27	5.58	3.91	4.97	5.27	4.83	4.06	6.35	5.58	5.03	6.52	5.70	4.79	3.88
Fe_2O_3	0.55	0.58	0.44	0.40	0.57	0.75	0.90	0.84	0.47	0.52	0.52	0.51	0.49	0.54	0.52	0.53
CaO	0.02	0.03	0.01	-	0.01	0.01	-	0.01	0.01	0.03	0.01	0.01	0.02	0.03	-	0.01
Rb_2O	0.01	-	-	-	-	-	-	-	0.02	-	0.02	0.02	-	0.01	0.04	0.04
BaO	0.03	-	0.01	-	0.02	-	0.06	0.01	-	0.01	0.02	-	-	-	0.02	-
PbO	-	-	0.01	0.01	0.01	0.01	0.02	0.03	0.01	0.01	0.01	-	0.01	0.01	0.03	0.02
Total	100.79	101.28	100.64	100.53	100.20	100.66	100.10	100.58	100.56	100.07	100.34	100.75	100.80	100.55	100.91	100.33
X_{Or}	0.50	0.47	0.55	0.50	0.66	0.57	0.53	0.58	0.64	0.45	0.52	0.56	0.43	0.50	0.58	0.66

Table 6-2: Perthitic alkali feldspar microprobe analyses (continued)

Unit	Hypersolvus granite north (5/6)															
Sample	204756	204756	204756	204756	204756	204756	204756	204756	204756	204756	204756	204756	204756	204756	204756	204756
Grain/line	gr5-2	gr5-3	gr5-4	gr5-5	gr5-6	gr5-7	gr6-line1	gr6-line2	gr6-line3	gr6-line4	gr6-line5	gr6-line6	gr6-line7	gr6-line8	gr6-line9	gr6-line10
(wt. %)																
SiO_2	66.62	66.35	66.97	67.60	68.00	67.34	66.75	67.44	67.49	67.66	67.88	68.03	67.06	67.44	67.59	67.64
Al_2O_3	17.84	17.87	18.16	18.01	18.44	18.06	17.87	18.14	17.87	18.10	17.95	18.19	18.13	17.98	17.75	17.60
K_2O	12.22	9.82	8.90	9.68	8.35	8.54	8.43	8.33	7.46	7.92	7.45	7.28	8.57	8.71	8.22	8.00
Na_2O	3.30	4.88	5.26	5.27	5.89	5.93	5.89	5.93	6.37	6.24	6.74	7.06	5.79	5.77	5.97	6.24
Fe_2O_3	0.54	0.56	0.51	0.50	0.51	0.56	0.54	0.60	0.89	0.93	0.95	0.87	0.84	0.95	0.94	0.92
CaO	0.01	0.05	-	0.03	0.02	0.02	-	0.03	0.04	0.03	0.01	-	-	-	0.03	0.04
Rb_2O	-	-	-	-	-	-	0.01	-	0.03	-	-	-	0.01	-	-	-
BaO	0.06	-	-	-	-	0.01	-	0.03	-	-	-	0.06	0.03	0.02	-	0.04
PbO	0.02	-	0.02	0.02	0.02	0.02	0.04	0.02	0.01	-	0.02	0.02	-	-	-	0.03
Total	100.60	99.52	99.82	101.10	101.23	100.48	99.52	100.53	100.15	100.87	101.00	101.50	100.43	100.87	100.50	100.50
X_{Or}	0.71	0.57	0.53	0.55	0.48	0.49	0.48	0.48	0.44	0.46	0.42	0.40	0.49	0.50	0.48	0.46

Unit	Hypersolvus granite north (6/6)									
Sample	204756	204756	204756	204756	204756	204756	204756	204756		
Grain/line	gr6-line11	gr6-line12	gr6-line13	gr6-line14	gr6-line15	gr6-line16	gr6-line17	gr6-line18	Mdn	MAD
(wt. %)										
SiO_2	68.17	67.97	68.03	68.09	68.75	67.32	67.57	67.86	67.05	0.55
Al_2O_3	17.92	17.87	17.97	18.00	18.26	17.91	17.91	17.86	17.96	0.17
K_2O	6.82	6.80	8.66	7.64	6.51	9.22	7.97	7.75	9.08	0.85
Na_2O	6.95	7.00	5.96	6.44	7.18	5.37	6.06	6.33	5.34	0.59
Fe_2O_3	0.96	0.87	0.96	0.86	0.92	0.91	0.93	0.80	0.51	0.10
CaO	0.01	0.02	0.02	-	0.01	0.03	0.03	-	0.02	0.01
Rb_2O	-	-	-	-	-	-	-	0.05	-	-
BaO	0.01	-	-	-	0.01	-	0.02	-	-	-
PbO	0.01	-	0.01	0.01	-	0.02	-	0.01	0.01	0.01
Total	100.85	100.53	101.61	101.04	101.63	100.77	100.50	100.65	100.22	0.49
X_{Or}	0.39	0.39	0.49	0.44	0.37	0.53	0.46	0.45	0.53	0.05

Table 6-2: Perthitic alkali feldspar microprobe analyses (continued)

Unit	Transsolvus granite (1/4)															
Sample	204720	204720	204720	204720	204720	204720	204720	204720	204720	204720	204720	204720	204720	204720	204720	204720
Grain/line	gr1-line1	gr1-line2	gr1-line3	gr1-line4	gr1-line5	gr1-line6	gr1-line7	gr1-line8	gr1-line9	gr1-line10	gr1-line11	gr1-line12	gr2-line1	gr2-line2	gr2-line3	gr2-line4
(wt. %)																
SiO_2	64.60	64.57	66.18	66.88	65.45	67.04	65.63	65.95	66.50	66.41	65.07	66.56	66.25	66.59	66.21	68.08
Al_2O_3	17.32	17.57	17.80	18.00	17.74	18.07	17.84	18.00	17.85	17.85	17.60	18.24	18.04	17.98	17.58	17.42
K_2O	12.50	11.36	8.35	5.88	10.20	4.93	9.99	7.82	7.32	7.50	11.42	7.04	7.81	7.14	7.56	8.19
Na_2O	3.16	3.70	6.02	7.67	4.70	8.17	4.69	6.12	6.65	6.29	3.49	6.68	6.19	6.63	6.22	5.36
Fe_2O_3	0.87	0.81	0.89	0.88	1.03	1.04	0.82	0.83	0.93	0.95	0.62	0.94	0.70	0.77	0.83	0.78
CaO	0.02	-	-	0.01	0.03	-	0.03	0.01	0.03	0.05	0.03	0.02	0.05	0.03	0.02	0.02
Rb_2O	-	0.11	-	-	-	-	-	0.02	-	-	0.05	0.04	0.03	0.02	-	0.08
BaO	-	-	-	-	-	-	0.04	-	-	0.02	0.01	-	-	-	-	-
PbO	0.02	-	-	-	0.01	-	0.01	0.03	-	0.02	-	0.01	-	-	0.01	0.02
Total	98.49	98.12	99.24	99.31	99.16	99.25	99.06	98.79	99.27	99.09	98.29	99.53	99.06	99.16	98.43	99.93
X_{Or}	0.72	0.67	0.48	0.34	0.59	0.28	0.58	0.46	0.42	0.44	0.68	0.41	0.45	0.41	0.44	0.50

Unit	Transsolvus granite (2/4)															
Sample	204720	204720	204720	204720	204720	204720	204720	204720	204720	204720	204720	204720	204720	204720	204720	204720
Grain/line	gr2-line5	gr2-line6	gr2-line7	gr2-line8	gr2-line9	gr2-line10	gr2-line11	gr2-line12	gr2-line13	gr2-line14	gr3-line1	gr3-line2	gr3-line3	gr3-line4	gr3-line5	gr3-line6
(wt. %)																
SiO_2	66.54	66.50	65.78	66.23	66.80	66.86	67.08	65.91	66.47	65.08	66.83	67.56	66.60	67.64	67.60	67.62
Al_2O_3	18.24	18.24	17.86	18.03	18.07	17.98	17.15	17.57	17.82	17.58	18.11	18.33	18.25	17.97	18.47	18.10
K_2O	7.65	5.96	9.23	10.64	7.15	8.99	9.23	10.83	8.47	13.82	6.64	3.09	5.75	2.86	2.21	1.53
Na_2O	6.33	7.32	5.22	4.72	6.41	5.41	4.95	4.02	5.18	2.15	7.04	9.35	7.57	9.47	10.23	10.37
Fe_2O_3	0.93	0.96	0.93	0.85	0.94	0.84	0.93	0.85	0.83	0.83	0.77	0.89	0.77	0.76	0.73	0.84
CaO	0.03	0.03	0.01	0.01	0.02	0.01	-	-	0.02	-	0.01	0.01	0.03	0.02	0.02	0.02
Rb_2O	-	0.07	-	0.06	0.03	0.01	0.03	0.06	0.05	0.02	-	-	0.05	-	-	-
BaO	0.03	-	-	0.01	-	0.01	-	0.01	0.01	0.01	-	0.02	0.03	-	-	-
PbO	0.01	-	-	0.02	0.03	-	-	0.02	0.01	0.03	-	0.04	0.03	-	0.02	0.04
Total	99.75	99.08	99.03	100.57	99.45	100.10	99.37	99.25	98.85	99.51	99.39	99.29	99.07	98.71	99.26	98.51
X_{Or}	0.44	0.35	0.54	0.60	0.42	0.52	0.55	0.64	0.52	0.81	0.38	0.18	0.33	0.17	0.12	0.09

Table 6-2: Perthitic alkali feldspar microprobe analyses (continued)

Unit	Transsolvus granite (3/4)															
Sample	204720	204720	204720	204720	204720	204720	204715	204715	204715	204715	204715	204715	204715	204715	204715	204715
Grain/line	gr3-line7	gr3-line8	gr3-line9	gr3-line10	gr3-line11	gr3-line12	gr1-line1	gr1-line2	gr1-line3	gr1-line4	gr1-line5	gr1-line6	gr2-line1	gr2-line2	gr2-line3	gr2-line4
(wt. %)																
SiO_2	65.60	66.60	66.88	66.65	67.29	66.05	65.67	65.94	65.76	65.37	65.88	65.38	66.51	66.20	66.67	65.55
Al_2O_3	17.71	18.17	18.46	18.21	17.99	17.81	17.76	17.76	17.86	17.67	17.75	17.58	17.87	17.89	17.92	17.58
K_2O	10.42	4.74	4.95	5.12	6.64	11.12	10.48	10.65	11.56	12.60	10.07	12.08	10.43	7.53	6.59	11.44
Na_2O	3.91	7.98	8.53	7.85	7.34	3.89	4.14	4.38	3.93	2.68	4.69	2.90	4.61	6.29	6.56	3.89
Fe_2O_3	0.84	0.74	0.73	0.91	0.79	0.76	0.85	0.82	0.91	0.83	0.82	0.74	0.87	0.84	1.20	0.88
CaO	0.02	0.05	0.01	0.02	-	0.04	0.05	0.01	0.02	0.01	-	0.03	0.02	-	0.05	0.10
Rb_2O	0.13	-	-	-	-	0.05	0.20	0.06	0.05	0.15	0.01	0.17	0.11	-	0.05	0.05
BaO	0.02	-	0.03	0.04	0.01	0.01	-	-	-	-	-	0.05	-	-	-	-
PbO	0.02	0.01	0.02	-	-	0.03	0.01	-	-	0.04	-	0.02	0.02	0.03	0.02	-
Total	98.66	98.29	99.61	98.80	100.06	99.76	99.16	99.61	100.08	99.34	99.23	98.95	100.43	98.79	99.05	99.50
X_{Or}	0.64	0.28	0.28	0.30	0.37	0.65	0.62	0.62	0.66	0.76	0.59	0.73	0.60	0.44	0.40	0.66

Unit	Transsolvus granite (4/4)											
Sample	204715	204715	204715	204713	204713	204713	204713	204713	204713	204713		
Grain/line	gr2-line5	gr2-line6	gr2-line7	gr1	gr2	gr3	gr4	gr5	gr6	gr7	Mdn	MAD
(wt. %)												
SiO_2	66.27	66.78	64.83	64.88	67.52	67.46	65.98	66.27	64.91	65.44	66.27	0.55
Al_2O_3	17.66	18.05	17.68	17.39	18.37	18.21	17.90	17.98	17.71	17.69	17.86	0.19
K_2O	11.04	8.82	9.69	14.90	9.28	11.78	11.17	14.72	13.17	13.17	9.11	2.04
Na_2O	4.11	5.84	4.60	1.02	5.57	3.77	3.95	1.35	2.28	2.26	5.29	1.36
Fe_2O_3	0.92	0.86	0.82	0.77	0.41	0.60	0.52	0.82	0.67	0.60	0.83	0.06
CaO	0.05	0.03	0.02	0.02	0.04	0.01	0.03	0.01	0.06	0.08	0.02	0.01
Rb_2O	0.03	0.06	0.14	0.11	-	0.07	-	0.25	0.08	0.07	0.03	0.03
BaO	0.04	0.03	-	0.05	-	-	-	0.04	-	-	-	-
PbO	-	-	0.01	-	-	0.02	-	0.02	0.06	0.04	0.01	0.01
Total	100.09	100.46	97.79	99.14	101.19	101.92	99.54	101.45	98.94	99.35	99.25	0.31
X_{Or}	0.64	0.50	0.58	0.91	0.52	0.67	0.65	0.88	0.79	0.79	52	12

Table 6-2: Perthitic alkali feldspar microprobe analyses (continued)

Unit	Enclaves (1/2)															
Sample	204712	204712	204712	204712	204712	204712	204712	204712	204712	204712	204712	204712	204712	204712	204712	204712
Grain/line	gr1-1	gr1-2	gr1-3	gr1-4	gr2-1	gr2-2	gr2-3	gr2-4	gr2-5	gr3-line1	gr3-line2	gr3-line3	gr3-line4	gr3-line5	gr3-line6	gr4-1
(wt. %)																
SiO_2	66.44	64.87	65.96	66.78	66.98	66.31	66.23	65.57	65.65	66.57	66.30	67.65	67.24	67.51	66.75	65.64
Al_2O_3	18.11	17.47	18.32	18.19	17.32	17.86	17.86	17.95	17.85	17.82	17.76	18.01	18.14	17.87	17.91	17.61
K_2O	7.20	11.23	8.37	8.55	10.40	7.14	10.02	12.58	12.58	8.72	7.36	1.83	4.27	1.86	5.07	13.56
Na_2O	6.36	3.87	5.89	5.82	4.62	6.56	4.89	2.86	3.00	6.11	6.37	10.01	8.41	9.87	7.72	2.33
Fe_2O_3	0.62	0.50	0.53	0.56	0.58	0.59	0.48	0.69	0.58	0.79	0.69	0.80	0.79	0.79	0.67	0.56
CaO	0.08	0.60	0.07	0.41	0.05	0.10	0.06	0.06	0.08	0.05	0.09	0.06	0.12	0.09	0.07	0.03
Rb_2O	0.09	0.09	0.06	-	-	0.06	0.01	0.12	0.08	-	0.10	-	0.12	-	0.02	0.16
BaO	0.03	0.02	0.03	0.02	-	-	-	0.08	0.01	-	-	0.05	-	-	-	-
PbO	0.02	-	-	-	-	-	-	-	-	0.01	-	0.02	0.03	-	-	-
Total	98.93	98.65	99.22	100.32	99.96	98.61	99.54	99.91	99.82	100.06	98.67	98.41	99.12	97.99	98.22	99.89
X_{Or}	0.43	0.66	0.48	0.49	0.60	0.42	0.57	0.74	0.73	0.48	0.43	0.11	0.25	0.11	0.30	0.79

Unit	Enclaves (2/2)					Dark porphyritic granite (1/1)										
Sample	204712	204712	204712			10036	10036	10036	10036	10036	10036	10036	10036	10036		
Grain/line	gr4-2	gr4-3	gr4-4	Mdn	MAD	gr1-1	gr1-2	gr1-3	gr1-4	gr1-5	gr1-6	gr2-1	gr2-2	gr2-3	Mdn	MAD
(wt. %)																
SiO_2	65.66	65.72	67.11	66.31	0.65	66.28	66.85	66.69	66.60	67.31	66.61	66.34	66.55	65.25	66.60	0.25
Al_2O_3	17.70	17.46	17.79	17.86	0.15	17.92	18.13	17.96	18.35	18.04	17.98	17.79	17.96	17.77	17.96	0.08
K_2O	12.90	13.93	10.76	8.72	2.52	6.68	7.60	8.37	8.13	5.80	7.65	9.28	7.47	12.37	7.65	0.71
Na_2O	2.65	2.12	4.27	5.82	1.91	6.87	6.17	5.77	6.12	7.44	6.23	5.34	6.30	3.41	6.17	0.40
Fe_2O_3	0.53	0.62	0.53	0.59	0.06	0.79	0.67	0.65	0.64	0.67	0.75	0.78	0.77	0.70	0.70	0.06
CaO	0.21	0.08	0.05	0.08	0.02	0.02	0.05	-	0.04	0.03	-	0.03	0.02	0.01	0.02	0.01
Rb_2O	0.17	0.13	0.05	0.06	0.06	0.01	0.04	-	-	-	-	0.07	0.08	0.01	0.01	0.01
BaO	-	0.02	-	-	-	-	-	0.02	0.01	-	-	0.04	0.04	-	-	-
PbO	-	-	-	-	-	-	0.02	0.01	-	-	-	0.02	-	0.03	-	-
Total	99.81	100.09	100.57	99.54	0.55	98.56	99.53	99.47	99.88	99.29	99.23	99.68	99.17	99.55	99.41	0.20
X_{Or}	0.76	0.81	0.62	0.49	0.16	0.39	0.45	0.49	0.47	0.34	0.45	0.53	0.44	0.70	0.45	0.04

Table 6-3: Perthitic alkali feldspar LA-ICP-MS analyses

Unit	Hypersolvus granite south*															
Sample	204768-line1	204768-line2	204768-line3	204768-line4	204771-line1	204771-line2	204771-line3	204771-line4	204771-line5	204771-line6	204771-line7	10017-line1	10017-line2	10017-line3	Mdn	MAD
(ppm)																
Sc	23.6	24.2	24.4	23.3	21.5	21.2	21.8	21.0	21.2	21.7	21.4	25.6	26.1	25.6	22.5	1.3
Ti	79.1	54.0	25.9	48.9	17.8	19.2	18.0	30.2	37.5	14.0	24.6	69.6	50.2	46.0	33.9	15.5
Zn	18.4	16.3	14.5	15.1	10.1	15.1	7.7	34.4	27.8	3.6	23.3	11.4	11.0	14.1	14.8	3.7
Ga	70.7	61.9	63.3	73.6	67.1	76.9	78.5	89.3	87.5	55.7	84.2	74.7	70.3	54.5	72.2	7.6
Rb	535	527	585	539	538	354	449	518	394	730	432	430	352	706	523	82
Sr	4.2	3.0	1.4	2.1	1.9	0.74	2.3	0.33	0.45	14.1	0.6	7.8	7.7	2.6	2.2	1.5
Zr	24.4	17.1	12.8	12.7	8.2	7.3	5.5	14.9	23.9	5.6	17.8	37.6	68.1	40.1	16.0	8.2
Nb	6.4	5.3	4.3	12.9	2.3	2.3	3.2	2.1	3.2	0.7	8.6	9.9	7.7	8.4	4.8	2.6
Ba	14.0	15.1	17.5	13.5	14.5	12.2	9.9	7.7	7.2	28.7	9.5	13.3	36.4	129.0	13.7	3.8
La	0.7	0.7	0.3	2.0	0.6	0.4	0.8	0.3	0.3	1.6	0.5	2.3	1.8	1.6	0.7	0.4
Ce	3.1	7.4	9.2	4.0	1.9	1.0	2.5	1.1	1.3	3.2	2.0	5.6	5.5	6.2	3.2	2.0
Pr	0.4	0.4	0.2	0.7	0.3	0.2	0.4	0.1	0.2	0.3	0.3	0.8	0.8	0.8	0.3	0.2
Nd	1.8	3.1	2.9	3.2	1.5	0.7	1.9	0.7	0.9	1.8	1.4	4.2	3.5	3.6	1.9	1.1
Sm	0.51	0.56	0.24	1.01	0.70	0.34	0.88	0.26	0.37	0.43	0.41	1.18	1.12	1.13	0.54	0.24
Eu	0.11	0.09	0.04	0.09	0.12	0.04	0.16	0.03	0.04	0.95	0.05	0.14	0.15	0.14	0.10	0.05
Gd	0.62	0.69	0.35	1.3	0.78	0.47	1.0	0.31	0.36	0.48	0.44	1.3	1.3	1.4	0.66	0.30
Tb	0.20	0.18	0.09	0.21	0.18	0.11	0.23	0.07	0.09	0.12	0.10	0.26	0.29	0.29	0.18	0.07
Dy	1.1	1.1	0.63	1.3	1.0	0.57	1.4	0.40	0.52	0.91	0.62	1.5	1.9	2.1	1.0	0.4
Ho	0.36	0.26	0.16	0.33	0.25	0.15	0.34	0.11	0.14	0.23	0.15	0.35	0.52	0.52	0.25	0.10
Er	0.93	0.74	0.45	0.72	0.60	0.37	0.78	0.32	0.41	0.68	0.37	0.81	1.2	1.0	0.70	0.24
Tm	0.20	0.13	0.07	0.11	0.10	0.06	0.12	0.08	0.08	0.10	0.07	0.11	0.17	0.16	0.11	0.03
Yb	0.78	0.67	0.35	0.49	0.46	0.36	0.42	0.72	0.47	0.48	0.39	0.50	0.82	0.73	0.48	0.11
Y	5.9	5.4	3.2	7.1	4.8	2.9	7.4	1.9	2.7	7.5	3.0	7.6	8.9	8.0	5.6	2.2
Lu	0.12	0.08	0.04	0.05	0.05	0.04	0.05	0.12	0.07	0.04	0.06	0.06	0.10	0.08	0.06	0.01
Pb	50.0	23.9	9.2	10.4	33.4	30.2	39.2	20.5	19.6	18.5	28.1	8.6	9.1	9.9	20.1	10.2
Th	2.4	2.8	1.6	0.5	2.6	1.6	2.1	1.4	1.1	1.2	2.3	4.0	3.9	3.7	2.2	0.7
U	0.51	0.29	0.20	0.17	0.26	0.19	0.27	0.20	0.20	0.22	0.30	0.28	0.45	0.58	0.26	0.06
REE+Y	16.6	21.4	18.2	22.5	13.3	7.7	18.3	6.4	7.8	18.7	9.8	26.6	28.0	27.6	15.7	7.4

*Hypersolvus granite south in this table stands for the fine grained samples of the southern hypersolvus granite

Table 6-3: Perthitic alkali feldspar LA-ICP-MS analyses (continued)

Unit	Hypersolvus granite north																
Sample	204756-line1	204756-line2	204756-line3	204756-line4	204756-line5	204756-line6	204756-line7	204756-line8	10040-line1	10040-line2	10040-line3	10040-line4	10040-line5	10040-line6	10040-line7	Mdn	MAD
(ppm)																	
Sc	23.2	23.5	23.5	22.9	23.0	22.8	22.8	22.7	20.2	20.1	20.9	19.7	20.0	19.6	20.4	22.7	0.8
Ti	21.7	15.1	5.5	4.7	9.0	10.4	9.7	22.8	6.6	13.3	10.3	1.6	26.0	22.7	22.6	10.4	4.8
Zn	51.7	47.3	37.7	33.2	33.3	44.4	35.8	46.1	26.0	19.4	26.0	18.1	31.4	37.1	38.2	35.8	8.6
Ga	93.3	93.5	96.0	95.8	95.8	93.9	94.8	87.6	78.8	62.1	64.9	78.9	57.5	54.5	59.9	87.6	8.4
Rb	746	908	749	751	710	638	848	785	983	926	1020	779	1234	861	899	848	97
Sr	0.23	0.27	0.37	0.32	0.56	0.50	0.28	0.28	2.2	1.0	0.63	1.4	1.0	1.1	0.94	0.56	0.30
Zr	89.3	77.0	7.5	6.2	31.3	38.9	32.3	55.2	9.0	106	12.5	4.0	37.5	101	23.9	32.3	23.3
Nb	20.4	28.2	1.6	0.6	5.0	10.3	6.8	21.6	3.8	7.4	6.0	0.7	31.8	7.7	3.5	6.8	3.5
Ba	45.0	59.0	41.2	40.7	42.6	43.4	46.9	51.5	38.8	28.2	38.5	15.3	62.4	61.5	86.0	43.4	4.9
La	6.0	5.4	7.9	4.3	8.2	6.2	6.2	3.5	3.9	8.4	4.1	5.2	7.3	3.7	6.3	6.0	1.6
Ce	22.9	18.1	27.4	14.2	22.8	17.5	18.3	12.5	8.2	23.5	10.3	8.6	17.6	9.1	18.5	17.6	5.2
Pr	2.1	1.9	3.2	1.7	2.5	2.0	2.2	1.3	0.7	3.4	1.0	0.9	2.0	1.2	2.6	2.0	0.6
Nd	10.6	8.8	14.6	7.8	12.3	9.1	10.1	6.1	3.9	11.3	5.9	4.0	9.1	4.9	9.7	9.1	2.2
Sm	1.6	1.5	2.7	1.4	2.0	1.5	1.9	1.1	0.52	2.5	0.91	0.38	1.1	1.2	1.5	1.5	0.4
Eu	0.10	0.10	0.19	0.10	0.14	0.10	0.13	0.07	0.03	0.13	0.05	0.02	0.08	0.14	0.17	0.10	0.03
Gd	1.5	1.4	2.4	1.3	1.8	1.4	1.7	0.88	0.40	11.0	1.0	0.33	0.94	1.4	2.2	1.4	0.4
Tb	0.34	0.40	0.58	0.32	0.40	0.36	0.43	0.27	0.12	0.49	0.23	0.07	0.19	0.42	0.39	0.36	0.07
Dy	2.7	4.4	3.7	2.1	2.7	2.6	3.3	2.3	0.67	2.8	1.8	0.36	1.2	4.3	3.4	2.7	0.7
Ho	1.01	1.28	0.99	0.58	0.80	0.89	1.15	0.75	0.15	1.35	0.42	0.09	0.33	0.65	0.92	0.80	0.22
Er	3.4	5.5	2.9	1.7	2.7	3.7	4.4	3.5	0.43	2.1	1.3	0.28	1.0	3.4	2.6	2.7	0.9
Tm	0.81	1.33	0.52	0.30	0.54	1.01	1.05	0.96	0.09	0.45	0.14	0.06	0.25	0.61	0.40	0.52	0.29
Yb	5.4	7.2	2.6	1.5	3.3	6.9	6.1	6.5	0.5	1.3	0.5	0.3	1.5	3.1	2.1	2.6	2.0
Y	9.5	15.0	11.9	7.7	12.1	10.4	13.0	8.1	3.5	16.9	9.3	2.5	6.7	11.2	13.2	10.4	2.6
Lu	0.76	0.77	0.30	0.17	0.45	0.98	0.75	0.94	0.06	0.20	0.06	0.03	0.24	0.43	0.27	0.30	0.23
Pb	36.0	42.8	62.0	48.0	56.8	55.0	62.2	33.8	3.2	7.5	3.3	2.5	16.9	10.3	8.4	33.8	23.5
Th	13.1	22.2	8.2	7.3	11.5	22.3	14.6	22.2	1.6	1.7	0.5	0.9	27.3	5.5	2.4	8.2	6.5
U	0.82	1.22	0.42	0.32	0.37	0.61	0.57	0.88	0.27	0.61	0.26	0.16	1.22	0.86	0.27	0.57	0.29
REE+Y	67.7	72.2	81.5	44.9	72.2	63.7	70.1	47.8	23.2	85.6	37.1	23.1	49.2	45.2	63.9	57.5	17.3

Table 6-3: Perthitic alkali feldspar LA-ICP-MS analyses (continued)

Unit	Transsolvus granite																
Sample	204743 -line1	204743 -line2	204743 -line3	204743 -line4	204743 -line5	204743 -line6	10039-line	204713 -line1	204713 -line2	204715 -line1	204715 -line2	204715 -line3	204715 -line4	204715 -line5	204715 -line6	204715 -line7	204715 -line8
(ppm)																	
Sc	25.3	25.0	25.3	25.0	25.2	24.8	22.9	15.7	15.8	22.1	21.0	21.6	21.3	20.9	20.5	19.7	20.0
Ti	7.7	8.9	19.9	23.2	37.3	19.5	28.0	93.0	10.1	10.3	22.4	17.7	12.1	11.3	7.6	19.7	14.5
Zn	78.6	65.8	55.3	35.1	65.7	46.3	198	820	222	141	116	151	142	72.8	173	180	153
Ga	98.4	98.9	64.7	60.5	65.6	60.3	110	97.5	102.7	85.1	79.5	86.7	81.2	85.7	85.4	83.4	86.5
Rb	1431	1520	1703	1854	1677	1683	1935	3176	2548	3120	3160	2154	2480	3220	1682	1765	2650
Sr	0.68	0.63	0.82	1.4	0.89	1.6	0.78	3.5	0.51	3.4	11.4	13.4	2.1	5.9	1.2	1.2	0.87
Zr	100	77.0	128	90.0	46.0	26.3	52.6	109	23.6	1120	15.7	1060	32.5	67.0	30.1	82.0	35.0
Nb	17.8	32.0	30.1	32.5	25.0	10.8	35.2	49.0	18.9	13.1	250.0	49.3	19.8	22.8	8.0	33.7	12.6
Ba	39.0	44.7	74.0	85.9	88.8	74.5	30.7	7.5	6.4	20.4	29.0	18.5	14.8	17.1	10.7	16.6	14.4
La	5.9	8.8	7.5	17.9	8.4	11.3	18.6	9.6	13.2	24.6	27.0	25.4	19.0	23.6	17.4	26.3	29.0
Ce	17.0	27.1	25.2	29.9	22.6	34.0	53.3	9.7	14.1	22.9	43.0	19.7	13.0	28.0	18.5	39.4	30.1
Pr	1.8	2.8	2.7	3.3	2.5	3.7	4.7	1.9	2.7	3.4	4.6	4.3	2.9	4.3	3.4	6.3	4.6
Nd	8.2	12.9	12.4	19.2	10.0	16.5	23.3	9.5	13.4	17.8	23.1	19.2	10.6	20.5	15.3	30.8	20.9
Sm	1.7	2.2	3.0	3.1	1.5	3.5	3.9	2.6	3.8	3.8	2.3	5.0	2.4	3.7	3.2	7.7	3.0
Eu	0.12	0.14	0.24	0.24	0.16	0.25	0.24	0.19	0.28	0.25	0.17	1.02	0.18	0.23	0.24	0.56	0.21
Gd	1.9	2.6	3.8	3.6	1.9	3.0	3.9	3.5	5.6	4.6	4.7	6.4	3.0	4.3	4.9	11.2	3.6
Tb	0.72	0.76	1.32	1.25	0.46	1.13	0.80	0.70	1.31	0.97	0.65	1.34	0.60	0.68	1.13	2.82	0.78
Dy	5.4	5.5	11.0	9.8	2.9	8.2	4.5	5.7	10.2	8.3	5.6	10.3	5.0	5.8	9.6	22.8	6.0
Ho	1.66	1.7	3.3	2.8	1.1	2.9	1.0	1.3	2.3	1.7	1.4	2.3	1.2	1.3	2.4	5.6	1.4
Er	5.7	5.6	10.2	9.3	2.2	9.1	2.6	3.9	7.2	5.5	4.5	6.9	3.7	4.3	7.7	18.7	4.2
Tm	1.1	1.1	1.9	1.8	0.42	1.32	0.43	0.68	1.00	0.85	0.68	0.93	0.57	0.62	1.22	2.82	0.59
Yb	6.5	6.2	10.3	9.6	2.3	7.2	2.8	6.5	6.1	5.6	5.0	6.2	3.9	4.1	7.9	19.2	3.8
Y	27.0	26.0	48.0	44.2	11.8	38.6	24.9	50.7	82.6	55.7	47.5	80.0	37.2	41.6	72.8	179.0	42.5
Lu	0.87	0.80	1.31	1.3	0.30	0.95	0.33	0.95	0.68	0.70	0.59	0.73	0.52	0.49	0.96	2.20	0.43
Pb	22.6	61.0	42.1	51.7	35.4	13.5	96.0	58.8	90.0	25.8	34.1	75.0	14.6	49.7	36.0	53.0	19.8
Th	12.9	22.0	29.6	11.8	4.9	19.2	17.8	5.1	3.1	3.6	0.4	5.8	3.2	2.3	1.9	11.7	2.9
U	1.69	1.53	2.47	2.01	0.58	1.38	0.85	2.57	1.52	3.17	1.20	8.30	0.86	1.21	0.71	2.04	0.48
REE+Y	84.7	103	141	156	68.2	141	145	106	164	156	170	189	103	143	166	373	151

Table 6-3: Perthitic alkali feldspar LA-ICP-MS analyses (continued)

Unit	Transsolvus granite												
Sample	204715-line9	204720-line1	204720-line2	204720-line3	204720-line4	204720-line5	204720-line6	204720-line7	204720-line8	204720-line9	204720-line10	204720-line11	Mdn	MAD
(ppm)														
Sc	20.3	17.4	17.7	17.6	17.4	17.4	17.4	17.5	17.6	17.5	17.7	17.6	20.0	2.5
Ti	12.5	15.1	13.1	16.1	12.5	15.3	28.5	22.4	16.1	14.3	37.7	16.1	16.1	4.0
Zn	115.0	26.2	33.5	25.2	31.9	37.2	36.8	53.2	61.4	36.3	43.8	39.5	65.7	32.2
Ga	77.9	82.4	83.8	82.9	84.8	84.4	83.7	83.9	109.4	89.7	93.5	90.3	84.8	4.9
Rb	2895	1245	1008	1175	735	695	1076	1972	1880	2050	1766	1773	1773	381
Sr	3.4	0.87	0.87	0.69	0.68	0.89	0.64	0.66	0.34	0.38	0.45	0.61	0.87	0.33
Zr	68.0	35.2	41.9	11.2	61.2	35.9	48.0	85.0	219	74.0	260	101	67.0	32.0
Nb	5.9	11.6	7.7	6.2	6.4	14.7	12.0	43.6	46.6	12.5	28.3	20.5	19.8	10.3
Ba	25.0	18.9	19.7	16.1	13.3	20.2	16.8	25.9	19.6	29.1	20.9	20.2	20.2	5.7
La	21.7	40.2	21.7	27.1	28.6	35.8	23.2	28.9	36.0	28.3	21.2	28.1	23.2	5.3
Ce	19.1	70.1	39.1	42.4	53.4	62.4	45.9	48.3	71.9	56.5	49.0	57.1	34.0	14.3
Pr	4.4	9.4	5.1	5.9	6.5	8.1	5.7	6.0	6.9	6.6	5.4	6.1	4.6	1.4
Nd	18.6	49.7	28.2	28.4	35.8	43.2	30.9	32.5	39.5	33.9	31.4	34.9	20.9	8.5
Sm	5.2	8.6	5.0	4.8	5.8	7.4	5.3	5.1	5.5	5.2	4.8	4.8	3.9	1.2
Eu	0.41	0.43	0.26	0.25	0.27	0.39	0.27	0.27	0.29	0.26	0.27	0.25	0.25	0.02
Gd	8.1	8.3	4.6	4.6	5.8	7.2	5.0	5.1	5.5	5.1	5.1	4.8	4.7	1.0
Tb	1.87	1.41	0.80	0.78	0.89	1.24	0.83	0.92	0.93	0.87	0.80	0.76	0.87	0.18
Dy	17.4	9.7	5.7	5.4	6.1	8.9	5.9	7.0	6.9	5.9	5.8	5.2	6.0	1.0
Ho	4.3	2.1	1.2	1.1	1.3	1.9	1.3	1.6	1.6	1.3	1.2	1.1	1.6	0.4
Er	13.8	7.0	4.1	3.6	4.1	6.3	4.1	5.4	6.0	3.8	4.0	3.5	5.4	1.6
Tm	2.04	1.19	0.71	0.59	0.68	1.06	0.71	0.90	1.04	0.56	0.61	0.51	0.85	0.24
Yb	13.0	9.3	5.5	4.4	4.9	8.0	5.3	6.0	7.7	3.5	4.3	3.5	6.0	1.7
Y	132.0	43.0	25.4	25.0	26.9	40.9	26.6	38.1	38.3	30.4	29.0	28.0	38.6	11.6
Lu	1.52	1.09	0.68	0.51	0.59	0.94	0.64	0.67	0.88	0.41	0.50	0.40	0.68	0.20
Pb	54.0	34.5	24.7	17.6	25.2	35.6	34.8	31.8	66.0	39.2	87.0	76.3	36.0	15.7
Th	1.5	2.6	2.1	1.2	1.7	3.3	1.6	12.5	10.7	3.7	5.7	4.5	3.7	2.1
U	0.59	1.26	0.82	0.56	0.72	1.26	0.78	1.32	1.99	0.77	1.39	0.95	1.26	0.48
REE+Y	262	260	147	154	181	233	161	186	228	182	163	179	151	48

Table 6-3: Perthitic alkali feldspar LA-ICP-MS analyses (continued)

Unit	Enclaves									Dark porphyritic granite					
Sample	204712-line1	204712-line2	204712-line3	204712-line4	204712-line5	204720-EN-line1	204720-EN-line2	Mdn	MAD	10036-line1	10036-line2	10036-line3	10036-line4	Mdn	MAD
(ppm)															
Sc	24.7	24.1	24.0	24.4	24.0	25.4	25.2	24.4	0.4	27.8	27.7	26.8	26.6	27.2	0.5
Ti	56.4	37.7	24.4	47.6	64.8	24.4	30.4	37.7	13.3	5.4	5.9	7.2	6.8	6.3	0.7
Zn	70.7	73.5	56.7	64.3	43.2	60.8	63.4	63.4	6.7	35.3	53.5	27.8	76.0	44.4	12.8
Ga	55.7	80.1	84.1	78.6	56.4	80.9	82.0	80.1	1.9	77.9	75.2	75.3	76.9	76.1	0.8
Rb	1430	1280	472	1496	1782	651	863	1280	417	657	684	688	797	686	16
Sr	5.1	4.3	3.8	5.7	8.4	0.41	0.46	4.3	1.4	2.2	0.9	2.4	1.2	1.7	0.6
Zr	284	86.5	122	165	92.0	73.8	118	118	31	1.5	1.9	10.4	14.9	6.1	4.4
Nb	31.7	16.8	9.0	18.7	19.3	17.3	26.5	18.7	1.9	0.6	0.7	2.2	2.4	1.5	0.8
Ba	105	8.7	4.5	6.6	61.9	11.0	13.1	11.0	4.4	21.6	29.2	33.0	32.9	31.0	1.9
La	28.3	34.9	58.9	42.4	21.0	21.6	47.0	34.9	12.1	1.5	1.8	1.2	1.8	1.6	0.1
Ce	44.3	49.4	69.1	55.1	44.0	56.4	97.7	55.1	10.8	5.2	6.1	3.8	5.7	5.5	0.4
Pr	6.0	7.0	11.1	8.6	5.5	5.9	10.9	7.0	1.5	1.0	1.2	0.7	1.0	1.0	0.1
Nd	26.2	29.1	44.6	35.6	23.6	27.4	51.2	29.1	5.5	5.0	6.2	3.4	5.3	5.1	0.6
Sm	3.3	3.6	5.3	4.7	4.9	3.8	6.8	4.7	0.9	1.4	2.1	1.2	1.6	1.5	0.2
Eu	0.38	0.19	0.24	0.28	0.64	0.25	0.38	0.28	0.09	0.09	0.15	0.09	0.12	0.11	0.02
Gd	3.0	2.9	4.6	4.4	4.6	3.5	6.3	4.4	0.9	1.5	2.2	1.4	1.8	1.6	0.2
Tb	0.50	0.47	0.58	0.78	0.96	0.66	1.07	0.66	0.16	0.32	0.48	0.30	0.41	0.36	0.05
Dy	2.4	2.5	2.8	4.2	5.3	3.7	5.6	3.7	1.2	1.9	3.0	1.8	2.7	2.3	0.4
Ho	0.55	0.71	0.60	0.88	1.21	0.94	1.50	0.88	0.28	0.49	0.76	0.45	0.71	0.60	0.13
Er	1.2	2.8	1.4	2.0	2.7	2.5	3.7	2.5	0.5	1.5	2.2	1.4	2.1	1.8	0.3
Tm	0.20	0.92	0.23	0.28	0.39	0.44	0.61	0.39	0.16	0.29	0.45	0.34	0.42	0.38	0.06
Yb	1.0	9.6	1.2	1.5	1.9	2.5	3.3	1.9	0.8	1.6	2.6	2.2	2.3	2.3	0.2
Y	14.7	19.7	17.1	23.1	27.3	18.8	33.5	19.7	3.4	9.9	12.0	8.6	12.5	11.0	1.3
Lu	0.14	1.48	0.15	0.22	0.25	0.36	0.52	0.25	0.11	0.20	0.32	0.33	0.31	0.32	0.01
Pb	25.7	16.1	18.4	24.4	15.6	77.6	92.1	24.4	8.3	78	106	67	63	72	8
Th	5.5	5.3	7.2	12.2	4.3	7.1	7.3	7.1	1.6	1.3	0.6	1.9	3.1	1.6	0.6
U	0.86	0.54	0.46	0.54	0.46	0.89	0.97	0.54	0.08	0.45	0.82	0.54	0.54	0.54	0.05
REE+Y	132	164	218	184	144	148	270	165	38	21.8	29.5	18.6	26.3	24.0	3.8

K-feldspar (microcline)

Table 6-4: K-feldspar (microcline) microprobe analyses

Unit	Transsolvus granite (1/2)																
Sample	204722_ 2Ksp	204722_ 5Ksp	204722_ 6Ksp	204722_ 15Ksp	204722_ 16Ksp	204720_ 7Ksp	204720_ 8Ksp	204720_ 9Ksp	204720_ 10Ksp	204720_ 15Ksp	204720_ 16Ksp	204715_ 1Ksp	204715_ 2Ksp	204715_ 5Ksp	204715_ 6Ksp	204715_ 7Ksp	204715_ 8Ksp
(wt. %)																	
SiO_2	64.01	64.61	65.13	64.83	65.45	64.84	64.78	64.77	64.82	65.12	65.02	63.92	64.98	65.11	64.76	64.58	64.75
Al_2O_3	18.19	17.91	17.81	18.52	17.44	17.81	17.37	17.69	17.66	18.13	17.91	17.60	17.95	17.65	17.57	17.35	17.36
Fe_2O_3	1.12	1.40	0.75	0.15	0.34	0.61	1.03	0.81	0.67	0.45	0.65	0.76	0.64	1.22	1.20	1.47	1.47
BaO	-	0.04	-	0.02	0.05	0.01	0.02	-	0.01	0.01	0.01	-	0.02	0.02	0.02	-	-
PbO	0.01	0.03	-	-	0.02	-	0.02	-	-	-	0.01	-	-	0.03	-	0.02	0.03
CaO	0.04	0.02	-	0.01	-	0.03	0.01	-	0.01	-	-	-	-	0.01	0.02	-	0.01
Na_2O	0.26	0.25	0.63	0.09	0.26	0.45	0.60	0.48	0.66	0.34	0.64	0.61	0.56	0.46	0.51	0.53	0.56
Rb_2O	0.23	0.28	0.21	0.28	0.31	0.22	0.19	0.22	0.15	0.17	0.18	0.27	0.25	0.36	0.32	0.30	0.35
K_2O	15.89	16.01	15.96	16.80	16.04	16.17	15.98	16.07	15.85	16.50	16.06	16.01	15.84	16.04	15.99	15.94	15.75
Total	99.7	100.5	100.5	100.7	99.9	100.1	100.0	100.1	99.8	100.7	100.5	99.2	100.2	100.9	100.4	100.2	100.3
Apfu (based on 8 oxygens)																	
Si	2.98	2.99	3.00	2.99	3.03	3.00	3.01	3.00	3.01	3.00	3.00	2.99	3.00	3.00	3.00	3.00	3.00
Al	1.00	0.98	0.97	1.01	0.95	0.97	0.95	0.97	0.97	0.98	0.97	0.97	0.98	0.96	0.96	0.95	0.95
Fe^{3+}	0.04	0.05	0.03	0.01	0.01	0.02	0.04	0.03	0.02	0.02	0.02	0.03	0.02	0.04	0.04	0.05	0.05
Na	0.02	0.02	0.06	0.01	0.02	0.04	0.05	0.04	0.06	0.03	0.06	0.06	0.05	0.04	0.05	0.05	0.05
Rb	0.01	0.02	0.01	0.02	0.02	0.01	0.01	0.01	0.01	0.01	0.01	0.01	0.01	0.02	0.02	0.02	0.02
K	0.94	0.94	0.94	0.99	0.95	0.96	0.95	0.95	0.94	0.97	0.95	0.96	0.93	0.94	0.94	0.94	0.93

Table 6-4: K-feldspar (microcline) microprobe analyses (continued)

Unit	Transsolvus granite (2/2)																	
Sample	204715_ 13Ksp	204715_ 14Ksp	204715_ 15Ksp	204715_ 16Ksp	204713_ 1Ksp	204713_ 2Ksp	204713_ 3Ksp	204713_ 4Ksp	204713_ 9Ksp	204713_ 10Ksp	204713_ 13Ksp	204713_ 15Ksp	204713_ 17Ksp	204713_ 18Ksp	204713_ 19Ksp	204713_ 20Ksp	Mdn	MAD
(wt. %)																		
SiO_2	64.83	64.81	64.63	64.75	64.57	64.85	64.85	64.92	64.81	64.92	64.83	64.62	65.10	65.05	64.63	64.72	64.82	0.10
Al_2O_3	17.77	17.78	17.88	17.89	17.50	17.44	17.67	17.58	17.43	17.72	17.90	17.84	17.86	17.66	17.64	17.71	17.71	0.15
Fe_2O_3	0.71	0.77	0.68	0.71	0.80	0.85	0.82	1.03	1.15	0.71	0.61	0.73	0.75	0.78	0.93	0.87	0.77	0.12
BaO	-	0.04	0.04	-	0.01	0.01	-	-	0.01	-	-	0.02	-	-	-	-	0.01	0.01
PbO	0.01	-	0.02	-	0.01	-	0.03	-	-	0.01	-	0.03	-	-	-	0.02	-	-
CaO	-	-	-	-	-	-	-	0.01	0.01	0.01	0.16	0.02	-	-	-	0.01	-	-
Na_2O	0.45	0.62	0.50	0.65	0.47	0.66	0.48	0.57	0.39	0.48	0.51	0.50	0.58	0.59	0.36	0.41	0.50	0.09
Rb_2O	0.19	0.22	0.27	0.18	0.31	0.19	0.34	0.24	0.36	0.30	0.25	0.24	0.27	0.24	0.35	0.34	0.25	0.05
K_2O	15.85	15.83	16.00	15.88	16.14	15.97	16.07	15.94	16.21	16.06	16.08	16.08	16.21	15.92	16.32	16.01	16.01	0.07
Total	99.8	100.1	100.0	100.1	99.8	100.0	100.3	100.3	100.4	100.2	100.3	100.1	100.8	100.2	100.2	100.1	100.1	0.17
Apfu (based on 8 oxygens)																		
Si	3.01	3.00	3.00	3.00	3.00	3.01	3.00	3.00	3.00	3.00	3.00	3.00	3.00	3.01	3.00	3.00	3.00	0.00
Al	0.97	0.97	0.98	0.98	0.96	0.95	0.96	0.96	0.95	0.97	0.98	0.98	0.97	0.96	0.96	0.97	0.97	0.01
Fe^{3+}	0.02	0.03	0.02	0.02	0.03	0.03	0.03	0.04	0.04	0.02	0.02	0.03	0.03	0.03	0.03	0.03	0.03	0.00
Na	0.04	0.06	0.04	0.06	0.04	0.06	0.04	0.05	0.03	0.04	0.05	0.05	0.05	0.05	0.03	0.04	0.05	0.01
Rb	0.01	0.01	0.01	0.01	0.02	0.01	0.02	0.01	0.02	0.02	0.01	0.01	0.01	0.01	0.02	0.02	0.01	0.00
K	0.94	0.94	0.95	0.94	0.96	0.95	0.95	0.94	0.96	0.95	0.95	0.95	0.95	0.94	0.97	0.95	0.95	0.01

Albite

Table 6-5: Albite microprobe analyses

Unit	Transsolvus granite (1/3)																		
Sample	204722 _3Ab	204722 _4Ab	204722 _7Ab	204722 _8Ab	204722 _9Ab	204722 _10Ab	204722 _11Ab	204722 _12Ab	204722 _13Ab	204722 _14Ab	204722 _17Ab	204722 _18Ab	204720 _11Ab	204720 _12Ab	204720 _13Ab	204720 _17Ab	204720 _18Ab	204715 _3Ab	204715 _4Ab
(wt. %)																			
SiO_2	68.42	68.94	68.82	68.74	68.64	68.47	65.52	68.40	68.80	68.51	68.65	69.04	68.27	68.33	68.01	68.64	67.87	68.48	68.59
Al_2O_3	18.78	19.02	19.65	19.66	18.89	19.05	18.12	19.25	19.22	18.78	18.98	19.46	18.69	18.86	18.60	19.02	18.98	19.11	18.88
Fe_2O_3	1.52	0.80	0.28	0.10	0.78	0.96	0.73	0.30	0.43	0.91	0.37	0.23	0.46	0.71	0.91	0.94	0.53	0.45	0.88
BaO	-	-	0.04	0.01	0.04	-	0.01	-	0.01	0.03	-	0.03	0.04	-	-	0.09	0.02	0.08	0.01
PbO	0.01	-	-	0.01	-	-	-	0.02	-	0.02	0.01	-	0.01	-	-	-	0.03	0.01	0.02
CaO	-	-	-	-	-	-	-	0.01	-	-	0.01	-	-	0.02	-	-	0.02	0.08	-
K_2O	0.08	0.09	0.04	0.02	0.10	0.11	0.12	0.06	0.08	0.14	0.07	0.09	0.13	0.16	0.08	0.08	0.10	0.08	0.11
Na_2O	11.72	11.65	11.79	11.76	11.78	11.76	11.47	11.76	11.77	11.66	11.71	11.69	11.82	11.56	11.67	11.66	11.62	11.60	11.79
Total	100.5	100.5	100.6	100.3	100.2	100.3	96.0	99.8	100.3	100.0	99.8	100.5	99.4	99.6	99.3	100.4	99.2	99.9	100.3
Apfu (based on 8 oxygens)																			
Si	2.99	3.00	2.99	2.99	3.00	2.99	2.99	3.00	3.00	3.00	3.01	3.00	3.01	3.00	3.00	2.99	3.00	3.00	3.00
Al	0.97	0.98	1.01	1.01	0.97	0.98	0.98	0.99	0.99	0.97	0.98	1.00	0.97	0.98	0.97	0.98	0.99	0.99	0.97
Fe^{3+}	0.05	0.03	0.01	-	0.03	0.03	0.03	0.01	0.01	0.03	0.01	0.01	0.02	0.02	0.03	0.03	0.02	0.01	0.03
Na	0.99	0.98	0.99	0.99	1.00	1.00	1.02	1.00	1.00	0.99	0.99	0.98	1.01	0.98	1.00	0.99	0.99	0.99	1.00
K	-	0.01	-	-	0.01	0.01	0.01	-	-	0.01	-	-	0.01	0.01	-	-	0.01	-	0.01

Table 6-5: Albite microprobe analyses (continued)

Unit	Transsolvus granite (2/3)																			
Sample	204715 _17Ab	204715 _18Ab	204715 _19Ab	204715 _20Ab	204713 _5Ab	204713 _6Ab	204713 _7Ab	204713 _8Ab	204713 _11Ab	204713 _12Ab	204713 _14Ab	204713 _16Ab	10035-2	10035-7	10035-9	10035-11	10035-12	10039-2	10039-4	10039-6
(wt. %)																				
SiO_2	68.34	68.38	68.64	68.26	68.01	68.58	68.30	68.28	70.55	68.16	68.26	68.35	68.27	67.87	67.20	68.17	68.28	69.85	69.03	68.36
Al_2O_3	18.88	18.91	18.76	18.88	18.71	18.87	18.14	18.72	18.53	18.89	18.70	18.93	19.91	19.98	20.19	20.17	20.07	20.33	20.45	20.81
Fe_2O_3	0.93	0.80	1.01	1.10	0.92	0.75	2.27	0.98	0.55	0.99	1.24	0.95	0.68	0.31	0.61	0.96	0.82	1.08	0.58	0.82
BaO	-	-	0.02	0.01	-	-	-	-	0.04	0.03	-	0.05	-	-	0.06	0.04	-	0.03	-	0.02
PbO	-	-	-	-	-	-	-	-	-	0.03	0.01	0.03	0.02	0.02	-	-	-	0.02	-	-
CaO	0.01	0.01	-	-	0.02	0.01	0.06	0.04	0.02	-	0.02	0.02	0.01	0.04	0.01	-	0.01	0.01	0.02	-
K_2O	0.11	0.13	0.09	0.09	0.09	0.10	0.08	0.09	0.08	0.08	0.08	0.18	0.15	0.07	0.09	0.11	0.22	0.14	0.06	0.12
Na_2O	11.64	11.78	11.62	11.66	11.51	11.87	11.32	11.61	11.29	11.71	11.68	11.71	11.54	11.59	11.67	11.57	11.52	11.59	11.63	11.70
Total	99.9	100.0	100.1	100.0	99.3	100.2	100.2	99.7	101.0	99.9	100.0	100.2	100.6	99.9	99.8	101.0	100.9	103.0	101.8	101.8
Apfu (based on 8 oxygens)																				
Si	3.00	3.00	3.00	2.99	3.00	3.00	3.00	3.00	3.04	2.99	2.99	2.99	2.97	2.97	2.95	2.96	2.96	2.97	2.97	2.94
Al	0.98	0.98	0.97	0.98	0.97	0.97	0.94	0.97	0.94	0.98	0.97	0.98	1.02	1.03	1.04	1.03	1.03	1.02	1.04	1.06
Fe^{3+}	0.03	0.03	0.03	0.04	0.03	0.02	0.07	0.03	0.02	0.03	0.04	0.03	0.02	0.01	0.02	0.03	0.03	0.03	0.02	0.03
Na	0.99	1.00	0.99	0.99	0.98	1.01	0.96	0.99	0.94	1.00	0.99	0.99	0.97	0.98	0.99	0.97	0.97	0.96	0.97	0.98
K	0.01	0.01	0.01	0.01	0.01	0.01	-	-	-	-	-	0.01	0.01	-	-	0.01	0.01	0.01	-	0.01

Table 6-5: Albite microprobe analyses (continued)

Unit	Transsolvus granite (3/3)																			
Sample	10039-7	10039-8	10039-10	10039-11	204764-4	204764-6	204764-8	204764-10	204764-12	WOC3-1	WOC3-2	WOC3-3	WOC3-4	WOC3-5	WOC3-6	WOC3-7	WOC3-8	WOC3-9	WOC3-10	Mdn	MAD
(wt. %)																				
SiO_2	69.93	70.38	68.74	68.66	66.48	67.08	69.93	71.30	60.91	72.60	66.78	71.06	71.02	71.41	70.63	70.51	72.94	71.09	72.21	68.54	0.38
Al_2O_3	20.35	20.66	21.23	20.76	18.16	21.25	19.68	20.25	24.24	20.84	20.25	21.32	20.88	21.14	19.59	20.94	20.31	22.11	20.80	19.35	0.65
Fe_2O_3	0.84	0.93	0.30	0.98	0.34	0.19	0.85	0.55	0.18	0.25	1.14	0.78	0.95	0.85	0.65	1.07	1.19	0.39	1.01	0.81	0.20
BaO	-	-	0.04	0.03	-	-	0.01	0.03	0.01	0.01	-	0.04	0.02	0.04	0.03	-	-	0.02	0.02	0.01	0.01
PbO	0.01	-	0.01	0.02	-	0.01	-	0.02	0.02	-	0.01	-	0.01	-	-	0.01	0.02	0.01	0.03	-	-
CaO	0.01	0.01	-	0.01	0.01	0.01	-	-	0.05	0.01	-	-	0.01	0.01	0.02	-	-	0.01	0.01	0.01	0.01
K_2O	0.13	0.10	0.13	0.14	0.08	0.08	0.11	0.09	0.06	0.01	0.11	0.13	0.09	0.11	0.12	0.15	0.12	0.10	0.11	0.10	0.02
Na_2O	11.70	11.61	11.91	11.74	11.02	11.65	11.41	11.52	9.72	10.97	10.93	11.63	11.43	11.57	10.41	11.47	10.67	11.59	10.51	11.63	0.09
Total	103.0	103.7	102.4	102.4	96.1	100.3	102.0	103.8	95.2	104.7	99.2	105.0	104.4	105.1	101.4	104.2	105.2	105.3	104.7	100.5	0.65
Apfu (based on 8 oxygens)																				
Si	2.97	2.97	2.94	2.94	3.02	2.93	3.00	3.00	2.79	3.01	2.95	2.96	2.97	2.97	3.02	2.96	3.02	2.95	3.00	2.99	0.01
Al	1.02	1.03	1.07	1.05	0.97	1.09	0.99	1.00	1.31	1.02	1.05	1.05	1.03	1.04	0.99	1.04	0.99	1.08	1.02	0.99	0.02
Fe^{3+}	0.03	0.03	0.01	0.03	0.01	0.01	0.03	0.02	0.01	0.01	0.04	0.02	0.03	0.03	0.02	0.03	0.04	0.01	0.03	0.03	0.01
Na	0.96	0.95	0.99	0.98	0.97	0.99	0.95	0.94	0.86	0.88	0.94	0.94	0.93	0.93	0.86	0.93	0.85	0.93	0.85	0.98	0.01
K	0.01	0.01	0.01	0.01	-	-	0.01	0.01	-	-	0.01	0.01	-	0.01	0.01	0.01	0.01	0.01	0.01	0.01	0.00

Zirconosilicate minerals and zircon

Table 6-6: Zirconosilicate minerals microprobe analyses

Mineral	Catapleiite						Elpidite (1/2)								
Unit	Hypersolvus granite south			TS			Hypersolvus granite south								
Sample	10032-6	10032-7	10032-8	204715-2	Mdn	MAD	10016-1	10016-2	10016-5	10016-6	10016-7	10016-8	10016-9	10016-10	204771-3
(wt.%)															
SiO_2	49.70	51.45	50.63	48.97	50.16	0.83	64.83	60.30	66.83	64.30	64.88	65.68	66.23	64.33	63.77
ZrO_2	31.25	31.26	32.08	29.82	31.25	0.42	19.16	18.64	19.59	19.07	19.35	19.40	19.87	19.56	20.65
Na_2O	1.66	2.20	2.35	4.29	2.27	0.34	0.91	1.77	4.43	3.95	5.02	4.06	5.09	4.30	3.47
CaO	1.70	2.19	2.26	4.14	2.22	0.28	0.01	-	0.03	-	0.01	0.02	0.03	0.01	0.11
K_2O	0.05	0.03	0.04	0.17	0.05	0.01	0.10	0.08	0.10	0.19	0.23	0.09	0.21	0.28	0.05
Al_2O_3	0.11	0.03	-	-	0.01	0.01	0.09	0.05	0.03	0.03	0.02	-	0.02	0.05	0.02
FeO	0.37	0.33	0.21	0.25	0.29	0.06	0.21	0.06	0.15	0.03	0.02	0.09	0.17	0.17	0.22
HfO_2	1.17	1.61	0.85	0.74	1.01	0.21	0.33	0.11	0.30	0.39	0.41	0.32	0.26	0.29	1.10
SnO_2	0.42	0.36	0.47	0.26	0.39	0.06	1.04	1.84	1.18	1.18	1.49	1.38	0.42	0.47	0.16
TiO_2	1.29	0.27	0.15	0.09	0.21	0.09	0.23	0.15	0.31	0.30	0.14	0.05	0.17	0.29	0.06
F	-	-	0.39	-	-	-	0.03	-	-	-	-	-	-	-	-
Total	87.72	89.72	89.27	88.71	88.99	0.50	86.93	83.01	92.94	89.43	91.57	91.07	92.46	89.75	89.61
Apfu (based on T-site = 3 apfu)							*Apfu (based on T-site = 6 apfu)*								
Si	3.00	3.00	3.00	3.00			6.00	6.00	6.00	6.00	6.00	6.00	6.00	6.00	6.00
Al	0.01	-	-	-			0.01	0.01	-	-	-	-	-	0.01	-
∑ *T-site*	3.00	3.00	3.00	3.00			6.00	6.00	6.00	6.00	6.00	6.00	6.00	6.00	6.00
Zr	0.92	0.89	0.93	0.89			0.86	0.90	0.86	0.87	0.87	0.86	0.88	0.89	0.95
Hf	0.02	0.03	0.01	0.01			0.01	-	0.01	0.01	0.01	0.01	0.01	0.01	0.03
Ti	0.06	0.01	0.01	-			0.02	0.01	0.02	0.02	0.01	-	0.01	0.02	-
Fe	0.02	0.02	0.01	0.01			0.02	0.01	0.01	-	-	0.01	0.01	0.01	0.02
Sn	0.01	0.01	0.01	0.01			0.04	0.07	0.04	0.04	0.05	0.05	0.02	0.02	0.01
∑ *Zr-site*	1.03	0.95	0.97	0.92			0.94	1.00	0.94	0.95	0.95	0.93	0.92	0.95	1.00
Na	0.19	0.25	0.27	0.51			0.16	0.34	0.77	0.71	0.90	0.72	0.89	0.78	0.63
Ca	0.11	0.14	0.14	0.27			-	-	-	-	-	-	-	-	0.01
K	-	-	-	0.01			0.01	0.01	0.01	0.02	0.03	0.01	0.02	0.03	0.01
∑*alkali*	0.31	0.39	0.42	0.79			0.18	0.35	0.79	0.74	0.93	0.73	0.92	0.81	0.65
F	-	0.07	-	-			0.01	-	-	-	-	-	-	-	-
H_2O	2.00	2.00	2.00	2.00			3.00	3.00	3.00	3.00	3.00	3.00	3.00	3.00	3.00
∑*anions*	2.00	2.07	2.00	2.00			3.01	3.00	3.00	3.00	3.00	3.00	3.00	3.00	3.00

Table 6-6: Zirconosilicate minerals microprobe analyses (continued)

Mineral	Elpidite (2/2)															
Unit	Hypersolvus granite south (cont.)						Hypersolvus granite north						Transsolvus granite			
Sample	204771-5	204771-7	204771-8	204771-10	10032-3	10032-5	10040-3	10040-4	10040-11	10040-12	10040-13	10040-14	WOC2-2	WOC2-9	Mdn	MAD
(wt.%)																
SiO_2	65.50	66.23	63.30	63.29	63.95	63.70	63.98	63.47	62.00	61.69	64.86	64.55	64.54	66.40	64.33	0.87
ZrO_2	19.90	19.47	19.71	19.73	20.11	20.79	20.71	20.20	19.67	20.15	21.07	21.37	18.72	19.44	19.71	0.40
Na_2O	3.35	2.91	2.93	3.40	2.30	2.37	2.82	2.30	2.00	3.14	3.17	2.81	2.96	3.07	3.07	0.70
CaO	0.06	0.06	0.10	0.04	0.24	0.07	0.31	0.48	1.04	0.21	0.16	0.14	0.02	0.04	0.06	0.05
K_2O	0.02	0.02	0.23	0.07	0.04	0.21	0.09	0.13	0.17	0.27	0.08	0.12	0.39	0.10	0.10	0.07
Al_2O_3	-	0.01	0.06	0.06	0.01	0.02	0.30	0.22	0.21	0.20	0.06	0.12	0.22	0.13	0.05	0.04
FeO	0.19	0.03	1.17	0.64	-	0.12	0.11	0.16	1.34	1.48	0.01	0.01	0.01	0.11	0.12	0.09
HfO_2	1.27	1.02	0.73	0.86	0.32	0.41	-	-	0.34	0.26	0.37	0.43	0.45	0.23	0.34	0.09
SnO_2	0.94	1.67	1.43	1.26	0.53	0.29	0.37	0.41	0.03	0.28	0.22	0.04	0.19	1.53	0.53	0.49
TiO_2	0.02	0.05	0.05	0.01	0.10	0.24	0.16	0.26	0.08	0.01	0.02	0.02	0.05	0.10	0.10	0.07
F	-	-	0.07	-	-	0.02	0.10	0.07	0.13	0.05	0.18	-	-	-	-	-
Total	91.25	91.46	89.75	89.35	87.60	88.21	88.89	87.66	86.96	87.71	90.11	89.61	87.55	91.15	89.61	1.64
Apfu (based on T-site = 6 apfu)																
Si	6.00	6.00	6.00	6.00	6.00	6.00	5.98	5.99	5.99	5.99	6.00	5.99	5.99	5.99		
Al	-	-	0.01	0.01	-	-	0.03	0.02	0.02	0.02	0.01	0.01	0.02	0.01		
∑ *T-site*	6.00	6.00	6.00	6.00	6.00	6.00	6.02	6.01	6.01	6.01	6.00	6.01	6.01	6.01		
Zr	0.89	0.86	0.91	0.91	0.92	0.95	0.94	0.93	0.93	0.95	0.95	0.97	0.85	0.86		
Hf	0.03	0.03	0.02	0.02	0.01	0.01	-	-	0.01	0.01	0.01	0.01	0.01	0.01		
Ti	-	-	-	-	0.01	0.02	0.01	0.02	0.01	-	-	-	-	0.01		
Fe	0.01	-	0.09	0.05	-	0.01	0.01	0.01	0.11	0.12	-	-	-	0.01		
Sn	0.03	0.06	0.05	0.05	0.02	0.01	0.01	0.02	-	0.01	0.01	-	0.01	0.05		
∑ *Zr-site*	0.97	0.95	1.08	1.03	0.96	1.00	0.98	0.98	1.05	1.09	0.97	0.98	0.87	0.93		
Na	0.59	0.51	0.54	0.62	0.42	0.43	0.51	0.42	0.37	0.59	0.57	0.51	0.53	0.54		
Ca	0.01	0.01	0.01	-	0.02	0.01	0.03	0.05	0.11	0.02	0.02	0.01	-	-		
K	-	-	0.03	0.01	-	0.02	0.01	0.02	0.02	0.03	0.01	0.01	0.05	0.01		
∑*alkali*	0.60	0.52	0.58	0.64	0.45	0.47	0.55	0.49	0.50	0.65	0.59	0.53	0.58	0.55		
F	-	-	0.02	-	-	-	0.03	0.02	0.04	0.02	0.05	-	-	-		
H_2O	3.00	3.00	3.00	3.00	3.00	3.00	3.00	3.00	3.00	3.00	3.00	3.00	3.00	3.00		
∑*anions*	3.00	3.00	3.02	3.00	3.00	3.00	3.03	3.02	3.04	3.02	3.05	3.00	3.00	3.00		

Table 6-6: Zirconosilicate minerals microprobe analyses (continued)

Mineral	Vlasovite (1/6)															
Unit	Hypersolvus granite north															
Sample	10011-1	10011-2	10011-3	10011-4	10011-5	10011-6	10011-7	10011-8	10011-9	10011-10	10011-11	10010-1	10010-2	10010-3	10010-4	10010-5
(wt. %)																
SiO_2	60.28	60.67	61.14	61.34	62.03	61.08	60.90	60.54	60.50	51.29	61.88	54.71	59.49	61.69	61.64	60.65
ZrO_2	28.90	28.05	29.18	29.17	29.17	29.07	28.62	29.66	29.13	29.40	28.63	27.30	26.98	29.01	28.58	28.45
Na_2O	6.53	6.17	7.72	4.63	7.74	5.54	5.96	6.62	8.58	5.47	6.67	10.24	10.95	8.36	3.85	3.84
CaO	0.02	0.02	-	-	0.02	0.05	-	0.02	0.03	0.01	0.04	-	0.03	0.01	-	0.03
K_2O	0.16	0.38	0.16	0.15	0.15	0.23	0.16	0.28	0.13	0.13	0.10	0.05	0.17	0.21	0.28	0.73
Al_2O_3	0.03	-	0.04	-	0.03	0.01	0.01	0.02	0.01	-	-	-	0.01	0.02	0.01	-
FeO	0.16	0.11	0.04	-	-	0.01	0.01	-	-	-	-	-	0.05	-	0.01	-
HfO_2	0.65	0.67	0.72	0.96	0.34	0.52	0.54	0.39	0.25	0.53	0.60	0.78	1.02	0.78	0.67	0.43
SnO_2	0.06	0.14	0.07	0.19	0.07	0.13	0.20	0.15	0.07	0.08	0.13	0.05	0.14	0.21	0.32	0.46
TiO_2	0.05	0.08	0.05	0.15	0.07	0.18	0.20	0.07	0.05	0.13	0.04	0.08	0.10	0.07	-	-
F	0.22	0.24	0.17	0.02	-	0.14	-	0.24	0.17	0.03	0.09	-	-	0.09	-	0.48
Total	96.98	96.43	99.22	96.60	99.62	96.89	96.60	97.88	98.83	87.05	98.16	93.20	98.94	100.42	95.34	94.88
Apfu (based on T-site = 4 apfu)																
Si	4.00	4.00	4.00	4.00	4.00	4.00	4.00	4.00	4.00	4.00	4.00	4.00	4.00	4.00	4.00	4.00
Al	-	-	-	-	-	-	-	-	-	-	-	-	-	-	-	-
∑ *T-site*	4.00	4.00	4.00	4.00	4.00	4.00	4.00	4.00	4.00	4.00	4.00	4.00	4.00	4.00	4.00	4.00
Zr	0.93	0.90	0.93	0.93	0.92	0.93	0.92	0.96	0.94	1.12	0.90	0.97	0.88	0.92	0.90	0.91
Hf	0.01	0.01	0.01	0.02	0.01	0.01	0.01	0.01	-	0.01	0.01	0.02	0.02	0.01	0.01	0.01
Ti	-	-	-	0.01	-	0.01	0.01	-	-	0.01	-	-	-	-	-	-
Fe	0.01	0.01	-	-	-	-	-	-	-	-	-	-	-	-	-	-
Sn	-	-	-	0.01	-	-	0.01	-	-	-	-	-	-	0.01	0.01	0.01
∑ *Zr-site*	0.96	0.93	0.95	0.96	0.93	0.95	0.94	0.97	0.95	1.14	0.92	1.00	0.92	0.94	0.93	0.94
Na	0.84	0.79	0.98	0.59	0.97	0.70	0.76	0.85	1.10	0.83	0.84	1.45	1.43	1.05	0.48	0.49
Ca	-	-	-	-	-	-	-	-	-	-	-	-	-	-	-	-
K	0.01	0.03	0.01	0.01	0.01	0.02	0.01	0.02	0.01	0.01	0.01	-	0.01	0.02	0.02	0.06
∑*alkali*	0.86	0.82	0.99	0.60	0.98	0.72	0.77	0.87	1.11	0.84	0.85	1.46	1.44	1.07	0.51	0.55
F	0.05	0.05	0.03	-	-	0.03	-	0.05	0.04	0.01	0.02	-	-	0.02	-	0.10
H_2O	-	-	-	-	-	-	-	-	-	-	-	-	-	-	-	-
∑*anions*	0.05	0.05	0.03	-	-	0.03	-	0.05	0.04	0.01	0.02	-	-	0.02	-	0.10

Table 6-6: Zirconosilicate minerals microprobe analyses (continued)

Mineral	Vlasovite (2/6)															
Unit	Hypersolvus granite north															
Sample	10010-6	10010-7	10010-8	10010-9	10010-10	10010-11	10010-12	10010-13	10010-14	10010-15	10010-16	10010-17	10010-18	10010-19	10010-20	10010-21
(wt. %)																
SiO_2	62.37	60.51	60.57	58.63	59.91	60.27	53.94	61.50	60.74	61.37	61.10	61.00	60.45	60.18	61.35	61.74
ZrO_2	28.50	27.98	28.46	28.28	27.86	27.96	28.22	28.47	28.16	29.11	28.24	27.86	28.61	28.71	28.74	28.91
Na_2O	4.76	10.86	7.24	10.27	11.42	10.68	12.66	10.53	10.86	9.55	9.01	10.32	6.78	9.92	8.41	8.87
CaO	0.01	0.02	0.01	0.01	-	0.01	0.01	0.01	0.02	-	-	-	0.36	-	-	-
K_2O	0.36	0.17	0.16	0.19	0.15	0.08	0.07	0.07	0.12	0.06	0.10	0.09	0.16	0.10	0.12	0.17
Al_2O_3	-	-	-	0.06	-	0.01	0.01	0.04	-	-	-	-	0.14	0.03	0.03	-
FeO	0.04	-	-	0.01	-	-	0.02	-	-	0.04	-	-	0.05	0.02	0.01	0.02
HfO_2	0.64	0.97	0.79	0.77	0.90	0.73	0.85	0.91	0.86	0.89	0.89	0.86	0.96	0.76	0.86	0.65
SnO_2	0.30	0.08	0.18	0.04	0.06	0.16	0.12	0.14	-	0.10	0.21	0.18	0.09	0.12	0.05	0.20
TiO_2	0.04	0.06	0.01	0.06	0.07	0.08	0.05	0.03	0.07	0.09	0.05	0.18	0.04	0.04	0.09	0.05
F	0.31	0.25	0.15	0.05	0.17	-	0.09	0.32	0.28	0.10	-	0.11	0.16	-	-	0.20
Total	97.21	100.80	97.51	98.35	100.46	99.98	96.01	101.87	101.00	101.26	99.60	100.56	97.73	99.87	99.67	100.71
Apfu (based on T-site = 4 apfu)																
Si	4.00	4.00	4.00	4.00	4.00	4.00	4.00	4.00	4.00	4.00	4.00	4.00	3.99	4.00	4.00	4.00
Al	-	-	-	0.01	-	-	-	-	-	-	-	-	0.01	-	-	-
∑ *T-site*	4.00	4.00	4.00	4.00	4.00	4.00	4.00	4.00	4.00	4.00	4.00	4.00	4.01	4.00	4.00	4.00
Zr	0.89	0.90	0.92	0.94	0.91	0.90	1.02	0.90	0.90	0.93	0.90	0.89	0.92	0.93	0.91	0.91
Hf	0.01	0.02	0.01	0.02	0.02	0.01	0.02	0.02	0.02	0.02	0.02	0.02	0.02	0.01	0.02	0.01
Ti	-	-	-	-	-	-	-	-	-	-	-	0.01	-	-	-	-
Fe	-	-	-	-	-	-	-	-	-	-	-	-	-	-	-	-
Sn	0.01	-	-	-	-	-	-	-	-	-	0.01	-	-	-	-	0.01
∑ *Zr-site*	0.91	0.93	0.94	0.96	0.93	0.93	1.05	0.92	0.92	0.95	0.93	0.92	0.95	0.95	0.94	0.93
Na	0.59	1.39	0.93	1.36	1.48	1.37	1.82	1.33	1.39	1.21	1.14	1.31	0.87	1.28	1.06	1.11
Ca	-	-	-	-	-	-	-	-	-	-	-	-	0.03	-	-	-
K	0.03	0.01	0.01	0.02	0.01	0.01	0.01	0.01	0.01	-	0.01	0.01	0.01	0.01	0.01	0.01
∑*alkali*	0.62	1.41	0.94	1.38	1.49	1.38	1.83	1.33	1.40	1.21	1.15	1.32	0.91	1.29	1.07	1.13
F	0.06	0.05	0.03	0.01	0.03	-	0.02	0.07	0.06	0.02	-	0.02	0.03	-	-	0.04
H_2O	-	-	-	-	-	-	-	-	-	-	-	-	-	-	-	-
∑*anions*	0.06	0.05	0.03	0.01	0.03	-	0.02	0.07	0.06	0.02	-	0.02	0.03	-	-	0.04

Table 6-6: Zirconosilicate minerals microprobe analyses (continued)

Mineral	Vlasovite (3/6)															
Unit	cont.	Dark porphyritic granite														
Sample	10010-22	10204-1	10204-2	10204-3	10204-4	10204-5	10204-6	10204-7	10201-1	10201-2	10201-3	10204-8	10204-11	10204-12	10204-13	10204-14
(wt. %)																
SiO_2	61.70	62.24	60.32	61.23	60.78	61.41	59.12	60.44	62.85	55.64	56.24	59.79	60.99	61.54	61.66	61.02
ZrO_2	27.84	28.74	28.54	28.57	27.82	28.60	27.07	28.47	28.17	28.39	28.00	28.51	28.52	27.93	28.53	28.36
Na_2O	9.66	8.26	8.12	11.40	10.82	11.24	10.68	8.25	11.33	10.12	9.54	11.84	6.33	6.25	8.44	8.73
CaO	0.01	-	0.01	-	0.01	0.02	0.03	0.02	-	-	0.02	0.02	-	-	-	-
K_2O	0.08	0.07	0.16	0.07	0.12	0.12	0.08	0.18	0.14	0.14	0.10	0.10	0.13	0.17	0.01	0.01
Al_2O_3	-	0.02	0.02	0.02	-	-	0.01	-	-	0.01	-	-	-	-	-	-
FeO	-	-	0.02	-	0.03	-	-	-	0.04	0.02	0.17	0.02	0.02	-	0.01	-
HfO_2	0.85	0.79	0.68	0.75	0.61	0.81	0.77	0.79	0.81	0.58	0.73	0.83	0.58	0.81	0.80	0.68
SnO_2	0.22	0.22	0.21	0.15	0.13	0.17	0.18	0.23	0.15	0.12	0.10	0.11	0.46	0.34	0.10	0.16
TiO_2	0.19	0.12	0.06	0.05	0.06	0.07	0.10	0.13	0.05	0.04	0.07	0.05	0.11	0.17	0.07	0.05
F	-	0.02	-	-	0.08	0.08	-	0.13	0.21	-	0.05	0.18	0.23	0.18	0.07	-
Total	100.52	100.46	98.14	102.24	100.42	102.49	98.04	98.58	103.66	95.06	94.98	101.38	97.27	97.33	99.66	99.01
Apfu (based on T-site = 4 apfu)																
Si	4.00	4.00	4.00	4.00	4.00	4.00	4.00	4.00	4.00	4.00	4.00	4.00	4.00	4.00	4.00	4.00
Al	-	-	-	-	-	-	-	-	-	-	-	-	-	-	-	-
∑ *T-site*	4.00	4.00	4.00	4.00	4.00	4.00	4.00	4.00	4.00	4.00	4.00	4.00	4.00	4.00	4.00	4.00
Zr	0.88	0.90	0.92	0.91	0.89	0.91	0.89	0.92	0.87	1.00	0.97	0.93	0.91	0.89	0.90	0.91
Hf	0.02	0.01	0.01	0.01	0.01	0.02	0.01	0.01	0.01	0.01	0.01	0.02	0.01	0.02	0.01	0.01
Ti	0.01	0.01	-	-	-	-	-	0.01	-	-	-	-	0.01	0.01	-	-
Fe	-	-	-	-	-	-	-	-	-	-	0.01	-	-	-	-	-
Sn	0.01	0.01	0.01	-	-	-	-	0.01	-	-	-	-	0.01	0.01	-	-
∑ *Zr-site*	0.91	0.93	0.95	0.93	0.91	0.93	0.92	0.95	0.90	1.01	1.00	0.95	0.94	0.92	0.92	0.93
Na	1.21	1.03	1.04	1.44	1.38	1.42	1.40	1.06	1.40	1.41	1.32	1.54	0.80	0.79	1.06	1.11
Ca	-	-	-	-	-	-	-	-	-	-	-	-	-	-	-	-
K	0.01	0.01	0.01	0.01	0.01	0.01	0.01	0.01	0.01	0.01	0.01	0.01	0.01	0.01	-	-
∑*alkali*	1.22	1.03	1.06	1.45	1.39	1.43	1.41	1.07	1.41	1.42	1.33	1.55	0.81	0.80	1.06	1.11
F	-	-	-	-	0.02	0.02	-	0.03	0.04	-	0.01	0.04	0.05	0.04	0.01	-
H_2O	-	-	-	-	-	-	-	-	-	-	-	-	-	-	-	-
∑*anions*	-	-	-	-	0.02	0.02	-	0.03	0.04	-	0.01	0.04	0.05	0.04	0.01	-

Table 6-6: Zirconosilicate minerals microprobe analyses (continued)

Mineral	Vlasovite (4/6)															
Unit	Dark porphyritic granite (cont.)				Transsolvus granite											
Sample	10204-15	10204-16	10204-17	10204-18	204715-1	204715-3	204715-4	204715-5	204715-6	204715-7	204715-8	204715-9	204715-10	204715-11	204722-1	204722-3
(wt. %)																
SiO_2	62.56	61.62	61.94	60.73	58.72	62.37	61.80	62.05	61.23	61.47	62.48	62.11	61.35	60.94	61.75	63.19
ZrO_2	28.78	28.50	29.15	28.34	28.01	28.53	28.91	27.99	28.56	29.19	28.96	28.46	29.05	29.12	29.11	29.44
Na_2O	7.33	8.03	7.76	7.86	13.45	8.62	7.01	9.31	10.44	8.29	8.23	8.52	9.92	7.34	5.70	7.96
CaO	-	0.03	0.02	-	0.02	0.03	-	-	-	0.01	0.03	0.03	0.01	0.68	0.07	0.16
K_2O	0.08	0.17	0.11	0.08	0.09	0.16	0.20	0.15	0.03	0.09	0.12	0.12	0.10	0.13	0.16	0.11
Al_2O_3	-	0.02	-	0.01	-	0.03	0.03	0.02	0.03	0.02	-	0.02	0.03	0.01	0.48	-
FeO	0.05	0.01	0.03	-	-	0.03	0.03	-	-	-	-	-	-	0.07	0.01	0.02
HfO_2	0.84	0.68	0.90	0.96	0.86	0.96	0.93	0.75	0.94	0.97	0.84	0.87	0.85	0.77	0.73	0.75
SnO_2	0.28	0.29	0.15	0.03	0.13	0.13	0.24	0.09	0.08	0.09	0.18	0.14	0.08	0.14	0.10	0.14
TiO_2	0.16	0.17	0.09	0.05	0.01	0.10	0.07	0.11	0.05	0.11	-	0.06	0.04	0.07	0.02	0.03
F	-	-	-	0.21	0.21	0.16	0.22	-	0.14	-	0.07	-	0.03	0.14	-	0.17
Total	100.09	99.51	100.15	98.18	101.41	101.04	99.35	100.48	101.42	100.25	100.89	100.33	101.45	99.35	98.13	101.89
Apfu (based on T-site = 4 apfu)																
Si	4.00	4.00	4.00	4.00	4.00	4.00	4.00	4.00	4.00	4.00	4.00	4.00	4.00	4.00	3.98	4.00
Al	-	-	-	-	-	-	-	-	-	-	-	-	-	-	0.04	-
∑ *T-site*	4.00	4.00	4.00	4.00	4.00	4.00	4.00	4.00	4.00	4.00	4.00	4.00	4.00	4.00	4.02	4.00
Zr	0.90	0.90	0.92	0.91	0.93	0.89	0.91	0.88	0.91	0.93	0.90	0.89	0.92	0.93	0.92	0.91
Hf	0.02	0.01	0.02	0.02	0.02	0.02	0.02	0.01	0.02	0.02	0.02	0.02	0.02	0.01	0.01	0.01
Ti	0.01	0.01	-	-	-	0.01	-	0.01	-	0.01	-	-	-	-	-	-
Fe	-	-	-	-	-	-	-	-	-	-	-	-	-	-	-	-
Sn	0.01	0.01	-	-	-	-	0.01	-	-	-	-	-	-	-	-	-
∑ *Zr-site*	0.93	0.93	0.94	0.93	0.95	0.92	0.94	0.90	0.93	0.95	0.92	0.92	0.94	0.96	0.93	0.93
Na	0.91	1.01	0.97	1.00	1.78	1.07	0.88	1.16	1.32	1.05	1.02	1.06	1.25	0.93	0.71	0.98
Ca	-	-	-	-	-	-	-	-	-	-	-	-	-	0.05	0.01	0.01
K	0.01	0.01	0.01	0.01	0.01	0.01	0.02	0.01	-	0.01	0.01	0.01	0.01	0.01	0.01	0.01
∑*alkali*	0.92	1.03	0.98	1.01	1.79	1.09	0.90	1.18	1.32	1.05	1.03	1.08	1.26	0.99	0.73	1.00
F	-	-	-	0.04	0.05	0.03	0.04	-	0.03	-	0.01	-	0.01	0.03	-	0.03
H_2O	-	-	-	-	-	-	-	-	-	-	-	-	-	-	-	-
∑*anions*	-	-	-	0.04	0.05	0.03	0.04	-	0.03	-	0.01	-	0.01	0.03	-	0.03

Table 6-6: Zirconosilicate minerals microprobe analyses (continued)

Mineral	Vlasovite (5/6)															
Unit	Transsolvus granite															
Sample	204722-4	204722-5	204722-6	204722-7	204722-8	204722-9	204722-10	204722-11	WOC2-4	WOC2-5	WOC2-6	WOC2-7	WOC2-10	WOC2-11	10034-1	10034-2
(wt. %)																
SiO_2	63.03	63.39	61.95	62.11	60.15	62.79	62.91	62.39	63.03	62.97	62.91	61.82	62.82	62.75	62.82	62.17
ZrO_2	29.61	28.79	29.28	29.63	27.65	29.50	28.85	28.02	28.91	29.06	29.03	29.02	29.57	29.65	28.19	29.15
Na_2O	6.46	9.52	7.49	5.99	7.88	6.63	7.92	5.50	5.84	5.88	6.90	7.02	5.16	6.26	5.42	7.15
CaO	-	0.01	0.03	0.01	0.01	-	-	0.47	-	-	-	0.04	0.04	0.01	0.02	-
K_2O	0.14	0.12	0.15	0.16	0.08	0.15	0.13	0.19	0.08	0.14	0.11	0.10	0.12	0.20	0.11	0.02
Al_2O_3	0.07	-	-	0.01	0.01	0.04	-	0.01	0.03	0.01	-	-	-	-	0.04	-
FeO	-	0.01	-	0.08	0.02	-	-	0.16	0.03	-	-	0.01	-	0.02	0.08	0.02
HfO_2	0.61	0.90	0.85	0.88	0.65	0.74	0.89	0.96	0.88	0.78	0.81	0.50	0.78	0.53	0.80	0.79
SnO_2	0.16	0.15	0.20	0.17	0.11	0.19	0.19	0.22	0.21	0.24	0.28	0.14	0.30	0.30	0.47	0.08
TiO_2	0.09	0.04	0.11	0.08	0.06	0.15	0.10	0.11	0.10	0.02	0.22	0.05	0.08	0.04	0.14	0.07
F	0.03	0.33	-	-	0.02	0.02	-	0.43	0.07	-	-	-	-	0.04	-	-
Total	100.18	103.11	100.06	99.12	96.62	100.19	101.00	98.26	99.15	99.10	100.26	98.70	98.87	99.76	98.09	99.44
Apfu (based on T-site = 4 apfu)																
Si	4.00	4.00	4.00	4.00	4.00	4.00	4.00	4.00	4.00	4.00	4.00	4.00	4.00	4.00	4.00	4.00
Al	0.01	-	-	-	-	-	-	-	-	-	-	-	-	-	-	-
∑ *T-site*	4.00	4.00	4.00	4.00	4.00	4.00	4.00	4.00	4.00	4.00	4.00	4.00	4.00	4.00	4.00	4.00
Zr	0.92	0.89	0.92	0.93	0.90	0.92	0.89	0.88	0.89	0.90	0.90	0.92	0.92	0.92	0.87	0.91
Hf	0.01	0.02	0.02	0.02	0.01	0.01	0.02	0.02	0.02	0.01	0.01	0.01	0.01	0.01	0.01	0.01
Ti	-	-	0.01	-	-	0.01	-	0.01	-	-	0.01	-	-	-	0.01	-
Fe	-	-	-	-	-	-	-	0.01	-	-	-	-	-	-	-	-
Sn	-	-	0.01	-	-	-	-	0.01	0.01	0.01	0.01	-	0.01	0.01	0.01	-
∑ *Zr-site*	0.93	0.91	0.95	0.96	0.92	0.94	0.92	0.91	0.92	0.92	0.93	0.93	0.94	0.94	0.91	0.94
Na	0.79	1.17	0.94	0.75	1.02	0.82	0.98	0.68	0.72	0.72	0.85	0.88	0.64	0.77	0.67	0.89
Ca	-	-	-	-	-	-	-	0.03	-	-	-	-	-	-	-	-
K	0.01	0.01	0.01	0.01	0.01	0.01	0.01	0.02	0.01	0.01	0.01	0.01	0.01	0.02	0.01	-
∑*alkali*	0.81	1.18	0.95	0.76	1.02	0.83	0.99	0.73	0.73	0.74	0.86	0.89	0.65	0.79	0.68	0.89
F	0.01	0.07	-	-	-	-	-	0.09	0.01	-	-	-	-	0.01	-	-
H_2O	-	-	-	-	-	-	-	-	-	-	-	-	-	-	-	-
∑*anions*	0.01	0.07	-	-	-	-	-	0.09	0.01	-	-	-	-	0.01	-	-

Table 6-6: Zirconosilicate minerals microprobe analyses (continued)

Mineral	Vlasovite (6/6)										
Unit	Transsolvus granite										
Sample	10034-3	10034-4	10034-5	10034-6	10034-7	10034-8	10034-9	10034-10	10034-11	Mdn	MAD
(wt. %)											
SiO_2	62.45	61.07	61.05	60.15	62.98	62.38	61.69	62.14	62.76	61.41	0.83
ZrO_2	29.72	29.04	28.59	29.58	29.40	29.48	29.17	29.38	29.55	28.63	0.44
Na_2O	6.72	2.84	2.12	1.75	5.63	4.96	5.13	4.46	5.02	7.86	1.69
CaO	0.01	0.01	0.01	0.02	-	0.02	-	-	0.01	0.01	0.01
K_2O	0.02	0.14	0.15	0.18	0.03	0.06	0.09	0.08	0.13	0.13	0.03
Al_2O_3	-	0.01	0.04	-	0.01	-	-	-	-	-	-
FeO	-	-	0.01	0.01	0.10	0.15	-	-	0.02	0.01	0.01
HfO_2	0.86	0.72	0.72	0.66	0.89	0.84	0.86	1.06	0.80	0.79	0.09
SnO_2	0.12	0.68	0.45	0.39	0.14	0.08	0.12	0.07	0.12	0.14	0.05
TiO_2	0.02	0.23	0.21	0.13	0.10	0.03	0.07	0.04	0.14	0.07	0.03
F	-	-	-	0.10	0.02	0.02	-	0.28	-	0.03	0.03
Total	99.93	94.72	93.34	92.93	99.28	97.99	97.13	97.39	98.55	99.28	1.24
Apfu (based on T-site = 4 apfu)											
Si	4.00	4.00	4.00	4.00	4.00	4.00	4.00	4.00	4.00		
Al	-	-	-	-	-	-	-	-	-		
∑ *T-site*	4.00	4.00	4.00	4.00	4.00	4.00	4.00	4.00	4.00		
Zr	0.93	0.93	0.91	0.96	0.91	0.92	0.92	0.92	0.92		
Hf	0.02	0.01	0.01	0.01	0.02	0.02	0.02	0.02	0.01		
Ti	-	0.01	0.01	0.01	-	-	-	-	0.01		
Fe	-	-	-	-	0.01	0.01	-	-	-		
Sn	-	0.02	0.01	0.01	-	-	-	-	-		
∑ *Zr-site*	0.95	0.97	0.95	0.99	0.94	0.95	0.94	0.95	0.94		
Na	0.83	0.36	0.27	0.23	0.69	0.62	0.65	0.56	0.62		
Ca	-	-	-	-	-	-	-	-	-		
K	-	0.01	0.01	0.02	-	-	0.01	0.01	0.01		
∑*alkali*	0.84	0.37	0.28	0.24	0.70	0.62	0.65	0.56	0.63		
F	-	-	-	0.02	-	-	-	0.06	-		
H_2O	-	-	-	-	-	-	-	-	-		
∑*anions*	-	-	-	0.02	-	-	-	0.06	-		

Table 6-7: Zircon microprobe analyses

Unit	Hypersolvus granite north													
Sample	10205-55	10205-56	10205-57	10205-60	10205-61	10205-62	10205-63-1	10205-64	10205-65	10205-65-1	10205-67	10205-68	10205-68-1	10205-69-1
(wt. %)														
SiO_2	32.46	32.29	32.53	32.28	32.17	32.44	32.47	32.43	32.56	32.82	32.81	32.84	32.61	32.64
ZrO_2	64.31	64.37	63.76	63.39	62.93	63.56	63.57	64.68	64.33	64.94	65.05	64.71	64.34	63.71
HfO_2	1.07	1.09	1.12	1.20	1.20	1.10	1.11	1.12	1.15	1.19	1.18	1.19	1.15	1.13
P_2O_5	0.15	0.20	0.18	0.12	0.33	0.17	0.17	0.17	0.27	0.15	0.10	0.18	0.20	0.21
CaO	-	0.02	0.03	0.03	0.06	0.01	0.03	0.03	0.03	0.02	0.06	-	0.02	-
Dy_2O_3	0.12	0.11	0.09	0.09	0.12	0.12	0.14	0.10	0.08	0.08	0.06	0.06	0.09	0.13
Er_2O_3	0.21	0.19	0.16	0.14	0.14	0.18	0.18	0.14	0.16	0.11	0.18	0.13	0.14	0.16
Yb_2O_3	0.23	0.23	0.24	0.11	0.19	0.25	0.21	0.13	0.13	0.16	0.22	0.21	0.16	0.25
Y_2O_3	1.22	1.23	1.14	0.94	1.17	1.47	1.41	1.16	1.11	1.01	1.00	1.10	1.13	1.35
Total	99.78	99.72	99.24	98.29	98.30	99.30	99.28	99.95	99.83	100.48	100.65	100.42	99.83	99.58
REE+Y-ox.	1.78	1.75	1.64	1.28	1.61	2.02	1.94	1.52	1.49	1.37	1.46	1.50	1.51	1.89
Apfu (based on 4 anions)														
Si	1.00	1.00	1.01	1.01	1.00	1.00	1.00	1.00	1.00	1.00	1.00	1.00	1.00	1.01
Zr	0.97	0.97	0.96	0.96	0.96	0.96	0.96	0.97	0.96	0.97	0.97	0.96	0.96	0.96
Hf	0.01	0.01	0.01	0.01	0.01	0.01	0.01	0.01	0.01	0.01	0.01	0.01	0.01	0.01
P	-	0.01	-	-	0.01	-	-	-	0.01	-	-	-	0.01	0.01
Y	0.02	0.02	0.02	0.02	0.02	0.02	0.02	0.02	0.02	0.02	0.02	0.02	0.02	0.02
Sum Zr	1.00	1.00	0.99	0.99	1.00	1.00	1.00	1.00	1.00	1.00	1.00	1.00	1.00	0.99

Table 6-7: Zircon microprobe analyses (continued)

Unit	Hypersolvus granite north						
Sample	10205-69-2	10205-70-1	10205-70-2	10205-71	10205-72	10205-72-1	Mdn
(wt. %)							
SiO_2	32.62	32.79	32.78	32.66	32.32	32.49	32.55
ZrO_2	64.49	64.09	64.48	64.25	62.97	63.77	64.28
HfO_2	1.06	1.15	1.20	1.17	1.09	1.12	1.14
P_2O_5	0.18	0.14	0.15	0.15	0.28	0.18	0.17
CaO	0.04	-	0.02	0.04	0.02	0.05	0.02
Dy_2O_3	0.11	0.02	0.07	0.10	0.14	0.12	0.10
Er_2O_3	0.17	0.13	0.13	0.12	0.21	0.19	0.16
Yb_2O_3	0.25	0.15	0.14	0.17	0.22	0.20	0.20
Y_2O_3	1.40	0.92	0.99	1.08	1.75	1.26	1.15
Total	100.33	99.39	99.94	99.75	98.99	99.37	99.78
REE+Y-ox.	1.94	1.22	1.32	1.48	2.32	1.76	1.61
Apfu (based on 4 anions)							
Si	1.00	1.01	1.01	1.00	1.00	1.00	
Zr	0.96	0.96	0.96	0.96	0.95	0.96	
Hf	0.01	0.01	0.01	0.01	0.01	0.01	
P	-	-	-	-	0.01	-	
Y	0.02	0.02	0.02	0.02	0.03	0.02	
∑*Zr-site*	1.00	0.99	0.99	1.00	1.00	1.00	

Monazite-(Ce)

Table 6-8: Monazite-(Ce) microprobe analyses

Unit	Hypersolvus granite south													Hypersolvus granite north					
Sample	10017 -1	10017 -2	10017 -3	10017 -5	10017 -6	10017 -7	10017 -8	10032 -8	20477 1-1	20477 1-9	20477 3-5	20477 3-6	20477 3-7	10011 -3	10011 -14	10011 -15	10011 -16	10011 -17	10040 -2
(wt. %)																			
P_2O_5	30.67	30.71	30.64	30.47	29.01	30.08	30.25	30.46	30.00	30.25	30.09	29.85	29.93	30.89	29.43	30.30	30.49	26.27	30.61
SiO_2	0.57	0.55	0.64	0.83	1.51	0.54	0.61	0.52	0.35	0.45	0.76	1.06	0.74	0.29	3.36	0.39	0.51	7.29	0.45
CaO	0.02	0.01	0.06	-	0.04	0.02	-	0.04	-	0.01	0.03	0.05	0.02	0.02	0.09	0.02	0.07	0.29	0.02
Na_2O	-	-	-	-	-	-	-	-	-	-	-	0.01	-	-	0.12	-	-	1.23	-
SrO	-	0.02	-	0.01	-	-	0.02	-	-	-	-	0.03	-	-	-	0.05	-	0.03	-
PbO	0.06	0.03	-	0.03	0.08	0.06	0.02	0.02	0.01	0.03	0.05	0.03	0.03	0.03	0.05	0.04	0.03	0.05	0.02
ThO_2	0.34	0.67	0.65	0.85	1.77	0.31	0.37	0.93	0.48	0.34	0.78	0.74	0.37	0.66	1.30	1.04	0.42	0.72	0.75
UO_2	-	-	-	0.01	-	-	-	0.01	-	-	-	-	-	-	0.04	-	0.03	0.07	-
F	0.70	0.56	0.57	0.50	0.55	0.67	0.56	0.64	0.62	0.56	0.54	0.47	0.55	0.53	0.49	0.53	0.58	1.85	0.59
Cl	0.02	0.01	-	0.01	0.01	0.01	0.02	0.01	0.01	0.01	0.01	0.02	0.01	0.02	0.02	0.02	-	0.01	0.02
Y_2O_3	0.02	0.02	0.10	0.03	0.14	0.07	0.10	0.17	0.12	0.15	0.06	0.01	0.07	0.06	0.45	0.13	0.07	0.09	0.09
La_2O_3	17.03	18.43	19.00	17.71	17.42	17.91	17.67	24.74	25.14	24.07	22.54	22.52	25.29	22.06	16.28	20.00	23.42	21.13	19.94
Ce_2O_3	35.92	35.57	36.47	36.63	34.48	37.05	37.21	35.90	33.29	33.77	35.51	35.40	33.13	34.58	32.42	34.20	36.41	32.02	35.52
Pr_2O_3	4.02	3.71	3.57	3.93	3.75	3.80	3.83	2.65	2.98	2.94	3.20	3.19	3.05	3.23	3.71	3.40	2.99	2.48	3.46
Nd_2O_3	11.93	10.24	8.72	9.38	10.73	9.19	9.23	4.87	7.42	8.00	6.99	6.98	7.43	7.67	11.46	9.72	5.99	5.23	9.08
Sm_2O_3	1.16	0.82	0.49	0.60	1.07	0.85	0.62	-	0.38	0.48	0.26	0.28	0.25	0.66	1.36	0.92	0.17	0.09	0.62
Eu_2O_3	-	-	-	-	-	-	0.03	0.01	0.05	-	-	-	-	-	-	-	-	-	0.05
Gd_2O_3	0.32	0.33	0.32	0.28	0.46	0.31	0.13	0.13	0.19	0.09	0.15	0.07	0.16	0.30	0.62	0.30	0.05	0.07	0.34
Dy_2O_3	-	0.02	0.03	-	0.05	-	-	-	-	0.04	-	-	-	-	-	0.08	-	0.04	-
Total	102.5	101.4	101.0	101.1	100.8	100.6	100.4	100.8	100.8	101.0	100.7	100.5	100.8	100.8	101.0	100.9	101.0	98.2	101.3
Apfu (based on 4 anions)																			
P	0.99	1.00	1.00	0.99	0.96	0.99	0.99	0.99	0.99	0.99	0.99	0.98	0.98	1.01	0.94	0.99	0.99	0.84	1.00
Si	0.02	0.02	0.02	0.03	0.06	0.02	0.02	0.02	0.01	0.02	0.03	0.04	0.03	0.01	0.13	0.02	0.02	0.28	0.02
Th	-	0.01	0.01	0.01	0.02	-	-	0.01	-	-	0.01	0.01	-	0.01	0.01	0.01	-	0.01	0.01
F	0.08	0.07	0.07	0.06	0.07	0.08	0.07	0.08	0.08	0.07	0.07	0.06	0.07	0.06	0.06	0.07	0.07	0.22	0.07
La	0.24	0.26	0.27	0.25	0.25	0.26	0.25	0.35	0.36	0.34	0.32	0.32	0.36	0.31	0.23	0.29	0.33	0.29	0.28
Ce	0.50	0.50	0.51	0.51	0.49	0.53	0.53	0.51	0.47	0.48	0.50	0.50	0.47	0.49	0.45	0.49	0.51	0.44	0.50
Pr	0.06	0.05	0.05	0.05	0.05	0.05	0.05	0.04	0.04	0.04	0.05	0.05	0.04	0.05	0.05	0.05	0.04	0.03	0.05
Nd	0.16	0.14	0.12	0.13	0.15	0.13	0.13	0.07	0.10	0.11	0.10	0.10	0.10	0.11	0.15	0.13	0.08	0.07	0.12
Sm	0.02	0.01	0.01	0.01	0.01	0.01	0.01	-	0.01	0.01	-	-	-	0.01	0.02	0.01	-	-	0.01
Gd	-	-	-	-	0.01	-	-	-	-	-	-	-	-	-	0.01	-	-	-	-
∑REE	0.98	0.97	0.96	0.96	0.97	0.98	0.97	0.97	0.99	0.98	0.97	0.97	0.98	0.96	0.91	0.97	0.97	0.85	0.97

Table 6-8: Monazite-(Ce) microprobe analyses (continued)

Unit	Hypersolvus granite north													Dark grey porphyritic granite						
Sample	1004 0-6	1004 0-9	1004 0-11	1004 0-12	1004 0-14	1004 0-16	1001 0-3	1001 0-5	1001 0-8	1001 0-12	2047 56-1	2047 56-4	2047 56-5	1003 4-1	1003 4-2	1003 6-1	1003 6-2	1003 6-3	1003 6-11	Mdn
(wt. %)																				
P_2O_5	28.81	30.55	30.21	30.09	26.90	30.57	30.04	30.23	30.52	30.26	30.28	29.72	28.61	30.16	30.66	30.95	31.02	30.80	30.66	30.26
SiO_2	3.74	0.45	0.46	0.58	0.53	0.45	0.88	0.33	0.65	0.36	0.60	0.87	0.52	0.45	0.16	0.29	0.21	0.21	0.30	0.52
CaO	0.12	-	0.01	0.02	0.04	0.01	0.03	0.02	0.03	-	0.02	0.02	0.01	-	-	0.01	0.02	0.02	0.03	0.02
Na_2O	0.06	-	-	-	-	-	-	-	-	-	-	-	-	-	-	-	-	-	-	-
SrO	0.02	0.07	0.01	-	0.04	-	-	0.02	0.03	-	-	-	-	-	-	0.03	-	0.03	0.02	-
PbO	0.11	0.06	0.03	0.10	0.06	0.03	0.04	0.03	0.02	0.03	0.07	0.08	0.09	0.03	0.04	0.03	-	0.04	0.02	0.03
ThO_2	0.88	0.75	0.99	0.93	0.83	1.07	0.73	0.24	0.55	0.55	1.38	1.71	1.05	0.99	0.35	0.17	0.13	0.21	0.20	0.73
UO_2	0.05	-	-	0.03	-	0.02	-	-	-	-	0.02	-	-	0.03	-	-	-	-	0.01	-
F	0.47	0.62	0.52	0.54	0.55	0.56	0.53	0.62	0.53	0.61	0.48	0.53	0.49	0.54	0.49	0.48	0.58	0.50	0.56	0.55
Cl	0.01	0.02	0.01	0.01	0.01	-	0.01	0.03	-	-	0.01	0.02	0.03	0.02	0.01	0.01	0.01	0.01	0.01	0.01
Y_2O_3	0.14	-	-	0.06	0.31	0.07	0.20	-	0.13	0.15	0.17	0.37	0.09	0.03	0.05	0.05	0.01	0.01	-	0.07
La_2O_3	17.77	22.75	22.45	22.71	17.69	23.47	21.89	25.68	23.51	22.92	21.48	17.79	19.27	25.45	25.96	24.59	24.79	24.61	24.56	22.49
Ce_2O_3	33.26	35.50	35.92	35.25	30.61	35.28	33.45	34.09	34.01	34.29	34.32	33.79	34.28	33.39	35.33	35.91	35.86	35.92	35.87	35.27
Pr_2O_3	3.58	3.05	3.29	3.03	3.07	2.92	3.61	2.95	3.03	3.18	3.19	3.44	3.32	2.89	2.78	2.79	2.55	2.85	2.81	3.19
Nd_2O_3	9.84	6.85	6.94	7.25	9.55	6.17	8.61	6.45	7.74	8.13	8.66	10.83	9.10	6.73	4.96	5.86	5.98	5.78	5.93	7.70
Sm_2O_3	0.75	0.19	0.17	0.44	0.77	0.16	0.53	0.04	0.26	0.37	0.54	1.20	0.46	0.06	-	0.12	0.09	0.01	0.23	0.41
Eu_2O_3	-	0.13	-	-	-	-	-	-	-	-	-	-	-	-	-	-	-	-	-	-
Gd_2O_3	0.34	0.03	0.12	0.13	0.39	0.09	0.23	0.23	0.17	0.21	0.24	0.57	0.24	0.31	-	0.26	-	0.18	0.17	0.22
Dy_2O_3	-	0.07	-	-	0.04	0.07	0.06	0.06	-	-	0.02	0.03	0.10	-	-	-	-	-	-	-
Total	99.8	100.8	100.9	100.9	91.2	100.7	100.6	100.7	100.9	100.8	101.3	100.7	97.5	100.8	100.6	101.3	101.0	100.9	101.1	100.8
Apfu (based on 4 anions)																				
P	0.93	1.00	0.99	0.99	0.98	1.00	0.98	0.99	0.99	0.99	0.99	0.98	0.98	0.99	1.00	1.00	1.01	1.00	1.00	0.99
Si	0.14	0.02	0.02	0.02	0.02	0.02	0.03	0.01	0.03	0.01	0.02	0.03	0.02	0.02	0.01	0.01	0.01	0.01	0.01	0.02
Th	0.01	0.01	0.01	0.01	0.01	0.01	0.01	-	-	-	0.01	0.02	0.01	0.01	-	-	-	-	-	0.01
F	0.06	0.08	0.06	0.07	0.07	0.07	0.06	0.08	0.06	0.07	0.06	0.06	0.06	0.07	0.06	0.06	0.07	0.06	0.07	0.07
La	0.25	0.32	0.32	0.32	0.28	0.33	0.31	0.37	0.33	0.33	0.31	0.26	0.29	0.36	0.37	0.35	0.35	0.35	0.35	0.32
Ce	0.46	0.50	0.51	0.50	0.48	0.50	0.47	0.48	0.48	0.49	0.48	0.48	0.51	0.47	0.50	0.50	0.50	0.51	0.51	0.50
Pr	0.05	0.04	0.05	0.04	0.05	0.04	0.05	0.04	0.04	0.04	0.04	0.05	0.05	0.04	0.04	0.04	0.04	0.04	0.04	0.05
Nd	0.13	0.09	0.10	0.10	0.15	0.08	0.12	0.09	0.11	0.11	0.12	0.15	0.13	0.09	0.07	0.08	0.08	0.08	0.08	0.11
Sm	0.01	-	-	0.01	0.01	-	0.01	-	-	-	0.01	0.02	0.01	-	-	-	-	-	-	0.01
Gd	-	-	-	-	0.01	-	-	-	-	-	-	0.01	-	-	-	-	-	-	-	-
∑REE	0.91	0.97	0.98	0.98	0.98	0.96	0.97	0.99	0.97	0.98	0.97	0.97	0.99	0.98	0.98	0.98	0.97	0.98	0.98	0.98

Pyrochlore group minerals

Table 6-9: Fluornatropyrochlore, fluorcalciopyrochlore’ and hydroxynatro-/calciopyrochlore microprobe analyses

EMP analyses

Unit	Hypersolvus granite south										Hypersolvus granite north										
Sample	10018-1	10018-3	10018-4	10018-5	10018-6	10018-1	10018-2	10018-3	10013-4	10013-8	10010-1	10010-2	10010-3	10010-4	10010-5	10010-6	10010-7	10010-9	10011-4	10011-5	10011-6
Species	fn*	fn	fn	fn	fn	fn	fn	fn	ch	nh	fn	fn	fn	fc	fn	fn	fn	fn	hc	hc	fc
(wt. %)																					
Na_2O	1.65	3.72	8.50	4.90	3.44	4.00	4.48	1.76	0.10	1.19	2.99	4.43	4.79	1.92	4.12	5.02	8.14	5.09	0.80	0.71	1.05
CaO	2.65	3.68	4.05	3.83	3.60	3.92	3.99	2.60	1.39	1.92	3.30	3.72	1.47	3.61	3.49	3.57	3.88	3.66	2.48	2.84	2.41
BaO	0.86	0.24	0.04	0.07	0.14	0.09	0.14	0.31	0.53	0.18	0.31	0.09	0.12	0.65	0.08	0.11	0.02	0.11	0.38	0.68	0.41
SrO	-	0.02	0.04	0.05	0.03	0.04	0.07	0.05	0.03	-	0.19	0.03	-	0.21	0.05	0.03	-	0.06	0.06	0.13	0.06
SiO_2	2.82	1.43	1.55	0.97	0.90	0.89	1.73	2.11	2.67	2.56	2.12	0.54	2.65	1.99	0.32	1.44	0.06	1.20	0.92	0.68	0.91
Nb_2O_5	52.26	53.11	52.10	53.73	54.69	53.05	52.51	54.80	54.33	51.37	55.96	57.45	55.00	52.37	57.76	55.67	56.64	55.22	51.47	55.88	52.08
Ta_2O_5	1.69	2.37	2.36	2.53	1.61	2.52	2.32	1.81	2.83	3.08	2.77	2.87	1.51	2.34	2.99	3.09	2.80	3.28	2.00	1.52	2.48
FeO	0.87	0.34	-	0.05	0.20	0.11	0.04	0.52	1.90	1.80	0.24	0.09	0.05	0.04	0.03	0.28	-	0.22	0.29	0.16	0.29
MnO	0.09	0.02	0.01	-	0.01	-	0.02	0.02	0.13	0.02	-	-	-	-	-	-	-	-	0.01	-	-
TiO_2	7.80	8.03	8.50	8.13	7.76	8.88	8.61	7.59	5.21	4.93	5.61	5.43	5.36	8.72	5.07	5.32	5.23	5.18	10.8	8.65	10.2
ZrO_2	0.24	0.31	0.39	0.37	0.27	0.28	0.45	0.14	2.98	3.15	0.15	0.16	0.47	0.16	0.18	0.22	0.11	0.33	0.65	0.10	0.80
PbO	2.41	0.24	0.23	0.36	0.36	0.19	0.15	0.21	2.69	4.32	0.12	0.15	0.11	0.24	0.17	0.12	0.17	0.15	0.63	0.26	0.86
ThO_2	0.36	0.03	0.05	0.07	0.03	0.03	0.08	0.10	0.15	0.16	0.02	0.09	-	0.06	0.07	0.02	0.03	0.03	0.12	0.22	0.05
UO_2	0.58	0.46	0.41	0.36	0.41	0.32	0.28	0.51	1.10	1.13	0.85	0.61	0.35	1.09	0.55	0.38	0.49	0.50	0.94	1.25	0.95
F	2.52	4.11	4.46	4.31	4.06	4.27	4.35	3.14	0.58	1.29	3.14	3.66	3.35	3.10	3.49	3.48	4.04	3.60	2.05	1.87	2.46
Y_2O_3	0.25	0.20	0.27	0.26	0.22	0.27	0.23	0.25	0.18	0.11	0.22	0.17	0.07	0.24	0.13	0.24	0.17	0.16	0.32	0.28	0.22
La_2O_3	3.54	3.82	3.61	3.74	3.78	4.00	3.69	3.62	3.90	3.62	3.83	4.03	3.71	4.05	3.87	3.79	4.06	3.68	4.18	3.99	4.24
Ce_2O_3	9.89	9.92	9.59	9.99	10.08	10.05	9.71	10.43	9.07	8.33	9.18	9.49	10.94	9.86	10.08	9.53	9.50	9.57	11.20	10.39	10.86
Pr_2O_3	1.08	0.90	0.93	1.02	0.94	0.92	0.93	1.11	0.86	0.78	0.92	0.87	1.19	0.87	1.00	0.91	0.93	0.96	1.13	1.00	1.03
Nd_2O_3	2.64	2.21	2.30	2.38	2.27	2.06	2.44	3.04	2.28	2.11	2.24	2.21	3.03	2.22	2.58	2.19	2.31	2.26	2.91	2.71	2.95
Sm_2O_3	-	-	-	-	-	0.21	0.29	0.36	-	-	-	-	-	-	-	-	-	-	-	-	-
Total	93.1	93.41	97.49	95.29	93.08	94.30	94.66	93.15	92.7	91.5	92.82	94.54	92.75	92.43	94.56	93.95	96.88	93.73	92.47	92.52	93.3

Table 6-9: Fluornatropyrochlore, fluorcalciopyrochlore’ and hydroxynatro-/calciopyrochlore microprobe analyses (continued)

Formulae

Unit	Hypersolvus granite south										Hypersolvus granite north										
Sample	1001 8-1	1001 8-3	1001 8-4	1001 8-5	1001 8-6	1001 8-1	1001 8-2	1001 8-3	1001 3-4	1001 3-8	1001 0-1	1001 0-2	1001 0-3	1001 0-4	1001 0-5	1001 0-6	1001 0-7	1001 0-9	1001 1-4	1001 1-5	1001 1-6
Apfu (based on 7 anions)																					
Na	0.23	0.50	1.09	0.65	0.46	0.53	0.59	0.24	0.01	0.17	0.41	0.60	0.66	0.26	0.56	0.68	1.08	0.70	0.11	0.10	0.15
Ca	0.20	0.27	0.29	0.28	0.27	0.29	0.29	0.20	0.11	0.16	0.25	0.28	0.11	0.27	0.26	0.27	0.28	0.28	0.19	0.22	0.18
Ba	0.02	0.01	-	-	-	-	-	0.01	0.02	0.01	0.01	-	-	0.02	-	-	-	-	0.01	0.02	0.01
Fe	0.05	0.02	-	-	0.01	0.01	-	0.03	0.12	0.11	0.01	0.01	-	-	-	0.02	-	0.01	0.02	0.01	0.02
Pb	0.05	-	-	0.01	0.01	-	-	-	0.05	0.09	-	-	-	-	-	-	-	-	0.01	-	0.02
U	0.01	0.01	0.01	0.01	0.01	-	-	0.01	0.02	0.02	0.01	0.01	0.01	0.02	0.01	0.01	0.01	0.01	0.02	0.02	0.02
Y	0.01	0.01	0.01	0.01	0.01	0.01	0.01	0.01	0.01	-	0.01	0.01	-	0.01	-	0.01	0.01	0.01	0.01	0.01	0.01
La	0.09	0.10	0.09	0.09	0.10	0.10	0.09	0.09	0.11	0.10	0.10	0.10	0.10	0.11	0.10	0.10	0.10	0.10	0.11	0.11	0.11
Ce	0.26	0.25	0.23	0.25	0.26	0.25	0.24	0.27	0.25	0.23	0.24	0.24	0.28	0.25	0.26	0.24	0.24	0.25	0.30	0.28	0.28
Pr	0.03	0.02	0.02	0.03	0.02	0.02	0.02	0.03	0.02	0.02	0.02	0.02	0.03	0.02	0.03	0.02	0.02	0.02	0.03	0.03	0.03
Nd	0.07	0.05	0.05	0.06	0.06	0.05	0.06	0.08	0.06	0.06	0.06	0.06	0.08	0.06	0.07	0.05	0.06	0.06	0.07	0.07	0.08
□/H_2O	0.97	0.75	0.20	0.62	0.79	0.72	0.67	1.02	1.21	1.02	0.87	0.67	0.73	0.97	0.70	0.59	0.19	0.57	1.11	1.13	1.10
A-site	2.00	2.00	2.00	2.00	2.00	2.00	2.00	2.00	2.00	2.00	2.00	2.00	2.00	2.00	2.00	2.00	2.00	2.00	2.00	2.00	2.00
Nb	1.69	1.66	1.56	1.66	1.73	1.65	1.61	1.74	1.83	1.76	1.78	1.82	1.75	1.67	1.84	1.76	1.76	1.76	1.68	1.83	1.69
Ta	0.03	0.04	0.04	0.05	0.03	0.05	0.04	0.03	0.06	0.06	0.05	0.05	0.03	0.04	0.06	0.06	0.05	0.06	0.04	0.03	0.05
Ti	0.42	0.42	0.42	0.42	0.41	0.46	0.44	0.40	0.29	0.28	0.30	0.29	0.28	0.46	0.27	0.28	0.27	0.27	0.59	0.47	0.55
Si	0.01	0.01	0.01	0.01	0.01	0.01	0.01	-	0.11	0.12	0.01	0.01	0.02	0.01	0.01	0.01	-	0.01	0.02	-	0.03
Zr	0.20	0.10	0.10	0.07	0.06	0.06	0.12	0.15	0.20	0.19	0.15	0.04	0.19	0.14	0.02	0.10	-	0.08	0.07	0.05	0.06
B-site	2.35	2.24	2.14	2.20	2.23	2.22	2.23	2.33	2.48	2.41	2.29	2.20	2.27	2.33	2.20	2.21	2.09	2.19	2.40	2.38	2.38
F	0.57	0.90	0.93	0.93	0.90	0.93	0.93	0.70	0.14	0.31	0.70	0.81	0.75	0.69	0.78	0.77	0.88	0.80	0.47	0.43	0.56
OH, O	0.43	0.10	0.07	0.07	0.10	0.07	0.07	0.30	0.86	0.69	0.30	0.19	0.25	0.31	0.22	0.23	0.12	0.20	0.53	0.57	0.44
Y-site	1.00	1.00	1.00	1.00	1.00	1.00	1.00	1.00	1.00	1.00	1.00	1.00	1.00	1.00	1.00	1.00	1.00	1.00	1.00	1.00	1.00
∑REE	0.46	0.43	0.41	0.44	0.44	0.44	0.43	0.48	0.44	0.41	0.42	0.43	0.49	0.45	0.46	0.43	0.43	0.43	0.52	0.49	0.51

*Species: fn = fluornatropyrochlore, fc = fluorcalciopyrochlore, hn** = hydroxy-natropyrochlore, hc** = hydroxy-calciopyrochlore (**Y-site non-F-dominant)

Table 6-9: Fluornatropyrochlore, fluorcalciopyrochlore’ and hydroxynatro-/calciopyrochlore microprobe analyses (continued)

EMP analyses

Unit	Dark grey porphyritic granite																				
Sample	1003 6-1	1003 6-2	1003 6-3	1003 6-4	1003 6-5	1003 6-6	1003 6-7	1003 6-8	1003 4-1	1003 4-2	1003 4-6	1020 1-1	1020 1-2	1020 1-3	1020 1-4	1020 1-5	1020 1-6	1020 1-7	1020 1-8	1020 1-9	1020 1-10	1020 4-1
Species	fn	fn	fn	fn	fn	fn	fn	fn	fn	hc	fn	fn	fn	fn	Fn	fn	fn	hn	fn	fn	fn	hn
(wt. %)																						
Na_2O	2.45	3.28	2.91	3.46	4.55	3.06	2.82	5.57	2.23	1.16	2.11	4.75	5.56	3.40	5.38	5.88	4.58	2.13	6.24	7.58	6.72	2.47
CaO	3.29	3.62	2.15	3.32	2.87	3.42	2.88	3.44	2.49	2.20	2.59	2.79	2.88	2.70	2.88	2.85	2.67	3.28	2.96	3.15	3.12	2.48
BaO	0.29	0.03	0.25	0.08	0.04	0.04	0.08	0.05	0.81	0.93	0.57	0.02	0.06	0.02	0.01	0.01	0.03	0.16	0.06	0.01	0.05	0.82
SrO	0.07	0.04	0.08	0.05	0.08	0.02	0.08	0.01	0.12	0.19	0.11	0.01	0.06	0.04	0.03	0.04	-	0.11	0.06	-	0.01	0.05
SiO_2	1.14	0.29	4.93	0.11	0.20	0.98	0.35	0.19	1.22	2.26	0.76	0.31	0.39	0.38	0.24	0.34	0.47	2.45	0.35	0.50	0.26	1.09
Nb_2O_5	54.20	55.56	53.65	57.61	59.91	57.28	59.25	57.66	57.74	55.68	60.08	57.99	57.75	57.88	58.25	57.77	59.35	52.43	58.96	56.71	59.54	58.13
Ta_2O_5	2.18	2.21	2.48	3.05	2.08	1.73	2.14	3.18	2.28	2.09	2.34	3.07	2.88	2.91	2.95	2.90	2.82	2.93	2.89	3.08	1.35	2.68
FeO	0.56	0.41	0.91	0.04	0.15	0.36	0.29	0.11	0.37	0.92	0.22	0.13	0.06	0.16	0.12	0.19	0.20	0.81	0.11	0.04	0.42	0.17
MnO	0.03	-	0.04	-	-	-	-	-	0.01	0.01	0.01	-	-	-	-	-	-	0.12	0.01	-	0.01	0.04
TiO_2	7.49	7.91	4.25	5.37	4.54	6.17	4.48	4.84	4.21	4.65	3.84	5.82	5.91	5.27	5.67	5.64	5.16	6.37	4.43	5.66	5.61	4.88
ZrO_2	0.18	0.14	0.45	0.26	0.15	0.09	0.18	0.23	-	0.30	0.02	0.32	0.26	0.22	0.32	0.29	0.26	0.57	0.40	0.33	0.20	0.34
PbO	3.05	0.18	2.34	0.17	0.27	0.16	0.02	0.20	0.56	1.88	0.36	0.15	0.12	0.15	0.03	-	0.15	5.34	0.14	0.09	0.17	0.10
ThO_2	0.10	0.03	1.17	0.08	0.08	-	-	-	0.10	0.13	0.06	-	-	0.01	-	0.04	-	0.07	-	-	-	0.10
UO_2	0.60	0.67	0.56	0.62	0.74	0.60	0.65	0.47	0.61	0.74	0.72	0.48	0.54	0.68	0.46	0.50	0.63	0.45	0.44	0.40	0.42	0.49
F	2.22	4.30	2.62	3.91	3.62	4.01	3.63	3.76	2.24	1.62	2.33	4.27	4.04	3.86	4.18	3.95	3.93	1.85	4.18	4.02	4.31	2.08
Y_2O_3	0.14	0.12	0.24	0.16	0.11	0.10	0.15	0.11	0.25	0.28	0.20	0.22	0.12	0.19	0.13	0.12	0.17	0.18	0.13	0.17	0.18	0.21
La_2O_3	4.22	4.48	3.88	4.33	4.24	4.32	4.20	4.29	4.68	4.49	4.82	4.35	4.43	4.39	4.48	4.42	4.27	4.15	4.54	4.34	4.48	4.18
Ce_2O_3	9.58	9.83	8.93	9.89	9.93	9.62	9.93	9.79	9.80	9.56	10.03	10.18	10.15	9.86	10.06	9.88	10.04	9.19	9.61	9.97	9.95	9.72
Pr_2O_3	0.85	0.87	0.94	0.94	1.04	0.90	1.03	0.90	0.76	0.84	0.87	0.91	0.98	0.89	0.92	0.98	0.93	0.90	0.93	0.80	0.88	0.85
Nd_2O_3	2.30	2.24	2.27	2.37	2.47	2.20	2.34	2.29	1.96	2.02	2.02	2.27	2.29	2.29	2.26	2.22	2.41	1.94	2.00	2.20	1.99	2.10
Sm_2O_3	-	-	-	-	-	-	-	-	-	-	-	-	-	-	-	-	-	-	-	-	-	-
Total	94.0	94.4	94.0	94.1	95.6	93.4	93.0	95.5	91.5	91.3	93.1	96.2	96.8	93.7	96.6	96.4	96.4	94.6	96.7	97.4	97.8	92.1

Table 6-9: Fluornatropyrochlore, fluorcalciopyrochlore, and hydroxynatro-/calciopyrochlore microprobe analyses (continued)

Formulae

Unit	Dark grey porphyritic granite																					
Sample	1003 6-1	1003 6-2	1003 6-3	1003 6-4	1003 6-5	1003 6-6	1003 6-7	1003 6-8	1003 4-1	1003 4-2	1003 4-6	1020 1-1	1020 1-2	1020 1-3	1020 1-4	1020 1-5	1020 1-6	1020 1-7	1020 1-8	1020 1-9	1020 1-10	1020 4-1
Apfu (based on 7 anions)																						
Na	0.34	0.44	0.40	0.47	0.62	0.41	0.39	0.75	0.32	0.17	0.30	0.63	0.74	0.47	0.71	0.78	0.61	0.30	0.83	1.00	0.87	0.35
Ca	0.25	0.27	0.16	0.25	0.21	0.26	0.22	0.26	0.20	0.18	0.20	0.20	0.21	0.21	0.21	0.21	0.20	0.25	0.22	0.23	0.22	0.19
Ba	0.01	-	0.01	-	-	-	-	-	0.02	0.03	0.02	-	-	-	-	-	-	-	-	-	-	0.02
Fe	0.03	0.02	0.05	-	0.01	0.02	0.02	0.01	0.02	0.06	0.01	0.01	-	0.01	0.01	0.01	0.01	0.05	0.01	-	0.02	0.01
Pb	0.06	-	0.04	-	0.01	-	-	-	0.01	0.04	0.01	-	-	-	-	-	-	0.10	-	-	-	-
U	0.01	0.01	0.01	0.01	0.01	0.01	0.01	0.01	0.01	0.01	0.01	0.01	0.01	0.01	0.01	0.01	0.01	0.01	0.01	0.01	0.01	0.01
Y	0.01	-	0.01	0.01	-	-	0.01	-	0.01	0.01	0.01	0.01	-	0.01	-	-	0.01	0.01	-	0.01	0.01	0.01
La	0.11	0.11	0.10	0.11	0.11	0.11	0.11	0.11	0.13	0.12	0.13	0.11	0.11	0.11	0.11	0.11	0.11	0.11	0.11	0.11	0.11	0.11
Ce	0.25	0.25	0.23	0.26	0.25	0.25	0.26	0.25	0.27	0.26	0.27	0.26	0.25	0.26	0.25	0.25	0.25	0.24	0.24	0.25	0.24	0.26
Pr	0.02	0.02	0.02	0.02	0.03	0.02	0.03	0.02	0.02	0.02	0.02	0.02	0.02	0.02	0.02	0.02	0.02	0.02	0.02	0.02	0.02	0.02
Nd	0.06	0.06	0.06	0.06	0.06	0.05	0.06	0.06	0.05	0.05	0.05	0.06	0.06	0.06	0.06	0.05	0.06	0.05	0.05	0.05	0.05	0.05
□/H_2O	0.83	0.81	0.88	0.79	0.68	0.86	0.89	0.52	0.93	1.04	0.97	0.69	0.58	0.84	0.61	0.54	0.72	0.83	0.50	0.33	0.43	0.95
A-site	2.00	2.00	2.00	2.00	2.00	2.00	2.00	2.00	2.00	2.00	2.00	2.00	2.00	2.00	2.00	2.00	2.00	2.00	2.00	2.00	2.00	2.00
Nb	1.77	1.74	1.70	1.84	1.89	1.81	1.91	1.82	1.93	1.88	1.98	1.80	1.79	1.85	1.80	1.80	1.85	1.72	1.83	1.74	1.81	1.92
Ta	0.04	0.04	0.05	0.06	0.04	0.03	0.04	0.06	0.05	0.04	0.05	0.06	0.05	0.06	0.05	0.05	0.05	0.06	0.05	0.06	0.02	0.05
Ti	0.41	0.41	0.22	0.29	0.24	0.32	0.24	0.25	0.23	0.26	0.21	0.30	0.30	0.28	0.29	0.29	0.27	0.35	0.23	0.29	0.28	0.27
Si	0.01	-	0.02	0.01	0.01	-	0.01	0.01	-	0.01	-	0.01	0.01	0.01	0.01	0.01	0.01	0.02	0.01	0.01	0.01	0.01
Zr	0.08	0.02	0.35	0.01	0.01	0.07	0.02	0.01	0.09	0.17	0.06	0.02	0.03	0.03	0.02	0.02	0.03	0.18	0.02	0.03	0.02	0.08
B-site	2.30	2.22	2.34	2.20	2.19	2.24	2.23	2.16	2.30	2.36	2.29	2.19	2.18	2.23	2.18	2.17	2.21	2.33	2.15	2.13	2.14	2.33
F	0.51	0.94	0.58	0.87	0.80	0.89	0.82	0.83	0.52	0.38	0.54	0.93	0.88	0.87	0.91	0.86	0.85	0.42	0.91	0.87	0.91	0.48
OH, O	0.49	0.06	0.42	0.13	0.20	0.11	0.18	0.17	0.48	0.62	0.46	0.07	0.12	0.13	0.09	0.14	0.15	0.58	0.09	0.13	0.09	0.52
Y-site	1.00	1.00	1.00	1.00	1.00	1.00	1.00	1.00	1.00	1.00	1.00	1.00	1.00	1.00	1.00	1.00	1.00	1.00	1.00	1.00	1.00	1.00
∑REE	0.45	0.45	0.42	0.46	0.46	0.44	0.46	0.45	0.47	0.47	0.48	0.45	0.45	0.46	0.45	0.44	0.45	0.44	0.43	0.44	0.43	0.46

Table 6-9: Fluornatropyrochlore, fluorcalciopyrochlore’ and hydroxynatro-/calciopyrochlore microprobe analyses (continued)

EMP analyses

Unit	Dark grey porphyritic granite							Transsolvus granite											
Sample	1020 4-3	1020 4-4	1020 4-5	1020 4-6	1020 4-7	1020 4-8	1020 4-10	WO C2-2	WO C2-3	WO C2-4	WO C2-5	WO C2-6	WO C2-7	WO C2-8	2047 15-1	2047 15-2	2047 15-3	2047 15-5	2047 15-7	2047 15-8	2047 15-1	
Species	fn	fn	fn	fn	fn	fn	fn	fn	fn	fn	fn	fn	fn	fn	Fn	fn	fn	fn	fn	fn	fn	Mdn
(wt. %)																						
Na_2O	4.48	4.01	4.99	4.78	3.93	4.58	6.08	7.32	4.57	5.87	6.46	5.17	6.98	7.12	7.93	7.99	8.05	8.83	7.99	8.20	8.01	4.76
CaO	2.62	3.17	2.48	3.36	3.35	2.05	3.64	2.99	2.71	3.31	3.58	2.89	3.63	3.66	3.23	3.45	3.64	3.97	2.96	3.02	3.61	3.13
BaO	0.22	0.44	0.11	0.06	0.44	0.26	0.05	0.03	0.96	0.28	0.04	0.37	0.06	0.01	0.06	0.03	0.04	0.03	0.04	0.03	0.03	0.07
SrO	0.02	-	0.04	-	0.02	0.01	0.03	0.03	0.02	0.07	0.01	0.02	0.04	-	0.04	-	-	0.03	0.01	0.02	0.02	0.04
SiO_2	0.65	1.08	0.70	0.80	0.90	1.33	0.98	2.44	3.12	3.33	1.51	2.00	1.46	1.62	1.84	1.42	1.42	2.20	0.98	1.07	2.70	0.98
Nb_2O_5	58.84	56.64	58.79	55.83	56.90	58.83	55.36	55.89	54.72	53.16	55.21	56.32	57.25	55.85	56.22	56.82	56.27	54.67	58.15	55.74	54.31	56.64
Ta_2O_5	2.37	2.92	2.59	2.91	2.85	1.89	2.96	2.08	2.23	1.96	2.29	2.05	2.67	2.71	1.78	2.60	2.83	2.96	2.24	2.50	2.75	2.63
FeO	0.18	0.10	0.04	0.08	0.08	0.46	0.01	0.15	0.69	0.39	0.66	0.89	0.13	0.18	0.31	0.07	0.06	-	0.02	0.26	0.04	0.16
MnO	0.02	0.01	-	0.01	-	0.02	-	-	-	-	-	0.01	-	0.01	-	-	-	-	-	-	-	0.01
TiO_2	4.58	5.91	4.36	6.02	5.82	3.97	6.10	4.39	3.78	4.67	4.27	4.00	4.64	5.19	4.58	4.77	4.95	5.27	4.12	4.42	4.97	5.18
ZrO_2	0.32	0.40	0.30	0.47	0.45	0.25	0.37	0.48	0.39	0.36	0.48	0.30	0.49	0.45	0.27	0.38	0.38	0.49	0.28	0.29	0.51	0.30
PbO	0.08	0.20	0.10	0.28	0.21	0.41	0.18	0.19	2.47	2.42	0.11	1.04	0.06	0.10	0.28	0.22	0.24	0.17	0.10	0.15	0.17	0.17
ThO_2	-	-	0.04	-	0.01	0.04	0.03	-	-	0.01	-	0.05	-	-	0.06	-	0.01	-	-	0.01	-	0.04
UO_2	0.37	0.48	0.40	0.33	0.35	0.37	0.33	0.24	0.37	0.37	0.27	0.35	0.17	0.19	0.30	0.22	0.17	0.09	0.25	0.14	0.14	0.47
F	3.82	3.34	3.59	4.03	3.45	3.37	4.13	3.95	2.24	3.02	2.80	2.72	3.97	3.99	3.98	3.96	3.86	3.83	3.73	4.18	3.70	3.68
Y_2O_3	0.13	0.17	0.15	0.18	0.18	0.13	0.12	0.10	0.28	0.31	0.12	0.41	0.15	0.16	0.14	0.12	0.09	0.11	0.12	0.09	0.15	0.16
La_2O_3	4.22	4.22	4.28	4.25	4.12	4.10	4.14	4.27	4.36	3.99	3.97	4.20	4.18	4.18	4.58	4.56	4.48	4.17	4.76	4.54	4.30	4.24
Ce_2O_3	9.75	9.59	10.15	9.71	9.56	10.53	9.49	9.70	9.53	9.40	9.17	9.57	9.58	9.58	9.62	9.63	9.66	9.23	9.94	9.58	9.38	9.70
Pr_2O_3	0.96	0.90	0.95	0.86	0.97	1.02	0.82	1.03	0.95	0.84	0.95	0.96	0.85	0.89	0.99	0.93	0.80	0.83	0.95	0.96	0.89	0.92
Nd_2O_3	2.28	2.09	2.45	2.03	2.03	2.45	1.96	2.54	2.39	2.32	2.15	2.48	2.43	2.37	2.30	2.48	2.31	2.29	2.46	2.42	2.27	2.29
Sm_2O_3	-	-	-	-	-	-	-	-	-	-	-	-	-	-	-	-	-	-	-	-	0.18	0.18
Total	94.3	94.3	95.0	94.3	94.2	94.6	95.0	96.2	94.8	95.0	93.0	94.7	97.1	96.6	96.8	98.0	97.7	97.6	97.5	95.9	96.6	94.6

Table 6-9: Fluornatropyrochlore, fluorcalciopyrochlore’ and hydroxynatro-/calciopyrochlore microprobe analyses (continued)

Formulae

Unit	Dark grey porphyritic granite							Transsolvus granite														
Sample	1020 4-3	1020 4-4	1020 4-5	1020 4-6	1020 4-7	1020 4-8	1020 4-10	WO C2-2	WO C2-3	WO C2-4	WO C2-5	WO C2-6	WO C2-7	WO C2-8	2047 15-1	2047 15-2	2047 15-3	2047 15-5	2047 15-7	2047 15-8	2047 15-1	Mdn
Apfu (based on 7anions)																						
Na	0.61	0.54	0.68	0.65	0.53	0.63	0.81	0.96	0.63	0.80	0.89	0.71	0.92	0.94	1.04	1.04	1.05	1.14	1.06	1.10	1.05	0.64
Ca	0.20	0.24	0.19	0.25	0.25	0.15	0.27	0.22	0.21	0.25	0.27	0.22	0.26	0.27	0.23	0.25	0.26	0.28	0.22	0.22	0.26	0.23
Ba	0.01	0.01	-	-	0.01	0.01	-	-	0.03	0.01	-	0.01	-	-	-	-	-	-	-	-	-	-
Fe	0.01	0.01	-	-	-	0.03	-	0.01	0.04	0.02	0.04	0.05	0.01	0.01	0.02	-	-	-	-	0.01	-	0.01
Pb	-	-	-	0.01	-	0.01	-	-	0.05	0.05	-	0.02	-	-	0.01	-	-	-	-	-	-	-
U	0.01	0.01	0.01	0.01	0.01	0.01	-	-	0.01	0.01	-	0.01	-	-	-	-	-	-	-	-	-	0.01
Y	-	0.01	0.01	0.01	0.01	-	-	-	0.01	0.01	-	0.02	0.01	0.01	-	-	-	-	-	-	0.01	0.01
La	0.11	0.11	0.11	0.11	0.11	0.11	0.11	0.11	0.11	0.10	0.10	0.11	0.10	0.10	0.11	0.11	0.11	0.10	0.12	0.12	0.11	0.11
Ce	0.25	0.25	0.26	0.25	0.25	0.27	0.24	0.24	0.25	0.24	0.24	0.25	0.24	0.24	0.24	0.24	0.24	0.23	0.25	0.24	0.23	0.25
Pr	0.02	0.02	0.02	0.02	0.02	0.03	0.02	0.03	0.02	0.02	0.02	0.02	0.02	0.02	0.02	0.02	0.02	0.02	0.02	0.02	0.02	0.02
Nd	0.06	0.05	0.06	0.05	0.05	0.06	0.05	0.06	0.06	0.06	0.05	0.06	0.06	0.06	0.06	0.06	0.06	0.05	0.06	0.06	0.05	0.06
□/H_2O	0.72	0.75	0.66	0.65	0.75	0.70	0.49	0.36	0.58	0.44	0.36	0.52	0.38	0.36	0.25	0.26	0.24	0.16	0.26	0.22	0.26	0.66
A-site	2.00	2.00	2.00	2.00	2.00	2.00	2.00	2.00	2.00	2.00	2.00	2.00	2.00	2.00	2.00	2.00	2.00	2.00	2.00	2.00	2.00	2.00
Nb	1.87	1.79	1.86	1.76	1.80	1.87	1.72	1.72	1.77	1.68	1.78	1.80	1.75	1.71	1.72	1.73	1.72	1.65	1.79	1.74	1.66	1.79
Ta	0.05	0.06	0.05	0.06	0.05	0.04	0.06	0.04	0.04	0.04	0.04	0.04	0.05	0.05	0.03	0.05	0.05	0.05	0.04	0.05	0.05	0.05
Ti	0.24	0.31	0.23	0.32	0.31	0.21	0.32	0.22	0.20	0.25	0.23	0.21	0.24	0.26	0.23	0.24	0.25	0.27	0.21	0.23	0.25	0.27
Si	0.01	0.01	0.01	0.02	0.02	0.01	0.01	0.02	0.01	0.01	0.02	0.01	0.02	0.01	0.01	0.01	0.01	0.02	0.01	0.01	0.02	0.01
Zr	0.05	0.08	0.05	0.06	0.06	0.09	0.07	0.17	0.22	0.23	0.11	0.14	0.10	0.11	0.12	0.10	0.10	0.15	0.07	0.07	0.18	0.07
B-site	2.21	2.25	2.20	2.20	2.24	2.22	2.17	2.16	2.25	2.21	2.18	2.21	2.15	2.15	2.12	2.12	2.13	2.13	2.12	2.10	2.16	2.20
F	0.85	0.74	0.80	0.89	0.77	0.75	0.90	0.85	0.51	0.67	0.63	0.61	0.85	0.85	0.85	0.84	0.82	0.81	0.80	0.91	0.79	0.81
OH, O	0.15	0.26	0.20	0.11	0.23	0.25	0.10	0.15	0.49	0.33	0.37	0.39	0.15	0.15	0.15	0.16	0.18	0.19	0.20	0.09	0.21	0.19
Y-site	1.00	1.00	1.00	1.00	1.00	1.00	1.00	1.00	1.00	1.00	1.00	1.00	1.00	1.00	1.00	1.00	1.00	1.00	1.00	1.00	1.00	1.00
∑REE	0.45	0.44	0.46	0.44	0.43	0.47	0.42	0.44	0.46	0.43	0.43	0.46	0.43	0.43	0.44	0.44	0.43	0.41	0.46	0.44	0.42	0.45

Table 6-10: Zero-valent-dominant pyrochlore microprobe analyses

EMP analyses

Unit	Hypersolvus granite south		Hypersolvus granite north								Dark pp gr	Transsolvus granite						
Sample	10018-2	10018-8	10010-8	10011-1	10011-2	10011-3	10011-7	10011-8	10011-9	10011-10	10204-2	WOC2-1	10034-3	10034-4	10034-5	10034-7	10034-8	Mdn
(wt. %)																		
Na_2O	0.68	2.44	1.12	0.31	1.05	0.13	0.18	1.59	0.14	0.40	1.87	3.94	0.71	0.28	1.42	0.33	1.24	0.71
CaO	2.19	2.90	3.28	2.33	2.59	2.45	2.66	2.39	2.35	2.42	2.42	2.67	2.42	1.52	2.21	1.68	2.29	2.42
BaO	1.11	1.42	2.99	3.31	1.98	5.48	3.04	1.34	2.50	3.17	1.77	1.23	2.61	4.33	1.57	2.65	1.17	2.50
SrO	-	0.05	0.57	0.20	0.27	0.32	0.21	0.23	0.22	0.26	0.01	0.03	0.38	0.52	0.22	0.36	0.18	0.22
SiO_2	3.81	2.93	4.24	4.36	2.02	9.69	4.43	12.20	2.37	4.65	2.64	4.26	2.81	6.76	2.91	5.09	2.29	4.24
Nb_2O_5	50.57	48.49	49.71	50.75	53.31	42.53	50.12	51.97	52.83	52.50	53.66	51.29	57.18	46.01	55.42	48.75	57.05	51.29
Ta_2O_5	1.91	1.50	2.48	1.17	1.33	1.37	1.56	1.24	1.22	0.87	2.85	2.23	2.16	1.72	2.09	2.01	2.13	1.72
FeO	1.13	1.99	0.81	0.76	0.36	1.71	0.69	0.30	0.60	0.67	0.21	0.37	0.82	0.70	1.23	1.64	0.72	0.72
MnO	0.20	0.22	0.03	0.11	0.05	0.01	0.06	0.01	0.04	0.06	0.12	-	0.02	0.05	0.02	0.02	-	0.04
TiO_2	8.23	7.50	8.31	8.03	8.65	6.73	8.00	8.04	8.36	6.94	5.22	3.98	3.89	2.86	4.25	4.13	3.83	6.94
ZrO_2	0.44	0.18	0.15	0.19	0.22	0.24	0.20	0.20	0.26	0.13	0.49	0.45	-	0.49	0.31	0.75	0.20	0.22
PbO	4.97	3.52	0.26	3.76	0.16	5.79	3.77	1.94	1.15	2.05	3.67	4.72	0.10	7.73	2.19	7.83	2.58	3.52
ThO_2	0.38	0.04	0.11	0.21	0.19	0.31	0.50	0.18	0.22	0.55	0.12	0.02	0.05	0.33	0.15	0.16	0.13	0.18
UO_2	0.63	0.46	1.14	1.39	0.91	0.77	1.12	0.70	1.26	1.17	0.51	0.29	0.70	0.80	0.86	0.72	0.66	0.77
F	1.44	2.41	1.29	0.78	1.60	0.48	0.38	2.74	0.56	0.50	2.06	2.01	1.20	0.95	1.47	1.10	1.56	1.29
Y_2O_3	0.21	0.20	0.23	0.29	0.24	0.48	0.25	0.17	0.22	0.22	0.15	0.53	0.36	0.63	0.24	0.30	0.25	0.24
La_2O_3	3.40	3.24	3.85	3.63	3.87	2.97	3.91	3.36	3.93	3.66	3.84	4.17	4.69	3.75	4.31	3.71	4.31	3.84
Ce_2O_3	9.45	8.04	9.46	9.64	10.18	8.37	9.69	8.58	10.44	9.50	9.06	9.06	9.76	7.49	9.41	8.29	9.58	9.45
Pr_2O_3	0.83	0.74	0.96	0.86	0.94	0.77	0.91	0.71	0.98	0.86	0.82	0.98	0.88	0.56	0.89	0.71	0.88	0.86
Nd_2O_3	2.25	1.66	2.22	2.27	2.23	2.05	2.13	1.75	2.46	2.04	1.92	2.39	2.00	1.55	1.81	1.73	1.94	2.04
Sm_2O_3	-	-	-	-	-	-	-	-	-	0.14	-	-	-	-	-	-	-	0.14
Total	93.19	88.92	92.65	93.98	91.47	92.44	93.65	98.48	91.85	92.53	92.53	93.78	92.24	88.61	92.37	91.50	92.32	93.34

Table 6-10: Zero-valent-dominant pyrochlore microprobe analyses (continued)

Formulae

Unit	Hypersolvus granite south		Hypersolvus granite north								Dark pp gr	Transsolvus granite						
Sample	10018-2	10018-8	10010-8	10011-1	10011-2	10011-3	10011-7	10011-8	10011-9	10011-10	10204-2	WOC2-1	10034-3	10034-4	10034-5	10034-7	10034-8	Mdn
Apfu (based on 7 anions)																		
Na	0.10	0.35	0.16	0.04	0.15	0.02	0.03	0.19	0.02	0.06	0.27	0.56	0.10	0.04	0.20	0.05	0.18	0.27
Ca	0.17	0.23	0.25	0.18	0.20	0.19	0.21	0.16	0.19	0.19	0.19	0.21	0.19	0.13	0.17	0.14	0.18	0.19
Ba	0.03	0.04	0.08	0.09	0.06	0.16	0.09	0.03	0.07	0.09	0.05	0.04	0.08	0.14	0.05	0.08	0.03	0.05
Sr	-	-	0.02	0.01	0.01	0.01	0.01	0.01	0.01	0.01	-	-	0.02	0.02	0.01	0.02	0.01	-
Fe	0.07	0.12	0.05	0.05	0.02	0.10	0.04	0.02	0.04	0.04	0.01	0.02	0.05	0.05	0.08	0.11	0.04	0.01
Mn	0.01	0.01	-	0.01	-	-	-	-	-	-	0.01	-	-	-	-	-	-	0.01
Pb	0.10	0.07	0.01	0.07	-	0.11	0.07	0.03	0.02	0.04	0.07	0.09	-	0.17	0.04	0.16	0.05	0.07
U	0.01	0.01	0.02	0.02	0.01	0.01	0.02	0.01	0.02	0.02	0.01	-	0.01	0.01	0.01	0.01	0.01	0.01
Y	0.01	0.01	0.01	0.01	0.01	0.02	0.01	0.01	0.01	0.01	0.01	0.02	0.01	0.03	0.01	0.01	0.01	0.01
La	0.09	0.09	0.10	0.10	0.10	0.08	0.11	0.08	0.11	0.10	0.10	0.11	0.13	0.11	0.12	0.11	0.12	0.10
Ce	0.25	0.22	0.25	0.26	0.27	0.22	0.26	0.19	0.28	0.25	0.24	0.24	0.26	0.22	0.25	0.23	0.26	0.24
Pr	0.02	0.02	0.03	0.02	0.03	0.02	0.02	0.02	0.03	0.02	0.02	0.03	0.02	0.02	0.02	0.02	0.02	0.02
Nd	0.06	0.04	0.06	0.06	0.06	0.05	0.06	0.04	0.07	0.05	0.05	0.06	0.05	0.04	0.05	0.05	0.05	0.05
□/H_2O	1.08	0.77	0.97	1.07	1.07	0.99	1.07	1.23	1.13	1.10	0.96	0.62	1.07	1.02	0.98	1.01	1.02	0.96
A-site	2.00	2.00	2.00	2.00	2.00	2.00	2.00	2.00	2.00	2.00	2.00	2.00	2.00	2.00	2.00	2.00	2.00	
Nb	1.66	1.64	1.61	1.67	1.75	1.40	1.66	1.44	1.78	1.73	1.79	1.69	1.91	1.66	1.85	1.70	1.92	1.79
Ta	0.04	0.03	0.05	0.02	0.03	0.03	0.03	0.02	0.02	0.02	0.06	0.04	0.04	0.04	0.04	0.04	0.04	0.06
Ti	0.45	0.42	0.45	0.44	0.47	0.37	0.44	0.37	0.47	0.38	0.29	0.22	0.22	0.17	0.24	0.24	0.21	0.29
Si	0.28	0.22	0.30	0.32	0.15	0.70	0.32	0.75	0.18	0.34	0.20	0.31	0.21	0.54	0.22	0.39	0.17	0.20
Zr	0.02	0.01	0.01	0.01	0.01	0.01	0.01	0.01	0.01	-	0.02	0.02	-	0.02	0.01	0.03	0.01	0.02
B-site	2.44	2.32	2.42	2.45	2.41	2.51	2.47	2.58	2.45	2.47	2.35	2.28	2.37	2.42	2.36	2.40	2.35	2.35
F	0.33	0.57	0.29	0.18	0.37	0.11	0.09	0.53	0.13	0.12	0.48	0.46	0.28	0.24	0.34	0.27	0.37	0.48
OH, O	0.67	0.43	0.71	0.82	0.63	0.89	0.91	0.47	0.87	0.88	0.52	0.54	0.72	0.76	0.66	0.73	0.63	0.52
Y-site	1.00	1.00	1.00	1.00	1.00	1.00	1.00	1.00	1.00	1.00	1.00	1.00	1.00	1.00	1.00	1.00	1.00	
∑REE	0.43	0.38	0.44	0.45	0.47	0.39	0.46	0.33	0.49	0.44	0.43	0.46	0.48	0.42	0.45	0.42	0.46	0.43

Fluorite

Table 6-11: Fluorite microprobe analyses

Unit	Hypersolvus granite south (fine grained)															Hypersolvus granite north						
Sample	1001 7-9-Fl	1001 7-10-Fl	1001 7-11-Fl	1001 7-12-Fl	1003 2-1-Fl	1003 2-2-Fl	1003 2-3-Fl	1003 2-4-Fl	1003 2-5-Fl	1003 2-6-Fl	1003 2-9-Fl	1003 2-10-Fl	2047 71-7-Fl	2047 71-6-Fl	2047 71-14-Fl	1004 0-1-Fl	1004 0-4-Fl	1004 0-5-Fl	1004 0-13-Fl	2047 56-6-Fl	2047 56-7-Fl	Mdn
(wt. %)																						
SiO_2	-	0.02	2.54	0.02	0.01	0.01	0.01	0.02	0.01	-	0.01	-	0.01	0.01	0.20	0.04	0.01	0.02	0.02	0.02	0.01	0.01
CaO	50.59	51.09	45.74	50.23	50.42	50.32	50.25	50.58	49.71	50.04	50.52	50.28	50.23	49.90	49.82	50.53	50.42	49.32	50.48	50.29	50.11	50.28
Na_2O	0.06	0.07	0.56	0.10	0.08	0.11	0.13	0.16	0.21	0.13	0.08	0.15	0.09	0.08	0.11	0.10	0.13	0.15	0.09	0.21	0.13	0.11
SrO	-	-	-	-	-	-	-	-	-	-	-	-	-	-	-	-	-	-	-	-	-	-
PbO	-	-	-	-	-	0.01	-	-	-	-	-	-	-	-	-	0.01	-	-	-	-	-	-
ThO_2	-	-	0.03	0.06	-	-	0.03	0.03	0.04	-	-	-	0.02	0.01	0.01	-	-	-	-	0.02	0.04	-
P_2O_5	0.01	0.01	-	0.01	0.02	0.01	-	-	0.01	-	0.02	0.01	0.02	0.02	0.01	0.01	0.02	0.02	0.01	-	0.01	0.01
F	49.14	49.05	44.42	48.68	48.78	48.47	48.78	49.18	48.35	49.02	49.37	49.03	49.76	49.38	48.98	48.96	48.85	47.94	48.69	49.50	49.14	48.98
Y_2O_3	0.15	0.15	0.20	0.19	0.16	0.24	0.27	0.36	0.48	0.30	0.25	0.36	0.27	0.20	0.20	0.28	0.32	0.28	0.25	0.48	0.28	0.27
La_2O_3	-	0.02	0.01	-	0.03	0.06	0.07	-	0.06	-	0.02	0.03	0.01	0.01	0.05	0.04	-	0.05	0.06	0.04	0.08	0.03
Ce_2O_3	0.03	-	0.05	-	0.13	0.12	0.13	0.13	0.17	0.14	0.01	0.14	0.04	0.05	0.11	0.10	0.04	0.17	0.10	0.15	0.08	0.10
Pr_2O_3	-	-	0.04	-	0.05	0.07	0.10	0.04	-	-	0.08	0.07	0.03	0.03	0.05	0.18	0.07	-	0.06	-	-	0.04
Nd_2O_3	0.07	0.04	-	0.03	-	0.12	0.12	0.14	0.17	0.07	0.04	0.18	0.03	-	0.03	0.12	0.10	0.09	0.05	0.16	0.12	0.07
Sm_2O_3	-	0.02	0.10	-	-	0.09	0.07	0.09	-	0.04	0.01	0.02	0.05	0.03	-	0.06	0.10	0.11	0.05	0.06	0.06	0.05
Eu_2O_3	-	-	-	-	-	-	-	-	0.05	0.09	-	-	0.01	0.01	-	0.06	0.02	-	0.01	-	0.02	-
Gd_2O_3	-	-	0.01	0.08	-	-	0.03	0.10	0.14	0.05	0.04	0.13	-	0.01	-	0.03	-	0.01	-	-	0.04	0.01
Dy_2O_3	0.04	-	-	-	-	-	-	0.01	0.04	-	-	0.05	-	0.07	0.01	-	0.02	0.12	0.08	0.02	-	-
Total	100.1	100.5	93.7	99.4	99.7	99.6	100.0	100.8	99.4	99.9	100.5	100.4	100.6	99.8	99.6	100.5	100.1	98.3	100.0	101.0	100.1	100.0
Apfu (based on 2 anions)																						
Si	-	-	0.04	-	-	-	-	-	-	-	-	-	-	-	-	-	-	-	-	-	-	-
Ca	0.70	0.71	0.70	0.70	0.70	0.70	0.70	0.70	0.70	0.69	0.69	0.69	0.68	0.68	0.69	0.70	0.70	0.70	0.70	0.69	0.69	0.70
Na	-	-	0.02	-	-	-	-	-	0.01	-	-	-	-	-	-	-	-	-	-	0.01	-	-
F	2.00	2.00	2.00	2.00	2.00	2.00	2.00	2.00	2.00	2.00	2.00	2.00	2.00	2.00	2.00	2.00	2.00	2.00	2.00	2.00	2.00	2.00

Fluorite-fluocerite solid solution

Table 6-12: Fluorite-fluocerite solid solution microprobe analyses

Unit	HS south	Hypersolvus granite north																
Sample	10032-7-Fl	10010-1-Fl	10010-2-Fl	10010-4-Fl	10010-6-Fl	10010-7-Fl	10010-11-Fl	10011-19-Fl	10011-20-Fl	10011-24-Fl	10040-3-Fl	10040-8-Fl	10040-15-Fl	204749-1-Fl	204749-2-Fl	204749-3-Fl	204749-4-Fl	204749-5-Fl
(wt. %)																		
SiO_2	0.01	0.02	0.01	0.01	0.01	-	-	0.01	0.88	-	-	0.03	0.02	0.01	0.01	0.01	0.01	0.01
CaO	46.24	43.76	42.52	44.73	42.48	42.45	43.00	43.07	38.21	48.08	48.10	41.43	47.15	42.88	43.15	44.70	42.31	42.46
Na_2O	0.97	1.54	1.79	1.23	1.83	1.87	1.68	1.45	1.87	0.53	0.46	1.88	0.78	1.74	1.72	1.41	1.80	1.72
SrO	-	-	-	-	-	-	-	-	0.05	-	-	-	-	-	-	-	-	-
PbO	-	-	-	-	-	-	-	-	0.21	-	-	-	-	-	-	0.02	-	-
ThO_2	0.01	-	0.03	0.01	-	-	-	-	1.07	-	-	0.01	0.01	-	0.02	0.01	0.01	0.04
P_2O_5	0.02	0.02	0.01	0.02	0.01	0.01	0.02	0.02	0.01	0.01	0.01	0.01	0.01	0.01	0.02	-	0.03	0.02
F	48.10	47.68	46.82	47.40	46.82	47.73	47.15	47.69	44.87	48.46	48.90	46.59	49.11	47.47	47.02	48.23	47.42	47.75
Cl	0.01	-	0.01	0.01	-	-	0.01	0.01	0.02	-	-	-	-	-	0.01	0.01	-	-
Y_2O_3	1.98	4.05	4.19	3.64	4.20	4.30	4.02	3.41	3.78	1.38	1.32	4.63	2.15	3.70	3.78	3.14	3.56	3.60
La_2O_3	0.37	0.17	0.36	0.08	0.53	0.39	0.48	0.42	1.10	0.09	0.08	0.70	0.08	0.54	0.49	0.38	0.68	0.56
Ce_2O_3	0.96	0.72	1.23	0.39	1.47	1.36	1.22	1.10	2.65	0.25	0.37	1.71	0.24	1.64	1.47	1.08	1.74	1.69
Pr_2O_3	0.14	0.13	0.31	0.06	0.19	0.27	0.17	0.24	0.26	0.10	0.13	0.40	0.04	0.15	0.27	0.22	0.22	0.24
Nd_2O_3	0.76	0.79	0.89	0.43	1.09	0.92	0.90	0.85	1.66	0.29	0.25	1.15	0.34	1.09	1.13	0.99	1.20	1.20
Sm_2O_3	0.14	0.34	0.30	0.22	0.23	0.18	0.16	0.31	0.48	0.08	0.14	0.26	0.13	0.30	0.41	0.24	0.33	0.44
Eu_2O_3	0.03	0.15	0.04	0.13	0.03	0.10	0.09	0.04	-	-	-	0.20	0.06	0.14	0.10	-	0.20	0.06
Gd_2O_3	0.22	0.54	0.49	0.42	0.55	0.48	0.51	0.48	0.52	0.14	0.18	0.49	0.20	0.49	0.49	0.34	0.43	0.36
Dy_2O_3	-	0.21	0.21	0.15	0.11	0.11	0.06	0.15	0.40	0.11	-	0.13	0.21	0.24	0.23	0.20	0.25	0.17
Total	100.0	100.1	99.2	98.9	99.6	100.2	99.5	99.2	98.0	99.5	99.9	99.5	100.5	100.4	100.3	101.0	100.2	100.3
Apfu (based on 2 anions)																		
Ca	0.65	0.62	0.62	0.64	0.61	0.60	0.62	0.61	0.58	0.67	0.67	0.60	0.65	0.61	0.62	0.63	0.60	0.60
Na	0.02	0.04	0.05	0.03	0.05	0.05	0.04	0.04	0.05	0.01	0.01	0.05	0.02	0.04	0.04	0.04	0.05	0.04
F	2.00	2.00	2.00	2.00	2.00	2.00	2.00	2.00	2.00	2.00	2.00	2.00	2.00	2.00	2.00	2.00	2.00	2.00
Y	0.01	0.03	0.03	0.03	0.03	0.03	0.03	0.02	0.03	0.01	0.01	0.03	0.01	0.03	0.03	0.02	0.03	0.03
La	-	-	-	-	-	-	-	-	0.01	-	-	-	-	0.01	0.01	0.01	0.01	0.01
Ce	-	-	0.01	-	0.01	0.01	0.01	0.01	0.01	-	-	0.01	-	0.01	0.01	-	0.01	0.01
Nd	-	-	-	-	0.01	-	-	-	0.01	-	-	0.01	-	0.05	0.05	0.04	0.05	0.05

Table 6-12: Fluorite-fluocerite solid solution microprobe analyses (continued)

Unit		Dark grey porphyritic granite								Transsolvus granite				
Sample	204756-2-Fl	10034-3-Fl	10034-4-Fl	10034-5-Fl	10034-6-Fl	10201-1-Fl	10201-2-Fl	10201-3-Fl	10201-4-Fl	204720-1-Fl	204720-6-Fl	204720-8-Fl	204720-9-Fl	Mdn
(wt. %)														
SiO_2	0.01	0.01	0.01	0.02	0.02	0.01	0.02	0.01	0.01	0.01	-	0.02	0.07	0.01
CaO	45.13	41.60	41.79	43.72	47.08	41.97	42.22	42.08	42.43	38.13	40.85	38.76	37.94	42.47
Na_2O	0.92	1.95	1.89	1.47	0.75	1.94	1.99	1.91	1.90	2.36	2.07	1.88	1.98	1.80
SrO	0.01	-	-	-	-	-	-	-	-	-	-	-	-	-
PbO	0.01	-	0.03	0.02	0.01	-	-	-	-	-	-	0.02	-	-
ThO_2	0.04	-	0.01	-	0.01	0.02	-	0.06	-	-	-	0.02	-	0.01
P_2O_5	0.02	0.02	0.02	0.01	0.01	0.01	0.03	-	0.01	0.03	0.01	0.01	0.01	0.01
F	47.10	46.92	47.92	48.29	48.60	47.20	47.49	47.11	47.35	47.77	47.25	47.52	47.33	47.48
Cl	-	0.01	-	-	-	-	0.01	0.01	-	0.01	-	0.01	0.01	-
Y_2O_3	1.95	4.38	4.24	3.54	1.61	4.17	4.72	4.71	4.72	4.17	4.90	3.70	4.01	3.89
La_2O_3	0.36	0.61	0.53	0.45	0.17	0.76	0.41	0.41	0.39	1.01	0.45	0.70	0.63	0.45
Ce_2O_3	0.88	1.60	1.70	1.11	0.61	1.82	1.44	1.43	1.22	2.57	1.34	1.86	1.71	1.40
Pr_2O_3	0.20	0.13	0.26	0.26	0.16	0.39	0.28	0.30	0.22	0.40	0.21	0.41	0.25	0.23
Nd_2O_3	0.73	1.17	1.12	0.85	0.66	1.27	0.91	0.97	0.89	1.60	0.98	1.22	1.31	0.97
Sm_2O_3	0.08	0.32	0.42	0.29	0.20	0.35	0.29	0.35	0.31	0.40	0.35	0.29	0.29	0.29
Eu_2O_3	0.11	0.05	-	0.06	0.01	0.12	0.03	0.13	0.02	0.08	0.08	0.12	-	0.06
Gd_2O_3	0.13	0.62	0.51	0.38	0.27	0.51	0.50	0.47	0.48	0.61	0.54	0.48	0.45	0.48
Dy_2O_3	0.02	0.20	0.24	0.21	0.06	0.06	0.15	0.31	0.36	0.21	0.24	0.32	0.20	0.20
Total	97.7	99.6	100.7	100.7	100.2	100.6	100.5	100.2	100.3	99.4	99.3	97.3	96.2	100.0
Apfu (based on 2 anions)														
Ca	0.65	0.60	0.59	0.61	0.66	0.60	0.60	0.61	0.61	0.54	0.59	0.55	0.54	0.61
Na	0.02	0.05	0.05	0.04	0.02	0.05	0.05	0.05	0.05	0.06	0.05	0.05	0.05	0.05
F	2.00	2.00	2.00	2.00	2.00	2.00	2.00	2.00	2.00	2.00	2.00	2.00	2.00	2.00
Y	0.01	0.03	0.03	0.02	0.01	0.03	0.03	0.03	0.03	0.03	0.03	0.03	0.03	0.03
Ce	-	-	-	-	-	0.01	0.01	0.01	0.01	0.01	0.01	0.01	0.01	0.01
Nd	-	0.01	0.01	0.01	-	0.01	-	-	-	0.01	-	0.01	0.01	-

Gagarinite-(Ce)

Table 6-13: Gagarinite-(Ce) microprobe analyses

Unit	Transsolvus granite					
Sample	204720-2-Gag	204720-3-Gag	204720-4-Gag	204720-5-Gag	204722-13-Gag	Mean
(wt. %)						
SiO_2	0.02	0.02	0.02	0.02	0.02	0.02
CaO	10.5	10.7	10.4	10.1	10.5	10.4
Na_2O	6.24	5.09	8.35	5.86	6.73	6.45
SrO	0.08	0.04	0.07	0.05	0.09	0.07
PbO	-	-	0.01	0.02	-	0.01
ThO_2	0.01	-	-	-	0.01	0.01
UO_2	0.02	0.01	0.01	-	0.02	0.01
P_2O_5	0.02	0.02	0.01	0.02	0.02	0.01
F	35.4	34.5	36.4	34.9	35.6	35.4
Cl	0.01	0.02	0.01	-	0.01	0.01
Y_2O_3	4.07	4.67	3.13	3.14	3.38	3.68
La_2O_3	9.66	9.87	10.0	10.6	10.6	10.2
Ce_2O_3	18.6	19.5	19.4	19.6	19.6	19.3
Pr_2O_3	2.47	2.46	2.23	2.44	2.39	2.40
Nd_2O_3	8.16	8.63	8.30	8.69	8.22	8.40
Sm_2O_3	1.35	1.24	1.22	1.25	1.17	1.25
Eu_2O_3	0.03	0.08	-	0.05	0.23	0.10
Gd_2O_3	1.17	1.43	1.16	1.22	1.29	1.26
Dy_2O_3	0.49	0.45	0.44	0.33	0.34	0.41
Total	98.2	98.7	101.1	98.3	100.2	99.3
Apfu (based on 6 anions)						
Ca	0.60	0.63	0.58	0.59	0.60	0.60
Na	0.32	0.27	0.42	0.31	0.35	0.33
F	6.00	6.00	6.00	6.00	6.00	6.00
Y	0.06	0.07	0.04	0.05	0.05	0.05
La	0.10	0.10	0.10	0.11	0.10	0.10
Ce	0.18	0.20	0.18	0.19	0.19	0.19
Pr	0.02	0.02	0.02	0.02	0.02	0.02
Nd	0.08	0.08	0.08	0.08	0.08	0.08
Sm	0.01	0.01	0.01	0.01	0.01	0.01
Gd	0.01	0.01	0.01	0.01	0.01	0.01
∑ REE	0.47	0.50	0.45	0.48	0.47	0.47

Fluorbritholite-(Ce)

Table 6-14: Fluorbritholite-(Ce) microprobe analyses

Unit	Transsolvus granite					
Sample	204715-7-Fbr	204715-8-Fbr	204715-9-Fbr	204715-10-Fbr	204715-11-Fbr	Mean
(wt. %)						
SiO_2	22.09	20.48	20.66	20.57	20.83	20.93
CaO	2.41	3.18	3.01	3.05	3.19	2.97
Na_2O	1.29	1.59	1.67	1.66	1.82	1.60
SrO	0.11	0.07	0.03	0.08	0.08	0.07
PbO	0.61	1.01	0.99	0.91	0.30	0.77
ThO_2	0.04	0.31	0.28	0.29	0.03	0.19
UO_2	0.01	-	-	0.01	-	-
P_2O_5	0.17	1.10	1.48	1.66	0.07	0.89
F	1.73	2.35	2.11	1.97	2.09	2.05
Cl	0.04	0.07	0.03	0.03	0.01	0.04
Y_2O_3	3.27	2.55	2.07	2.19	1.32	2.28
La_2O_3	15.62	14.03	14.32	14.07	19.58	15.52
Ce_2O_3	29.14	30.47	30.53	30.93	31.01	30.41
Pr_2O_3	3.37	3.73	3.66	3.97	3.70	3.69
Nd_2O_3	12.15	12.24	12.37	12.17	13.75	12.54
Sm_2O_3	1.79	1.75	1.89	1.98	1.89	1.86
Eu_2O_3	-	0.04	-	0.04	-	0.01
Gd_2O_3	1.60	1.55	1.22	1.43	1.44	1.45
Dy_2O_3	0.27	0.42	0.66	0.58	0.08	0.40
Total	94.95	95.92	96.09	96.74	100.31	96.80
Apfu (based on 12.5 anions)						
Si	3.11	2.86	2.87	2.85	2.88	2.91
Ca	0.36	0.48	0.45	0.45	0.47	0.44
Na	0.35	0.43	0.45	0.45	0.49	0.43
Sr	0.01	0.01	-	0.01	0.01	0.01
Pb	0.02	0.04	0.04	0.03	0.01	0.03
Th	-	0.01	0.01	0.01	-	0.01
P	0.02	0.13	0.17	0.19	0.01	0.11
F	0.77	1.04	0.93	0.86	0.91	0.90
Cl	0.01	0.02	0.01	0.01	-	0.01
Y	0.24	0.19	0.15	0.16	0.10	0.17
La	0.81	0.72	0.73	0.72	1.00	0.80
Ce	1.50	1.56	1.55	1.57	1.57	1.55
Pr	0.17	0.19	0.19	0.20	0.19	0.19
Nd	0.61	0.61	0.61	0.60	0.68	0.62
Sm	0.09	0.08	0.09	0.09	0.09	0.09
Gd	0.07	0.07	0.06	0.07	0.07	0.07
Dy	0.01	0.02	0.03	0.03	-	0.02
∑REE	3.27	3.26	3.26	3.27	3.59	3.33

APPENDIX 3: PARTITIONING COEFFICIENTS AND MELT COMPOSITIONS

Table 6-15: Partitioning coefficients (after White, 2003)

Unit	Hypersolvus granite south*			Hypersolvus granite north		Transsolvus granite					Enclaves	
Sample	204768	204771	10017	204756	10040	204743	10039	204713	204715	204720	204712	204720-EN
*Bulk rock (*and perthitic alkali feldspar) compositions*												
SiO_2 *(wt. %)*	69.07	70.42	67.64	70.68	71.16	70.66	71.61	70.75	71.33	69.73	69.33	69.33
CaO	0.89	0.55	0.99	0.55	0.61	0.56	0.55	0.43	0.31	0.32	0.66	0.66
Na_2O/K_2O	0.99	1.05	1.02	1.07	1.05	1.10	2.28	1.08	1.26	0.96	0.40	0.40
Alk. index	1.05	1.13	1.16	1.19	1.12	1.22	1.29	1.44	1.38	1.49	1.17	1.17
Avg. Xor*	0.50	0.45	0.47	0.50	0.56	0.57	0.78	0.75	0.60	0.44	0.49	0.24
Partitioning coefficients perthitic alkali feldspar-melt												
Rb	0.368	0.363	0.331	0.352	0.374	0.345	0.340	0.301	0.317	0.284	0.344	0.344
Y	0.024	0.040	0.017	0.039	0.040	0.037	0.039	0.037	0.048	0.038	0.031	0.031
Zr	0.044	0.053	0.034	0.054	0.060	0.053	0.060	0.049	0.055	0.041	0.044	0.044
Nb	0.041	0.049	0.029	0.050	0.057	0.048	0.055	0.043	0.049	0.035	0.039	0.039
Ba	12.57	11.32	11.82	12.57	14.07	14.32	19.57	18.82	15.07	11.07	12.32	6.07
La	0.054	0.061	0.038	0.058	0.069	0.055	0.057	0.041	0.049	0.034	0.049	0.049
Ce	0.042	0.053	0.028	0.050	0.058	0.047	0.048	0.036	0.046	0.031	0.041	0.041
Pr	0.036	0.053	0.023	0.053	0.061	0.052	0.061	0.047	0.058	0.038	0.038	0.038
Nd	0.031	0.046	0.022	0.045	0.048	0.044	0.047	0.042	0.052	0.039	0.036	0.036
Sm	0.018	0.034	0.012	0.034	0.034	0.032	0.034	0.034	0.046	0.036	0.025	0.025
Eu	1.456	0.752	1.238	0.548	0.676	0.467	0.079	0.194	0.178	0.225	1.675	1.675
Gd	0.020	0.036	0.014	0.035	0.034	0.034	0.035	0.036	0.048	0.039	0.027	0.027
Dy	0.022	0.039	0.015	0.038	0.038	0.036	0.038	0.038	0.050	0.040	0.029	0.029
Er	0.027	0.041	0.020	0.040	0.041	0.039	0.040	0.038	0.047	0.038	0.033	0.033
Yb	0.027	0.039	0.021	0.038	0.038	0.038	0.039	0.039	0.047	0.041	0.033	0.033

* fine grained samples of the southern hypersolvus granite

Table 6-16: Melt compositions

Unit	Hypersolvus granite south														
Sample	204768-1	204768-2	204768-3	204768-4	204771-1	204771-2	204771-3	204771-4	204771-5	204771-6	204771-7	10017-1	10017-2	10017-3	Mdn	MAD
(ppm)																
Rb	1456	1434	1592	1466	1480	974	1235	1425	1084	2008	1189	1301	1065	2136	1429	166
Y	241	222	130	292	120	72.4	183	47.5	67.9	185	74.9	439	511	460	184	108
Zr	549	385	288	286	154	136	103	280	449	105	335	1102	1996	1175	311	152
Nb	158	131	105	317	46.9	45.9	65.0	43.1	64.0	14.2	175	336	261	286	118	59
Ba	1.1	1.2	1.4	1.1	1.3	1.1	0.9	0.7	0.6	2.5	0.8	1.1	3.1	10.9	1.1	0.2
La	12.5	13.4	5.9	35.8	10.0	6.5	12.9	4.5	5.5	26.2	8.7	61.8	48.6	43.5	12.7	6.6
Ce	74.2	175	218	95.8	36.0	19.3	46.3	19.7	23.4	59.8	38.2	197	195	220	67.0	36.4
Pr	9.7	9.7	4.7	19.4	5.3	2.9	6.7	2.5	3.0	6.4	4.8	34.3	33.8	32.8	6.6	3.3
Nd	56.6	101	93.5	102	32.6	16.2	42.2	15.2	19.2	38.5	29.8	186	158	161	49.4	26.0
Sm	28.5	31.1	13.5	56.1	20.4	9.7	25.5	7.4	10.7	12.4	11.8	96.8	91.5	93.0	23.0	9.7
Eu	0.07	0.06	0.03	0.06	0.16	0.06	0.21	0.04	0.06	1.26	0.06	0.11	0.12	0.12	0.07	0.02
Gd	31.4	34.9	17.8	65.7	21.5	13.0	27.7	8.5	10.1	13.3	12.1	90.8	91.5	95.8	24.6	9.9
Dy	53.0	49.0	29.1	58.7	26.4	14.7	36.7	10.3	13.4	23.5	16.0	96.4	126	135	32.9	15.7
Er	33.8	26.8	16.5	26.3	14.6	8.8	18.8	7.8	9.9	16.5	9.0	40.0	58.0	51.1	17.6	7.6
Yb	29.5	25.2	13.2	18.5	11.7	9.3	10.9	18.3	12.1	12.2	9.9	23.5	38.2	34.0	15.8	3.9
∑REE	329	466	413	478	179	101	228	94	107	210	140	827	840	866	250	127

Table 6-16: Melt compositions (continued)

Unit	Hypersolvus granite north																
Sample	204756-1	204756-2	204756-3	204756-4	204756-5	204756-6	204756-7	204756-8	10040-1	10040-2	10040-3	10040-4	10040-5	10040-6	10040-7	Mdn	MAD
(ppm)																	
Rb	2118	2578	2126	2132	2016	1811	2408	2229	2627	2476	2727	2082	3298	2301	2403	2301	184
Y	242	384	305	196	309	267	332	208	87.0	423	234	62.6	168	281	331	267	64
Zr	1652	1424	139	114	579	720	597	1021	150	1774	209	66.7	625	1684	398	597	448
Nb	411	568	32.5	13.1	101	208	137	435	67.3	130	107	12.5	561	136	61.9	130	77
Ba	3.6	4.7	3.3	3.2	3.4	3.5	3.7	4.1	2.8	2.0	2.7	1.1	4.4	4.4	6.1	3.5	0.7
La	103	92.2	135	74.7	141	107	107	60.9	56.9	122	60.1	75.6	106	54.4	91.6	92.2	17.6
Ce	457	361	547	283	456	349	366	250	141	405	178	148	304	157	319	319	86
Pr	38.6	34.9	59.6	32.0	46.6	36.7	42.1	24.2	11.9	55.6	16.7	14.2	32.0	19.7	42.1	34.9	10.7
Nd	234	195	322	171	273	201	224	134	81.9	234	123	83.0	188	101	201	195	39
Sm	47.8	45.7	80.4	41.7	59.7	45.8	57.5	31.7	15.4	75.0	26.9	11.2	32.0	34.0	43.8	43.8	12.1
Eu	0.19	0.19	0.34	0.18	0.25	0.18	0.23	0.13	0.05	0.19	0.08	0.03	0.12	0.20	0.25	0.19	0.05
Gd	41.3	38.7	69.5	36.1	50.1	38.8	49.3	25.1	11.7	318	29.2	9.6	27.3	40.0	63.0	38.8	11.3
Dy	70.3	116	97.2	56.0	70.7	69.8	88.0	59.7	17.8	74.5	46.4	9.6	30.7	114	90.0	70.3	19.7
Er	83.9	137	71.7	42.7	66.0	92.8	109	86.6	10.3	50.6	31.0	6.8	24.3	82.1	62.5	66.0	23.3
Yb	139.5	186	66.2	37.7	85.5	179	158	170	14.1	35.2	14.3	8.0	39.3	80.5	56.1	66.2	52.0
∑REE	1215	1207	1450	775	1248	1121	1201	842	361	1370	526	366	784	682	970	927	246

Table 6-16: Melt compositions (continued)

Unit	Transsolvus granite (1/2)																
Sample	204743-1	204743-2	204743-3	204743-4	204743-5	204743-6	10039-1	204713-1	204713-2	204715-1	204715-2	204715-3	204715-4	204715-5	204715-6	204715-7	204715-8
(ppm)																	
Rb	4151	4410	4941	5379	4865	4883	5695	10558	8470	9838	9964	6792	7820	10154	5304	5566	8356
Y	721	695	1283	1181	315	1031	640	1356	2210	1153	983	1656	770	861	1507	3705	880
Zr	1880	1448	2406	1692	865	494	875	2204	477	20218	283	19135	587	1209	543	1480	632
Nb	368	661	622	671	517	223	639	1145	442	266	5074	1001	402	463	162	684	256
Ba	2.7	3.1	5.2	6.0	6.2	5.2	1.6	0.4	0.3	1.4	1.9	1.2	1.0	1.1	0.7	1.1	1.0
La	106	160	136	325	153	205	326	233	322	500	549	516	386	479	354	534	589
Ce	361	575	535	634	479	721	1103	268	390	503	944	432	285	615	406	865	661
Pr	35.7	53.9	52.6	63.8	47.5	71.8	77.6	39.5	57.5	58.5	78.7	73.7	49.1	73.6	57.8	107	78.7
Nd	188	295	284	440	229	378	496	227	321	344	446	371	205	396	295	595	404
Sm	52.4	69.5	92.7	95.2	47.1	109	112	74.4	112	81.2	49.1	108	50.8	79.7	68.2	166	65.2
Eu	0.25	0.29	0.51	0.51	0.35	0.52	2.99	0.96	1.44	1.41	0.97	5.74	0.99	1.31	1.35	3.13	1.18
Gd	56.1	76.1	111	106	56.4	90.0	114	97.6	156	95.8	99.3	134	63.6	90.3	102	235	75.6
Dy	150	152	303	270	80	226	119	148	267	164	110	204	99.3	115	190	453	119
Er	147	144	264	240	57	235	64.4	104	191	117	95.5	147	78.5	90.4	164	398	89.1
Yb	173	166	275	255	61.6	192	72.4	164	155	119	105	131	82.0	87.7	169	409	81.7
∑REE	1269	1692	2052	2430	1211	2228	2488	1357	1972	1984	2478	2123	1300	2028	1808	3764	2164

Table 6-16: Melt compositions (continued)

Unit	Transsolvus granite (2/2)													
Sample	204715-9	204720-1	204720-2	204720-3	204720-4	204720-5	204720-6	204720-7	204720-8	204720-9	204720-10	204720-11	Mdn	MAD
(ppm)														
Rb	9129	4392	3555	4144	2592	2451	3795	6956	6631	7231	6229	6254	5695	1536
Y	2732	1126	666	655	705	1072	697	999	1004	797	760	734	983	262
Zr	1228	851	1012	275	1478	867	1160	2053	5291	1788	6281	2440	1228	641
Nb	120	337	222	180	187	426	347	1263	1350	362	820	594	442	218
Ba	1.7	1.7	1.8	1.4	1.2	1.8	1.5	2.3	1.8	2.6	1.9	1.8	1.7	0.6
La	441	1196	646	807	851	1066	689	860	1072	842	631	838	516	194
Ce	419	2249	1254	1360	1712	2001	1472	1549	2306	1812	1571	1831	721	361
Pr	75.6	249	136	156	174	217	151	159	184	176	145	163	78	30
Nd	359	1269	719	725	913	1102	788	829	1008	865	801	890	440	211
Sm	112	239	140	133	162	205	146	141	152	143	134	133	112	32
Eu	2.32	1.93	1.16	1.10	1.22	1.73	1.22	1.20	1.27	1.14	1.20	1.11	1.20	0.22
Gd	170	210	118	117	147	183	127	129	140	131	130	122	117	22
Dy	345	240	140	133	152	220	145	174	172	147	143	128	152	32
Er	293	185	108	96.2	109	167	108	141	158	99.1	105	91.5	117	29
Yb	277	225	132	106	119	193	128	145	186	85.6	104	84.8	132	45
∑REE	2495	6064	3395	3633	4342	5354	3756	4130	5377	4302	3765	4283	2386	1121

Table 6-16: Melt compositions (continued)

Unit	Enclaves								
Sample	204712 -1	204712 -2	204712 -3	204712 -4	204712 -5	204720 EN-1	204720 EN-2	Mdn	MAD
(ppm)									
Rb	4155	3719	1371	4347	5178	1892	2508	3719	1212
Y	479	642	557	753	890	613	1092	642	111
Zr	6424	1957	2753	3732	2081	1669	2660	2660	703
Nb	803	425	229	474	489	438	671	474	48
Ba	8.5	0.7	0.4	0.5	5.0	1.8	2.2	1.8	1.3
La	576	711	1200	863	428	439	957	711	246
Ce	1076	1200	1679	1339	1069	1370	2374	1339	262
Pr	156	182	288	223	143	154	283	182	39
Nd	733	814	1247	995	660	766	1432	814	154
Sm	132	145	210	188	195	154	273	188	34
Eu	0.23	0.11	0.14	0.16	0.38	0.15	0.23	0.16	0.05
Gd	111	106	167	160	170	129	232	160	31
Dy	81.2	87.4	96.0	145	184	127	192	127	40
Er	36.4	85.9	43.7	61.1	81.0	76.7	112	76.7	15.6
Yb	30.0	295	35.7	44.6	59.3	75.5	102	59.3	23.7
∑REE	2932	3626	4966	4020	2989	3290	5957	3656	638